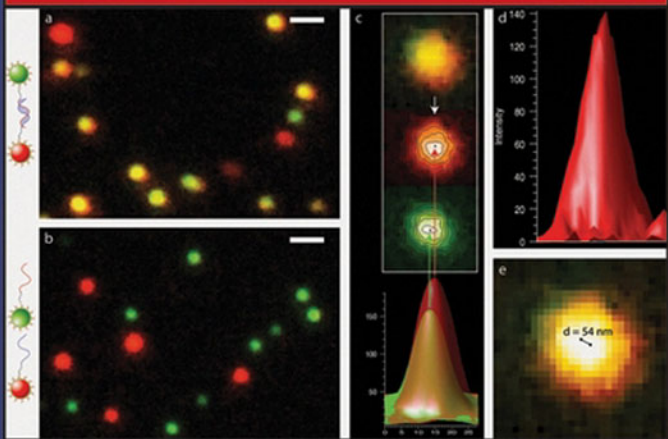


Biomedical Nanostructures



EDITED BY

KENNETH E. GONSALVES

CRAIG R. HALBERSTADT

CATO T. LAURENCIN

LAKSHMI S. NAIR

BIOMEDICAL NANOSTRUCTURES



THE WILEY BICENTENNIAL—KNOWLEDGE FOR GENERATIONS

Each generation has its unique needs and aspirations. When Charles Wiley first opened his small printing shop in lower Manhattan in 1807, it was a generation of boundless potential searching for an identity. And we were there, helping to define a new American literary tradition. Over half a century later, in the midst of the Second Industrial Revolution, it was a generation focused on building the future. Once again, we were there, supplying the critical scientific, technical, and engineering knowledge that helped frame the world. Throughout the 20th Century, and into the new millennium, nations began to reach out beyond their own borders and a new international community was born. Wiley was there, expanding its operations around the world to enable a global exchange of ideas, opinions, and know-how.

For 200 years, Wiley has been an integral part of each generation's journey, enabling the flow of information and understanding necessary to meet their needs and fulfill their aspirations. Today, bold new technologies are changing the way we live and learn. Wiley will be there, providing you the must-have knowledge you need to imagine new worlds, new possibilities, and new opportunities.

Generations come and go, but you can always count on Wiley to provide you the knowledge you need, when and where you need it!

WILLIAM J. PESCE
PRESIDENT AND CHIEF EXECUTIVE OFFICER

PETER BOOTH WILEY
CHAIRMAN OF THE BOARD

BIOMEDICAL NANOSTRUCTURES

Edited by

Kenneth E. Gonsalves

Polymer Nanotechnology Laboratory

Department of Chemistry and Center for Optoelectronics and Optical Communications, University of North Carolina at Charlotte

Craig R. Halberstadt

Department of Surgery

Carolinas Medical Center

Cato T. Laurencin

Department of Orthopaedic Surgery

Department of Biomedical & Chemical Engineering

University of Virginia

Lakshmi S. Nair

Department of Orthopaedic Surgery

University of Virginia



WILEY-INTERSCIENCE

A JOHN WILEY & SONS, INC., PUBLICATION

Copyright © 2008 by John Wiley & Sons, Inc. All rights reserved

Published by John Wiley & Sons, Inc., Hoboken, New Jersey
Published simultaneously in Canada

No part of this publication may be reproduced, stored in a retrieval system, or transmitted in any form or by any means, electronic, mechanical, photocopying, recording, scanning, or otherwise, except as permitted under Section 107 or 108 of the 1976 United States Copyright Act, without either the prior written permission of the Publisher, or authorization through payment of the appropriate per-copy fee to the Copyright Clearance Center, Inc., 222 Rosewood Drive, Danvers, MA 01923, (978) 750-8400, fax (978) 750-4470, or on the web at www.copyright.com. Requests to the Publisher for permission should be addressed to the Permissions Department, John Wiley & Sons, Inc., 111 River Street, Hoboken, NJ 07030, (201) 748-6011, fax (201) 748-6008, or online at <http://www.wiley.com/go/permission>.

Limit of Liability/Disclaimer of Warranty: While the publisher and author have used their best efforts in preparing this book, they make no representations or warranties with respect to the accuracy or completeness of the contents of this book and specifically disclaim any implied warranties of merchantability or fitness for a particular purpose. No warranty may be created or extended by sales representatives or written sales materials. The advice and strategies contained herein may not be suitable for your situation. You should consult with a professional where appropriate. Neither the publisher nor author shall be liable for any loss of profit or any other commercial damages, including but not limited to special, incidental, consequential, or other damages.

For general information on our other products and services or for technical support, please contact our Customer Care Department within the United States at (800) 762-2974, outside the United States at (317) 572-3993 or fax (317) 572-4002.

Wiley also publishes its books in a variety of electronic formats. Some content that appears in print may not be available in electronic formats. For more information about Wiley products, visit our web site at www.wiley.com.

Wiley Bicentennial Logo: Richard J. Pacifico

Library of Congress Cataloging-in-Publication Data:

Biomedical nanostructures / by Kenneth E. Gonsalves ... [et al.].

p. : cm.

Includes bibliographical references and index.

ISBN 978-0-471-92552-1 (cloth)

1. Nanotechnology. 2. Nanostructures. 3. Nanostructured materials. 4.

Biomedical engineering. I. Gonsalves, Kenneth E.

[DNLM: 1. Nanostructures. 2. Biocompatible Materials. 3. Biomedical Technology. QT 36.5 B61525 2008]

R857.N34B5568 2008

610.28-dc22

2007019895

Printed in the United States of America

10 9 8 7 6 5 4 3 2 1

CONTENTS

Contributors	xix
Part I. Nanostructure Fabrication	1
1 Nanofabrication Techniques	3
<i>Joseph W. Freeman, Lee D. Wright, Cato T. Laurencin, and Subhabrata Bhattacharyya</i>	
1.1 Introduction	3
1.2 Photolithography	4
1.2.1 Cleaning of the Substrate	4
1.2.2 Application of the Photoresist Material	5
1.2.3 Soft Baking	5
1.2.4 Exposure	6
1.2.4.1 Contact Printing	6
1.2.4.2 Proximity Printing	6
1.2.4.3 Projection Printing	6
1.2.5 Developing	6
1.2.6 Hard Baking	6
1.2.7 Limitations of Photolithography	7
1.3 Specialized Lithography Techniques	7
1.3.1 Electron Beam Lithography	7
1.3.2 Nanosphere Lithography	8
1.3.3 Soft Lithography	8
1.3.4 Dip Pen Lithography	8
1.3.5 LIGA	10
1.3.5.1 Deep X-Ray Lithography	10
1.3.5.2 Electroplating	11
1.3.5.3 Molding	11
1.4 Thin Film Deposition	11
1.5 Electrospinning	13
1.6 Nanospheres	15
1.7 Carbon Nanotubes	16
1.7.1 Electric Arc Discharge	17

1.7.2	Laser Ablation	17
1.7.3	Chemical Vapor Deposition	17
1.7.4	Photolytic Laser-Assisted Chemical Vapor Deposition	18
1.7.5	Pyrolytic Laser-Assisted Chemical Vapor Deposition	19
1.7.6	Substrate-Site-Selective Growth	19
1.8	Self-Assembled Nanostructures	20
1.9	Conclusions	21
	References	22
2	Micro/Nanomachining and Fabrication of Materials for Biomedical Applications	25
	<i>Wei He, Kenneth E. Gonsalves, and Craig R. Halberstadt</i>	
2.1	Introduction	25
2.2	Overview of Ion Implantation Process	26
2.3	Micro/Nanomachining of “Soft” Polymeric Biomaterials	27
2.3.1	Orthopedic Applications	27
2.3.2	Blood-Contacting Devices	32
2.3.3	Other Applications	33
2.4	Micro/Nanomachining of “Hard” Metallic Biomaterials	35
2.4.1	Orthopedic Applications	36
2.4.2	Dental Implants	38
2.4.3	Blood-Contacting Devices	38
2.4.4	Other Applications	39
2.5	Novel Biocompatible Photoresists	39
2.6	Three-Dimensional Lithography	41
2.7	Conclusions	41
	References	42
3	Novel Nanostructures as Molecular Nanomotors	49
	<i>Yan Chen, Jianwei Jeff Li, Zehui Charles Cao, and Weihong Tan</i>	
3.1	Introduction	49
3.2	Multi-DNA Nanomotors	51
3.3	Single DNA Nanomotors	55
3.4	Conclusions	59
	References	60
4	Bioconjugation of Soft Nanomaterials	61
	<i>Neetu Singh, William H. Blackburn, and Andrew Lyon</i>	
4.1	Introduction	61
4.1.1	Definition of Hydrogels	62
4.1.2	Classification of Hydrogels	62

4.1.3	Stimuli-Sensitive Polymers	62
4.1.4	Microgels and Nanogels	64
4.2	Core/Shell Structured Materials	66
4.2.1	Block Copolymer Micelles	68
4.3	Bioconjugated Hydrogel Particles in Nanotechnology	70
4.3.1	Drug/Gene Delivery	70
4.3.2	Analytical Applications	77
4.3.3	Biomaterials	80
4.4	Conclusions	83
	References	84
5	Nanotechnology and Drug Delivery	93
	<i>Xiaojun Yu, Chandra M. Valmikinathan, Amanda Rogers, and Junping Wang</i>	
5.1	Introduction	93
5.2	Advantages of Nanostructured Delivery Systems	94
5.2.1	Localized and Targeted Delivery	95
5.2.2	Controlled Delivery	95
5.2.3	Enhanced Circulation Time and Biodistribution	95
5.2.4	Drug Solubility	95
5.2.5	Intracellular Drug Delivery	96
5.2.6	Ability to Cross Biological Membranes	96
5.2.7	Enhanced Surface Areas	96
5.3	Activation and Targeting of Nanotechnology-Based Drug Delivery Systems (Externally and Internally)	97
5.3.1	Activation and Targeting through PhysicoChemical Stimuli	97
5.3.1.1	pH-Sensitive Carriers	97
5.3.1.2	Thermally Responsive Carriers	99
5.3.1.3	Photochemically Controlled Delivery System	100
5.3.1.4	Magnetic Targeted Drug Delivery of Nanocarriers	101
5.3.1.5	Ultrasound-Mediated Drug Delivery and Targeting	101
5.3.2	Drug Targeting through Targeting Molecules	101
5.3.2.1	Monoclonal Antibodies	101
5.3.2.2	Folate Ligands	102
5.3.2.3	Transferrin Ligands	102
5.3.2.4	Aptamers	103
5.3.2.5	Lectins	103
5.3.2.6	Synthetically Modified and Designed Peptide Ligands	104
5.3.2.7	Other Targeting Ligands	104
5.4	Multifunctional Nanoparticle Systems	105
5.4.1	Multivalent Strategies	105

5.4.1.1	Dendrimers	105
5.4.1.2	Polymeric Nanocarriers	105
5.4.1.3	Carbone Nanotubes (CNT)	107
5.4.2	Exploiting Inherent Material Properties	107
5.4.2.1	Electrical Properties	107
5.4.2.2	Optical Properties	108
5.4.2.3	Magnetic Properties	108
5.4.2.4	Thermal Properties	108
5.4.2.5	Structural Properties	108
5.4.2.6	Polymeric Micelles as Nanoreactors	109
5.5	Conclusions	109
	References	109
6	Polymeric Nanoparticles and Nanopore Membranes for Controlled Drug and Gene Delivery	115
	<i>Jingjiao Guan, Hongyan He, Bo Yu, and L. James Lee</i>	
6.1	Introduction	115
6.2	Nanoparticles for Drug/Gene Delivery	116
6.2.1	Why is Size Important for NPs in Drug/Gene Delivery?	116
6.2.1.1	Drug/Gene Protection	117
6.2.1.2	Delivery of Poorly Soluble Drugs	117
6.2.1.3	Sustained Release	117
6.2.1.4	Extended Blood Circulation	117
6.2.1.5	Targeted Delivery	118
6.2.1.6	Enhanced Cellular Uptake	118
6.2.1.7	Barrier Penetration	118
6.2.2	NPs prepared from Water-Insoluble Polymers	119
6.2.2.1	NPs Prepared by Precipitation of Polymers	119
6.2.2.2	NPs Prepared by Polymerization of Monomers	120
6.2.3	NPs Prepared from Water-Soluble Polymers	121
6.2.3.1	NPs Prepared by Cross-Linking of Polymers	121
6.2.3.2	NPs Prepared by Self-Assembling of Block Copolymers	124
6.2.3.3	NPs Prepared by Polymerization of Monomers	125
6.3	Nanopore Membranes for Drug Delivery	125
6.3.1	Overview of Nanopore-Based Devices for Sustained Drug Delivery	125
6.3.2	Polymeric Nanopore Membranes for Drug Delivery	126
6.4	Electrospun Polymeric Nanofibers (EPNFs) for Drug Delivery	129
6.5	Conclusions	130
	References	131

7	Development of Nanostructures for Drug Delivery Applications	139
	<i>Nikhil Dube, Joydeep Dutta, and Dharendra S. Katti</i>	
7.1	Introduction	139
7.2	Nanosystems for Drug Delivery	141
7.3	Polymeric Nanoparticles	142
7.3.1	Synthesis	142
7.3.1.1	Structure and Property	143
7.3.1.2	Applications of Nanoparticles for Drug Delivery	143
7.4	Nanofibers	145
7.4.1	Fabrication	146
7.4.1.1	Electrospinning	146
7.4.1.2	Applications of Nanofibers	147
7.5	Dendrimers	152
7.5.1	Properties of Dendrimers	153
7.5.2	Applications of Dendrimers in Drug Delivery	154
7.6	Liposomes and Lipid Nanoparticles	157
7.6.1	Synthesis of Liposomes and Lipid Nanoparticles	158
7.6.1.1	High Pressure Homogenization (HPH)	158
7.6.1.2	Microemulsion Method	159
7.6.1.3	High Speed Stirring and/or Ultrasonication	159
7.6.2	Drug Delivery Applications of Liposomes	159
7.6.3	Drug Delivery Applications of Lipid Nanoparticles	161
7.7	Nanotubes and Fullerenes	162
7.7.1	Synthesis	162
7.7.1.1	Chemical Vapor Deposition (CVD)	162
7.7.1.2	Electric Arc Discharge	163
7.7.1.3	Laser Ablation	163
7.7.2	Purification of Carbon Nanotubes	163
7.7.3	Toxicity of Carbon Nanotubes	164
7.7.4	Functionalization of Carbon Nanotubes	164
7.7.5	Biomedical Applications of Carbon Nanotubes	165
7.7.5.1	Drug Delivery by Carbon Nanotubes	166
7.7.5.2	Nucleic Acid Delivery by Carbon Nanotubes	166
7.7.5.3	Protein Delivery by Carbon Nanotubes	167
7.7.5.4	Vaccine and Peptide Delivery by Carbon Nanotubes	168
7.7.6	Biomedical Applications of Fullerenes	168
7.8	Nanogels	170
7.8.1	Synthesis of Nanogels	170
7.8.1.1	Emulsion Polymerization	171
7.8.1.2	Cross-Linking Reaction of Preformed Polymer Fragments	171

7.8.2	Nanogels for Drug Delivery	171
7.9	Viral Vectors and Virus-Like Particles (VLPs)	174
7.9.1	Recombinant Virus Vectors	175
7.9.1.1	Adenovirus Vectors	175
7.9.1.2	Retrovirus Vectors	175
7.9.1.3	Adeno Associated Virus Vectors	175
7.9.2	Applications of Recombinant Virus Vectors	176
7.9.3	Virus-Like Particles	177
7.9.4	Applications of Virus-Like Particles	178
7.9.4.1	Papillomavirus-Like Particles	178
7.9.4.2	Polyomavirus-Like Particles	178
7.10	Nanocrystal Technology	179
7.10.1	Approaches for the Production of Drug Nanocrystals	180
7.10.2	Preparation of Tablets from Nanosuspensions of Poorly Soluble Drugs	182
7.11	Conclusions	182
	References	183
8	Bioconjugated Nanoparticles for Ultrasensitive Detection of Molecular Biomarkers and Infectious Agents	207
	<i>Amit Agrawal, May Dongmei Wang, and Shuming Nie</i>	
8.1	Introduction	207
8.2	Novel Properties of Nanoparticles	208
8.3	Single-Molecule Detection	210
8.3.1	Instrumental Setup and Principles	210
8.3.2	Color-Coded Nanoparticles	213
8.3.3	Single-Molecule Imaging	215
8.4	Applications	216
8.4.1	Detection of Single Respiratory Syncytial Virus Particles	216
8.4.2	Single-Molecule Detection by Two-Color Imaging	218
8.5	Conclusion and Outlook	219
	References	220
	Part II. Bio-Nano Interfaces	223
9	ECM Interactions with Cells from the Macro- to Nanoscale	225
	<i>Steve Mwenifumbo and Molly M. Stevens</i>	
9.1	Introduction	225
9.2	Cell Microenvironment	226
9.2.1	ECM Compositional Diversity	226

9.2.1.1	Constituent Macromolecules	226
9.2.1.2	Developmental Diversity	227
9.2.1.3	Tissue-Specific Diversity	227
9.2.2	Nanoscaled Structures of the ECM	228
9.2.2.1	Proteins—Collagens and Elastins	229
9.2.2.2	GAGs	235
9.2.2.3	Proteoglycans	236
9.2.2.4	Glycoproteins	236
9.2.3	Putting It All Together—Hierarchical Assembly	239
9.3	Cell—ECM Interactions—The Multidimensional Map	241
9.3.1	Signaling Gradients	242
9.3.2	Soluble Factors	243
9.3.3	Growth Factors	244
9.3.4	ECM Components	245
9.3.4.1	Binding Domains	245
9.3.4.2	Cryptic Sites	246
9.3.4.3	Underlying Surface Chemistry	247
9.3.4.4	Topography	247
9.3.5	Environmental Stresses—Mechanical Stresses	248
9.3.6	Cell Surface Receptors	248
9.3.6.1	Integrins	249
9.3.6.2	Cell Adhesion—Adhesion Complexes	249
9.3.6.3	Integrin Signaling	249
9.3.7	Guided Activities of Cells—ECM Remodeling	250
9.3.7.1	ECM Remodeling	250
9.4	Conclusions	251
	Acknowledgments	252
	References	252
10	Cell Behavior Toward Nanostructured Surfaces	261
	<i>Sangamesh G. Kumbar, Michelle D. Kofron, Lakshmi S. Nair, and Cato T. Laurencin</i>	
10.1	Introduction	261
10.2	Nanotopographic Surfaces: Fabrication Techniques	264
10.2.1	Cell Behavior Toward Nanotopographic Surfaces Created by Electron Beam Lithography	270
10.2.2	Cell Behavior Toward Nanotopographic Surfaces Created by Photolithography	271
10.2.3	Cell Behavior Toward Nanotopographic Surfaces Composed of Aligned Nanofibers by Electrospinning	272
10.2.4	Cell Behavior Toward Nanotopographic Surfaces Created by Nanoimprinting	274

10.2.5	Cell Behavior Toward Nanotopographic Surfaces Created by Self-Assembly	276
10.2.6	Cell Behavior Toward Nanotopographic Surfaces Created by Phase Separation	277
10.2.7	Cell Behavior Toward Nanotopographic Surfaces Created by Colloidal Lithography	278
10.2.8	Cell Behavior Toward Nanotopographic Surfaces Composed of Random Nanofibers Created by Electrospinning	279
10.2.9	Cell Behavior Toward Nanotopographic Surfaces Created by Chemical Etching	280
10.2.10	Cell Behavior Toward Nanotopographic Surfaces Created by Incorporating Carbon Nanotubes/Nanofibers	282
10.2.11	Cell Behavior Toward Nanotopographic Surfaces Created by Polymer Demixing	283
10.3	Conclusions	287
	References	287

11 Cellular Behavior on Basement Membrane Inspired Topographically Patterned Synthetic Matrices **297**

Joshua Z. Gasiorowski, John D. Foley, Paul Russell, Sara J. Liliensiek, Paul F. Nealey, and Christopher J. Murphy

11.1	Introduction	297
11.2	Basement Membrane	298
11.2.1	Significance of Basement Membranes in Disease	298
11.2.2	Biochemical Attributes	299
11.2.3	Physical Characteristics: Compliance	300
11.2.3.1	Physical Characteristics: Topography	301
11.3	History of Biomimetic Synthetic Matrices	303
11.3.1	Matrigel and Randomly Ordered Arrays	304
11.3.2	Nanogroove Synthesis	305
11.4	Cell Behavior on Manufactured Nanogroove Surfaces	307
11.4.1	Nanoscale Topography Affects Cell Proliferation	307
11.4.2	Cellular Adhesive Strength on Nanogrooved Surfaces	308
11.4.3	Cellular Migration Rates on Nanogroove Surfaces	309
11.4.4	Focal Adhesion Structure and Orientation are Dictated by Nanogroove Dimensions	309
11.5	Cell Signaling and Expression on Topographical Surfaces	311
11.5.1	Cell Morphology Changes Induced by Topography May Influence Gene Expression	311
11.5.2	Macrophages Are Stimulated by Nanoscale Topography	312

11.5.3	Osteoblast Expression on Nanoscale Surfaces	312
11.5.4	The Addition of Soluble Factors Can Change Cellular Behavior on Nanogrooves	313
11.6	Conclusions	314
	References	314
12	Focal Adhesions: Self-Assembling Nanoscale Mechanochemical Machines that Control Cell Function	321
	<i>Tanmay Lele and Donald E. Ingber</i>	
12.1	Introduction	321
12.2	Solid-State Biochemistry in Focal Adhesions	322
12.3	Focal Adhesion as a Mechanotransduction Machine	324
12.4	Mechanical Control of Molecular Binding Interactions in Focal Adhesions	326
12.5	The Focal Adhesion as a Multifunctional Biomaterial	328
12.6	Conclusions	329
	References	331
13	Controlling Cell Behavior via DNA and RNA Transfections	337
	<i>Jaspreet K. Vasir and Vinod Labhassetwar</i>	
13.1	Introduction	337
13.2	Methods of DNA/RNA Transfection	337
13.3	Barriers to Transfection	339
13.4	DNA Transfection	340
13.4.1	Gene Therapy	340
13.4.2	Tissue Engineering	343
13.4.3	Functional Genomics	343
13.5	RNA Transfection	344
13.5.1	As a Tool to Understand Gene Function	344
13.5.2	As a Therapeutic	345
13.5.3	RNA Transfection—Delivering siRNA Inside Cells	347
13.5.3.1	<i>In vitro</i>	347
13.5.3.2	<i>In vivo</i>	348
13.5.4	Issues	352
13.5.4.1	Specificity	352
13.5.4.2	Resistance	352
13.5.4.3	Stability	352
13.6	Conclusions	353
	Acknowledgments	353
	References	353

14 Multiscale Coculture Models for Orthopedic Interface Tissue Engineering	357
<i>Helen H. Lu and I-Ning E. Wang</i>	
14.1 Introduction	357
14.2 Cellular Interactions and the Soft Tissue-to-Bone Interface	358
14.3 Types of Coculture Models	359
14.3.1 Coculture System with Cell–Cell Contact	359
14.3.1.1 Mixed Coculture	359
14.3.1.2 Temporary Dividers	360
14.3.2 Coculture System Without Cell–Cell Contact	360
14.3.2.1 Segregated Coculture	360
14.3.2.2 Porous Membrane Inserts	361
14.3.2.3 Conditioned Media Studies	361
14.4 Coculture Models for Orthopedic Interface Tissue Engineering	362
14.4.1 Coculture Models of Osteoblasts and Fibroblasts	362
14.4.2 Coculture Models of Osteoblasts and Chondrocytes	363
14.4.3 Coculture and Triculture Models of Osteoblasts, Chondrocytes, and Fibroblasts	364
14.5 Macro- and Microscale Coculture	364
14.6 Two-Dimensional (2D) and Three-Dimensional (3D) Cocultures	365
14.7 Mechanism of Cellular Interactions During Coculture	366
14.8 Conclusions	368
Acknowledgments	368
References	368
 Part III. Clinical Applications of Nanostructures	 375
 15 Nanostructures for Tissue Engineering/Regenerative Medicine	 377
<i>Syam P. Nukavarapu, Sangamesh G. Kumbar, Lakshmi S. Nair, and Cato T. Laurencin</i>	
15.1 Introduction	377
15.1.1 Tissue Engineering/Regenerative Medicine	377
15.1.2 Scaffolds for Tissue Engineering	378
15.1.3 Nanofeatures of ECM	379
15.2 Nanofibrous Scaffolds	381
15.2.1 Electrospinning	381
15.2.2 Phase Separation	384
15.2.3 Molecular Self-Assembly	385

15.3	Surface Patterned Scaffolds	386
15.3.1	Micro/Nanocontact Printing	387
15.3.2	Capillary Force Lithography	387
15.3.3	Biomolecular Patterning	389
15.4	Relevance of Nanostructured Scaffolds in Regenerative Medicine	390
15.5	Role of Nanostructured Scaffolds in Tissue Engineering	391
15.5.1	Bone and Cartilage Tissue Engineering	392
15.5.2	Vascular Tissue Engineering	394
15.5.3	Neural Tissue Engineering	397
15.5.4	Cardiac Tissue Engineering	399
15.6	Conclusions	401
	References	401
16	Nanostructures for Cancer Diagnostics and Therapy	409
	<i>Kumerash S. Soppimath and Guru V. Betageri</i>	
16.1	Introduction	409
16.1.1	Cancer and Early Diagnosis	409
16.1.2	Cancer and Chemotherapy	411
16.1.3	Why Nanotechnology for Treating Cancer?	413
16.2	Nanotools for Early Cancer Detection	414
16.2.1	Quantum Dots	414
16.2.2	Nanoshells	415
16.2.3	Gold Nanoparticles	416
16.2.4	Paramagnetic Nanoparticles	416
16.3	Nanomedicine for Cancer Treatment	417
16.3.1	Liposomes	417
16.3.1.1	Long-Circulating Liposomes	419
16.3.1.2	Size and Tumor Delivery	420
16.3.1.3	Doxil	420
16.3.1.4	Stealth Cisplatin Liposomes	423
16.3.1.5	Vincristine Sphingomyelin Liposomes	424
16.3.1.6	Sustained Release Liposomes	424
16.3.1.7	Liposome Vaccine	425
16.3.1.8	Liposomes as Solubilizing Carrier for Water Insoluble Anticancer Drugs	426
16.4	Polymeric Nanoparticles	427
16.4.1	Albumin Nanoparticles	427
16.4.2	Micellar Nanoparticles	428
16.5	Conclusions	430
	References	430

17 Clinical Applications of Micro- and Nanoscale Biosensors	439
<i>David W.G. Morrison, Mehmet R. Dokmeci, Utkan Demirci, and Ali Khademhosseini</i>	
17.1 Introduction	439
17.2 Classes of Biosensors	440
17.2.1 Method of Biological Signaling	440
17.2.2 Method of Transduction	442
17.3 Types of <i>In Vitro</i> Diagnostics	442
17.3.1 Cantilever-Based Biosensors	442
17.3.2 Cell and Protein Arrays	445
17.3.3 Nanoparticles	445
17.4 <i>In Vivo</i> Diagnostics	446
17.4.1 Quantum Dots	447
17.4.2 MRI Contrast Agents	448
17.5 Current and Emerging Clinical Applications of Micro- and Nanoscale Biosensors	448
17.5.1 Glucose Detection <i>In Vivo</i>	448
17.5.2 Bacterial Urinary Tract Infections	449
17.5.3 Human Immunodeficiency Virus (HIV) Detection	450
17.5.4 Cancer Cell Targeting	451
17.6 Conclusions	454
Acknowledgments	454
References	454
18 Nanoscale Iron Compounds Related to Neurodegenerative Disorders	461
<i>Joanna F. Collingwood and Jon Dobson</i>	
18.1 Introduction	461
18.2 Iron in the Human Brain	461
18.2.1 General Overview	461
18.2.2 Iron Storage	462
18.2.2.1 Ferritin	463
18.2.2.2 Hemosiderin	464
18.2.2.3 Magnetite	465
18.2.2.4 Neuromelanin	466
18.2.3 Regional Distribution of Iron Compounds	466
18.2.4 Iron Transport	467
18.3 Iron Compounds in Neurodegenerative Disorders	468
18.3.1 Overview	468
18.3.2 Alzheimer's Disease	470
18.3.3 Huntington's Disease	471
18.3.4 Parkinson's Disease	471

18.3.5 Neurodegeneration with Brain Iron Accumulation	473
18.3.6 Aceruloplasminemia	473
18.3.7 Neuroferritinopathy	473
18.3.8 Other Neurodegenerative Conditions	474
18.3.9 Hemochromatosis	474
18.4 Magnetic Properties of Nanoscale Brain Iron Compounds	475
18.5 Experimental Techniques	476
18.5.1 Sample Integrity	476
18.5.2 Microscopy and Spectroscopy	476
18.5.3 Magnetic Characterization	477
18.5.4 Clinical Imaging	478
18.6 Applications	478
18.6.1 Iron Chelation	478
18.6.2 Detection and Diagnosis	479
18.6.3 Nanoparticle Synthesis	480
18.6.4 Iron Nanoparticles as Contrast Agents	480
18.7 Conclusions	481
References	481
19 Application of Nanotechnology into Life Science: Benefit or Risk	491
<i>Yoon-Sik Lee and Myung-Haing Cho</i>	
19.1 Introduction	491
19.2 Drug or Gene Delivery	492
19.3 Rapid Bioassay	494
19.4 Tissue Engineering	496
19.5 Potential Safety Issues	497
19.6 Conclusions	498
Acknowledgments	498
References	498
Index	503

CONTRIBUTORS

Agrawal Amit, Department of Biomedical Engineering, 101 Woodruff Circle, Suite 2001, Emory University, Atlanta, GA, USA. E-mail: amit.agrawal@bme.gatech.edu

Betageri Guru V., Chair Department of Pharmaceutical Sciences, College of Pharmacy Western University of Health Sciences, 309 E Second Street, Pomona, CA, USA. E-mail: gbetageri@westernu.edu

Bhattacharyya Subhabrata, Department of Chemistry, University of Virginia, VA, USA. E-mail: sb4st@cms.mail.virginia.edu

Blackburn William H., Georgia Institute of Technology, School of Chemistry and Biochemistry and Petit Institute for Bioengineering & Bioscience, Atlanta, GA, USA. E-mail: bart.blackburn@chemistry.gatech.edu

Cao Zehui Charles, Center for Research at the Bio/Nano Interface, Department of Chemistry, Shands Cancer Center, University of Florida, Gainesville, FL, USA. E-mail: zcao@uiuc.edu

Chen Yan, Center for Research at the Bio/Nano Interface, Department of Chemistry, Shands Cancer Center, University of Florida, Gainesville, FL, USA. E-mail: ychen@chem.ufl.edu

Cho Myung-Haing, Laboratory of Toxicology, College of Veterinary Medicine, Seoul National University, Sillim-dong, Kwanak-gu, Seoul 151-742, Korea Nano Systems Institute-National Core Research Center, Seoul National University, Seoul 151-742, Korea. E-mail: mchotox@snu.ac.kr

Collingwood Joanna F., Institute for Science & Technology in Medicine, Keele University, Hartshill, Stoke-on-Trent, UK. E-mail: j.f.collingwood@pmed.keele.ac.uk

Demirci Utkan, Harvard-MIT Division of Health Sciences and Technology, Massachusetts Institute of Technology, Cambridge, MA, USA; Center for Biomedical Engineering, Department of Medicine, Brigham and Women's Hospital, Cambridge, MA, USA. E-mail: utkan@mit.edu

Dobson Jon, Institute for Science & Technology in Medicine, Keele University, Hartshill, Stoke-on-Trent, UK. E-mail: j.p.dobson@bemp.keele.ac.uk

- Dokmeci Mehmet R.**, Department of Electrical Engineering, Northeastern University, Boston, MA, USA. E-mail: mehmetd@ece.neu.edu
- Dube Nikhil**, Department of Biological Sciences and Bioengineering, Indian Institute of Technology, Kanpur, India. E-mail: nikhil.dube@gmail.com
- Dutta Joydeep**, Department of Biological Sciences and Bioengineering, Indian Institute of Technology, Kanpur, India. E-mail: joydeep_dutta@relbio.com
- Foley John D.**, Department of Surgical Sciences, School of Veterinary Medicine, University of Wisconsin, Madison, WI, USA. E-mail: j.d.foley@hotmail.com
- Freeman Joseph W.**, School of Biomedical Engineering and Sciences, Virginia Tech, Blacksburg, VA, USA. E-mail: jwfreeman@vt.edu
- Gasiorowski Joshua Z.**, Department of Surgical Sciences, School of Veterinary Medicine, University of Wisconsin, Madison, WI, USA. E-mail: gasiorowski@svm.vetmed.wisc.edu
- Gonsalves Kenneth E.**, Polymer Nanotechnology Laboratory, Department of Chemistry and Center for Optoelectronics and Optical Communication, University of North Carolina, Charlotte, NC, USA. E-mail: kegonsal@email.uncc.edu
- Guan Jingjiao**, NSF Nanoscale Science and Engineering Center for Affordable Nanoengineering of Polymeric Biomedical Devices, The Ohio State University, Columbus, OH, USA. E-mail: guan.13@osu.edu
- Halberstadt Craig**, Tengion, Inc., Winston Salem, NC, USA. E-mail: craig.halberstadt@tengion.com
- He Hongyan**, NSF Nanoscale Science and Engineering Center for Affordable Nanoengineering of Polymeric Biomedical Devices, Department of Chemical and Biomolecular Engineering, The Ohio State University, Columbus, OH, USA. E-mail: he.60@osu.edu
- He Wei**, Department of Biomedical Engineering, Georgia Institute of Technology, Atlanta, GA, USA. E-mail: weihe@u.washington.edu
- Ingber Donald E.**, Vascular Biology Program, Departments of Pathology & Surgery, Children's Hospital and Harvard Medical School, Boston, MA, USA. E-mail: Donald.Ingber@childrens.harvard.edu
- Katti Dharendra S.**, Department of Biological Sciences and Bioengineering, Indian Institute of Technology, Kanpur, India. E-mail: dsk@iitk.ac.in
- Khademhosseini Ali**, Harvard-MIT Division of Health Sciences and Technology, Massachusetts Institute of Technology, Cambridge, MA, USA; Center for Biomedical Engineering, Department of Medicine, Brigham and Women's Hospital, Cambridge, MA, USA. E-mail: alik@mit.edu
- Kofron Michelle D.**, Department of Biomedical Engineering, University of Virginia, VA, USA. E-mail: mdk8g@virginia.edu

- Kumbar Sangamesh G.**, Department of Orthopaedic Surgery, University of Virginia, VA, USA. E-mail: sgk4d@virginia.edu
- Labhasetwar Vinod**, Department of Biomedical Engineering/ND20, Lerner Research Institute, The Cleveland Clinic Foundation, 9500 Euclid Avenue, Cleveland, OH, USA. E-mail: labhasv@ccf.org
- Laurencin Cato T.**, Department of Orthopaedic Surgery, Biomedical and Chemical Engineering, University of Virginia, VA, USA. E-mail: Laurencin@virginia.edu
- Lee L. James**, NSF Nanoscale Science and Engineering Center for Affordable Nanoengineering of Polymeric Biomedical Devices, Department of Chemical and Biomolecular Engineering, The Ohio State University, Columbus, OH, USA. E-mail: lee.31@osu.edu
- Lee Yoon-Sik**, Organic Synthesis Laboratory, School of Chemical and Biological Engineering, Seoul National University, Sillim-dong, Kwanak-gu, Seoul 151-742; Korea Nano Systems Institute-National Core Research Center, Seoul National University, Seoul 151-742, Korea. E-mail: yslee@snu.ac.kr
- Lele Tanmay**, Department of Chemical Engineering, University of Florida, Gainesville, FL, USA. E-mail: tlele@che.ufl.edu
- Li Jianwei Jeff**, Center for Research at the Bio/Nano Interface, Department of Chemistry, Shands Cancer Center, University of Florida, Gainesville, FL, USA. E-mail: li6@fas.harvard.edu
- Liliensiek Sara J.**, Department of Surgical Sciences, School of Veterinary Medicine, University of Wisconsin, Madison, WI, USA. E-mail: sjlilien@students.wisc.edu
- Lu Helen H.**, Biomaterials and Interface Tissue Engineering Laboratory, Department of Biomedical Engineering, Columbia University, New York, NY 10027; College of Dental Medicine, Columbia University, New York, NY, USA. E-mail: hl2052@columbia.edu
- Lyon Andrew**, Georgia Institute of Technology, School of Chemistry and Biochemistry and Petit Institute for Bioengineering & Bioscience, Atlanta, GA, USA. E-mail: LL62@mail.gatech.edu
- Morrison David W.G.**, Harvard-MIT Division of Health Sciences and Technology, Massachusetts Institute of Technology, Cambridge, MA, USA. E-mail: morrisdw@mit.edu
- Murphy Christopher J.**, Department of Surgical Sciences, School of Veterinary Medicine, University of Wisconsin, Madison, WI, USA. E-mail: murphyc@svm.vetmed.wisc.edu
- Mwenifumbo Steve**, Department of Materials, Imperial College London, London, SW7 2AZ, UK; Institute of Biomedical Engineering, Imperial College London, London, SW7 2AZ, UK. E-mail: s.mwenifumbo@imperial.ac.uk

Nair Lakshmi S., Department of Orthopaedic Surgery, University of Virginia, VA, USA. E-mail: nair@virginia.edu

Nealey Paul F., Department of Chemical and Biological Engineering, School of Veterinary Medicine, University of Wisconsin, Madison, WI, USA. E-mail: nealey@engr.wisc.edu

Nie Shuming, Department of Biomedical Engineering, 101 Woodruff Circle, Suite 2001, Emory University, Atlanta, GA, USA. E-mail: snie@emory.edu

Nukavarapu Syam P., Department of Orthopaedic Surgery, University of Virginia, VA, USA. E-mail: spn2b@virginia.edu

Rogers Amanda, Department of Chemical, Biomedical and Materials Engineering, Stevens Institute of Technology, Hoboken, NJ, USA. E-mail: arogers@stevens.edu

Russell Paul, Department of Surgical Sciences, School of Veterinary Medicine, University of Wisconsin, Madison, WI, USA. E-mail: russellp@scm.vetmed.wisc.edu

Singh Neetu, Georgia Institute of Technology, School of Chemistry and Biochemistry and Petit Institute for Bioengineering & Bioscience, Atlanta, GA, USA. E-mail: gtg149n@mail.gatech.edu

Soppimath Kumerash S., Collage of Pharmacy, Western University of Health Sciences, 309 E Second Street, Pomona, CA, USA. E-mail: ksoppimath@westernu.edu

Stevens Molly M., Department of Materials, Imperial College London, London, SW7 2AZ, UK; Institute of Biomedical Engineering, Imperial College London, London, SW7 2AZ, UK. E-mail: m.stevens@imperial.ac.uk

Tan Weihong, Center for Research at the Bio/Nano Interface, Department of Chemistry, Shands Cancer Center, University of Florida, Gainesville, FL, USA. E-mail: tan@chem.ufl.edu

Valmikinathan Chandra M., Department of Chemical, Biomedical and Materials Engineering, Stevens Institute of Technology, Hoboken, NJ, USA. E-mail: cvalmiki@stevens.edu

Vasir Jaspreet K., Department of Pharmaceutical Sciences, College of Pharmacy, University of Nebraska Medical Center, Omaha, NE, USA. E-mail: jvasir@unmc.edu

Wang Junping, Department of Chemical, Biomedical and Materials Engineering, Stevens Institute of Technology, Hoboken, NJ, USA. E-mail: jwang16@stevens.edu

Wang I-Ning E., Biomaterials and Interface Tissue Engineering Laboratory, Department of Biomedical Engineering, Columbia University, New York, NY, USA. E-mail: iw2102@columbia.edu

Wang May Dongmei, Department of Biomedical Engineering, 313 Ferst Drive, UA Whitaker Building 4106, Georgia Institute of Technology, Atlanta, GA, USA. E-mail: maywang@bme.gatech.edu

Wright Lee D., School of Biomedical Engineering and Sciences, Virginia Tech, Blacksburg, VA, USA. E-mail: ldw80@vt.edu

Yu Bo, NSF Nanoscale Science and Engineering Center for Affordable Nanoengineering of Polymeric Biomedical Devices, Department of Chemical and Biomolecular Engineering, The Ohio State University, Columbus, OH, USA. E-mail: yu.304@osu.edu

Yu Xiaojun, Department of Chemical, Biomedical and Materials Engineering, Stevens Institute of Technology, Hoboken, NJ, USA. E-mail: xyu@stevens.edu

PART I

Nanostructure Fabrication

Nanofabrication Techniques

JOSEPH W. FREEMAN, LEE D. WRIGHT, CATO T. LAURENCIN, and SUBHABRATA BHATTACHARYYA

1.1 INTRODUCTION

Interest in the study and production of nanoscaled structures is increasing. The incredibly small sizes of nanoscaled devices and functionality of nanoscaled materials allow them to potentially change every aspect of human life. This technology is used to build the semiconductors in our computers; nanoscaled materials are studied for drug delivery, DNA analysis, use in cardiac stents, and other medical purposes. Layers of molecules can be placed on machine parts to protect them from wear or aid in lubrication; monolayers of molecules can be added to windows to eliminate glare. Although we are already greatly affected by this technology, new advances in nanofabrication are still being made.

Microelectromechanical systems (MEMS) and nanoelectromechanical systems (NEMS) have the potential to perform tasks and study the human body (BioMEMS and BioNEMS) at the molecular level. BioMEMS have existed for decades and were first used in neuroscience. In the 1970s, Otto Prohaska developed the first planar microarray sensor to measure extracellular nerve activity [1]. Prohaska and his group developed probes used for research in nerve cell interactions and pathological cell activities in the cortical section of the brain [1]. In the future, NEMS and other nanoscaled structures may be able to perform more advanced tasks. This technology may allow us to cure diseases or heal tissues at the molecular level. Computers may be even more powerful, while taking up less space.

Many of the fabrication methods for nanoscaled devices used today are actually based on previously conceived methods. Others take advantage of new technologies to make nanoscaled structures. Still others combine several

different methods to produce new technologies. This section will describe several technologies commonly used in nanofabrication. These methods produce a large variety of structures from fibers, to columns, to layers of materials that are a single molecule thick.

1.2 PHOTOLITHOGRAPHY

Originally, lithography was a printing method invented in 1798 by Alois Senefelder in Germany. At that time, there were only two printing techniques: relief printing and intaglio printing [2]. In relief printing, a raised surface is inked and an image is taken from this surface by placing it in contact with paper or cloth. The intaglio process relies on marks engraved onto a plate to retain the ink [2]. Lithography is based on the immiscibility of oil and water. Designs are drawn or painted with an oil-based substance (greasy ink or crayons) on specially prepared limestone. The stone is moistened with water, which the stone accepts in areas not covered by the crayon. An oily ink, applied with a roller, adheres only to the drawing and is repelled by the wet parts of the stone. The print is then made by pressing paper against the inked drawing.

Optical lithography began in the early 1970s when Rick Dill developed a set of mathematical equations to describe the process of lithography [3]. These equations published in the “Dill papers” marked the first time that lithography was described as a science and not an art. The first lithography modeling program SAMPLE was developed in 1979 by Andy Neureuther (who worked for a year with Rick Dill) and Bill Oldman [3].

Photolithography is a technique used to transfer shapes and designs onto a surface of photoresist materials. Over the years, this process has been refined and miniaturized; microlithography is currently used to produce items such as semiconductors for computers and an array of different biosensors. To date, photolithography has become one of the most successful technologies in the field of microfabrication [4]. It has been used regularly in the semiconductor industry since the late 1950s; a great deal of integrated circuits have been manufactured by this technology [4]. Photolithography involves several generalized steps, cleaning of the substrate, application of the photoresist material, soft baking, exposure, developing, and hard baking [5]. Each step will be explained briefly below.

1.2.1 Cleaning of the Substrate

During substrate preparation, the material onto which the pattern will be developed is cleaned to remove anything that could interfere with the lithography process including particulate matter and impurities. After cleaning, the substrate is dried, usually in an oven, to remove all water [3].

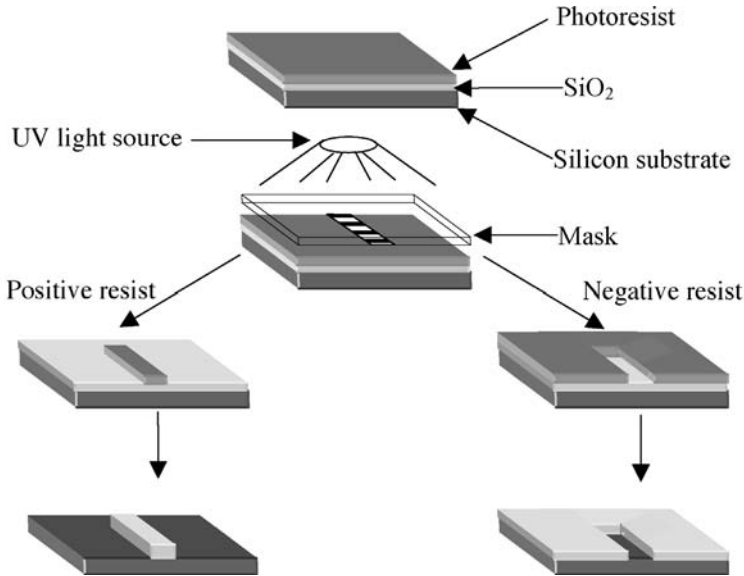


FIGURE 1.1 Steps in photolithography using positive and negative photoresists.

1.2.2 Application of the Photoresist Material

There are two types of photoresist materials, positive and negative. Positive photoresists become more soluble when they are exposed to UV light (Fig. 1.1). So in photolithography, when the mask is laid down onto the positive photoresist, the exposed areas (those not covered by the mask) will be removed by the developing solution leaving only the shape of the mask and the underlying substrate (Fig. 1.1) [5].

Negative photoresist materials work in the opposite manner (Fig. 1.1). These photoresist materials polymerize with exposure to UV light, making them less soluble after exposure. Once the mask has been lifted and the material has been washed with developing solution, the photoresist covered by the mask is washed away (Fig. 1.1). Therefore, using a negative photoresist creates the photographic negative of your mask [5].

Photoresists commonly used in the production of microelectronics include ethylene glycol, monoethyl ether propylene glycol and methyl ether acetate [6].

1.2.3 Soft Baking

The soft baking step is used to remove the solvents from the photoresist coating. Soft baking also makes the coating photosensitive [3].

1.2.4 Exposure

In this step, the mask is placed onto or over the substrate so that the pattern can be placed onto the surface of the substrate (Fig. 1.1). There are three different techniques used to position the mask prior to exposing the photoresist to UV light; these techniques are contact printing, proximity printing, and projection printing [5].

1.2.4.1 Contact Printing During contact printing, the substrate surface is covered with the photoresist and the mask physically touches the surface. The substrate is exposed to UV light while it is in contact with the mask. The contact between the mask and the substrate makes micron resolution possible. Unfortunately, if debris is trapped between the mask and the substrate, it can damage the mask and cause defects in the pattern [5].

1.2.4.2 Proximity Printing In proximity printing, the mask and the substrate are separated by a small distance (10–25 μm) before exposure to UV light. This technique protects the mask and the pattern from some debris damage that could occur during contact printing. The distance between the mask and the substrate lowers the resolution to 2–4 μm [5].

1.2.4.3 Projection Printing In projection printing, an image of the mask is projected onto the substrate after it is covered with the photoresist. This method can produce patterns with high resolution (1 μm) by projecting a small section of the mask at a time. Once the mask is in the correct position, the photoresist is exposed to high intensity UV light through the pattern in the mask [5].

1.2.5 Developing

Through developing, the photoresist becomes more soluble (positive photoresists) or less soluble (negative photoresists). When using a positive photoresist, an increase in energy causes an increase in the solubility of the resist until the threshold energy is reached. At this energy, all of the resist is soluble. In negative photoresists, the material becomes less and less soluble with increased energy. At the threshold energy, the material is even less soluble; as the energy is raised above the threshold energy, more of the photoresist is insoluble and more of it will remain after developing. The amount of time and energy necessary to complete the developing step depends on a variety of factors such as the prebaking conditions, amount of photoresist material, and developing chemistry. After the developing, a solvent is used to wash the sample [5].

1.2.6 Hard Baking

This is the final step of photolithography. Hard baking is used to harden the photoresist and improve bonding between the photoresist layer and the substrate underneath [5].

1.2.7 Limitations of Photolithography

Current photolithography techniques used in microelectronics manufacturing use a projection printing system (known as a stepper). In this system, the image of the mask is reduced and projected, via a high numerical aperture lens system, onto a thin film of photoresist that has been spin coated onto a wafer [4]. The resolution that the stepper is capable of is based on optical diffraction limits set in the Rayleigh equation (Eq. 1.1).

$$R = k_1 \lambda / \text{NA} \quad (1.1)$$

In the Rayleigh equation, k_1 is a constant that is dependent on the photoresist, λ is the wavelength of the light source, and NA is the numerical aperture of the lens.

The minimum feature size that can be achieved with this technique is approximately the wavelength of the light used, λ ; although theoretically, the lower limit is $\lambda/2$. So, in order to produce micro- or nanoscaled patterns and structures, light sources with shorter wavelengths must be used. This also makes manufacturing more difficult and expensive [4].

1.3 SPECIALIZED LITHOGRAPHY TECHNIQUES

In order to produce patterns at the nanometer scale, which is necessary for the fabrication of semiconductor integrated circuits, nanoelectromechanical systems, or lab-on-a-chip applications, specialized lithography techniques are used. Some of these techniques involve steps similar to those seen in photolithography; the differences lie in the use of energy sources with smaller wavelengths and smaller masks (both changes are used to produce nanoscaled patterns and structures). Such specialized lithography techniques include electron beam lithography, nanosphere lithography, and focused ion beam lithography (FIB). Other specialized techniques are more reminiscent of original lithography in that they transfer the pattern of molecules directly onto the substrate as a print. These techniques include types of soft lithography (such as microcontact printing, replica molding, microtransfer molding, and solvent-assisted micromolding), nanoimprint lithography, and dip pen lithography (a type of scanning probe lithography) [4, 7]. Other techniques, such as LIGA, combine elements from both categories. A few of these techniques will be briefly discussed below.

1.3.1 Electron Beam Lithography

Electron beam lithography has been used in the production of semiconductors and the patterning of masks for other types of lithography (such as X-ray and optical lithography). In electron beam lithography, the exposed substrate is modified by the energy from a stream of electrons.

1.3.2 Nanosphere Lithography

Nanosphere lithography is similar to other types of lithography. In this type of lithography, the mask is replaced with a layer of nanospheres. After exposure and developing, the uncovered resin is washed away leaving behind nanoscale vertical columns.

1.3.3 Soft Lithography

Soft lithography is called “soft” because an elastomeric stamp or mold is the part that transfers patterns to the substrate and this method uses flexible organic molecules and materials rather than the rigid inorganic materials commonly used during the fabrication of microelectronic systems [4]. This process, developed by George Whitesides, does not depend on a resist layer to transfer a pattern onto the substrate. Soft lithography can produce micropatterns of self-assembled monolayers (SAMs) through contact printing or form microstructures in materials through imprinting (embossing) or replica molding [4].

In this process, a self-assembled monolayer is stamped onto the substrate [4]. The molecular impressions left by the monolayer can be used to seed crystal growth or bind strands of DNA for bioanalysis. Soft lithography techniques are not subject to the limitations set by optical diffraction, as discussed earlier (the edge definition is set by van der Waals interactions and the properties of the materials used) [4]. They offer procedurally simple, less expensive alternatives to the production of nanoscaled structures through photolithography.

1.3.4 Dip Pen Lithography

Dip pen lithography is a type of scanning probe lithography. In this lithographic technique, the tip of an atomic force microscope (AFM) is used to create micro- and nanoscaled structures by depositing material onto a substrate. The AFM tip delivers the molecules to the substrate surface using a solvent meniscus that forms in ambient atmospheres. Structures with features ranging from several hundreds of nanometers to sub-50 nm can be generated using this technique [7].

Dip pen lithography is a direct-write method that yields high resolution and has been used to create microscale and nanoscale patterns with a variety of “inks” (such as biomolecules, organic molecules, polymers, and inorganic molecules) on a number of substrates. The AFM tip was first used to form patterns of octadecanethiols in ethanol on the mica surfaces [8]. The technology can now be used to construct protein arrays for proteomics, pharmaceutical screening processes, and panel immunoassays [9].

Dip pen lithography involves several steps. The first is substrate preparation: the substrate is cleaned and rinsed to remove all impurities and produce a

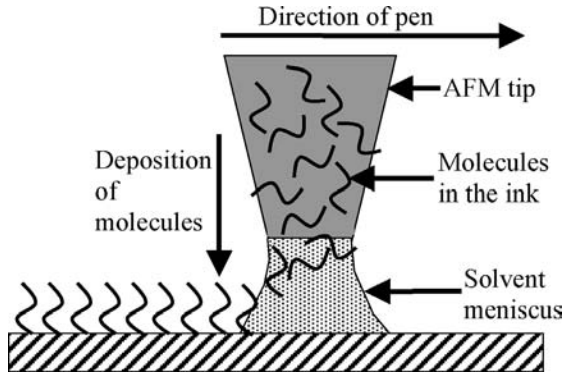


FIGURE 1.2 Dip pen lithography, transferring the molecules from the pen to the substrate surface.

flawless surface. In order to aid in adhesion of the material being deposited, a self-assembled monolayer may be added to the surface. The AFM tip is then coated with the “ink” to be deposited onto the substrate. Finally, the tip is used to produce the desired pattern (Fig. 1.2) [7].

The formation, structure, and stability of the deposited material depend on several different variables. The formation and stability of the structure are subject to the strength of the adhesion between the substrate and the deposited material and the amount of adhesion between the material being deposited and the AFM tip [9]. One source of this adhesion is surface charge. The static interaction between a charged substrate surface and oppositely charged nanospecies will lead to the successful deposition onto the substrate surface [7].

If the adhesion between the material and the AFM tip is too strong, it may prevent material deposition; if it is too weak, the material will not stay on the tip long enough to be deposited onto the substrate and the amount on the tip may not be enough to produce the structure. The deposition of material from the tip to the substrate is also influenced by the cohesion between the material already deposited and the material on the tip [8].

Temperature is also an important factor in dip pen lithography. When working with biomolecules and organic molecules, temperature affects the solubility and diffusion rate of the molecules, which influences the size of the nanopatterns. The solvent used is also a factor in stability. The amount of solvent in the material can influence the shape of the deposit. As the solvent evaporates from the material after deposition, the deposits could harden [8]. Temperature can also influence solvent evaporation rates.

The speed of tip can change the dimensions of the pattern. Increasing speed causes a decrease in pattern size. Humidity can also affect this process. The proper humidity is necessary for the transfer of the material to the substrate [7].

Progress has been made in using dip pen lithography in nanopatterning biomolecules and organic molecules by modulating interactions between target surfaces and the molecules being deposited [8]. Very few inorganic materials have been successfully patterned with this technique; successes include pure metals and metal oxides [7].

1.3.5 LIGA

LIGA is a German acronym for Lithographie, Galvanoformung, Abformung. This process for creating three-dimensional microstructures was developed in the 1980s by W. Ehrfeld [10, 11]. It is an early technique for producing micro- and nanoscaled structures and involves lithography, electroforming, and plastic molding. LIGA was one of the first techniques used to create microstructures with high aspect ratios and depths of hundreds of nanometers [10, 11]. LIGA is a valuable tool for the production of micro- or nanoscaled molds; these molds can aid in the mass production of micromachine parts. The basic steps of LIGA (Fig. 1.3) are explained below [10–12].

1.3.5.1 Deep X-Ray Lithography In LIGA, a several hundred microns thick radiation sensitive polymer layer is applied to a substrate (a metallic base plate or a silicon wafer). This layer is either glued to the substrate or polymerized onto it; polymethyl methacrylate (PMMA) is an example of a polymer that can

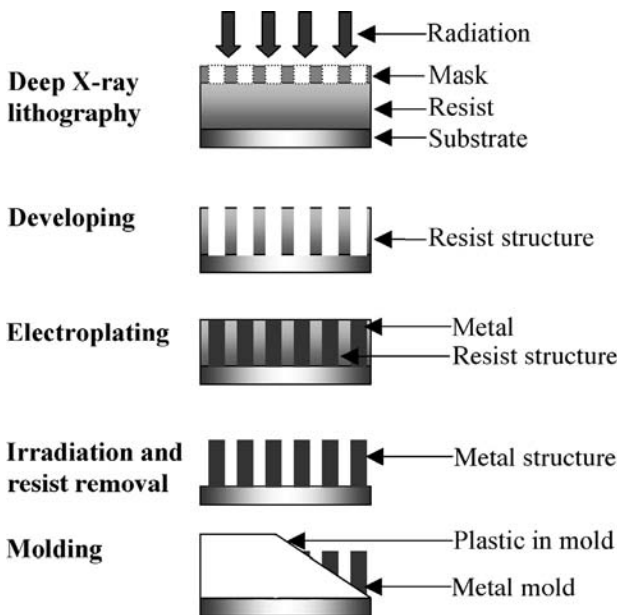


FIGURE 1.3 Diagram of the LIGA technique.

be bonded to the substrate. A mask is placed over the polymer layer and the mask pattern is then transferred onto the polymer layer using deep X-ray exposure with wavelengths from 0.2 to 0.6 nm (using Synchrotron radiation) [11].

1.3.5.2 Electroplating After irradiation, the exposed polymer is removed by solvent during development leaving behind the polymer micro- or nanostructures with high aspect ratios. The cavities between three-dimensional structures are typically filled in with metals such as gold, copper, or nickel by electroplating. Alloys, such as nickel–iron or nickel–cobalt, can also be used to fill in the cavities left after development [8].

1.3.5.3 Molding The structure is exposed to X-ray radiation a second time (without the mask) and the remaining polymer (from the structures with the high aspect ratio) is removed with solvent or developer. This step creates metal micro- or nanostructures with a high aspect ratio. These metal structures are used as a mold for plastic parts using injection molding, hot embossing, or resin casting [8].

1.4 THIN FILM DEPOSITION

Thin film deposition techniques allow one to deposit a thin layer of material onto a surface or a substrate. Typically, the thicknesses of these thin films are in the nanometer scale. Some techniques even allow the addition of single atom layers of a material to the substrate. These techniques are used to create a wide variety of devices including coatings for optics components, conductors, semiconductors, and insulators for electronic devices, and films for packaging. Although thin film deposition includes a broad range of technologies and methodologies, a generalized process can be described in three steps: (1) creation of the flux of condensable species, this includes either neutral atoms or ions, (2) transportation of the created species to the substrate, and (3) growth of the film onto the substrate. Thin film deposition has a wide variety of applications including the manufacture of reflective coatings for optics, the manufacture of electronics, and the purification of metals such as copper through electroplating. Electronics is perhaps the most well-known field that requires thin film deposition. The technology is continually allowing the electronics industry to create smaller and smaller electronic components including insulators, semiconductors, and integrated circuits, allowing developers to increase the speed and efficiency of their products without increasing the product size. Thin film deposition can be divided into two broad categories: physical deposition and chemical deposition. Only a few thin film deposition techniques do not fit completely into these categories; they will be described later. Many methods of thin film deposition do not rely on one technology to attain their goals; often a combination of techniques and technologies are used.

Physical deposition, as the name implies, involves thin film deposition techniques that use physics, typically in terms of mechanical or thermodynamic means, to deposit the desired film onto the substrate. Physical deposition includes three primary classes: evaporation, sputtering, and ion beam. Evaporation thin film deposition employs the ability to evaporate the material to be deposited by physical heating to create the flux of material. The species created through the heating process is then transported to the substrate to be deposited onto the surface. Although rather simple in concept, many different methods to heat the materials have been used, including resistance heating, electron beam heating, arc evaporation, induction heating, and flash evaporation.

An example of arc evaporation is cathodic arc plasma deposition (CAPD). This technique utilizes vacuum arcs to produce the condensable species. The source material to be deposited is created from the cathode in the arc discharge circuit. The condensable species is created from the source material through flash evaporation as the arc spots move along the surface of the target. The arc spots are sustained by the plasma being formed by the arc itself [13].

The second class of physical thin film deposition is the sputtering technique. This process involves the synthesis of the condensation species by bombardment of the source (target) with positive ions of an inert gas. The collisions cause the atoms on the target to be knocked off through momentum transfer and result in the creation of ions on the target as well. This technique is typically called plasma-assisted (enhanced) deposition, which encourages the atoms to be knocked off and collected onto substrates [13]. The sputtering technique has an advantage over the aforementioned evaporation technique because it can occur at lower temperatures (heating is not required) and because the process is independent of the evaporation rate of the material.

Another class of physical thin film deposition utilizes ion beam technology. These techniques employ the use of an ion beam to ionize the material to be deposited. An example is gas cluster ion beam technology (GCIB). Neutral gas clusters are produced by the expansion of atoms or molecules at high pressure through a room temperature nozzle into a vacuum. The neutral gas cluster is ionized by the bombardment of electrons and is accelerated by a high voltage to impact a substrate. The impact causes all of the atoms to nearly interact simultaneously and deposit a very high energy density into a small volume of the target material [14].

The second large category of thin film deposition techniques is chemical deposition. As the name implies, chemical deposition causes a chemical change of the fluid material that results in the deposition. Chemical vapor deposition (CVD) is a class of chemical deposition where the condensable species is formed from gases or vapors that are, without energy input, not condensable. The substrates are heated at high temperature to cause the gases to decompose resulting in deposition. Plasma-enhanced chemical vapor deposition (PECVD) utilizes plasma that is created through the action of an electric field. Ionization, dissociation, and gas phase reactions occur as the reactant gases are passed

through the low pressure plasma. The addition of plasma to the technique allows the process to occur at much lower temperatures, not entirely relying on the reactions to be driven thermally [13]. This method will be discussed in more depth later in Section 1.7.

Plating is another class of chemical deposition used to produce thin films. The plating technique distinguishes itself because of its use of liquid precursors. The material to be deposited is initially dissolved in an aqueous solution. Although the process can be driven entirely by the reagents within the solution, usually an electric current or ion beam is used to drive the reaction to form the layer of desired material.

The final two techniques of thin film deposition to be discussed are molecular beam epitaxy (MBE) and reactive sputtering. MBE and reactive sputtering do not entirely fit into either chemical or physical deposition categories, being more of a combination of chemical and physical. During MBE, ultrapure elements are heated until they begin to slowly evaporate. The evaporated elements do not react with one another until they condense onto the substrate. The process occurs in a high vacuum, which allows a slow deposition rate. The slow deposition rate allows the material to grow epitaxially, meaning instead of many randomly arranged grains being formed, as in higher deposition rates, the material tends to grow in larger grains with a more uniform orientation. The slow deposition rate also allows the element to be deposited one layer at a time [15].

The last technique to be discussed is reactive sputtering. In reactive sputtering, a small amount of non-noble gas (such as oxygen or nitrogen) is mixed with the plasma forming gas. The material is then sputtered from the target to the substrate reacting with the gas. The result is the deposition of a different material. If the gas used is either oxygen or nitrogen, an oxide or nitride can be formed. The method is not limited to oxygen or nitrogen; a wide variety of compounds can be created via this method [16].

1.5 ELECTROSPINNING

Electrospinning is a technique used to create polymeric fibers with diameters in the nanometer range. This process involves the ejection of a charged polymer fluid onto an oppositely charged surface. One of the first investigations into the flow of conducting liquid through a charged tube with a counterelectrode some distance away was conducted by Zeleny [17]. A great deal of these experiments used aqueous electrolyte solutions with high electrical conductivity and low viscosity. The addition of a charge to this solution caused it to form a fine spray of charged droplets that were attracted to the counterelectrode. These droplets quickly evaporated in the air; this process was later called electrospaying.

Electrospinning is very similar to electrospaying; a charge is applied to a polymer solution or melt and ejected toward an oppositely charged target (Fig. 1.4). A typical electrospinning experimental setup is shown in Fig. 1.4.

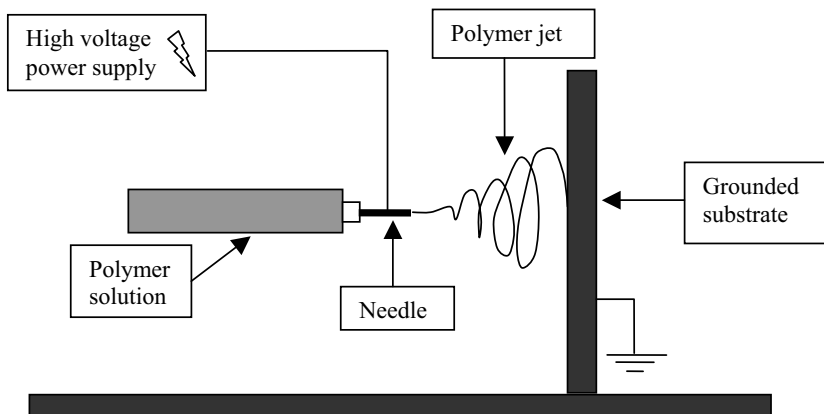


FIGURE 1.4 A typical electrospinning setup.

In both processes, the surface tension and viscoelastic forces of the polymer solution cause drops at the tip of the syringe to retain their hemispherical shape. The charge induced by the electric field causes the droplet to deform into a “Taylor cone” at the tip of the tube [18]. When the applied voltage is increased beyond a threshold value, the electric forces in the droplet overcome the opposing surface tension forces and a narrow charged jet is ejected from the tip of the Taylor cone. In electrospaying, the strength of the electric field and low viscosity of a solution cause droplets to separate from the cone and spray onto the target. In electrospinning, the concentration of the solution, viscosity of the solution, and the entanglement of the polymer chains cause a fiber to be extruded from the tip of the cone. The polymer jet begins as a nearly straight line because of the stabilization from the longitudinal stress of the external electrical field on the charge carried by the jet. However, the polymer jet quickly becomes unstable because of the repulsive forces from the opposite charges in the polymer jet. The jet experiences electrically driven bending instabilities and the jet is whipped around in a spiral, as demonstrated by Reneker et al., using high speed videography [19]. The polymer jet is stretched while it bends and travels through the spiral causing a significant decrease in fiber diameter and rapid evaporation of the solvent resulting in the formation of nanoscale thin fibers. These fibers land randomly onto the grounded target forming a nonwoven fiber mat (Fig. 1.5).

Electrospinning produces fibers with submicron diameters [19]. The diameter of the fibers can be adjusted by altering the distance between the polymer source and the target, the polymer concentration, and the voltage. The orientation of the fibers onto the target can be changed by employing various external mechanical or electrostatic forces [20]. The mechanical properties of the fiber mat can be altered by changing the diameter and orientation of the fibers.

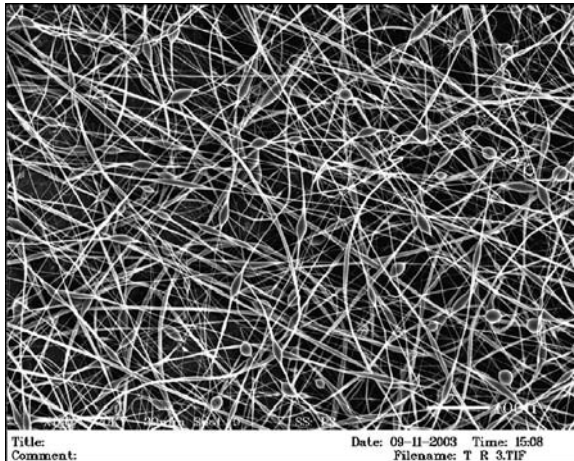


FIGURE 1.5 Electrospun poly(lactic acid-co-glycolic acid) nanofibers.

Cellulose acetate was one of the first solutions electrospun; Formhals was given a U.S. patent for this process in 1934 [21]. In another early study, molten wax was observed to form threads when subjected to high electrical field [17]. Presently, a wide variety of polymers have been electrospun from natural polymers such as type I collagen or elastin to synthetic polymers such as polyphosphazenes.

Several parameters affect the electrospinning process. These parameters can be split into different groups, polymer solution properties, processing parameters, and environmental parameters. Polymer solution properties include solution viscosity, polymer molecular weight, polymer concentration, surface tension, solution conductivity, and dielectric effect of the solvent [22–24]. Processing parameters that affect electrospinning include voltage, distance from needle to collector, flow rate, needle/orifice diameter, and type of collector [22, 23, 25, 26]. The environmental parameters that can affect electrospinning of nanofibers include humidity, pressure, and type of atmosphere [22, 25].

1.6 NANOSPHERES

Nanosphere technology revolves around the creation of polymeric spheres that are hundreds of nanometers in diameter. Their tiny size and ability to absorb or bind to (through surface chemistry) drugs or growth factors make them ideal vehicles for drug or growth factor delivery.

Polymeric nanospheres can be created by emulsion solvent diffusion. The polymer is dissolved into a volatile organic solvent (such as chloroform, ethyl acetate, or methylene chloride). This solution is then poured into an aqueous phase with a surfactant or stabilizer and agitated usually with a sonicator. The

nanospheres are then collected by evaporating the solvent (this may be done with mixing) or dilution with water.

Drugs and growth factors may be added to the organic or aqueous phase in order to incorporate them into the nanospheres. Scanning electron microscopy is used for nanosphere characterization. The size and density of the spheres can be altered by changing the amount of polymer added to the surfactant or stabilizer solution and the speed with which the solution is agitated.

1.7 CARBON NANOTUBES

Carbon is the building block for all organic life. It is found in a variety of structures that display vastly different properties. In nature, pure carbon is found in a variety of forms from the soft, flexible, and conductive graphite to the hard, inflexible insulating diamond. The properties of these materials stem from the arrangement of their carbon atoms. In graphite, the carbon atoms are arranged into sheets of honeycomb-shaped matrices; these matrices are held together by covalent bonds between the carbon atoms. The sheets are held to one another by weak van der Waals forces; this allows graphite to flake off into layers (sheets of carbon atoms slide over one another when force is applied) making graphite a good lubricant. In contrast, the carbon atoms in a diamond are arranged into a tetrahedral pattern. This arrangement makes diamonds hard and prevents them from flaking like graphite. Similarly, it is the arrangement of their atoms and their nanoscale size that give carbon nanotubes their mechanical, chemical, and electrical properties.

Carbon nanotubes (CNTs) are fullerenes that are structurally similar to long rolls of graphite. Fullerenes are molecules composed entirely of carbon that exist as hollow objects (spheres, ellipsoids, or tubes); they are named after Buckminster Fuller, an American architect, designer, and author known for his work on geodesic domes.

CNTs are created as single-walled nanotubes (SWNTs) or multiwalled nanotubes (MWNTs). SWNTs have only one wall whereas MWNTs have many walls formed around one another. The walls of MWNTs are held to one another by van der Waals forces. The properties of CNTs depend on their length, diameter, and chirality (the direction in which the graphite sheet is rolled up).

Carbon filaments were first noticed under gaseous conditions in the presence of metal catalysts in the 1950s after the development of the electron microscope. Carbon filaments up to several hundred nanometers long were noticed extending from catalytic particles of transition metals [27]. Tibbetts was the first to document these structures and speculate about their growth mechanism [27]. In the 1990s, Iijima observed the formation of MWNTs through the electric arc discharge method and later documented the synthesis of SWNTs via laser ablation [28].

SWNTs are very strong and very stiff because of the strength of the carbon–carbon bond and the seamless structure of the nanotube; the modulus of an SWNT has been calculated as 0.64 TPa with an ultimate tensile stress of approximately 37 GPa [29]. The electrical properties of SWNTs can range from metallic to semiconducting with various band gaps depending on the chirality and diameter of the tube [29]. CNTs have been used in a variety of applications including increasing mechanical properties of polymers through composite reinforcement, use in nanosensing devices, and in bioimaging.

CNTs have been made using a variety of fabrication methods; some of the more common methods will be mentioned in this section. These methods include electric arc discharge, laser ablation of carbon, and chemical vapor deposition, techniques that are also used to create thin films, as mentioned in an earlier section.

1.7.1 Electric Arc Discharge

The electric arc discharge method was one of the first methods used to fabricate CNTs [30]. An electric arc is a discharge of current that occurs when a current jumps between two electrodes or a gap in a circuit; to form CNTs, high purity carbon electrodes are used. During this process, the anode, the source of the carbon, is consumed throughout the process. As the nanotubes are formed from the material in the anode, they are deposited onto the cathode. The composition of the electrodes affects the type of CNTs produced. MWNTs are produced when pure carbon electrodes are used. To produce SWNTs, a small hole is drilled into the anode and filled with metallic catalyst particles and graphite powder. Mixtures of Ni and Y have been shown to produce high quality SWNTs [31].

1.7.2 Laser Ablation

Ablation is the melting or vaporizing of a substance; in laser ablation for the fabrication of CNTs, a graphite target is subjected to a laser at high temperatures. The graphite target is ablated with a powerful laser in the presence of an inert gas. The gas collects the ablated carbon powder and deposits it onto a cooled substrate. The powder consists of CNTs and onion-like structures [30]. Similar to the electric arc discharge method, MWNTs are produced when pure carbon (graphite) is used and SWNTs are produced when the target is mixed with catalytic metals (<1%) such as Co–Ni powder [30].

1.7.3 Chemical Vapor Deposition

Unlike the previously mentioned techniques for CNT production (electric arc discharge and laser ablation), chemical vapor deposition allows the user to deposit the CNTs directly onto a substrate. Chemical vapor deposition is commonly used in the manufacturing of metals and ceramics [27]. This technique can produce CNTs at a continuous rate and is easily scalable to

produce large amounts of CNTs for commercial distribution [30]. By changing growth conditions such as growth temperature, carbon source, catalyst, catalyst-to-carbon ratio, and type of substrate, CNTs can grow in a variety of ways, including randomly oriented and aligned.

There are several ways to perform chemical vapor deposition, including hot-wall chemical vapor deposition, cold-wall chemical vapor deposition, high pressure CO conversion (HiPCO) chemical vapor deposition, and laser-assisted chemical vapor deposition; both hot-wall and cold-wall chemical vapor deposition are forms of thermal chemical vapor deposition. In hot-wall chemical vapor deposition processes, such as thermal chemical vapor deposition, the process takes place in a high temperature tube furnace. The substrate that the CNTs will be deposited on is placed inside of the tube and the entire tube is heated (heating the substrate to the growth temperature). A hydrocarbon source, such as benzene, xylene, or hexane, is also introduced into the tube. Once in the tube, it decomposes and deposits onto the substrate. In cold-wall chemical vapor deposition processes, including plasma-enhanced chemical vapor deposition, the temperature of the sample holder is raised and the rest of the system is left at a lower temperature. In HiPCO chemical vapor deposition, high pressure carbon monoxide is fed into the system and used as the carbon source.

Laser-assisted chemical vapor deposition is a technique that is used for thin film deposition and can be adopted to produce films of CNTs. In laser-assisted chemical vapor deposition, the global energy source that warms the furnace is replaced by a localized energy source, the laser. In this method, the source of the energy on the substrate is localized, so the growth of the CNTs can be limited to the area over which the laser passes.

Laser-assisted chemical vapor deposition is controlled by two mechanisms: photolytic laser-assisted chemical vapor deposition and pyrolytic laser-assisted chemical vapor deposition. Depending on the conditions, such as temperature and position of the laser beam, both mechanisms can take place simultaneously. In such cases, one mechanism for CNT deposition may dominate the other. Only the photolytic process can occur at low temperatures, but at high temperatures both the photolytic and pyrolytic processes can occur simultaneously [32]. Pyrolytic or photolytic reactions are caused by the laser radiation wavelength, precursor compounds used, and chosen substrate material [33].

1.7.4 Photolytic Laser-Assisted Chemical Vapor Deposition

Photolytic laser-assisted chemical vapor deposition can be performed at low wavelengths and with short pulse durations. This combination of conditions creates a low temperature during processing, eliminating damage that can be caused by thermal reactions with the substrate, such as recrystallization, oxidation, and crack formation. This allows for exact processing of materials for use in microelectronics [34]. Since it does not produce high temperatures, photolytic laser-assisted chemical vapor deposition is used in conjunction with

temperature-sensitive substrates. Lasers or lamps can be used as a source for photons, but the increased power densities of lasers lead to a 100-fold increase in growth rate when compared to lamps [35].

Resonant absorption of the laser radiation by the precursor causes bonds in the precursor molecules to break freeing them for deposition onto the substrate [30]. In photolytic laser-assisted chemical vapor deposition, the laser beam is parallel to the substrate and passes just above it. The photons from the laser are absorbed by the gas phase starting the reaction [36]. This arrangement allows for the control of the substrate temperature independent from the laser radiation [30]. Photolytic laser-assisted chemical vapor deposition may also occur in a perpendicular laser–substrate arrangement, but this geometry also introduces pyrolytic laser-assisted chemical vapor deposition [33].

1.7.5 Pyrolytic Laser-Assisted Chemical Vapor Deposition

In pyrolytic laser-assisted chemical vapor deposition, the thermal energy produced by the laser causes molecules of the reagent to disassociate and deposit as CNTs on the substrate. The laser beam strikes the substrate at perpendicular incidence and the chemical reaction is driven thermally by the local heating of the substrate by the laser radiation. If the substrate is moved throughout the process, single-step patterns can be made. If the substrate is stationary, this process can produce three-dimensional structures [33]. Since this method is essentially a type of thermal chemical vapor deposition, the same conditions used for thermal chemical vapor deposition can be used with pyrolytic chemical vapor deposition. The major difference is the heat source; the use of a localized heat source (the laser) changes the reaction kinetics. This improves the deposition rate and allows three-dimensional objects to be produced [37].

Pyrolytic laser-assisted chemical vapor deposition was first performed by Lydtin in 1972 [33] using an IR laser to deposit carbon onto aluminum substrates. Now any commercially available laser can be used as a radiation source for this technique. Typically, argon and krypton lasers are used for submicron-sized patterns (necessary for nanofabrication and microelectronics) [30]. Otherwise, other types of lasers, such as CO₂ lasers, can be used since most gases do not absorb the infrared or visible wavelengths emitted.

Pyrolytic laser-assisted chemical vapor deposition can also be performed with an IR laser through vibration excitation. In this technique, the gas phase is excited through collisional and vibrational relaxation processes. This heats up the gas phase and the substrate, leading to the deposition of the film. Examples of laser and gas phase systems used in this technique include CO₂ lasers and BCl₃, SiH₄, or NH₃ gas [33].

1.7.6 Substrate-Site-Selective Growth

There are other techniques that can deposit CNTs into precise shapes and patterns. One of these techniques is substrate-site-selective growth. This

procedure combines lithography with chemical vapor deposition to achieve targeted nanotube deposition for pattern production. In this process, a pattern is placed onto the substrate using lithography; Wei and colleagues developed a pattern of SiO_2 on top of a silicon substrate [30]. After the pattern has been laid down, the nanotubes are deposited using a chemical vapor deposition technique. In previous work, Wei and colleagues used a conventional tube furnace with ferrocene ($\text{Fe}(\text{C}_5\text{H}_5)_2$) as the nanotube nucleation initiator and xylene as the carbon source [30]. The furnace was gradually heated to 800°C and the ferrocene–xylene solution was fed into the reactor at 150°C . The choice of precursors is extremely important because it dictates the length of the nanotubes deposited onto the substrate. The combination of ferrocene and xylene produced vertically aligned MWCNTs that were 20–30 μm in length onto the SiO_2 pattern; there was no CNT deposition on the silicon surface [30]. This technique has great potential for the design of mesoscale systems similar to those in MEMS [30].

1.8 SELF-ASSEMBLED NANOSTRUCTURES

The self-assembly of molecules into structures is a phenomena seen frequently in nature; type I collagen molecules are examples of molecules that can orient and arrange themselves to form two-dimensional and three-dimensional structures. Among the nanofabrication methods discussed in this chapter, self-assembly of molecules is one of the most promising ways to form a large variety of nanostructures [38]. This technique relies on the noncovalent interactions between molecules (electrostatic, van der Waals, hydrogen bonding, π – π interactions, and capillary force) to organize groups of molecules into larger, regular structures [38].

Self-assembled monolayers are among the most commonly studied self-assembled structures. SAMs are surfaces covered by a thin film consisting of a single layer of molecules. Typically, they are formed when surfactant molecules are absorbed onto a substrate as a monomolecular layer. Among the most common and widely studied SAM systems are gold–alkylthiolate ($\text{CH}_3(\text{CH}_2)_n\text{S}$) and silicon oxide–alkylsilane monolayer systems (Fig. 1.6).

In typical SAM fabrication, a group with a strong attraction to a particular substrate is attached to the head of a long molecule, an alkane chain with about 10–20 methylene units. The head group absorbs easily onto the substrate surface, creating a monolayer with the tails pointing away from the substrate surface [39]. An example of this is the gold–thiol SAM; thiol (S–H) head groups in solution absorb readily onto gold. In work with methyl-terminated thiols, Krishnan and colleagues first cleaned the substrate, silicon wafers, in hot 1:4 H_2O_2 (30%)/ H_2SO_4 and then rinsed them in distilled–deionized water and absolute alcohol. Next, a layer of gold was added in order to allow the thiol groups to bind. The wafers were covered in gold using vapor deposition of chromium and gold from heated tungsten boats in a cryogenically pumped deposition chamber [39].

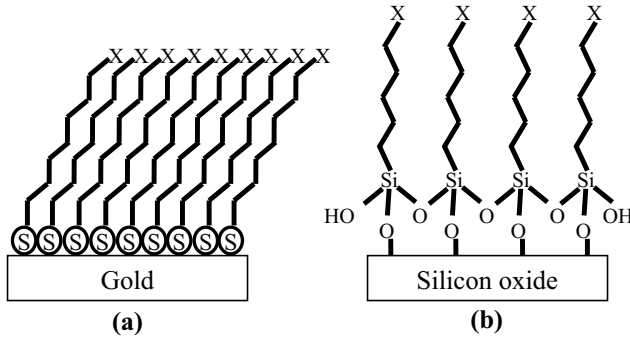


FIGURE 1.6 A diagram of (a) gold–alkylthiolate and (b) silicon oxide–alkylsilane SAMs.

The layer of chromium was deposited before the layer of gold to enhance adhesion to the substrate. The gold-coated samples were removed and placed into 1 mM solutions of 1-hexadecanethiol in ethanol, contained at ambient temperature, for 3 days. Afterward, the wafers were placed into the thiol solution. Before experimental use, they were rinsed with ethanol and air dried [39]. In this method, the thiol heads form a dense layer (1 molecule thick) on the gold surface whereas the tails of the molecules point outward forming another layer covering the substrate surface.

By changing the group attached to the tail of the absorbed molecules (or using different molecules), you can tailor the functionality of the new surface. Functionality can also be added to that tail groups after the SAM is formed. The tail groups and molecules can be selected to form SAMs for specific applications. Adding short oligomers of ethylene glycol groups to the tail decreases protein adhesion [40]. Methyl-terminated groups can increase plasma and protein binding [39], which could increase the biocompatibility of the substrate. Creating a monolayer of fluoroalkylsilane (FAS) onto silicon surfaces reduces neural cell growth [41]. The use of 1-octadecanethiol, 1-dodecanethiol, and 1-hexanethiol groups protects copper from corrosion [42]. Absorbing a layer of octadecyltrichlorosilane (OTS) increases wear resistance of polysilicon, a technique that may increase the durability of MEMS or NEMS [43].

1.9 CONCLUSIONS

Nanotechnology is an exciting field that has seen tremendous growth and has advanced into the biomedical and electronics arena. Nanotechnology has become an integrated part of our everyday lives. From medicine, to clothing, to electronics, breakthroughs in nanofabrication have lead to new products. There are a plethora of techniques for creating nanoscaled devices for biomedical engineering. Many of these, such as lithography-based techniques,

are applications of older techniques with more modern and powerful equipment. All of these techniques produce patterns, structures, and surface morphologies at the nanoscale that lead to devices and materials with unique surface properties and functionality. These techniques impart unique chemical, mechanical, electrical, and optical properties to materials for use in electronics, materials science, and medicine. Nanofabrication has led to major advances in these fields and holds promise for the creation of new technologies.

REFERENCES

1. Urban GA, Prohaska O, Olcaytug F. In: Urban GA, editor. *BioMEMS*. Dordrecht, The Netherlands: Springer; 2006. p 1–14.
2. Henshaw M. First impressions: the early history of lithography—a comparative survey. *Artonview* 2003;(33):33–38.
3. Mack CA. Optical lithography modeling. In: Sheats JR, Smith BW, editors. *Microolithography Science and Technology*. New York: Marcel Dekker, Inc.; 2006. 109–170.
4. Xia YN and Whitesides GM. Soft lithography. *Annu Rev Mater Sci* 1998;28: 158–184.
5. Madou MJ. *Fundamentals of Microfabrication: The Science of Miniaturization*. Boca Raton, FL: CRC Press LLC; 2002.
6. Atkinson GA and Ounaies Z. Polymer systems: materials and fabrication. In: Gadel-Hak M, editor. *MEMS Design and Fabrication*. Boca Raton, FL: Taylor & Francis; 2006. p 9-1–9-39.
7. Ding L, Li Y, Chu HB, Li XM, Liu J. Creation of cadmium sulfide nanostructures using AFM dip-pen nanolithography. *J Phys Chem B* 2005;109:22337–22340.
8. Jaschke M and Butt HJ. Deposition of organic material by the tip of a scanning force microscope. *Langmuir* 1995;11:1061–1064.
9. Lee KB, Lim JH, Mirkin CA. Protein nanostructures formed via direct-write dip-pen nanolithography. *J Am Chem Soc* 2003;125:5588–5589.
10. Becker EW, Ehrfeld W, Haggmann P, Maner A, Münchmeyer D. Fabrication of microstructures with high aspect ratios and great structural heights by synchrotron radiation lithography, galvanofarming, and plastic moulding (LIGA process). *Microelectron Eng* 1986;4:35–36.
11. Kathuria YP. L^3 : laser, LIGA and lithography in microstructuring. *Indian Inst Sci J* 2004;84:77–87.
12. Menz W, Mohr J, Paul O. The LIGA process. In: Menz W, Mohr J, Paul O, editors. *Microsystem Technology*. Wiley-VCH; 2001. p 285–350.
13. Randhawa H. Review of plasma-assisted deposition processes. *Thin Solid Films* 1991;196:329–349.
14. Yamada I and Toyoda N. Recent advances in R&D of gas cluster ion beam processes and equipment. *Nucl Instrum Methods Phys Res B: Beam Interact Mater Atoms* 2005;241:589–593.
15. Ota Y. Silicon molecular beam epitaxy. *Thin Solid Films* 1983;106:1–136.

16. Brodsky MH. Plasma preparations of amorphous silicon films. *Thin Solid Films* 1978;50:57–67.
17. Zeleny J. Electric discharge from points. *Phys Rev* 1917;9:562–563.
18. Yarin AL, Koombhongse S, Reneker DH. Taylor cone and jetting from liquid droplets in electrospinning of nanofibers. *J Appl Phys* 2001;90:4836–4846.
19. Reneker DH, Yarin AL, Fong H, Koombhongse S. Bending instability of electrically charged liquid jets of polymer solutions in electrospinning. *J Appl Phys* 2000;87:4531–4547.
20. Huang ZM, Zhang YZ, Koraki M, Ramakrishna S. A review on polymer nanofibers by electrospinning and their applications in nanocomposites. *Composites Sci Technol* 2003;63:2223–2253.
21. Formhals A. Apparatus for producing artificial filaments from material such as cellulose acetate. US patent 1,975,504. 1934.
22. Ramakrishna S, Fujihara K, Teo W, Lim T, Ma Z. An introduction to electrospinning and nanofibers. Singapore: World Scientific Publishing Co.
23. Buchko CJ, Chen LC, Shen Y, Martin DC. Processing and microstructural characterization of porous biocompatible protein polymer thin films. In: 1999. p 7397–7407.
24. Fong H and Reneker DH. Elastomeric nanofibers of styrene-butadiene-styrene triblock copolymer. *Journal of polymer science. Part B-Polymer Physics* 1999;37:3488–3493.
25. Baumgarten PK. Electrostatic spinning of acrylic microfibers. *Journal of colloid and interface science* 1971;36:71–79.
26. Deitzel JM, Kleinmeyer J, Harris D, Tan NCB. The effect of processing variables on the morphology of electrospun nanofibers and textiles. *Polymer*. 2001;42:261–272.
27. Tibbetts GG. Why are carbon filaments tubular. *J Crystal Growth* 1984;66:632–638.
28. Iijima S. Helical microtubules of graphitic carbon. *Nature* 1991;354:56–58.
29. Baughman RH, Zakhidov AA, de Heer WA. Carbon nanotubes—the route toward applications. *Science* 2002;297:787–792.
30. Wei B, Vajtai R, Ajayan PM. Synthetic approaches for carbon nanotubes. In: Kumar CSSR, Hormes J, Leuschner C, editors. *Nanofabrication Towards Biomedical Application Techniques, Tools, Applications and Impact*. Weinheim: Wiley-VCH; 2005. p 33–55.
31. Journet C, et al. *Nature* 1997;388:756–758.
32. Mogyorosi P and Carlsson JO. Growth characteristics of photolytic laser-induced chemical vapor-deposition of tungsten from WF₆. *J Vac Sci Technol A: Vac Surf Films* 1992;10:3131–3135.
33. Conde O and Silvestre AJ. Laser-assisted deposition of thin films from photoexcited vapour phases. *App Phys A: Mater Sci Process* 2004;79:489–497.
34. Jantunen H. Electronics materials, packing and reliability techniques (EMPART). INFOTECH OULU Annual Report; 2005. p 16–24.
35. Gonzales P, et al. Photo-induced chemical vapour deposition of silicon oxide thin films. *Thin Solid films* 1992;218:170–181.

36. Heszler P, Landstrom L, Lindstam M, Carlsson JO. Light emission from tungsten nanoparticles during laser-assisted chemical vapor deposition of tungsten. *J Appl Phys* 2001;89:3967–3970.
37. Lehmann O and Stuke M. 3-Dimensional laser direct writing of electrically conducting and isolating microstructures. *Mater Lett* 1994;21:131–136.
38. Wei B, Vajtai R, Ajayan PM. Molecular Biomimetics: Building Materials Nature's Way, One Molecule at a time. In: Kumar CSSR, Hormes J, Leuschner C, editors. *Nanofabrication Towards Biomedical Applications Techniques, Tools, Applications, and Impact*. Weinheim: Wiley-VCH; 2005, p 119–134.
39. Krishnan A, Cha P, Liu YH, Allara D, Vogler EA. Interfacial energetics of blood plasma and serum adsorption to a hydrophobic self-assembled monolayer surface. *Biomaterials* 2006;27:3187–3194.
40. Senaratne W, Andruzzi L, Ober CK. Self-assembled monolayers and polymer brushes in biotechnology: current applications and future perspectives. *Bio-macromolecules* 2005;6:2427–2448.
41. Patel KR, et al. Evaluation of polymer and self-assembled monolayer-coated silicone surfaces to reduce neural cell growth. *Biomaterials* 2006;27:1519–1526.
42. Li G, Ma H, Jiao Y, Chen S. An impedance investigation of corrosion protection of copper by self-assembled monolayers of alkanethiols in aqueous solution. *J Serb Chem Soc* 2004;69:791–805.
43. Baker MA and Li J. The influence of an OTS self-assembled monolayer on the wear-resistant properties of polysilicon based MEMS. *Surf Interface Anal* 2006;38:863–867.

Micro/Nanomachining and Fabrication of Materials for Biomedical Applications

WEI HE, KENNETH E. GONSALVES, and CRAIG R. HALBERSTADT

2.1 INTRODUCTION

In 1965, Intel cofounder Gordon Moore observed that innovations in technology would allow a doubling of the number of transistors on a chip about every 2 years [1]. The reality of Moore's prediction, popularly known as Moore's law, is being driven into the future, thanks to the advances in technologies such as lithography. Apart from traditional optical lithography, intense interest has been devoted to what is considered next generation lithography (NGL), that is, extreme UV (EUV), X-ray, electron, and ion beam lithographies, to produce sub-100 nm features. Advances in the lithographic process have not only impacted the semiconductor manufacturing industry, but also provide excellent tools/resources for the growth of the exciting interdisciplinary field of biomedical engineering.

One of the most widely known applications of lithography in the biomedical field is micro/nanofabrication of biomaterials. Biomaterials are a class of materials intended to interface with biological systems to evaluate, treat, augment, or replace any tissue, organ, or function of the body [2]. In general, biomaterials can be divided into the following categories: polymers, metals, ceramics, composites, and natural materials. One of the key factors in determining the successful performance of materials in biomedical applications is the property of the surface, where the material and the biological system meet and interact. Intense effort has been invested into engineering the biomaterial surface to achieve the optimum and desired interactions between cells and materials, while keeping intact the materials bulk properties. For

Biomedical Nanostructures, Edited by Kenneth E. Gonsalves, Craig R. Halberstadt, Cato T. Laurencin, and Lakshmi S. Nair

Copyright © 2008 John Wiley & Sons, Inc.

example, cell adhesion to surfaces can be either promoted by immobilizing cell adhesive peptides, such as RGD [3] and IKVAV [4], and proteins, such as fibronectin [5] and laminin [6], or prohibited by attaching macromolecules such as poly(ethylene glycol) [7]. Besides surface chemistry, surface morphology is of paramount importance in determining the biological responses to biomaterials. It is well known that cell orientation and the direction of cell movement are affected by the morphology of the substrate, a phenomenon known as “contact guidance.” The ability to control cell orientation and connection is especially important for tissue engineering applications, as an intricate network of cells and extracellular matrix proteins modulates tissue functions. The advent of lithographic methods as used in microelectronics for making structures on the same scale as biological cells has opened up the possibility of precise surface engineering of biomaterials down to the nanometer scale [8].

The focus of this chapter will be placed on using ion beam lithography/ion implantation to enhance performances of both “soft” polymeric biomaterials and “hard” metallic biomaterials. Throughout this chapter, we will use specific examples for applications such as hard tissue replacements, blood contacting implants, and other products. A brief summary on the recent developments of novel biocompatible photoresists, aiming at improving the compatibility of the conventional photolithography with biomolecular (i.e., attachment of cell-specific peptides and proteins) and cellular patterning, is also included.

2.2 OVERVIEW OF ION IMPLANTATION PROCESS

Ion implantation refers to the bombardment of material surfaces with ions with a minimum exposure of 10–20 keV of energy [9]. It is a process whereby energetic dopant ions are made to impinge on silicon or other targets, resulting in the penetration of these ions below the target surface and thereby giving rise to controlled, predictable dopant distributions. Due to high initial energy, ions penetrate the surface layer of the material losing their energy in two types of interactions: elastic collisions with target nuclei and inelastic collisions with the electrons [10]. Because the ions do not penetrate too deeply, usually less than a micrometer, the implantation and modifications are confined to the near-surface region, and only surface properties are changed.

Ion implantation offers numerous advantages for treating component surfaces. A primary benefit is the ability to selectively modify the surface without detrimentally affecting material's bulk properties, largely because the process is carried out at low substrate temperature. It is useful for generating surface layers that are integrated with the substrate and have a specified composition, thus avoiding the risk of delamination associated with techniques such as coating. The process is extremely controllable and reproducible, and offers high concentration of the dopants. It can be tailored to modify different surfaces in desired ways. The technique is highly versatile, allowing selection of the types of ions used according to the characteristics to be modified. When used in combination with an electroformed screen mesh mask, it can transfer

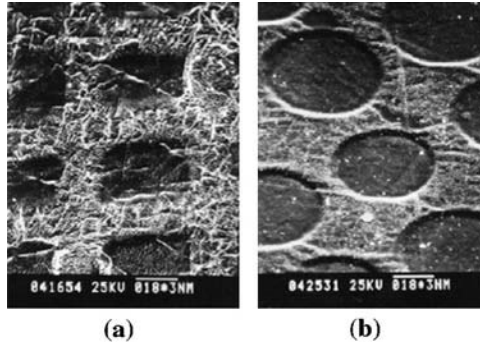


FIGURE 2.1 SEM morphology of silicon rubber that had the ion-beam texturing process performed using an electroformed screen mesh mask with either a square (a) or a round (b) pattern. The energy of the Ar ion beam used was 1 keV. (Reprinted from Reference [11], with permission from Elsevier.)

the patterns from the mask to the surface by removing the atoms from the unmasked area (Fig. 2.1) [11]. It is an attractive micro/nanofabrication technique as it allows patterning and surface chemistry modification to occur simultaneously in a single-step process. This approach is distinct from the mechanical transfer of micropatterns of a die into a polymer, as well as conventional photolithography. The limitations of the former are that the polymer has to be a thermally stable thermoplastic material and the surface chemistry cannot be modified. In the latter case, the surface and bulk chemistry are difficult to modify simultaneously while applying a specific pattern.

2.3 MICRO/NANOMACHINING OF “SOFT” POLYMERIC BIOMATERIALS

Polymers have enjoyed widespread use in many biomedical applications, ranging from contact lenses, intraocular lenses, dental implants, vascular grafts, artificial hearts, breast implants, biodegradable sutures, pacemakers, artificial skin, and joint replacements. As pointed out earlier, it is very important that the polymeric biomaterials have the “correct” surface properties to ensure the successful functional outcome. Depending on the applications, the “correct” surface properties could be corrosion and/or wear resistance, support of cell adhesion and differentiation, antimicrobial, antithrombogenic, and so on.

2.3.1 Orthopedic Applications

Poly(methyl methacrylate) (PMMA) is used extensively as bone cement, which is primarily used to adhere the stems of total joint prostheses in the medullary cavity of bone [12]. As it acts as an interface between the prostheses component and bone tissue, it is necessary that this material is biologically compatible with

osteoblasts (bone-forming cells) in order to enhance matrix formation and mineralization that will ultimately support osseointegration of the implant with the surrounding tissue. Applying masked ion beam lithography (MIBL), He et al. [13, 14] investigated the potential of this technique for bone tissue engineering. Compared to conventional patterning techniques such as photolithography, MIBL produced patterns without using any harsh chemicals that are toxic to the cells and could denature biologically active molecules such as proteins and peptides (biomolecules). In these studies, PMMA films were exposed to masked Ca^+ ion (85 keV , $1 \times 10^{14} \text{ ions/cm}^2$), P^+ ion (85 keV , 1×10^{15} and $1 \times 10^{16} \text{ ions/cm}^2$), and Ar^+ ion (115 keV , $1 \times 10^{15} \text{ ions/cm}^2$) implantations, respectively. The surface morphology of the PMMA films was studied using atomic force

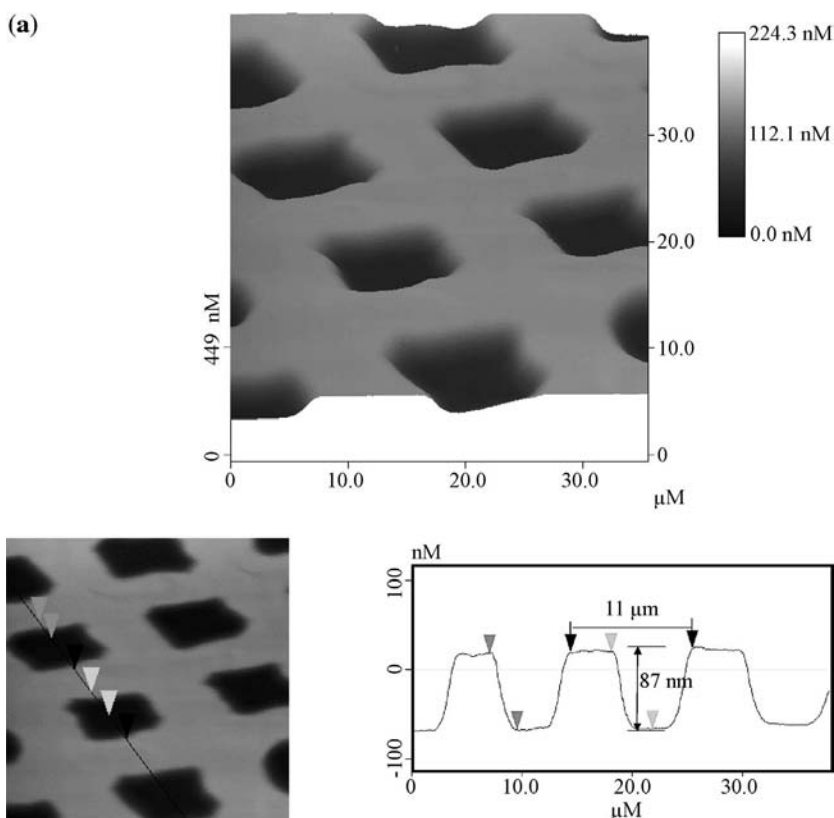


FIGURE 2.2 AFM images of the PMMA film surfaces, recorded in the tapping mode with typical surface features characterized by a cross-section analysis. (a) 85 keV , $1 \times 10^{14} \text{ ions/cm}^2$ Ca^+ ions; (b) 85 keV , $1 \times 10^{15} \text{ ions/cm}^2$ P^+ ions; (c) 85 keV , $1 \times 10^{16} \text{ ions/cm}^2$ P^+ ions; and (d) 115 keV , $1 \times 10^{15} \text{ ions/cm}^2$ Ar^+ ions. (a–c, reprinted from Reference [14], with permission from Elsevier; d, reprinted from Reference [13], with kind permission of Springer Science and Business Media.)

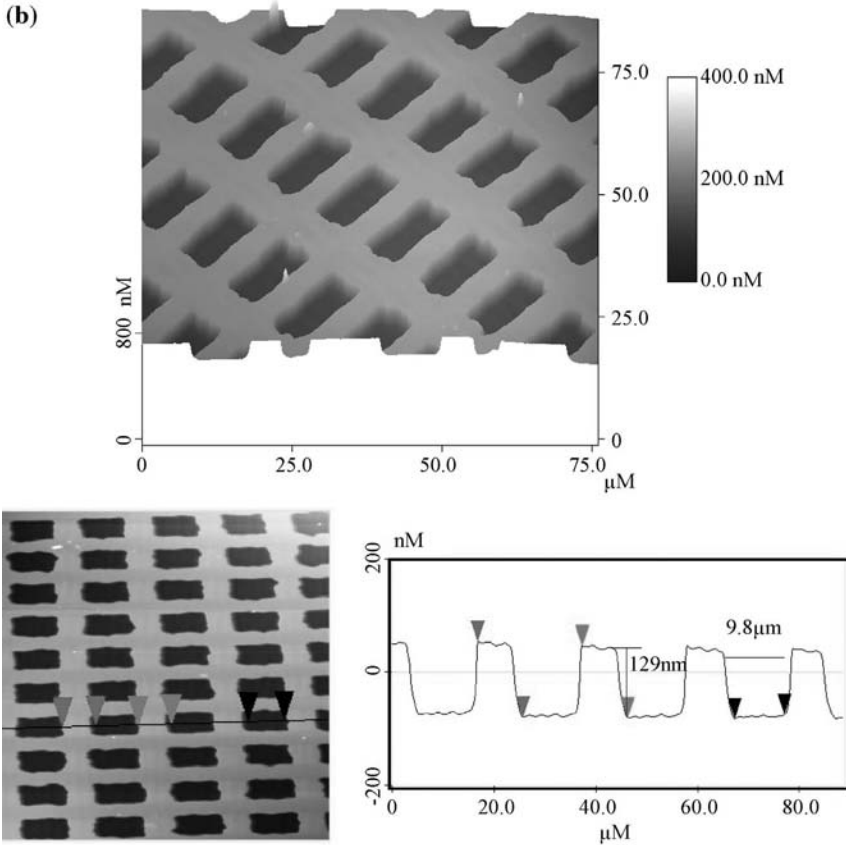


FIGURE 2.2 (Continued)

microscopy (AFM) after irradiation. As shown in Fig. 2.2, the patterns generated on the films were characterized as arrays of holes with nanoscale depth and microscale width. The AFM results of cross-section analysis on the Ca^+ ions irradiated sample showed that the distance between the two left edges of the isolated islands is about $11 \mu\text{m}$, and the height of each island is about 87 nm . In the lower dose P^+ ions treated sample, the distance is $9.8 \mu\text{m}$ and the depth is 129 nm . When the dose of P^+ ion was increased, the distance increased to $11.3 \mu\text{m}$ while the depth became 95 nm . Due to erosion of the walls from the sides, the walls became thinner when the dosage of the ions was increased. Initially, only the region that is under the opening of the mask is etched, but as those areas recede, the walls stick up higher than the eroded areas. Even though the mask shades the walls, ions that sputter off the center of each region can come off at a shallow angle and strike the wall, which results in the sputtering from the sides of the walls.

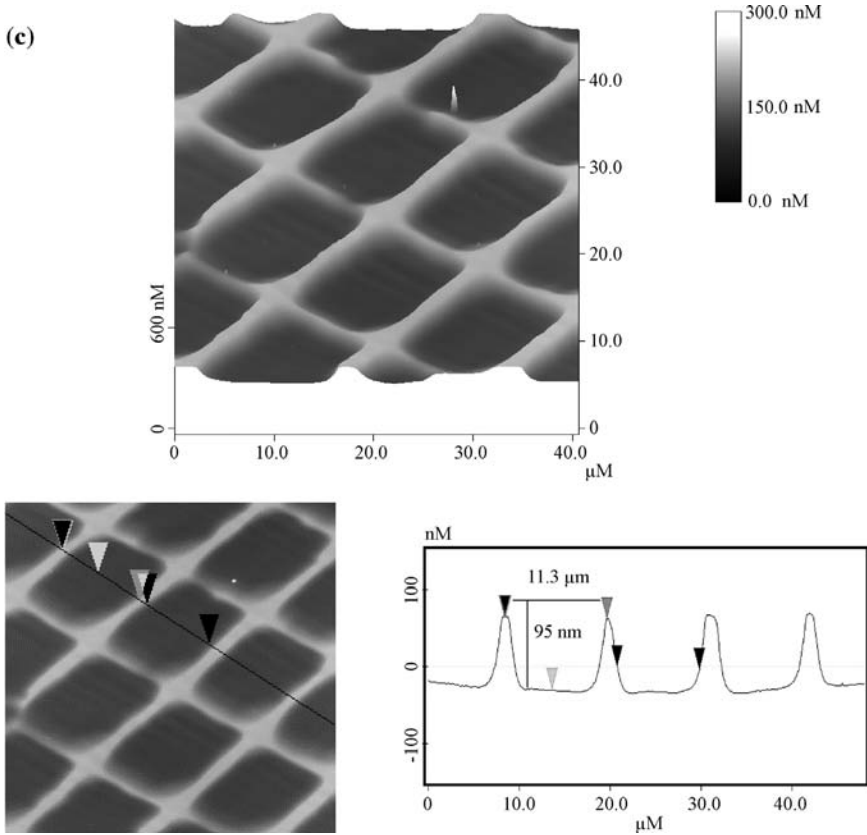


FIGURE 2.2 (Continued)

In order to evaluate the influence of the ion beam treatments on cell adhesion, primary rat calvaria osteoblast cells were cultured on nonirradiated, P^+ ion irradiated, and Ar^+ ion irradiated PMMA surfaces [13]. Both P^+ ions and Ar^+ ions implanted PMMA samples had greater cell attachment than the untreated PMMA, indicating that ion irradiation improves osteoblast adhesion on polymeric substrate, most likely due to the increased surface roughness. This is consistent with the literature on strong correlations between increased surface roughness and enhanced osteoblast adhesion [15]. Furthermore, despite the similarity in surface topography and surface roughness in both treated samples, the extent of cell attachment was higher for the P^+ irradiated samples than the Ar^+ irradiated samples. This observed difference may be due to not only a surface morphological difference but may also be due to that P^+ ions influence on osteoblast behavior. The depth profile of P in the treated PMMA film was investigated by dynamic secondary ion mass spectroscopy (SIMS). The majority of P ions are distributed in the area that is about 100 nm from the

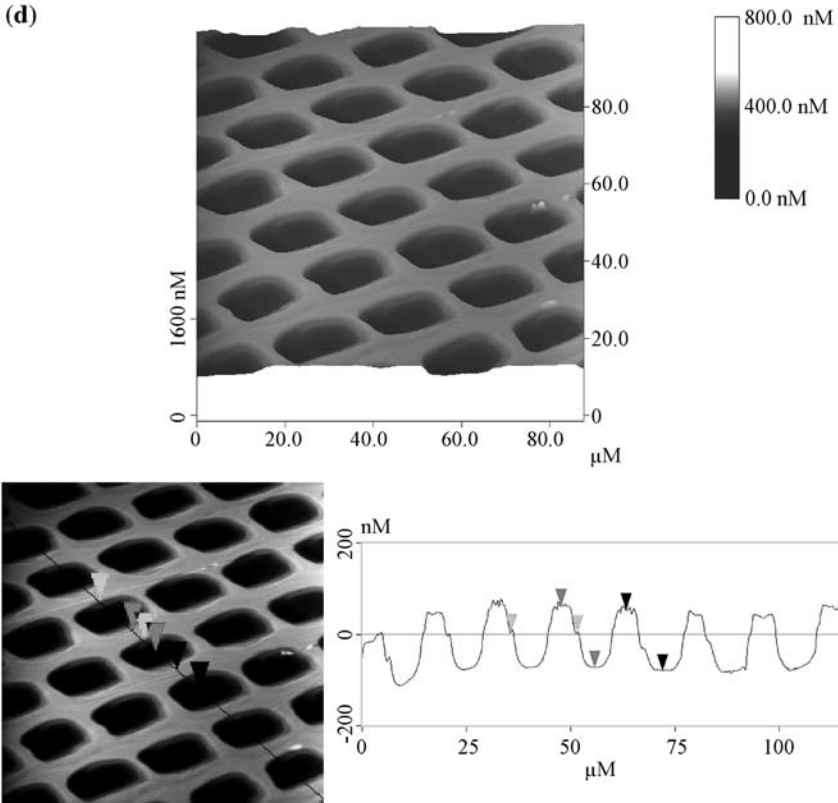


FIGURE 2.2 (Continued)

surface, with the maximum concentrations of 1.1×10^{20} ions/cm³ at 121 nm. The result suggested that MIBL is capable of achieving a nanoscale elemental composition/distribution.

In summary, the advantages of using ion implantation as a microfabrication technique are as follows: (a) since it is a one-step process, the patterns can be “micromachined” into the material in a controlled manner through specific masks; and (b) by selecting a specific ion to implant, such as Ca or P, the surface chemistry of the biocompatible material can be tailored, which may influence certain biological processes. In addition, nanostructures can be controlled to allow for distinct cellular pattern adhesion. MIBL could be a viable and novel technique for patterning and doping soft materials simultaneously for potential biomedical applications.

The other type of commonly used polymeric orthopedic product is ultrahigh molecular weight polyethylene (UHMWPE), which is generally used in total joint replacement because of its superior properties such as ductility, impact load damping, and excellent biocompatibility [16, 17]. However, the generated

wear debris at the articular surface compromises the long-term use of UHMWPE, as it is considered the major cause of loosening and premature failure of the total joint replacement [18]. Ion implantation has provided an effective means to improve the wear properties of UHMWPE. For example, UHMWPE was subjected to nitrogen ion implantation [19, 20]. Wear resistance of UHMWPE after nitrogen implantation was improved by 68 times over control samples, due to cross-linking of UHMWPE that reduces the sliding between the molecules. In addition, the load-bearing capacity of UHMWPE was increased, which could be partially attributed to the harder and tougher surface-modified layer produced by nitrogen ion implantation. Valenza et al. [21] studied the effect of ions other than nitrogen on wear resistance of UHMWPE. UHMWPE was implanted using H^+ , He^+ , Ar^+ , and Xe^+ ion beams at 300 keV. The irradiation was performed with an ion flux ranging between 10^{14} and 10^{17} ions/cm². Using traditional pin-on-disk wear tests, the authors found that the surface wear resistance increases with increasing irradiation dose: a reduction of about 76% is observed after 72 h in a UHMWPE sample treated with 3×10^{15} Xe^+ /cm².

2.3.2 Blood-Contacting Devices

Synthetic polymers are widely used in blood-contacting implants and devices. Using vascular prostheses for instance, clinically used artificial blood vessels are constructed most frequently from expanded polytetrafluoroethylene (ePTFE) or poly(ethylene terephthalate) (PET), also known as Dacron. Major concerns associated with blood-contacting devices are infection, thrombosis, and stenosis. Ion implantation has been successfully used to improve the antithrombogenicity and hemocompatibility of polymeric biomaterials [22–30]. The reduction of thrombogenicity of silicon rubber for catheters was achieved by treating the surface with ions, such as hydrogen, nitrogen, argon and neon, leading to increases in its hydrophilicity and significantly changing the long-term ability of its surface to resist biodeposits [25, 30]. The other approach to improve the biocompatibility of artificial vascular grafts is to develop surfaces that support endothelialization. This is crucial since endothelial cells are responsible for the formation of a nonthrombogenic interface between blood and tissue. In the early 1990s, Lee et al. [22] reported that the adhesion and proliferation of endothelial cells could be drastically improved when the surface of segmented polyurethane (SPU) was modified by neon or sodium ion implantation (Fig. 2.3). *In vivo*, the neon ion implanted SPU tubes demonstrated superior graft patency when replacing the femoral artery [24] Kurotobi et al. [31] prepared hybrid-type small vascular grafts of ePTFE in three steps: Ne ion bombardment of the inner walls of small tubes, plasma protein coating on implanted surfaces, and He ion bombardment through proteins coated on inner walls. The graft was implanted in the carotid artery of a mongrel dog and the health of the dog was followed for 180 days. The graft exhibited

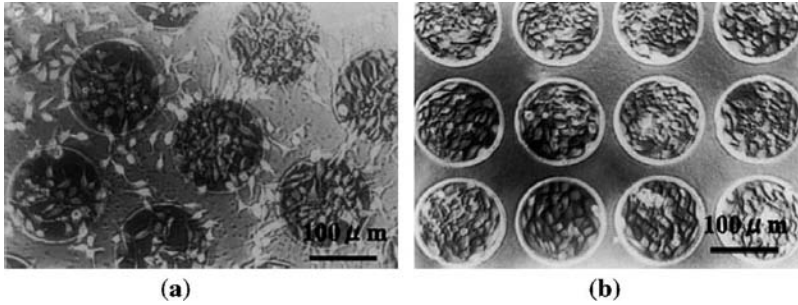


FIGURE 2.3 Morphology of endothelial cell attachment to Ne^+ ion implanted (a) polystyrene and (b) segmented polyurethane with a fluence of 1×10^{15} ions/cm² after incubation of 3 days.(Reprinted from Reference [30], with permission from Elsevier.)

great antithrombogenicity, possibly as a result of low plasma protein adsorption. Oxygen [28], silver [26, 27], and fluorine [29] ion implantations have also been demonstrated to affect endothelial cell adhesion and growth on polymer substrates.

2.3.3 Other Applications

Recently, ion implantation has also been used to treat polymers for nervous system repair. Polydimethylsiloxane (PDMS) rubber tubes, commonly used for peripheral nerve regeneration, were treated by carbon negative-ion implantation [32]. The PDMS rubber surface was found to have more hydrophilic properties due to the formation of functional groups such as hydroxyl at the surface by the radiation effect of ion implantation. The carbon-implanted PDMS rubber tube was effective in “tubulation” of rat sciatic nerve, where 15-mm-long sciatic nerve was regenerated to conduct nerve stimulation. Okuyama et al. [33] investigated neurite outgrowth on a fluorinated polyimide film micropatterned by ion beam. The ability to control the interaction of neurons with a biomaterial surface in a specific manner is important for both the investigation of basic neuron cellular function and the design of advanced bioelectronics such as biosensors and neural computers. To demonstrate the importance of the surface topography and chemistry on neuron cell behavior, micropatterns with 120 or 160 μm width (Fig. 2.4) were prepared on polyimide surface using an ion-beam mask by irradiation with He^+ , Ne^+ , or Kr^+ at 1×10^{14} ions/cm². Neurons preferentially attached to areas exposed to the ion beams. Interestingly, although most attachment was found on Kr^+ treated surface and the least was on He^+ treated, the extent of neurite outgrowth was the opposite; that is, He^+ surface supported the longest neurite extension while cells on the Kr^+ surface showed the shortest neurite length. These results imply that ion implantation could be used to

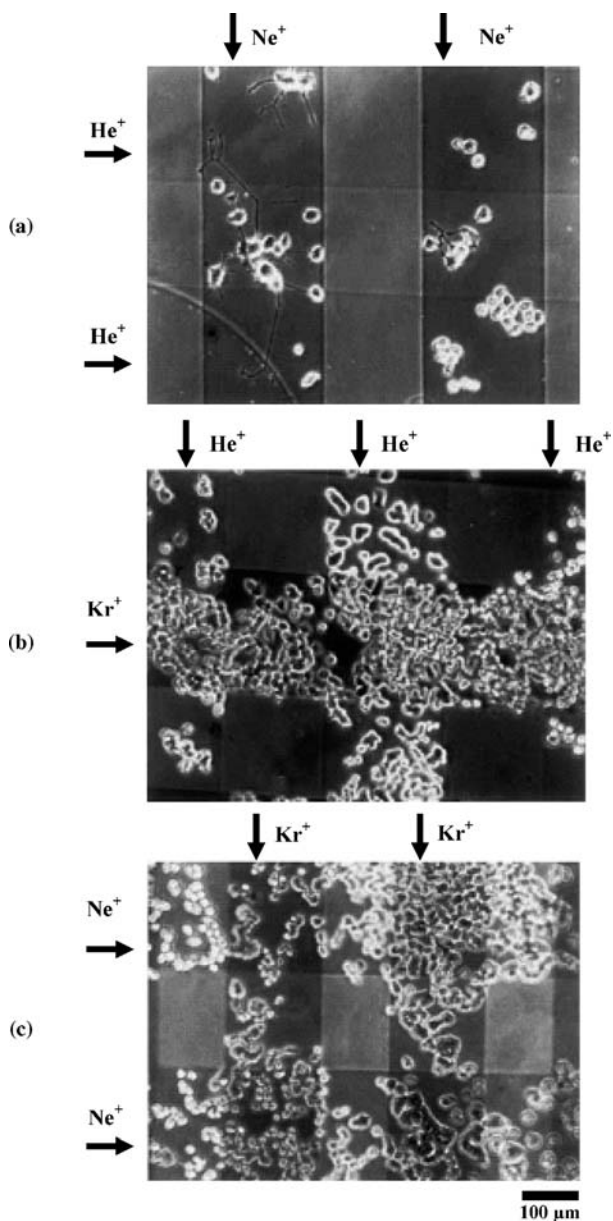


FIGURE 2.4 Images of phase contrast microscopy of PC12 cells cultured on ion-irradiated fluorinated polyimide films for 72 h. (a) He^+ + Ne^+ irradiation; (b) He^+ + Kr^+ irradiation; (c) Ne^+ + Kr^+ irradiation. (Reprinted from Reference [33], with permission from Elsevier.)

pattern specific cellular growth on a biomaterial substrate. Another example of the possibilities offered by ion implantation for biomedical applications is the development of a dural substitute in restorative cranial surgery. The ideal synthetic dural substitute requires two different surfaces: a cell adhesive external side and a nonadhesive cerebral side. Commonly, the nonabsorbable, nonadhesive ePTFE is used for this purpose. Ne^+ ion implantation of one side of ePTFE led to excellent bone attachment and tissue in-growth without altering the properties of the nonadhesive cerebral side [30]. In another study, ePTFE was exposed to Ar^+ ion implantation and exhibited excellent closure of the dural defect without the postoperative leakage of the cerebrospinal fluid (CSF) [34]. The improvement was believed to be due to fibroblast-like cell invasion and anchoring into the gaps of the ePTFE surface created by ion-beam irradiation that enhanced the cell adhesiveness of the material.

Examples of using ion implantation for other biomedical applications of polymers include F^+ ion implantation to induce cell attachment onto the PMMA intraocular lens [35], ion beam modifications of polyethylene for a skin coverage substitute [36, 37], and Ar^+ ion implantation to reduce tissue inflammatory response to polyurethanes [38]. In addition to these applications, the prevention of medical device related infections remains a main obstacle due to the high rate of complications, increasing health care costs and causing high rate of mortality and morbidity. Therefore, it is of great interest to the biomedical industry that the medical polymers possess anti-infective properties. Studies have shown that ion implantation provides an effective yet simple approach to minimize bacterial adhesion to polymers. Silver ion implantation has been studied due to its antimicrobial properties [39, 40]. Boldyryeva et al. demonstrated that negative silver ion implantation into PMMA not only resulted in the formation of silver nanoparticles with the diameter of less than 10 nm, but also created surface-exposed gradient of such nanostructures [40]. Other ions, such as argon [41] and acetylene [42], have also been shown to improve the antibacterial performance of polymeric biomaterials.

2.4 MICRO/NANOMACHINING OF “HARD” METALLIC BIOMATERIALS

Metallic materials are no strangers to the biomedical field. In fact, metal implants are widely used for orthopedics, dental, and cardiovascular applications, examples of which include total hip replacement, total knee replacement, bone plates, and stents. In the field of orthopedics, metals are popular primarily because of their ability to bear significant loads, withstand fatigue loading, and undergo plastic deformation prior to failure. Currently, the most commonly used metal implants include stainless steels, cobalt–chromium–molybdenum alloys, commercially pure titanium, and titanium alloys [12]. However, the use of metallic implants is not short of problems, and

ion implantation has been widely used to improve the performance of metallic implants. This section will review studies involving ion implantation of hard metals.

2.4.1 Orthopedic Applications

As mentioned above, metals are used in orthopedic applications because of their good biocompatibility and their excellent mechanical and tribological properties. However, there are still limitations associated with their applications. For example, a typical concern with titanium is its relatively poor wear resistance. Among various procedures used to enhance the performance of metallic orthopedic products, ion implantation has been the most commonly used treatment. Ion implantation can harden the surface and reduce the friction coefficient, ultimately improving the wear resistance [43]. Buchanan's work [44] demonstrated that impregnation of Ti6Al4V with nitrogen ion significantly improved the material's resistance to wear-accelerated corrosion in both saline and serum solutions at all applied stress levels. Other researchers observed order-of-magnitude improvements in the wear resistance of nitrogen ion implanted titanium alloys [45, 46], using traditional pin-on-disk wear tests. Besides nitrogen, several other elements have also been used to improve wear-corrosion and corrosion behavior of metals. Tan et al. [47] modified nickel–titanium with oxygen at three levels of implantation doses (5×10^{16} , 1×10^{17} , and 3×10^{17} ions/cm²). Topographical changes were induced by oxygen ion implantation. Grooves that were originally present on the NiTi surface were smoothed by low and medium dose oxygen ion implantation, and the medium dose oxygen-implanted samples (1×10^{17} ions/cm²) showed the best corrosion resistance; however, nanopores appeared on the surface of the modified materials at the high dose (3×10^{17} ions/cm²), which acts as the source of pitting corrosion and impairing the resistance of pitting corrosion. Krupa et al. [48] studied how the modification of titanium surfaces by calcium ion implantation affects the corrosion resistance of titanium. It was found that calcium ion implantation at a dose of 1×10^{17} ions/cm² increases the corrosion resistance of titanium under stationary conditions, but, at longer exposure times, the susceptibility of calcium ion implanted titanium to pitting corrosion under anodic polarizations increases. In a subsequent study [49], phosphorous ion implantation was performed on titanium surface at a dose of 1×10^{17} ions/cm². The process led to amorphization of the surface layer and the formation of TiP. It also increased the corrosion resistance after short-term as well as long-term exposures, suggesting the advantageous effect of phosphorous ion implantation.

Great effort has also been devoted to improve the integration of metallic implants with the surrounding bone tissue. It is widely known that ceramic materials bind well to bone tissue due to the advantageous effect of their components CaO and P₂O₅, which are capable of nucleating hydroxyapatite

(HA). HA has many crystallographic features similar to those of the natural apatite present in bone, and therefore has been frequently used as coatings to create the bone-like surface chemistry that will be beneficial for osseointegration. Metals such as titanium do not support precipitation of HA intrinsically. In order to endow the metal surface with factors capable of being actively involved in the osseointegration process, researchers have studied how calcium ion implantation and phosphorous ion implantation modify surface chemistry and bioactivity both *in vitro* and *in vivo*. Hanawa et al. [50] demonstrated *in vivo* that the implantation of Ca^+ ions into Ti surfaces enhanced osseointegration and the formation of new osteoid tissue, possibly as a result of more rapid calcium phosphate precipitation on the implanted surface. Pham et al. [51] studied surface-induced reactivity for Ti by ion implantation of Ca and P, respectively, at several implantation energy steps. Needle-like HA crystallites were found on all implanted surfaces, but absent on the control samples without any ion implantation, suggesting that Ca and P ion implantation rendered the Ti surface active in the biomineralization process. *In vitro* culturing of bone cells on the Ca ion implanted Ti samples showed that the cell-material interaction was altered and was dependent on the ion implantation dosage [52–54]. High dose of Ca ions (1×10^{17} ions/cm²) significantly enhanced cell spreading, formation of focal adhesion plaques, and expression of integrins, despite the initial decrease in cell adhesion. Several groups [55–57] also studied the effect of dual ion implantation of Ca and P into Ti and its alloys. It was found that the binding energies of the Ca 2p, P 2p, and O 1s peaks of the modified surface layer about 100 nm thick are the same as the hydroxyapatite standard, indicating the formation of an apatite-like nanocoating on the surface by the successive implantation of calcium and phosphorous. The improved biocompatibility was further confirmed by the growth of bone marrow cells on the treated surfaces.

Sodium has also been implanted into titanium to improve its bone conductivity [58–60]. The implantation induced a modification in chemistry and morphology, producing morphologically rugged surfaces and showing sodium titanate incorporated within the surface layer with concentration, depth distribution, and morphology depending on the parameters of the ion implantation. The growth of bone-forming cells on the Na ion implanted surfaces was significantly improved from that on the untreated samples, evidenced by the high alkaline phosphatase activity and better spreading of cells [60].

Amino groups (NH_2^+) have been implanted to modify Ti surfaces [61, 62]. Because of the formation of TiN during the implantation process and the ability to create depths as deep as 61 nm, properties of the Ti, such as wear, corrosion, and fatigue resistance, have been improved. In addition, the attachment and spreading of cultured osteoblasts onto NH_2^+ implanted Ti was better than on hydroxyapatite and there was also an increased calcification on its surface.

2.4.2 Dental Implants

Dental applications use metallic implants for several therapies, including root form implants, endodontic stabilizers, and dental blades. Similar to orthopedic applications, it is also desirable to have faster and stronger bone bonding to the dental implant. Surface modification by ion implantation has been used to enhance the efficacy of these metallic implants. De Maeztu et al. [63] evaluated bone integration of dental implants habitually used in clinical practice and subjected to ion implantation surface treatment. Both commercially pure titanium dental implants and Ti6Al4V alloy implants, untreated or treated with either one of the following ions, carbon oxide (CO^+), nitrogen (N^+), carbon (C^+), and neon (Ne^+), were examined. The study found that surface treatment of dental implant surfaces by ion implantation to improve bone integration not only quantitatively (higher percentage contacts between bone and implant), but also qualitatively (with strong and more stable binding). There was a statistical difference found between the treated implants and controls, especially for C^+ ion implantation in Ti, and for CO^+ implantation in Ti6Al4V where the existence of covalent bonding between the Ti–O–C atoms was confirmed by X-ray photoelectron spectroscopy. Lee et al. [64] tried to successfully improve the surface hardness of endodontic Nitinol (nickel–titanium alloy) root canal instruments using boron implantation. Alternatively, Rapisarda et al. [65] implanted nitrogen ions into nickel–titanium endodontic instrument at an implantation dosage of 2×10^{17} ions/cm² and demonstrated that the ion implantation process makes NiTi endodontic instruments more resistant to wear and, therefore, able to shape more pulp canals before being discarded. It has also been shown that the ion implantation of nitrogen onto the surface of orthodontic wires decreases the frictional forces produced during tooth movement, thereby improving the efficiency of tooth movement [66].

2.4.3 Blood-Contacting Devices

Metals can also be used in blood-contacting devices. For example, coronary stents are mostly made from 316L stainless steel. Carbon ion implantation on the stainless steel stents was suggested to have the potential of reducing restenosis caused by inflammatory reaction after coronary revascularization [67]. Recent work by Yang et al. [68] demonstrated that phosphorous doping is an effective way to improve the blood compatibility of titanium oxide film, and it is related to the changes of electron structure and surface properties caused by phosphorous doping. On the contrary, ion implantation can also be used to improve thrombogenicity. Murayama et al. [69] modified Guglielmi detachable platinum coils (GDCs) that are used for endovascular treatment of wide-necked aneurysms, using a combination of protein coating and Ne^+ ion implantation at a dose of 1×10^{15} ions/cm². They found an intensive blood cellular response on ion-implanted coil surfaces, indicating that ion implantation combined with protein coating of GDCs improved cellular adhesion and

proliferation. This technology may provide early wound healing at the necks of embolized, wide-necked, cerebral aneurysms.

2.4.4 Other Applications

As discussed above, ion implantation can also generate antibacterial properties on the metallic implant surfaces. It has been shown that F^+ implanted titanium significantly inhibited the growth *in vitro* of both bacteria *Porphyromonas gingivalis* and *Actinobacillus actinomycetemcomitans* than nonion implanted control polished titanium samples [70]. Other ions such as silver and copper also have favorable effects on antibacterial property of the surfaces. Dan et al. [71] demonstrated that implantation of copper ions into AISI 420 stainless steel with a dose of 5×10^{17} ions/cm² greatly improved its antibacterial property against both *Escherichia coli* and *Staphylococcus aureus*.

2.5 NOVEL BIOCOMPATIBLE PHOTORESISTS

As mentioned earlier, the application of conventional photolithography for cellular and biomolecular patterning is greatly hampered due to the fact that organic solvents are normally utilized to dissolve the photoresist in order to reveal the pattern on the surface of the material. Such processes can lead to the denaturation of biomolecules, and thus, it is not suitable for application in biomolecular surface patterning. For example, the commonly used negative photoresist SU8, a multifunctional epoxy derivative of a bis-phenol-A novolac, requires the use of developers such as ethyl acetate or diacetone alcohol. Therefore, in order to create specific biocompatible surfaces using photolithography, a new class of photoresists will need to be developed. After all, photolithography is the current workhorse for the microelectronics industry, and it is a very mature and developed technology, with the capability of generating very precise, highly reproducible, and large-scale patterns. To date, two types of new biocompatible photoresist materials have been developed: one is based on poly(*t*-butyl acrylate) [72–74], and the other is based on poly(3-(*t*-butoxycarbonyl)-*N*-vinyl-2-pyrrolidone) [75, 76].

Both photoresists share the chemical amplification mechanism; that is, the photogenerated acid deprotects the *t*-butyl ester groups resulting in changes in solubility/hydrophilicity. It has been demonstrated that with the poly(*t*-butyl acrylate) type photoresist, it is possible to pattern biomolecules directly while the resist is being processed because the biomolecules can tolerate the low temperatures and the concentrations of the developer applied. Instead of the commercially common developer of base concentration in the range of 0.27N, diluted aqueous base developers of 0.0026N or lower base concentration were sufficient to reveal the pattern, making the processes both environment and

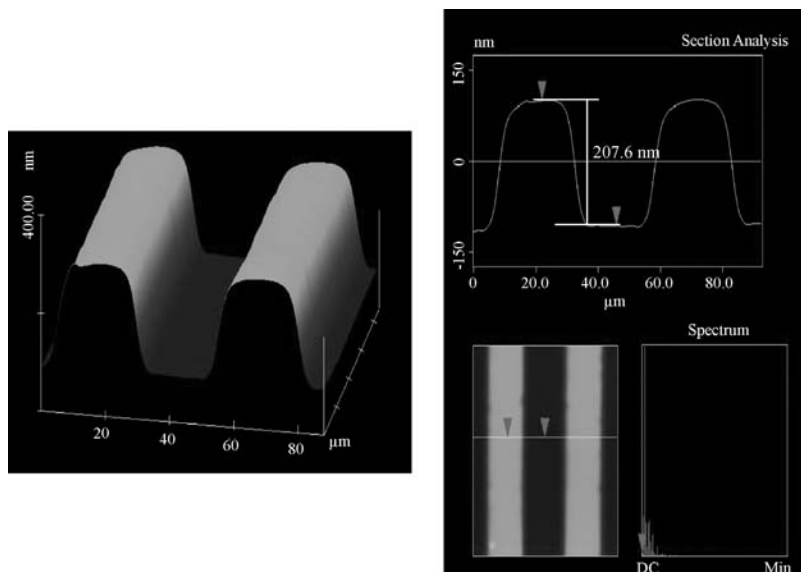


FIGURE 2.5 AFM micrographs of patterned poly(MMA-co-*t*-BOC-NVP) surface (25 μm line \times 50 μm space) showing section analysis.

biomolecular friendly. On the contrary, the development of poly(3-(*t*-butoxycarbonyl)-*N*-vinyl-2-pyrrolidone) type photoresists has further improved the biocompatibility of the lithographic patterning processes, as the usual step of feature development by organic solvents that normally denature biomolecules was eliminated. Upon exposure to UV light, the *t*-BOC groups undergo photolysis and become carboxylic groups, resulting in a change of surface property from hydrophobic to hydrophilic. Consequently, upon seeding fibroblast cells onto these patterned surfaces, the cells aligned along the hydrophilic patterned grooves. The preferential adhesions to the patterns are most likely due to the preferential adsorption of serum proteins from culture media onto the UV exposed area, which is more hydrophilic. The newly formed carboxyl groups also provide possibilities to couple specific peptides or proteins that will guide cell interaction with the substrate in a specific manner. In addition, these photolithographic techniques can control the depth and the pitch of the surface structures at the nanometer scale. As shown in Fig. 2.5, the patterned surface presents topography of nanogrooves with resolution around 200 nm, which may contribute to the observed oriented cellular growth. These important components coupled with the ability to mask different patterns of cell adhesive and nonadhesive peptides may allow for the tailoring of complex cell adhesive patterns onto the surface for the creation of complex tissues and organs.

2.6 THREE-DIMENSIONAL LITHOGRAPHY

A major interest in the field of tissue engineering is creating three-dimensional scaffold that will mimic the extracellular matrix (ECM) and accommodate mammalian cells by guiding their growth in three dimensions. ECM consists of numerous topographical features at the nanoscale, such as nanofibers, pores, bands, and bridges [77]. Thus, it is important to replicate these features to ensure the creation of functional tissues *in vitro*. Currently, techniques that can produce nanopatterns on biomedically relevant surfaces are limited. Ideally, such techniques should satisfy the requirements of nanoscale resolution, high throughput, reproducibility, high controllability of 3D nanostructures, low cost, and ability to pattern large area [78]. Nanoimprint lithography (NIL) has emerged as a versatile technique to meet these requirements. NIL can generate sub-10 nm resolution features on either flat or nonflat surfaces and has been widely used in nanodevice fabrications ranging from electronic to biological applications [79, 80]. Recently, Hu et al. [78] have demonstrated that NIL can be applied to fabricate three-dimensional scaffolds consisting of multiple-layer nanostructures on biomedically relevant substrates. Motivated by the natural 3D nanostructures on collagens, which have a 400 nm fibrillar width and 70 nm cross-striation, they developed a multiple-NIL process to generate similar 3D nanostructures on tissue-culture polystyrene. Bovine pulmonary artery smooth muscle cells were cultured on the scaffolds and the results show that these imprinted polymer scaffolds with nanotopographical features can effectively direct the cell orientation.

The other approach to generate 3D nanostructures is UV nanoembossing. UV embossing offers many advantages; for example, it is usually performed at room temperature and low pressure. This is critical to the patterning of delicate substrates such as encapsulated protein-in-polymer or water-containing hydrogels for biomedical applications [81]. Yue's group has demonstrated the use of UV embossing to create high aspect ratio submicrometer-scale 3D structures on biocompatible polymers, that is, poly(ethylene glycol) diacrylate hydrogel, with faithful replication, and the feasibility of incorporating proteins into the patterned structures that will have potential in many biological applications such as protein and drug delivery, as well as tissue engineering [81, 82].

2.7 CONCLUSIONS

Advances in the lithographic processes are providing powerful and versatile tools for biomedical engineering research. In a recent review by Khademhosseini et al. [83], the impact of micro/nanoscale engineering enabled by the widespread use and availability of lithographic technologies has been

summarized, especially for tissue engineering and biological applications. An impressive body of research has demonstrated that surface structures even down to the nanometer scale can regulate cell behavior and fate both *in vitro* and *in vivo*. Therefore, the ability of generating biologically relevant structures with dimensions ranging from nanometer to millimeter and providing exquisite control over the composition and properties at the interface is very attractive for biomedical engineering research. Because of its unique capabilities of generating surface chemistry alterations and micro/nanoscale topography simultaneously, ion implantation/lithography are becoming increasingly important in enhancing biomaterial–cell interactions. It can be envisioned that micro/nanoscale technologies will play a critical role in advancing many clinical applications.

REFERENCES

1. Moore G. Cramming more components onto integrated circuits. *Electronics* 1965; 38(8):114–117.
2. Boretos JW and Eden M. *Contemporary Biomaterials, Material and Host Response, Clinical Applications, New Technology and Legal Aspects*. Park Ridge: Noyes Publications; 1984. p 232–233.
3. Massia SP and Hubbell JA. Covalent surface immobilization of Arg-Gly-ASP- and Tyr-Lle-Gly-Ser-Arg-containing peptides to obtain well-defined cell-adhesive substrates. *Anal Biochem* 1990;187(2):292–301.
4. Kam L, Shain W, Turner JN, Bizios R. Selective adhesion of astrocytes to surfaces modified with immobilized peptides. *Biomaterials* 2002;23(2):511–515.
5. Kobayashi H and Ikada Y. Covalent immobilization of proteins onto the surface of poly(vinyl alcohol) hydrogel. *Biomaterials* 1991;12(8):747–751.
6. Chandy T, Das GS, Wilson RF, Rao GHR. Use of plasma glow for surface-engineering biomolecules to enhance blood compatibility of Dacron and PTFE-vascular prosthesis. *Biomaterials* 2000;21(7):699–712.
7. Han DK, Jeong SY, Kim YH. Evaluation of blood compatibility of PEO-grafted and heparin-immobilized polyurethanes. *J Biomed Mater Res* 1989;23(A2 Suppl.): 211–228.
8. Clark P. Cell behavior on micropatterned surfaces. *Biosens Bioelectron* 1994;9 (9–10):657–661.
9. Williams JM. Ion implantation for implantable devices. *Biomed Sci Instrum* 1986; 22:75–76.
10. Jagielski J, et al. Ion implantation for surface modifications of biomaterials. *Surf Coat Technol* 2006; 200(22–23):6355–6361.
11. Cui FZ and Luo ZS. Biomaterials modification by ion-beam processing. *Surf Coat Technol* 1999;112(1–3):278–285.

12. Agrawal CM. Reconstructing the human body using biomaterials. *JOM* 1998;50(1): 31–35.
13. He W, et al. Micro/nanomachining of polymer surface for promoting osteoblast cell adhesion. *Biomed Microdevices* 2003;5(2):101–108.
14. He W, Poker DB, Gonsalves KE, Batina N. Micro/nanomachining of polymeric substrates by ion beam techniques. *Microelectron Eng* 2003;65(1–2): 153–161.
15. Webster TJ, Siegel RW, Bizios R. Nanoceramic surface roughness enhances osteoblast and osteoclast functions for improved orthopedica/dental implant efficacy. *Scra Mater* 2001;44(8–9):1639–1642.
16. Lappalainen R, Anttila A, Heinonen H. Diamond coated total hip replacements. *Clin Orthop Relat Res* 1998;352:118–127.
17. Kostov KG, et al. Structural effect of nitrogen plasma-based ion implantation on ultra-high molecular weight polyethylene. *Surf Coat Technol* 2004;186(1–2): 287–290.
18. Derbyshire B, Fisher J, Dowson D, Hardaker C, Brummit K. Comparative study of the wear of UHMWPE with zirconia ceramics and stainless steel femoral heads in artificial hip joints. *Med Eng Phys* 1994;16(3):229–236.
19. Chen J, et al. Surface modification of ion implanted ultra high molecular weight polyethylene. *Nucl Instrum Methods Phys Res* 2000;169(1–4):26–30.
20. Shi W, Li XY, Dong H. Preliminary investigation into the load bearing capacity of ion beam surface modified UHMWPE. *J Mater Sci* 2004;39(9):3183–3186.
21. Valenza A, Visco AM, Torrisi L, Campo N. Characterization of ultra-high-molecular-weight polyethylene (UHMWPE) modified by ion implantation. *Polymer* 2004;45(5):1707–1715.
22. Lee JS, et al. Selective adhesion and proliferation of cells on ion-implanted polymer domains. *Biomaterials* 1993;14(12):958–960.
23. Sioshansi P. New processes for surface treatment of catheters. *Artif Organs* 1994; 18(4):266–271.
24. Iwaki M, et al. Ion bombardment into inner wall surfaces of tubes and their biomedical applications. *Nucl Instrum Methods Phys Res B* 1995; 106(1–4):618–623.
25. Bambauer R, Mestres P, Schiel R, Klinkmann J, Sioshansi P. Surface-treated catheters with ion beam-based process evaluation in rats. *Artif Organs* 1997;21(9): 1039–1041.
26. Sato H, et al. Enhanced growth of human vascular endothelial cells on negative ion (Ag^-)-implanted hydrophobic surfaces. *J Biomed Mater Res* 1999;44(1): 22–30.
27. Tsuji H, et al. Negative-ion beam surface modification of tissue-culture polystyrene dishes for changing hydrophilic and cell attachment properties. *Nucl Instrum Methods Phys Res B* 1999;148 (1–4):1136–1140.
28. Xu G, et al. Oxygen ion implantation at 20 to 2000 keV into polysulfone for improvement of endothelial cell adhesion. *Colloids Surf B* 2000;19(3): 237–247.

29. Bačáková L, Mareš V, Lisá V, Švorčík V. Molecular mechanisms of improved adhesion and growth of an endothelial cell line cultured on polystyrene implanted with fluorine ions. *Biomaterials* 2000;21(11):1173–1179.
30. Suzuki Y. Ion beam modification of polymers for the application of medical devices. *Nucl Instrum Methods Phys Res B* 2003;206:501–506.
31. Kurotobi K, Kaibara M, Suzuki Y, Iwaki M, Nakajima. Plasma protein adsorption onto cell attachment controlled ion implanted collagen. *Nucl Instrum Methods Phys Res B* 2001;175–177:791–796.
32. Tsuji H, et al. Improvement of polydimethylsiloxane guide tube for nerve regeneration treatment by carbon negative-ion implantation. *Nucl Instrum Methods Phys Res B* 2003;206:507–511.
33. Okuyama Y, et al. Neurite outgrowth on fluorinated polyimide film micropatterned by ion irradiation. *Nucl Instrum Methods Phys Res B* 2003;206:543–547.
34. Takahashi N, et al. Biocompatibility of modified ePTFE for an artificial dura mater. *Nucl Instrum Methods Phys Res B* 2006;242(1–2):61–64.
35. Li D, Cui F, Gu H. F^+ ion implantation induced cell attachment on intraocular lens. *Biomaterials* 1999;20(20):1889–1896.
36. Švorčík V, et al. Adhesion and proliferation of keratinocytes on ion beam modified polyethylene. *J Mater Sci Mater Med* 2000;11(10):655–660.
37. Švorčík V, et al. Fibroblasts adhesion on ion beam modified polyethylene. *Nucl Instrum Methods Phys Res B* 2004;215:366–372.
38. Melnig V, Apetroaei N, Dumitrascu N, Suzuki Y, Tura V. Improvement of polyurethane surface biocompatibility by plasma and ion beam techniques. *J Optoelectron Adv Mater* 2005;7(5):2521–2528.
39. Davenas J, Thévenard P, Philippe F, Arnaud M. Surface implantation treatments to prevent infection complications in short term devices. *Biomol Eng* 2002;19(2–6): 263–268.
40. Boldyryeva H, Umeda N, Plaksin O, Takeda Y, Kishimoto N. High-fluence implantation of negative metal ions into polymers for surface modification and nanoparticle formation. *Surf Coat Technol* 2005;196(1–3):373–377.
41. Zhang W, et al. Plasma surface modification of polyvinyl chloride for improvement of antibacterial properties. *Biomaterials* 2006;27(1):44–51.
42. Wang J, et al. The effect of amorphous carbon films deposited on polyethylene terephthalate on bacterial adhesion. *Biomaterials* 2004;25(16):3163–3170.
43. Chu PK, Chen JY, Wang LP, Huang N. Plasma-surface modification of biomaterials. *Mater Sci Eng R* 2002;36(5–6):143–206.
44. Buchanan RA, Rigney ED Jr, Williams JM. Wear-accelerated corrosion of Ti-6Al-4V and nitrogen-ion-implanted Ti-6Al-4V: mechanisms and influence of fixed-stress magnitude. *J Biomed Mater Res* 1987;21(3):367–377.
45. Oliver WC, Hutchings R, Pethica JB. The wear behavior of nitrogen-implanted metals. *Metall Trans* 1984;15A(12):2221–2229.
46. Sioshansi P, Oliver RW, Matthews FD. Wear improvement of surgical titanium alloys by ion implantation. *J Vac Sci Technol* 1985;3(6):2670–2674.

47. Tan L, Dodd RA, Crone WC. Corrosion and wear-corrosion behavior of NiTi modified by plasma source ion implantation. *Biomaterials* 2003;24(22):3931–3939.
48. Krupa D, et al. Effect of calcium-ion implantation on the corrosion resistance and biocompatibility of titanium. *Biomaterials* 2001;22(15):2139–2151.
49. Krupa D, et al. Effect of phosphorous-ion implantation on the corrosion resistance and biocompatibility of titanium. *Biomaterials* 2002;23(16):3329–3340.
50. Hanawa T, et al. Early bone formation around calcium-ion-implanted titanium inserted into rat tibia. *J Biomed Mater Res* 1997;36(1):131–136.
51. Pham MT, et al. Surface induced reactivity for titanium by ion implantation. *J Mater Sci Mater Med* 2000;11(6):383–391.
52. Nayab SN, et al. Adhesion of bone cells to ion-implanted titanium. *J Mater Sci Mater Med* 2003;14(11):991–997.
53. Nayab SN, Jones FH, Olsen I. Human alveolar bone cell adhesion and growth on ion-implanted titanium. *J Biomed Mater Res* 2004;69(4):651–657.
54. Nayab SN, Jones FH, Olsen I. Effects of calcium ion implantation on human bone cell interaction with titanium. *Biomaterials* 2005;26(23):4717–4727.
55. Krupa D, et al. Effect of dual ion implantation of calcium and phosphorous on the properties of titanium. *Biomaterials* 2005;26(16):2847–2856.
56. Tsyganov I, Wieser E, Matz W, Reuther H, Richter E. Modification of the Ti-6Al-4V alloy by ion implantation of calcium and/or phosphorous. *Surf Coat Technol* 2002;158–159:318–323.
57. Baumann H, Bethge K, Bilger G, Jones D, Symietz I. Thin hydroxyapatite surface layers on titanium produced by ion implantation. *Nucl Instrum Methods Phys Res B* 2002;196(3–4):286–292.
58. Pham MT, et al. Solution deposition of hydroxyapatite on titanium pretreated with a sodium ion implantation. *J Biomed Mater Res* 2002;59(4):716–724.
59. Maitz MF, et al. Ion beam treatment of titanium surfaces for enhancing deposition of hydroxyapatite from solution. *Biomol Eng* 2002;19(2–6):269–272.
60. Maitz MF, Poon RWY, Liu XY, Pham MT, Chu PK. Bioactivity of titanium following sodium plasma immersion ion implantation and deposition. *Biomaterials* 2005;26(27):5465–5473.
61. Yang YZ, Tian JM, Tian JT, Chen ZQ. Surface modification of titanium through amino group implantation. *J Biomed Mater Res* 2001;55(3):442–444.
62. Yang YZ, Tian JM, Deng L, Ong JL. Morphological behavior of osteoblast-like cells on surface-modified titanium in vitro. *Biomaterials* 2002;23(5):1383–1389.
63. De Maezta MA, Alava JI, Gay-Escoda C. Ion implantation: surface treatment for improving the bone integration of titanium and Ti6Al4V dental implants. *Clin Oral Implants Res* 2003;14(1):57–62.
64. Lee DH, Park B, Saxena A, Serene TP. Enhanced surface hardness by boron implantation in Nitinol alloy. *J Endod* 1996;22(10):543–546.

65. Rapisarda E, Bonaccorso A, Tripi TR, Condorelli GG, Torrisi L. Wear of nickel–titanium endodontic instruments evaluated by scanning electron microscopy: effect of ion implantation. *J Endod* 2001;27(9):588–592.
66. Ryan R, Walker G, Freeman K, Cisneros GJ. The effects of ion implantation on rate of tooth movement: an *in vitro* model. *Am J Orthod Dentofac Orthop* 1997; 112(1):64–68.
67. Jung JH, et al. Does a carbon ion implanted surface reduce the restenosis rate of coronary stents? *Cardiology* 2005;104(2):72–75.
68. Yang P, et al. Blood compatibility improvement of titanium oxide film modified by phosphorous ion implantation. *Nucl Instrum Methods Phys Res B* 2006;242(1–2): 15–17.
69. Murayama Y, et al. Ion implantation and protein coating of detachable coils for endovascular treatment of cerebral aneurysms: concepts and preliminary results in swine models. *Neurosurgery* 1997;40(6):1233–1243.
70. Yoshinari M, Oda Y, Kato T, Okuda K. Influence of surface modifications to titanium on antibacterials activity *in vitro*. *Biomaterials* 2001;22(14): 2043–2048.
71. Dan ZG, Ni HW, Xu BF, Xiong J, Xiong PY. Microstructure and antibacterial properties of AISI 420 stainless steel implanted by copper ions. *Thin Solid Films* 2005;492(1–2):93–100.
72. Douvas A, et al. Photolithographic patterning of proteins with photoresists processable under biocompatible conditions. *J Vac Sci Technol B* 2001;19(6): 2820–2824.
73. Douvas A, et al. Biocompatible photolithographic process for the patterning of biomolecules. *Biosens Bioelectron* 2002;17(4):269–278.
74. Diakoumakos CD, et al. Dilute aqueous base developable resists for environmentally friendly and biocompatible processes. *Microelectron Eng* 2002;61–62: 819–827.
75. He W, Gonsalves KE, Pickett JH, Halberstadt CR. Synthesis, characterization, and preliminary biological study of poly(3-(*t*-butoxycarbonyl)-*N*-vinyl-2-pyrrolidone). *Biomacromolecules* 2003;4(1):75–79.
76. He W, Halberstadt CR, Gonsalves KE. Lithography application of a novel photoresist for patterning of cells. *Biomaterials* 2004;25(11):2055–2063.
77. Abrams GA, Goodman SL, Nealey PF, Franco M, Murphy CJ. Nanoscale topography of the basement membrane underlying the corneal epithelium of the rhesus macaque. *Cell Tissue Res* 2000;299(1):39–46.
78. Hu W, Yim EKF, Reano RM, Leong KW, Rang SW. Effects of nanoimprinted patterns in tissue-culture polystyrene on cell behavior. *J Vac Sci Technol B* 2005;23(6):2984–2989.
79. Chou SY. Nanoimprint lithography and lithographically induced self-assembly. *MRS Bull* 2001;26(7):512–517.
80. Bao LR, et al. Nanoimprinting over topography and multiplayer three-dimensional printing. *J Vac Sci Technol B* 2002;20(6):2881–2886.
81. Chan-Park MB, et al. Fabrication of high aspect ratio poly(ethylene glycol)-containing microstructures by UV embossing. *Langmuir* 2003;19:4371–4380.

82. Gao JX, et al. UV embossing of sub-micrometer patterns on biocompatible polymeric films using a focused ion beam fabricated TiN mold. *Chem Mater* 2004; 16:956–958.
83. Khademhosseini A, Langer R, Borenstein J, Vacanti JP. Microscale technologies for tissue engineering and biology. *Proc Natl Acad Sci USA* 2006;103(8): 2480–2487.

Novel Nanostructures as Molecular Nanomotors

YAN CHEN, JIANWEI JEFF LI, ZEHUI CHARLES CAO, and WEIHONG TAN

3.1 INTRODUCTION

Nanotechnology is the design, characterization, production, and application of structures, devices, and systems by controlling shape and size at the nanometer scale. It produces and exploits moieties whose valuable properties are attributable to their precise nanoscale architectures, and promises to be among the most important emerging scientific areas of the twenty-first century as Richard Feynman predicted early in 1959. Recently, nanotechnology has addressed many important problems from basic sciences to biomedicine to space technology. Today, a variety of nanoscale-structured materials and devices can be manufactured. For example, the burgeoning interest in the medical applications of nanotechnology has led to the emergence of a new field called nanomedicine, which greatly improves or even revolutionizes medical diagnosis, treatment, and prevention of diseases by using molecular tools and molecular knowledge of the human body [1]. Most of these studies include the interaction of nanostructured materials with biological systems.

The ability to systematically modify the properties of biological nanostructures by controlling their structure and their chemical properties at a nanoscale level makes them extremely attractive candidates for use in contexts from fundamental scientific studies to commercially viable technologies. Also, various nanostructures have been investigated to determine their properties and possible applications in biosensors. These structures include nanotubes, nanofibers, nanorods, nanoparticles, and thin films. The use of nanomaterials in biosensors allows the application of many new signal transduction technologies for rapid

analysis of multiple substances *in vivo*. Besides biosensors, nanotechnology also aims to exploit biomolecules and the processes carried out by them for the development of novel functional materials and devices and more speculatively, nanomachines and perhaps nanorobots. In the long term, the earliest molecular machine systems and nanodevices may be effective in scientific and medical applications, giving scientists and physicians the most potent tools imaginable to conquer scientific problems, human disease, ill health, and aging.

Hence, one of the questions arising from nanotechnology development is: “How to provide energy for nanodevices?” Similar to conventional equipments and devices, nanodevices also need energy to function properly and consistently. This leads to the idea of constructing nanomotors from biological molecules. So far, several types of nanomotors have been developed based on protein, DNA, and RNA molecules, and their efficiency to convert biological or chemical energy into mechanical energy has been demonstrated and characterized.

Ideal for engineering purposes, proteins represent fertile territory for nanotechnology. They possess sophisticated architectures at nanoscale dimensions, rich chemistry, and versatile enzymatic activities. They are also capable of carrying out complex tasks in cells. Nanodevices could use motor proteins to move linearly, by rotation, or in a more complex three-dimensional manner. Nanodevices might also respond to the environment through proteins with built-in switches that operate in a simple on–off way or through more finely tuned and complex logic gates with graded or multiple inputs. In this way, nanodevices will be able to sense their environment.

More advanced functions might include transport (uptake, movement, and delivery of cargoes utilizing protein transporters and pores) and chemical transformation, by enzymatic catalysis, for example. Most molecular motor proteins perform actual physical work by actively transporting or moving other molecules or proteins within cellular systems. Examples of these type of proteins are the kinesin motor proteins that “walk” on “tubulin-rails” transporting vesicles along given pathways in the cell. Similarly, certain members of the myosin family transport cargo using actin filaments as a track to run on. In addition to intracellular transport directed by microtubule tracks, proteins like dynein together with tubulin are also involved in the movement of whole, free cells like sperm cells and protozoa [2].

Besides proteins, nanomotors can be constructed with various biomotifs. In this chapter, we mainly focus on DNA nanomotors. Despite its central importance in biology, the applications of DNA are not restricted to biological sciences. DNA functions successfully as genetic material because of its chemical properties. Its capabilities to form duplex via Watson–Crick base pairing, as well as its diversity in adopting different conformations due to external stimuli, which can be mediated by small molecules or ions [3], promise its potential in the development of nanomotors.

3.2 MULTI-DNA NANOMOTORS

Conformational changes induced by intermolecular hybridization of complementary DNA molecules can be translated into a nanomechanical response to construct various types of nanomotors. The first DNA hybridization-based nanomotor was the DNA tweezer built by Yurke and his colleagues [4]. Based on the concept of chemical fuel by strand-exchange reactions, the DNA tweezer involves the intermolecular hybridization of three oligonucleotides as shown in Fig. 3.1. Strand A, doubly labeled with a 3'-TAMRA (carboxy-tetramethylrhodamine) and a 5'-TET (tetrachlorofluorescein) fluorogenic group, consists of two 18-base sequences that hybridize with complementary sequences at the ends of strands B and C to form two stiff arms; the hinge is formed from a four-base single-stranded region of A between the regions hybridized to strands B and C. In this conformation, termed as "rest state," the remaining two unhybridized 24-base portions of 42-mer strands B and C dangle floppily from the end of the tweezer. In this rest state, the two fluorophores are spatially separated and no intermolecular resonant energy transfer from TET to TAMRA, and therefore, no quenching of TET fluorescence occur. The assembled tweezers are opened and closed with fuel strands F and \bar{F} . The closing strand F consists of three regions, two of which are 24-mer base sections complementary to the dangle end of the tweezer on strands B and C. The other region of F locates at one end with an additional eight-base overhang section. The hybridization of F and the tweezer in the dangle end areas brings the two ends of the tweezer together. In this closed form, the fluorescence signal of TET is quenched by intramolecular resonant energy transfer from TET to TAMRA. When adding the opening strand \bar{F} , which is fully complementary to strand F, the strand-exchange reaction occurs and F is displaced from the tweezer by branch migration and forms a more stable

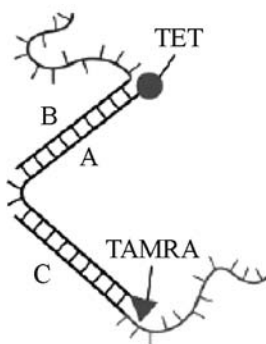


FIGURE 3.1 Construction of the molecular tweezers. Molecular tweezer structure formed by hybridization of oligonucleotide strands A, B, and C.

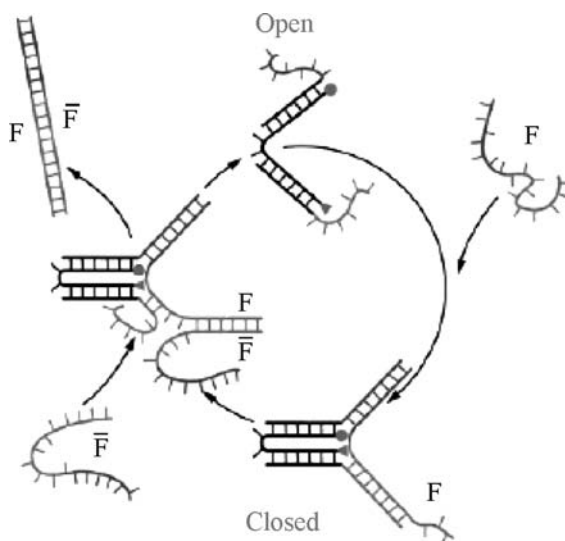


FIGURE 3.2 Operation of the molecular tweezers. Closing strand F hybridizes with the dangling ends of strands B and C (shown in blue and green) to pull the tweezers closed. Hybridization with the overhang section of F (red) allows F strand to remove F from the tweezers, forming a double-stranded waste product FF and allowing the tweezers to open. Complementary sections of B , C , F , and \bar{F} that hybridize to close and open the tweezers are colored.

duplex with \bar{F} . Released from the hybridization with F , the tweezer returns to its “rest state” and gives the fluorescence signal again. The above process completes one cycle of opening and closing of the nanomotor with a waste product as FF duplex, and this cycling of the motor is fully reversible. The operation of the molecular tweezers is shown in Fig. 3.2. The switching time is about 13 s. For each cycle, the fluorescence signal drops by a factor of 6 when the tweezer is closed by F and climbs back to the original level when opened by \bar{F} . The closing force for the tweezer is about 15 pN, which is at the upper end of the range of measured forces exerted by single-group kinesin and myosin motors.

One problem of this DNA tweezer design is the lack of robustness due to the formation of dimer or other oligomers between cycles [5]. The first robust nanomotor device based on multiple DNA hybridization topology was the PX–JX2 nanomotor developed by Yan et al. [6] (Fig. 3.3). They improved the robustness via the Yurke mechanism [4] by introducing two topological motifs—paranemic crossover (PX) DNA and its topoisomer (JX2) DNA, the latter of which can be converted to the other by removal of the internal strands and rotating by 180° , as shown in Fig. 3.4. The PX motif consists of two helical domains formed by four strands that flank a central dyad axis,

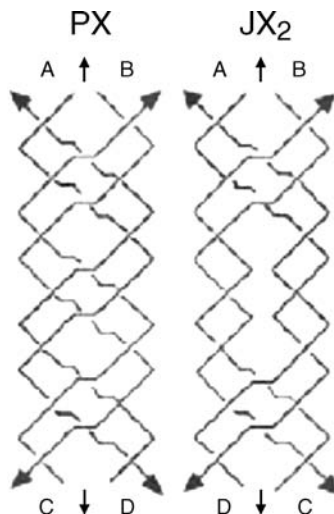


FIGURE 3.3 Schematic drawings of the device. The PX and JX₂ motifs. The PX motif, postulated to be involved in genetic recombination, consists of two helical domains formed by four strands that contain a central dyad axis (indicated by the vertical black arrows). Two strands are drawn in red and two in blue, where the arrowheads indicate the 3' ends of the strands. The Watson–Crick base pairing in which every nucleotide participates is indicated by the thin horizontal lines within the two double helical domains. Every possible crossover occurs between the two helical domains. The same conventions apply to the JX₂ domain, which lacks two crossovers in the middle. The letters A, B, C, and D, along with the color coding, show that the bottom of the JX₂ motif (C and D) are rotated 180° relative to the PX motif.

while its topoisomer, JX₂, contains two adjacent sites where backbones juxtapose without crossing over. Both of them are constructed by internal “set” strands, which have single-stranded extension to allow branch migration. The green set strand can set the motor in its PX conformation, while the pale-purple one can fix it in JX₂ form. In the presence of biotinylated fueling strands and with the aid of streptavidin-coated magnetic beads, the green set strands can be eliminated from the PX, producing an unstructured intermediate. The addition of pale-purple set strands converts the intermediate to JX₂ conformation. Reversed conformational change can also be achieved via the same mechanism.

The robustness and effectiveness of this nanomotor are demonstrated by gel electrophoresis, but the most convincing evidence for its operation is derived from atomic force microscopy (AFM) data [7]. DNA trapezoids are connected to the nanomotor to form three edge-sharing DNA triangles. The conformational change between PX and JX₂ brings the trapezoids to parallel form or opposite orientation, which can be observed by an atomic force microscope. The AFM images, shown in Fig. 3.5, demonstrate the effective conversation of the nanomotor.

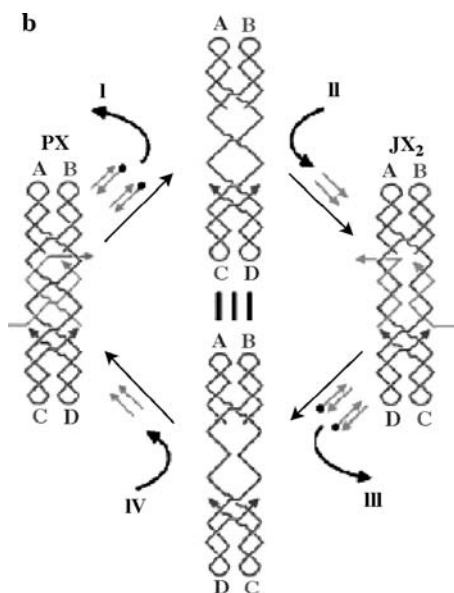


FIGURE 3.4 Principles of device operation. On the left is a PX molecule. The green set strands are removed by the addition of biotinylated green “fuel” strands (biotin indicated by black circles) in process I. The unstructured intermediate is converted to the JX2 motif by the addition of the pale-purple set strands in process II. The JX2 molecule is converted to the unstructured intermediate by the addition of biotinylated pale-purple “fuel” strands in process III. The identity of this intermediate and the one above it is indicated by the identity symbol between them. The cycle is completed by the addition of green set strands in process IV, restoring the PX device.

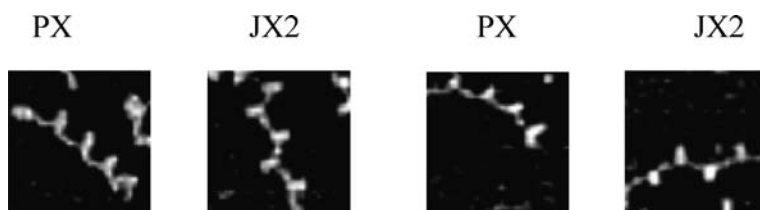


FIGURE 3.5 Cycling of the device. This panel shows three steps of the operation of the device, sampling aliquots from each cycle. The system originates in the PX state and is then converted (left to right) to the JX2 state, back to PX, and then back to JX2. The PX linear arrays are clearly in the *cis* arrangement, and the JX2 linear arrays are clearly in the *trans* arrangement. All images show an area 200 nm \times 200 nm.

3.3 SINGLE DNA NANOMOTORS

While people have employed DNA hybridization to construct DNA nanomotors with multiple DNA molecules, a single DNA molecule can also accomplish this. The development of a “molecular beacon” is one of the examples, which makes the fabrication of DNA nanomotor simple and convenient. Molecular beacon is a single-stranded DNA (ssDNA) that can form an intramolecular hairpin structure due to a specially designed nucleotide sequence. The two ends of the beacon are labeled with a fluorophore F and a quencher Q, respectively. Prior to hybridization with target nucleic acids, the beacon takes on a stem–loop structure and keeps the F and Q in close proximity, which results in minimal fluorescence signal due to static quenching of the fluorophore by the quencher. After introducing the target, the loop sequence of the molecular beacon hybridizes to the target and opens up the stem duplex. Consequently, the two moieties are spatially separated, leading to the restoration of the fluorescence.

Tan et al. [8] made use of this kind of special DNA structure and constructed an artificial molecular motor made of a single-strand DNA molecular beacon.

Based on the same principle of natural protein motors to switch between two different conformations, they have constructed a single-strand DNA motor that can change between its shrunken and extended forms. The DNA molecule is a 17-mer DNA oligonucleotide with a sequence of 5'-TGGTTGGTGTGGTTGGT-3'. This ssDNA adopts a highly compact and symmetrical tetraplex (TE) structure that consists of two tetrads of guanine base pairs and three loops, as shown in Fig. 3.6. The shrunken state of the

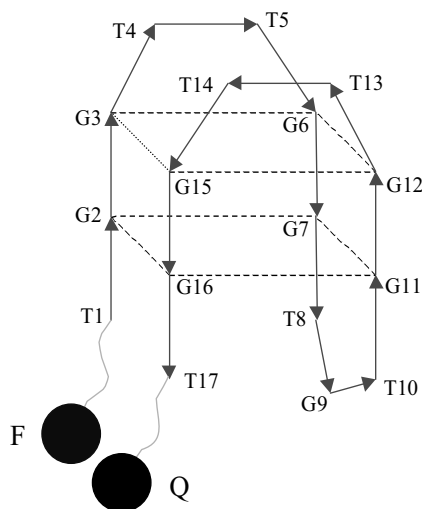


FIGURE 3.6 The structural conformation of the DNA motor. The red ball and the black ball represent the fluorophore and the quencher, respectively. The rectangular plains represent two layers of G-quartet structures.

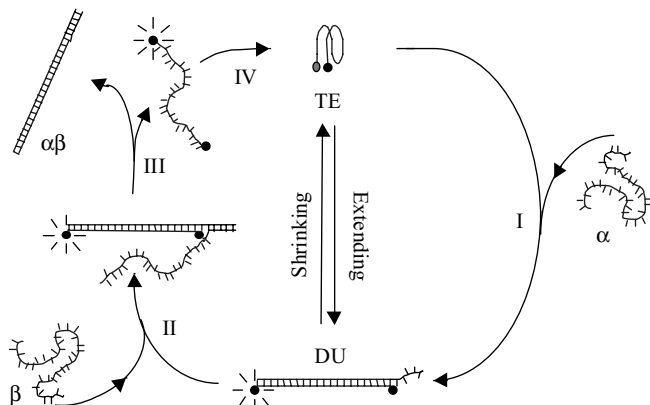


FIGURE 3.7 The working principle of the DNA motor. (I) In the presence of α strand, the 17-mer forms a duplex with α , which straightens the tetraplex and separates F and Q, changing the TE conformation into the DU form. (II) The addition of β strand initiates the strand-exchange reaction by DNA sticky end pairing and forms a longer duplex with the α strand. (III) The strand-exchange reaction releases the 17-mer from the DU structure. (IV) The 17-mer shrinks and forms back the tetraplex structure again.

molecule brings the two ends close to each other. Therefore, the fluorophore F and quencher Q come to spatial proximity and consequently the nanomotor is in its dark state. The working principle of this nanomotor is shown in Fig. 3.7. In the presence of a complementary oligonucleotide, strand α , the 17-mer nanomotor and α will form a DNA duplex (DU) that straightens the tetraplex and separates the two ends of the motor. This extended form of the DNA molecule motor will give approximately fourfold of enhanced fluorescence, which reflects the conformational change of the DNA. This motor is also named “DUTE motor” since it is switched between a duplex form (DU) and a tetraplex form (TE). Similar to some natural motors, the DUTE motor returns to its original shrunken state via a DNA strand-exchanging reaction [9] using a new single strand β that is fully complementary to the α strand. The strand-exchanging reaction is initiated by DNA sticky end pairing [10] and proceeds through a branch migration [11] to form duplex $\alpha\beta$. Consequently, the 17-mer oligonucleotide comes back to its original tetraplex shrunken form and completes one extending–shrinking cycle. Further addition of α will initiate a new cycle of the molecular motor, which reveals that the process is fully reversible. Figure 3.8 records 10 cycles, which clearly shows that the shrinking–extending cycle can be easily and accurately controlled. The net product in each cycle, a duplex DNA molecule $\alpha\beta$, releases energy during hybridization and is the driving force to produce mechanic movements of cargoes when the motor is loaded.

By calculating the Gibbs free energy change for each cycle, the energy conversion efficiency can be estimated as 0.63, and can be further improved by

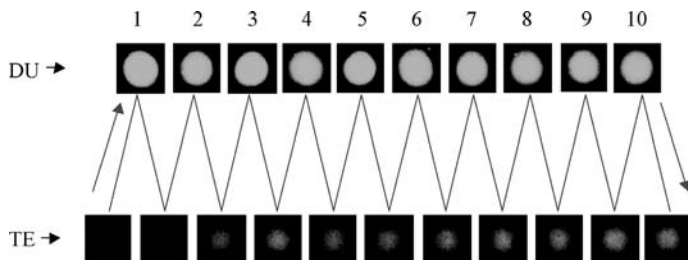


FIGURE 3.8 Cycling of the DNA motor. During the motor's cycling, the motor molecules are imaged by a digital camera. Ten cycles were recorded here.

reducing the length of the β strand. With the help of multivalent ions such as polyamines, the strand exchange still takes place when the sticky end is as short as one-base-long. In this case, the ideal energy conversion efficiency can reach 0.94.

Furthermore, the reversible cycling between the shrinking and extending forms of the DUTE motor makes it possible to use this design to manipulate the distance between two nanoelements in a nanosystem. While the shrinking force of the DUTE motor is calculated to be 2.2 pN, the extending force is 20.7 pN, about 10-fold greater than those determined for kinesin and myosin protein nanomotors. The extending force can be further increased by decreasing the temperature and by changing metal ion type and concentration.

With a molecular weight of only 7.8 kDa, this single DNA nanomotor is the smallest among DNA/protein molecular motors. In addition, this single DNA molecule is easily produced and can be operated in a more predictable fashion. It is thus believed to have great potential in functioning effectively as a nanomotor and in powering nanoscale devices with efficient force generation.

Although chemical-fueled nanomotors have the advantages of easy synthesis and regulation, the accumulation of DNA "waste" can change the composition of the solution, leading to reduced efficiency. The necessity to add DNA "fuel" in each cycle causes inconvenience and makes remote control impossible. In comparison, approaches using external energy sources such as optical energy may solve the problems associated with chemical-fueled nanomotors. Therefore, light-driven nanomotors will have great potential to improve practicability and efficiency of nanodevices.

Initial success has been demonstrated using light to control DNA hybridization by Asanuma et al. at the University of Tokyo [12]. They incorporated photoswitchable azobenzene moieties into DNA strands to reversibly photo-regulate the formation and dissociation of the corresponding duplex. The azobenzene moieties in the DNA strands adopt *trans* form before UV radiation. Since the *trans*-azobenzene is nonpolar and planar, it favorably stacks with the adjacent DNA bases, stabilizing the duplex. Upon UV radiation ($300 < \lambda < 400$ nm), azobenzenes promptly isomerize to the polar and nonplanar *cis* form, making the hybridization unstable, which then causes the duplex to open up. Such isomerization is reversible, since the *cis*-azobenzene moiety is

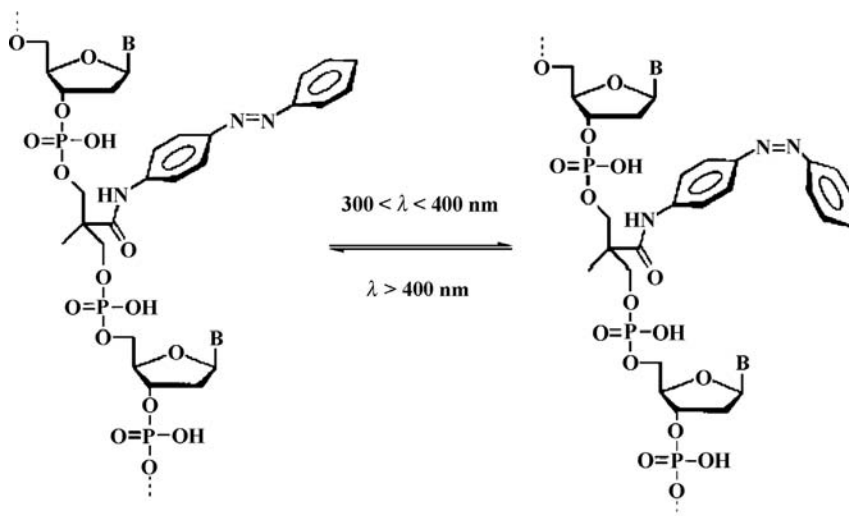


FIGURE 3.9 Incorporation of azobenzene into DNA strand. On UV radiation ($300 < \lambda < 400\text{ nm}$), the *trans*-azobenzene is converted into *cis* form. When irritated by visible light ($\lambda > 400\text{ nm}$), the *cis* isomer is changed back to *trans* form.

switched back to the *trans* form by radiation of visible light ($\lambda > 420\text{ nm}$) (Fig. 3.9). With the azobenzene being in a different conformation, the DNA strands can have different melting temperature (T_m). A D-threosinol-tethered azobenzene moiety is chosen as the linker since it induces relatively large melting temperature change (ΔT_m , $\sim 14.3^\circ\text{C}$) upon photoisomerization. An even higher ΔT_m is possible by introducing two or more D-threosinol-tethered azobenzene groups to the DNA strands. An additional advantage is that the D-threosinol linked azobenzene shown in Fig. 3.10 can be directly coupled to a DNA strand on a DNA synthesizer.

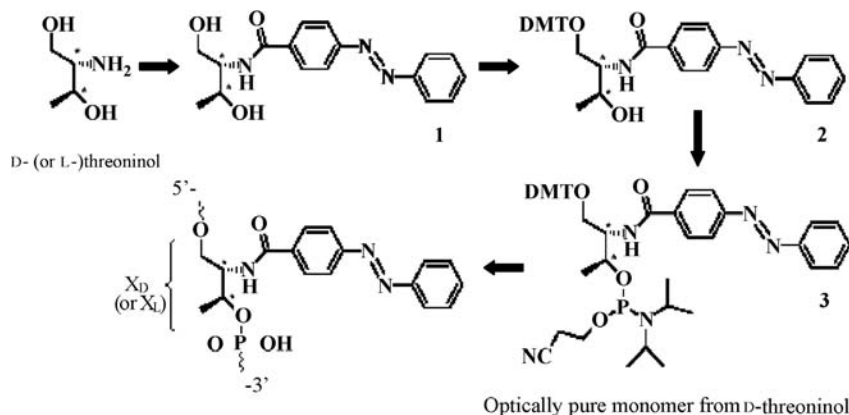


FIGURE 3.10 Modified ODN carrying an azobenzene moiety attached by a chiral diol linker. DMT = 4,4-dimethoxytrityl.

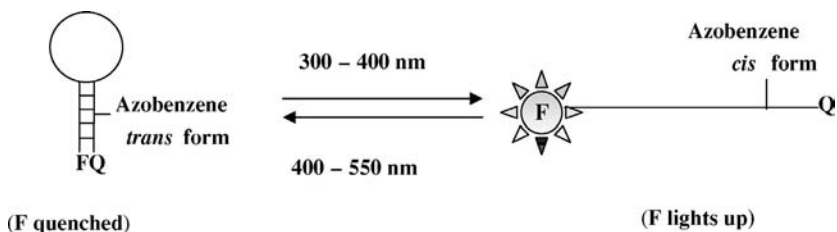


FIGURE 3.11 The working principle of the light-driven molecular beacon.

Based on this work, Tan et al. have made further steps by incorporating the photoswitchable azobenzene moiety into a hairpin structure of a molecular beacon and using fluorescence change to monitor the process in real time. Taking advantage of the large difference in T_m between perfect match stem and one-base-mismatch stem, a sequence GAGXGACTGGTATCCTAAATCTCGCTC with an azobenzene base (X) in the stem was designed. Texas Red was selected as the fluorophore for the molecular beacon for its longer excitation wavelength (>550 nm). The Black Hole Quencher (BHQ) is used as the quencher on the other end of the beacon. Implanted into the stem, the *trans*-azobenzene stabilizes the hairpin structure with irradiation of visible light and keeps the MB motor nonfluorescent. Upon radiation of UV light, the *cis*-azobenzene destabilizes the stem and causes restoration of the fluorescence (Fig. 3.11). The initial T_m results show that the MB nanomotor has a 20° difference between the *trans* and *cis* forms of the azobenzene. This should ensure sufficient difference between the stability of these two forms, which results in complete transition between open and closed forms of the MB upon UV or visible radiations. Atomic force microscopy will be used to characterize the open–close force and energy conversion efficiency of this nanomotor. It is expected that when linked to two nanoelements at the two ends of the nanomotor, this motor will provide effective and well-controlled manipulations at the nanometer level for desired applications.

Single DNA nanomotors can convert biochemical or optical energy to mechanical energy to provide energy sources on the molecular level, which features comparable or greater forces than protein nanomotors. Moreover, they also have potentials in manipulating molecules or nanoelements via controlled intracellular movements.

3.4 CONCLUSIONS

Here we describe a new architectural system on the nanoscale that is derived from the central biological molecule, DNA. Instead of discussing its biological functions, we mainly focus on its chemical properties for the development of nanoscale energy devices. These DNA molecule based nanomotors have been shown to have great robustness and potential as the power source for

nanomachines. Incorporated into fixed positions in periodic arrays, these nanomotors can also be used to manipulate elements on the nanoscale with interaction forces comparable or even greater than protein motors. Although here we stress on Watson–Crick base-paired motifs, nanomotors based on other interactions, such as DNA structural transition, may also lead to new generation of structural nucleic acid based nanodevices [13]. This field is still in its early stage, and increasing number of new concepts as well as applications of some proven designs are expected to emerge in the near future.

REFERENCES

1. Freitas RA, Jr. Current status of nanomedicine and medical nanorobotics. *J Comput Theor Nanosci* 2005;2(1):1–25.
2. Vogel PD. Nature's design of nanomotors. *Eur J Pharm Biopharm* 2005;60: 267–277.
3. Astier Y, Bayley H, Howorka S. Protein components for nanodevices. *Curr Opin Chem Biol* 2005;9:576–584.
4. Yurke B, Turberfield AJ, Mills AP Jr., Simmel FC, Neumann JL. A DNA-fuelled molecular machine made of DNA. *Nature* 2000;406:605–608.
5. Simmel FC and Yurke B. Using DNA to construct and power a nanoactuator. *Phys Rev E* 2001;#041913.
6. Yan H, Zhang XP, Shen ZY, Seeman NC. A robust DNA mechanical device controlled by hybridization topology. *Nature* 2002;415:62–65.
7. Seeman NC. From genes to machines: DNA nanomechanical devices. *Trends in Biochem Sci* 2005;30:119–125.
8. Li JJ and Tan W. A single DNA molecule nanomotor. *Nano Lett* 2002;2(4): 315–318.
9. Kmiec EB and Holloman WK. DNA strand exchange in the absence of homologous pairing. *J Biol Chem* 1994;269:10163–10168.
10. Li JJ and Tan W. Real time observation of DNA sticky end pairing by using fluorescence energy transfer. Forthcoming.
11. Thompson BJ, Camien MN, Warner RC. Kinetics of branch migration in double-stranded DNA. *Proc Natl Acad Sci USA* 1976;73:2299–2303.
12. Asanuma H, et al. Enantioselective Incorporation of Azobenzenes into Oligodeoxyribonucleotide for Effective Photoregulation of Duplex Formation, *Angew Chem Int Ed* 2001;40(14):2671–2673.
13. Seeman NC. At the crossroads of chemistry, biology, and materials: structural DNA nanotechnology. *Chem Biol* 2003;10:1151–1159.

Bioconjugation of Soft Nanomaterials

NEETU SINGH, WILLIAM H. BLACKBURN, and ANDREW LYON

4.1 INTRODUCTION

The last decade of research in the physical sciences has seen a dramatic increase in the study of nanoscale materials, and in their application to problems in biotechnology. The intriguing optical, electrical, magnetic, and mechanical properties of many nanostructures can be exploited for sensing, imaging, and therapeutics. However, much of the work has focused on “hard” materials such as carbon nanostructures, magnetic materials, metals, and semiconductors, since these are the materials that display the most profound and advantageous nanoscale phenomena. Despite the continued interest in these established areas of nanoscience, new classes of soft nanomaterials are being developed from more traditional polymeric constructs. Specifically, nanostructured hydrogels and their conjugates with biomolecular entities are emerging as a promising group of materials for multiple biotech applications. This chapter will present some of the recent advances in the marriage between bioconjugated, nanoscale, water-swallowable networks and the biosciences.

The relevance of “nano” to a soft material can be very different from that of an optically, magnetically, or electrically active material, since most hydrogels are mainly interesting from a structural or physicochemical standpoint. Therefore, the goal of this chapter is simply to explore current research in polymeric hydrogel particles, where the nanoscale dimensions of the hydrogel have particular relevance to the length scales of the biological system under study. The focus on polymer particles is important, as these discrete structures bridge the gap between more traditional areas of nanoscience and the world of soft matter. The focus on hydrogels arises from the growing need to understand how hydrophilic polymers can affect emerging areas of biotechnology.

4.1.1 Definition of Hydrogels

As a classification of materials, gels escape a rigid definition as they combine the properties of solids and fluids. They have structural integrity and do not flow when removed from their container. However, for molecules that are significantly smaller than the gel pore size, the transport of material through a gel is similar to mass transport in a fluid. Hydrogels, as the name implies, are gels that swell in aqueous media. They are composed of a hydrophilic polymer component that is cross-linked into a network by either covalent or noncovalent interactions [1–3]. Cross-linking provides dimensional stability, while the high solvent content gives rise to the fluid-like transport properties. The particular physical properties associated with these materials make hydrogels ideal candidates for a number of applications. However, to make an impact in areas such as *in vivo* diagnostics, drug/gene delivery, chemical separations, or chemical and biological sensors, many groups have pushed toward the synthesis of more complex polymer architectures that often contain one or more biomolecular components. Such materials may be designed for biocompatibility, biodegradation, encapsulation, biorecognition, or environmentally switchable payload release. In this chapter, we will focus on a wide variety of approaches toward bioconjugated, hydrogel nanomaterials.

4.1.2 Classification of Hydrogels

Hydrogels can be classified in many ways but in this chapter we will deal mostly with the classification based on type of cross-links. Based on the type of cross-links there are two classes of hydrogels: physically and chemically cross-linked networks [4]. A detailed discussion of the synthesis and physiochemical properties, of these networks is beyond the scope of this chapter. For more detailed information on the physical and chemical behaviors of noncrystalline polymer networks, the reader is referred to the excellent review by Dušek and Prins [5].

The most typical form of a hydrogel is in a macroscopic form [6–8]. These “bulk” gels can be anywhere from millimeters in dimension or larger. The subject of this chapter is largely related to smaller entities, which are typically called microgels [9, 10]. Microgels are colloiddally stable hydrogels whose size can vary from tens of nanometers to micrometers. Perhaps the earliest report of microgel synthesis was by Staudinger in 1935 [11], but interest in such materials for biotechnology applications has only flourished recently. For recent reviews on the subject of colloidal hydrogels, the reader is referred to excellent compilations of Pelton [12], and Saunders and Vincent [13].

4.1.3 Stimuli-Sensitive Polymers

A large body of research has recently been devoted to the study of gels that respond to their environment; such materials offer the possibility to design

tunable or triggered devices. These stimuli-responsive gels are often called “smart” materials, as a result of their responsivity [14, 15]. However, such a moniker is unwarranted, as the gel behavior can be simply described as a polymer phase transition or phase separation. There is no more “intelligence” in these materials than that of a melting ice cube. Nonetheless, there is a broad range of stimuli available, as hydrogels can be made responsive to temperature [7], pH [10,16], ionic strength [17–19], light [20–24], electric field [25], and biomolecules [26–30]. The responsive behavior of the hydrogels is inherited from the type of the polymer used in making the gel and/or any modifications made postpolymerization.

The use of stimuli-sensitive polymers in fabricating hydrogels has led to many interesting applications, including those using bioconjugated materials; in this section we will discuss some fundamentals of stimuli-responsive materials to lay the groundwork for later discussions. One of the most widely studied stimuli-sensitive polymers is poly(*N*-isopropylacrylamide) (pNIPAm) formed from the monomer *N*-isopropylacrylamide. Since most of our group’s work is based on pNIPAm, and also to facilitate the understanding of some of the later parts of this chapter, it is appropriate to provide a brief background on this polymer. For an in-depth understanding, the reader is referred to a comprehensive review by Schild [31]. One of the earliest studies on the solution properties of pNIPAm was carried out by Heskins and Guillet [32], where they observed that the phase transition of pNIPAm is endothermic and entropy driven. Due to this striking thermal behavior in aqueous media, pNIPAm has been widely used to make responsive hydrogels. As with most olefin-based monomers, pNIPAm has been synthesized by a variety of techniques: redox initiation, free radical initiation, ionic initiation, and also using radiation [31]. Various functional groups have also been added to the polymer via copolymerization and postpolymerization modification, thereby making multiresponsive and multifunctional polymers.

The behavior of any polymer in a solvent is related to the balance between solvent–solvent, solvent–polymer, and polymer–polymer interactions. For stimuli-sensitive polymers, the polymer solvation can be “switched” by enforcing one of these interactions or by weakening another. Figure 4.1 illustrates this concept schematically. For the case of pNIPAm in water, the polymer hydrogen bonds to water via the amide side chains. However, the isopropyl group on the side chain induces hydrophobic structuring of the

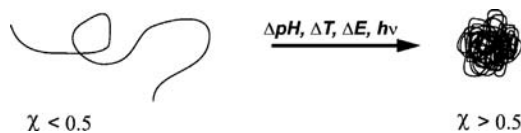


FIGURE 4.1 Schematic of a stimuli-sensitive polymer undergoing phase transition due to a change in the solvent quality. Factors such as pH, temperature, electric field, and light can cause these phase transitions depending on the polymer composition.

water. This structured water leads to entropically driven polymer–polymer interactions via the hydrophobic effect [31]. Under the conditions where pNIPAm has a random coil structure, the solvent–polymer interactions are stronger than the polymer–polymer interactions. At higher temperatures, the hydrogen bonds with the water molecules break and there is an entropically favored release of bound and structured water, leading to the formation of a globular polymer conformation. In this case, the polymer–polymer hydrophobic interactions become stronger than the polymer–solvent interactions, and the polymer phase separates. The temperature at which this phase separation occurs is called the lower critical solution temperature (LCST). It is this behavior that makes pNIPAm a very attractive candidate for the fabrication of stimuli-responsive hydrogels. It is worthwhile noting, however, that one must consider more than simply hydrophilic and hydrophobic side chain contributions to polymer solvation when describing LCST behavior. For example, the polymer formed from *N*-isopropylmethacrylamide (NIPMAm) [33–38], which differs from NIPAm by only a single methyl group, has a higher LCST in water, which suggests that it is more hydrophilic despite a greater organic content. Apparently, this “increased hydrophilicity” does not arise from an increase in polymer polarity, but instead comes from a decrease in chain flexibility. This changes the entropic contribution to the free energy of mixing, and thus increases the LCST.

4.1.4 Microgels and Nanogels

Colloidally stable particles made from hydrogels, also referred to as micro- or nanogels, have similar properties as their macrogel counterparts; that is, a pNIPAm microgel, like the bulk gel, will also undergo a volume phase transition temperature (VPTT) near the LCST of the parent polymer [13, 39]. In addition to these properties, microgels have other characteristics of colloidal dispersions such as zeta potentials [13, 40, 41] and can also form ordered phases when prepared as a highly monodispersed sol [42–45].

Some very important studies have focused on the differences between macro- and microgels with respect to their phase behavior [13, 39, 43, 46–58]. These are too numerous to describe in detail here, so we offer a single example of the complexity of these materials. Wu et al. have shown that the VPTT of the microgels is slightly higher than the LCST of pNIPAm (Fig. 4.2), and also that the transition region is less sharp than that of bulk gels [46]. The reason for this continuous transition is due to a greater heterogeneity in the subchain lengths of the microgels as compared to traditionally prepared macrogels. When the microgels are subjected to $T > \text{VPTT}$, the regions of the particle with longer subchain lengths collapse at a lower temperature than the regions with shorter subchains. Thus, one can think of the observed phase transition for a microgel as being the summation of the phase transitions of the different subnetworks in the particle. We have also observed this behavior in core/shell

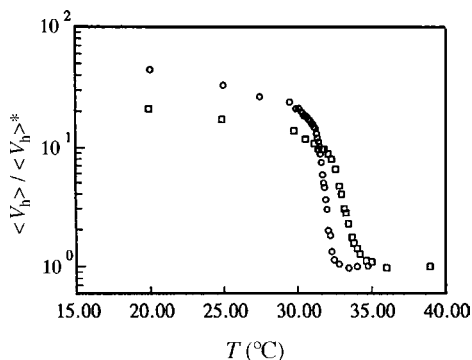


FIGURE 4.2 Deswelling ratio of linear pNIPAm chains (○) and cross-linked microgels (□) in water. Due to the heterogeneity in the cross-links, microgels have a broader phase transition region as compared to linear pNIPAm chains. Reprinted with permission from Reference [46]. Copyright 1997 American Chemical Society.

structured microgels using fluorescent probes to interrogate cross-linker gradients [50].

Chemical functionalization of microgels not only facilitates control over the volume phase transition but also allows postpolymerization modifications and provides handles to trigger response to external stimuli like pH, ionic strength, or light. However, to achieve efficient design of functional microgels based on chemical modification, it is important to understand how the functional groups are distributed in the polymer network. A recent report by Hoare and Pelton gives an insight into this aspect. The researchers describe two different methods of obtaining controllable distribution of the functional groups in the system [59]. As the first method, acrylic acid (AAc) groups were incorporated in acrylamide/NIPAm microgels by hydrolyzing the acrylamide blocks. The second method involved direct copolymerization of methacrylic acid (MAA) with NIPAm. The distribution of the acid functional groups obtained by the two methods had different topochemical distributions. Another factor that influenced the distribution was the temperature of acrylamide hydrolysis, that is, whether it was above or below the LCST of the microgel. Based on potentiometric and conductometric titrations as well as electrophoretic mobility evaluations of the microgels, it was found that at a temperature below the LCST, most of the carboxyl groups were located throughout the microgel, whereas at a temperature above the LCST, a high percentage of carboxyl groups were found to be located at or near the surface of the microgels. In case of pMAA-co-pNIPAm microgels, there exists a core/shell kind of a structure with MAA mostly forming the shell. This difference in the distribution of the carboxyl groups in the microgels produced by the two different comonomers is because of the difference in the polymerization kinetics due to different reactivity ratio of the monomers. The copolymer of

acrylamide and NIPAm is expected to have random incorporation of the monomers resulting in acrylamide and hence carboxyl groups on hydrolysis, throughout the bulk of the microgel. On the contrary, the reactivity ratios of MAA and NIPAm suggest that there is greater affinity for the homopolymerization of NIPAm, which is followed by MAA monomer polymerization resulting in the core/shell-like structure.

4.2 CORE/SHELL STRUCTURED MATERIALS

The synthesis and behaviors of hydrogel latexes have been extensively reviewed in the literature [12, 13]. In this chapter, we would like to focus on the synthesis and applications of particles with higher order complexities. Core/shell structured materials represent one example of such particles. Core/shell hydrogel particles can broadly be divided in two classes: one where the core is made from nonhydrogel material and the shell is made from hydrogel, and the second being where both the core and the shell are made of a hydrogel-like material. In the first class of materials, the core is usually made of solid material such as polystyrene, silica, or gold nanoparticles. Dingenouts et al. synthesized a polystyrene core with small amount of NIPAm as a comonomer by surfactant-free emulsion polymerization (SFEP) [60]. The polystyrene-co-pNIPAm particles were stabilized by the sulfate groups from the initiator. These cores were then used as seeds for polymerizing a cross-linked shell of pNIPAm. For the shell synthesis the reaction was carried out at 80°C, which provided a core particle with a deswollen pNIPAm-rich periphery, onto which pNIPAm polymerizing in solution aggregated by a precipitation polymerization mechanism. Xiao et al. synthesized similar particles where pNIPAm chains were grafted on the polystyrene core resulting in a “hairy” particle [61]. Similar approaches have been used by other groups to prepare particles with silica [62] and gold cores [63].

The second type of core/shell materials is the one that has hydrogel in both the core and the shell. Our group first reported the synthesis of this type of hydrogel particles by two-stage precipitation polymerization [10]. In this method, a polymer shell with the same or different structure or functionality to that of the core is added onto preformed core particles, thereby allowing control over the radial distribution of the functional groups in the particle. In a typical synthesis, preformed pNIPAm core particles are heated to $\sim 70^\circ\text{C}$, followed by addition and initiation of the shell monomer solution. Since the reaction temperature is well above the VPTT of the core particles, the particles are in a collapsed state. The collapsed particles are hydrophobic and hence tend to capture the growing oligomers, which results in the formation of the shell.

Core/shell particles prepared in this fashion can exhibit very interesting properties [9, 33, 34, 50, 64–67]. Since the shell can be synthesized using different comonomers than the core, the particles can show multiple phase transition behavior with temperature [10, 33, 34]. Furthermore, depending

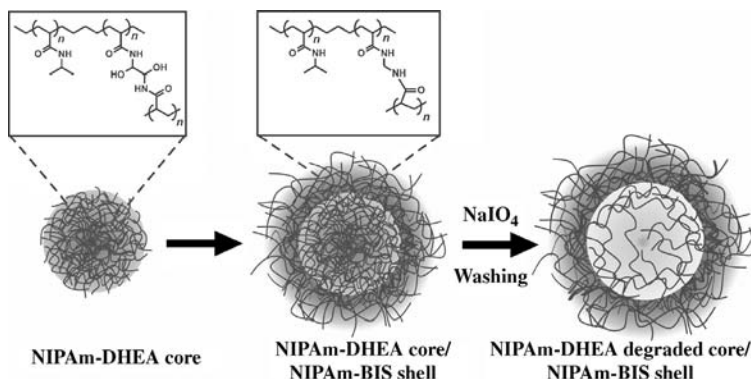


FIGURE 4.3 Preparation of thermosensitive hollow microgels via oxidation of core cross-links. Reprinted with permission from Reference [68].

upon the cross-linker density of the shell, compression or “shrink-wrapping” of the core can be observed due to a cross-link gradient in the shell [64, 65, 67]. We have also used this synthetic method to make hollow hydrogel capsules (Fig. 4.3) [68]. To accomplish this, the core is fabricated with a degradable cross-linker and the shell with a nondegradable one. The degradable cross-linker that we have used contains a vicinal diol, which can be degraded by stoichiometric addition of periodate. After core degradation, the particles were cleaned extensively by centrifugation, after which dynamic light scattering (DLS) and fluorescence were used to confirm the hollow structure.

Berndt and Richtering have also synthesized core/shell particles having two different polymers in the core and the shell [33]. In their demonstration, the core was made of pNIPAm and the shell consisted of poly(*N*-isopropylmethacrylamide) (pNIPMAm), which has an LCST of 45°C in water. They studied the thermoresponsivity of these particles and found, in a similar fashion to previous work from our group, that the particles had two transitions corresponding to the LCSTs of the two polymers (Fig. 4.4). In a recent study, the researchers investigated the effect of shell thickness and cross-linking density on the structure of the doubly temperature-sensitive core/shell microgel networks using small angle neutron scattering (SANS) techniques [69, 70]. It was observed that variation of cross-linking density in the shell mainly affects the dimensions of the shell without affecting the core. However, increase in the shell-to-core mass ratio, leads to increased expansion of the core with a broader core-shell interface between the LCSTs, thus indicating the elastic force exerted on the core by expanding shell. Studies at a temperature below the LCST of the core suggested that the core of the core/shell particle was unable to swell to the same extent as a free core (with no shell), thus indicating that the expanded shell prohibits the swelling of the core. In another report, the same research group observed that an increased shell thickness shifts the core transition toward higher temperatures while the collapse of the core can shift

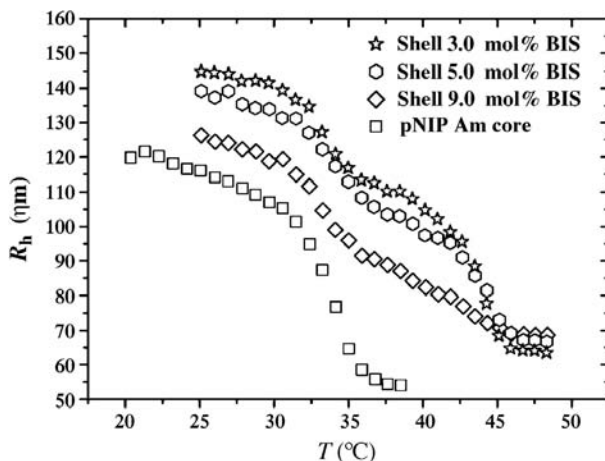


FIGURE 4.4 Hydrodynamic radius as a function of temperature for pNIPAm core/pNIPMAm shell microgels with different shell cross-linker concentrations. The sample containing 3.0 mol% BIS clearly shows that the particle is undergoing two phase transitions, the first transition corresponding to the LCST of pNIPAm and the second to that of pNIPMAm. Reprinted with permission from Reference [33]. Copyright 2003 American Chemical Society.

the transition of a thin shell to lower temperatures [71]. They also observed an additional thermal transition in these core/shell microgels, which was attributed to the formation of additional hydrogen bonds near the core–shell interface, resulting from the overcompensation of the thermodynamic forces during the core transitions by the elastic forces in the shell.

4.2.1 Block Copolymer Micelles

Hydrogel nanoparticles can also be formed by using the ability of block copolymers to self-assemble into micelles [72]. Micelle-forming block copolymers, like surfactants, have both hydrophobic and hydrophilic domains. By controlling the polarity of the solvent and the concentration of the polymers, block copolymers can be formed into spherical micelles. In hydrophilic solvents, the hydrophobic block forms the core and the hydrophilic block is exposed to the solvent. A potentially powerful aspect of this approach is that, in the same vein as micelles or liposomes, one can imagine making “mix-and-match” assemblies, where functional units can be co-assembled with structural units to prepare nanoparticles with good control over the display, number, and spacing of the bioconjugation sites.

In some cases, these micelles can be cross-linked to form stable nanoparticles. For example, Zhu and Napper used pNIPAm-*b*-PEO to form microgels [73,74]. Initially, the block copolymer was synthesized using the ceric ion redox system in nitric acid at 50°C, followed by addition of the cross-linker

N,N'-methylenebis(acrylamide) (BIS) to form cross-linked microgels. The authors observed that the size of the microgels, as measured by DLS, was dependent on the concentration of NIPAm and PEO, and also on the rate of heating during polymerization.

The group of Karen Wooley has extensively studied cross-linked block copolymer micelles, which they refer to as shell cross-linked knedels (SCK) [72, 75–88]. The size range for SCKs is ~ 5 –200 nm. They are prepared from amphiphilic block copolymers, which self-assemble into polymeric micelles. The micelles are further stabilized by cross-linking of the side chain functionalities in the shell of the micelles, as shown in Fig. 4.5. The first SCK reported was fabricated from polystyrene and poly(4-vinylpyridine) block copolymer [75]. Before self-assembling the polymer into micelles, the pyridyl nitrogen was quaternized by reaction with *p*-chloromethylstyrene to impart hydrophilicity to the polymer. Once the polymer formed micelles, the styrene moiety in the shell was polymerized to give the cross-linked structure. The dimensions and topologies of the particles can be controlled by varying the length of the hydrophilic and hydrophobic blocks. The Wooley group has used similar approaches to prepare hydrogel containing SCKs [85, 88], as well as core degradable nanoparticles [77, 81].

Akiyoshi et al. have found that polysaccharides partly modified by hydrophobic groups such as cholesterol can form nanoparticles in water [89]. The sizes of these particles typically range from 20 to 30 nm with excellent monodispersity, according to size exclusion chromatography, DLS, and TEM. These particles are not true block copolymer micelles but are closely related to this class of particles, since the association forces are similar. They first reported the synthesis of these particles in 1993 by using hydrophobized

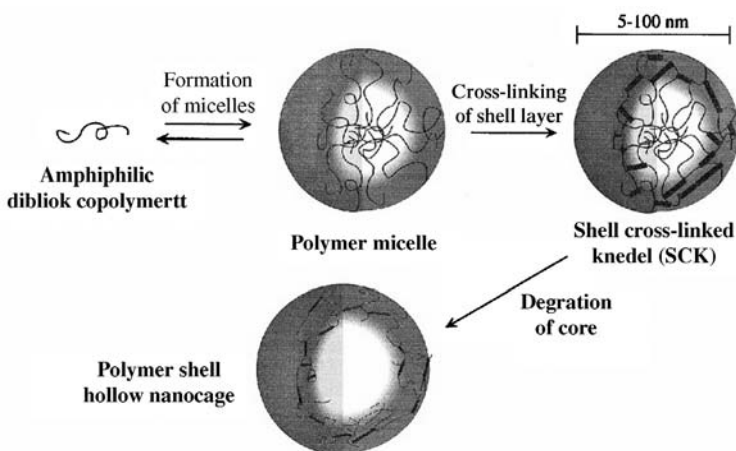


FIGURE 4.5 General synthetic approach for synthesizing shell cross-linked knedel (SCK) nanoparticles. The degradation step is used for the preparation of hollow particles. Reprinted with permission from Reference [82].

pullulan having 1.6 cholesterol groups per 100 glucose units [89], which aggregated intermolecularly to form nanoparticles. These nanoparticles are considered to be hydrogels in which the cross-links are provided by the associated hydrophobic groups. The size of the particles can be controlled by the number of the hydrophobic groups and also by the structure of the polymers. The group has also made particles in which pNIPAm was incorporated to create thermoresponsive pullulan particles. These particles can capture and entrap macromolecules such as proteins in the gel network [90–93]. The self-assembly of these polymers can be controlled from the molecular level (association of hydrophobic groups) to the nanoscale level (association of hydrophobized polymers) and macroscopic level (association of nanoparticles). The hierarchy of pullulan assembly is shown in Fig. 4.6.

A general strategy to synthesize polymeric nanoparticles derived from peptide di- and triblock copolymers has been demonstrated by Wooley and coworkers [94]. In their strategy, they coupled peptide tritrypticin having antimicrobial activity to living radical macroinitiators on a solid-phase resin. The initiators further allowed nitroxide-mediated radical polymerization (NMRP) and atom transfer radical polymerization (ATRP) of acrylate monomers on the solid support, resulting in copolymers end-functionalized with tritrypticin. The peptide-containing block copolymer was finally cleaved from the resin and self-assembled into micellar nanoparticles. Additional micellar stability was achieved by cross-linking of the copolymer chains using carbodiimide-coupling chemistry. The micellar nanoparticles were found to possess antimicrobial activity suggesting that the peptide had retained bioactivity and bioavailability following the conjugation and nanoparticles formation. Another example of this strategy was provided by Wooley and coworkers, which involved the use of an antigen-functionalized ATRP macroinitiator to form amphiphilic diblock copolymer possessing antigen biofunctionality [95].

4.3 BIOCONJUGATED HYDROGEL PARTICLES IN NANOTECHNOLOGY

The synthetic methods described in the previous sections have enabled the field to advance toward the application of hydrogel nano- and microparticles in more complex biotech and nanotech applications. In this section, we will describe some of these applications, highlighting systems where the ability to create synthetically and topologically complex hydrogels has led to successful incorporation into advanced nanosystems.

4.3.1 Drug/Gene Delivery

Recently, significant efforts have been put into devising colloidal drug carriers. It has been hypothesized that an actively targeted particulate drug carrier will

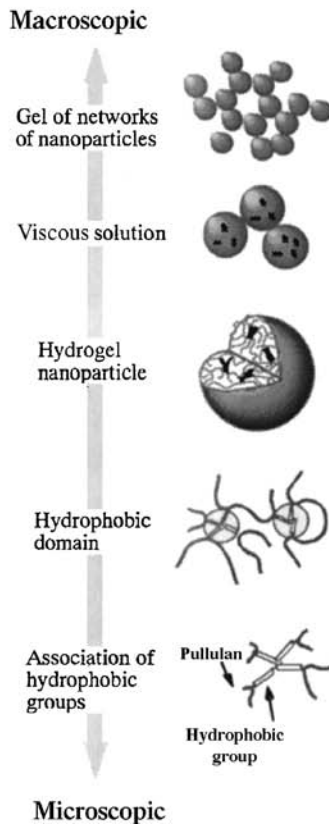
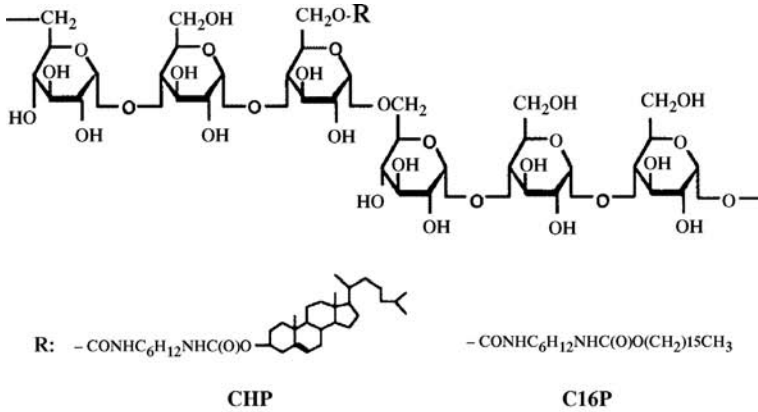


FIGURE 4.6 Chemical structure and the hierarchical self-assembly of hydrophobically modified pullulan. Reprinted with permission from Reference [93]. Copyright 2002 American Chemical Society.

increase the therapeutic efficacy of a drug by delivering that drug to the diseased site, while also reducing systemic side effects of the drug. An ideal drug carrier should be able to target and deliver only to the diseased sites, it should not induce immune response, and it should be degradable and produce nontoxic degradation products [96].

The particulate carriers that have been most widely studied are liposomes and polymer nanoparticles. Liposomal drug carriers have been studied extensively, with a few liposomal formulations currently being available in the market, while many others are in the development “pipeline.” One important drawback of liposomes is payload leakage. Since the boundary of the liposomes is a simple lipid bilayer, performance can be hampered by passive diffusion of drugs across that boundary [97]. Among polymer particles, the most widely studied are poly(lactic acid-co-glycolic acid) (PLGA) particles [98]. The popularity of this material largely stems from its degradation into nontoxic by-products, which can be removed from the body via the renal system. However, this construct suffers from numerous drawbacks, as it is a very hydrophobic, immunogenic polymer with acidic degradation products. The increase in acidity associated with polymer degradation can induce nonspecific inflammatory responses, which can be very detrimental in targeted delivery applications. Nonviral gene delivery systems have been proposed as a safer alternative to viral vectors, since they will induce host immune response to a lesser extent than viral vectors. Several cationic polymers such as polyethyleneimine, polyamidoamine, and polylysine have been used for nonviral gene delivery, but they all lack the biocompatibility needed for *in vivo* use [99]. Conversely, hydrogel nanoparticles represent a potentially useful class of materials as drug/gene carrier systems, but have been studied much less extensively. Here we report a few examples of recent efforts involving nanoparticulate hydrogel delivery vehicles.

In an effort to employ biodegradable polymers as delivery vehicles, Kim et al. used glycidyl methacrylate dextran as the major comonomer and dimethacrylate poly(ethylene glycol) as a covalent cross-linker [100]. In this case, the particles were prepared by free radical polymerization and a hydrophobic drug, clonazepam, was then loaded in the particles. It was found that the release rate was dependent on the pH as well as the concentration of the enzyme dextranase, which degraded the dextran and eroded the particles. Na and Bae have used self-assembled hydrogel particles of pullulan acetate and sulfonamide conjugates to study the release of the drug adriamycin [101]. In this case, the pullulans had pH-responsive polymer incorporated in the structure, which caused the particles to shrink and aggregate at $\text{pH} < 7$. The shrinking of the particles in turn caused the expulsion of the drug into the surrounding medium.

Peppas and coworkers have used hydrogels as a delivery vehicle to carry insulin. Poly(methacrylic acid) and poly(ethylene glycol) were used to synthesize the hydrogels by UV-initiated free radical polymerization [102]. Insulin was then conjugated to the protein transferrin, and this complex was

loaded into the hydrogels. The insulin–transferrin conjugate was used as it has been shown to cross the intestinal epithelium. Peppas and coworkers suggested the use of the insulin–transferrin-loaded hydrogels as an insulin oral delivery system due to its increased stability against proteolytic degradation. Insulin was conjugated to transferrin by reacting it with dimethylmaleic anhydride (DMMA). The transferrin was conjugated with succinimidyl 3-(2-pyridyl-dithio)propionate (SDSP). The DMMA and SDSP were then reacted to form the insulin–transferrin conjugate, which were then loaded into the hydrogels. A 22-fold increase in transport of insulin across Caco-2 cell monolayers was seen with conjugate-loaded hydrogels versus insulin alone.

While the previous examples were simple demonstrations of *ex vivo* controlled release from hydrogel particles, others have applied nanoparticulate hydrogels to *in vivo* delivery. For example, Hsiue et al. have used pNIPAm nanoparticles for ocular delivery [103]. Two formulations were used, where one was composed of a solution of linear pNIPAm, while the other was mixture of linear pNIPAm and pNIPAm particles. The drug release and cytotoxicity studies were carried out on rabbits. The drug epinephrine, which reduces intraocular pressure, was then delivered from each of the two formulations. It was observed that the intraocular pressure was decreased for ~24 h when the linear pNIPAm system was used, while the mixed system extended the therapeutic effect to ~32 h. Systems such as these are therefore potentially interesting for the clinical treatment of glaucoma.

As mentioned above, an ideal drug carrier should not induce an immune response in the host. This is commonly achieved by making the surface of the particle hydrophilic, which can prevent opsonization (i.e., adhesion enhanced phagocytosis) by macrophages [104]. For example, Gaur et al. synthesized cross-linked polyvinylpyrrolidone hydrogel nanoparticles (~100 nm diameter) [105]. The surface of these particles was then made hydrophilic by attaching poloxamers and poloxamines, which are examples of polyethylene glycol/polypropylene glycol block copolymers. *In vivo* studies in mice indicated that less than 1% of the dose was retained by the macrophages in the liver, and even after 8 h of injection ~5–10% of these particles were still circulating in the vasculature. This enhanced circulation time, and the lack of liver accumulation, could enable the use of such particles in drug delivery. They also reported that increase in size and hydrophobicity increased their uptake by reticuloendothelial system, suggesting that both factors may play a role in the ability of the body's defense mechanisms to recognize the particles as foreign invaders.

Targeting is an important property for a drug carrier, as one can potentially enhance the uptake and retention of the nanocarrier at the site of disease via active targeting. We have synthesized a folic acid labeled pNIPAm core/shell microgel that can target cancer cells [106]. Folic acid is a well-known ligand for targeting cancer cells because most tumors overexpress folate receptors. In this demonstration, pNIPAm core/shell hydrogel particles were synthesized, where the pNIPAm core was fluorescently labeled and the pNIPAm shell contained a small amount of a comonomer containing a primary amine. We then

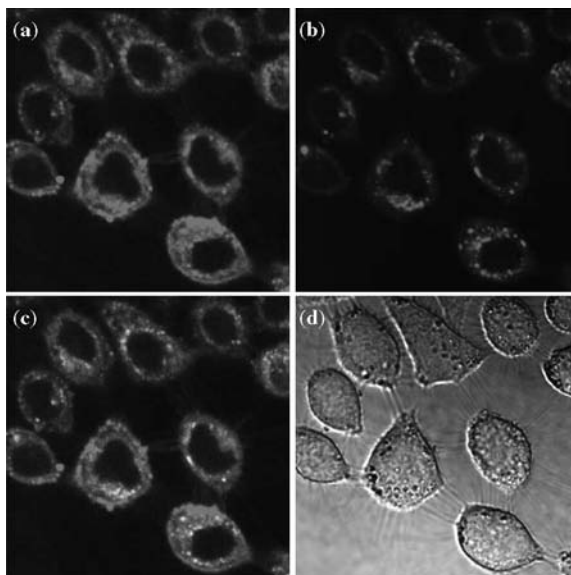


FIGURE 4.7 Confocal images of HeLa cells incubated with folate-conjugated nanoparticles. (a) Green fluorescent particle channel, (b) lysotracker red dye channel, (c) overlap of both the channels, and (d) transmittance image of the cells. Experiments performed in collaboration with Jean Chmielewski at Purdue University.

covalently coupled folic acid to the amine-containing hydrogel shell in order to surface localize the targeting ligand. When these particles were incubated with cancer cells that overexpressed the folate receptor, the hydrogel nanoparticles were taken up by receptor-mediated endocytosis (Fig. 4.7). It was also observed that the particles exhibited thermal cytotoxicity above the phase transition temperature. The exact reason for this effect is not known, but is suspected to be intracellular aggregation and protein adsorption on deswollen, hydrophobic pNIPAm particles. Since these particles apparently retain their thermoresponsivity in the cytosol, it was hypothesized that they could enable thermally triggered delivery of chemotherapeutic payloads, thereby enabling both active targeting and triggered delivery in one vehicle.

In another example of active targeting, Choi et al. used pNIPAm microgels for targeting liver cells [107]. They used pNIPAm-co-AAc microgels that were tagged with fluorescein, while the targeting moiety in this case was galactose, which is a ligand for asialoglycoproteins. It was observed that galactosylated microgels were internalized in the cells via this ligand–receptor interaction. Furthermore, since these particles are thermoresponsive, they studied temperature–dependent uptake of these particles. The uptake efficiency increased with the increase in temperature, which they suggested was due to enhanced uptake efficiency for smaller particles, although the increase in

particle hydrophobicity could also enhance uptake. The Wooley group has investigated SCKs with targeting ligands like folic acid, integrins, and peptides [108–110]. They have also demonstrated that nanoparticles coupled with a short peptide belonging to a protein transduction domain of HIV exhibited targeting ability to CHO and HeLa cell lines.

Kumacheva and coworkers describe another hydrogel design to be used for cancer targeting [111]. In this work, pNIPAm-co-AAc hydrogel particles averaging 150 nm in diameter were synthesized. Hydrogel nanoparticles were conjugated with transferrin, a targeting ligand, by carbodiimide coupling. The transferrin-conjugated particles were then targeted to HeLa cells. Transferrin receptors that are present on the cellular surface enable receptor-mediated endocytosis of the targeted nanoparticles. These hydrogels were loaded with Rhodamine 6G (R6G) and later with doxorubicin to study uptake and delivery. The transferrin-conjugated particles delivered 100 times more R6G to cells than bare microgels, and cell mortality was greatly enhanced over bare, doxorubicin-loaded microgels ($72.6 \pm 5.0\%$ versus $33.8 \pm 2.8\%$).

Synthetic/viral composite systems have also been explored. For example, Jana et al. prepared polyvinylpyrrolidone nanoparticles and encapsulated them in a reconstituted Sendai viral envelope containing only the fusion proteins [112]. These particles were incubated with human hepatoblastoma cell lines, which resulted in internalization of the polymer particles, as confirmed by fluorescence. Na et al. have used self-assembled polysaccharide (curdlan) particles for targeting [113]. Curdlan was hydrophobically modified with a carboxylated sulfonylurea derivative. The targeting ligand was lactobionic acid, which targets HepG2 cells. As expected, the degree of nontargeted uptake was significantly diminished relative to that for particles targeted to HepG2 cells.

Many groups have used cationic polymers such as chitosan for gene delivery. Chitosan is a natural cationic polysaccharide consisting of D-glucosamine and N-acetyl-D-glucosamine. This polymer has been shown to be biocompatible, nonimmunogenic, and degradable, thereby making it potentially suitable as a delivery vehicle. In the presence of polyanions, chitosan can form hydrogel nanoparticles by complex coacervation. For example, chitosan–DNA nanoparticles have been widely studied for their application in gene delivery. Mao et al. have synthesized chitosan–DNA nanoparticles and studied the transfection efficiency [99]. Targeting agents, like transferrin, have also been conjugated to these particles to increase the internalization, while drugs like chloroquine have been encapsulated within these particles to investigate controlled release. Mitra et al. have used chitosan to encapsulate doxorubicin, a highly toxic chemotherapeutic drug [114]. For encapsulation, they first conjugated doxorubicin with dextran. This drug–dextran conjugate readily formed particles when mixed with chitosan. *In vivo* studies then showed that the chitosan–drug conjugate circulated in the blood longer than the drug alone and also that the conjugate decreased the tumor size to a larger extent than the free drug.

In a very recent example of using soft polymeric nanoparticles bioconjugates for targeted drug delivery *in vivo*, Langer and coworkers used a nanoparticle construct of biocompatible and biodegradable poly(D,L-lactic-co-glycolic acid)-block-poly(ethylene glycol) (PLGA-b-PEG) [115]. PLGA-b-PEG copolymers having terminal carboxyl groups were precipitated into nanoparticles in the presence of the cancer therapy agent docetaxel, resulting in the encapsulation of the drug within the nanoparticles. With an aim to target the particles specifically to cancer cells, the terminal carboxyl groups on the nanoparticles surface were conjugated to RNA oligonucleotide aptamers (specific to PSMA proteins expressed on the surface of LNCaP prostate epithelial cancer cell) by carbodiimide coupling chemistry. Animal studies showed that the aptamer bioconjugate nanoparticle resulted in complete shrinkage of the tumor after a single intratumoral injection of maximal tolerated dose for i.v. administered docetaxel (Fig. 4.8). The nanoparticle synthesis involves FDA approved materials and the technique thus holds promise for clinical trials of the effectiveness of polymeric nanoparticles bioconjugates in cancer therapy. Additional advantages for clinical studies include small size, facile synthesis, relative stability, and immunogenic nature of the targeting agents.

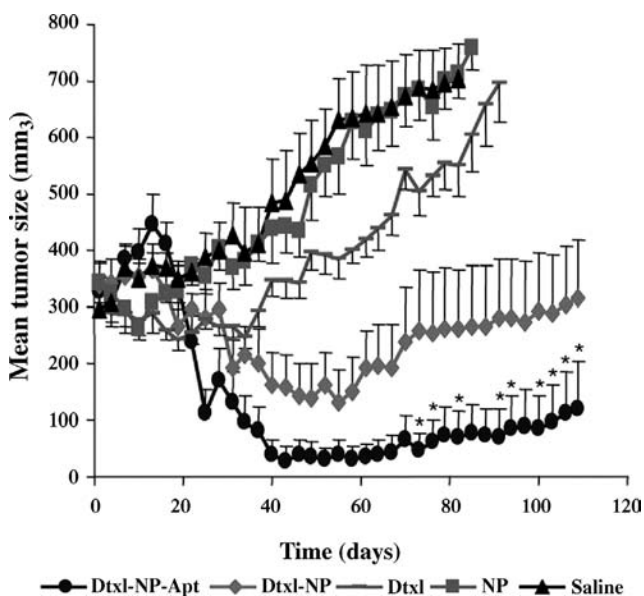


FIGURE 4.8 Effect of a single intratumoral injection on tumor size. Saline (black); pegylated PLGA NP without drug (NP, brown); emulsified Dtxl (Dtxl, green); Dtxl-encapsulated NPs (Dtxl-NP, red); or Dtxl-encapsulated NP-Apt bioconjugates (Dtxl-NP-Apt, blue); * indicates groups that were statistically significant compared with all other groups. Reprinted with permission from Reference [115]. Copyright 2006 National Academy of Sciences, USA.

4.3.2 Analytical Applications

Given the ability to synthesize a variety of responsive hydrogel structures, chemical and biological sensing application remains an intriguing application. One of the earliest types of hydrogel nanoparticle employed in “sensing” was a pH-responsive particle. The simplest method of fabrication involves the use of a pH-responsive moiety, such as a weak acid, which can be copolymerized into the polymer network. At low pH, the acid groups are protonated and the particles will be in a somewhat condensed form, while at a higher pH where the acid groups are deprotonated, the particles adopt a swollen structure due to Coulombic repulsion among the negatively charged regions and a change in the free energy of mixing with water. Similarly, charged microgels are responsive to ionic strength, where an oppositely charged ion neutralizes the charge and causes the gel to shrink. Similar approaches have enabled the fabrication of cross-linked block copolymer micelles with pH responsivity. While this approach appears to be a generalizable motif by which one can imagine designing hydrogel nanoparticles that “sense” their surroundings, very little has been done on creating hydrogel nanoparticles for real chemical sensing applications. However, a few examples are beginning to emerge. For example, we have demonstrated that hydrogel microstructures can be rendered sensitive to protein binding provided the interaction is multivalent and therefore results in an increase in the microgel cross-link density [30]. This approach has been extended to reversible biosensors based on antibody–antigen displacement or competitive binding. In this example, we have first incubated antigen-presenting microgels with antibodies, which then bind to the microgel surface. These microgels also possess a photoaffinity label (benzophenone), which can then be photoactivated, thereby photocoupling the antibodies to the microgels. The antibody–antigen-based cross-links can then be reversibly switched by exposure to free antigen, which displaces the cross-link and swells the particle. This approach has been coupled to a microlensing technology that allows for rapid, label-free readout of the sensor response [116].

In addition to these applications, microgels have been used for the separation of proteins from complex media. Kawaguchi et al. reported that proteins could be separated using thermoresponsive microgels [117]. They used regular pNIPAm microgels and observed that at $T > VPTT$ larger amounts of protein bound to the particles than at $T < VPTT$. The higher degree of protein adsorption at $T > VPTT$ was attributed to hydrophobic interaction between the protein and dehydrated polymer. In an approach that utilized Coulombic interactions, Elaissari et al. used cationically charged pNIPAm microgels for extraction of RNA. It was observed that the interaction between the cationic particles and negatively charged RNA decreased with an increase in pH, ionic strength, and temperature, thereby indicating that adsorption was mainly governed by electrostatics [118]. In an immunoseparation study, Kondo et al. synthesized poly(styrene/NIPAm/glycidyl methacrylate) microgels. These particles were designed such that they flocculated at high temperature and at

high ionic strength. Using the glycidyl methacrylate comonomer as a chemical handle for chemoligation, BSA was coupled to the particles, which were then used for immunoseparation of anti-BSA from serum. After incubation with the serum, the particles were separated by flocculation [119]. Similarly, particles that contained magnetite were used by this group for separation and purification using a magnetic field to collect the particles [120].

Hydrogel nanoparticles have also been employed in a molecularly imprinted polymer (MIP) scheme. The principle behind MIP is based on both shape and molecular-recognition templating. When the polymerization is carried out in the presence of “template” molecules, it is envisioned that the polymer will rigidify around that template, forming a cavity that is optimized for binding of that molecule. After the templates are removed, it is hoped that the cavity retains that shape and is able to bind and detect that particular molecule or similar molecules in a complex mixture. Ye et al. have synthesized hydrogel nanoparticles in the presence of theophylline and 17 β -estradiol. The sensing molecules were dissolved in the mixture of methacrylic acid and trimethylolpropane trimethacrylate and then polymerized either thermally or by UV irradiation. In these studies, they used radioligand binding analysis to determine the sensitivity and selectivity of analyte binding [121]. Competitive binding experiments showed high selectivity for the analyte.

Daunert and coworkers in a recent report showed how biological processes can be used to tailor the response of hydrogels [122]. A biological recognition unit was incorporated into the hydrogel structure and conformational changes in the unit, in response to external factors, resulted in volume changes in the hydrogel. Calmodulin (CaM) is a protein that undergoes different conformational changes on binding with Ca²⁺ (native to dumbbell-like), certain peptides, or a certain class of drugs like phenothiazines (native to more constricted). CaM was incorporated in the hydrogel by genetically engineering the protein to have a cysteine residue at the C-terminus, which was further conjugated to an allylamine in order to attain oriented immobilization of the protein in the hydrogel network. For incorporating phenothiazine in the polymer network, a derivative having polymerizable acrylate group was synthesized. Free radical polymerization of the polymerizable protein and drug, an acrylamide monomer, and cross-linker BIS resulted in the desired hydrogels. The hydrogel showed reversible swelling that was dependent on the concentration of Ca²⁺. On saturating the hydrogel with Ca²⁺, the resulting conformational change in CaM and the phenothiazine binding site of CaM became accessible to the immobilized drug, resulting in the increased cross-linking and shrinkage of the hydrogel. The gel swelled on Ca²⁺ removal, resulting from the release of the drug derivative from the binding site and also since the water uptake property of the polymer was changed due to modification of the hydrophobic surface of the protein. The hydrogel also showed response to phenothiazines. When the hydrogel was treated with free phenothiazine (chlorpromazine), the hydrogel swelled due the competitive binding of the free drug replacing the bound immobilized drug from the binding site of the conjugated protein. These protein- and drug-modified

hydrogel biomaterials hold promise for microactuators and in microfluidics, as also demonstrated by the authors.

Miyata et al. have demonstrated gels that respond to tumor markers [123]. The gels were prepared by biomolecular imprinting (Fig. 4.9). In this work, the gels responded to the tumor-specific marker α -fetoprotein, AFP, which is a glycoprotein used for serum diagnosis of primary hepatoma. Lectin (Con A)

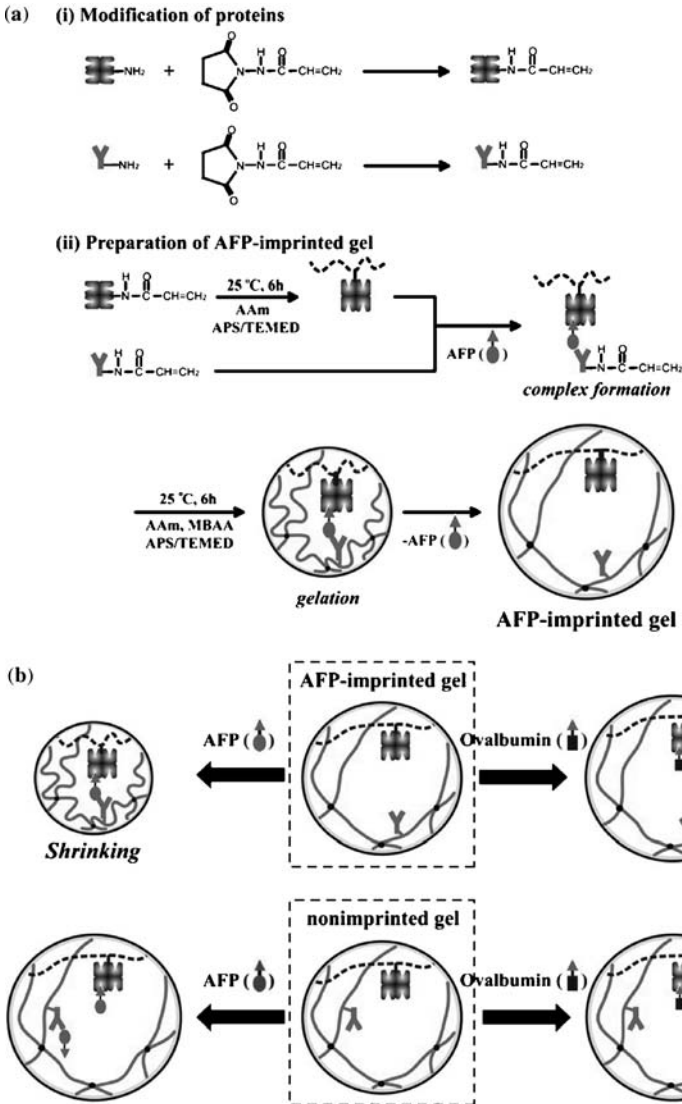


FIGURE 4.9 Schematic representation of tumor marker responsive hydrogel preparation. (a) Synthesis of the tumor marker responsive hydrogels. (b) Representation of hydrogel behavior in response to tumor markers. Reprinted with permission from Reference [123]. Copyright 2006 National Academy of Sciences, USA.

and polyclonal anti-AFP antibody were conjugated with *N*-succinimidylacrylate to form polymerizable vinyl groups and the gels were formed by copolymerizing these groups with acrylamide in the presence of template AFP. This formed a lectin–AFP–antibody complex, and the removal of the AFP created the AFP-imprinted gel. It was shown that AFP-imprinted gels shrank upon exposure to AFP, as the lectin–AFP–antibody forms a gel cross-linking complex. Nonimprinted gels experienced slight swelling in AFP solutions. The gels were also shown to be specific to the glycoprotein, as the gels did not shrink, but swelled in ovalbumin solutions.

4.3.3 Biomaterials

Perhaps the broadest definition of biomaterials comes from the National Institutes of Health Consensus Development Conference: “[a biomaterial is] any substance (other than a drug) or combination of substances, synthetic or natural in origin, which can be used for any period of time, as a whole or part of a system which treats, augments or replaces any tissue, organ or function of the body” [124]. Research in the field of biomaterials is often linked to developing a more biocompatible system, such as making an implant or surgical device less damaging to the body. In the case of hydrogels, much of the effort has been put in coating the surface of the implants or devices with polymers or bulk gels. With the advent of responsive hydrogels, many researchers began working on making “smarter biomaterials,” where these materials can sense a change in the environment and respond to it in a programmed fashion. In this section, we describe a few of those examples pertaining specifically to hydrogel nanoparticles.

As mentioned previously, Kawaguchi has studied the interaction of proteins with microgels extensively [117,125,126]. For example, the group has studied the effect of temperature on the nonspecific adsorption of proteins to thermo-responsive microgels. They have also investigated the activity of enzymes that are covalently bound to the microgels. In one example, they attached trypsin peroxidase to pNIPAm microgels and studied its activity as a function of temperature [127]. The enzyme activity decreased with increase in temperature due to the decrease in the pore size. This caused the decrease in the rate of diffusion of the substrate to the enzyme. They also studied a similar system with a small molecule, ubiquinone, attached to the particle and observed similar temperature-dependent results. Duracher et al. have studied the adsorption of HIV-1 capsid protein p24 on polystyrene core–pNIPAm shell particles [128]. As predicted by numerous studies, they observed higher adsorption at $T > VPTT$ of pNIPAm due to hydrophobic interactions. Similarly, Urakami et al. studied the phagocytosis of polystyrene-co-polyacrylamide gel particles as a function of hydrophobicity. They observed that phagocytosis by granulocytes increased with the increase in polystyrene content of the particles, again presumably due to an increase in hydrophobic association with the granulocyte [129]. In similar studies, Kimhi and Bianco-Peled used isothermal titration calorimetry to study

the adsorption of small molecules (aspartic acid and valine) to pNIPAm microgels as a function of temperature [130]. They found that at 25°C aspartic acid binds strongly to the polymer particles due to formation of hydrogen bonds and at 37°C valine binds strongly due to the hydrophobic effect.

More advanced architectures can be prepared that take advantage of biocatalytic systems. For example, Ogawa et al. have synthesized pNIPAm microgels containing a pendant vinyl imidazole side chain, which again allows for pH-tunable gel swelling [28]. The enzyme urease, which catalyses the hydrolysis of urea into ammonia, was then physically entrapped in the particles. As the enzyme produced ammonia, the pH of the medium decreased. Hence, in the presence of urea, the particles shrank due to increase in pH and subsequent deprotonation of the imidazole unit. When the substrate was removed, the particles swelled to their original size as the local pH equilibrated with the pH of the surrounding bath. To demonstrate the potential utility of such a biomechanical system, the authors incorporated these particles into a membrane. Upon introduction of urea to one of the solvent reservoirs, they observed that the permeability of the membrane increased as the particles shrank.

An important aspect of many implanted biomaterials relates to the ability of cells to adsorb and proliferate on the material surface. It is clear that even materials with low surface energies and hence low degrees of nonspecific protein adsorption can tend to foul over time in cell culture or following implantation. Therefore, it is important to evaluate fouling of biomaterials as well as to arrive at new strategies for mediating cellular recruitment at synthetic surfaces. Thus, in addition to the aforementioned protein adsorption studies, Kawaguchi and coworkers have also studied the effect of cell binding to thermoresponsive particles on a solid surface [117]. They first deposited pNIPAm microspheres on a plate to produce a 2D array upon which the cell culture medium was seeded. They observed that the cells produced more reactive oxygen species at 37°C than at 25°C, indicating that the cells are under more mechanical stress at the higher temperature. This is presumably due to stronger attachment at $T > VPTT$. They also observed that the amount of reactive oxygen species produced when the system was heated from 25 to 37°C was much higher than just incubation at 37°C. This they attributed to the stimulus inflicted by the dynamic deswelling process. In addition to this system, they have also used a ligand–receptor system to study the mechanical stress on the cells [117]. Our group has fabricated particles in which the adsorption of the proteins to the particles is reduced by using PEG grafting [131]. In this report, we used pNIPAm core/pNIPAm shell particles and attached PEG either to the core or to the shell by copolymerisation of PEG-monomethacrylate. Reduced protein adsorption was observed for both the core- and shell-grafted PEG particles. It was further observed by NMR and protein adsorption measurements that at high temperature the PEG chains phase separate to the particle surface, and because of the polymer's hydrophilicity reduce protein adsorption. In the case of the particles in which the PEG is attached to the core, the PEG chains are able to penetrate the shell and phase separate to the surface, thus reducing the surface energy of the deswollen particles.

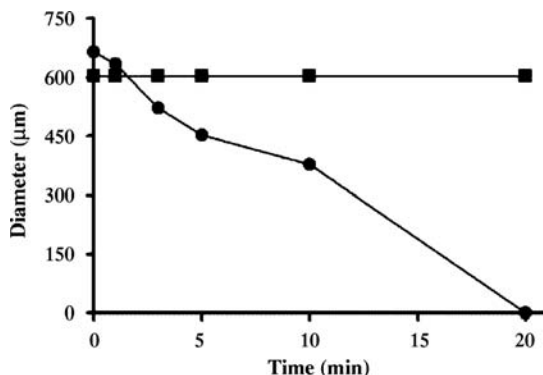


FIGURE 4.10 Diameter of hydrogels cross-linked with CYKC (●) and CSKC (■) upon exposure to 0.5 mg mL^{-1} α -chymotrypsin. Tyrosine containing hydrogels degraded within 20 min, while hydrogels containing serine do not degrade. Reprinted with permission from Reference [132]. Copyright 2005 American Chemical Society.

The development of materials that can interact with cells and proteins is important for drug delivery devices and extracellular matrix (ECM) mimicking. Protease responsive hydrogels have been described in the literature, such as those developed by Moore and coworkers [132]. In this work, hydrogel particles that are degraded by α -chymotrypsin were developed. They described a conjugation technique by which a disulfide transfer reaction under acidic conditions allows for a cross-linker that contains peptide sequences to be synthesized. A methacrylamide containing a chymotrypsin-sensitive sequence, CYKC, was incorporated into polyacrylamide hydrogels. Hydrogels containing the CYKC cross-linker completely degraded in 20 min in the presence of chymotrypsin, while hydrogels containing a chymotrypsin-insensitive CSKC cross-linker remained intact (Fig. 4.10). Kim and Healy have also synthesized pNIPAm gels with peptide cross-links. These gels can be used as an extracellular matrix mimic, where the peptide can be cleaved by a metalloproteinase, which subsequently leads to gel erosion. Figure 4.11 shows a schematic depiction of this process [133].

In another example of core/shell particles that may have utility in biomaterials applications, we have prepared a system in which the shell acts a barrier between the protein in the solution and a core-localized ligand buried under the shell [134]. In this case, we have synthesized a core to which biotin is attached, followed by addition of a shell containing a degradable cross-linker. Initially, the cross-linker density is high enough that the pore sizes are smaller than the size of the protein avidin. As the cross-linker is degraded, the average pore size increases and allows permeation of avidin to the core, where it can bind to biotin (Fig. 4.12). We have also observed protein size dependent permeation; that is, for larger proteins, more cross-links have to be degraded to allow for binding. These systems are interesting from the view of the topological complexity and also because they may be a model system for a particle that can “express” a particular functionality at the surface following a biological or chemical signal, which disrupts shell-localized cross-links.

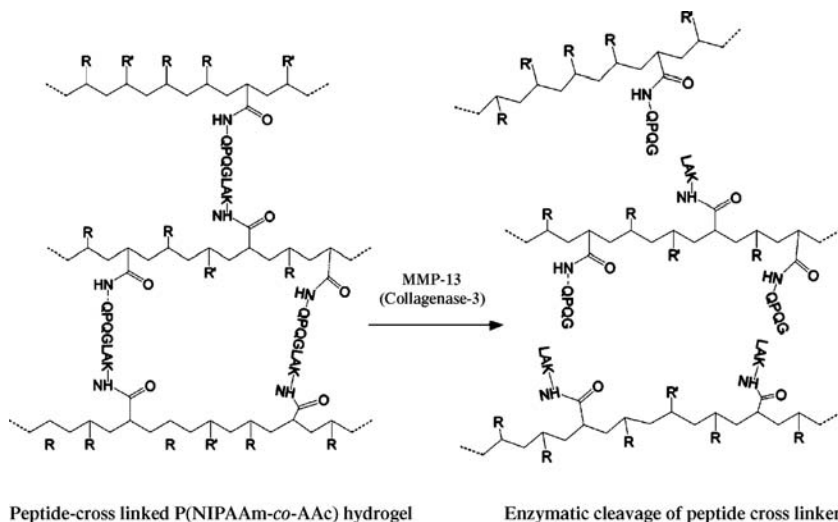


FIGURE 4.11 Schematic of peptide cross-linked hydrogel degradation by MMP-13 (collagenase-3). The letters indicate the single-letter amino acid designations. Reprinted with permission from Reference [133]. Copyright 2003 American Chemical Society.

4.4 CONCLUSIONS

Toward the end of the last century, it was commonly thought that the term “nanotechnology” was coined exclusively for “hard materials,” but this changed as polymeric materials became more common ingredients in nanometric systems. In this chapter, we have discussed various types of hydrogel nanoparticles and their applications in nanotechnology. As more and more research is carried out in this field, it becomes clearer that these materials hold great promise on their own, and as a bridge between more traditional nanostructures and biological systems. For example, gels that respond to a

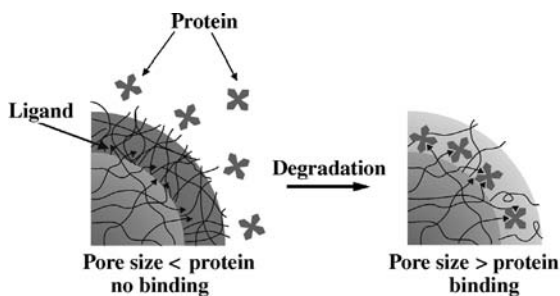


FIGURE 4.12 Schematic of permselective core/shell microgels. The particles exhibit shell cross-linker density-dependent permeation of the protein. Reprinted with permission from Reference [134].

change in their environment are potentially useful in the context of truly bioresponsive structures that may enable us to manipulate natural systems in a rational fashion.

Although many groups have worked in this field, we believe that most of the potential resources are untapped. There are opportunities for new efforts in advanced synthetic approaches to complex hydrogel nanomaterials, both in colloid synthesis (e.g., size and shape control) and in new chemoligation methods for controlled bioconjugate synthesis. The rational design of multifunctional architectures will be enabled by such efforts, thereby allowing the improvement of current applications areas, as well as the implementation of hydrogels in new arenas. In the case of core/shell particles reported by our group and others, the range of potential applications in which such materials can be applied is just beginning to be uncovered. Early studies of the detailed structure/function relationships in hydrogel particles are now leading to the design of primitive applications-oriented nanomaterials. These proof-of-concept studies can then feed back into the synthetic labs and provide guidance for the synthesis of the second generation of materials. In parallel, it will become increasingly important to perform detailed studies of cytotoxicity, immunogenicity, and pharmacokinetics, if these materials are to be employed in biotech applications. Finally, ground level integration between chemists, biochemists, engineers, and clinicians is desired to enable the design, synthesis, and testing of structures that are truly applicable in clinical applications such as drug delivery devices, implantable biomaterials, biosensors/assays, and targeted chemotherapeutic formulations.

REFERENCES

1. Gehrke SH. Synthesis, equilibrium swelling, kinetics, permeability and applications of environmentally responsive gels. *Adv Polym Sci* 1993;110:82.
2. Hoffman AS. Hydrogels for biomedical applications. *Adv Drug Deliv Rev* 2002;54:3–12.
3. Yeomans K. Hydrogels—very versatile materials. *Chem Rev* 2000;10:2–5.
4. Hennink WE and van Nostrum CF. Novel crosslinking methods to design hydrogels. *Adv Drug Deliv Rev* 2002;54:13–36.
5. Dušek K and Prins W. Structure and elasticity of non-crystalline polymer networks. *Fortschritte der Hochpolymeren-Forschung* 1969;6:1–102.
6. Li Y and Tanaka T. Study of the universality class of the gel network system. *J Chem Phys* 1989;90:5161–5166.
7. Li Y and Tanaka T. Kinetics of swelling and shrinking of gels. *J Chem Phys* 1990; 92:1365–1371.
8. Tanaka T. Kinetics of phase transition in polymer gels. *Physica A* 1986;140A: 261–268.
9. Gan D and Lyon LA. Tunable swelling kinetics in core-shell hydrogel nanoparticles. *J Am Chem Soc* 2001;123:7511–7517.

10. Jones CD and Lyon LA. Synthesis and characterization of multiresponsive core-shell microgels. *Macromolecules* 2000;33:8301–8306.
11. Staudinger H and Husemann E. *Ber Dtsch Chem Ges* 1935;68:1618.
12. Pelton RH. Temperature-sensitive aqueous microgels. *Adv Colloid Interface Sci* 2000;85:1–33.
13. Saunders BR and Vincent B. Microgel particles as model colloids: theory, properties and applications. *Adv Colloid Interface Sci* 1999;80:1–25.
14. Tanaka T. Collapse of gels and the critical endpoint. *Phys Rev Lett* 1978;40: 820–823.
15. Dusek K and Patterson K. Transition on swollen polymer networks induced by intramolecular condensation. *Polym Sci Polym Phys Ed* 1968;6:1209–1216.
16. Moselhy J, Wu XY, Nicholov R, Kodaria K. *In vitro* studies of the interaction of poly(NIPAM/MAA) nanoparticles with proteins and cells. *J Biomater Sci Polym Ed* 2000;11:123–147.
17. Duracher D, Sauzedde F, Elaissari A, Perrin A, Pichot C. Cationic amino-containing *n*-isopropylacrylamide–styrene copolymer latex particles: 1. Particle size and morphology vs. polymerization process. *Colloid Polym Sci* 1998;276:219–231.
18. Duracher D, Sauzedde F, Elaissari A, Pichot C, Nabzar L. Cationic amino-containing *n*-isopropyl-acrylamide–styrene copolymer particles: 2. Surface and colloidal characteristics. *Colloid Polym Sci* 1998;276:920–929.
19. Snowden MJ, Chowdhry BZ, Vincent B, Morris GE. Colloidal copolymer microgels of *n*-isopropylacrylamide and acrylic acid: pH, ionic strength and temperature effects. *J Chem Soc Faraday Trans.* 1996;92:5013–5016.
20. Sershen SR, Westcott SL, Halas NJ, West JL. Temperature-sensitive polymer–nanoshell composites for photothermally modulated drug delivery. *J Biomed Mater Res* 2000;51:293–298.
21. Sershen SR, Westcott SL, Halas NJ, West JL. Independent optically addressable nanoparticle-polymer optomechanical composites. *Appl Phys Lett* 2002;80:4609–4611.
22. Sershen SR, Westcott SL, West JL, Halas NJ. An opto-mechanical nanoshell–polymer composite. *Appl Phys B* 2001;73:379–381.
23. Suzuki A, Ishii T, Maruyama Y. Optical switching in polymer gels. *J Appl Phys* 1996;80:131–136.
24. Suzuki A and Tanaka T. Phase-transition in polymer gels induced by visible-light. *Nature* 1990;346:345–347.
25. Tanaka T, Nishio I, Sun ST, Ueno-Nishio S. Collapse of gels in an electric field. *Science* 1982;218:467–469.
26. Miyata T, Asami N, Uragami T. A reversibly antigen-responsive hydrogel. *Nature* 1999;399:766–769.
27. Ogawa K, Nakayama A, Kokufuta E. Preparation and characterization of thermo-sensitive polyampholyte nanogels. *Langmuir* 2003;19:3178–3184.
28. Ogawa K, Wang B, Kokufuta E. Enzyme-regulated microgel collapse for controlled membrane permeability. *Langmuir* 2001;17:4704–4707.
29. Ogawa Y, Ogawa K, Wang B, Kokufuta E. A biochemo-mechanical system consisting of polyampholyte gels with coimmobilized glucose oxidase and urease. *Langmuir* 2001;17:2670–2674.

30. Kim J, Nayak S, Lyon LA. Bioresponsive hydrogel microlenses. *J Am Chem Soc* 2005;127:9588–9592.
31. Schild HG. Poly(*n*-isopropylacrylamide): experiment, theory and application. *Prog Polym Sci* 1992;17:163–249.
32. Heskins M and Guillet JE. Solution properties of poly(*n*-isopropylacrylamide). *J Macromol Sci Chem* 1968;A2:1441–1455.
33. Berndt I and Richtering W. Doubly temperature sensitive core–shell microgels. *Macromolecules* 2003;36:8780–8785.
34. Berndt I, Pedersen JS, Richtering W. Structure of multiresponsive “intelligent” core–shell microgels. *J Am Chem Soc* 2005;127:9372–9373.
35. Matsumoto A, Ikeda S, Harada A, Kataoka K. Glucose-responsive polymer bearing a novel phenylborate derivative as a glucose-sensing moiety operating at physiological pH conditions. *Biomacromolecules* 2003;4:1410–1416.
36. Duracher D, Elaissari A, Mallet F, Pichot C. Preparation of thermosensitive latexes by copolymerization of *n*-isopropylmethacrylamide with a chelating monomer. *Macromol Symp* 2000;150:297–303.
37. Duracher D, Elaissari A, Pichot C. Characterization of cross-linked poly(*n*-isopropylmethacrylamide) microgel latexes. *Colloid Polym Sci* 1999;277:905–913.
38. Duracher D, Elaissari A, Pichot C. Preparation of poly(*n*-isopropylmethacrylamide) latexes kinetic studies and characterization. *J Polym Sci A Polym Chem* 1999;37:1823–1837.
39. Pelton R. Temperature-sensitive aqueous microgels. *Adv Colloid Interface Sci* 2000;85:1–33.
40. Daly E and Saunders BR. Temperature-dependent electrophoretic mobility and hydrodynamic radius measurements of poly(*n*-isopropylacrylamide) microgel particles: structural insights. *Phys Chem Chem Phys* 2000;2:3187–3193.
41. Ohshima H, et al. Electrophoretic mobility of latex-particles covered with temperature-sensitive hydrogel layers. *J Colloid Interface Sci* 1993;159:512–514.
42. Debord JD and Lyon LA. Thermoresponsive photonic crystals. *J Phys Chem B* 2000;104:6327–6331.
43. Senff H and Richtering W. Temperature sensitive microgel suspensions colloidal phase behavior and rheology of soft spheres. *J Chem Phys* 1999;111:1705–1711.
44. Hu Z, Lu X, Gao J. Hydrogel opals. *Adv Mater* 2001;13:1708–1712.
45. Hellweg T, Dewhurst CD, Bruckner E, Kratz K, Eimer W. Colloidal crystals made of poly(*n*-isopropylacrylamide) microgel particles. *Colloid Polym Sci* 2000;278:972–978.
46. Wu C and Zhou S. Volume phase transition of swollen gels: discontinuous or continuous? *Macromolecules* 1997;30:574–576.
47. Wu C and Zhou S. Light scattering study of spherical poly(*n*-isopropylacrylamide) microgels. *J Macromol Sci Phys* 1997;B36:345–355.
48. Yi YD, Oh KS, Bae YC. Phase transition of submicron sized *n*-alkylacrylamide-derivative copolymer particles: applicability of photon correlation spectroscopy. *Polymer* 1997;38:3471–3476.
49. Varga I, et al. Effect of cross-link density on the internal structure of poly(*n*-isopropylacrylamide) microgels. *J Phys Chem B* 2001;105:9071–9076.
50. Gan D and Lyon LA. Interfacial nonradiative energy transfer in responsive core–shell hydrogel nanoparticles. *J Am Chem Soc* 2001;123:8203–8209.

51. Guillermo A, et al. NMR investigations into heterogeneous structures of thermosensitive microgel particles. *J Polym Sci Part B Polym Phys* 2000;38:889–898.
52. Saunders BR. On the structure of poly(*n*-isopropylacrylamide) microgel particles. *Langmuir* 2004;20:3925–3932.
53. Woodward NC, et al. Calorimetric investigation of the influence of cross-linker concentration on the volume phase transition of poly(*n*-isopropylacrylamide) colloidal microgels. *Langmuir* 2003;19:3202–3211.
54. Senff H and Richtering W. Influence of crosslink density on rheological properties of temperature-sensitive microgel suspensions. *Colloid Polym Sci* 2000;278:830–840.
55. Senff H, Richtering W, Norhausen C, Weiss A, Ballauff M. Rheology of a temperature sensitive core–shell latex. *Langmuir* 1999;15:102–106.
56. Meyer S and Richtering W. Influence of polymerization conditions on the structure of temperature-sensitive poly(*n*-isopropylacrylamide) microgels. *Macromolecules* 2005;38:1517–1519.
57. Stieger M, Richtering W, Pedersen JS, Lindner P. Small-angle neutron scattering study of structural changes in temperature sensitive microgel colloids. *J Chem Phys* 2004;120:6197–6206.
58. Wu X, Pelton RH, Hamielec AE, Woods DR, McPhee W. The kinetics of poly(*n*-isopropylacrylamide) microgel latex formation. *Colloid Polym Sci* 1994;272:467–477.
59. Hoare T and Pelton R. Functional group distribution in carboxylic acid containing poly(*n*-isopropylacrylamide) microgels. *Langmuir* 2004;20:2123–2133.
60. Dingenouts N, et al. Analysis of thermosensitive core–shell colloids by small-angle neutron scattering including contrast variation. *Phys Chem Phys* 2001;3:1169–1174.
61. Xiao XC, Chu LY, Chen WM, Wang S, Xie R. Preparation of submicrometer-sized monodispersed thermoresponsive core–shell hydrogel microspheres. *Langmuir* 2004;20:5247–5253.
62. Zha L, Zhang Y, Yang W, Fu S. Monodisperse temperature-sensitive microcontainers. *Adv Mater* 2002;14:1090–1092.
63. Kim JH and Lee TR. Thermo- and pH-responsive hydrogel-coated gold nanoparticles. *Chem Mater* 2004;16:3647–3651.
64. Jones CD and Lyon LA. Dependence of shell thickness on core compression in acrylic acid modified poly(*n*-isopropylacrylamide) core/shell microgels. *Langmuir* 2003;19:4544–4547.
65. Jones CD and Lyon LA. Shell-restricted swelling and core compression in poly(*n*-isopropylacrylamide) core-shell microgels. *Macromolecules* 2003;36:1988–1993.
66. Gan D and Lyon LA. Fluorescence nonradiative energy transfer analysis of crosslinker heterogeneity in core–shell hydrogel nanoparticles. *Anal Chim Acta* 2003;496:53–63.
67. Jones CD, McGrath JG, Lyon LA. Characterization of cyanine dye-labeled poly(*n*-isopropylacrylamide) core/shell microgels using fluorescence resonance energy transfer. *J Phys Chem B* 2004;108:12652–12657.
68. Nayak S, Gan D, Serpe MJ, Lyon LA. Hollow thermoresponsive microgels. *Small* 2005;1:416–421.

69. Berndt I, Pedersen JS, Lindner P, Richtering W. Influence of shell thickness and cross-link density on the structure of temperature-sensitive poly-*n*-isopropylacrylamide–poly-*n*-isopropylmethacrylamide core–shell microgels investigated by small-angle neutron scattering. *Langmuir* 2006;22:459–468.
70. Berndt I, Pedersen JS, Richtering W. Temperature-sensitive core–shell microgel particles with dense shell. *Angew Chem Int Ed* 2006;45:1737–1741.
71. Berndt I, Popescu C, Wortmann F-J, Richtering W. Mechanics versus thermodynamics: swelling in multiple-temperature-sensitive core-shell microgels. *Angew Chem Int Ed* 2006;45:1081–1085.
72. Wooley KL. From dendrimers to knedel-like structures. *Chem-Eur J* 1997;3: 1397–1399.
73. Zhu PW and Napper DH. Aggregation of block copolymer microgels of poly-*(n*-isopropylacrylamide) and poly(ethylene glycol). *Macromolecules* 1999;32: 2068–2070.
74. Zhu PW and Napper DH. Effect of heating rate on nanoparticle formation of poly(*n*-isopropylacrylamide)–poly(ethylene glycol) block copolymer microgels. *Langmuir* 2000;16:8543–8545.
75. Thurmond KB, II Kowalewski T, Wooley KL. Water-soluble knedel-like structures: the preparation of shell-cross-linked small particles. *J Am Chem Soc* 1996;118:7239–7240.
76. Thurmond KB, II Kowalewski T, Wooley KL. Shell cross-linked knedels: a synthetic study of the factors affecting the dimensions and properties of amphiphilic core–shell nanospheres. *J Am Chem Soc* 1997;119:6656–6665.
77. Huang H, Remsen EE, Kowalewski T, Wooley KL. Nanocages derived from shell cross-linked micelle templates. *J Am Chem Soc* 1999;121:3805–3806.
78. Huang H, Wooley KL, Remsen EE. Amphiphilic core–shell nanospheres obtained by intramicellar shell crosslinking of polymer micelles with poly(ethylene oxide) linkers. *Chem Commun* 1998;1415–1416.
79. Remsen EE, Thurmond KB, II Wooley KL. Solution and surface charge properties of shell cross-linked knedel nanoparticles. *Macromolecules* 1999;32: 3685–3689.
80. Zhang Q, Clark CG Jr., Wang M, Remsen EE, Wooley KL. Thermally-induced (re)shaping of core–shell nanocrystalline particles. *Nano Lett* 2002;2:1051–1054.
81. Zhang Q, Remsen EE, Wooley KL. Shell cross-linked nanoparticles containing hydrolytically degradable, crystalline core domains. *J Am Chem Soc* 2000;122: 3642–3651.
82. Wooley KL. Shell crosslinked polymer assemblies: nanoscale constructs inspired from biological systems. *J Polym Sci A* 2000;38:1397–1407.
83. Liu J, Zhang Q, Remsen EE, Wooley KL. Nanostructured materials designed for cell binding and transduction. *Biomacromolecules* 2001;2:362–368.
84. Ma Q, Remsen EE, Clark CG Jr., Kowalewski T, Wooley KL. Chemically induced supramolecular reorganization of triblock copolymer assemblies: trapping of intermediate states via a shell-crosslinking methodology. *Proc Natl Acad Sci USA* 2002;99:5058–5063.

85. Ma Q, Remsen EE, Kowalewski T, Schaefer J, Wooley KL. Environmentally-responsive, entirely hydrophilic, shell cross-linked (sck) nanoparticles. *Nano Lett* 2001;1:651–655.
86. Ma Q, Remsen EE, Kowalewski T, Wooley KL. Two-dimensional, shell-cross-linked nanoparticle arrays. *J Am Chem Soc* 2001;123:4627–4628.
87. Shanmugananda Murthy K, Ma Q, Clark CG Jr., Remsen EE, Wooley KL. Fundamental design aspects of amphiphilic shell-crosslinked nanoparticles for controlled release applications. *Chem Commun* 2001;773–774.
88. Huang H, Kowalewski T, Remsen EE, Gertzmann R, Wooley KL. Hydrogel-coated glassy nanospheres: a novel method for the synthesis of shell crosslinked knedels. *J Am Chem Soc* 1997;119:11653–11659.
89. Akiyoshi K, Deguchi S, Moriguchi N, Yamaguchi S, Sunamoto J. Self-aggregates of hydrophobized polysaccharides in water. Formation and characteristics of nanoparticles. *Macromolecules* 1993;26:3062–3068.
90. Akiyoshi K, et al. Self-assembled hydrogel nanoparticle of cholesterol-bearing pullulan as a carrier of protein drugs: complexation and stabilization of insulin. *J Control Release* 1998;54:313–320.
91. Akiyoshi K, Nishikawa T, Shichibe S, Sunamoto J. Stabilization of insulin upon supramolecular complexation with hydrophobized polysaccharide nanoparticle. *Chem Lett* 1995;24:707–708.
92. Akiyoshi K, Sasaki Y, Sunamoto J. Molecular chaperone-like activity of hydrogel nanoparticles of hydrophobized pullulan: thermal stabilization with refolding of carbonic anhydrase b. *Bioconjugate Chem* 1999;10:321–324.
93. Kuroda K, Fujimoto K, Sunamoto J, Akiyoshi K. Hierarchical self-assembly of hydrophobically modified pullulan in water: gelation by networks of nanoparticles. *Langmuir* 2002;18:3780–3786.
94. Becker ML, Liu J, Wooley KL. Functionalized micellar assemblies prepared via block copolymers synthesized by living free radical polymerization upon peptide-loaded resins. *Biomacromolecules* 2005;6:220–228.
95. Joralemon MJ, Smith NL, Holowka D, Baird B, Wooley KL. Antigen-decorated shell crosslinked nanoparticles: synthesis, characterization, and antibody interactions. *Bioconjugate Chem* 2005;16:1246–1256.
96. Marcucci F and Lefoulon F. Active targeting with particulate drug carriers in tumor therapy: fundamentals and recent progress. *Drug Discov Today* 2004;9:219–228.
97. Barratt G. Colloidal drug carriers: achievements and perspectives. *Cell Mol Life Sci* 2003;60:21–37.
98. Hirose S, Muller BG, Mulligan RC, Langer R. Plasmid DNA encapsulation and release from solvent diffusion nanospheres. *J Control Release* 2001;70:231–242.
99. Mao HQ, et al. Chitosan–DNA nanoparticles as gene carriers: synthesis, characterization and transfection efficiency. *J Control Release* 2001;70:399–421.
100. Kim IS, Jeong YI, Kim SH. Self-assembled hydrogel nanoparticles composed of dextran and poly(ethylene glycol) macromer. *Int J Pharm* 2000;205:109–116.
101. Na K and Bae YH. Self-assembled hydrogel nanoparticles responsive to tumor extracellular pH from pullulan derivative/sulfonamide conjugate:

- characterization, aggregation, and adriamycin release *in vitro*. *Pharm Res* 2002;19:681–688.
102. Kavimandan NJ, Losi E, Peppas NA. Novel delivery system based on complexation hydrogels as delivery vehicles for insulin–transferrin conjugates. *Biomaterials* 2006;27:3846–3854.
 103. Hsiue G-H, Hsu S-h, Yang C-C, Lee S-H, Yang IK. Preparation of controlled release ophthalmic drops, for glaucoma therapy using thermosensitive poly-*n*-isopropylacrylamide. *Biomaterials* 2001;23:457–462.
 104. Ghosh PK. Hydrophilic polymeric nanoparticles as drug carriers. *Indian J Biochem Bio Phys* 2000;37:273–282.
 105. Gaur U, et al. Biodistribution of fluoresceinated dextran using novel nanoparticles evading reticuloendothelial system. *Int J Pharm* 2000;202:1–10.
 106. Nayak S, Lee H, Chmielewski J, Lyon LA. Folate-mediated cell targeting and cytotoxicity using thermoresponsive microgels. *J Am Chem Soc* 2004;126:10258–10259.
 107. Choi SH, Yoon JJ, Park TG. Galactosylated poly(*n*-isopropylacrylamide) hydrogel submicrometer particles for specific cellular uptake within hepatocytes. *J Colloid Interface Sci* 2002;251:57–63.
 108. Becker ML, Remsen EE, Pan D, Wooley KL. Peptide-derivatized shell-crosslinked nanoparticles. 1. Synthesis and characterization. *Bioconjugate Chem* 2004;15:699–709.
 109. Becker ML, Bailey LO, Wooley KL. Peptide-derivatized shell-crosslinked nanoparticles. 2. Biocompatibility evaluation. *Bioconjugate Chem* 2004;15:710–717.
 110. Pan D, Turner JL, Wooley KL. Folic acid-conjugated nanostructured materials designed for cancer cell targeting. *Chem Commun* 2003;2400–2401.
 111. Das M, Mardyani S, Chan WCW, Kumacheva E. Biofunctionalized pH-responsive microgels for cancer cell targeting: rational design. *Adv Mater (Weinheim, Germany)*, 2006;18:80–83.
 112. Jana SS, et al. Targeted cytosolic delivery of hydrogel nanoparticles into HepG2 cells through engineered Sendai viral envelopes. *FEBS Lett* 2002;515:184–188.
 113. Na K, Park KH, Kim SW, Bae YH. Self-assembled hydrogel nanoparticles from curdlan derivatives: characterization, anti-cancer drug release and interaction with a hepatoma cell line (HepG2). *J Control Release* 2000;69:225–236.
 114. Mitra S, Gaur U, Ghosh PC, Maitra AN. Tumor targeted delivery of encapsulated dextran–doxorubicin conjugate using chitosan nanoparticles as carrier. *J Control Release* 2001;74:317–323.
 115. Farokhzad OC, et al. Targeted nanoparticle-aptamer bioconjugates for cancer chemotherapy *in vivo*. *Proc Nat Acad Sci USA* 2006;103:6315–6320.
 116. Kim J, Singh N, Lyon LA. Label-free biosensing with hydrogel microlenses. *Angew Chem Int Ed* 2006;45:1446–1449.
 117. Kawaguchi H, et al. Versatility of thermosensitive particles. *Macromol Symp* 2000;151:591–598.
 118. Elaissari A, et al. Hydrophilic and cationic latex particles for the specific extraction of nucleic acids. *J Biomater Sci Polym Ed* 1999;10:403–420.

119. Kondo A, Kaneko T, Higashitani K. Development and application of thermo-sensitive immunospheres for antibody purification. *Biotechnol Bioeng* 1994;44:1–6.
120. Kondo A, Kamura H, Higashitani K. Development and application of thermosensitive magnetic immunospheres for antibody purification. *Appl Microbiol Biotechnol* 1994;41:99–105.
121. Ye L, Cormack PAG, Mosbach K. Molecularly imprinted monodisperse microspheres for competitive radioassay. *Anal Commun*. 1999;36:35–38.
122. Ehrick JD, et al. Genetically engineered protein in hydrogels tailors stimuli-responsive characteristics. *Nat Mater* 2005;4:298–302.
123. Miyata T, Jige M, Nakaminami T, Uragami T. Tumor marker-responsive behavior of gels prepared by biomolecular imprinting. *Proc Nat Acad Sci USA* 2006;103:1190–1193.
124. Boretos JW and Eden M. *Contemporary Biomaterials, Material and Host Response, Clinical Applications, New Technology and Legal Aspects*. Park Ridge, New Jersey: Noyes Publications; 1984. p 232.
125. Kawaguchi H. Functional polymer microspheres. *Prog Polym Sci* 2000;25: 1171–1210.
126. Kawaguchi H, Fujimoto K, Mizuhara Y. Hydrogel microspheres. 3. Temperature-dependent adsorption of proteins on poly-*n*-isopropylacrylamide hydrogel microspheres. *Colloid Polym Sci* 1992;270:53–57.
127. Shiroya T, Tamura N, Yasui M, Fujimoto K, Kawaguchi H. Enzyme immobilization on thermosensitive hydrogel microspheres. *Colloid Surface B* 1995;4:267–274.
128. Duracher D, Elaissari A, Mallet F, Pichot C. Adsorption of modified HIV-1 capsid p24 protein onto thermosensitive and cationic core-shell poly(styrene)-poly(*n*-isopropylacrylamide) particles. *Langmuir* 2000;16:9002–9008.
129. Urakami Y, Kasuya Y, Fujimoto K, Miyamoto M, Kawaguchi H. Phagocytosis of microspheres with modified surfaces. *Colloid Surface B* 1994;3:183–190.
130. Kimhi O and Bianco-Peled H. Microcalorimetry study of the interactions between poly(*n*-isopropylacrylamide) microgels and amino acids. *Langmuir* 2002;18:8587–8592.
131. Gan D and Lyon LA. Synthesis and protein adsorption resistance of peg-modified poly(*n*-isopropylacrylamide) core/shell microgels. *Macromolecules* 2002;35:9634–9639.
132. Plunkett KN, Berkowski KL, Moore JS. Chymotrypsin responsive hydrogel: application of a disulfide exchange protocol for the preparation of methacrylamide containing peptides. *Biomacromolecules* 2005;6:632–637.
133. Kim S and Healy KE. Synthesis and characterization of injectable poly(*n*-isopropylacrylamide-co-acrylic acid) hydrogels with proteolytically degradable cross-links. *Biomacromolecules* 2003;4:1214–1223.
134. Nayak S and Lyon LA. Ligand-functionalized core/shell microgels with permselective shells. *Angew Chem Int Ed* 2004;43:6706–6709.

Nanotechnology and Drug Delivery

XIAOJUN YU, CHANDRA M. VALMIKINATHAN, AMANDA ROGERS,
and JUNPING WANG

5.1 INTRODUCTION

With the advent of science and technology, the ability to understand biology and medicine has improved tremendously. As almost all biological components or entities have structures that originate at the submicron level, understanding and modifications at this level could effect the final performance of such systems. The simple word “nano” has changed the way that people look at the environment around them. Nanotechnology is a multidisciplinary scientific field that applies engineering and manufacturing principles to the design, synthesis, characterization, and application of materials and devices on nanoscale [1, 2].

In the last several decades, nanotechnology has been developed in several areas, which include drug delivery, bioMEMS, tissue engineering, biosensors, microfluidics, microarrays, and bioimaging [3]. The nanotechnology-based drug delivery system has emerged to be the mainstream research among all the applications because it offers an extraordinary opportunity to make significant advances in medical diagnosis and treatment. Corporate investment on nanotechnology for drug delivery and medical diagnostics is increasing year by year and nanotechnology-based drug delivery has already been commercialized by a lot of companies.

Nanotechnology-based drug delivery is generating continuing interest among researchers at the federal government agencies as well as private industrial sectors. According to statistics published in 2002 [1], several foundations and government agencies like NIH, NSF, and NASA have increased funding new research ideas and interests in the field of nanotechnology-based drug delivery systems for targeted and controlled release of therapeutic elements. The field of

nanotechnology-based drug delivery system that started as a small division in 2001 by National Nanotechnology Initiative with funding of \$116 million is expected to reach \$82 billion by the end of 2007 [4] and is expected to grow stronger and attract further investments [5]. On the industrial side, pharmaceutical companies have started to invest into projects that modify existent delivery systems. The demand for drug delivery systems in the United States has grown rapidly and bounds to create a niche for itself in the market for innovative technologies that will change the face of science and technology. There are around 150 companies that have active research divisions working on targeted controlled drug delivery and this number is bound to increase in the near future owing to tremendous developments in the field of medicine and increased understanding of the human anatomy and diseases associated with it [6].

Traditional nanotechnology for drug delivery mainly referred to those nanoscale vehicles which were mainly utilized to improve the drug bioavailability and minimize the side effects of the drug by holding or transporting the drug molecules to the desired locations. Recently, new nanoscale platforms have been under development for not only therapeutic purpose but also diagnostic applications [7]. In addition to the traditional function of drug delivery, these nanotools have been utilized for medical diagnostics via fluorescent imaging [8] or magnetic resonance imaging (MRI) [9], as well as for some new therapeutic strategies such as the photothermal therapeutics in clinical oncology [10]. Investigations on multifunctional nanoparticles with the combination of therapeutic, targeting, and imaging functions for advanced drug delivery systems have drawn more and more attention from current researchers [11–13].

5.2 ADVANTAGES OF NANOSTRUCTURED DELIVERY SYSTEMS

Once a stable and effective active pharmaceutical ingredient (API) has been identified, there are several ways to administer it into the human body. The most common ways of administration are oral, transdermal, and nasal delivery methods [14]. The oral delivery pathway is the easiest and most sought-after delivery method but has its own disadvantages with the current designs. The limitations include reduced bioavailability and ineffective way to deliver proteins and peptides due to the effects of pH in the digestive system, the effect of passage through various organs, and the effects of stress from the intestines [15]. The nasal and transdermal methods cause patient discomfort and also have reduced efficiency and availability in the system [16]. Other challenges involved in conventional drug delivery systems include difficulties for providing reproducible amounts of release per fixed time frame, poor solubility of drugs, and difficulties for targeting specific regions without affecting healthy tissues [6]. Nanotechnology-based drug delivery systems have many advantages and provide the insight for solving the problems associated with conventional drug delivery systems.

5.2.1 Localized and Targeted Delivery

Nanotechnology-based drug delivery systems can be controlled to deliver drugs to specific sites and target drugs to certain cells only, without affecting neighboring normal cells [17, 18]. Several external stimuli such as ultrasound and magnetic field have been able to influence drug targeting in nanocarriers for tumor eradication. Several biologically relevant molecules such as transferrin [19], folate [20], and antibodies [21] play important roles in internal targeting and internalization of drugs. The localized and targeted delivery greatly helps in reducing systemic toxicity and largely increases effectiveness of the therapeutic ingredients [6].

5.2.2 Controlled Delivery

The nanotechnology-based drug delivery platform provides researchers with options to deliver highly toxic drug intermediates and complexes, as well as DNA and viral vectors at optimum dosages at controlled intervals of time [16]. Release profile from materials largely depends upon the nature of the delivery system. By choosing the correct type of materials for preparation of nanoparticles, the release profile can be modified [22]. In addition, nanotechnology opens the door to modify the property of materials at the atomic scale leading to creation of materials with varied delivery rates that are extremely controllable [23].

5.2.3 Enhanced Circulation Time and Biodistribution

Nanocarriers may increase the circulation time of drugs within the body. Particle size is intrinsically related to rate of clearance from the circulation. Larger particles tend to be removed much faster than smaller particles. In addition to increased circulation time, nanoparticles also exhibit enhanced biodistribution over their larger counterparts. When administered to test animals, larger particles tend to be found in high concentrations in the spleen and liver rather than in the target locations. Smaller particles are more likely to be taken up by other cells within the body, including target cells [24].

5.2.4 Drug Solubility

Nanotechnology allows for the delivery of all types of drugs. Particularly, it has been especially effective for the delivery of drugs exhibiting poor solubility in water to living tissues. Micelles, which are typically assembled from amphiphilic materials, possess a hydrophobic core surrounded by a hydrophilic outer layer, known as a corona. Hydrophobic molecules may be easily encapsulated in the microenvironment of the core. The hydrophilic corona facilitates travel of the nanoparticles through water-based solutions. This

allows for increased delivery of hydrophobic compounds in aqueous environments of the human body [25–27].

5.2.5 Intracellular Drug Delivery

Intracellular drug delivery helps in reducing toxicity and improving dosage efficiency [28]. Hydrophobic drug carriers at the nanoscale are able to easily pass the cell membrane [29]. Endocytosis in cells is limited by particle size and targeting issues. The maximum size of a material that can penetrate the cell membrane is about 500 nm. The internalization of nanomaterials into the cell is also affected by the ability of the material to be activated and targeted to specific cell organelles such as the nucleus or the mitochondria [30].

The delivery of hydrophilic and genetic components into the cell poses the greatest challenge. The common methods for cellular internalization of the nanoparticles include direct diffusion through the cell membrane owing to concentration gradients, crossing the voltage-gated channels and receptor-mediated endocytosis. Lipid- and micelle-based delivery systems provide various opportunities to encapsulate or bind to specific hydrophilic and hydrophobic constituents, hence producing nanoparticles that can be modified on the surface to cause endocytosis [30].

5.2.6 Ability to Cross Biological Membranes

The difficulties in crossing the biological membranes like the blood–brain barrier (BBB), gastrointestinal system, and the vascular endothelial system have posed great challenges for drug delivery. Conventional delivery methods such as intravenous delivery, oral delivery, or transdermal delivery of microparticles have failed in regions that need to penetrate the BBB or the gastrointestinal systems owing to various physiological environmental aspects including the pH differences and the size properties. Nanotechnology-based drug delivery devices have the ability to cross biological membranes when tailored with appropriate properties. Metallic nanomaterials, polymeric drug carriers, and lipid-based delivery systems have provided the researchers with opportunities to drive the drug through biological membranes.

5.2.7 Enhanced Surface Areas

It has been a long known fact that size reduction per unit volume of material increases the surface area of materials. This fundamental concept is valid for drug delivery technologies employing nanoscale entities. As compared to the conventional drug delivery systems, nanotechnology-based drug delivery systems have improved surface areas. This increased surface area per unit volume leads to improvement on loading and releasing efficiency of drugs.

5.3 ACTIVATION AND TARGETING OF NANOTECHNOLOGY-BASED DRUG DELIVERY SYSTEMS (EXTERNALLY AND INTERNALLY)

5.3.1 Activation and Targeting Through PhysicoChemical Stimuli

5.3.1.1 pH-Sensitive Carriers pH-sensitive carriers are of particular interest in chemotherapy and for the delivery of molecules that will be delivered into cells via an endosomal mechanism. This is due to the fact that tumor sites and endosomes used in intracellular trafficking tend to have lower pH than normal interstitial fluids [31]. Thus, pH-sensitive delivery systems are ideal for intracellular delivery of drugs, genes, proteins, and other compounds [20, 31–36].

Some pH-responsive delivery systems depend on interactions between drugs and the materials from which the delivery systems are made. These systems depend on drug/carrier conjugation, including the formation of acid-cleavable bonds between drug and carrier molecules. For instance, Bae et al. [37] have reported the formation of polymeric micelles for adriamycin (ADR) delivery. ADR was conjugated to a polymeric backbone via an acid-labile hydrazone bond. Significant and rapid ADR release was exhibited at low pH (pH 3.0), whereas release was much slower at pH 7.4 [37]. Similar studies using doxorubicin (DOX) found that doxorubicin release from polymeric micelles was also affected by acid-cleavable bonds between the polymer and the drug. Drug release was not found to be minimal at pH 7.4, whereas considerable release was exhibited at pH 5.0 [31, 38].

Drug–drug interactions that are pH sensitive may also play a role in modulating drug release from pH-responsive delivery systems. DOX-loaded particles prepared by Kataoka et al. [38], displayed a drug release that depended upon conjugation not only between drug and polymer molecules but also between the drug molecules themselves. It was found that some of the DOX encapsulated in polymeric micelles actually formed a dimer referred to as DOX–DOX via the formation of an azomethine bond. Release was, in part, dependent on the type of DOX being released. DOX monomer was released preferentially in the initial release phase, whereas DOX–DOX was found to play a role in the sustained release of the drug. DOX–DOX also showed a pH-dependent release. Under acidic conditions, the azomethine bond in DOX–DOX may be cleaved to release additional DOX monomer. Thus, the formation of DOX–DOX dimers via acid-labile bonds may play a role in the pH sensitivity of DOX-loaded polymeric micelles [38].

Another effective way to design a pH-dependent delivery system involves exploiting the properties of the materials from which the delivery systems are made. Amphiphilic and titratable lipids and polymers have been examined extensively for the creation of pH-responsive delivery systems.

pH-sensitive liposomes have been prepared using combinations of cationic and anionic lipids in conjunction with titratable weakly basic (cationic) or weakly acidic (anionic) amphiphiles. Typically, these liposomes are negatively

charged at neutral pH and stable in neutral or basic environments. As pH is decreased, the amphiphilic component of the bilayer is protonated until the bilayer is no longer charged. This results in a loss of electrostatic stabilization of the liposomes, causing them to aggregate and fuse with nearby membranes. The pH at which liposomes are destabilized depends on factors including the anionic to cationic lipid ratio and the pK_a of the titratable component. Shi et al. [32] have combined the use of pH-sensitive liposomes with antibody/antigen targeting methods. Folate receptor targeting ligands were added to pH-sensitive liposomes. These systems were investigated for their ability to deliver both drugs and genes to tumor sites and showed promise as vehicles for intracellular drug and gene trafficking [32].

pH-responsive polymers typically contain ionizable components that are capable of acting as proton donors or acceptors. Weak polyacids like poly (acrylic acid) (PAAc) are proton acceptors at low pH, and proton releasers at neutral pH, while the opposite is true of weak polybases like poly (4-vinylpyridine) [39]. Nanoparticulate drug delivery systems that are pH responsive typically incorporate weak polyacids or polybases in conjunction with hydrophobic components. When the ionizable components are charged, electrostatic interactions keep the nanoparticles intact and separate in solution. As pH is modulated, the charge on the ionizable component is modified until hydrophobic interactions are more significant than electrostatic ones. When this occurs, the nanoparticles tend to aggregate and fuse with one another and with nearby membranes. The deformation of the nanoparticle matrix results in release of molecules being carried therein [33, 35, 39].

One of the most popular applications for pH-sensitive polymeric nanoparticles is delivery of cancer therapy to tumor sites. For instance, 5-fluorouracil (5-FU)-loaded pH-sensitive nanoparticles comprised of pullulan acetate/sulfonamide (PA/SDM) conjugates have been synthesized by Liang et al. [33]. Pullulan acetate is a hydrophobic component whereas SDM is weakly acidic with pH-dependent solubility. 5-FU is a chemotherapy drug that is currently used clinically for cancer treatment. The properties of the PA/SDM components allowed for self-assembly of nanoparticles containing 5-FU. It was found that nanoparticles comprised of PA/SDM conjugates aggregated as pH was decreased from 7.5 to 6.0. The ambient pH in tumors tends to be approximately 6.8. Release studies indicated that drug release was significantly greater at lower pH (6.0 and 6.8) than at higher pH (7.4 and 8.2). The decrease in pH caused the SDM group to deionize, resulting in more hydrophobic behavior and causing structural deformation and aggregation of the nanoparticles. As a result, overall 5-FU release was greater at pH 6.8 (tumor pH) than at pH 7.4 (ambient physiological pH). This study highlights the potential for the use of pH-sensitive carriers for delivery of chemotherapeutic agents to tumors [33].

While most pH-sensitive delivery systems currently under investigation involve release at low pH, some systems have been designed specifically for release at high pH. Meissner et al. [35] have reported the creation of

pH-sensitive nanoparticles for the delivery of tacrolimus, a drug that has been proven effective in the treatment of irritable bowel disease. Nanoparticles were prepared from a pH-sensitive polymer known as Eudragit P-4135F (EP4135F). Unlike the particles previously discussed, these particles were stable at lower pH and released at higher pH. This was due to the pH-dependent degradation rate of the polymer matrix. The polymer matrix was found to disintegrate much more quickly at pH 7.4 than at pH 6.8. This allows for the delivery of drugs to the distal ileum, where the release of tacrolimus is facilitated by the luminal pH [35].

5.3.1.2 Thermally Responsive Carriers Thermoresponsive nanocarriers may be prepared by incorporation of heat-sensitive polymers. Such polymers exhibit a property known as critical solution temperature (CST). At this temperature, a temperature-responsive polymer undergoes a phase transition in solution. Polymers that are water soluble below a certain temperature and phase separate above that temperature are said to have a lower critical solution temperature (LCST). The opposite is true for polymers with a higher. Most applications to drug delivery involve the use of LCST polymers. The general form of such polymers is represented by poly(*N*-substituted acrylamide) and the most popular variety is poly(*N*-isopropylacrylamide) (PNIPAAm). This polymer undergoes a very obvious, reversible phase transition in water at its LCST of approximately 32 °C. Modifications to this polymer have allowed for the modulation of the LCST [39].

Temperature-responsive polymers may be incorporated into drug delivery systems in a variety of fashions. One method of incorporation involves the synthesis of core–shell nanoparticles in which the outermost shell consists of a heat-sensitive polymer. For instance, Cammas et al. [40] have reported the formation of polymeric micelles from amphiphilic block copolymers of *N*-isopropylacrylamide (IPAAm) and styrene. The heat-sensitive IPAAm was used to form the outer core while styrene was used to form the hydrophobic inner core of the micelles. It was found that nanoparticles formed from copolymers of IPAAm with styrene exhibited reversible transition at approximately 32 °C. In other words, the micelles remained intact below the LCST and aggregated to form a turbid solution above the LCST only to disperse into micelles again upon subsequent temperature reduction below the LCST. The hydrophobic agent adriamycin, used in cancer treatment, was incorporated into the micelles without the observation of significant changes in their properties, thereby indicating the potential for the use of such vessels for delivery of hydrophobic drugs [40].

Graft copolymers of PNIPAAm with other polymers have also been investigated for their sensitivity to temperature change. Various graft copolymers can be formed in order to adjust the LCST and the release properties of the resulting nanoparticle systems. Cammas et al. [40] claimed to have prepared poly (IPAAm) copolymers with LCST values as low as 26 and as high as 39 °C. In another report, Chaw et al. [36] have reported the use of

nanoparticles synthesized from cholesteryl end-capped poly(*N*-isopropylacrylamide-co-*N,N*-dimethylacrylamide) [P(NIPAAm-co-DMAAm)] and cholesteryl grafted poly[*N*-isopropylacrylamide-co-*N*-(hydroxymethyl) acrylamide] [P(NIPAAm-co-NHMMAAm)] for the delivery of hydrophobic drugs, including cyclosporine A (CyA) and indomethacin (IND). They found that the presence of hydrophilic NHMMAAm and DMAAm segments increased the LCST of polymer systems [36]. Similarly, copolymers of NIPAAm with methacrylic acid (MAA) prepared by Lo et al. were found to exhibit higher LCST than pure PNIPAAm polymers at neutral pH [34]. Both studies also indicated that, at physiological pH, drug release was greater at temperatures above the LCST [34, 36].

Nanoparticles that are capable of being controlled by multiple external stimuli have also been prepared. Lo et al. [34] have prepared “intelligent” nanoparticles that are both thermal and pH responsive. These nanoparticles were synthesized from poly(D,L-lactide)-*g*-poly(*N*-isopropylacrylamide-co-methacrylic acid) and (PLA-*g*-P(NIPAm-co-MAA)) graft copolymer by dialyzing an organic polymer solution against distilled water. Copolymers of NIPAm with methacrylic acid (MAA) were designed to increase LCST and add pH sensitivity to nanoparticle systems. At neutral pH, the MAA molecules are ionised, thereby preventing aggregation of nanoparticles. The LCST of nanoparticles at neutral pH was shown to be above 37 °C. At lower pH, eventual deionization of the MAA molecules results in decreased LCST and eventual aggregation of nanoparticles. Nanoparticles were tested for the delivery of both hydrophobic and hydrophilic agents, pyrene and 5-fluoroacil, respectively. In both instances, it was found that drug release was controlled by both environmental pH and ambient temperature [34].

5.3.1.3 Photochemically Controlled Delivery System Photochemical technology, named photochemical internalization (PI), was initially reported as a method for enhancing the delivery of macromolecules into cytosol [41, 42]. This method explored the potential use of photosensitizers that localize primarily to the endosomes and lysosomes of cells to rupture endosomes and lysosomes and thereby deliver endocytosed macromolecules into the cytosol when exposure to light. This strategy was developed specifically for drug and gene delivery [43]. In the drug delivery system, with the aid of tumor focused light, the photosensitizer acted as the enhancer for the uptake of hydrophilic anticancer drugs, such as bleomycin that are easily metabolized [44]. This strategy significantly improves the drug bioavailability as well as provides the whole system targeting property, thus enhancing the antitumor effect.

The photosensitizers can also be used for anticancer drugs loaded in actively targeted liposomes [45–47] or polymeric micelles [48] delivered to tumor sites of patients. Since these anticancer agents are light sensitive, they would be kept harmless in light-free states. During treatment, a tumor-focused light is used to induce the photosensitizers eradicating the tumor cells. This method is called photodynamic therapy (PDT).

5.3.1.4 Magnetic Targeted Drug Delivery of Nanocarriers Magnetically induced drug delivery involves encapsulation of magnetic material, usually magnetite (Fe_2O_3) inside a polymer container that has a drug either tagged or trapped. The magnetic particles aid in targeting of the drug to the site and slow degradation of the polymer carrier causes the slow release of the drug [49]. Magnetic targeting and eradication of cancerous tissues can also be performed by increasing temperature of the metallic magnetic nanoparticles once they have been internalized into tissue or cells where a tumor is located [50].

5.3.1.5 Ultrasound-Mediated Drug Delivery and Targeting Ultrasound has for long been a tool in diagnostic medicine and imaging applications. Recently, owing to widespread developments in the field of medicine and engineering, the ultrasound-mediated drug delivery and targeting have been explored. The ability to use ultrasound as a targeting tool has been termed as *Sonophoresis* and this field of science has aided in the delivery of high molecular weight drugs through several barriers, including the skin. Several therapeutic classes of drugs like gene-based drug, chemotherapeutic, and thrombolytic drugs have been successfully delivered across barriers [51]. The common approach is to create a contrast agent that aids in targeting tumor by using a microbubble. These microbubbles are formed by agitation of gases through solutions. Recent developments in technologies enable researchers to make nanobubbles from biologically relevant polymers, lipid bilayers, and gases [52].

5.3.2 Drug Targeting through Targeting Molecules

Targeting molecules may be conjugated onto nanoparticles to actively target them to particular sites for the delivery of their payloads. Many of these molecules are comprised of peptides or peptide fragments. Multiple targeting molecules may be attached to the surface of a nanoparticle in order to increase its chances of coming into contact with a receptor-bearing cell. This is particularly the case when target cells over express surface receptors for certain molecules. Targeting molecules are also valuable in the context of intracellular drug trafficking via receptor-mediated endocytosis [19, 20, 32, 40, 53–58]. Some of the most commonly used targeting molecules include monoclonal antibodies, folate, transferrin, and a category of peptide ligands known as aptamers. This section will discuss their potential applications for drug targeting.

5.3.2.1 Monoclonal Antibodies Over the last decade, extensive studies have been conducted on targeting monoclonal antibodies (mAb) to receptors on the surface of tumor cells. This type of antibody-based therapy could potentially target the tumor cells with little or no impact on normal cells surrounding the tumor [59].

Several research groups have designed bispecific antibodies (BiAbs) [60]. The design of BiAbs was based on the fusion of two independent antibodies with one that binds to the tumor and the other that binds to the drug via a sulfhydryl- or maleimide-based linkage. This method has been modified to create specifically designed delivery units or carriers where the antibody and a drug bound to a spacer or a polymer backbone, which eventually degrades. This method has also been employed for binding one arm of the BiAbs to the target cells and the other arm to a killer cell or a T cell that acts on the tumors [30]. The antibody targets the specific site and causes the docking of the polymer backbone containing the drug [61]. The degradation or the breakdown of the polymer chain causes the internalization of the drug that breaks and eventually destroys the tumor.

5.3.2.2 Folate Ligands Folate receptors (FR) bind folate and folate–drug conjugates. These folate molecules are subsequently taken up by FR-bearing cells via endocytosis. An acidic endosomal compartment is created around the folate molecule as it is taken into the target cell. Folate ligands have been conjugated to a variety of compounds for delivery to FR-bearing cells. Folate-based delivery systems are advantageous for a variety of reasons. FR bind folate conjugates with an extremely high affinity, which guarantees selectivity. In addition, folate-bearing molecules are internalized by target cells without exposure to harsh conditions [20, 32].

Molecules that have been conjugated to folate ligands thus far include radioactive pharmaceutical agents, MRI contrast agents, proteins, oligonucleotides, ribozymes, drug loaded nanocarriers, and other therapeutic agents. Folate conjugates have been particularly beneficial in cancer therapy, as tumor cells are known to express large numbers of folate receptors [32]. Folate conjugates of several chemotherapeutic agents including taxol, maytansine, nitroheterocyclic bis(haloethyl) phosphoramidite, and 5V-hydroxyl of 5-fluoro-2V-deoxyuridine-5V-omonophosphate (FdUMP) have been created [20].

5.3.2.3 Transferrin Ligands Transferrin (TF) is an iron-transporting serum glycoprotein. TF receptors are expressed in significant quantity on erythroblasts and cancer cells. After binding to TF receptors, TF-bearing particles are taken into cells via endocytosis and contained in endosomes. The endosomal pH causes TF to release its iron [57].

Polymeric nanoparticles conjugated to polyethylene glycol-coupled transferrin (PEG-TF) were prepared by Li et al. [57] for the delivery of pDNA to K562 cells. Their results indicated that TF-PEG nanoparticles delivered an initial burst of pDNA followed by a controlled release over the course of several days with a cumulative release of 67.1–81.3% of encapsulated compound after the first week. Nanoparticle uptake was proven to depend on TF receptor-mediated endocytosis because the presence of free TF in solution decreased the binding efficiency of TF-PEG nanoparticles [57].

Transferrin may also be used as a means of crossing the BBB. Visser et al. [19] have reported the use of pegylated liposomes conjugated to transferrin to deliver protein drugs to brain capillary epithelial cells (BCEC), which bear TF receptors. TF-PEG liposomes were loaded with horseradish peroxidase (HRP) as a sample drug and incubated with BCEC. A comparison of TF-bearing pegylated liposomes with non-TF-bearing carriers was conducted at 37 and 4 °C. At 37 °C, the TF-bearing liposomes showed a two to four times greater association with BCEC cells than liposomes without TF ligands. These results indicate that the potential exists for the creation of TF-bearing liposomes that are capable of releasing peptide drugs within the endothelial cells of the BBB [19].

5.3.2.4 Aptamers Aptamers are nucleic acid ligands formed from DNA and RNA oligonucleotides. Their unique structures enable them to bind specifically to target sites in a fashion similar to antibodies. Aptamers are optimal targeting molecules for a number of reasons. They are typically submicron sized and highly biocompatible. Synthesis via the SELEX procedure (see Reference [55] for more details) allows for the synthesis, selection, purification, and amplification of aptamers suited for a wide variety of targets. Most aptamers are not immunogenic and can achieve prolonged circulation time and *in vivo* stability. Stability may be further enhanced through chemical modification of aptamers [53, 54].

Farokhzad et al. [53] have synthesized nanoparticle–aptamer bioconjugates with the ability to target prostate cancer cells. Polymeric nanoparticles containing the model drug rhodamine-labeled dextran were conjugated to RNA aptamers that bind to the prostate-specific membrane antigen (PSMA), which is present in prostate cancer cells more so than in healthy cells. The nanoparticle–aptamer conjugates were taken up by cells containing PSMA receptors to a much greater extent than they were by cells lacking the receptor. Thus, the results indicated that nanoparticle–aptamer conjugates could be effectively used to target drug-loaded nanoparticles to cancerous cells [53]. In subsequent studies, nanoparticles were loaded with the chemotherapeutic agent docetaxel and conjugated to PSMA aptamers. *In vivo* tests were performed using mouse xenograft models of prostate cancer. The results showed that aptamer–drug-loaded nanoparticle conjugates were more effective than drug-loaded nanoparticles without aptamers, drug injections, or empty nanoparticles in effecting complete tumor regression. Thus, the use of aptamers for targeting can increase the efficacy of nanoparticle-based drug delivery systems [55].

5.3.2.5 Lectins Certain biologically active molecules must be protected from proteolysis within the gastrointestinal (GI) tract when delivered orally. This may be accomplished by encapsulating them in nanoparticles that are stable in the presence of proteases. However, these encapsulating materials may also discourage passage of molecules into circulation through the

intestinal epithelial lining. This problem has been addressed by coating such nanoparticles with lectins that can bind to the intestinal lining. Lectins are proteins that have the ability to bind to particular carbohydrates. They are fairly resistant to acidic conditions and enzymatic degradation. In addition, some lectins like wheat germ agglutinin (WGA) can bind to the intestinal mucosa [56, 62]. For instance, Russell-Jones et al. [56] have reported the use of lectin-coated nanoparticles for oral delivery systems. The coatings were successfully used to encourage nanoparticle uptake by epithelial cells. Lectin coatings could thus be used to facilitate the transport of biodegradable drug-loaded nanoparticles through the intestinal wall and into the circulation [56, 62].

5.3.2.6 Synthetically Modified and Designed Peptide Ligands A variety of other peptide ligands have been explored for targeting of nanosized drug delivery and imaging systems. Some of these are based on modifications of naturally occurring peptides. For instance, Nah et al. [58] have reported the use of the short peptide chain known as artery wall binding peptide (AWBP) for the delivery of genes to cells of the arterial wall. The AWBP group was added to a synthetically created peptide chain that was then conjugated to a nanosized polymeric gene delivery vector. Results indicated that particles conjugated to AWBP were taken up by receptor-mediated endocytosis [58].

Other ligands, like RGD peptide ligands, can be designed entirely through synthetic chemistry. These molecules are formed from cyclized Arg-Gly-Asp chains and have been shown to bind specifically to certain integrins. RGD ligands may be tailored to bind specifically to integrins that are present at target sites. For instance, Mitra et al. [63] have reported the use of a polymer–RGD complex to target the $\alpha v \beta 3$ integrin. This integrin is present on the luminal surface of tumor vasculature only during angiogenesis. The use of RGD ligands allows for the destruction of tumor vasculature by chemotherapeutic agents, thereby limiting tumor growth potential [63]. Another group, Dharap et al. [64], has reported the development of synthetic peptides similar to luteinizing hormone-releasing hormone (LHRH) for the delivery of drug–polymer conjugates to ovarian cancer cells. These cells tend to overexpress LHRH receptors, which are not present in most healthy human tissues. Thus, synthetically designed LHRH ligands may be attached to drug delivery systems in order to direct chemotherapeutic agents to ovarian cancer cells without affecting healthy tissues [64].

5.3.2.7 Other Targeting Ligands Aside from those mentioned above, numerous small molecular ligands have been used for targeting purposes. Insulin, NGR peptide, NGF peptide, and gelatinase inhibitory peptide CTTHWGFTLC have all been explored for their ability to bind to specific target receptors. These ligands have been coupled with delivery vehicles ranging from liposomes and polymeric nanoparticles to quantum dots and have the potential to function as targeting agents for therapeutic and imaging purposes [6].

5.4 MULTIFUNCTIONAL NANOPARTICLE SYSTEMS

Research into nanotechnology goes far beyond drug delivery. The future looks toward the creation of multifunctional nanoparticles capable of performing other tasks in conjunction with drug delivery as shown in Fig. 5.1. Several strategies exist for the creation of multifunctional nanoparticles. Prominent among these are the simultaneous attachment of several molecules to multivalent systems and combination of drug molecules with nanocarriers that have inherently advantageous properties.

5.4.1 Multivalent Strategies

Some systems allow for the incorporation of multiple compounds via encapsulation, conjugation, or some combination of the two. This is particularly true of polymeric systems, including those based on dendrimers and carbon nanotubes.

5.4.1.1 Dendrimers Dendrimers are ideal systems for performing multiple functions due to their ability to encapsulate drugs in both covalent and noncovalent fashions. The branched nature of dendrimers allows for the conjugation of multiple compounds. As unimolecular micelle, dendrimers have the added capacity to carry molecules via encapsulation in their hydrophobic cores. Thus, multifunctional systems can be created by encapsulating one molecule within the micelle core and covalently linking a second molecule to the micelle surface. For example, dendrimer carriers containing contrast agents like fluorescein isothiocyanate (FITC) have been prepared and conjugated to folates in order to target them to cancer cells. These FITC/folate conjugated dendrimers have been subsequently conjugated with drugs, including methotrexate and taxol. Such dendrimer systems serve the dual purpose of imaging cancer cells and delivering cancer therapies. In doing so, they take advantage of the capacity for multiple covalent attachments in addition to non covalent encapsulation [65, 66]. Small dendrimer carriers for gadolinium have also been designed for delivery of this MRI contrast agent. In the future perhaps the surfaces of these nanocarriers may be conjugated to chemicals for the purpose of targeting or drug delivery in conjunction with imaging [6].

5.4.1.2 Polymeric Nanocarriers Nanocarriers formed from straight-chain polymers like PLGA and PCL possess multivalent potential as well. While compounds may be loaded into the hydrophobic core of polymeric micelles or into the matrix of polymeric nanospheres, their surfaces may be modified and conjugated to other substances. These substances could include targeting agents, drugs, or additional polymeric substances to modify the release properties of the system. This opens avenues for polymeric carriers with function in imaging in conjunction with drug delivery, delivery of multiple drugs at once, or delivery of drugs in conjunction with biomolecules like

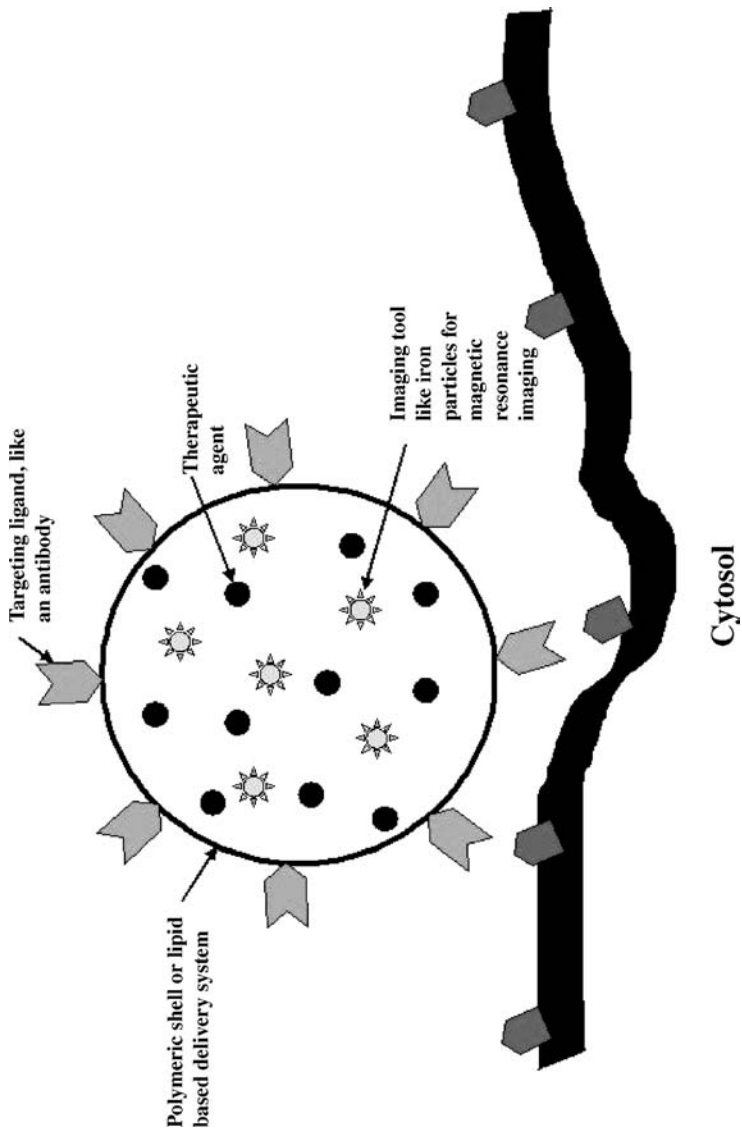


FIGURE 5.1 Schematic drawing of multifunctional nanoparticles.

peptides or nucleic acids. In addition, some surface modifications may allow for the use of polymeric micelles as coating materials for scaffolds in tissue engineering. Studies with the sample drug pyrene have indicated that polymeric micelle coatings can exhibit controlled drug release from surfaces [27]. Thus, it is possible that tissue engineering scaffolds may be coated with drug-loaded micelles in order to release drugs or growth factors to prevent infection or enhance tissue regeneration.

5.4.1.3 Carbon Nanotubes (CNT) Carbon nanotubes are essentially rolled graphite sheets. They may be single or multilayered, SWNT and MWNT, respectively. Both are commercially available with varying structures and purities [67–69]. Bianco et al. [67] have reviewed at length the potential of CNT for drug, peptide, and gene delivery.

Carbon nanotubes may be covalently or noncovalently functionalized in order to increase their biocompatibility, solubility, and drug-loading capacity. Thus, far most research into multifunctional CNT has focused on covalent attachment of multiple molecules. Covalent strategies to enhance solubility and drug-loading capacity typically involve surface modifications to the external CNT walls and tips to create carboxylic functionality. Addition reactions to CNT external walls create functionalized, soluble nanotubes. Targeting antigens, fluorescent probes, drug molecules, peptides, and other biomolecules may all be covalently linked to functionalized CNT surfaces [67–70].

Linking multiple agents to the same CNT creates the potential for multifunctional systems. For instance, Wu et al. [70] have used multiple covalent attachments to create CNT that are useful in both drug delivery and imaging. Amphotericin B, an antifungal agent, was covalently linked to amino groups on the surface of the nanotubes. Fluorescein, a fluorescent probe, was also covalently attached to the CNT surface. A strategy of orthogonal protecting groups was used to ensure that both molecules were successfully incorporated. The chemicals were shown to retain their advantageous properties when taken up by mammalian cells, with fluorescein maintaining its optical properties and amphotericin retaining its antifungal properties [70].

5.4.2 Exploiting Inherent Material Properties

Some materials, particularly metals and ceramics, possess properties that are clinically useful. For instance, many metals can easily be magnetized, heated, or made to fluoresce by the introduction of a magnetic or an electric field [71]. Ceramics have structural properties that render them useful in tissue engineering [72]. These materials may be used to deliver biologically active molecules. The resulting delivery systems are multifunctional due to the inherent properties of the nanocarrier materials.

5.4.2.1 Electrical Properties The ability of metallic particles to act as conductors has rendered them useful for the purpose of biomolecule delivery

and activation. In several studies, gold nanoparticles have been functionalized with the redox enzymes. The gold particles were shown to enhance electron transfer, thereby increasing enzymatic activity. Thus, it is possible for gold nanoparticles to act both as delivery vehicles for the enzymes and as electron conduits for enzymatic activity [71, 73]. Nanowire assemblies formed from redox enzymes and gold nanoparticles may also be used as very precise biosensors [73].

Some studies have investigated the electron-transfer potential of block copolymers [74]. Polymeric micelles derived from such copolymers might serve to both deliver and activate enzymes in a fashion similar to gold nanoparticles.

5.4.2.2 Optical Properties The optical properties of some metals allow for the creation of nanoparticulate systems that serve both imaging and drug delivery purposes. Quantum dots are smaller semiconductor nanocrystals that have been used for imaging since the 1980s. Quantum dots have been conjugated to a variety of biological materials, including peptides, antibodies, and oligonucleotides. Thus far, these particles have been used to image living tissues, including cancer cells and genes. However, it is feasible that drug molecules might also be attached to quantum dots, thereby creating a system for drug delivery in combination with imaging [75].

5.4.2.3 Magnetic Properties Magnetic metallic nanoparticles have already been used extensively for MRI. Iron oxide associated with dextran has been used clinically as a contrast agent for MRI. Iron oxide particles have also been successfully associated with insulin to reduce cellular internalization of the somewhat toxic magnetic particles. In the future, these particles may also be coupled to drug molecules, creating magnetic nanoparticles that function in imaging and drug delivery [4, 6].

5.4.2.4 Thermal Properties Some metals can be heated via the introduction energy from an electric field or via irradiation. Such metals have already been used for tumor ablation via hyperthermia [76]. Gold nanoparticles have already been loaded with anticancer drugs [77]. It is feasible that gold or other metallic nanoparticles containing anticancer agents might be used in the future for the treatment of tumors via drug delivery in conjunction with hyperthermia [76–78].

5.4.2.5 Structural Properties Ceramic nanoparticles are primarily used for the creation of bone scaffolds or biocompatible coatings in the field of tissue engineering. It is possible, however, for these particles to perform additional functions. For instance, capsules formed from nanohydroxyapatite and nanocrystalline calcium sulfate have been investigated for the delivery of vancomycin and gentamicin. Such materials could be used in bone scaffolds to provide structural support and prevent or treat the bone infection osteomyelitis [79]. The incorporation of growth factors into ceramic nanoparticles for use in

tissue engineering has also been reported. In this instance, the particles serve the dual function of providing structural support as part of the bone scaffold and encouraging bone regeneration via growth factor delivery [72].

5.4.2.6 Polymeric Micelles as Nanoreactors Polymeric micelles have been investigated for the entrapment of metallic nanoparticles for use as contrast agents in MRI and other imaging techniques. In some instances, the polymers may entrap a metal salt and interact with it in such a way as to cause metal chelation to occur. The micelle thus provides a microenvironment that serves as a reactor for the production of metallic particles [74]. The microenvironment provided by the core of polymeric micelles may in the future be modified in such a way that it is capable of acting as a microreactor for the synthesis or activation of a biologically active compound like a drug or growth factor.

5.5 CONCLUSIONS

The ability to manipulate materials at the atomic length scale has led to diversified applications in the field of biomedical engineering, including drug delivery. Several techniques and materials for the synthesis of nanoparticles like dendrimers, liposomes, micelles, and metallic and polymeric nanoparticles have been in use over the last few years. More recently, understanding of molecular biology has shown that various targeting mechanisms and imaging and diagnostic tools play a major role in the success of these nanotechnology-based delivery systems. The efficiency of the therapeutic application will dramatically improve by performing multiple functions using the same nanotherapeutic platform.

The application of nanotechnology in the field of medicine has attracted attention from the federal and the industrial sectors around the globe. The annual international nanotechnology funding in 2004 had reached approximately 3 billion and is bound to increase several fold over the next decade. Several nanotechnology based-drug delivery products have recently been available in the market and several others are in clinical trials. These products will change the face of the biomedical therapies and will attract further attention from researchers, federal funding agencies, and venture capitalists.

REFERENCES

1. Roco M. Nanotechnology: convergence with modern biology and medicine. *Cur Opin Biotechnol* 2003;14:337–346.
2. National nanotechnology initiatives Advisory on nanobiotechnology. National Science Foundation (NNI); 2003; p. 1–108.

3. Gourley P. Brief overview of biomicronano technologies. *Biotechnol Prog* 2005;21(1):2–10.
4. Sahoo AK and Labhasetwar V. Nanotech approaches to drug delivery and imaging. *Drug Discov Today* 2003;24:1112–1120.
5. Sinkula M and Paul R. Investing in nanobiotechnology. *Nat Biotechnol* 2003;10:1144–1147.
6. Koo OM, Rubinstein I, Onyuksel H. Role of nanotechnology in targeted drug delivery and imaging: a concise review. *Nanomed Nanotechnol Biol Med* 2005;1:193–212.
7. Loo C, Lowery A, Halas N, West J. Immunotargeted nanoshells for integrated cancer imaging and therapy. *Nanolett* 2005;5(4):709–711.
8. Trehin R, et al. Fluorescent nanoparticle uptake for brain tumor visualization. *Neoplasia* 2006;8(4):302–311.
9. Cyrus T, et al. Three-dimensional molecular imaging of intramural biomarkers with targeted nanoparticles. *J Cardiovasc Magn Reson* 2006;8(3):535–541.
10. Zharov V, Mercer K, Galitovskaya E, Smeltzer M. Photothermal nanotherapeutics and nanodiagnostics for selective killing of bacteria targeted with gold nanoparticles. *Biophys J* 2006;90(2):619–627.
11. Sullivan D and Ferrari M. Nanotechnology, tumor imaging—seizing an opportunity. *Mol Imaging* 2004;3(4):364–369.
12. Bertin P, et al. Multifunctional polymeric nanoparticles from diverse bioactive agents. *J Am Chem Soc* 2006;128(13):4168–9.
13. Grodzinski P, Silver M, Molnar L. Nanotechnology for cancer diagnostics: promises and challenges. *Expert Rev Mol Diagn* 2006;6(3):307–318.
14. Orive G and Pedraz JL. Drug delivery in biotechnology: present and future. *Curr Opin Biotechnol* 2003;14:659–664.
15. Carino G and Edith M. Oral-insulin delivery. *Adv Drug Deliv Rev* 1999;35:249–257.
16. McAllister D and Prausnitz M. Microfabricated microneedles for gene and drug delivery. *Annu Rev Biomed Eng* 2000;2:289–313.
17. Khademhosseini A and Langer R. Nanobiotechnology for tissue engineering and drug delivery, *Chemical Engineering Program*, 2006;102:38–42.
18. Otilia K and Onyuksel H. Role of nanotechnology in targeted drug delivery and imaging: a concise review. *Nanomedicine* 2005;1:193–212.
19. Visser CC, et al. Nanoparticles bearing polyethylene glycol-coupled transferrin as gene carriers: preparation and *in vitro* evaluation. *Int J Pharm* 2005;25:299–305.
20. Leamon CP and Reddy JA. Folate-targeted chemotherapy. *Adv Drug Deliv Rev* 2004;80:1127–1141.
21. Alvarez V and Sanz L. Antibody engineering: facing new challenges in cancer therapy. *Acta Pharmacol Sin* 2005;6:641–648.
22. Majeti RK. Nano and micro particles as controlled drug delivery devices. *J Pharm Pharm Sci* 2000;3(2):234–258.
23. Saltzman W and Baldwin S. Materials for protein delivery in tissue engineering. *Adv Drug Deliv Rev* 1998;(33):71–86.

24. Owens DE and III Peppas NA. Opsonization, biodistribution, and pharmacokinetics of polymeric nanoparticles. *Int J Pharm* 2006;307:93–102.
25. Kataoka K, Harada A, Nagasaki Y. Block copolymer micelles for drug delivery: design, characterization and biological significance. *Adv Drug Deliv Rev* 2001;47: 113–131.
26. Teixeira M, Alonson MJ, Pinto MMM, Barbosa CM. Development and characterization of PLGA nanospheres and nanocapsules containing xanthaone and 3-methoxyanthone. *Eur J Pharm Biopharm* 2005;59:491–500.
27. Otsuka H, Nagasaki Y, Kataoka K. PEGylated nanoparticles for biological and pharmaceutical applications. *Adv Drug Deliv Rev* 2003;44:402–419.
28. Kearsey J. Strategies for intracellular drug delivery. *The Drug Delivery Companies Report*, 2004. p. 43–46.
29. Hoffman A. Design of smart polymers that can direct intracellular drug delivery. *Polym Adv Technol* 2002;13:992–999.
30. Torchilin V. Recent approaches to intracellular delivery of drugs and dNA and organelle targeting. *Annu Rev Biomed Eng* 2006;8:343–375.
31. Nishiyama N, Bae Y, Miyata K, Fukuchima S. Smart polymeric micelles for gene and drug delivery. *Drug Discov Today: Technol* 2005;2:21–26.
32. Shi G, Gui W, Stephenson SM, Lee RJ. Efficient intracellular drug and gene delivery using folate receptor-targeted pH-sensitive liposomes composed of cationic/anionic lipid combinations. *J Control Rel* 2002;80:309–319.
33. Liang L, Ping J, Ming C, Guoliang Z, Fengbao Z. 5-Fluorouracil-loaded self-assembled pH-sensitive nanoparticles as novel drug carrier for treatment of malignant tumors. *Chin J Chem Eng* 2006;14:377–382.
34. Lo CL, Lin KM, Hsiue GH. Preparation and characterization of intelligent core–shell nanoparticles based on poly(D,L-lactide)-g-poly(*N*-isopropyl acrylamide-co-methacrylic acid). *J Control Rel* 2005;104:477–488.
35. Meissner Y, Pellequer Y, Lamprecht A. Nanoparticles in inflammatory bowel disease: particle targeting versus pH-sensitive delivery. *Int J Pharma* 2006;316: 138–143.
36. Chaw CS, et al. Thermally responsive core–shell nanoparticles self-assembled from cholesteryl end-capped and grafted polyacrylamides: drug incorporation and *in vitro* release. *Biomaterials* 2004;25:4297–4308.
37. Bae Y, Fukushima S, Harada A. Design of environment-sensitive supramolecular assemblies for intracellular drug delivery: polymeric micelles that are responsive to intracellular pH change. *Angew Chem Int Ed* 2003;42:4640–4643.
38. Kataoka K, et al. Doxorubicin-loaded poly(ethylene glycol)–poly(β -benzyl-L-aspartate) copolymer micelles: their pharmaceutical characteristics and biological significance. *J Control Rel* 2000;64:143–153.
39. Gil ES and Hudson SM. Stimuli-responsive polymers and their bioconjugates. *Prog Polym Sci* 2004;29:1173–1222.
40. Cammas S, et al. Thermo-responsive polymer nanoparticles with a core-shell micelle structure as site-specific drug carriers. *J Control Rel* 1997;48:157–164.
41. Berg K, et al. Photochemical internalization: a novel technology for delivery of macromolecules into cytosol, *Cancer Res*, 1999;59(6):1180–1183.

42. Engesaeter B, et al. PCI-enhanced adenoviral transduction employs the known uptake mechanism of adenoviral particles. *Can Gen Ther* 2005;12(5):439–448.
43. Berg K, Selbo P, Prasmickaite L, Hogset A. Photochemical drug and gene delivery. *Curr Opin Mol* 2004;6(3):279–287.
44. Berg K, Dietze A, Kaalhus O, Hogset A. Site-specific drug delivery by photochemical internalization enhances the antitumor effect of bleomycin. *Clin Canc Res* 2005;11(23):8476–85.
45. Derycke A and De Witte P. Liposomes for photodynamic therapy. *Adv Drug Deliv Rev* 2004;56(1):17–30.
46. Chen B, Pogue B, Hasan T. Liposomal delivery of photosensitising agents. *Expert Opin Drug Deliv* 2005;2(3):477–487.
47. Konan Y, Gurny R, Allemann E. State of the art in the delivery of photosensitizers for photodynamic therapy. *J Photochem Photobiol B* 2002;66(2):89–106.
48. Ideta R, et al. Nanotechnology-based photodynamic therapy for neovascular disease using a supramolecular nanocarrier loaded with a dendritic photosensitizer. *Nanoletters* 2005;5(12):2426–31.
49. Leach J. Thesis on magnetic targeted drug delivery. Virginia Polytechnic; 2003. p 83.
50. Hofer K. Hyperthermia and cancer, In: Fourth International Conference on Scientific and Clinical Applications of Magnetic Carriers. 2002;12:78–80.
51. Ng K-Y and Matsunaga T. Ultrasound Mediated Drug Delivery. In: Wang B, editor. *Drug Delivery: Principles and Application*. Wiley; 2005.
52. Rapaport N. Cancer therapy by micellar-encapsulated drug and ultrasound. *Int J Pharm* 2004;277:155–162.
53. Farokhzad OC, et al. Nanoparticle-aptamer bioconjugates: a new approach for targeting prostate cancer cells. *Can Res* 2004;64:7668–7672.
54. Pestourie C, Tavitian B, Duconge F. Aptamers against extracellular targets for *in vivo* applications. *Biochimie* 2005;87:921–930.
55. Farokhzad OC, et al. Targeted nanoparticle-aptamer bioconjugates for cancer chemotherapy *in vivo*. *Proc Nat Acad Sci USA* 2006;103:6315–6320.
56. Russell-Janes GJ, Veitch H, Arthur L. Lectin-mediated transport of nanoparticles across Caco-2 and OK cells. *Int J Pharm* 1999;190:165–174.
57. Li Y, Ogris M, Wagner E, Pelisek J, Rueffer M. Nanoparticles bearing polyethylene glycol-coupled transferrin as gene carriers: preparation and *in vitro* evaluation. *Int J Pharm* 2003;229:93–101.
58. Nah JW, Yu L, Han So, Ahn CH, Kim SW. Artery wall binding peptide-poly(ethylene glycol)-grafter- poly(L-lysine)-based gene delivery to artery wall cells. *J Control Rel* 2002;78:273–284.
59. Malavasi F and Funaro A. Monoclonal antibodies for therapy of human cancers. *Biotechnol Adv* 2000;18:385–401.
60. Lee R and Lawrence L. Bispecific antibodies: targeting cancer and much more. *Exp Hematol* 2006;34:1–6.
61. Rong-Lu Z and Kopecek J. Design of novel bioconjugates for targeted drug delivery. *J Control Release* 2001;78:165–173.

62. Peppas NA and Kavimandan NJ. Nanoscale analysis of protein and peptide absorption: insulin absorption using complexation and pH-sensitive hydrogels as delivery vehicles. *Eur J Pharm Sci* 2006 (1):83–87.
63. Mitra A, et al. Targeting tumor angiogenic vasculature using polymer-RGD conjugates. *J Control Release* 2005;102:191–201.
64. Dharap SS, et al. Molecular targeting of drug delivery systems to ovarian cancer by BH3 and LHRH peptides. *J Control Release* 2003;91:61–73.
65. Gillies ER and Frechet MJJ. Dendrimers and dendritic polymers in drug delivery. *Drug Disc Today* 2005;10:35.
66. Patri AK, Majoros IJ, Baker JR. Dendritic polymer macromolecular carriers for drug delivery. *Curr Opin Chem Biol* 2002;6:466–471.
67. Bianco A, Kostarelos K, Prato M. Applications of carbon nanotubes in drug delivery. *Curr Opin Chem Biol* 2005;9:674–679.
68. Pantarotto D, et al. Immunization with peptide-functionalized carbon nanotubes enhances virus-specific neutralizing antibody responses. *Chem Biol* 2003;10:961–966.
69. Klumpp C, Kostarelos K, Prato M, Bianco A. Functionalized carbon nanotubes as emerging nanovectors for the delivery of therapeutics. *Biochim Biophys Acta* 2006;1758:404–412.
70. Wu W, et al. Targeted delivery of amphotericin B to cells by using functionalized carbon nanotubes. *Angew Chem Int Ed* 2005;44:6358–6362.
71. Penn SG, He L, Natan MJ. Nanoparticles for bioanalysis. *Curr Opin Chem Biol* 2003;7:609–615.
72. Ben N. Natural, bioceramics: from coral to bone and beyond. *Curr Opin Solid State Mater Sci* 2003;7:283–288.
73. Yeh JI, Zimmt MB, Zimmerman AL. Nanowiring of a redox enzyme by metallized peptides. *Biosens Bioelectron* 2005;21:973–978.
74. Riess G. Micellization of block copolymers. *Prog Polym Sci* 2003;12:87–91.
75. Chan W. Bionanotechnology progress and advances. *Am Soc Blood Marrow Transpl* 2006;12:87–91.
76. Shinkai M, et al. Intracellular hyperthermia for cancer using magnetite cationic liposomes. *J Magn Magn Mater* 1999;194:176–184.
77. Myer L, et al. Colloidal gold: a novel nanoparticle vector for tumor directed drug delivery. *Drug Deliv* 2004;11:169–183.
78. Yang YC WC, Hwu YK, Je JH. Synchrotron X-ray synthesis of colloidal gold particles for drug delivery. *Mater Chem Phys* 2006.
79. Rauschmann MA, et al. Nanocrystalline hydroxyapatite and calcium sulphate as biodegradable composite carrier material for local delivery of antibiotics in bone infections. *Biomaterials* 2005;26:2677–2684.

Polymeric Nanoparticles and Nanopore Membranes for Controlled Drug and Gene Delivery

JINGJIAO GUAN, HONGYAN HE, BO YU, and L. JAMES LEE

6.1 INTRODUCTION

Drugs range from conventional small-molecule therapeutics to emerging protein/peptide-based macromolecular biopharmaceuticals. Although the therapeutic effects of a drug are of paramount importance, the way to deliver it is also critical. Nucleic acids have also been used to treat/prevent diseases in gene therapy which holds potential to revolutionize medicine. But its development is significantly hampered by a lack of efficient and safe delivery techniques. During the past four decades, considerable effort has been made to develop systems to facilitate delivery of drugs and nucleic acids. Such a system is called a drug/gene delivery system (DGDS). A successful DGDS should offer at least one of three benefits: enhancing therapeutic outcome, improving patient compliance, or reducing therapeutic cost. Specific goals for developing a novel drug delivery technique may vary, but generally include targeting diseased organs, tissues, or cells; reducing side effects such as infection, systemic toxicity, and unwanted immune reactions; increasing drug bioavailability; optimizing pharmacokinetics; minimizing risk and/or discomfort associated with administration such as injection; enabling self-administration and lowering involvement of health care workers; and lowering the cost of drug/gene delivery systems [1]. A primary driving force for developing advanced DGDSs is associated with many emerging protein, peptide, and nucleic acid based therapeutics. They are potent, but expensive and labile. Delivering them to target tissues or cells in an efficient, controlled, safe, and patient-friendly manner remains a major challenge for drug/gene delivery research.

Recently, polymer-based DGDSs with critical structural features at the nanometer scale have attracted immense interest. Polymers are macromolecules composed of a large number of identical or similar repeating units organized in a chain-like molecular architecture. They exhibit a wide diversity of compositions, structures, and properties. Some characteristics of polymers, such as biocompatibility, biodegradability, a broad range of mechanical properties, and ease of processing, make them extensively useful in drug delivery. Besides material, size is another determining factor for a DGDS. A cell can be regarded as a combination of numerous nanomachines such as ion channels and ribosomes, and a majority of drugs/genes fall into the nanometer range in terms of molecular size. It is obvious that a DGDS with nanoscale-sized features would have better potential to be more effective in interacting with both the biological systems and the drugs/genes. Such a system therefore would be more likely to achieve controlled drug/gene delivery. In this chapter, three types of polymeric nanostructures for drug/gene delivery are described, including particulate nanostructures or nanoparticles (NPs), nanopore membranes, and fibrous nanostructures or nanofibers. Fabrication of these polymeric nanostructures and their applications in drug/gene delivery will be introduced first, followed by a brief discussion on the future trends in this dynamic field.

6.2 NANOPARTICLES FOR DRUG/GENE DELIVERY

NPs have been widely studied for drug/gene delivery, and some products such as Doxil[®] and Abraxane[®], have reached clinics. A very important factor of drug/gene delivery NPs is their nanometer size. In the following section, we will first discuss why the size of NPs is critical in drug/gene delivery. Different types of polymeric NPs will then be introduced. Because drug delivery polymeric NPs are used in biological fluids and most of the NPs are produced in the presence of water, the water solubility of polymers plays a major role in the fabrication, structures, properties, and functions of the NPs. We therefore classify NPs based on the water solubility of the polymers used. In some cases, different types of polymers are used together to manufacture NPs. The polymer that plays a major role in determining the preparation method and properties of the NPs is taken as a standard for classification.

6.2.1 Why is Size Important for NPs in Drug/Gene Delivery?

Drugs are conventionally administered in the form of free, unassociated molecules. This strategy is simple, but it is becoming increasingly limited in many conditions, especially in those involving the use of highly cytotoxic chemotherapeutics and environmentally sensitive biopharmaceuticals. In recent decades, particulate systems at the micrometer scale, or microparticles (MPs), have been under active study for controlled drug/gene delivery. For example,

porous MPs of 20 μm diameter were used for deep lung drug delivery via inhalation [2] and particles larger than 40 μm for embolization therapy [3]. Between free drug molecules and MPs lie particles between 10 and 1000 nm in size. This size range offers considerable advantages over free drugs and MPs in view of drug/gene protection, delivery of poorly soluble drugs, sustained release, blood circulation time, organ/tissue/cell targeting, cellular uptake, and barrier penetration. These benefits are discussed in the following sections.

6.2.1.1 Drug/Gene Protection For optimum therapeutic efficacy and patient compliance, drug/gene release from NPs over a sustained period of time is often desired. Many drugs, especially protein, peptide, and nucleic acid based agents, however, are subject to rapid clearance and degradation in the body. Protection of these drugs from degradation and unwanted interactions is thus needed before they are released. Protection is also necessary for targeted delivery through intravascular or oral routes because the drug/gene must pass a series of biological and physiological barriers before reaching its target.

6.2.1.2 Delivery of Poorly Soluble Drugs Many potent drugs are poorly soluble in water, resulting in either low bioavailability or a need for a dosage form causing significant adverse side effects. One such example is paclitaxel, a widely used anticancer drug with very low water solubility. It is currently delivered with Cremophor EL, a solvent associated with acute hypersensitivity reactions. In addition, a large number of potent candidate drugs are discarded during drug discovery process because of their low water solubility, resulting in significant waste of efforts [4]. Polymeric NPs may represent a general and simple solution to this problem.

6.2.1.3 Sustained Release Sustained drug release is desired in many conditions to achieve optimized therapeutic outcomes and improved patient compliance. An *in vivo* study on diabetic rats showed that subcutaneously injected insulin-loaded polymeric NPs of 85–185 nm exerted a much longer hypoglycemic effect than free insulin [5]. In another study, intramuscularly delivered 600 nm PLGA NPs loaded with plasmid DNA showed sustained gene expression [6]. Although MPs may also offer sustained release, only NPs can be used as circulation depot [7].

6.2.1.4 Extended Blood Circulation For intravenously administered NPs, long circulation time is a prerequisite for targeted drug delivery and sustained drug release in blood. The smallest capillaries set the upper limit for the size of circulating rigid particles at approximately 5 μm . However, particles at the micron scale are rapidly taken up by the reticuloendothelial system (RES), while particles less than 200 nm in size with appropriate surface properties have significantly low RES uptake and can circulate in blood for considerably prolonged periods of time [7, 8].

6.2.1.5 Targeted Delivery Targeted delivery is one of the most pursued goals in drug/gene therapy. NPs are capable of targeting at many different levels, from organs, to tissues and cells, to even subcellular compartments. Organ and tissue targeting can be achieved because vasculatures of different organs and tissues have fenestrations of different sizes. For example, blood vessels in the liver contain fenestrations of approximately 106–175 nm [9]. These organs can thus be selectively targeted by controlling the size and surface properties of the NPs. Many types of tumors are characterized by porous blood vessels. The pore cutoff size is between 380 and 780 nm. Circulating NPs between 100 and 300 nm would thus leak through the nanopores and accumulate in the tumor because of the enhanced permeation and retention (EPR) effect [10]. Moreover, by attaching ligands, NPs can actively target virtually any type of accessible cells with identified cellular receptors.

6.2.1.6 Enhanced Cellular Uptake While phagocytic cells can take up micron-sized particles more efficiently, nonphagocytic cells—the targets of most therapies—preferentially internalize particles at the nanometer scale. One study showed that NPs of 100 nm were taken up at 2.5-fold and 6-fold greater rates than 1 and 10 μm particles, respectively, in a Caco-2 cell line [11]. Similar results have been observed with other cell lines [12]. A gene transfection study also showed that DNA-loaded particles of less than 100 nm size had 27-fold greater transfection than particles larger than 100 nm in a COS-7 cell line [13]. The size of the NPs affected the pathway of particle internalization as well [14], implying that the intracellular fate of NPs can be controlled. This is particularly important for drugs or genes that need to function in specific cellular compartments.

6.2.1.7 Barrier Penetration The extremely small size of NPs facilitates their penetration across various biological barriers for drug delivery. Oral administration is generally the most preferred drug delivery method, but it is not applicable to many drugs because of their susceptibility to degradation in the GI tract and low permeability through the intestinal barrier. Polymeric NPs can not only protect the encapsulated drugs from degradation and prolong the residence time of drugs in the absorption site of the GI tract but also efficiently penetrate the mucosal layer covering the intestinal lumen [15]. As a result, increased bioavailabilities of drugs such as heparin, insulin, peptides, and paclitaxel have been obtained [5, 16–18]. The blood/brain barrier (BBB) is another formidable barrier for drug delivery. It is formed by tight junctions between the capillary endothelial cells and protects the central nervous system (CNS) from harmful agents in the blood. A large number of drugs are precluded from entering the CNS. Overcoming the BBB is thus a major challenge for treating many devastating brain diseases such as brain tumors. Studies have shown that NPs could efficiently cross the BBB [19] and a recent study concluded that NPs less than 100 nm in diameter crossed the BBB much more efficiently than larger NPs [20].

6.2.2 NPs Prepared from Water-Insoluble Polymers

NPs made of water-insoluble polymers can be prepared from either preformed polymers or monomers. Poly(lactic acid) (PLA) and poly(lactic-co-glycolic acid) (PLGA) are the most widely used hydrophobic polymers for this application because they are biocompatible, biodegradable, and approved by the US Food and Drug Administration (FDA) for internal use in humans. To render NPs' desired surface properties which are critical in determining their interactions with biological systems and performance as drug/gene carriers, amphiphilic copolymers are commonly incorporated into them. Poly(ethylene glycol) (PEG), a hydrophilic polymer extensively used in drug delivery has been coupled with various hydrophobic polymers to form amphiphilic block copolymers, for example, PLA-PEG and PLGA-PEG. They are commonly used for the preparation of PEG-coated NPs. NPs are also prepared from many other hydrophobic polymers and their derivatives, such as polycaprolactone (PCL) and polyalkylcyanoacrylate (PACA). A number of methods have been developed to fabricate NPs from these hydrophobic polymers, and they are introduced in this section.

6.2.2.1 NPs Prepared by Precipitation of Polymers

Emulsion/Solvent Evaporation In this method, the polymer is dissolved in a water-immiscible organic solvent like dichloromethane, chloroform, or ethyl acetate. The drug is also dissolved or dispersed in the polymer solution. When this solution is added to a large amount of aqueous solution and homogenized, small droplets of the polymer solution form in the water, resulting in a system termed oil-in-water emulsion. Surfactants such as poly(vinyl alcohol) (PVA) are commonly used as emulsifying agents to stabilize the droplets. Solid polymeric NPs form after the organic solvent evaporates. To encapsulate a water-soluble drug, the drug is usually dissolved in water and emulsified in an oil phase, forming a water-in-oil emulsion. This water-in-oil emulsion is then emulsified again in water, forming a water-in-oil-in-water emulsion [21]. PEG-coated PLGA NPs of 200 nm size were prepared using this method to encapsulate protein and peptide drugs [7]. The formation of a nanosized emulsion usually requires sonication or high speed homogenization. In a modified emulsion/solvent evaporation method, a semipolar water-miscible solvent such as acetone was added in the organic phase. Pouring this organic phase into water resulted in the spontaneous formation of nanosized droplets, probably caused by the decreased interfacial tension between the organic and the aqueous phases and interfacial turbulence induced by the rapid diffusion of acetone into water. PLGA NPs of 200–300 nm size incorporating 5-FU were produced using this method [22].

Solvent Displacement In contrast with the emulsion/solvent evaporation method, a water-miscible solvent such as acetone or ethanol is used to dissolve the polymer and the drug in this method. The drug needs to be insoluble or only

slightly soluble in water. By pouring the solution into an aqueous solution, rapid diffusion of the organic solvent into the aqueous phase leads to the precipitation of the polymer and the drug as NPs. A surfactant like poloxamer 188, a triblock copolymer of poly(ethylene oxide)–poly(propylene oxide)–poly(ethylene oxide), and soy lecithin may be used to facilitate the formation and stabilization of NPs [23]. One example of applying this approach is the production of 100 nm PLGA NPs incorporating a model drug of coumarin-6 [24]. To increase the loading capacity for a lipophilic drug, an oil solvent for the drug can be included in the organic phase. The resulting NPs have an oily core surrounded by a polymer coat and are thus called nanocapsules. PLA nanocapsules of 180 nm diameter containing halofantrine were prepared using this method [23].

Salting Out In this method, a solution of a polymer and a drug in a water-miscible solvent, for example, acetone, is added to an aqueous phase containing PVA and saturated salt such as magnesium chloride or magnesium acetate [25]. Although acetone is miscible in water, an oil-in-water emulsion forms under mechanical stirring because of the salting out of the organic solvent induced by the salt. By adding pure water to the system, acetone diffuses out of the oil phase into the aqueous phase and solid polymeric NPs form. Using this method, drug-loaded PLA NPs ranging from 230 to 730 nm were produced [25]. In another study, PLA and PLGA NPs with a mean size below 200 nm were formed [26].

Supercritical Fluid CO₂ Technology Supercritical carbon dioxide (scCO₂) is attracting considerable interest for producing particulate drug delivery systems because it is nontoxic, nonflammable, inexpensive, and biologically and environmentally benign [27]. ScCO₂ has been used as a solvent to dissolve drugs and polymers together. When such a solution is atomized through a nozzle into a low pressure chamber, drug-loaded polymeric microparticles are formed [28]. This technique is attractive because of the complete elimination of organic solvents, but it is significantly limited by the low solubility of high molecular weight polymers in scCO₂. On the contrary, the low solubility of scCO₂ for polymers can be utilized in another particle manufacturing method called supercritical antisolvent precipitation (SAS). In SAS, a drug and polymer solution in an organic solvent is atomized into scCO₂. Rapid extraction of the organic solvent into the scCO₂ phase leads to the precipitation of drug-loaded polymeric NPs [29].

6.2.2.2 NPs Prepared by Polymerization of Monomers PACA NPs are prepared using this method. PACA is a biodegradable polymer used as tissue adhesive in surgery. Thus, this polymer attracts great interest for drug delivery applications. To prepare PACA NPs, an alkylcyanoacrylic monomer such as isobutylcyanoacrylate (IBCA) or isohexylcyanoacrylate (IHCA) is added to an acidic aqueous solution to form an emulsion via vigorous mechanical stirring. This is followed by polymerization. Surfactants such as

Dextran 70 or polysorbates may be used as a colloidal stabilizer. The produced NPs are approximately 70–350 nm in size [5,20,30]. Many drugs have been incorporated with PACA NPs. They can be added either during or after the polymerization process. Encouraging results have been obtained with PACA-NP-based drug delivery systems. Doxorubicin-loaded PACA NPs were shown to be able to overcome cancer's multidrug resistance (MDR), which is responsible for a significant portion of the failure of chemotherapy [30,31]. Insulin-loaded PACA NPs also showed both a sustained hypoglycemic effect when delivered via subcutaneous injection and enhanced absorption via oral administration compared with free insulin [5]. When formulated with PACA NPs, the antitumor effect of antisense oligonucleotides was also significantly enhanced [32].

6.2.3 NPs Prepared from Water-Soluble Polymers

Like water-insoluble polymers, water-soluble polymers are also widely used to prepare NPs for drug/gene delivery. These polymers are of either natural or synthetic origin and include highly engineered copolymers. The water solubility of polymers offers the potential to produce NPs in water without the need of organic solvents, which are toxic and can denature labile macrobiomolecules such as proteins. Many hydrophilic polymers are charged in water. They can interact with ionic drugs, allowing controlled association and release of the drugs. Many of these polymers also carry reactive groups, permitting the modification and grafting of functional molecules. On the contrary, because of their water solubility, the polymer chains need to be associated with one another to maintain distinct NPs in water. Based on whether preformed polymers or monomers are used as precursors and the fabrication methods, NPs prepared from water-soluble polymers are divided into three groups: cross-linked preformed polymers, self-assembled block copolymers, and polymerized monomers.

6.2.3.1 NPs Prepared by Cross-Linking of Polymers A variety of hydrophilic polymers have been used to prepare drug/gene delivery NPs by cross-linking of polymer chains. Production processes usually start with dissolving the polymers in water and are followed by forming an intermediate distinct phase via various approaches such as ionic gelation, emulsification, solvent displacement, complex coacervation, or salt-induced desolvation. Cross-linking is then carried out to form NPs. In some cases, the intermediate step is skipped, and the polymers dissolved in water are cross-linked directly to generate NPs. The cross-links can be either chemical bonds or physical interactions.

Chemical-bond-based cross-linking has been used to generate gelatin and polyethylenimine (PEI) NPs for drug/gene delivery. Gelatin is a protein product traditionally obtained by the partial hydrolysis of collagen. It is a “generally regarded as safe (GRAS)” material and has a long history of safe use in pharmaceuticals and food. Gelatin is a polyampholyte and is positively charged at an acidic pH. To form NPs, the distinct phase is often formed in the first step

by water-in-oil emulsification, solvent displacement, complex coacervation, or salt-induced desolvation. It is followed by the chemical cross-linking of gelatin with various agents such as glutaraldehyde and glyoxal. Anticancer drugs such as doxorubicin [33], paclitaxel [34], cytarabine [35], and methotrexate [36], and ophthalmic drugs such as pilocarpine HCl and hydrocortisone [37] have been incorporated into the gelatin NPs, and the biodistribution of the paclitaxel-loaded NPs in the body has been studied [34]. Plasmid DNA was also incorporated into gelatin NPs using this method [38, 39]. In one study, gene-loaded gelatin and pegylated gelatin NPs with an average size of 200 nm were delivered through both intravenous and intratumoral routes into mice, which showed significant expression of the reporter gene [39]. Recently, gelatin NPs conjugated with the antibody for targeting human T-cell leukemia cells and primary T-lymphocytes have been produced, showing promise for using gelatin NPs for delivering drugs and genes to specific cell types [40, 41]. PEI NPs were produced by covalently cross-linking PEI with poly(ethylene oxide) (PEO) in a water-in-oil emulsion system [42]. The formed NPs, called nanogels, had diameters of 20–220 nm and were slightly positively charged at pH 7 before the drug was loaded [43]. The cationic nature of the nanogel was utilized to form complexes with negatively charged drugs such as retinoic acid, indomethacin, oligonucleotides, and nucleoside analogs [42–45]. Ligands such as folate, transferrin, or insulin have been conjugated to the nanogels to achieve receptor-mediated delivery [44, 45]. Drug-loaded nanogel particles were found to transport across polarized monolayers of human intestinal epithelial cells and bovine brain microvessel endothelial cells through transcellular pathways. An *in vivo* study also showed substantially enhanced brain accumulation of oligonucleotides carried by nanogel compared with free oligonucleotides following intravenous injection to mice [45]. These results indicate the potential use of nanogels for delivering poorly soluble and high molecular weight drugs through oral routes and across the BBB.

Since many water-soluble polymers are polyelectrolytes, ionic interaction is widely used for cross-linking the polymers. Alginate NPs were prepared by cross-linking anionic sodium alginate with cationic calcium ions and/or polymers such as chitosan or poly-L-lysine. In one study, alginate NPs measuring approximately 235 nm in diameter and encapsulating several antitubercular drugs were produced and administered to guinea pigs through the pulmonary route [46]. They showed significantly higher bioavailabilities and much longer efficacy than the orally administered free drugs. Plasmid DNA and oligonucleotides were also encapsulated into alginate NPs by this method [47–49]. This method has also been applied to chitosan, an inexpensive, biodegradable, biocompatible, and bioadhesive polysaccharide carrying a high density of positively charged primary amino groups in water at an acidic pH. Calvo et al. produced chitosan NPs by using tripolyphosphate anions as cross-linking agents [50]. These NPs had high loading capacity for proteins like bovine serum albumin [51], tetanus toxoid, diphtheria toxoid [50, 52], and insulin [53, 54]. An immunosuppressant drug, cyclosporin A [55], and

an anticancer drug, doxorubicin [56], have also been formulated into chitosan NPs using this method. Encouraging results were obtained using these NPs in nasal and ocular drug delivery [53, 55].

Plasmid DNA is a large polymer carrying a high density of negative charges in water. It can act as both a therapeutic agent in gene delivery and a cross-linking agent for polycations such as chitosan and PEI. Leong et al. prepared DNA–chitosan NPs by simply mixing DNA and chitosan solutions in the presence of sodium sulfate [57]. The NPs formed spontaneously in water and were generally 100–300 nm in diameter with a narrow size distribution. Oral administration of the chitosan NPs containing an allergen gene to mice showed a substantial immunization effect compared with the treatment with naked DNA [58]. In another study, chitosan–DNA NPs were delivered to the livers of rats through bile duct and portal vein infusions. A relatively high level of gene expression was observed with low toxicity [59].

Perhaps, the most extensively and intensively investigated polymer for nonviral gene delivery is PEI. PEI is highly positively charged at a neutral pH. It therefore binds DNA in water, forming PEI–DNA complexes. The morphology of the complexes is highly dependent on the charge ratio of PEI to DNA, which, in turn, is equivalent to the ratio of the nitrogen atoms of PEI to the phosphates of DNA (N/P ratio), as shown in Fig. 6.1. Compact PEI–DNA NPs called polyplexes form within an appropriate range of the N/P ratio, generally from 3 to 20. These NPs are preferred for gene transfection. Besides primary amines, PEI also has a large amount of secondary and tertiary amines. Following the cellular uptake of the NPs via

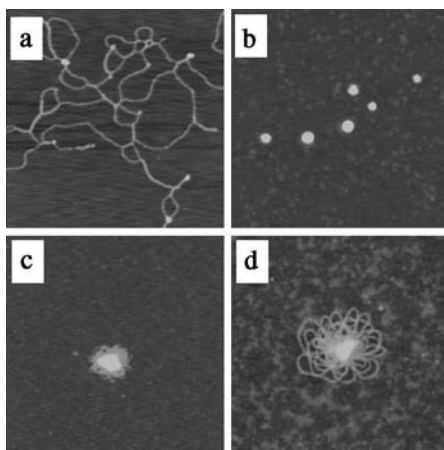


FIGURE 6.1 Atomic force microscopy (ambient tapping mode) images of complexes formed by branched 25 kDa PEI and λ -DNA in water at N/P ratios of (a) 1:10, (b) 3:1, (c) 30:1, and (d) 300:1. Highly compact PEI–DNA NPs form at an N/P ratio of 3:1. Scan areas = $1\mu\text{m} \times 1\mu\text{m}$.

endocytosis, these amines can probably act as a “proton sponge,” eventually leading to the escape of the NPs from the endosomes and subsequent lysosomal degradation [60, 61]. Besides the intrinsic capabilities for DNA condensation and endosomal escape, PEI has been modified with additional features for enhanced biocompatibility and transfection efficiency [62, 63]. For *in vivo* gene delivery, PEG has been coupled with PEI to achieve improved water solubility, reduced immunogenicity, and extended circulation time. A number of ligands such as galactose [64], folate [65], transferrin [66], and antibody [67] have been conjugated to PEI to attain receptor-mediated targeting. PEI–DNA NPs have shown therapeutic promise in many animal studies. Significant transgene expressions in the lung have been observed following delivery of PEI–DNA NPs via various routes, including intravenous delivery [68], nasal instillation [69], intratracheal instillation [70], and pulmonary delivery [71], indicating a great potential of PEI–DNA NPs for treating lung diseases such as cystic fibrosis. The expression of the therapeutic bcl-2 gene in CNS neurons was also achieved by the peripheral intramuscular injection of PEI–DNA NPs [72]. In addition, the intravenous delivery of transferrin-coated PEI–DNA NPs into mice bearing tumors resulted in preferential transgene expression in distant tumors as compared with the major organs [73]. Tumor-preferential transgene expression was also observed following the intraperitoneal injection of PEI–DNA complexes [74].

6.2.3.2 NPs Prepared by Self-Assembling of Block Copolymers

Block copolymers can form polymeric micelles with core–shell architecture by self-assembly in water. Such copolymers must contain a hydrophilic segment that forms the outer shell. PEG or PEO is the most commonly used polymer for this purpose. When administered into the blood circulation, the outer shell provides steric repulsion against adsorption of plasma proteins and avoids rapid clearance by the RES. The other segment(s) of the copolymer must be able to segregate in water as the solid core. It can be made from various types of polymers, such as PLA, PLGA, PCL, poly(glutamic acid), PEI, and poly(benzyl aspartate). The core formation can be driven and stabilized by different interactions, including electrostatic attraction, hydrophobic interaction, chemical bonds, and polymer–metal complexation [75]. The chemical composition, molecular size, and block lengths of the copolymers can be changed easily, allowing versatile manipulation of the structure and properties of polymeric micelles. More importantly, ligands can be easily conjugated to the end of the outer hydrophilic segment of the copolymers to provide an active targeting capability [76].

Polymeric micelles are usually between 10 and 50 nm in diameter [77]. This size range is generally smaller than other drug delivery NPs. Because of their small size, polymeric micelles are less likely to be recognized and taken up by the RES compared with larger NPs. Moreover, they may be

particularly suitable for passive targeting of tumors with a small vasculature cutoff size [10]. Polymeric micelles also have a narrow size distribution, which is desirable for controlling their distribution and drug release rate in the body. Drug molecules are entrapped in the core of the micelles and are protected from hydrolytic and enzymatic degradation. A wide variety of drugs with diverse characteristics have been formulated with polymeric micelles and tested *in vitro* and *in vivo*. Enhanced antitumor activity was observed with different anticancer drugs, including doxorubicin [76], cisplatin [75], paclitaxel [78], and camptothecin [79]. Polymeric micelles were also found to be able to cross the intestinal barrier and release poorly soluble drugs over a sustained period of time [80]. In addition encouraging results have been obtained when polymeric micelles were used to deliver oligonucleotides [81].

6.2.3.3 NPs Prepared by Polymerization of Monomers Peppas et al. developed a free-radical precipitation/dispersion method to synthesize hydrogel NPs of cross-linked methacrylic acid (MAA) grafted with PEG. Since poly(methacrylic acid) and poly(acrylic acid) are pH-sensitive polymers, the produced poly(MAA-g-PEG) and poly(AA-g-PEG) NPs exhibited a considerable change in size, upon a change in pH ranging in diameter from 200 nm (pH 2.0) to 2 μm (pH 6.0) [82, 83]. The poly(MAA-g-PEG) hydrogel NPs were tested for oral delivery of insulin. Insulin was loaded into the NPs by expanding the polymer network at a high pH. While in the stomach, which is characterized by a low pH because of the gastric acid, the NPs shrank and the insulin was physically entrapped and protected from the acid. As the NPs entered the intestine—the major site for drug and nutrient absorption—the pH increased up to 8.0. As a result, the NPs swelled and insulin was released. A significant reduction of serum glucose compared with that of control animals was observed after the insulin-loaded poly (MAA-g-PEG) hydrogel NPs were delivered orally to diabetic rats [83].

6.3 NANOPORE MEMBRANES FOR DRUG DELIVERY

6.3.1 Overview of Nanopore-Based Devices for Sustained Drug Delivery

Depot systems for sustained drug delivery have gained interest in recent years. Polymer-based formulations such as Lupron Depot[®] and Gliadel[®] Wafer are in clinical use for cancer treatment. Many other technologies are currently under development. Notable examples are chip-based devices containing well-defined reservoirs for the controlled release of multiple drugs [84, 85]. Another promising technique for this application is nanopore-mediated drug release. Silicon-based membranes containing arrays of

uniform channel-like nanopores have been created using microfabrication techniques [86, 87]. The pore size was extremely uniform across the entire membrane and could be precisely controlled down to a width as small as 7 nm. Capsules have been built on these membranes with a high drug-loading capacity, and the release kinetics of encapsulated drugs could be controlled by the pore size. The silicon-based nanopore membranes have also been used in biocapsules for the immunoisolation of transplanted pancreatic islet cells for the treatment of diabetes [88]. By precisely controlling the pore size, these membranes would allow the free passage of small molecules such as water, oxygen, nutrients, and insulin, produced by the encapsulated cells, while preventing the entrance of larger and harmful entities such as host antibodies and other immune system constituents. Alumina nanopore membranes with densely packed pores 46–75 nm in diameter produced by anodization have also been tested for immunoisolation [89]. When implanted in the body of a diabetic patient, the encapsulated cells are expected to produce insulin in response to the blood glucose level of the patient for an extended period of time without the need for immunosuppressants.

While the above two techniques can produce chemically inert and mechanically stable nanopore membranes with highly uniform and well-defined pore structures, silicon and alumina are intrinsically nonbiodegradable. If implanted, they must be removed by surgery after use. Polymers such as PLGA, on the contrary, can be fully biodegradable and biocompatible. Compared with silicon-based materials and micro/nanofabrication, polymers are also inexpensive and a variety of low cost techniques are available for the creation of polymeric micro/nanostructures, including nanopore membranes. This section will summarize the fabrication methods for polymeric nanopore membranes and their applications in drug delivery, including a recently developed method for the preparation of a polymeric nanopore membrane. This is followed by a design of the drug delivery device based on this nanopore fabrication technique.

6.3.2 Polymeric Nanopore Membranes for Drug Delivery

Track etching is a well-established process for generating nanopores in a polymer film via swift heavy ion irradiation and subsequent selective etching to remove the polymer in the latent tracks [90]. Polycarbonate (PC) and poly(ethylene terephthalate) (PET) are the polymers primarily used in this technique, though others include polypropylene, poly(vinylidene fluoride), and polyimides. The produced nanopores range from 10 nm to hundreds of nanometers in diameter with a density from 1 to $10^{10}/\text{cm}^2$. Compared with the phase-inversion technique, track etching produces a relatively uniform pore size over a large size range. Sustained drug release through PC membranes with 200–300 nm pores has been demonstrated [91].

The phase-inversion technique may create nanopores based on liquid–liquid diffusion between the polymer-rich and the polymer-poor phase [92]. Within the

membranes, the polymer-rich phase is solidified into a solid matrix, while the polymer-poor phase develops into the pores. The membrane structure elements such as pore size and pore size distribution can be controlled by adjusting the experimental conditions. Phase inversion is a simple process with low cost. However, the relatively wide pore size distribution limits its applications. Phase inversion has been employed to prepare porous membranes for controlled drug delivery [93, 94].

A novel technique, sacrificial template imprinting, has recently been developed in our laboratory to produce polymeric nanonozzle arrays [95]. A bundle of optical fibers was first etched to create an array of extremely sharp tips or nanotips. The nanotip array was used as a master to create a negative poly(dimethyl siloxane) (PDMS) mold by nanoimprinting. It was followed by another nanoimprinting step to produce a PVA nanotip array. A final nanoimprinting step was performed by applying a PLGA film on the PVA nanotips by spin coating the PLGA solution. Parameters such as the spin rate and polymer concentration were carefully controlled to allow for a minimum exposure of the PVA nanotips through the PLGA film. By dissolving the PVA template in water, a PLGA film with an array of well-defined nozzle-like nanopores was created (Fig. 6.2). The pore geometries can be controlled by a number of variables. For example, the fiber diameter can be reduced from 3 μm to less than 200 nm by pulling the optic fibers. This allows for the creation of high density nanotip arrays. The angle of the cone-shaped nanotips depends on the differential etching rates of the fiber and the surrounding cladding material. The size of the small end of the nozzles depends on the tip shape and the imprinting depth. The dimension of the larger end of the nozzles depends on the angle of the tip and the layer thickness. Replication accuracy requires complete wetting between the mold and the casting fluid (i.e., between optic fiber and PDMS resin, or cured PDMS and PVA/water solution, or dry PVA and PLGA solution). Compared with other polymer nanopore

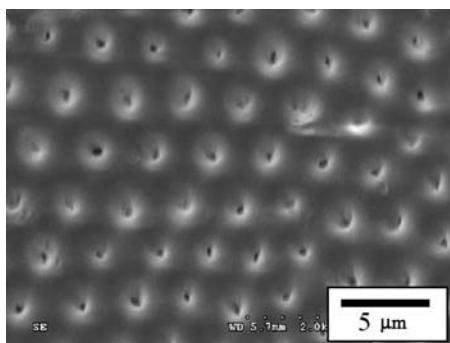


FIGURE 6.2 Scanning electron microscopy image of PLGA nanonozzle array. Pore size: 250 nm.

fabrication techniques, this method can produce high density nanopores with very uniform size from a biodegradable or many other nonbiodegradable polymers. Efforts on the integration of the nanopore membranes into functional devices are ongoing in our laboratory.

To incorporate the nanopore membrane into a practical drug delivery device, we have designed a fabrication procedure for a capsule-like microdevice, as shown in Fig. 6.3. The device consists of two parts: a drug reservoir and a nanonozzle gate. The manufacturing process integrates three modules: (1) microfabrication of the drug reservoir and drug loading, (2) fabrication of the nanonozzle gate by integrating a nanonozzle membrane with a supporting microporous membrane, and (3) device assembly by bonding the two parts together. The entire device, including the drug reservoir, microporous support, and nanonozzle membrane, can be made of biocompatible and biodegradable polymers. It is thus advantageous as an implantable device. A biologically and environmentally benign technique based on CO_2 has been developed in our laboratory for bonding polymers, including PLGA [96]. It can be performed at room temperature in the absence of any organic solvent. Biomolecules such as enzymes and even cells can withstand the bonding conditions and remain active after the treatment [97]. In principle, devices of different sizes ranging from micrometer to centimeter scale can be produced, depending on the intended use. The pore size of the nanonozzles can also be tailored to control the drug release rate. Nanoclay has been added into PLGA to enhance the mechanical stability of

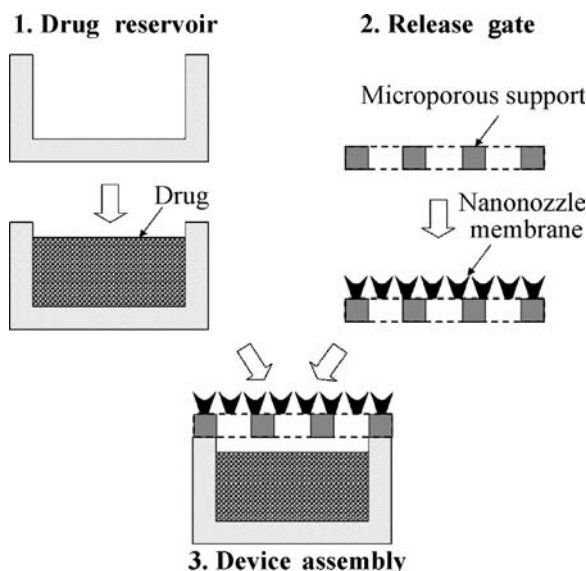


FIGURE 6.3 Schematic representation of fabrication of a nanopore-based micro-device for controlled drug release.

the nanopore membrane [98]. One envisioned application of such a device is sustained release of interferon- α in tumors.

6.4 ELECTROSPUN POLYMERIC NANOFIBERS (EPNFs) FOR DRUG DELIVERY

Besides nanoparticles and nanopore membranes, another class of polymeric nanostructures that have attracted considerable interest for drug delivery is nanofibers, which will be discussed in detail in Chapter 7. Electrospinning is currently the most widely used method for the production of polymeric nanofibers. It can be simply carried out by applying a high voltage (several thousand volts/cm) to a capillary filled with polymer fluid (solution or melt), which is ejected out toward a counterelectrode serving as the collector. The liquid jet undergoes a whipping process and splaying occurs in a region where the repulsive force from the electric charges carried by the jet becomes larger than its cohesive force. This splaying and solvent evaporation, together with a large elongation because of the acceleration of the polymer jet by the electric force, are responsible for the formation of nanometer-sized polymeric fibers [99]. This method is highly versatile, allowing the incorporation of multiple ingredients into single fibers by simply dispersing them into a precursor solution or suspension. Coaxial electrospinning has been used to produce core–shell nanofibers that incorporate proteins [100]. A wide range of polymers have been electrospun to form nanofibers, including the polymers widely used in drug delivery, such as PEO/PEG [101], PLGA [102–104], PCL [105], chitosan [106], PVA [107], and gelatin [108]. Compared with other methods for nanofiber fabrication, such as self-assembly and template synthesis, electrospinning is simple, cost-effective, and suitable to yield very long fibers from various polymers.

EPNFs can form nonwoven scaffolds (Fig. 6.4) that are morphologically similar to the extracellular matrix (ECM) of natural tissues. The ECM is characterized by a high porosity, wide distribution of pore size, and a broad range of mechanical properties. These attributes contribute greatly to the structures and functions of tissues and organs. EPNFs provide an excellent platform for cell growth and tissue formation. As a result, EPNFs are widely studied as structural elements in tissue engineering [109] and wound healing [102, 104, 105]. Biologically and therapeutically active compounds are usually incorporated into the EPNFs for synergistic effects. Such compounds include antibiotics [102, 104, 110], antifungal drugs [110], heparin for prevention of vascular smooth-muscle-cell proliferation [105], proteins [100, 107], and plasmid DNA [103]. Currently, research on drug delivery EPNFs is focused on the demonstration of drug incorporation, the effect of drug loading on nanofiber properties, and the characterization of drug release from the nanofibers. Encouraging results have been obtained, making EPNFs promising as future drug delivery carriers.

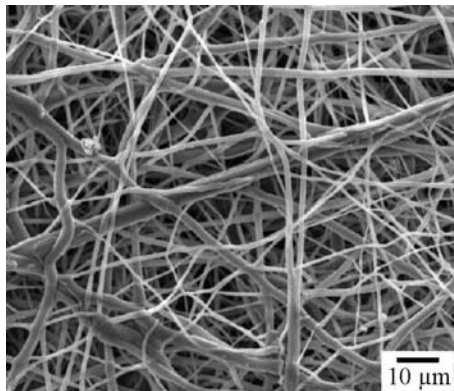


FIGURE 6.4 SEM image of electrospun PCL nanofibers. Courtesy of Dr. John Lannutti in the Department of Materials Science and Engineering at The Ohio State University.

6.5 CONCLUSIONS

Since major diseases such as cancer, diabetes, Alzheimer's disease, and cardiovascular diseases will continue to deteriorate human health in the foreseeable future, new genomic and proteomic drugs are emerging at an accelerated pace with the use of high throughput drug discovery technologies. However, the full realization of the potential of these new therapeutics will need powerful drug/gene delivery technologies. At the same time, polymer nanotechnology is rapidly expanding. Its application to drug/gene delivery has offered unprecedented opportunities for the creation of a variety of polymeric nanostructures. Among them, multifunctional NPs will remain as a major focus in the near future. Besides their therapeutic effects, these NPs should possess functions such as drug protection, targeting, controlled release, stimuli reactivity, barrier penetration, in vivo imaging, and result reporting. Polymers likely will be the major structural materials for the NPs, but they will be joined by many other functional materials such as magnetic particles, quantum dots, and biomolecules for additional functionalities. Simple mixing of the multiple components into a nanosized particle is not enough to achieve the desired functionalities. The organization of the various components into a well-defined and predesigned structure will be essential. One such example is a virus, which can be regarded as a nanomachine that is designed, produced, and optimized by nature specifically for gene delivery. A virus consists of proteins, nucleic acids, and other molecules precisely arranged in the highly organized 3D structure necessary for the execution of a series of functions in a well-defined order. Virus-based vectors have been engineered for gene delivery, but their usage is restricted by high toxicity and immunogenicity. As a result, the "artificial virus" is widely regarded as the next-generation gene delivery vector. It is a virus-like structure, but built

with synthetic materials and capable of efficient gene transfer without the viral toxicity and immunogenicity. Constructing a functioning artificial virus is extremely challenging. The conventional bottom-up approaches carried out in bulk solution for the production of NPs will not be sufficient to achieve all the structures and functions. Nanoengineering techniques such as single-molecule manipulation at the nanoscale likely will be essential for manufacturing such artificial viruses. Other than NPs, many other multifunctional, nanostructured DGDSs likely will be developed. These systems may consist of components such as nanopores for controlled drug release, micro/nanosensors for disease detection, ligands for targeting, and functional NPs for imaging and external activation. The success of such a comprehensive DGDS will require a deep understanding of diseases and biological/physiological systems as well as the integration of knowledge across engineering, science, and medicine.

REFERENCES

1. Langer R. Drug delivery and targeting. *Nature* 1998;392:5–10.
2. Edwards DA, et al. Large porous particles for pulmonary drug delivery. *Science* 1997;276:1868–1871.
3. Bastian P, Bartkowski R, Koehler H, Kissel T. Chemo-embolization of experimental liver metastases. Part 1. Distribution of biodegradable microspheres of different sizes in an animal model for the locoregional therapy. *Eur J Pharm Biopharm* 1998;46:243–254.
4. Lipinski CA, Lombardo F, Dominy BW, Feeney PJ. Experimental and computational approaches to estimate solubility and permeability in drug discovery and development settings. *Adv Drug Deliv Rev* 2001;46:3–26.
5. Mesiha MS, Sidhom MB, Fasipe B. Oral and subcutaneous absorption of insulin poly(isobutylcyanoacrylate) nanoparticles. *Int J Pharm* 2005;288:289–293.
6. Cohen H, et al. Sustained delivery and expression of DNA encapsulated in polymeric nanoparticles. *Gene Ther* 2000;7:1896–1905.
7. Li YP, et al. PEGylated PLGA nanoparticles as protein carriers: synthesis, preparation and biodistribution in rats. *J Control Release* 2001;71:203–211.
8. Moghimi SM, Hunter AC, Murray JC. Long-circulating and target-specific nanoparticles: theory to practice. *Pharmacol Rev* 2001;53:283–318.
9. Ballet F. Hepatic circulation: potential for therapeutic intervention. *Pharmacol Ther* 1990;47:281–328.
10. Hobbs SK, et al. Regulation of transport pathways in tumor vessels: role of tumor type and microenvironment. *Proc Natl Acad Sci USA* 1998;95:4607–4612.
11. Desai MP, Labhasetwar V, Walter E, Levy RJ, Amidon GL. The mechanism of uptake of biodegradable microparticles in Caco-2 cells is size dependent. *Pharm Res* 1997;14:1568–1573.
12. Zauner W, Farrow NA, Haines AMR. *In vitro* uptake of polystyrene microspheres: effect of particle size, cell line and cell density. *J Control Release* 2001;71:39–51.

13. Prabha S, Zhou W-Z, Panyam J, Labhassetwar V. Size-dependency of nanoparticle-mediated gene transfection: studies with fractionated nanoparticles. *Int J Pharm* 2002;244:105–115.
14. Rejman J, Oberle V, Zuhorn IS, Hoekstra D. Size-dependent internalization of particles via the pathways of clathrin- and caveolae-mediated endocytosis. *Biochem J* 2004;377:159–169.
15. Desai MP, Labhassetwar V, Amidon GL, Levy RJ. Gastrointestinal uptake of biodegradable microparticles: effect of particle size. *Pharm Res* 1996;13:1838–1845.
16. Jiao Y, et al. *In vitro* and *in vivo* evaluation of oral heparin-loaded polymeric nanoparticles in rabbits. *Circulation* 2002;105:230–235.
17. Feng S-S. Nanoparticles of biodegradable polymers for new-concept chemotherapy. *Expert Rev Med Devices* 2004;1:115–125.
18. Takeuchi H, Yamamoto H, Kawashima Y. Mucoadhesive nanoparticulate systems for peptide drug delivery. *Adv Drug Deliv Rev* 2001;47:39–54.
19. Olivier J-C. Drug transport to brain with targeted nanoparticles. *NeuroRx* 2005;2:108–119.
20. Gao K and Jiang X. Influence of particle size on transport of methotrexate across blood brain barrier by polysorbate 80-coated polybutylcyanoacrylate nanoparticles. *Int J Pharm* 2006;310:213–219.
21. Zambaux MF, et al. Influence of experimental parameters on the characteristics of poly(lactic acid) nanoparticles prepared by a double emulsion method. *J Control Release* 1998;50:31–40.
22. Niwa T, Takeuchi H, Hino T, Kunou N, Kawashima Y. Preparations of biodegradable nanospheres of water-soluble and insoluble drugs with DL-lactide/glycolide copolymer by a novel spontaneous emulsification solvent diffusion method, and the drug release behavior. *J Control Release* 1993;25:89–98.
23. Mosqueira VCF, et al. Efficacy and pharmacokinetics of intravenous nanocapsule formulations of halofantrine in *Plasmodium berghei*-infected mice. *Antimicrob Agents Chemother* 2004;48:1222–1228.
24. Dailey LA, et al. Nebulization of biodegradable nanoparticles: impact of nebulizer technology and nanoparticle characteristics on aerosol features. *J Control Release* 2003;86:131–144.
25. Allemann E, Leroux JC, Gurny R, Doelker E. *In vitro* extended-release properties of drug-loaded poly(DL-lactic acid) nanoparticles produced by a salting-out procedure. *Pharm Res* 1993;10:1732–1737.
26. Konan YN, Gurny R, Allemann E. Preparation and characterization of sterile and freeze-dried sub-200 nm nanoparticles. *Int J Pharm* 2002;233:239–252.
27. Subramaniam B, Rajewski RA, Snavely K. Pharmaceutical processing with supercritical carbon dioxide. *J Pharm Sci* 1997;86:885–890.
28. Mishima K, et al. Microencapsulation of proteins by rapid expansion of supercritical solution with a nonsolvent. *AIChE J* 2000;46:857–865.
29. Randolph TW, Randolph AD, Mebes M, Yeung S. Sub-micrometer-sized biodegradable particles of poly(L-lactic acid) via the gas antisolvent spray precipitation process. *Biotechnol Prog* 1993;9:429–435.

30. Soma CE, Dubernet C, Bentolila D, Benita S, Couvreur P. Reversion of multidrug resistance by co-encapsulation of doxorubicin and cyclosporin A in polyalkylcyanoacrylate nanoparticles. *Biomaterials* 1999;21:1–7.
31. Barraud L, et al. Increase of doxorubicin sensitivity by doxorubicin-loading into nanoparticles for hepatocellular carcinoma cells *in vitro* and *in vivo*. *J Hepatol* 2005;42:736–743.
32. Schwab G, et al. Antisense oligonucleotides adsorbed to polyalkylcyanoacrylate nanoparticles specifically inhibit mutated Ha-ras-mediated cell proliferation and tumorigenicity in nude mice. *Proc Natl Acad Sci USA* 1994;91:10460–10464.
33. Leo E, Angela Vandelli M, Cameroni R, Forni F. Doxorubicin-loaded gelatin nanoparticles stabilized by glutaraldehyde: involvement of the drug in the crosslinking process. *Int J Pharm* 1997;155:75–82.
34. Yeh TK, Lu Z, Wientjes MG, Au JLS. Formulating paclitaxel in nanoparticles alters its disposition. *Pharm Res* 2005;22:867–874.
35. Bajpai AK and Choubey J. *In vitro* release dynamics of an anticancer drug from swellable gelatin nanoparticles. *J Appl Polym Sci* 2006;101:2320–2332.
36. Cascone MG, Lazzeri L, Carmignani C, Zhu Z. Gelatin nanoparticles produced by a simple W/O emulsion as delivery system for methotrexate. *J Mater Sci Mater Med* 2002;13:523–526.
37. Vandervoort J and Ludwig A. Preparation and evaluation of drug-loaded gelatin nanoparticles for topical ophthalmic use. *Eur J Pharm Biopharm* 2004;57: 251–261.
38. Truong-Le VL, et al. Gene transfer by DNA–gelatin nanospheres. *Arch Biochem Biophys* 1999;361:47–56.
39. Kaul G and Amiji M. Tumor-targeted gene delivery using poly(ethylene glycol)-modified gelatin nanoparticles: *in vitro* and *in vivo* studies. *Pharm Res* 2005;22: 951–961.
40. Balthasar S, et al. Preparation and characterization of antibody modified gelatin nanoparticles as drug carrier system for uptake in lymphocytes. *Biomaterials* 2005;26:2723–2732.
41. Dinauer N, et al. Selective targeting of antibody-conjugated nanoparticles to leukemic cells and primary T-lymphocytes. *Biomaterials* 2005;26:5898–5906.
42. Vinogradov S, Batrakova E, Kabanov A. Poly(ethylene glycol)–polyethylenimine NanoGel particles: novel drug delivery systems for antisense oligonucleotides. *Colloid Surf B* 1999;16:291–304.
43. Vinogradov SV, Bronich TK, Kabanov AV. Nanosized cationic hydrogels for drug delivery: preparation, properties and interactions with cells. *Adv Drug Deliv Rev* 2002;54:135–147.
44. Vinogradov SV, Zeman AD, Batrakova EV, Kabanov AV. Polyplex nanogel formulations for drug delivery of cytotoxic nucleoside analogs. *J Control Release* 2005;107:143–157.
45. Vinogradov SV, Batrakova EV, Kabanov AV. Nanogels for oligonucleotide delivery to the brain. *Bioconj Chem* 2004;15:50–60.
46. Zahoor A, Sharma S, Khuller GK. Inhalable alginate nanoparticles as anti-tubercular drug carriers against experimental tuberculosis. *Int J Antimicrob Agents* 2005;26:298–303.

47. You J-O and Peng C-A. Calcium-alginate nanoparticles formed by reverse microemulsion as gene carriers. *Macromol Symp* 2004;219:147–153.
48. Gonzalez Ferreiro M, Tillman L, Hardee G, Bodmeier R. Characterization of alginate/poly-L-lysine particles as antisense oligonucleotide carriers. *Int J Pharm* 2002;239:47–59.
49. Aynie I, Vauthier C, Chacun H, Fattal E, Couvreur P. Spongelike alginate nanoparticles as a new potential system for the delivery of antisense oligonucleotides. *Antisense Nucleic Acid Drug Dev* 1999;9:301–312.
50. Calvo P, Remunan-Lopez C, Vila-Jato JL, Alonso MJ. Novel hydrophilic chitosan–polyethylene oxide nanoparticles as protein carriers. *J Appl Polym Sci* 1997;63:125–132.
51. Zhang H, Oh M, Allen C, Kumacheva E. Monodisperse chitosan nanoparticles for mucosal drug delivery. *Biomacromolecules* 2004;5:2461–2468.
52. Calvo P, Remunan-Lopez C, Vila-Jato JL, Alonso MJ. Chitosan and chitosan/ethylene oxide–propylene oxide block copolymer nanoparticles as novel carriers for proteins and vaccines. *Pharm Res* 1997;14:1431–1436.
53. Fernandez-Urrusuno R, Calvo P, Remunan-Lopez C, Vila-Jato JL, Alonso MJ. Enhancement of nasal absorption of insulin using chitosan nanoparticles. *Pharm Res* 1999;16:1576–1581.
54. Grenha A, Seijo B, Remunan-Lopez C. Microencapsulated chitosan nanoparticles for lung protein delivery. *Eur J Pharm Sci* 2005;25:427–437.
55. De Campos AM, Sanchez A, Alonso MJ. Chitosan nanoparticles: a new vehicle for the improvement of the delivery of drugs to the ocular surface. Application to cyclosporin A. *Int J Pharm* 2001;224:159–168.
56. Janes KA, Fresneau MP, Marazuela A, Fabra A, Alonso MJ. Chitosan nanoparticles as delivery systems for doxorubicin. *J Control Release* 2001;73:255–267.
57. Leong KW, et al. DNA–polycation nanospheres as non-viral gene delivery vehicles. *J Control Release* 1998;53:183–193.
58. Roy K, Mao H-Q, Huang SK, Leong KW. Oral gene delivery with chitosan–DNA nanoparticles generates immunological protection in a murine model of peanut allergy. *Nat Med* 1999;5:387–391.
59. Jiang X, et al. Chitosan-g-PEG/DNA complexes deliver gene to the rat liver via intrabiliary and intraportal infusions. *J Gene Med* 2006;8:477–487.
60. Boussif O, et al. A versatile vector for gene and oligonucleotide transfer into cells in culture and *in vivo*: polyethylenimine. *Proc Natl Acad Sci USA* 1995;92:7297–7301.
61. Akinc A, Thomas M, Klibanov AM, Langer R. Exploring polyethylenimine-mediated DNA transfection and the proton sponge hypothesis. *J Gene Med* 2005;7:657–663.
62. Lungwitz U, Breunig M, Blunk T, Goepferich A. Polyethylenimine-based non-viral gene delivery systems. *Eur J Pharm Biopharm* 2005;60:247–266.
63. Neu M, Fischer D, Kissel T. Recent advances in rational gene transfer vector design based on poly(ethylene imine) and its derivatives. *J Gene Med* 2005;7:992–1009.

64. Kunath K, von Harpe A, Fischer D, Kissel T. Galactose-PEI-DNA complexes for targeted gene delivery: degree of substitution affects complex size and transfection efficiency. *J Control Release* 2003;88:159-172.
65. Bennis JM, Mahato RI, Kim SW. Optimization of factors influencing the transfection efficiency of folate-PEG-folate-graft-polyethylenimine. *J Control Release* 2002;79:255-269.
66. Kircheis R, Blessing T, Brunner S, Wightman L, Wagner E. Tumor targeting with surface-shielded ligand-polycation DNA complexes. *J Control Release* 2001;72:165-170.
67. Chiu S-J, Ueno NT, Lee RJ. Tumor-targeted gene delivery via anti-HER2 antibody (trastuzumab, Herceptin) conjugated polyethylenimine. *J Control Release* 2004;97:357-369.
68. Dif F, Djediat C, Alegria O, Demeneix B, Levi G. Transfection of multiple pulmonary cell types following intravenous injection of PEI-DNA in normal and CFTR mutant mice. *J Gene Med* 2006;8:82-89.
69. Kichler A, Chillon M, Leborgne C, Danos O, Frisch B. Intranasal gene delivery with a polyethylenimine-PEG conjugate. *J Control Release* 2002;81:379-388.
70. Kleemann E, et al. Nano-carriers for DNA delivery to the lung based upon a TAT-derived peptide covalently coupled to PEG-PEI. *J Control Release* 2005;109:299-316.
71. Gautam A, Densmore CL, Golunski E, Xu B, Waldrep JC. Transgene expression in mouse airway epithelium by aerosol gene therapy with PEI-DNA complexes. *Mol Ther* 2001;3:551-556.
72. Wang S, Ma N, Gao SJ, Yu H, Leong KW. Transgene expression in the brain stem effected by intramuscular injection of polyethylenimine/DNA complexes. *Mol Ther* 2001;3:658-664.
73. Kircheis R, et al. Polyethylenimine/DNA complexes shielded by transferrin target gene expression to tumors after systemic application. *Gene Ther* 2001;8:28-40.
74. Aoki K, et al. Polyethylenimine-mediated gene transfer into pancreatic tumor dissemination in the murine peritoneal cavity. *Gene Ther* 2001;8:508-514.
75. Uchino H, et al. Cisplatin-incorporating polymeric micelles (NC-6004) can reduce nephrotoxicity and neurotoxicity of cisplatin in rats. *Br J Cancer* 2005;93:678-687.
76. Yoo HS and Park TG. Folate receptor targeted biodegradable polymeric doxorubicin micelles. *J Control Release* 2004;96:273-283.
77. Lavasanifar A, Samuel J, Kwon GS. Poly(ethylene oxide)-block-poly(L-amino acid) micelles for drug delivery. *Adv Drug Deliv Rev* 2002;54:169-190.
78. Le Garrec D, et al. Poly(*N*-vinylpyrrolidone)-block-poly(DL-lactide) as a new polymeric solubilizer for hydrophobic anticancer drugs: *in vitro* and *in vivo* evaluation. *J Control Release* 2004;99:83-101.
79. Kawano K, et al. Enhanced antitumor effect of camptothecin loaded in long-circulating polymeric micelles. *J Control Release* 2006;112:329-332.
80. Mathot F, Van Beijsterveldt L, Preat V, Brewster M, Arien A. Intestinal uptake and biodistribution of novel polymeric micelles after oral administration. *J Control Release* 2006;111:47-55.

81. Vinogradov S, Batrakova E, Li S, Kabanov A. Polyion complex micelles with protein-modified corona for receptor-mediated delivery of oligonucleotides into cells. *Bioconjug Chem* 1999;10:851–860.
82. Robinson DN and Peppas NA. Preparation and characterization of pH-responsive poly(methacrylic acid-g-ethylene glycol) nanospheres. *Macromolecules* 2002;35:3668–3674.
83. Foss AC, Goto T, Morishita M, Peppas NA. Development of acrylic-based copolymers for oral insulin delivery. *Eur J Pharm Biopharm* 2004;57:163–169.
84. Santini JT Jr, Cima MJ, Langer R. A controlled-release microchip. *Nature* 1999;397:335–338.
85. Grayson ACR, et al. Multi-pulse drug delivery from a resorbable polymeric microchip device. *Nat Mater* 2003;2:767–772.
86. Martin F, et al. Tailoring width of microfabricated nanochannels to solute size can be used to control diffusion kinetics. *J Control Release* 2005;102:123–133.
87. Walczak RJ, et al. Long-term biocompatibility of NanoGATE drug delivery implant. *Nanobiotechnology* 2005;1:35–42.
88. Desai TA, et al. Nanopore technology for biomedical applications. *Biomed Microdevices* 1999;2:11–40.
89. La Flamme KE, et al. Nanoporous alumina capsules for cellular macroencapsulation: transport and biocompatibility. *Diabetes Technol Ther* 2005;7:684–694.
90. Fleischer RL, Price PB, Walker RM. *Nuclear Tracks in Solids: Principles and Applications*. Berkeley:University of California Press;1975. p 3–118.
91. Rao V, Amar JV, Avasthi DK, Narayana Charyulu R. Etched ion track polymer membranes for sustained drug delivery. *Radiat Meas* 2003;36:585–589.
92. Kim SY, Kanamori T, Noumi Y, Wang P-C, Shinbo T. Preparation of porous poly(D,L-lactide) and poly(D,L-lactide-co-glycolide) membranes by a phase inversion process and investigation of their morphological changes as cell culture scaffolds. *J Appl Polym Sci* 2004;92:2082–2092.
93. Thombre AG, Cardinal JR, DeNoto AR, Herbig SM, Smith KL. Asymmetric membrane capsules for osmotic drug delivery. I. Development of a manufacturing process. *J Control Release* 1999;57:55–64.
94. Thombre AG, Cardinal JR, DeNoto AR, Gibbes DC. Asymmetric membrane capsules for osmotic drug delivery II. *In vitro* and *in vivo* drug release performance. *J Control Release* 1999;57:65–73.
95. Wang S, et al. Polymeric nanonozzle array fabricated by sacrificial template imprinting. *Adv Mater* 2005;17:1182–1186.
96. Yang Y, Zeng C, Lee LJ. Three-dimensional assembly of polymer microstructures at low temperatures. *Adv Mater* 2004;16:560–564.
97. Yang Y, Xie Y, Kang X, Lee LJ, Kniss D. Assembly of three-Dimensional polymeric constructs containing cells/biomolecules using carbon dioxide. *J Am Chem Soc* 2006;128:14040–14041.
98. He H, Yen C, Ho W, Lee LJ. Preparation of nanoporous PLGA membranes by phase inversion and investigation of their morphological changes for drug delivery. *Forthcoming*.

99. Frenot A and Chronakis IS. Polymer nanofibers assembled by electrospinning. *Curr Opin Colloid Interface Sci* 2003;8:64–75.
100. Jiang H, et al. A facile technique to prepare biodegradable coaxial electrospun nanofibers for controlled release of bioactive agents. *J Control Release* 2005;108:237–243.
101. Son WK, Youk JH, Lee TS, Park WH. The effects of solution properties and polyelectrolyte on electrospinning of ultrafine poly(ethylene oxide) fibers. *Polymer* 2004;45:2959–2966.
102. Kim K, et al. Incorporation and controlled release of a hydrophilic antibiotic using poly(lactide-co-glycolide)-based electrospun nanofibrous scaffolds. *J Control Release* 2004;98:47–56.
103. Luu YK, Kim K, Hsiao BS, Chu B, Hadjiargyrou M. Development of a nanostructured DNA delivery scaffold via electrospinning of PLGA and PLA-PEG block copolymers. *J Control Release* 2003;89:341–353.
104. Katti DS, Robinson KW, Ko FK, Laurencin CT. Bioresorbable nanofiber-based systems for wound healing and drug delivery: optimization of fabrication parameters. *J Biomed Mater Res B Appl Biomater* 2004;70B:286–296.
105. Luong-Van E, et al. Controlled release of heparin from poly(ϵ -caprolactone) electrospun fibers. *Biomaterials* 2006;27:2042–2050.
106. Bhattarai N, Edmondson D, Veisoh O, Matsen FA, Zhang M. Electrospun chitosan-based nanofibers and their cellular compatibility. *Biomaterials* 2005;26:6176–6184.
107. Zeng J, et al. Poly(vinyl alcohol) nanofibers by electrospinning as a protein delivery system and the retardation of enzyme release by additional polymer coatings. *Biomacromolecules* 2005;6:1484–1488.
108. Zhang Y, Ouyang H, Lim CT, Ramakrishna S, Huang Z-M. Electrospinning of gelatin fibers and gelatin/PCL composite fibrous scaffolds. *J Biomed Mater Res B Appl Biomater* 2005;72B:156–165.
109. Venugopal J and Ramakrishna S. Applications of polymer nanofibers in biomedicine and biotechnology. *Appl Biochem Biotechnol* 2005;125:147–157.
110. Verreck G, et al. Incorporation of drugs in an amorphous state into electrospun nanofibers composed of a water-insoluble, nonbiodegradable polymer. *J Control Release* 2003;92:349–360.

Development of Nanostructures for Drug Delivery Applications

NIKHIL DUBE, JOYDEEP DUTTA, and DHIRENDRA S. KATTI

7.1 INTRODUCTION

The prevalent methods for drug administration, namely oral and intravenous routes, are not always the most efficient routes for a particular treatment. These conventional free drug therapy methods have some disadvantages such as the low bioavailability of the drug at the target site, toxic side effects of the drug on healthy tissues, and degradation of the drug in the body before reaching the desired site of action [1]. Blood concentration of a drug, which is administered in a conventional manner, rapidly increases after administration and then decreases as it gets metabolized, and in due course its therapeutic effect comes to an end [2]. The key point in drug administration is that the blood concentration of the bioactive agent should remain between a maximum value (which represents the drug toxic level) and a minimum value (below which the drug is not effective) and this range of concentration is often referred to as the “therapeutic range” [3]. In controlled drug delivery systems designed for long-term administration, the drug level in the blood remains almost constant between the desired maximum and minimum for an extended period of time. Bioactive agents (such as drugs, proteins, nucleic acids) administered through oral or intravenous routes can be degraded prematurely by metabolism as well as by the destructive acidic and enzymatic conditions existing in gastrointestinal tracts in the body. The circulation time of these molecules in the body can be increased by entrapping them in appropriate high molecular weight materials, of which most commonly used are polymers. Hydrophobic drugs do not dissolve in the blood and do not reach their target, and this reduces their pharmacological efficacy. They can be more efficiently

delivered by encapsulation in hydrophilic drug carriers [4]. Drug delivery systems are designed to ensure the drug distribution in a manner such that its major fraction interacts exclusively with the target tissue at the cellular and subcellular level in addition to providing the desired kinetics for a specific duration. Therefore, problems associated with the administration of free drugs, such as limited solubility, poor biodistribution, lack of selectivity, unfavorable pharmacokinetics, and healthy tissue damage, can be overcome or ameliorated by the use of drug delivery systems. Drug delivery systems are designed to provide methods for targeting and releasing desired quantities of therapeutic compounds in well-defined regions in the body. In the process of delivery, the drug of interest is encapsulated in different forms like nano- and microstructures or macroscale drug releasing implants, which leads to controlled release of the drug. This enhances the therapeutic efficacy of the drugs and reduces the side effects. A variety of delivery systems have been developed to incorporate and release drugs, ranging from classical small molecules to large DNA fragments and proteins.

The main advantage of drug delivery systems is their ability to modify pharmacokinetics and biodistribution of the drug in the body as required [5]. The rate of drug release from the carrier determines its therapeutic effect. The rate of release from a drug carrier is controlled by the properties of the carrier material, the properties of the drug used, and the type of drug carrier system. The release rate can also be controlled using external stimulants like pH, ionic strength, temperature, magnetism, and ultrasound, depending on the type of delivery vehicle used. The mechanism of drug release can be either (a) diffusion of the drug from the carrier, (b) biodegradation of the material of encapsulation, (c) swelling of the encapsulating carrier followed by diffusion of the drug, or (d) a combination of the aforementioned mechanisms (a–c) [3].

Through proper targeting, drugs can be selectively delivered to the target site in requisite doses without affecting healthy tissues and organs. The biodistribution of the drugs can be improved primarily by two mechanisms, passive and active targeting. The natural tendency of particulate drug delivery systems to localize in the mononuclear phagocyte system (MPS), particularly, in liver and spleen macrophages, and enhanced permeability and retention (EPR) effect [5] observed in solid tumors are examples of passive targeting. In active or ligand-mediated targeting, the site-specific actions of drug delivery systems are achieved by combining them with ligands targeted against cell surface antigens or receptors. The drugs are combined with antibodies or ligands having specificity for the cell type of interest, therefore enabling active drug targeting. For example, cells of multiple cancer types including liver, kidney, and breast have been reported to overexpress folic acid receptors [6]. Hence, drug delivery systems can be surface modified to incorporate folic acid, which leads to greater accumulation of the drug inside the cancerous cells as against healthy ones. Thus, targeted drug delivery is a promising for the treatments of a variety of diseases [7–9].

The advent of nanotechnology has brought a revolution in the area of drug delivery. In the nanoworld, dimensions in the range from 0.1 to 100 nm play a vital role and the knowledge of the materials/mechanisms at the nanoscale may accelerate the improvement of drug delivery systems [10]. It is improving the capability of biomedical devices, which could offer ways of treating life-threatening conditions, including cancer and heart diseases. Nano- and microcarriers, due to their unique features, occupy a special niche in drug delivery technology. Therefore, it would be appropriate to discuss “what is that makes these nanoscale delivery systems unique?”

7.2 NANOSYSTEMS FOR DRUG DELIVERY

Over the years, drug delivery systems have had an enormous impact on medical technology, greatly improving the performance of many existing drugs and enabling the use of entirely new therapies. The delivery systems can vary in size ranging from macro- (>1 mm) to micro- to nanoscale. A considerable amount of research has been conducted for the preparation of macroscopic implants and microscale drug delivery systems [11, 12]. The various microfabrication techniques for drug delivery systems as well as the prospects of coupling drug delivery to macroscale sensors and implants have been discussed elsewhere [11, 12]. Nanosystems offer a variety of advantages as compared to micro- and larger scale delivery systems. The smaller sized nanostructures can easily be engulfed by various cells in the body (endocytosis), and hence offer the advantage of easy transport across the cell membrane. The average diameter of human cells spans 10–20 μm and the size of cell organelles is limited to a few hundred nanometers. Nanoscale devices offer a significant advantage as they can readily interact with biomolecules on the cell surface and within the cells, without having an adverse effect on the behavior and biochemical properties of those molecules [13]. Anatomical features such as the blood–brain barrier (BBB), the branching pathways of the pulmonary system, and the tight epithelial junctions of the skin make it difficult for larger sized carriers to reach many desired physiological targets [14]. Due to their subcellular sizes, nanocarriers can penetrate through fenestrations of blood capillaries, accumulate within the interstitial space, and be taken up by cells via endocytosis [15]. Hence, nanostructured drug carriers help to overcome the barriers imposed by the anatomical features of human body to allow for efficient delivery of drug molecules to otherwise unreachable diseased cells and tissues.

A wide variety of therapeutic molecules like hydrophilic and hydrophobic drugs, peptides, nucleic acids, DNA, vaccines, and other biological macromolecules can be delivered using nanocarriers [16–40]. Similar to their microscale counterparts, nanoscale carriers can be administered via the oral, intravenous, transdermal, nasal, intratumoral, and ocular routes of administration.

This chapter discusses the synthesis, properties, and drug delivery applications of a variety of nanoscale drug delivery vehicles including nanoparticles,

nanofibers, dendrimers, liposomes, nanotubes, fullerenes, nanogels, nanocrystals, viral vectors, and virus-like particles (VLP).

7.3 POLYMERIC NANOPARTICLES

Polymeric nanoparticles have received a considerable attention worldwide for their potential in controlled and targeted drug delivery systems. Nanoparticles are generally made from silica [16, 17], carbon [18], and metals like gold [19], platinum [20], and polymers [21]. Amongst these, polymeric nanoparticles have been the most promising drug carriers due to their structural and functional characteristics. Polymers offer greater flexibility in terms of method of preparation and the type of bioactive agents that can be encapsulated. The use of several polymeric materials as promising drug carriers is due to their biocompatibility, biodegradability, bioresorbability, and their ability to be functionalized [3]. Encapsulation of the drug within a polymeric carrier allows for greater control on the pharmacokinetics of the drug molecule [21]. The availability of a variety of polymers and the ability to modify the kinetics of drug release make polymeric nanoparticles potential candidates for a wide number of therapeutic applications. Due to the above advantages, the discussion of this section is focused on polymeric nanoparticles and their potential uses in drug delivery systems. A large number of synthetic polymers such as poly(lactic acid) (PLA) [22], poly(glycolic acid) (PGA) [23], and their copolymers poly(lactide-co-glycolide) (PLGA) [24], polyacrylates [25], poly(caprolactone) (PCL) [26], and poly(ethyleneoxide) (PEO) [27], and natural polymers like albumin [28], gelatin [29], alginate [30], collagen [31], and chitosan [6] have been exploited in formulating drug containing nanoparticles.

7.3.1 Synthesis

Several methods have been used for the preparation of polymeric nanoparticles. The emulsion methods employed are single (oil-in-water) emulsion method [24–26, 32–34], double emulsion (water-in-oil-in-water (w/o/w)) method [35–37], and emulsification–solvent diffusion method [38–40]. Several other methods like self-assembly of copolymers to polymeric micelles [41–43], spray drying [44], and salting out [45, 46] have also been reported for the synthesis of nanoparticles used in drug delivery applications. Polymeric nanoparticles can also be formed by the polymerization of monomers instead of using preformed polymers as in the methods mentioned above. The most common route is emulsion polymerisation, and nanoparticles formed by this method are uniformly dispersed in the aqueous phase and are stabilized by emulsifier molecules [47, 48]. The choice of the process for the formulation of drug-loaded nanoparticles depends on many factors like type of polymer, drug, interaction between the polymer and the drug, and final properties desired [49]. However, this chapter will not focus on all the available methods for

nanoparticle synthesis. For more information, the readers are directed to some excellent papers published on the various methods of nanoparticle synthesis.

7.3.1.1 Structure and Property The most important characteristics of nanoparticles that influence their eventual performance as drug delivery systems are particle size, encapsulation efficiency, and zeta potential.

Size and Shape The size of nanoparticles is very crucial for successful use as a drug delivery device. A smaller size is required for rapid dissolution in the body or arterial uptake [50, 51]. Larger particles are preferred for prolonged dissolution or targeting of MPS [34]. The factors that influence the size of polymeric nanoparticles are polymer concentration and molecular weight and the surfactant concentration [37, 52]. The shape of the nanoparticle has an important bearing on the drug release mechanism. The mechanism of drug release can be degradation, diffusion, or a combination of both [3]. For particles with a compact structure, drug release is controlled by the degradation of the polymer matrix, whereas for particles with pores and channels, release mainly depends on the diffusion of the drug [53].

Drug Encapsulation The drug loading efficiency largely depends upon the method of preparation, physicochemical properties of the drug, nature of polymer and surfactant used, and the interaction between the polymer, drug, and surfactant [32–34]. Drug can be incorporated in the nanoparticles using primarily two approaches, (i) incorporation during the preparation of particles or (ii) incubation/adsorption after the formation of particles [54]. In the first approach, the drug is chemically conjugated to the polymer matrix or physically entrapped in the polymer matrix, whereas the latter approach involves physical adsorption of the drug on the nanoparticle surface. The amount of drug encapsulated is higher when incorporated during the formation of particles; however, in this approach there is a possibility that drug stability gets affected by process parameters such as method of preparation and presence of additives [54].

Zeta Potential Another characteristic of polymeric nanoparticles that is of extreme interest is zeta potential. Zeta potential represents an index for particle stability. Particles with zeta potentials more positive than +30 mV or more negative than -30 mV are normally considered stable [55]. For the case of charged particles, as the zeta potential increases, the repulsive interactions will be larger leading to the formation of more stable particles with a more uniform size distribution. This stability is important in preventing aggregation. Surface modification is most commonly used approach for controlling zeta potential of nanoparticles and thereby improving their stability [56].

7.3.1.2 Applications of Nanoparticles for Drug Delivery Nanoparticles have been widely investigated for their drug and gene delivery applications.

Drug release from the nanoparticle eventually determines the therapeutic efficacy of the carrier. Broadly, the release characteristics of the nanocarriers can be modulated using the polymer and drug properties and external conditions such as pH, temperature, and magnetic field. The availability of a variety of parameters, which can be used to control the drug release profiles of the nanoparticles, has given rise to their applications in a number of biomedical areas. Some of the important applications of nanoparticles for therapeutic purposes are discussed in this section.

Cancer Chemotherapy Chemotherapy in cancer is often limited by the toxicity of the anticancer drugs used. This is because both the target cancerous cells and normal cells are nonselectively exposed to the drug, which can lead to undesired toxic side effects. Polymeric nanoparticles as drug carriers have been investigated in an attempt to increase the therapeutic efficacy and to reduce the undesired toxicity of anticancer drugs. The two most widely reported approaches for targeting cancer cells are passive [57, 58] and active targeting [59, 60]. One of the methods of active targeting is by the use of “stealth nanoparticles” that have been developed to avoid both the opsonization process and the recognition by macrophages [61]. This is achieved by modifying the surface of these nanoparticles so as to enable a hydrophilic nature to the surface. The hydrophilic coating prevents protein binding, complement activation, and preferential uptake by the reticuloendothelial system (RES) through steric repulsion mechanism [62]. The two polymers most widely used for coating nanoparticles to increase their blood circulation and accumulation in tumors after systemic delivery are PEG [63–65] and PEO [66–68]. More details on nanocarriers used for cancer therapy can be found in Chapter 16.

Drug Delivery to Brain The BBB represents an insurmountable obstacle for a large number of drugs, including antibiotics, antineoplastic agents, and a variety of drugs that act on central nervous system (CNS) active drugs. This barrier is formed at the level of endothelial cells of the cerebral capillaries and essentially comprises the major interface between the blood and the brain [69]. The brain blood vessel endothelial cells are characterized by having tight continuous circumferential junctions between them, thus abolishing any paracellular pathways between these cells. The presence of the tight junctions and the lack of employment of pathways between cells greatly restrict the movement of polar solutes across the cerebral endothelium. The diffusion of drugs from the blood into the brain mainly depends upon the ability of the biologically active molecule to traverse lipid membranes [70].

Polymeric nanoparticles can be advantageous in a number of ways for efficient delivery of drugs to brain and the central nervous system. The solid matrix of polymeric carriers protects the incorporated drugs against degradation, thus increasing the chances of the drug reaching the brain [71]. Furthermore, carriers can target delivery of drugs to the brain, and this targeted delivery can be controlled. Several studies have reported the use of polymeric

nanoparticles for targeted drug delivery to brain [72]. Several molecules like lectin [73], polysorbate-80 [74], apolipoprotein E [75], transferrin [76], and peptides [79] have been used as active agents for targeting brain capillary endothelial cell membranes and have been found to facilitate the drug transport across BBB. The surface properties of nanoparticles can be manipulated in a way so as to evade recognition by the macrophages of the RES, hence improving their likelihood of reaching the brain [71]. The mechanism of nanoparticle-mediated transport of drugs through BBB is believed to be endocytosis by the endothelial cells lining the brain blood capillaries [80].

Gene Delivery For effective gene delivery, plasmid DNA must be introduced into target cells, transcribed, and the genetic information ultimately translated into corresponding protein. The two main types of vectors that are used in gene therapy are based on viral or nonviral systems. The viral gene delivery system shows a high transfection yield, but it has many disadvantages such as oncogenic potential and immunogenicity [81]. Nonviral delivery systems have been increasingly proposed as alternatives to viral vectors because of potential advantages like ease of synthesis, cell and tissue targeting, low immune response, and unrestricted plasmid size [82].

Cationic polymers have been reported as promising carriers among the nonviral gene delivery systems. Polycation–DNA complexes are generally very stable and a number of cationic polymers have been investigated as gene carriers [81, 82]. Chitosan [83–85] and polyethyleneimine (PEI) [86, 87] have been used extensively to form nanoparticles (used for encapsulating DNA), and hence as a gene delivery vehicle. These polymers due to their cationic polyelectrolyte nature interact ionically with the negatively charged DNA and form polyelectrolyte complexes [86]. In these complexes, DNA is better protected against nuclease degradation, leading to better transfection efficiency. The chemical structure of polycations, size and composition of complexes, ligands used as targeting agents, plasmid dosage, and pH of transfection medium determine the suitability of polymeric nanoparticles for safe and efficient gene delivery.

7.4 NANOFIBERS

Conventionally, fibers having diameters less than 1 μm would be classified as nanofibers. However, most studies involving the use of nanofibers for drug delivery have made use of fibers with diameter ranging from a few nanometers to hundreds of nanometers [89]. The length of nanofibers can be as large as thousands of meters. Nanofibers can be made from carbon [90], organometallic compounds [91], inorganic compounds [92, 93], and organic polymers [94]. The high surface area and controlled pore size coupled with the ability to modify the release kinetics of the encapsulated bioactive molecules by modulation of composition and morphology of nanofibers make them very good candidates for the delivery of bioactive agents [95]. Due to several advantages such as

biodegradability, biocompatibility, and easy processability offered by many polymers, a variety of polymers in the form of nanofibers have been widely investigated for drug delivery applications [96]. Hence, the present discussion focuses on the methods of synthesis, and drug and gene delivery applications of polymeric nanofibers.

7.4.1 Fabrication

Nanofibers can be fabricated by a variety of methods such as drawing [97, 98], template synthesis [99–102], self-assembly [103–107], phase separation [108], and electrospinning [109–112]. Of these methods, electrospinning has been found to be the most suitable method for the synthesis of nanofibers to be used in drug delivery applications. Therefore, in this section, the discussion on synthesis is limited to electrospinning. However, for an elaborate discussion on other techniques, the reader is directed to some excellent reviews [96, 113, 114]. Electrospinning is relatively versatile, straightforward, cost-effective, and fast technique [110]. Depending on the bioactive agent to be encapsulated (small drug molecules or macromolecules like proteins and nucleic acids), suitable polymers from a variety of synthetic and natural polymers can be chosen to synthesize nanofibers by electrospinning [109]. Moreover, it seems to be the only method, which can be further developed for large-scale production of nanofibers for industrial applications [113]. The above advantages offered by electrospinning make it a very attractive technique for the synthesis of nanofibers for drug delivery applications.

7.4.1.1 Electrospinning An electrospinning system comprises a polymer solution, contained in a syringe with a connected needle [109]. The polymer solution is usually provided a charge using a high voltage power source. The positive output of the power supply unit is connected to the needle of syringe containing the polymer solution, whereas the negative output is connected to a grounded plate [109]. In the process, a high voltage electric field is applied to the tip of the needle connected to the syringe containing the polymer solution. During this process, the polymer droplet gets charged and mutual charge repulsion within the droplet gives rise to a force that opposes the surface tension at the tip of the needle. At a critical voltage, the droplet elongates to form a cone at the tip of the needle known as the “Taylor cone” [110]. When the applied voltage exceeds a critical voltage, the electrical force within the liquid overcomes the surface tension and a fine jet of polymer emerges from the cone. The charged polymer jet is directed to the grounded collector. It has been reported that the path taken by the jet to the grounded electrode is not straight, but undergoes whipping motion/bending instabilities resulting in a progressive decrease in the diameter of the jet [109]. As the jet travels in air, the solvent evaporates, resulting in formation of polymer fibers, which are collected as a nonwoven fiber mesh on the grounded collector. The viscosity of the polymer solution/melt plays a very crucial role in producing nanofibers from the emerging jet [112]. In case of

solutions with low viscosity, the jet breaks into droplets and the process is called electrospraying [115]. Polymer solutions with higher viscosity and long-chain molecules are required to obtain continuous fibers [113]. The parameters that affect electrospinning can be classified into three categories: (i) solution parameters such as viscosity, conductivity/polarity, and surface tension, (ii) process parameters such as applied electric voltage, tip-to-collector distance, diameter of the needle tip, feed rate, and the hydrostatic pressure applied to the polymer solution, and (iii) ambient parameters such as temperature, air velocity, and humidity of the electrospinning chamber [116].

A more detailed understanding of the electrospinning process and the influence of different fabrication parameters on the properties of polymeric nanofibers can be found in the reports by Frenot and Chronakis [109], Zong et al. [116], and Huang et al. [117].

7.4.1.2 Applications of Nanofibers Polymeric nanofibers have been used in a wide variety of applications, including industrial air filtration [118], protective clothing with a desired pore size [119], biomedical and pharmaceutical applications such as tissue engineering [96], and drug and gene delivery [98, 111]. The potential medical application of nonwoven polymeric nanofibers in the area of tissue engineering is to act as a scaffold for cells to attach and organize into tissue. The ideal tissue engineering scaffold should mimic the extracellular matrix, the natural abode of cells. The structure and morphology of nonwoven nanofibers can be manipulated to match the components of the extracellular matrix of natural tissues [96]. Previous studies have demonstrated that cells seeded on biodegradable polymeric nanofibers, when supplied with suitable nutrients and growth factors, can attach, proliferate, and maintain their phenotypic expression [120]. Electrospun nanofibrous scaffolds can also be used as carriers for hydrophilic and hydrophobic drugs and large molecules like DNA and proteins, and the release profile can be finely controlled by the modulation of the scaffold's morphology, porosity, and composition [113]. Due to their small diameter, nanofibers have a very high surface area to volume ratio. An advantage of the delivery of bioactive agents via polymer nanofibers is that the dissolution rate of the agent increases with increasing surface area of the corresponding carrier [117]. The large surface area also makes nanofibers amenable to surface functionalization with cell-specific ligands and antibodies. Thus, nanofibers with the encapsulated bioactive agent can be used for active targeting to specific cells and tissues for therapeutic applications [121]. In this section, the applications of polymeric nanofibrous matrices as delivery vehicles for bioactive agents are divided into two parts (low molecular weight drugs and macromolecules) based on the class of the therapeutic agent used.

Drug Delivery from Nanofibers Polymeric nanofibers have been widely reported for their use in the delivery of small drug molecules. The variety of advantages offered by electrospun nanofibers as discussed in the previous

sections have been exploited in a number of studies to investigate the application of nanofibers as drug carriers.

Kenawy et al. [122] reported electrospun nanofibers (as drug delivery vehicles) made from PLA and poly(ethylene-co-vinyl acetate) (PEVA). In these studies, the antibiotic tetracycline hydrochloride was used as a model drug. It was found that electrospun PEVA showed a higher drug release rate in Tris buffer than the fibers derived from 50/50 PLA/PEVA or pure PLA. This is due to the partial crystallinity of PLA, which limits the diffusion of the drug from the fibers. Similarly, Zeng et al. [123] studied the preparation of PLA nanofibers containing antituberculosis drug rifampin. The effect of ionic and nonionic surfactants on the properties of nanofibers and drug release kinetics in Tris buffer were investigated. The drug was perfectly included in the fibers and no burst release of the drug was observed. The release was attributed mainly to PLA degradation in the medium containing proteinase K, which degrades PLA, and not to the diffusion or permeation of drug through PLA carrier. Zong et al. [114] reported the formation of PLA nanofiber meshes containing a hydrophilic antibiotic, mefoxin, which is commonly used for the prevention of infections after surgery. The drug was completely released from the matrix within 48 h, with a burst release in the first 3 h. In a similar study, Kim et al. [122] prepared nanofibrous scaffolds made of PLGA containing mefoxin. Due to limited physical interactions between mefoxin and PLGA matrix, the majority of the drug localized on the surface of the nanofibers. Hence, the drug molecules on the fiber surface were easily washed away in aqueous solutions, resulting in a large initial burst and minimum sustained release for prolonged time. In order to achieve sustained drug release, amphiphilic PEG-b-PLA block copolymer was added to the existing drug-polymer solution. In this case, some drug molecules were encapsulated within the hydrophilic block of PEG-b-PLA and the initial burst release was reduced. The functionality of the released drug was investigated using *Staphylococcus aureus* bacteria inhibition. The antibiotic released from these electrospun scaffolds was effective in inhibiting bacterial growth. The influence of fiber diameter and the initial drug loading on the release profiles of drug-loaded electrospun PLA nanofibers was studied by Cui et al. [123]. Paracetamol, an analgesic drug, was chosen as a model drug. The results demonstrated that the release profiles of the electrospun meshes were biphasic, with an initial burst release followed by a constant release of the drug. The pores formed after the diffusion of drug molecules from the outer layer led to the subsequent constant release of the drug from the inner part. It was found that the initial burst release increased with the amount of drug loaded in the fibers. In case of fibers with lower drug entrapment, the lower porosity of fibers created by initial diffusion of the drug led to slower release in later stages. This study demonstrated the ability to modulate the kinetics of drug release from electrospun fiber for their applications as drug delivery systems. In yet another study, Katti et al. [124] reported the encapsulation of a broad-spectrum antibiotic, cefazolin, in PLGA nanofibers. They investigated the influence of

electrospinning fabrication parameters on the morphology and diameter of drug-loaded nanofibers. The study demonstrated the feasibility of incorporating different concentrations of cefazolin in PLGA nanofibrous matrices.

Verreck et al. [125] studied the formation of electrospun nanofibers made of polyurethane in which water-insoluble drugs were incorporated in an amorphous state. Itraconazole and ketanserin were chosen as the model drugs. The effect of drug/polymer ratio and polymer concentration on fiber morphology was investigated. Fiber diameter decreased with increasing drug/polymer ratio and decreasing polymer concentration. Itraconazole was released without an initial burst. The release time for higher drug loading was greater and the mechanism of drug release was diffusion from the polymer matrix. Ketanserin release showed a biphasic profile with a faster initial release rate compared to itraconazole. The differences in the rate of release between the two drugs were due to different solubility and diffusivity of drugs in the polymer. Rosen et al. [126] studied the formation of bioerodible nanofibrous matrices made from poly[bis(carboxyphenoxy)methane] (PCPM) by phase separation with a steroid as model drug. The drug release was characterized by an initial induction period where no erosion occurred and was followed by a near linear drug release. It was found that PCPM completely degraded into its monomer under physiological conditions and the drug was released at the rates useful for therapeutic applications. The study suggested the use of PCPM as a prototype polyanhydride for use in bioerodible drug delivery systems. In another study, Taepaiboon et al. [127] synthesized drug-loaded PVA nanofibrous matrices by electrospinning. Four model drugs with different degrees of solubility in the polymer were used in this study. The properties of the drug influenced both the morphology of the nanofibers and release kinetics of encapsulated drugs from the nanofibers. The results demonstrated that the release rate and the amount of drug released were mainly governed by the molecular weight of the drugs, with both parameters (release rate and the amount of drug released) decreasing with increasing molecular weight.

In a novel method reported by Huang et al. [128], PCL nanofibers containing drugs were synthesized using a coaxial/core–shell electrospinning process [129], wherein the core consisted of a drug solution and the shell consisted of a polymer solution. Resveratrol (an antioxidant) and gentamicin sulfate (an antibiotic) were used as model drugs. The morphology of the electrospun fibers was influenced by the concentration of the encapsulated drug and its interaction with the polymer. The results demonstrated that the drug release from the fibers was smooth with no burst release, indicating a perfect inclusion of drugs inside the fibrous matrix. The release kinetics mainly depended on the degradation of the PCL carrier and not on the diffusion of the drug through the carrier. Therefore, this study demonstrated the feasibility of synthesizing core–shell-type nanofibers using the electrospinning technique and the possibility of using the same for drug delivery applications.

In a recent study by Jiang et al. [130], polyethylene glycol-grafted chitosan (PEG-g-CS) and PLGA were electrospun to form nanofibrous scaffolds and

their potential as drug delivery carrier was investigated. Ibuprofen was used as a model drug and the effect of interaction between the drug and the polymer on the drug release was studied. The drug was loaded by two methods, covalent conjugation to PEG-g-CS component or by the electrostatic interaction between the charged carboxylic acid group of ibuprofen and amino groups of chitosan. Drug-loaded PLGA fibers showed burst release, whereas the (PEG-g-CS)/PLGA nanofibers containing drug showed a slower and sustained release. The reason for this observation was attributed to the electrostatic or covalent interaction between the drug and the polymer in (PEG-g-CS)/PLGA nanofibers, which limited the diffusion of the drug from the matrix.

Macromolecular Delivery from Nanofibers The high surface area and high permeability with interconnected pores make nanofibers promising candidates to provide local and sustained delivery of macromolecules like proteins, enzymes, growth factors, and DNA. In the construction of nanofibrous matrices as macromolecule carriers, properties such as structural stability and biochemical activity of the bioactive agent need to be engineered into the design. Nanofibrous meshes designed as scaffolds for drug delivery should be able to offer site-specific delivery of bioactive macromolecules in a controllable and sustainable manner [119]. Additionally, the scaffold should be able to protect the active agent from the biological system until it is released. Various studies have shown the possibility of several polymers to be processed into nanofibrous scaffolds for macromolecular delivery using electrospinning [131–138]. The retention of the bioactivity of released agents and their cell transfection capability has been confirmed by these studies. Some of these have been discussed in this section.

In a study conducted by Luu et al. [131], nanofibrous matrix composed of PLGA and PLA–PEG–PLA triblock copolymer were evaluated for DNA encapsulation. The results of their study demonstrated that an increase in the concentration of the amphiphilic copolymer lead to an increase in the thickness of the nanofibers, and as a consequence, slower release of DNA. The structural integrity of the DNA encapsulated was found to be intact after the electrospinning. The transfection efficiency of released DNA was accessed using preosteoblastic cells. Their results indicated that pCMV β plasmid released from the fibers was taken up by the cells, and subsequently, the β -gal gene was successfully expressed and translated into protein β -galactosidase by the cells. In a similar study by Liang et al. [132], pCMV β plasmid DNA was formulated in a core–shell structure. The DNA was condensed in dimethylformamide, with subsequent encapsulation of the condensed DNA globule in PLA–PEG–PLA triblock copolymer and PLGA was used in the shell. The mixture of encapsulated DNA and PLGA was electrospun to form a nanofibrous scaffold. The polylactide shell protected the encapsulated DNA from degradation during electrospinning. The bioactive plasmid DNA was found to exhibit a controlled release rate and could transfect preosteoblastic cells *in vitro*.

In a recent study, Zeng et al. [133] investigated the release kinetics of a model protein from nanofibrous scaffolds made of PVA (containing bovine serum albumin (BSA)). A hydrophobic coat of poly(*p*-xylene) (PPX) was applied to the electrospun fibers to control the protein release rate from the fibers. The authors observed that PPX-coated nanofibers exhibited a significantly retarded release of BSA, depending on the coating thickness of PPX, in contrast to the burst release of BSA from uncoated PVA nanofibers. In the same study, luciferase was used as a model enzyme to assess the activity of enzymes after their release from the fibers. Continuous release of the enzyme from nanofibers was observed and its structure was found to be intact as determined by gel electrophoresis. In another study, Jiang et al. [134] reported core-shell nanofibers made of PCL as the shell and PEG as the core containing BSA and lysozyme for their application in protein delivery. The fibers were synthesized by coaxial electrospinning in which the two polymers were simultaneously spun to form the coaxial fibers. The size of the core and shell and the protein release rate were controlled by the feed rate of the solution. The electrospinning process did not affect the structure and stability of the proteins. In a similar study by the same group [135], nanofibrous meshes of dextran were evaluated for macromolecular delivery. Uniform nanofibers of dextran were formed with the use of various solvents like water, dimethylsulfoxide, and dimethylformamide, and appropriate process conditions. The structure and activity of the bioactive agents used (BSA and lysozyme) were retained postelectrospinning. Thus, the results of the above studies demonstrated the potential of encapsulating water-soluble macromolecules in nanofibrous matrices for macromolecular delivery applications.

Proteins such as growth factors are often the most important biochemical signals for tissue engineering applications. Growth factors are important for controlling cellular activities of growth and proliferation and stimulating tissue formation. They can be delivered directly in their original form, or their expression can be induced through gene delivery. Growth factors often have short half-lives and are rapidly degraded or cleared, thereby minimizing their biological effect [136]. Numerous studies have investigated the feasibility of developing nanofibrous scaffolds loaded with growth factors and the results have demonstrated their potential as delivery vehicles with retained bioactivity of the agent [137–149]. In one of the studies aimed to assess the potential of delivering growth factors for therapeutic applications in nervous system, a copolymer of caprolactone and ethyl ethylene phosphate (PCLEEP) was electrospun to obtain fibrous scaffolds [137]. Human nerve growth factor (NGF) was encapsulated in the fiber and its sustained release via diffusion was observed for 3 months. Their results demonstrated that NGF released stimulated the growth of neurons *in vitro*. Therefore, such a sustained release system for NGF would be useful, as NGF is known to have a short half-life *in vivo* [137]. In a similar study, Beatty et al. [138] investigated the delivery of NGF from PEVA nanofibrous matrix. The dynamics and bioactivity of NGF released from the polymer matrix were studied using mammalian cells. The

results of their *in vitro* cell culture studies demonstrated that the released NGF stimulated the growth of neurons. In another study by Elbert et al., fibrin matrices were studied as NGF delivery systems [139, 140]. Their results suggested that these nanofiber matrices could enhance peripheral nerve regeneration, thereby indicating that fibrin nanofiber-based carrier devices for NGF delivery hold promise for therapeutic applications in central nervous system disorders like Alzheimer's disease and Parkinson's disease [141]. Delivery of growth factors required for bone repair and regeneration from nanofibrous matrices has also been studied [142–148]. Some of the growth factors that are important in the process of bone regeneration are beta transforming growth factor (TGF- β), platelet-derived growth factor (PDGF), and vascular endothelial growth factor (VEGF) [142]. Delivery of TGF- β [143, 144], PDGF [145–147], and VEGF [148, 149] from polymeric nanofibrous scaffolds has been investigated and the results of these studies demonstrated the controlled release of the growth factors from the nanofibrous scaffolds, and hence suggest their potential use as carriers of growth factors required for bone growth and regeneration.

The results of the aforementioned studies on the use of nanofibrous scaffolds as delivery vehicles for biological agents seem promising and pave the way for the investigations to be conducted so as to develop nanofibers as carriers of therapeutic agents for the treatment of various diseases.

7.5 DENDRIMERS

Dendrimers are highly branched, globular, macromolecules possessing a three-dimensional architecture [150, 151]. The term dendrimers originated from the Greek words dendron and mers, where “dendron” means tree and “mers” means part. Therefore, dendrimers would mean part of a tree and relates to the symmetrical branch-like structure of these polymers (Fig. 7.1). Technically, a dendrimer is a polymer, which is a large molecule consisting of many smaller chemical units linked together. There are two major strategies that are available for the synthesis of dendrimers. The first, introduced by Tomalia, was the “divergent method,” wherein the growth of a dendron originates from a central core. This approach involves assembling monomeric modules in a radial, branch-upon-branch motif [152]. The second method, pioneered by Hawker and Frchet, follows a “convergent growth process” [153]. It proceeds inward from what will become the dendrimer surface to a reactive focal point, leading to the formation of a single reactive dendron. The convergent approach is particularly well suited for the preparation of dendrimers to be used as building blocks for larger functional nanostructures as it provides access to dendritic “wedges” with differentiated reactivity at their focal point and chain ends. Fig. 7.1 provides a schematic representation of the synthetic route followed in the above two methods [154]. Dendrimers can be synthesized in a stepwise manner, which allows controlling their size by manipulating the

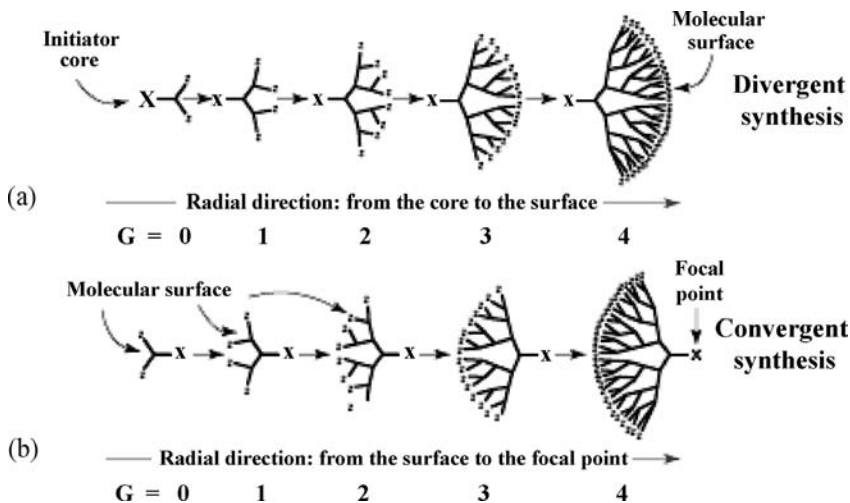


FIGURE 7.1 Schematic representation of the two methods for synthesizing dendritic macromolecules (dendrons): (a) the divergent method, in which the synthesis begins from a polyfunctional core and continues radially outward by successive stepwise activation and condensation, and (b) the convergent method in which the synthesis begins at what will be the periphery of the final macromolecule and proceeds inward. (Reprinted from Reference [154], with permission from Elsevier.)

monomer concentration used for its synthesis [150]. In this way, dendrimers with well-defined size in nanoscale from 70 to 300 nm can be synthesized [151–154].

7.5.1 Properties of Dendrimers

Dendrimers possess unique properties such as high degree of branching, multivalency, globular architecture, and well-defined molecular weight [155,156]. Appropriate manipulation of these properties allows for the design of reproducible and effective drug delivery systems [157,158]. The stepwise synthesis of dendrimers affords molecules with a highly regular branching pattern, a low polydispersity index, and control over the number of peripheral groups. Therefore, dendrimers resulting from stepwise synthetic processes are distinct with perfect branching as compared to the more readily accessed dendrimers obtained by polymerization processes that are often less well-defined hyperbranched polymers with irregular branching. The dendrimer structure/architecture also possesses some interesting properties [159]. Cavities in the core structure and folding of the branches create cages and channels that may be either hydrophilic or hydrophobic in nature depending on the chemical nature of the monomeric units. Specific binding sites may also be incorporated during synthesis. The surface groups of dendrimers are amenable to modification and can be customized for specific applications. Therefore, the

choice of the method of dendrimer synthesis and the monomers used in its synthesis permit control over properties such as shape, size, density, polarity, reactivity, and solubility.

7.5.2 Applications of Dendrimers in Drug Delivery

Structures based on dendrimers have made a significant impact in the area of nanotechnology as they provide for well-controlled functional building blocks. They can be used for a wide variety of applications [155,160,161] ranging from unimolecular devices or nanoreactors to sensors to medical technology including targeted drug and gene delivery. Many potential applications of dendrimers are based on their unparalleled molecular uniformity, multi-functional surface, and presence of internal cavities. These specific properties make dendrimers ideal carriers in biomedical applications such as drug delivery and gene transfection. The bioactive agents may either be encapsulated into the interior of the dendrimers or they may be chemically attached or physically adsorbed onto the dendrimer surface. The surface, interior, and core of the carrier can be tailored for the specific needs of the active material and its therapeutic applications.

There are now more than 50 families of dendrimers [162], with each family possessing unique properties. Poly(amidoamine) (PAMAM) dendrimers are the first complete dendrimer family to be synthesized, characterized, and commercialized [154]. The internal tertiary amines of PAMAM dendrimers are available for acid–base interactions and hydrogen bonding as well as for other noncovalent interactions with encapsulated guest molecules, thus making the polymers effective agents for encapsulating various drugs [163]. Patri et al. [164] investigated the drug delivery potential of PAMAM dendrimers to reduce toxicity and to increase aqueous solubility. The dendrimer surface was functionalized with hydroxyl groups to obtain highly soluble dendrimers. The drug methotrexate was covalently conjugated to the dendrimer. The drug inclusion complex, in which the drug was entrapped in the cage of the dendrimer core by noncovalent interaction, was also evaluated for its release kinetics. The results of this study demonstrated that methotrexate was immediately released from the inclusion complex as opposed to the methotrexate–dendrimer conjugates, which were stable in both water and PBS buffer solution. Therefore, this study indicated that a cleavable, covalently linked drug–dendrimer conjugate is probably more appropriate for drug delivery as it does not release the drug prematurely in biological conditions.

One of the simplest ways to construct dendrimer–drug conjugates is to couple drug molecules directly to the surface of the dendrimer. Because of its multiple surface functionalities, one dendrimer molecule has the capacity to carry multiple drug molecules. The number of drug molecules per conjugate can be varied by changing the coupling conditions. There are several reports on the preparation of dendrimer–drug conjugates via the covalent attachment of

drugs to the dendrimer surface [165, 166]. In a study by Malik et al. [165], a PAMAM dendrimer–platinate conjugate was examined for its antitumor activity. The results of the study demonstrated that the conjugate showed antitumor activity in all the tumor models tested, including a platinum-resistant tumor model. In another study, Zhuo et al. [166] prepared PAMAM dendrimers and attached 5-fluorouracil to the dendrimers to form conjugates. Their results demonstrated hydrolysis of the conjugates in a phosphate buffer solution and the consequent release of free 5-fluorouracil.

Nonsteroidal antiinflammatory drugs (NSAIDs) are among the most frequently used drugs in the world, especially for symptoms associated with osteoarthritis and other chronic musculoskeletal conditions [167]. Some of the NSAIDs widely used are ketoprofen, ibuprofen, diflunisal, and naproxen. NSAIDs cause a wide variety of reported adverse effects, including renal dysfunction, gastrointestinal hemorrhage, and hypersensitivity reactions [168]. These undesired effects have limited the use of NSAIDs. Drug conjugation, cellular transport, and cellular therapeutic activity of NSAIDs-based dendrimer conjugates as drug delivery vehicles have been widely investigated [169–171]. Denis et al. [168] studied the aqueous solubility of NSAIDs ketoprofen, ibuprofen, diflunisal, and naproxen in the presence of the ethylenediamine (EDA) core PAMAM dendrimers. The study demonstrated that PAMAM dendrimers have the potential to significantly enhance the solubility of NSAIDs. The results also demonstrated that the solubility of NSAIDs in the dendrimer solutions increased in an approximately linear manner with an increase in dendrimer concentration. The authors also proved that the bioavailability of the drugs increased with an increase of drug solubility. The reason for the enhancement of solubility of NSAIDs is believed to be an electrostatic interaction and hydrogen bond formations between the surface amine groups on the dendrimer molecule and the carboxyl group of NSAIDs. In another study, Kolhe et al. [169] reported the synthesis and evaluation of hydroxylated PAMAM dendrimer–ibuprofen conjugates with a high drug payload to improve intracellular delivery and to minimize systemic side effects. The study demonstrated the potential of drug–dendrimer conjugates to enter lung epithelial cell lines rapidly and localize predominantly in the cytoplasm. The high drug payload dendritic nanodevices translate into rapid pharmacological response with improved efficacy. Future studies are warranted to evaluate the pharmacokinetic and pharmacodynamic aspects of these nanomaterials in animal models. In yet another study, Na et al. [172] investigated the potential of polyamidoamine (PAMAM) dendrimers as carriers of ketoprofen. Their results demonstrated that the *in vitro* release of ketoprofen from the drug–dendrimer complex is significantly slower compared to pure ketoprofen. The blood distribution studies were conducted with mice and the results demonstrated a prolonged pharmacodynamic behavior for the ketoprofen–PAMAM dendrimer complex. Therefore, this study indicated that PAMAM dendrimers might be considered as potential drug carriers with the capability to provide a sustained release along with reduced side effects.

Dendrimers can also act as carriers, to transfer genes through the cell membrane into the nucleus. PAMAM dendrimers have been investigated as genetic material carriers [173–175]. The terminal amino groups of PAMAM dendrimers interact with phosphate groups of nucleic acids. This ensures consistent formation of transfection complexes. A transfection agent called SuperFect, consisting of activated dendrimers, is now commercially available. Activated dendrimers can carry a larger amount of genetic material than viruses. SuperFect–DNA complexes are characterized by high stability and provide efficient transport of DNA into the nucleus. The high transfection efficiency of dendrimers may not only be due to their well-defined shape, but may also be caused by the low pK of the amines (3.9 and 6.9). The low pK permits the dendrimer to buffer the pH change in the endosomal compartment [176]. The unique properties of dendrimers such as their well-defined size within nanoscale and multiple attachment sites that allow for the attachment of ligand and bioactive agents simultaneously make them suitable candidates for gene delivery. Compounds, which can facilitate nuclear localization, can be incorporated in the dendrimer surface. The above factors suggest that dendrimers can be used as potential transfection agents at the cellular and systemic levels [177].

Dhanikula and Hildgen [178] reported novel polyester-co-polyether dendrimers consisting of a hydrophilic core synthesized by a combination of convergent and divergent syntheses. PEO was incorporated in the interior of the dendrimers to provide a hydrophilic interior region. The dendrimers demonstrated the ability to encapsulate both hydrophilic and hydrophobic model compounds, with sufficiently high drug loading. Rhodamine and β -carotene were used as model hydrophilic and hydrophobic compounds, respectively. It was demonstrated that the physical entrapment and/or hydrogen bonding by PEO in the interior and branches of the dendrimer is responsible for drug encapsulation. The release of both types of encapsulated compounds (hydrophilic and hydrophobic) in phosphate buffer was found to be slow and sustained, with approximately 90% of drug being released in 170 h. Therefore, this study suggested that these dendrimers could be designed to serve as potential delivery vehicles. In another study for both hydrophilic and hydrophobic drugs, Bhadra et al. [179] reported the synthesis of a novel PEGylated peptide dendrimers for the delivery of an antimalarial drug, artemether. In this study, a peptide dendrimer on a PEG core with L-lysine as a repeating unit was synthesized. Artemether was found to form a complex with the dendritic interior as a result of hydrogen bonding and hydrophobic interactions. Chondroitin sulfate A (CSA) was conjugated to the system, which increased drug loading depending on the degree of conjugation. It was observed that CSA conjugation reduced hemolytic toxicity and macrophage toxicity. CSA-conjugated systems proved to be effective in removing ring and trophozooidal forms of *Plasmodium falciparum* culture *in vitro*. Their *in vivo* studies on mice demonstrated prolonged release of artemether from both CSA-coated and uncoated systems up to 13 h after the intramuscular administration

of the drug carriers. This study suggested the suitability of dendrimers for possible controlled delivery of antimalarials.

Therefore, dendrimers provide a uniform platform for drug attachment that has the ability to bind and release drugs through several mechanisms. The features discussed earlier in the text make dendrimers promising candidates for the development of drug delivery systems.

7.6 LIPOSOMES AND LIPID NANOPARTICLES

A liposome is a microscopic spherical vesicle with a membrane composed of a phospholipid bilayer used to deliver drugs, vaccines, or genetic material into a cell [180,181]. Depending on the number of bilayers, liposomes are classified as multilamellar (MLV), small unilamellar (SUVs), or large unilamellar (LUVs) [182]. The sizes of liposome can range from 25 nm to 10 μm in diameter. The size and morphology of liposomes can be regulated by the method of preparation and the concentration of the lipid. Liposomes, as interesting parenteral carrier systems, were described for the first time by Bangham and Horne in the 1960s and were introduced as drug carriers in the 1970s [183]. Liposomes have been widely explored as drug delivery vehicles due in part to the ease with which their assembly can be manipulated to produce specifically designed carriers for a variety of applications. Additionally, liposomes are also appealing because of their biocompatibility, ability to deliver both hydrophilic and hydrophobic drugs, including small molecules and large biomolecules such as DNA, and their ability to accommodate various ligands/coatings on their surface. Some of the obstacles for the development of liposomal formulations are limited physical stability of the lipid dispersions, possibility of drug leakage, low activity due to the absence of specific cell/tissue targeting, nonspecific clearance by the MPS, and difficulties in scaling up of the process [184–187].

Biodegradable and nonbiodegradable polymeric nanoparticles are of great importance for their potential uses in controlled and sustained drug release [188]. Nevertheless, the cytotoxicity of the polymers after internalization into cells is a crucial and often less discussed aspect [189]. Also, large-scale production of polymeric nanoparticles can be challenging. Therefore, polymeric nanoparticle-based carrier systems have had limited success in terms of their commercialization. Therefore, considerable attention has been directed toward the development of solid lipid nanoparticles (SLNs) and nanostructured lipid carriers (NLCs) for their application as controlled delivery systems [190]. SLNs and NLCs consist of matrix prepared with biocompatible and biodegradable lipids or lipidic substances, which are solid, at both room and physiological temperatures [191]. SLNs based on pure triglycerides or waxes exhibit limited drug payloads due to the solubility of drug in the lipid that can lead to potential drug expulsion from the crystal lattice upon polymorphic transitions into perfect crystals [192]. These

disadvantages of SLNs can be overcome by the design of NLCs, which are produced by preparing a blend of a solid and liquid lipid (oil), which leads to an imperfect matrix structure. The matrix of NLCs by virtue of these imperfections can accommodate drugs in molecular form or as amorphous clusters [193]. Compared to other delivery systems such as liposomes, microemulsions, and polymeric nanoparticles, SLNs and NLCs possess specific advantages that include production without organic solvents, long time physical stability, and the possibility of protection of chemically labile moieties inside the particles [190–198]. SLN formulations for various application routes including parenteral, oral, dermal, ocular, pulmonar, and rectal have been developed [199–210].

7.6.1 Synthesis of Liposomes and Lipid Nanoparticles

Liposomes are formed by the self-assembly of phospholipid molecules in an aqueous environment. The approaches for liposome synthesis include extrusion [211], reversed-phase evaporation [212], and detergent-based procedures [213]. For more details on these methods, readers are directed to the review article by Watwe and Bellare [214]. As in the case of liposomes, multiple preparative methods have been established for the production of finely dispersed lipid nanoparticle dispersions. In this section, some of these methods are described briefly keeping in view the possibility of scaling up, a prerequisite for commercialization purposes.

7.6.1.1 High Pressure Homogenization (HPH) HPH is a suitable method for the preparation of SLNs and NLCs and can be performed at elevated temperatures (hot HPH technique) or at low temperatures (cold HPH technique) [215–217]. The particle size in this approach is decreased by cavitation and turbulence. Briefly, for the hot HPH, the lipid and drug are melted (approximately 5°C above the melting point of the lipid) and combined with an aqueous surfactant solution having the same temperature. High speed stirring forms a hot preemulsion. The hot preemulsion is then processed in a temperature-controlled high pressure homogenizer. Generally, a maximum of three cycles at 500 bar are sufficient to form a nanoemulsion. The obtained nanoemulsions are crystallized upon cooling down to room temperature forming SLNs or NLCs. The cold HPH is more suitable for processing temperature-labile drugs or hydrophilic drugs. In this approach, the lipid and drug are melted together and then rapidly ground under liquid nitrogen forming solid lipid nanoparticles. A presuspension is formed by high speed stirring of the particles in a cold aqueous surfactant solution. This presuspension is then homogenized at or below ambient temperature forming SLNs or NLCs. The homogenizing conditions are generally five cycles at 500 bar. Both the aforementioned HPH techniques are suitable for processing lipid concentrations of up to 40% and generally yield very narrow particle size distributions (polydispersity index < 0.2) [218–219]. Scale-up feasibility for the

large-scale production of SLNs using this technique has also been reported [220–221].

7.6.1.2 Microemulsion Method In this method [220, 222], first, a warm microemulsion is prepared by stirring a solution containing typically 10% molten solid lipid, 15% surfactant, and 10% cosurfactant. This warm microemulsion is then dispersed under stirring in excess cold water (typical ratio 1:50) using a specially developed thermostated syringe. The excess water is removed either by ultrafiltration or by lyophilization in order to increase the particle concentration followed by ultrafiltration to finally arrive at SLN. The disadvantages of the process are the removal of excess water from the prepared SLN dispersion and the high concentrations of surfactants and cosurfactants that could enhance cost and pose regulatory hurdles during scale-up.

7.6.1.3 High Speed Stirring and/or Ultrasonication Another method for the production of SLN is from lipid microparticles (produced by spray congealing) using high speed stirring or sonication [223]. The advantages of this method are the ease of production and the use of simple equipments with easy availability. The problem associated with high speed stirring is that it results in particles of broader size distribution, which in turn can lead to physical instabilities such as particle growth upon storage. This difficulty can be overcome through the use of higher surfactant concentrations; however, this could then lead to toxicological problems. A further disadvantage of this approach is the potential metal contamination due to ultrasonication. In order to overcome the problems associated with the two methods, high speed stirring and ultrasonication have been combined to enable the formation of physically stable particles with narrow size distributions [224, 225].

Some other methods like w/o/w double emulsions [226] and solvent emulsification–evaporation/diffusion [227, 228] are also employed for the preparation of drug-loaded SLNs and NLCs.

7.6.2 Drug Delivery Applications of Liposomes

Liposomes have been extensively investigated as potential drug delivery systems due to the enormous diversity of structure and compositions that they provide [184]. They can encapsulate water-soluble drugs in their aqueous spaces and lipid-soluble drugs within the membrane itself [180]. They release their contents by interacting with cells in one of the four ways: adsorption, endocytosis, lipid exchange, or fusion [186]. They are capable of targeting drugs by passive as well as active means. Unmodified liposomes undergo rapid clearance from blood stream due to sequestration by macrophages of the RES. This property and the flexibility of altering size of liposomes have enabled their use in passive targeting of a number of drugs. The possibility of liposomes to passively target the RES and to encapsulate drugs with toxic side effects has

been studied [229]. The use of antibiotic amphotericin B in the treatment of systemic fungal infections is associated with extensive renal toxicity [229]. The toxicity associated with this compound is probably the result of its interaction with cholesterol in mammalian cells. Liposomal amphotericin B (Ambisome) [230], the first liposomal preparation to be licensed for clinical use, is used for the treatment of systemic fungal infections. Ambisome, by passively targeting the liver and spleen, reduces the renal toxicity of the drug at normal doses, although renal toxicity appears to remain unaffected when the formulation is administered at elevated doses [231]. Ambisome may also be used to treat drug-resistant leishmaniasis, a parasitic infection of the reticuloendothelial system [232]. The ability of liposomes to be taken up by macrophages and to concentrate in the liver and spleen undoubtedly makes them ideal for the treatment of diseases of the liver and spleen.

Liposomes have been established as immunoadjuvants (enhancers of the immunological response), potentiating both cell-mediated and humoral immunity [233]. Liposomal vaccines can be made by associating them with cytokines [233], microbes [234], soluble antigens [235], or DNA [236]. Several investigations have reported that liposomes encapsulating antigens have been found to stimulate an immune response for the antigen used in delivery. Another advantage of liposomal vaccines is that they can be stored under dry conditions at low temperatures for up to 12 months and still retain their adjuvanticity [237]. Hence, liposomes hold promise for vaccine therapy as they can be used for effective antigen/peptide delivery and are able to elicit immune response against the antigen delivered.

The use of liposomes as carriers for DNA has also been explored [238, 239]. Such liposomes are prepared from phospholipids with an amine hydrophilic head group. The amine groups of liposomes interact with the phosphate group of DNA molecules to form the gene carrier. Liposomes prepared in this way are commonly referred to as cationic liposomes, because they possess a positive surface charge at physiological pH. The use of cationic liposomes as gene delivery systems was pioneered in the late 1980s when it was demonstrated that the complexation of genes with liposomes promoted gene uptake by cells *in vitro* [240]. Cationic liposomes have also been actively pursued as a potential tool for gene delivery to specific cells in the body [241–244]. Although the experimental data indicate that cationic liposomes are able to facilitate the transfer of DNA into live mammalian cells, there are still hurdles that need to be overcome in order to achieve successful gene transfection. These include a reduction in the rapid clearance of cationic liposomes, production of efficiently targeted liposomes, ability to transfer the gene to the nucleus of a cell, and the ability to provide a sustained long-term expression of the genes. At the cellular level, the problems may be overcome by improving receptor-mediated uptake using appropriate ligands, the endowment of liposomes with endosomal escape mechanisms, a more efficient translocation of DNA to the nucleus, and the efficient dissociation of the liposome complex just before the entry of free DNA into the nucleus [245].

7.6.3 Drug Delivery Applications of Lipid Nanoparticles

During the past decade, the interest in lipid nanoparticle technology has been growing rapidly. Several studies have been reported to evaluate the potential of SLNs as drug carriers for controlled delivery of drugs with reduced toxic side effects [202, 246, 247]. Cavalli et al. [246] have prepared stealth and nonstealth tripalmitin SLNs loaded with paclitaxel in order to provide an alternative for parenteral administration of paclitaxel. The commercially available product Taxol[®] is a toxicologically critical micellar solution of the drug in Cremophor EL. The release studies on the SLN formulation demonstrated that 0.1% of the paclitaxel was released into the receptor medium (phosphate buffer, pH 7.4) after 120 min. The same group had previously demonstrated similarly sustained *in vitro* release profiles for doxorubicin and idarubicin (0.1% after 120 min) in contrast to burst release from reference solutions [202]. Similarly, for stearic acid SLNs containing cyclosporin A, which is a drug with many adverse side effects, they determined an *in vitro* release of less than 4% drug release after 2 h compared to the release greater than 60% from solution [247]. The clinical use of ketoconazole, an antifungal drug, has been related to some adverse effects in healthy adults, especially local reactions such as severe irritation and stinging. In an attempt to minimize the adverse side effects and providing a controlled release of the drug, Souto and Müller [248] assessed the stability of ketoconazole in SLN and NLC dispersions. Lipid particles were prepared using Compritol[®]888 ATO as solid lipid. The natural antioxidant α -tocopherol was selected as liquid lipid compound for the preparation of NLCs. Ketoconazole loading capacity was identical for both SLN and NLC systems (5% of particle mass). The results of the study indicated that SLNs were physically stable as suspensions after 3 months of storage; however, the SLN matrix was not able to protect the chemically labile ketoconazole against degradation when exposed to light. In contrast, the NLCs were able to stabilize the drug.

In an attempt to explore the potential for delivery of active agents using SLN formulations to brain, Yang et al. [249][249] studied the release mechanism of camptothecin (CA)-loaded stearic acid SLNs in mice. The CA-SLN suspension was injected intravenously into the tail vein of the mice. CA-SLN was found to effectively target the brain by crossing the blood–brain barrier. In another study by Wang et al. [224], *in vitro* release profiles and brain biodistribution studies were performed with an SLN formulation containing 5-fluoro-2'-deoxyuridine (FUdR). The release profile from SLN formulation was biphasic, with an initial burst release that was followed by a prolonged release, whereas 100% drug was released from the FUdR solution after less than 2 h. The biodistribution studies with SLN–FUdR formulation in mice demonstrated that brain targeting of the drug-loaded SLNs was two times greater than FUdR solutions. The probable reason for greater brain targeting with SLN formulations was the increase in effective lipophilicity, which facilitates the transport through the endothelial cells forming the BBB.

For more details on lipid nanoparticles, the readers are directed to some recent review articles [210, 250].

7.7 NANOTUBES AND FULLERENES

Tubes having diameters ranging from a few nanometers to hundreds of nanometers are most often referred to as nanotubes. Nanotubes made of carbon are one of the most well investigated in terms of their structure, property, synthesis, and applications. Therefore, this section focuses on carbon nanotubes (CNTs) and their drug delivery applications and touches upon some of the biomedical applications of fullerenes.

The backbone of CNTs is composed solely of carbon atoms, arranged in form of benzene rings forming graphite sheets, rolled up to give seamless cylinders. There are two main types of CNTs, single-walled (SWNTs) and multiwalled carbon nanotubes (MWNTs), the latter being formed by several concentric layers of rolled graphite sheets. The dimensions of these tubular structures range from 0.4 to 2 nm in diameter for SWNTs and from 2 to 100 nm for MWNTs. Both type of tubes have lengths ranging from micrometers to millimeters. CNTs are generally composed of sp^2 hybridized hexagonal sheets and are perfectly cylindrical in shape [251]. The present discussion focuses on CNTs and their drug delivery applications.

Another closely related nanomaterial is fullerene, which is considered to be the third allotrope of carbon after graphite and diamond. Fullerenes have carbon atoms arranged in the form of a closed shell. It consists of 60 carbon atoms, arranged as 12 pentagons and 20 hexagons. The structure of fullerenes is similar to that of a soccer ball. The diameter of fullerene can be as small as 2 nm [252]. Just as in the case of CNTs, the hexagonal and pentagonal rings present in fullerenes are sp^2 hybridized. Due to their unique properties, both CNTs and fullerenes have been investigated for drug delivery applications.

7.7.1 Synthesis

The three most popular methods to synthesize CNTs are chemical vapor deposition, electric arc discharge, and laser ablation, which are briefly illustrated in the following sections.

7.7.1.1 Chemical Vapor Deposition (CVD) In this process, a hydrocarbon gas is passed through a tubular furnace. The metal catalyst in the furnace is heated to high temperatures (500–1000°C) over a period of time by the hot gases. The basic mechanism in the process involves the dissociation of hydrocarbon molecules catalyzed by the metal catalyst and saturation of carbon atoms in the metal particles [253]. Precipitation of carbon from the metal particle leads to the formation of tubular carbon solids in sp^2 structure.

The role of metal catalyst is to speed up the process, to lower the production costs, and to improve the quality of the final product [254]. Purification is needed to eliminate impurities formed during the process, such as graphite compounds, amorphous carbon, coal, and metal particles. This is achieved by oxidative treatments with acid, microfiltration, thermal treatment, and ultrasound methods. The characteristics of the CNTs produced by chemical vapor deposition (CVD) method depend on the working conditions such as the temperature, concentration of hydrocarbon, the size and the pretreatment of metal catalyst, and the time of reaction [255]. Methane and ethane are the most commonly used gases [253], whereas iron and nickel are the most commonly used metal catalysts.

7.7.1.2 Electric Arc Discharge In this method, an electric arc discharge is generated between two graphite electrodes under an inert atmosphere of helium or argon [256]. The high temperature attained allows the sublimation of carbon leading to the formation of nanotubes. Purification by gasification with oxygen or carbon dioxide is necessary to obtain CNTs [257]. Both SWNTs and MWNTs can be obtained using this technique [258, 259]; however, production of SWNTs usually requires a metal catalyst. The important process variables are distance between electrodes, electric current, voltage, and electrode dimensions [259]. Appropriate modulation of these variables leads to the synthesis of CNTs.

7.7.1.3 Laser Ablation In this process, a piece of graphite mixed with a catalytic metal is vaporized by laser irradiation under an inert atmosphere of helium or argon gas. The most commonly used metal catalysts are cobalt and nickel. As the laser ablates the target, CNTs form and are carried by the gas flow onto a cool copper collector [260]. A purification step by gasification is needed to eliminate carbonaceous material. The important process parameters are laser absorption depth, energy density of the beam, laser pulse duration, and wavelength of the beam. These parameters when appropriately adjusted can produce CNTs that possess relatively greater purity [256]. Therefore, this is a preferred technique for the synthesis of highly pure CNTs [256].

Other methods that are used for making nanotubes include use of solar energy [261] and plasma torch method [262]. Fullerenes are generally produced by laser ablation [263], arc discharge [264], and ion beam sputtering [265]. Generally, the conditions for the synthesis of fullerenes are less severe in terms of time and temperature. Heating of the carbon/graphite source at a lower temperature and for a relatively shorter period of time results in the predominant formation of fullerenes.

7.7.2 Purification of Carbon Nanotubes

After the production of CNTs, a significant amount of metal catalyst particles and amorphous carbon are left as residues. Hence, purification of the

nanotubes is essential prior to further applications. One of the most commonly used technique for the purification and eventual solubilization of CNTs in various solvents is oxidation using strong acid treatments, which permit removal of the metallic impurities [266]. However, the strong acid conditions cut the tubes into shorter pieces and generate carboxylic functions at the tips, which modify their chemical and physical properties [266]. In order to avoid this change in properties, alternative methods like chromatography, gasification, centrifugation, filtration, and chemical derivatization techniques have been explored [267–270].

7.7.3 Toxicity of Carbon Nanotubes

The toxicity and biocompatibility issues of CNTs are very crucial for drug delivery applications. CNTs exposed to human epidermal keratinocytes have been found to elicit inflammatory response, loss in cell viability, and morphological alterations to cellular structure [271, 272]. In addition to the aforementioned *in vitro* studies, there have been *in vivo* studies conducted on guinea pigs and rats, which have reported histological evidence of lung inflammation and granuloma formation on exposure of these animals to pristine CNTs [273–276]. The nanotubes utilized in the above-mentioned studies were not purified and the presence of metal ions attached to the tubes during their synthesis was postulated to be an important reason for their toxicity. The study by Garibaldi et al. [277] reported the administration of purified CNTs to rat heart cell lines and the results of the study demonstrated that highly purified CNTs possess no evident toxicity and can be considered biocompatible with cardiomyocytes. The toxicity of the CNTs is thought to be due to their insolubility; however, when molecules are covalently linked to CNTs to increase their solubility, their toxicity is significantly reduced and they are safe and suitable for biological applications [278]. Therefore, it is possible to modify CNTs so as to enable minimum to none adverse tissue response.

7.7.4 Functionalization of Carbon Nanotubes

A major drawback of CNTs, particularly relevant to their compatibility with biological systems, is their complete insolubility in all types of solvents. For drug delivery applications, CNTs must be well dispersed in water and other solvents. Therefore, intrinsically hydrophobic CNT surfaces can be functionalized to render the nanotubes soluble in a wide variety of solvents. This facilitates their use in biomedical applications [252].

One of the commonly used approaches consists of the noncovalent functionalization of CNTs with surfactants, nucleic acids, peptides, polymers, and oligomers [279–282]. The advantage of this kind of approach is that the aromatic structure and thus the electronic characteristics of CNTs are preserved. The hydrophobic or π - π interactions are responsible for

noncovalent functionalization. Anionic, cationic, and nonionic surfactants have all been proposed to disperse nanotubes [283]. In a study by Islam et al. [283], sodium dodecyl sulfate (SDS) and Triton X-100 were used to obtain CNT suspensions. Their results demonstrated that the combination of π - π interactions of aromatic moieties between CNT and SDS and the long lipid chains of SDS increase the stability of the complex. Triton-X was found to interact by π stacking. Although surfactants are efficient in the solubilization of CNTs, they are known to permeabilize plasma membranes and can induce toxicity [266]. Therefore, the implications stemming from the use of surfactants interacting with biological systems can limit the possible biomedical applications of surfactant stabilized CNT complexes. On the contrary, the solubilization of CNTs with biological components would certainly be more appropriate for integration of this new type of material with living systems. Hence, CNTs functionalized with polysaccharides [279], amino acids [280], proteins [281], and nucleic acids [282] have been explored. The results of these studies demonstrated an increased solubility in water medium postfunctionalization, thereby indicating that functionalization of CNTs with biological component is a promising approach for solubilizing CNTs.

Another approach for surface modification of CNTs is the covalent functionalization of CNTs. Two approaches have been widely employed for chemical modification of CNTs: (i) the use of acids to introduce hydrophilic functional groups and (ii) the addition reaction of nanotubes to render them soluble in a variety of solvents [283]. CNT can be oxidized using strong acids, resulting in reduction of their length while generating carboxylic groups, which increase their dispersion in aqueous solutions [284]. The most efficient way to functionalize CNTs is based on the 1,3-dipolar cycloaddition of azomethine ylides. In this scheme, CNTs undergo an addition reaction when heated in dimethylformamide in the presence of an α -amino acid and an aldehyde [285]. The scope of this reaction is very broad and produces functionalized CNTs (f-CNTs) that possess high solubility in a wide range of solvents [286]. The covalent modification has the disadvantage that it impairs the physical properties of the nanotubes due to modification of their structure and thus limits their application in electronic devices [266]. However, the covalent bonding approach can be used advantageously in drug delivery applications as CNTs can be derivatized with bioactive molecules for their use as delivery vehicles for therapeutic applications [287].

7.7.5 Biomedical Applications of Carbon Nanotubes

CNTs are unique nanostructures, which are known to have remarkable electronic, mechanical, thermal, and optical properties [256]. Several applications of CNTs have been reported, such as chemical sensors, field emission materials, catalyst support, electronic devices, nanotweezers, reinforcements in

high performance composites, anode for lithium ion batteries, nanoelectronic devices, supercapacitors, flat panel displays, and hydrogen storage devices [288–291]. However, the biomedical applications of CNTs as drug and gene delivery vehicles are emphasized in the present discussion. The development of new and efficient drug delivery systems is of fundamental importance to improve the pharmacological profiles of many classes of therapeutic molecules. Within the family of nanomaterials, CNTs have emerged as a new alternative and efficient tool for transporting bioactive molecules in the body. As f-CNTs display low toxicity and are not immunogenic, they hold great potential in the field of nanobiotechnology and nanomedicine [279]. CNTs have large inner volumes relative to the dimensions of the tube, which can be filled with desired bioactive species, ranging from small drug molecules to proteins, peptides, and nucleic acids, and the resulting carriers can be delivered to tissues and cells for therapeutic purposes [292].

7.7.5.1 Drug Delivery by Carbon Nanotubes The use of f-CNTs for drug delivery of small molecules like anticancer, antibacterial, or antiviral agents is still unexplored. The development of nanocarriers with the ability to carry one or more therapeutic agents with recognition capacity, optical signals for imaging, and specific targeting is of fundamental advantage in the treatment of different types of diseases [293]. Theoretically, the use of f-CNTs in this approach would require the introduction of different functionalities on the surface of CNTs. In an attempt to explore the possibility of CNTs as drug delivery vehicles, Wu et al. [293] investigated the possibility of double functionalization of nanotubes with fluorescein and an antibiotic amphotericin B (AmB), which is used in the treatment of chronic fungal infections. The double functionalization enabled simultaneous linking of the fluorescent probes for tracking the uptake of CNTs as well as an antibiotic moiety as the active molecule. In this study, the antifungal activity of the AmB–CNT conjugate was assessed against three species of fungi that infect humans. AmB bound to CNTs was found to preserve its high antifungal activity, thereby indicating that CNTs show promise for use as antifungal delivery systems. In another study, Pastorin et al. [294] studied the introduction of a fluorescent probe and anticancer drug methotrexate to amino-functionalized CNTs by covalent conjugation. The CNTs were found to internalize in the cytoplasm of cancer cells, and the limited cellular uptake of methotrexate was enhanced due to its conjugation to CNTs. In another approach, Yinghuai et al. [295] developed f-CNTs with substituted carborane cages to form a new water-soluble CNT delivery system for the treatment of cancer cells. The above studies indicate that CNTs can be a promising material for the development of drug delivery systems.

7.7.5.2 Nucleic Acid Delivery by Carbon Nanotubes The use of CNTs as nucleic acid delivery systems for therapeutics is another application that has been explored. Pantarotto et al. [282] reported the utilization of CNTs as components for engineering a novel nanotube-based gene delivery vector

system. They reported the formation of ammonium-functionalized CNTs associated with plasmid DNA through electrostatic interactions. Upon interaction with mammalian HeLa cells, the f-CNTs penetrated the cell membranes and were taken up into the cells. Their results demonstrated that nanotubes exhibited low cytotoxicity and f-CNT-associated plasmid DNA was delivered to cells efficiently. Gene expression levels up to 10 times higher than those achieved with naked DNA were observed. These findings revealed a novel combination of properties attributable to soluble CNTs and established the potential of these structures for delivery of nucleic acid. In another study, Chapana et al. [296] reported the delivery of plasmid pUC19 from water-dispersible CNTs to *Escherichia coli* bacterial cells. The nanotube–plasmid conjugate created temporary membrane disruptions that enabled plasmid permeability through the bacterial cell wall and hence facilitated plasmid delivery into the cells. The results of the study encourage further investigation of the potential of CNTs for targeted and controlled delivery of DNA molecules. In a related study, Singh et al. [297] investigated the physicochemical interactions between cationic f-CNTs and DNA and the transfection efficiency of DNA-bound nanotube carriers. Three types of nanotubes, ammonium-functionalized single-walled and multiwalled carbon nanotubes (SWNT-NH₃, MWNT-NH₃), and lysine-functionalized single-walled carbon nanotubes (SWNTLys-NH₃) were electrostatically conjugated to plasmid pCMV- β -gal. Their results demonstrated that nanotube surface area and charge density were the critical parameters that determined the formation of electrostatic complex between f-CNTs and DNA. Another important study by Kam et al. [298] investigated the transfection efficiency of CNTs conjugated to short interfering RNA (siRNA), used for gene delivery to mammalian cells. The noncovalent adsorption of phospholipid molecules and PEG resulted in stable aqueous suspension of nanotubes. The functionalized CNTs were conjugated to siRNA by cleavable disulfide linkage. The results of the study demonstrated the transport, release, and nuclear translocation of oligonucleotides in mammalian cells with nanotube transporters, thus suggesting their promise for applications in gene therapy.

7.7.5.3 Protein Delivery by Carbon Nanotubes The use of f-CNTs as protein delivery vehicle is another research area currently under investigation. Kam and Dai [299] reported the use of CNTs as protein delivery vehicles and assessed the functional efficiency of the protein *in vitro* using mammalian cells. Three proteins, BSA, protein A (spA), and cytochrome *c* (cyt-*c*), were noncovalently bound to the acid oxidized CNTs. The carriers were found to be biocompatible and were internalized in the endosome, and thereafter released into the cytoplasm. The *in vitro* biological functionality and activity of the protein delivered by the nanotube was evident by the programmed cell death induced by cyt-*c* transported inside the cells. In another investigation by Kam et al. [300], protein streptavidin (SA) used in clinical applications was chemically conjugated to the acid-functionalized SWNTs. The *in vitro* release

efficacy of the CNT delivery system was determined by studying the effect of protein–nanotube conjugates on human leukemia and human T cells. The results of the study demonstrated that the functionalized nanotubes did not exhibit toxicity to the cells. The SA–nanotube carrier entered the cell by endocytosis and resulted in dose-dependant cell death, whereas SA by itself could not enter the cells. These studies suggest the potential of CNTs to be developed as protein carriers for therapeutic applications. Hence, CNTs represent a new class of molecular transporters with potential for future protein delivery applications.

7.7.5.4 Vaccine and Peptide Delivery by Carbon Nanotubes The basic concept for utilizing CNTs in vaccine delivery is to link the antigen to CNTs, while retaining its conformation and thereby inducing specific antibody response. In addition, the CNTs themselves should not trigger any response by the immune system. In a study by Pantarotto et al. [301], CNTs functionalized with a pyrrolidine ring through the 1,3-dipolar cycloaddition of azomethine ylides were covalently linked to a peptide sequence derived from the foot-and-mouth disease virus (FMDV), generating mono- and bisconjugated peptide CNTs. Their results demonstrated that both the mono- and bispeptide-derivatized CNTs elicited strong antibody response in BALC/c mice, thereby indicating that the antigen conformation was retained during the delivery, which is essential for the induction of antibody responses with the right specificity. In addition, the authors determined that the CNTs did not have any detectable immunogenicity. These findings suggested the potential of CNTs to present biologically important antigens in an appropriate conformation, and hence open up the possibility for their use in vaccine delivery. In a more recent study by Rasenick et al. [302], synthetic oligodeoxynucleotides (ODNs) containing cytosine–phosphodiester–guanine (CpG) motifs have been shown to be effective immunoprotective agents in murine models for a variety of viral, bacterial, and protozoan infections. However, the biological activities of ODN-CpGs are often short-lived, and therefore, several administrations of high doses are normally required. Their intracellular delivery faces the challenge of low uptake by the cells because of the repulsion between the negative charges on cell membranes and ODNs. Bianco et al. [303] used ammonium f-CNTs for efficient delivery of ODN-CpGs to mice cell lines. Their results demonstrated that the negative charge of ODN-CpG was neutralized by f-CNTs, and hence, the repulsion by the negatively charged cell membrane presumably reduced and the cellular uptake of ODN-CpG was facilitated. These results indicated the potential of CNTs as carriers for peptides to be delivered into cells, and hence the possibility of their use in vaccine development.

7.7.6 Biomedical Applications of Fullerenes

For the past decade, the chemical and physical properties of fullerenes have been an important area of study. Because of their unique structure, fullerenes

present an attractive option to be used for drug and gene delivery applications. Bioactive molecules can be filled in their hollow structure, and subsequently the outer surface can be functionalized for active targeting in the body [304]. In their natural form, fullerenes are insoluble. However, functional groups such as carboxylic acid can be added to improve their solubility [304, 305].

Fullerenes have been used as actual therapeutic macromolecules. They are strong antioxidants, capable of scavenging a variety of free radicals associated with medical conditions such as neurodegenerative diseases. Oxygen free radicals use their unpaired electrons to break chemical bonds in critical molecules such as nucleic acids, thereby triggering cell damage and possible apoptosis [306]. Fullerenes are believed to interrupt this process essentially by absorbing the potentially damaging electrons. Fullerenes have been modified with malonic acid moieties, creating a compound, that showed strong activity in animal models of neurodegenerative diseases [306]. In an investigation by Dugan et al. [307], water-soluble carboxylic acid functionalized fullerene derivatives, containing three malonic acid groups per molecule, were synthesized and found to be efficient free radical scavengers. These data suggest that polar carboxylic acid fullerene derivatives may have attractive therapeutic properties in neurodegenerative diseases.

In vivo investigation of the oral and intravenous administration of water-soluble fullerenes to Fischer rats showed that they distributed rapidly to many tissues. This observation suggested that they might eventually be useful to deliver drugs to a target tissue for therapeutic purposes [252]. Foley et al. [308] proposed using fullerenes as drug delivery agents as a consequence of their structure closely resembling the clathrin scaffolds that mediate endocytosis. Their results demonstrated that a fullerene derivative can cross the external cellular membrane and is preferentially localized in mitochondria.

Fullerenes have been suggested to hold promise for the inhibition of HIV protease [309], as a target to bone tissues [310], and as an antibacterial agent [311]. In a study by Friedman et al. [309], a diamino diacid derivative of fullerene was demonstrated to be a potent inhibitor for the protease enzyme specific to the human immunodeficiency virus. The study concluded that the strong hydrophobic interactions between the fullerene derivative and enzyme led to the inhibition of the virus. Another study by Gonzalez et al. [310] demonstrated that fullerene functionalized with a bisphosphate could be successfully used for the targeting of the specific bone tissue. This ability could be an important step toward the development of future fullerene derivatives as bone therapeutic agents. The trimalonic acid derivative of fullerene, carboxyfullerene, is water soluble and has been studied for its antibacterial activity on Gram-positive bacteria, *Staphylococci* [311]. The lethal action of carboxyfullerene was achieved by its insertion into cell walls of bacteria and disruption of their structure. This study demonstrated the potential of carboxyfullerenes to be developed as antibacterial systems.

In a recent study, Isobe et al. [312] demonstrated that tetraamino-functionalized fullerenes could bind a plasmid DNA and transfect the plasmid

to mammalian cells with high transfection efficiency. The cell uptake of the fullerene–DNA complex was by the mechanism of endocytosis and the internalized DNA was protected by the fullerene against enzymatic digestion. In a related study, Ashcroft et al. [313] reported the synthesis and characterization of a water-soluble fullerene derivative designed to covalently attach to an antibody, which recognizes antigen on human tumor cells, thereby opening the possibility of targeted anticancer agent delivery using fullerenes. In addition, intracellular uptake of water-soluble fullerene derivatives by human cancer cells *in vitro* [314] and significant anticancer activity of a slow release drug delivery system comprising of the fullerene–paclitaxel conjugate [315] have also been reported.

Another possible application of fullerenes is found in nuclear medicine [316] in which water soluble metallofullerenes that contain metal atoms or ions inside, are used as an alternative to chelating compounds that prevent the direct binding of toxic metal ions to serum components. It is envisioned that metallofullerenes can provide a unique alternative to chelating compounds because of their resistance to metabolism and high kinetic stability in the body. Metallofullerenes have also demonstrated the potential in use as magnetic resonance imaging (MRI) contrast agents [317, 318].

The aforementioned studies indicate the potential of using functionalized CNTs and fullerenes in delivery of bioactive molecules for various medical applications. However, the research on their potential as delivery vehicles is still confined to the laboratory and further extensive investigation is required before they can be utilized in clinical applications.

7.8 NANOGELS

Nanogels are cross-linked polymeric particles of submicrometer size whose properties differ from linear macromolecules of similar molecular weight. Nanogels have a three-dimensional structure with the cross-linked polymer network immersed in a solvent to synthesize a structure similar to a sol–gel structure. The networks can be composed of homopolymers or copolymers and are insoluble due to the presence of chemical cross-links (tie points, junctions) or physical cross-links such as entanglements or crystallites [319]. Dispersed gel particles can be viewed as cross-linked latex particles, which are swollen by a good solvent. If the good solvent is water, these species belong to the hydrogel class.

7.8.1 Synthesis of Nanogels

Chemically cross-linked nanogels can be synthesized by emulsion polymerization [320–323], or by cross-linking reactions within the polymer molecules, or by cross-linking reactions between preformed polymer fragments [324, 325].

7.8.1.1 Emulsion Polymerization The most common method for the synthesis of nanogels is combined polymerization and cross-linking, usually in an emulsion. In emulsion polymerization, the monomer is dispersed in an aqueous phase and the emulsion is stabilized by surfactants. The free radical polymerization of monomers dissolved in these surfactants produces polymeric particles or gels with narrow size distribution. Recently, inverse microemulsion polymerization has received tremendous attention by researchers due to its ability to produce nonionic, hydrophilic nanogel particles for protein and enzyme delivery systems [326–330]. A drawback of the emulsion procedure, especially when the products are designed for biomedical use, is the presence of monomers, surfactants, and cross-linking agents that are usually toxic and have to be removed from the system after the synthesis.

7.8.1.2 Cross-Linking Reaction of Preformed Polymer Fragments

Another approach for preparing nanogel particles is by intramolecular cross-linking between several structural moieties. For instance, Harth et al. [331] described the preparation of nanogel particles by coupling reactions between benzocyclobutene units in benzyl ether. In another study, Mecerreyes et al. [332] investigated intramolecular cross-linking between acrylic moieties of multifunctional acrylic macromolecules during polymerization in ultradilute solution. Homopolymers and copolymers of acrylamide and alkyl acrylamides have been widely used for the preparation of temperature- and pH-sensitive nanogels by cross-linking with polyols and polyamines [333–335]. In addition to the above methods, there have been reports on the preparation of polyacrylic acid nanogels by generating carbon-centered radicals along a polymer chain using short pulses of fast electrons, followed by intramolecular recombination [336, 337]. This method eliminates the use of monomer and cross-linking agents.

7.8.2 Nanogels for Drug Delivery

Nanogels are currently being actively investigated due to their potential technological applications in a variety of fields. Applications of such materials include surface coating [338–340], uptake and release of heavy metal ions [341, 342], optoelectronic switches [343], and drug delivery systems [344, 345]. The properties of nanogels, which make them particularly useful for drug delivery applications, are their high drug/biomacromolecule loading capacity and their ability to respond reversibly to external stimuli such as temperature, pH, ionic strength, solvent nature, and external stress [346, 347]. Nanogel particles are of particular interest because they exhibit intrinsic properties of gels combined with the properties of colloids, such as microheterogeneous structure, small size, and high surface-to-volume ratio. Nanogels can be used to regulate drug release in reservoir-based, controlled release systems or as carriers in swelling-controlled release devices [348, 349]. On the forefront of

controlled drug delivery, nanogels can be designed for their release to occur within specific areas of the body (within a certain pH of the digestive tract) or active delivery by the functionalization of nanogel surface with a ligand for specific targeting of cell receptors.

Environmentally responsive nanogels have been applied in a wide variety of controlled drug delivery applications. The intelligent response of these systems allows for the release that is controlled by the conditions of the environment like temperature or pH of the medium. Temperature-responsive nanogels, which are mostly based on poly(*N*-isopropylacrylamide) (PNIPAAm) and its derivatives, undergo a reversible volume phase transition with a change in the temperature of the environmental conditions [350]. This type of behavior is related to polymer phase separation that occurs when the temperature is raised to a critical value, known as the lower critical solution temperature (LCST). Polymeric gels tend to shrink or collapse as the temperature is increased above LCST, and the gels swell upon lowering the temperature below the LCST. For example, PNIPAAm gels exhibit the LCST of 33°C above which they are collapsed and below which they are swollen. In a study by Shin et al. [351], they reported the use of PNIPAAm nanogels for positive thermosensitive delivery of a model drug, indomethacin. The approach to achieve positive thermosensitive drug delivery in this study was to use the squeezing mechanism of the polymeric gel when the temperature is maintained above the LCST to release the drug. The results of the study demonstrated a uniform drug release rate and sustained release over a long period of time. A uniform release profile over a defined period of time achieved using this system may be useful for antipyretic delivery in order to maintain the effectiveness of the drug as long as the biological system is infected. Therefore, temperature-responsive nanogels prepared from PNIPAAm show promise for the development of delivery systems that exhibit a controlled and sustained release of drug in response to temperature changes [352–353].

pH-sensitive nanogel particles composed of polymethacrylic acid-grafted-polyethylene glycol [P(MAA-g-EG)] have been investigated for the oral delivery of therapeutic proteins. Lowmann et al. [356, 357] reported the formation of insulin-loaded P(MAA-g-EG) nanogels and studied the release mechanism of insulin from the carrier. Their results demonstrated that in an acidic environment, which is similar to that of the stomach, the gels were unswollen due to the formation of intermolecular polymer complexes, thereby protecting the insulin from proteolytic degradation. However, in basic and neutral environments, which are present in the intestine, the complexes dissociated that resulted in rapid gel swelling and consequent insulin release. The results of the above studies indicated the use of nanogels as highly suitable oral carriers for peptide drugs such as insulin.

Glucose-sensitive nanogels prepared by the copolymerization of diethylaminoethyl methacrylate (DEAEM) and poly(ethylene glycol) monomethacrylate (PEGMA) have been reported by Podual et al. [358, 359]. The polymeric nanogels were incorporated with glucose oxidase within their network to

render pH sensitivity to the nanogels. The working principle of these nanogels is as follows. Glucose oxidase reacts with glucose to form gluconic acid, which in turn lowers the pH in the local environment, and hence, triggers the pH-sensitive swelling/deswelling of the nanogel. The results of their equilibrium swelling studies indicated that the nanogels showed a strong pH-dependent swelling behavior. The transition between the swollen and the collapsed states was at a pH of 7.0. The nanogels exhibited release kinetics that could be useful as smart materials for diabetes applications in which the materials can sense an increase in glucose concentration, and hence, release insulin in response.

ODNs have attracted significant interest as potential diagnostic and therapeutic agents for neurodegenerative disorders like, Alzheimer and Parkinson disease. However, the use of ODNs in the body is hindered by the lack of stability of ODNs against enzymatic degradation as well as rapid clearance of ODNs through renal excretion. Furthermore, the BBB severely restricts the entry of ODNs to the brain from the periphery, which represents a major obstacle for the use of ODNs for diagnostics and therapy of disorders of central nervous system. In an attempt to evaluate the potential of nanogels as drug carriers to brain, Vinogradov et al. [358] prepared cationic nanogels consisting of covalently cross-linked PEG and PEI chains, PEG-cross-PEI nanogels, for delivery of ODNs to brain. The nanogel-ODN complex was delivered to bovine brain microvessel endothelial cells (BBMECs) and the results demonstrated that the nanogels protected ODNs from enzymatic degradation in the cells. The *in vivo* biodistribution of nanogels and encapsulated ODNs was also studied using a mouse model. The *in vivo* biodistribution study suggested that following intravenous administration of nanogel-formulated ODNs in mice, substantial amounts of nanogels and ODNs accumulated in the brain of the treated mice. The potential application of nanogels for delivering drugs to the brain has also been suggested by Soni et al. [359]. In their study, nanogels were prepared from a copolymer of NIPAAm and *N*-vinylpyrrolidone and fluorouracil was used as a model drug, which was encapsulated in the nanogel. *In vivo* studies performed on rabbits suggested sufficient accumulation of the drug-loaded nanogels in brain and the results of the study indicated the potential use of nanogels as therapeutic carriers for the drugs to be delivered to the brain tissue. In another study, McAllister et al. [360] reported the synthesis of DNA containing nanogels prepared from polyacrylates to assess the potential of nanogels as gene delivery vehicles. *In vitro* studies of the nanogel vectors were performed on HeLa cell lines and the results demonstrated that nanogel particles were able to enhance cellular uptake of DNA. These studies suggest the potential use of nanogels for gene delivery applications.

Incorporation of amphiphilic molecules with low solubility into PEO-cross-PEI nanogels was evaluated using indomethacin and retinoic acid [361]. The fine dispersions of the complex particles were obtained, which were stable over a week. The kinetics of drug release from dispersion of nanogel loaded with indomethacin was evaluated using the equilibrium dialysis technique. The experiment suggested that during the first hour of dialysis over 17.5% of the

drug was released in the external solution. After 24 h, 82% of indomethacin was found in the external solution. The results of the study suggested that pharmaceutical formulations useful for drug delivery applications for relatively insoluble drugs could be prepared by the immobilization of these drugs in PEO-cross-PEI nanogel systems, which are stable at physiological pH and ionic strength.

The results from the studies discussed in the present section suggest that polymeric nanogels are promising candidates for drug and gene delivery applications.

7.9 VIRAL VECTORS AND VIRUS-LIKE PARTICLES (VLPs)

Viruses are intracellular obligate parasites, designed through the course of evolution to infect cells, often with great specificity to a particular cell type. At the most basic level, they consist of a genetic material encapsulated within a protective protein shell called the “capsid”. They tend to be very efficient at transfecting their own DNA into the host cell that is expressed to produce new virus particles. Viruses have evolved to generate strategies to conduct the various steps of binding and internalization to their target cells efficiently [362]. Further, they are capable of manipulating the host cell’s machinery to make viral proteins. These properties of viruses make them ideal candidates for gene delivery. Due to the infectious nature of viruses, they pose a safety threat, and hence, cannot be used for drug/gene delivery in their original form [363].

A virus particle, in which the pathogenicity can be eliminated, while the efficiency of gene transfer and expression is retained, would be a desirable system for gene therapy. This concept is utilized in making recombinant virus particles in which the genetic material of the original virus is modified so as to produce particles that resemble the actual virus, but cannot replicate and spread the infection in their host. In making recombinant viral vectors, genes that are needed for the replication phase (nonessential genes) of the virus are replaced with foreign genes of interest. In this way, the modified virus is still capable of transducing the cell type it would normally infect without the synthesis of infectious viral proteins [364]. Viral vectors have been widely used for gene therapy, as they are able to deliver genes efficiently and achieve long-term expression [364–367]. In spite of the above advantages of the elimination of pathogenicity due to viral replication, retention of viral genes and their continued expression pose a risk of eliciting an immune response, which rapidly clears the cells expressing virally encoded gene products [365]. These factors, in conjunction with problems of large-scale production of recombinant virus vectors, often limit their potential as gene carriers and have driven a search for alternative gene delivery systems.

The promising alternatives for gene delivery, which retain the advantage of high transfection efficiency of virus particles, but do not possess their infectious genes, are virus-like particles (VLPs). VLPs mimic the overall structure of viral

particles, but are devoid of infectious genetic material [366]. Indeed, VLPs completely lack the DNA or RNA genome of the virus, but have the authentic conformation of viral capsid proteins as in actual virus particles. VLP preparations are based on the observation that expression of capsid proteins of many viruses leads to the spontaneous assembly of particles that are structurally similar to the parental virus particle [367]. Unlike viruses, VLPs are composed of only capsid protein and are devoid of nucleic acid.

Recombinant virus vectors and VLPs are useful in vaccination and gene delivery applications and their uses in gene and immune therapy are discussed in the following sections.

7.9.1 Recombinant Virus Vectors

7.9.1.1 Adenovirus Vectors Adenoviruses are nonenveloped viruses containing a linear double-stranded DNA genome of about 35 kilobase pairs (kbp). The genome is packaged in a protein capsid with a diameter of 70 nm. Adenovirus-based vectors are relatively easy to manipulate, can be produced consistently and cost-effectively at high titer, and are highly infectious [365]. They can efficiently transfer genes into both dividing and nondividing cells [364]. Adenoviral vectors are being widely used for gene delivery *in vivo* and are in clinical trials for cancer therapy [368]. To generate a recombinant adenovirus for gene transfer application, the E1 gene, important for viral expression and replication, is removed and the resulting plasmid is propagated in producer cells, such as human embryonic cells [369]. Synthesis of adenoviral gene products often stimulates an immune response to the infected cells and results in a loss of gene expression 1–2 weeks after the injection, which often limits their use [370].

7.9.1.2 Retrovirus Vectors Retroviruses are a class of enveloped viruses containing a single-stranded RNA molecule as the genome. The diameter of a typical retrovirus particle ranges from 90 to 140 nm. Following infection, the viral genome, is reverse transcribed into double-stranded DNA, which integrates into the host genome, and is subsequently expressed as proteins. Retroviruses infect target cells through specific interactions between the viral envelope protein and the surface receptor on the target cell [371]. Recombinant retroviruses are produced by deletion of the viral replication genes from the genome and replacing them with a foreign gene of interest. The modified virus can still enter a target cell and insert its genome [372]. Retrovirus-based vectors are particularly attractive for treatment of genetic diseases, where stable long-term integration in the host genome is required [369]. Furthermore, in clinical settings, retroviruses appear to have the lowest toxicity profile. Retroviral vector gene delivery seems to be more suitable to allow potentially permanent gene expression [370].

7.9.1.3 Adeno Associated Virus Vectors Adeno associated virus (AAV) is a virus associated with adenovirus. AAV is a simple, nonpathogenic,

single-stranded DNA virus. Its genome consists of two genes namely *cap* and *rep*. The *cap* gene encodes viral capsid proteins, and the *rep* gene product is involved in viral replication and integration [370]. AAV cannot replicate on its own, it requires a cell to be coinfecting with adenovirus in order to replicate. To produce an AAV vector, the *rep* and *cap* genes are replaced with a transgene and the plasmid is transfected into adenovirus infected producer cells, which leads to the formation of AAV vectors [372].

Alternative recombinant virus vectors have been developed from vaccinia virus [373], herpes simplex virus [374], bovine herpesvirus [375], and Sindbis virus [376].

7.9.2 Applications of Recombinant Virus Vectors

The success of gene therapy depends on the proper cell internalization and the level of gene expression in the nucleus of the target cell. Due to their intrinsic property to target host cells, recombinant viruses prove promising for efficient gene transfection, which eventually affects the therapeutic efficacy of the gene.

Recombinant adenovirus vectors have been widely reported for their use as gene delivery and vaccine delivery [377–384]. In the study by Chou et al. [377], it was demonstrated that intrathecal injection of glial cell line-derived neurotrophic factor (GDNF) encoded in recombinant adenovirus led to sustained GDNF expression in the spinal cord of rats. The gene transfer significantly reduced the onset of paraplegia and preserved the locomotor functions in rats after spinal ischemia. The results of study indicated that gene delivery via adenoviruses is an efficient alternative for gene transfer in the central nervous system. In another study, recombinant adenovirus particles encoding a protein IL-1Ra, which acts as an anticytokine, were delivered to the lungs of pigs, and subsequent secretion of proteins into the lungs was studied [378]. The results demonstrated that adenovirus particles do not induce an inflammatory response and were successful in delivering and consequently transfecting the gene *in vivo* as evidenced by the expression of the protein encoded by the gene. The results of the study demonstrated the potential of recombinant adenovirus for *in vivo* delivery of cytokines modulating genes. In yet another study, the *in vivo* gene delivery in salivary glands of rats by recombinant adenoviruses was studied [379]. The results of this study indicated that the protein was efficiently expressed in the salivary glands following injection and the level of protein was found to increase with the amount of adenoviruses used in injection. Similarly, recombinant adenoviruses have been reported for successful immune therapy in several animal models like rats, mice, rabbits, pigs, chimpanzees, and dogs against a variety of infections [380–384].

Retroviral vectors have been used for gene therapy applications and have been demonstrated to be more suitable for permanent gene expression [370, 385]. Nagano et al. [386] studied *in vitro* gene transfer to mouse germ

line stem cells using a retrovirus vector. The results of this study laid the groundwork for the introduction of new genes directly into the germ line of many animal species, and hence suggested a method to address the potential of somatic cell gene therapy.

Recombinant vectors derived from AAVs have several advantages for gene therapy research due to their attractive features like lack of cytotoxicity, ability to transduce both dividing and nondividing cells, long-term transgene expression, and ability to be generated into high titer virus preparations in the laboratory [387]. *In vivo* studies demonstrating functional gene delivery using AAV vectors have shown promising results for transfection to multiple tissue types, including adult murine heart [387], skeletal muscle of mouse [388], primate somatic cells [389], mouse liver [390], and subretinal space of rats [391, 392].

Recombinant herpesvirus vectors have been widely used for gene delivery applications. Several molecular and biological characteristics of the virus, such as little or no pathogenicity, ability to accommodate large amounts of foreign genetic material, ability to infect several cellular types derived from different animal species, and ability to maintain transgene expression during differentiation, make it a suitable gene carrier [393, 394]. A study by Stevenson et al. [395] explored the potential of herpesvirus as human gene delivery vectors wherein they demonstrated that recombinant virus carrying the β -galactosidase gene was able to infect a wide variety of human cell types *in vitro*, resulting in the expression of the protein. Bovine herpesvirus 4 (BHV-4) has been suggested as an efficient vector for gene delivery [396]. In a study by Donofrio et al. [396], various animal cell lines were infected with recombinant BHV-4, and it was found that the majority of cells neither exhibited cytopathic effects nor supported viral replication, and the expression of protein was clearly observed. Several studies [397–399] have reported successful gene delivery to cultured neuron cells and even to the brain of living rats, thereby indicating the potential of recombinant herpesvirus vectors as a valuable tool in gene therapy for rat central nervous system.

The applications of recombinant virus vectors for gene therapy in neurodegenerative disorders [400, 401], cardiovascular diseases [402], and gene delivery to placenta in case of complications in pregnancy [403] have also been reported. From the several examples cited above, it can be concluded that recombinant vectors show promise in the area of gene and immune therapy. However, it is unlikely that one particular type of viral vector will be suitable for all gene therapy applications. Rather, the development of a range of vectors using a range of virus types would probably be more appropriate to fulfill the requirements for different types of treatments.

7.9.3 Virus-Like Particles

VLPs are produced by the insertion of the gene for the target protein (capsid protein of the virus of which the VLPs are required) into the genome of baculovirus [404] or vaccinia virus [373]. The transfection is conducted

via a homologous recombination between the virus DNA and a transfer vector carrying the foreign target gene [367]. The genetically engineered viruses are then injected into bioreactors containing insect or mammalian cells. The recombinant virus infects the host cells and replicates rapidly. The infected cells are supplied with nutrients and oxygen for sufficient duration of time during which they can produce the maximum yield of the desired protein [366]. The capsid proteins self-assemble into VLPs, which are similar to the actual viruses and have same transfection efficiency for targeting cells [367]. The most commonly studied VLPs are from papillomavirus and polyomavirus. The present discussion focuses on the application of the VLPs of these two viruses.

7.9.4 Applications of Virus-Like Particles

7.9.4.1 Papillomavirus-Like Particles Papillomaviruses are members of the papovaviridae family. They are nonenveloped DNA viruses, which infect humans as well as a variety of animals. The papillomavirus capsid consists of two proteins, L1 and L2. L1 is the major capsid protein, which when expressed in eukaryotic cells is able to self-assemble into VLPs [405]. Capsid proteins for a variety of human papilloma viruses have been expressed in insect cells using recombinant baculovirus vectors [406–408] and in mammalian cells with vaccinia virus [409, 410]

There are several reports on the use of papilloma VLPs for immune therapy. The L1 capsid protein of rabbit papilloma virus has been expressed in insect cells using recombinant baculovirus, and the capsids were found to self assemble into VLPs [411, 412]. The results of the study showed that the immunization of rabbits with the VLPs could produce high titers of virus neutralizing antibodies. Long-term protective ability against the virus was demonstrated as VLPs induced strong, long-lasting protection against experimental challenge with the rabbit papillomavirus. In another study, the major capsid protein of the canine papillomavirus [413] was expressed in insect cells in native form, which self-assembled into VLPs. The particles were injected intradermally into cattle and the vaccinated animals developed antibodies against the canine virus. The conformation of the protein was found to affect the success of immunization. The results of the study indicated the feasibility of developing a vaccine to prevent infection from mucosal papillomas, which can progress to malignancy. Multiple studies have reported that different types of papillomavirus-like particles elicit immune responses from B and T lymphocytes [414–416], and hence, offer the potential use of VLPs for immunization against different types of papillomaviruses. The aforementioned studies reported above demonstrate the promise of papilloma VLPs as effective agents for immune therapy for reducing the impact of several papillomavirus-associated diseases.

7.9.4.2 Polyomavirus-Like Particles The capsids of polyomaviruses are nonenveloped, and the diameter of these capsids is approximately 45 nm. They

are made up of three viral-encoded proteins, VP1, VP2, and VP3, which encapsulate the viral chromatin composed of virus DNA and the cellular histones. The three structural proteins VP1, VP2, and VP3 are found in different ratios. The outer shell of the capsid is composed of 72 pentameric VP1 proteins. VP1 acts as a major ligand for certain membrane receptors during virus infection. Furthermore, the N-terminus of the VP1 protein contains a DNA-binding domain [417]. Murine polyomavirus, simian virus 40 (SV40), human BK virus (BKV), human JC virus (JCV), and other animal viruses come under the genus of polyomavirus [418].

The coat proteins of the polyomavirus can be expressed in insect cells [419–421], *E. coli* [418, 422], and mammalian cells [423]. These expressed monomers immediately assemble into capsid aggregates when the ionic strength of the solution is increased [420]. The VLPs thus formed can be stabilized by the addition of calcium and the introduction of disulphide linkages between the particles [422].

Goldmann et al. [424] reported the formation of VLPs from the major structural viral protein, VP1, of the human polyomavirus JCV, and the formed particles were investigated for their efficiency as a gene transfection agent. The transfection capability of VLPs was studied by encapsulating plasmid pCMV- β -gal in the particles. The results of their study demonstrated that the VLP efficiently transduced the DNA and resulted in the expression of functional β -galactosidase in monkey kidney cell lines. In another study, Henke et al. [418] demonstrated efficient *in vitro* uptake of ODNs and larger DNA fragments in mouse fibroblasts and efficient plasmid DNA transfection with recombinant VP1 capsids was reported. The polyoma VLP system has demonstrated effective delivery of DNA to mice cells, both *in vitro* and *in vivo* that has eventually resulted in prolonged gene expression [418]. The mechanism of the uptake of the particle played a crucial role in the process. The study demonstrated that cell surface sialic acid residues and an intact microtubule network, which are required for viral infectivity, are also necessary for cell internalization and gene expression. Abbing et al. [425] reported the preparation of VLPs from polyomavirus by the self-assembly of VP1 capsid proteins and the encapsulation of fluorescent protein and a low molecular weight drug methotrexate in the particles. The protein and the drug containing VLPs were found to internalize *in vitro* in mouse fibroblasts. The results of the studies seemed promising for the application of polyoma VLPs for drug and protein delivery. Therefore, the polyoma VLPs show promise for use in gene delivery and hence therapeutic and vaccine applications.

7.10 NANOCRYSTAL TECHNOLOGY

Nanocrystal technology has received increased attention in recent years from both academic and industrial sectors due to its efficacy to improve the poor solubility of several drugs. The number of synthetic drugs that are poorly

soluble is steadily increasing [426]. This increasing number of poorly soluble drugs requires innovative formulation approaches to reach a sufficiently high bioavailability after oral or intravenous administration. The solubility of poorly soluble drugs can be improved by reducing the particle size of the bioactive/pharmaceutical ingredients. Increased solubility and subsequent increased bioavailability have been observed when the particle size has been reduced to nanometer scales [427–429]. Therefore, all water-insoluble drugs potentially stand to benefit from this approach, wherein the size of bioactive agents is reduced in an attempt to significantly enhance their dissolution and bioavailability. An important aspect of this technology is that the drug nanocrystals can be applied to various administration routes like oral, parenteral, and intravenous.

7.10.1 Approaches for the Production of Drug Nanocrystals

There are a number of formulation approaches for poorly soluble drugs in water, for example, the use of cyclodextrins [430] or oil-in-water (o/w) emulsions for intravenous administration [431]. The principle limitation of the above approaches is that the drug needs to possess certain physicochemical properties like solubility of the drugs in oils and the requirement of having the right molecular size to fit into the cyclodextrin ring. These formulation approaches are of limited success as clearly demonstrated by the relatively low number of products based on such technologies in the market.

Among preparation methods under development, wet comminution has produced successful formulation results [432]. In this process, the particle size of a drug usually decreases to a steady state value with time, which depends on the kind of polymeric stabilizer used to prevent the aggregation of the particles. Therefore, the stabilization effect of polymer is a critical parameter in this approach. However, the properties of the drugs determine the type of polymeric stabilizers required. As a consequence, this process is hampered from the lack of a systematic understanding for the selection of an appropriate polymer for a specific drug.

Drug nanocrystals can be produced by a bottom-up approach like precipitation [433], or alternatively, by a top-down approach, like disintegration and milling [434]. The bottom-up technique is the classical precipitation approach, wherein the drug is dissolved in a solvent, which is subsequently added to a nonsolvent to precipitate the crystals. The main disadvantage of this technique is the difficulty/inability to control the crystal growth that needs to be stopped at the desired stage to avoid the formation of microcrystals. In addition, this technology cannot be applied to the increasing number of drugs that are poorly soluble in nearly every solvent medium, aqueous or nonaqueous. Therefore, the bottom-up approach is not widely used for drug nanocrystal production.

As a consequence, the top-down approach for nanocrystal production has received more attention. There are two basic disintegration technologies for

drug nanocrystals, namely (i) pearl/ball milling and (ii) high pressure homogenization.

In pearl milling, the drug macrosuspension is generally filled into a milling container containing milling pearls made from materials like glass, zircon oxide, or special polymers such as hard polystyrene derivatives. The pearls are then moved by a stirrer and in the due process the drug is ground to nanocrystals due to the impact between the pearls. A general problem of pearl mills is the erosion of material from the milling pearls leading to product contamination [434]. The erosion mainly depends on the hardness of the drug and the milling material and the milling time required, which can be from few hours up to several days. Such problems have been circumvented by the use of pearls made from polymeric materials that tend to minimize the erosion. The possibility of scaling up with pearl mills does exist; however, there is a limitation on the size of the mill, due to its weight. Approximately two thirds of the mill volume is occupied by the pearls, leading to a heavy weight of the machinery, thus limiting the maximum batch size.

The second most commonly used disintegration method is milling by high pressure homogenization. The two types of homogenizers used are microfluidizer homogenizers and piston-gap homogenizers.

Microfluidizer homogenizers are based on the principle of microfluidization in which the drug suspension is accelerated and passes with a high velocity in a specially designed homogenization chamber. In the first part of the chamber (Z-type), the suspension changes the direction of its flow a few times, leading to particle collision and shear forces. In the second chamber (Y type), the suspension stream is divided into two streams, which then collide frontally. A disadvantage of this technology is that, at times, there are high numbers of passes through the microfluidizer, which lead to loss in productivity. Often, the products obtained by microfluidization contain a relatively large fraction of microparticles (especially in the case of hard drugs), thus losing the special benefits of a real homogeneous drug nanocrystal suspension.

Due to the technical problems associated with pearl/ball milling technology and the microfluidization technique, piston-gap homogenizers were developed as an alternative to produce drug nanocrystals. The original technology was based on homogenization of particles in pure water [435]. However, a second-generation technology involves the homogenization of drug particles in a nonaqueous medium or a dispersion medium with a reduced water content (mixtures of water with water-miscible liquids such as water–poly(ethylene glycol) (PEG) or water–glycerol) [436]. As stated earlier in this section, precipitation is the conventional approach to produce nanosized drug material; however, the problem of potential growth of drug nanocrystals to drug microcrystals limits its utility. In an attempt to overcome this problem, a combination technology has been developed wherein precipitation is followed by a second step of high pressure homogenization. Some of the nanocrystal technologies based on the homogenization approach have been summarized in Table 7.1 [437].

TABLE 7.1 An Overview of Some of the Nanocrystal Technologies and Patents Applications

Nanocrystal type	Company name	Patent/patent application
Hydrosol	Novartis (prev. Sandoz)	GB 2,269,536 GB 2,200,048
Nanomorph™	Soligs/Abbott	D 19,637,517
Nanocrystal™	e'lan Nanosystems	US 5,145,684
Dissocubes®	SkyePharma	US 5,858,410
Nanopure	PharmaSol	PCT/EP00/0635
Nanoedge™	Baxter	US 6,884,436

7.10.2 Preparation of Tablets from Nanosuspensions of Poorly Soluble Drugs

The most preferred approach for the preparation of nanosuspension formulations of poorly soluble drugs is the homogenization approach. In this approach, the drug powder is initially dispersed in an aqueous surfactant solution, using an overhead mechanical stirrer. The coarse predispersion obtained is then homogenized at pressures of 500–1500 bar using multiple cycles. The size reduction process results in a suspension having particle size in the nanometer range, which is the so-called nanosuspension [438]. For formulation of tablets and capsules, the obtained nanosuspensions can be directly filled into gelatin or hydroxypropylmethyl cellulose capsules, which are then sealed. The drug nanosuspension is subsequently solidified in the capsule. During the transfer of the aqueous nanosuspensions in a solid dosage form, care must be taken to avoid the release of the drug nanocrystals as ultrafine dispersion. This generally happens as a consequence of agglomeration or fusion of crystals under the compaction pressure used in tableting.

Therefore, the nanocrystal technology could be a promising approach to solubilize poorly soluble drugs as well as improve the poor bioavailability of these drugs. These improved properties of otherwise insoluble drugs can now open possibilities of formulating these drugs into delivery systems.

7.11 CONCLUSIONS

Nanotechnology is beginning to change the scale and methods of drug delivery, and it is expected that these technologies will lead to medical benefits that cannot be achieved using larger scale devices or technologies. Due to the potential advantages in the offering, nanoscale drug delivery systems such as nanoparticles, nanofibers, dendrimers, liposomes, nanotubes, nanogels, and viral vectors are being aggressively pursued. In this chapter, synthesis procedures, properties, and drug delivery applications of the aforementioned

nanoscale systems have been discussed. A clear understanding of both physicochemical and physiological processes, which form the basis of complex interactions between a drug nanocarrier and its microenvironment, would probably lead to an accelerated development of these nanoscale technologies. Therefore, it is essential that fundamental research be conducted to address issues such as structure, surface properties, design parameters (drug loading efficiency, drug release mechanism), and biocompatibility of the nanoscale drug formulation, for the successful and efficient application of these technologies. The future of nanomedicine will depend on rational design of nanoscale drug delivery systems based on a detailed and thorough understanding of the pathological conditions and the interaction of these nanoscale delivery systems with the biological environment.

REFERENCES

1. Mainardes RM and Silva LP. Drug delivery systems: past, present, and future. *Curr Drug Targets* 2004;5:449–455.
2. Ratner BD, Schoen FJ, Hoffman AS, Lemons JE. *Biomaterials Science*. St Louis: Elsevier Science & Technology Books; 2004. p 629–649.
3. Peppas LB. Polymers in controlled drug delivery. *Med Plast Biomater* Nov:1997; 34–40.
4. Vogelson CT. Advances in drug delivery systems. *Mod Drug Discov* 2001;4(52): 49–50.
5. Dreher MR, et al. Tumor vascular permeability, accumulation, and penetration of macromolecular drug carriers. *J Natl Cancer Inst* 2006;36:335–344.
6. Mansouri S, et al. Characterization of folate–chitosan–DNA nanoparticles for gene therapy. *Biomaterials* 2006;27:2060–2065.
7. Yang L. Development of tumor-targeted nanoparticles for *in vivo* tumor imaging and drug delivery. *Nanomed Nanotechnol, Biol Med* 2006;2(4):293–295.
8. Amiji MM. Nanotechnology for targeted drug and gene delivery. *Nanomed Nanotechnol Biol Med* 2006;2(4):299–300.
9. Gaillard PJ and Boer AG. A novel opportunity for targeted drug delivery to the brain. *J Controll Release* 2006;2(28):60–62.
10. Silva GA. Nanotechnology approaches for the regeneration and neuroprotection of the central nervous system. *Surg Neurol* 2005;63:301–306.
11. Lu Y and Chen SC. Micro and nano-fabrication of biodegradable polymers for drug delivery. *Adv Drug Deliv Rev* 2004;56:1621–1633.
12. Van D, McGuire T, Langer R. Small scale systems for *in vivo* drug delivery. *Nat Biotechnol* 2003;21(10):1184–1191.
13. Kim GJ and Nie S. Targeted cancer nanotherapy. *Nanotoday* August:2005;28–33.
14. Martin CR and Kohli P. The emerging field of nanotube biotechnology. *Nat Rev Drug Discov* 2003;2:29–37.
15. Xu P, et al. Highly stable core-surface-crosslinked nanoparticles as cisplatin carriers for cancer chemotherapy. *Colloids Surf B Biointerfaces* 2006;48:50–57.

16. Kneuer C, et al. Silica nanoparticles modified with aminosilanes as carriers for plasmid DNA. *Int J Pharm* 2000;196:257–261.
17. Luo D, Han E, Belcheva N, Saltzman WM. A self-assembled, modular DNA delivery system mediated by silica nanoparticles. *J Control Release* 2004;95:333–341.
18. Sergiienko R, et al. Carbon encapsulated iron carbide nanoparticles synthesized in ethanol by an electric plasma discharge in an ultrasonic cavitation field. *Mater Chem Phys* 2006;98(1):34–38.
19. Brust M, Walker M, Bethell D, Schiffrin DJ, Whyman R. Synthesis of thiol-derivatised gold nanoparticles in a two-phase system. *J Chem Soc Chem Commun* 1994;801–802.
20. Chen M, Feng Y, Wang L, Zhang L, Zhang J. Study of palladium nanoparticles prepared from water-in-oil microemulsion. *Colloids Surf A* 2006;281(1–3):119–124.
21. Kayser O, Lemke A, Trejo NH. The impact of nanobiotechnology on the development of new drug delivery systems. *Curr Pharm Biotechnol* 2005;6:3–5.
22. Fishbein I, et al. Nanoparticulate delivery system of a tyrophostin for the treatment of restenosis. *J Control Release* 2000;65:221–229.
23. Nishioka Y and Yoshino H. Lymphatic targeting with nanoparticulate system. *Adv Drug Deliv Rev* 2001;47:55–64.
24. Panagi Z, et al. Effect of dose on the biodistribution and pharmacokinetics of PLGA and PLGA–mPEG nanoparticles. *Int J Pharm* 2001;221:143–152.
25. Calvo P, et al. Quantification and localization of PEGylated polycyanoacrylate nanoparticles in brain and spinal cord during experimental allergic encephalomyelitis in the rat. *Eur J Neurosci* 2002;15(8):1317–1326.
26. Zhang Y and Zhuo R. Synthesis and *in vitro* drug release behavior of amphiphilic triblock copolymer nanoparticles based on poly(ethylene glycol) and polycaprolactone. *Biomaterials* 2005;26(33):6736–6742.
27. Calvo P, et al. Novel hydrophilic chitosan–polyethylene oxide nanoparticles as protein carriers. *J appl polym Sci* 1997;63(1):125–132.
28. Merodio M, Arnedo A, Renedo MJ, Irache JM. Ganciclovir-loaded albumin nanoparticles: characterization and *in vitro* release properties. *Eur J Pharm Sci* 2001;12(3):251–259.
29. Zwiorek K, Kloeckner J, Wagner E, Coester C. Gelatin nanoparticles as a new and simple gene delivery system. *J Pharm Pharm Sci* 2004;7(4):22–28.
30. Zahoor A, Sharma S, Khuller GK. Inhalable alginate nanoparticles as antitubercular drug carriers against experimental tuberculosis. *Int J Antimicrob Agents* 2005;26(4):298–303.
31. Samaligeys MS and Rohdewald P. Reconstituted collagen nanoparticles, a novel drug carrier delivery system. *J Pharm Pharmacol* 1983;35(8):537–539.
32. Hans ML and Lowman AM. Biodegradable nanoparticles for drug delivery and targeting. *Curr Opin Solid State Mater Sci* 2002;6:319–327.
33. Couvreur P and Vauthier C. Polyalkylcyanoacrylate nanoparticles as drug carrier: present state and perspectives. *J Control Release* 1991;17:187–198.

34. Jain RA. The manufacturing techniques of various drug loaded biodegradable poly(lactide-co-glycolide) (PLGA) devices. *Biomaterials* 2000;21:2475–2490.
35. Coombes AGA. Design of nano and micro-particulate controlled release systems. Drug delivery company's report 2001/02. PharmaVentures Ltd;2001.
36. Alonso MJ, Gupta RK, Min C, Siber GR, Langer R. Biodegradable microspheres as controlled-release tetanus toxoid delivery systems. *Vaccine* 1994;12(4): 299–306.
37. Zhang Z and Feng S. Nanoparticles of poly(lactide)/vitamin E TPGS copolymer for cancer chemotherapy: synthesis, formulation, characterization and *in vitro* drug release. *Biomaterials* 2006;27:262–270.
38. Niwa T, Takeuchi H, Hino T, Kunou N, Kawashima Y. Preparations of biodegradable nanospheres of water-soluble and insoluble drugs with D,L-lactide/glycolide copolymer by a novel spontaneous emulsification solvent diffusion method, and the drug release behavior. *J Control Release* 1993;25:89–98.
39. Guerrero DQ, Fessi H, Allemann E, Doelker E. Influence of stabilizing agents and preparative variables on the formation of poly(D,L-lactic acid) nanoparticles by an emulsification–diffusion technique. *Int J Pharm* 1996;143: 133–141.
40. Murakami H, Kobayashi M, Takeuchi H, Kawashima Y. Preparation of poly(DL-lactide-co-glycolide) nanoparticles by modified spontaneous emulsification solvent diffusion method. *Int J Pharm* 1999;187:143–152.
41. Kwon GS, et al. Block copolymer micelles as vehicles for hydrophobic drugs. *Colloids Surf B Biointerfaces* 1994;2:429–434.
42. Salvage JP, et al. Novel biocompatible phosphorylcholine-based self-assembled nanoparticles for drug delivery. *J Control Release* 2005;104:259–270.
43. Xu JP, Ji J, Chen WD, Shen JC. Novel biomimetic polymersomes as therapeutics for drug delivery. *J Control Release* 2005;107(3):502–512.
44. Fu YJ, Shyu SS, Su FH, Yu PC. Development of biodegradable co-poly(D,L-lactic/glycolic acid) microspheres for the controlled release of 5-FU by the spray drying method. *Colloids Surf B Biointerfaces* 2002;25:269–279.
45. Leroux JC, Allemann E, Jaeghere FD, Doelker E, Gurny R. Biodegradable nanoparticles—from sustained release formulations to improved site specific drug delivery. *J Control Release* 1996;39:339–350.
46. Allemann E, Gurny R, Doelker E. Preparation of aqueous polymeric nanodispersions by a reversible salting-out process: influence of process parameters on particle size. *Int J Pharm* 1992;87:247–253.
47. Lukowski R, Miiller H, Müller BW, Dittgen M. Acrylic acid copolymer nanoparticles for drug delivery: characterization of the surface properties relevant for *in vivo* organ distribution. *Int J Pharm* 1992;84:23–31.
48. Behan N, Birkinshaw C, Clarke N. Poly(*n*-butylcyanoacrylate) nanoparticles: a mechanistic study of polymerisation and particle formation. *Biomaterials* 2001;22: 1335–1344.
49. Reis CP, Neufeld RJ, Ribeiro AJ, Veiga F. Nanoencapsulation methods for preparation of drug-loaded polymeric nanoparticles. *Nanomed: Nanotechnol, Biol Med* 2006;2:8–21.

50. McNeil SE. Nanotechnology for the biologist. *J Leukoc Biol* 2005;78:1–10.
51. Soppimath KS, Aminabhavi TM, Kulkarni AR, Rudzinski WE. Biodegradable polymeric nanoparticles as drug delivery devices. *J Control Release* 2001;70:1–20.
52. Chawla JS and Amiji MM. Biodegradable poly(*o*-caprolactone) nanoparticles for tumor targeted delivery of tamoxifen. *Int J Pharm* 2002;249:127–138.
53. Perez C, et al. Poly(lactic acid)–poly(ethylene glycol) nanoparticles as new carriers for the delivery of plasmid DNA. *J Control Release* 2001;75:211–224.
54. Yoo HS, Lee KH, Oh JE, Park TG. *In vitro* and *in vivo* anti-tumor activities of nanoparticles based on doxorubicin–PLGA conjugates. *J Control Release* 2000;68:419–431.
55. Müller RH, Jacobs C, Kayser O. Nanosuspensions as particulate drug formulations in therapy: rationale for development and what we can expect for the future. *Adv Drug Deliv Rev* 2001;47:3–19.
56. Vila A, Sanchez A, Tobo M, Calvo P, Alonso MJ. Design of biodegradable particles for protein delivery. *J Control Release* 2002;78:15–24.
57. Zhang Z and Feng SS. The drug encapsulation efficiency, *in vitro* drug release, cellular uptake and cytotoxicity of paclitaxel-loaded poly(lactide)–tocopheryl polyethylene glycol succinate nanoparticles. *Biomaterials* 2006;27:4025–4033.
58. Liu M, Dong J, Yang Y, Yang X, Xu H. Characterization and release of triptolide-loaded poly (D,L-lactic acid) nanoparticles. *Eur Polym J* 2005;41:375–382.
59. Yamazaki N, et al. Endogenous lectins as targets for drug delivery. *Adv Drug Deliv Rev* 2000;43:225–244.
60. Brigger I, Dubernet C, Couvreur P. Nanoparticles in cancer therapy and diagnosis. *Adv Drug Deliv Rev* 2002;54:631–651.
61. Peracchia MT, et al. Stealth PEGylated polycyanoacrylate nanoparticles for intravenous administration and splenic targeting. *J Control Release* 1999;60:121–128.
62. Couvreur P, Gref R, Andrieux K, Malvy C. Nanotechnologies for drug delivery application to cancer and autoimmune diseases. *Prog Solid State Chem* 2006;34:231–235.
63. Kaul G and Amiji M. Biodistribution and targeting potential of polyethylene glycol- modified gelatin nanoparticles in subcutaneous murine tumor model. *J Drug Target* 2004;12:585–591.
64. Kaul G and Amiji M. Tumor targeted gene delivery using polyethylene glycol-modified gelatin nanoparticles: *in vitro* and *in vivo* studies. *Pharm Res* 2005;22(6):951–961.
65. Li YP, et al. Stealth polycyanoacrylate nanoparticles as tumor necrosis factor carriers: pharmacokinetics and anti-tumor effects. *Biol Pharm Bull* 2001;24(6):662–665.
66. Vittaz M, et al. Effect of PEO surface density on long circulating PLA–PEO nanoparticles which are very low complement activators. *Biomaterials* 1996;17:1575–1581.
67. Zeng Y and Pitt WG. Poly(ethylene oxide)-*b*-poly(*N*-isopropylacrylamide) nanoparticles with crosslinked cores as drug carriers. *J Biomater Sci Polym Ed* 2005;16(3):371–380.

68. Shenoy D, Little S, Langer R, Amiji M. Poly(ethylene oxide)-modified poly(β -amino ester) nanoparticles as a pH-sensitive system for tumor-targeted delivery of hydrophobic drugs. Part I. *In Vitro* evaluations. *Mol Pharmacol* 2005;2(5): 357–366.
69. Kreuter J. Nanoparticulate systems for brain delivery of drugs. *Adv Drug Deliv Rev* 2001;47:65–81.
70. Roney C, et al. Targeted nanoparticles for drug delivery through the blood–brain barrier for Alzheimer’s disease. *J Control Release* 2005;108:193–214.
71. Garcia EG, Andrieux K, Gil S, Couvreur P. Colloidal carriers and blood–brain barrier translocation: a way to deliver drugs to the brain. *Int J Pharm* 2005;298: 274–292.
72. Olivier JC. Drug transport to brain with targeted nanoparticles. *J Am Soc Exp Neurother* 2005;2:108–119.
73. Gao X, et al. Lectin-conjugated PEG–PLA nanoparticles: preparation and brain delivery after intranasal administration. *Biomaterials* 2006;27:3482–3490.
74. Gao K and Jiang X. Influence of particle size on transport of methotrexate across blood–brain barrier by polysorbate 80-coated polybutylcyanoacrylate nanoparticles. *Int J Pharm* 2006;310:213–219.
75. Michaelis K, et al. Covalent linkage of apolipoprotein e to albumin nanoparticles strongly enhances drug transport into the brain. *J Pharm Exp Ther* 2006;317(3): 1246–1253.
76. Mishra V, et al. Targeted brain delivery of AZT via transferrin anchored pegylated albumin nanoparticles. *J Drug Target* 2006;14(1):45–53.
77. Costantino L, et al. Peptide-derivatized biodegradable nanoparticles able to cross the blood–brain barrier. *J Control Release* 2005;108:84–96.
78. Lu W, et al. Cationic albumin-conjugated pegylated nanoparticles as novel drug carrier for brain delivery. *J Control Release* 2005;107:428–448.
79. Krauzewicz N, et al. Virus-like gene transfer into cells mediated by polyomavirus pseudocapsids. *Gene Ther* 2000;7:2122–2131.
80. Leong KW, et al. DNA–polycation nanospheres as non-viral gene delivery vehicles. *J Control Release* 1998;53:183–193.
81. Borchard G. Chitosans for gene delivery. *Adv Drug Deliv Rev* 2001;52:145–150.
82. Mansouri S, et al. Chitosan–DNA nanoparticles as non-viral vectors in gene therapy: strategies to improve transfection efficacy. *Eur J Pharm Biopharm* 2004;57:1–8.
83. Zhao X, Yu SB, Wu FN, Mao ZB, Yu CL. Transfection of primary chondrocytes using chitosan–pEGFP nanoparticles. *J Control Release* 2006;112: 223–228.
84. Lungwitz U, Breunig M, Blunk T, Gopferich A. Polyethylenimine-based non-viral gene delivery systems. *Eur J Pharm Biopharm* 2005;60:247–266.
85. Santos AG, et al. Oligonucleotide–polyethylenimine complexes targeting retinal cells: structural analysis and application to anti-TGF β -2 therapy. *Pharm Res* 2006;23(4):770–781.
86. Guliyeva U, Oner F, Ozsoy S, Haziroglu R. Chitosan microparticles containing plasmid DNA as potential oral gene delivery system. *Eur J Pharm Biopharm* 2006;62:17–25.

87. Silva GA. Introduction to nanotechnology and its applications to medicine. *Surg Neurol* 2004;61:216–220.
88. Yokoyama A, et al. Biological behaviour of hat stacked carbon nanofibers in subcutaneous tissue in rats. *Nano Lett* 2005;5(1):157–161.
89. Chen Z, et al. Structure of poly(ferrocenyldimethylsilane) in electrospun organometallic nanofibers. *Macromolecules* 2001;34(18):6164–6166.
90. Kameoka J, Verbridge SS, Lui H. Fabrication of suspended silica glass nanofibers using a scanned electrospinning source. *Nano Lett* 2004;4(11):2105–2108.
91. Zhang M, Bando Y, Wada K, Kurashima K. Synthesis of nanotubes and nanowires of silicon oxide. *J Mater Sci Lett* 1999;18(23):1911–1913.
92. Duncan R. The drawing era of polymer therapeutics. *Nat Rev Drug Discov* 2003;2:347–360.
93. Griffith LG. Polymeric biomaterials. *Acta Mater* 2000;48:263–277.
94. Zhang Y, Lim CT, Ramakrishna S, Huang ZM. Recent development of polymer nanofibers for biomedical and biotechnological applications. *J Mater Sci-Mater Med* 2005;16:933–946.
95. Ondarcuhu T and Joachim C. Drawing a single nanofiber over hundreds of microns. *Eur Phys Lett* 1998;42:215–220.
96. Thomson RC, Shung AK, Yaszemski MJ, Mikos AG. Polymer scaffold processing. In: Vacanti J, Lanza RP, Langer R, editors. *Principles of Tissue Engineering*. San Diego: Academic Press; 251–261.
97. Feng L, Li SJ, Song YL, Jiang L, Zhu DB. Template based synthesis of aligned polyacrylonitrile nanofibers using a novel extrusion method. *Synth Met* 2003; 136:817–818.
98. Martin CR. Template synthesis of electronically conductive polymer nanostructures. *Acc Chem Res* November:1995;28:61–68.
99. Martin CR. Membrane-based synthesis of nanomaterials. *Chem Mater* 1996;8: 1739–1746.
100. Martin CR and Hulteen JC. A general template-based method for the preparation of nanomaterials. *J Mater Chem* 1997;7:1075–1087.
101. Guler MO, Claussen RC, Stupp SI. Encapsulation of pyrene within self-assembled peptide amphiphile nanofibers. *J Mater Chem* 2005;15:4507–4512.
102. Chen P. Self-assembly of ionic-complementary peptides: a physicochemical viewpoint. *Colloids Surf A: Physicochem Eng Aspects* 2005;261:3–24.
103. Hartgerink JD, Beniash E, Stupp SI. Peptide-amphiphile nanofibers: a versatile scaffold for the preparation of self-assembling materials. *Proc Natl Acad Sci USA* 2002;99(8):5133–5138.
104. Hartgerink JD, Paramonov SE, Jun HW. Self-assembly of peptide-amphiphile nanofibers: the roles of hydrogen bonding and amphiphilic packing. *J Am Chem Soc* 2006;128:7291–7298.
105. Niece KL, Hartgerink JD, Donners JM, Stupp SI. Self-assembly combining two bioactive peptide-amphiphile molecules into nanofibers by electrostatic attraction. *J Am Chem Soc* 2003;125:7146–7147.
106. Ma PX and Zhang R. Synthetic nano-scale fibrous extracellular matrix. *J Biomed Mater Res* 1999;46:60–72.

107. Frenot A and Chronakis IS. Polymer nanofibers assembled by electrospinning. *Curr Opin Colloid Interface Sci* 2003;8:64–75.
108. Reneker DH and Chun I. Nanometre diameter fibres of polymer, produced by electrospinning. *Nanotechnology* 1996;7:216–223.
109. Inai R, Kotaki M, Ramakrishna S. Structure and properties of electrospun PLLA single nanofibers. *Nanotechnology* 2005;16:208–213.
110. Li M, et al. Electrospun protein fibers as matrices for tissue engineering. *Biomaterials* 2005;26:5999–6008.
111. Smith LA and Ma PX. Nano-fibrous scaffolds for tissue engineering. *Colloids Surf B Biointerfaces* 2004;39:125–131.
112. Vasita R and Katti DS. Nanofibers and their applications in tissue engineering. *Int J Nanomed* 2006;1(1):15–30.
113. Shorey JD and Michelson D. On the mechanism of electrospraying. *Nucl Instrum Methods* 1970;82:295–296.
114. Xinhua Zong X, et al. Structure and process relationship of electrospun bioabsorbable nanofiber membranes. *Polymer* 2002;43:4403–4412.
115. Huang ZM, Zhang YZ, Kotaki M, Ramakrishna S. A review on polymer nanofibers by electrospinning and their applications in nanocomposites. *Compos Sci Technol* 2003;63:2223–2253.
116. Kosmider K and Scott J. Polymeric nanofibers exhibit an enhanced air filtration performance. *Filtr Sep* 2002;39(6):20–22.
117. Gibson HL, Truong Q, Walker JD, Jones WE. Chemical and biological protection and detection in fabrics for protective clothing. *Mater Res Soc* 2003;228(8):123–128.
118. Pham QP, Sharma U, Mikos AG. Electrospinning of polymeric nanofibers for tissue engineering applications: a review. *Tissue Eng* 2006;12(5):1197–1211.
119. Salvay DM and Shea LD. Inductive tissue engineering with protein and DNA-releasing scaffolds. *Mol Biosyst* 2006;2:36–48.
120. Kenawy ER, et al. Release of tetracycline hydrochloride from electrospun poly(ethylene-co-vinylacetate), poly(lactic acid), and a blend. *J Control Release* 2002;81:57–64.
121. Zeng J, et al. Biodegradable electrospun fibers for drug delivery. *J Control Release* 2003;92:227–231.
122. Kim K, et al. Incorporation and controlled release of a hydrophilic antibiotic using poly(lactide-co-glycolide)-based electrospun nanofibrous scaffolds. *J Control Release* 2004;98:47–56.
123. Cui W, et al. Investigation of drug release and matrix degradation of electrospun poly(DL-lactide) fibers with paracetamol inoculation. *Biomacromolecules* 2006;7:1623–1629.
124. Katti DS, Robinson KW, Ko FK, Laurencin CT. Bioresorbable nanofiber-based systems for wound healing and drug delivery: optimization of fabrication parameters. *J Biomed Mater Res B Appl Biomater* 70(2):286–296.
125. Verreck G, et al. Incorporation of drugs in an amorphous state into electrospun nanofibers composed of a water-insoluble, nonbiodegradable polymer. *J Control Release* 2003;92:349–360.

126. Rosen HB, Chang J, Wnek GE, Linhardt RJ, Langer R. Bioerodible polyanhydrides for controlled drug delivery. *Biomaterials* 1983;4:131–133.
127. Taepai boon P, Rungsardthong U, Supaphol P. Drug-loaded electrospun mats of poly(vinyl alcohol) fibres and their release characteristics of four model drugs. *Nanotechnology* 2006;17:2317–2329.
128. Huang ZM, et al. Encapsulating drugs in biodegradable ultrafine fibers through co-axial electrospinning. *J Biomed Mater Res* 2006;77:169–179.
129. Sun Z, et al. Compound core–shell nanofibers by coelectrospinning. *Adv Mater* 2003;15(22):1929–1932.
130. Jiang H, et al. Preparation and characterization of ibuprofen-loaded poly(lactide-co-glycolide)/poly(ethylene glycol)-g-chitosan electrospun membranes. *J Biomater Sci Polym Ed* 2004;15(3):279–296.
131. Luu YK, Kim K, Hsiao BS, Chu B, Hadjiargyrou M. Development of a nanostructured DNA delivery scaffold via electrospinning of PLGA and PLA–PEG block copolymers. *J Control Release* 2003;89:341–353.
132. Liang D, et al. *In vitro* non-viral gene delivery with nanofibrous scaffolds. *Nucleic Acids Res* 2005;33(19):1–8.
133. Zeng J, et al. Poly(vinyl alcohol) nanofibers by electrospinning as a protein delivery system and the retardation of enzyme release by additional polymer coatings. *Biomacromolecules* 2005;6:1484–1488.
134. Jiang H, et al. A facile technique to prepare biodegradable coaxial electrospun nanofibers for controlled release of bioactive agents. *J Control Release* 2005;108:237–243.
135. Jiang H, Fang D, Hsiao BS, Chu B, Chen W. Optimization and characterization of dextran membranes prepared by electrospinning. *Biomacromolecules* 2004;5:326–333.
136. Vasita R and Katti DS. Growth factor-delivery systems for tissue engineering: a materials perspective. *Expert Rev Med Devices* 2006;1:29–47.
137. Chew SY, Wen J, Yim EF, Leong KW. Sustained release of proteins from electrospun biodegradable fibers. *Biomacromolecules* 2005;6:2017–2024.
138. Beaty CE and Saltzman MW. Controlled growth factor delivery induces differential neurite outgrowth in three-dimensional cell cultures. *J Control Release* 1993;24:15–23.
139. Elbert SS and Hubbell JA. Controlled release of nerve growth factor from a heparin-containing fibrin-based cell ingrowth matrix. *J Control Release* 2000;69:149–158.
140. Lee AC, et al. Controlled release of nerve growth factor enhances sciatic nerve regeneration. *Exp Neurol* 2003;184:295–303.
141. Haller MF and Saltzman MW. Nerve growth factor delivery systems. *J Control Release* 1998;53:1–6.
142. Luginbuehl V, Meinel L, Merkle HP, Gander B. Localized delivery of growth factors for bone repair. *Eur J Pharm Biopharm* 2004;58:197–208.
143. Holland TA, Tabata Y, Mikos AG. Dual growth factor delivery from degradable oligo(poly(ethyleneglycol) fumarate) hydrogel scaffolds for cartilage tissue engineering. *J Control Release* 2005;101:111–125.

144. Simmons CA, Alsberg E, Hsiong S, Kim WJ, Mooney DJ. Dual growth factor delivery and controlled scaffold degradation enhance *in vivo* bone formation by transplanted bone marrow stromal cells. *Bone* 2004;35:562–569.
145. Wei G, Jin Q, Giannobile WV, Ma PX. Nano-fibrous scaffold for controlled delivery of recombinant human PDGF-BB. *J Control Release* 2006;112:103–110.
146. Lee JY, et al. Enhanced bone formation by controlled growth factor delivery from chitosan-based biomaterials. *J Control Release* 2002;78:187–197.
147. Park YJ, et al. Controlled release of platelet-derived growth factor-BB from chondroitin sulfate–chitosan sponge for guided bone regeneration. *J Control Release* 2000;67:385–394.
148. Markkanen JE, Rissanen TT, Antti Kivel A, Herttuala SY. Growth factor-induced therapeutic angiogenesis and arteriogenesis in the heart-gene therapy. *Cardiovasc Res* 2005;65:656–664.
149. Sun Q, et al. Sustained vascular endothelial growth factor delivery enhances angiogenesis and perfusion in ischemic hind limb. *Pharm Res* 2005;22(7):1110–1116.
150. Frechet JMJ and Tomalia D. *Dendrimers and Other Dendritic Polymers*. New York: John Wiley & Sons, Inc.; 2001.
151. Newkome GR, Moorefield CN, Vogtle F. *Dendrimers and Dendrons: Concepts, Syntheses, Applications*. Wiley-VCH; 2002.
152. Tomalia DA. Starburst dendrimers—nanoscopic supermolecules according to dendritic rules and principles. *Macromol Symp* 1996;101:243–255.
153. Hawker CJ and Frechet JMJ. Preparation of polymers with controlled molecular architecture—a new convergent approach to dendritic macromolecules. *J Am Chem Soc* 1990;112:7638–7647.
154. Esfand R and Tomalia DA. Poly(amidoamine) (PAMAM) dendrimers: from biomimicry to drug delivery and biomedical applications. *Drug Discov Today* 2001;6:427–436.
155. Gillies ER and Frechet JMJ. Dendrimers and dendritic polymers in drug delivery. *Drug Discov Today* 2005;10:35–43.
156. Bosman AW, Janssen HM, Meijer EW. About dendrimers: structure, physical properties and applications. *Chem Rev* 1999;99:1665–1688.
157. Liu M and Frechet JMJ. Designing dendrimers for drug delivery. *Pharm Sci Technol Today* 1999;2(10):393–401.
158. Duncan R. Polymer conjugates for tumour targeting and intra-cytoplasmic delivery. the EPR effect as a common gateway? *Pharm Sci Technol Today* 1999;2:441–449.
159. Available at www.dekker.com/sdek/93432345-48443502/.
160. Svenson S and Tomalia DA. Dendrimers in biomedical applications—reflections on the field. *Adv Drug Deliv Rev* 2005;57:2106–2129.
161. Dufs C, Uchegbu IF, Schtzlein AG. Dendrimers in gene delivery. *Adv Drug Deliv Rev* 2005;57:2177–2202.
162. Klajnert B and Bryszewska M. Dendrimers: properties and applications. *Acta Biochim Pol* 2001;48:199–208.

163. Beezer AE, et al. Dendrimers as potential drug carriers; encapsulation of acidic hydrophobes within water-soluble PAMAM derivatives. *Tetrahedron* 2003;59: 3873–3880.
164. Patri AK, et al. Targeted drug delivery with dendrimers: comparison of the release kinetics of covalently conjugated drug and non-covalent drug inclusion complex. *Adv Drug Deliv Rev* 2005;57:2203–2214.
165. Malik N, Evagorou EG, Duncan R. Dendrimer–platinate: a novel approach to cancer chemotherapy. *Anticancer Drugs* 1999;10(8):767–776.
166. Zhuo RX, Du B, Lu ZR. *In vitro* release of 5-fluorouracil with cyclic core dendritic polymer. *J Control Release* 1999;57:249–255.
167. Marie RG. Epidemiology of nonsteroidal anti-inflammatory drug-associated gastrointestinal injury. *Am J Med* 1998;104:23–29.
168. Denis MM. Comparative toxicity of nonsteroidal anti-inflammatory drugs. *Am J Med* 1999;107:37–41.
169. Kolhe P, et al. Preparation, cellular transport, and activity of polyamidoamine-based dendritic nanodevices with a high drug payload. *Biomaterials* 2006;27: 660–669.
170. Kolhe P, Misra E, Kannan RM, Kannan S, Lieh-Lai M. Drug complexation, *in vitro* release and cellular entry of dendrimers and hyperbranched polymers. *Int J Pharm* 2003;259:143–160.
171. Yiyun C and Tongwen X. Dendrimers as potential drug carriers, Part I. Solubilization of non-steroidal anti-inflammatory drugs in the presence of polyamidoamine dendrimers. *Eur J Med Chem* 2005;40:1188–1192.
172. Na M, et al. Dendrimers as potential drug carriers. Part II. Prolonged delivery of ketoprofen by *in vitro* and *in vivo* studies. *Eur J Med Chem* 2006;41:670–674.
173. Bielinska AU, et al. Regulation of *in vitro* gene expression using antisense oligonucleotides or antisense expression plasmids transfected using starburst PAMAM dendrimers. *Nucleic Acids Res* 1996;24:2176–2182.
174. Kukowska-Latallo JF, et al. Intravascular and endobronchial DNA delivery to murine lung tissue using a novel, nonviral vector. *Hum Gene Ther* 2000;11: 1385–1395.
175. Eichman JD, Bielinska AU, Latallo JK, Baker JR. The use of PAMAM dendrimers in the efficient transfer of genetic material into cells. *Pharm Sci Technol Today* 2000;3(7):232–245.
176. Haensler J and Szoka FC. Polyamidoamine cascade polymers mediate efficient transfection of cells in culture. *Bioconjug Chem* 1993;4:372–379.
177. Dufes C, Uchegbu IF, Schatzlein AG. Dendrimers in gene delivery. *Adv Drug Deliv Rev* 2005;57:2177–2202.
178. Dhanikula RS and Hildgen P. Synthesis and evaluation of novel dendrimers with a hydrophilic interior as nanocarriers for drug delivery. *Bioconjug Chem* 2006; 17:29–41.
179. Bhadra D, Bhadra S, Jain NK. PEGylated peptide based dendritic nanoparticulate systems for delivery of artemether. *J Drug Deliv Sci Technol* 2005;15:65–73.
180. Ostro MJ and Cullis PR. Use of liposomes as injectable-drug delivery systems. *Am J Hosp Pharm* 1989;46:1576–1587.

181. Available at <http://en.wikipedia.org/wiki/Liposome>.
182. Kshirsagar NA. Drug delivery systems. *Indian J Pharma* 2000;32:54–61.
183. Bangham AD and Horne RW. Negative staining of phospholipids and their structural modification by surface-active agents as observed in the electron microscope. *J Mol Biol* 1964;8:660–668.
184. Lasic DD. Novel applications of liposomes. *Tibtech* 1998;16:307–321.
185. Diederichs JE and Müller RH. Liposomen in kosmetika und arzneimitteln. *Pharm Ind* 1994;56:267–275.
186. Heath TD. Liposome dependent drugs. In: Gregoriadis G, editor. *Liposomes as Drug Carriers: Trends and Progress*. New York: John Wiley & Sons, Inc.; 1988. p 709–718.
187. Allemann E, Gurny R, Doelker E. Drug loaded nanoparticles—preparation methods and drug targeting issues. *Eur J Pharm Biopharm* 1993;39:173–191.
188. Smith A and Hunneyball IM. Evaluation of polylactide as a biodegradable drug delivery system for parenteral administration. *Int J Pharm* 1986;30:215–230.
189. Siekmann B and Westesen K. Sub-micron sized parenteral carrier systems based on solid lipids. *Pharm Pharmacol Lett* 1992;1:123–126.
190. Schwarz C, Mehnert W, Lucks JS, Müller RH. Solid lipid nanoparticles (SLN) for controlled drug delivery. I. Production, characterization and sterilization. *J Control Release* 1994;30:83–96.
191. Westesen K, Siekmann B, Koch MHJ. Investigations on the physical state of lipid nanoparticles by synchrotron radiation X-ray diffraction. *Int J Pharm* 1993; 93:189–199.
192. Cavalli R, Marengo E, Rodriguez L, Gasco MR. Effects of some experimental factors on the production process of solid lipid nanoparticles. *Eur J Pharm Biopharm* 1996;43(2):110–115.
193. Müller RH, et al. Solid lipid nanoparticles (SLN) as an alternative colloidal carrier system for controlled drug delivery. *Eur J Pharm Biopharm* 1995;41(1):62–69.
194. Bunjes H, Westesen K, Koch MHJ. Crystallization tendency and polymorphic transitions in triglyceride nanoparticles. *Int J Pharm* 1996;129:159–173.
195. Gasco MR. Solid lipid nanospheres from warm microemulsions. *Pharm Technol Eur* 1997;9(11):52–58.
196. Heiati H, Phillips NC, Tawashi R. Evidence for phospholipids bilayer formation in solid lipid nanoparticles formulated with phospholipid and triglyceride. *Pharm Res* 1996;13(9):1406–1410.
197. Vringer T and Ronde HG. Preparation and structure of a water-in-oil cream containing lipid nanoparticles. *J Pharm Sci* 1995;84(4):466–472.
198. Sjostrom B, Kaplun A, Talmon Y, Cabane B. Structure of nanoparticles prepared from oil-in-water emulsions. *Pharm Res* 1995;12(1):39–48.
199. Dingler A, Blum RP, Niehus H, Gohla S, Müller RH. Solid lipid nanoparticles (SLN/Lipopearl): a pharmaceutical and cosmetic carrier for the application of vitamin E in dermal products. *J Microencapsul* 1999;16(6): 751–767.
200. Demirel M, Yazan Y, Müller RH, Kilic F, Bozan B. Formulation and *in vitro*–*in vivo* evaluation of piribedil solid lipid particles. *J Microencapsul* 2001; 18(3):359–371.

201. Wissing SA and Müller RH. Solid lipid nanoparticles as carrier for sunscreens: *in vitro* release and *in vivo* skin penetration. *J Control Release* 2002;81:225–233.
202. Cavalli R, Caputo O, Gasco MR. Solid lipospheres of doxorubicin and idarubicin. *Int J Pharm* 1993;89:9–12.
203. Morel S, Gasco MR, Cavalli R. Incorporation in lipospheres of [D-Trp-6]LHRH. *Int J Pharm* 1994;105:1–3.
204. Cavalli R, Morel S, Gasco MR, Chetoni P, Saettone MF. Preparation and evaluation *in vitro* of colloidal lipospheres containing pilocarpine as ion pair. *Int J Pharm* 1995;117:243–246.
205. Sznitowska M, Gajewska M, Janicki S, Radwanska A, Lukowski G. Bioavailability of diazepam from aqueous-organic solution, submicron emulsion and solid lipid nanoparticles after rectal administration to rabbits. *Eur J Pharm Biopharm* 2001;52:159–163.
206. Müller RH, Radtke M, Wissing SA. Solid lipid nanoparticles (SLN) and nanostructured lipid carriers (NLC) in cosmetic and dermatological preparations. *Adv Drug Deliv Rev* 2002;54:131–155.
207. Müller RH, Radtke M, Wissing SA. Nanostructured lipid matrices for improved microencapsulation of drugs. *Int J Pharm* 2002;242:121–128.
208. Radtke M and Müller RH. Comparison of structural properties of solid lipid nanoparticles (SLN) versus other lipid particles. *Proc Int Symp Control Release Bioact Mater* 2000;27:309–310.
209. Olbrich C, Gebner A, Kayser O, Müller RH. Lipid–drug conjugate (LDC) nanoparticles as novel carrier system for the hydrophilic antitrypanosomal drug diminazenediaceturate. *J Drug Target* 2002;10(5):387–396.
210. Müller RK, Mader K, Gohla S. Solid lipid nanoparticles (SLN) for controlled drug delivery—a review of the state of the art. *Eur J Pharm Biopharm* 2005;50:161–177.
211. Hoffman RM, Margolis LB, Bergelson LD. Binding and entrapment of high molecular weight DNA by lecithin liposomes. *FEBS Lett* 1978;33:365–368.
212. Ridder M, Wang Y, Hofschneider PH. Liposomes as gene carriers: efficient transformation of mouse L cells by thymidine kinase gene. *Science* 1982;215:166–168.
213. Liu F, Yang J, Huang L, Liu D. Effect of non-ionic surfactants on the formation of DNA/emulsion complex and the emulsion-mediated gene transfer. *Pharm Res* 1997;13:1642–1646.
214. Watwe RM and Bellare JR. Manufacture of liposomes: a review. *Curr Sci* 1995;68:715–724.
215. Cortesi R, Esposito E, Luca G, Nastruzzi C. Production of lipospheres as carriers for bioactive compounds. *Biomaterials* 2002;23:2283–2294.
216. Lim SJ and Kim CK. Formulation parameters determining the physicochemical characteristics of solid lipid nanoparticles loaded with all-*trans* retinoic acid. *Int J Pharm* 2002;243:135–146.
217. Siekmann B, Bunjes H, Koch MHJ, Westesen K. Preparation and structural investigations of colloidal dispersions prepared from cubic monoglyceride–water phases. *Int J Pharm* 2002;244:33–43.
218. Lippacher A, Müller RH, Mader K. Preparation of semisolid drug carriers for topical application based on solid lipid nanoparticles. *Int J Pharm* 2001;214:9–12.

219. Lippacher A, Müller RH, Mader K. Semisolid SLN dispersions for topical application: influence of formulation and production parameters on microstructure. *Eur J Pharm Biopharm* 2002;53(2):155–160.
220. Jenning V, Lippacher A, Gohla SH. Medium scale production of solid lipid nanoparticles (SLN) by high pressure homogenization. *J Microencapsul* 2002;19(1):1–10.
221. Dingler A and Gohla S. Production of solid lipid nanoparticles (SLN): scaling up feasibilities. *J Microencapsul* 2002;19(1):11–16.
222. Cavalli R, Caputo O, Marengo E, Pattarino F, Gasco MR. The effect of the components of microemulsions on both size and crystalline structure of solid lipid nanoparticles (SLN) containing a series of model molecules. *Pharmazie* 1998;53:392–396.
223. Eldem T, Speiser P, Hincal A. Optimization of spray-dried and congealed lipid micropellets and characterisation of their surface morphology by scanning electron microscopy. *Pharm Res* 1991;8:47–54.
224. Wang JX, Sun X, Zhang ZR. Enhanced brain targeting by synthesis of 3V,5V-dioctanoyl-5-fluoro-2V-deoxyuridine and incorporation into solid lipid nanoparticles. *Eur J Pharm Biopharm* 2002;54:285–290.
225. Hou DZ, Xie CS, Huang KJ, Zhu CH. The production and characteristics of solid lipid nanoparticles. *Biomaterials* 2003;24:1781–1785.
226. Cortesi R, Esposito E, Luca G, Nastruzzi C. Production of lipospheres as carriers for bioactive compounds. *Biomaterials* 2002;23:2283–2294.
227. Shahgaldian P, Silva ED, Coleman AW, Rather B, Zaworotko MJ. *Para*-acyl-calix-arene based solid lipid nanoparticles (SLN): a detailed study of preparation and stability parameters. *Int J Pharm* 2003;253:23–38.
228. Dubes A, et al. Scanning electron microscopy and atomic force microscopy imaging of solid lipid nanoparticles derived from amphiphilic cyclodextrins. *Eur J Pharm Biopharm* 2003;55:279–282.
229. Boswell GW, Buell D, Bekersky I. AmBisome (liposomal amphotericin B): a comparative review. *J Clin Pharmacol* 1998;38:583–92.
230. Gray A and Morgan J. Liposomes in hematology. *Blood Rev* 1991;5:258–271.
231. Longuet P, et al. Limited protection by small unilamellar liposomes against the renal tubular toxicity induced by repeated amphotericin B infusion in rats. *Antimicrob Agents Chemother* 1991;35:1303–1308.
232. Davidson RN, et al. Liposomal amphotericin B in drug-resistant leishmaniasis. *Lancet* 1991;337:1061–1062.
233. Gregoriadis G, Gursel I, Gursel M, McCormack B. Liposomes as immunological adjuvants and vaccine carriers. *J Control Release* 1996;41:49–56.
234. Gregoriadis G. Engineering liposomes for drug delivery: progress and problems. *Biotechnology* 1995;13:527–537.
235. Oussoren C and Storm G. Targeting to lymph nodes by subcutaneous administration of liposomes. *Int J Pharm* 1998;162:39–44.
236. Gregoriadis G, Saffie R, DaSouza JB. Liposome mediated DNA vaccination. *FEBS Lett* 1997;402:107–110.
237. Kim CK and Jeong EJ. Development of dried liposome as effective immuno-adjuvant for hepatitis B surface antigen. *Int J Pharm* 1995;115:193–199.

238. Zabner J. Cationic lipids used in gene transfer. *Adv Drug Deliv Rev* 1997;27:17–28.
239. Smith J, Zhang YL, Niven R. Toward development of a non-viral gene therapeutic. *Adv Drug Deliv Rev* 1997;26:135–150.
240. Felgner PL, et al. Lipofection—a highly efficient, lipid-mediated DNA-transfection procedure. *Proc Natl Acad Sci USA* 1987;84:7413–7417.
241. Reimer DL, et al. Formation of novel hydrophobic complexes between cationic lipids and plasmid DNA. *Biochemistry* 2001;44:12877–12883.
242. Wong FM, Reimer DL, Bally MB. Cationic lipid binding to DNA: characterization of complex formation. *Biochemistry* 2000;35:5756–5763.
243. Ferguson MR, et al. Delivery of double-stranded DNA thioaptamers into HIV-1 infected cells for antiviral activity. *Biochem Biophys Res Comm* 2006;344(3):792–797.
244. Wong J, et al. Liposome-mediated transient transfection reduces cholesterol-dependent coxsackievirus infectivity. *J Virol Methods* 2006;133(2):211–218.
245. Iwasa A, et al. Cellular uptake and subsequent intracellular trafficking of R8-liposomes. *Biochim Biophys Acta Biomembr* 2006;1758(6):713–720.
246. Cavalli R, Caputo O, Gasco MR. Preparation and characterization of solid lipid nanospheres containing paclitaxel. *Eur J Pharm Sci* 2000;10:305–309.
247. Ugazio E, Cavalli R, Gasco MR. Incorporation of cyclosporine A in solid lipid nanoparticles. *Int J Pharm* 2002;241:341–344.
248. Souto EB and Müller RH. SLN and NLC for topical delivery of ketoconazole. *J Microencapsul* 2005;22:501–510.
249. Yang SC, et al. Distribution in mice of intravenously injected camptothecin solid lipid nanoparticles and targeting effect on brain. *J Control Release* 1999;59:299–307.
250. Wissing SA, Kayser O, Müller RH. Solid lipid nanoparticles for parenteral drug delivery. *Adv Drug Deliv Rev* 2004;56:1257–1272.
251. Yamago S, et al. *In vivo* biological behavior of a water-miscible fullerene: C-14 labeling, absorption, distribution, excretion and acute toxicity. *Chem Biol* 1995;2(6):385–389.
252. Bianco A, et al. Biomedical applications of functionalized carbon nanotubes. *Chem Commun* 2005;571–577.
253. Dai H. Carbon nanotubes: opportunities and challenges. *Surf Sci* 2002;500:218–241.
254. Resasco DE, et al. A scalable process for production of single-walled carbon nanotubes by catalytic disproportionation of CO on a solid catalyst. *J Nanopart Res* 2002;4:131–136.
255. Qingwen L, Jin Y, Zhogfan L. Dependence of the formation of carbon nanotubes on the chemical structures of hydrocarbons. *Adv Nanomater Nanodevices* 2002; 59–71.
256. Journet C and Bernier P. Production of carbon nanotubes. *Appl Phys A* 1998;1–9.
257. Morishita K and Takarada T. Scanning electron microscope observation of the purification behavior of carbon nanotubes. *J Mater Sci* 1999;34(6):1169–1174.
258. Bethune DS, et al. Cobalt-catalysed growth of carbon nanotubes with single-atomic-layer walls. *Nature* 1993;363:605–607.

259. Ebbesen TW and Ajayan PM. Large-scale synthesis of carbon nanotubes. *Nature* 1992;358:220–222.
260. Chiang M, et al. Electron field emission properties of pulsed laser deposited carbon films containing carbon nanotubes. *J Vac Sci Technol* 2001;19(3):1034–1039.
261. Guillard T, et al. Scale up of a solar reactor for fullerene and nanotube synthesis. *J Sol Energy Eng* 2002;124:22–27.
262. Bilodeau JF, Alexakis T, Meuniery JL, Tzantrizosz PG. Model of the synthesis of fullerenes by the plasma torch dissociation of C_2Cl_4 . *J Phys D: Appl Phys* 1997; 30:2403–2410.
263. Kroto HW, Heath JR, Brien SC, Curl RF, Smalley RE. C_{60} : buckminsterfullerene. *Nature* 1985;318:162–165.
264. Kratschmer W, Lamb LD, Fostiropoulos K, Huffman DR. Solid C_{60} : a new form of carbon. *Nature* 1990;347:354–357.
265. Chuanchen S, Haibin G, Dufei F. Extraction of C_{60} cluster ion beam. *Rev Sci Instrum* 1994;65:1405–1409.
266. Sinha N and Yeow JW. Carbon nanotubes for biomedical applications. *IEEE Trans Nanobiosci* 2005;4(2):180–195.
267. Dyke CA, Stewart MP, Tour JM. Separation of single-walled carbon nanotubes on silica gel: materials morphology and Raman excitation wavelength affect data interpretation. *J Am Chem Soc* 2005;127:4497–4509.
268. Georgakilas V, et al. Purification of HiPCO carbon nanotubes via organic functionalization. *J Am Chem Soc* 2002;124:14318–14319.
269. Zhao B, et al. Chromatographic purification and properties of soluble single-walled carbon nanotubes. *J Am Chem Soc* 2001;123:11673–11677.
270. Niyogi S, et al. Chromatographic purification of soluble single-walled carbon nanotubes. *J Am Chem Soc* 2001;123:733–734.
271. Shvedova AA, Castranova V. Exposure to carbon nanotube material: assessment of nanotube cytotoxicity using human keratinocyte cells. *J Toxicol Environ Health* 2003;66(20):1909–1926.
272. Riviere NA, Nemanich RJ, Inman AO, Wang YY, Riviere JE. Multi-walled carbon nanotube interactions with human epidermal keratinocytes. *Toxicol Lett* 2005;155(3):377–384.
273. Lam C, James JT, McCluskey R, Hunter R. Pulmonary toxicity of single-wall carbon nanotubes in mice 7 and 90 days after intratracheal instillation. *Toxicol Sci* 2004;77(1):126–134.
274. Warheit DB, et al. Comparative pulmonary toxicity assessment of single-wall carbon nanotubes in rats. *Toxicol Sci* 2004;77(1):117–125.
275. Huczko A, Lange H, Bystrzejewski M, Baranowski. Pulmonary toxicity of 1-D nanocarbon materials. *Fullerenes Nanotubes Carbon Nanostruct* 2005;13(2): 141–145.
276. Müller J, et al. Respiratory toxicity of multi-wall carbon nanotubes. *Toxicol App Pharmacol* 2005;207(3):221–231.
277. Garibaldi S, Brunelli C, Bavastrello V, Ghigliotti G, Nicolini C. Carbon nanotube biocompatibility with cardiac muscle cells. *Nanotechnology* 2006;17:391–397.
278. Bianco A, et al. Applications of carbon nanotubes in drug delivery. *Curr Opin Chem Biol* 2005;9:674–679.

279. Star A, Steuerman DW, Heath JR, Stoddart JF. Starched carbon nanotubes. *Angew Chem Int Ed* 2002;41(14):2508–2512.
280. Zheng M, et al. DNA-assisted dispersion and separation of carbon nanotubes. *Nat Mater* 2003;2:338–342.
281. Chen RJ, Zhang Y, Wang D, Dai H. Noncovalent sidewall functionalization of single-walled carbon nanotubes for protein immobilization. *J Am Chem Soc* 2001;123:3838–3839.
282. Pantarotto D, et al. Functionalized carbon nanotubes for plasmid DNA gene delivery. *Angew Chem Int Ed* 2004;43:5242–5246.
283. Islam MF, Rojas E, Bergey DM, Johnson AT, Yodh AG. High weight fraction surfactant solubilization of single-wall carbon nanotubes in water. *Nano Lett* 2003;3:269–273.
284. Liu J, et al. Fullerene pipes. *Science* 1998;280:1253–1256.
285. Georgakilas V, et al. Organic functionalization of carbon nanotubes. *J Am Chem Soc* 2002;124:760–761.
286. Georgakilas V, et al. Amino acid functionalization of water-soluble carbon nanotubes. *Chem Commun* 2002;24:3050–3051.
287. Bianco A, et al. Carbon nanotubes: on the road to deliver. *Curr Drug Deliv Rev* 2005;2:253–259.
288. Planeix JM, et al. Application of carbon nanotubes as supports in heterogeneous catalysis. *J Am Chem Soc* 1994;116(17):7935–7936.
289. Saito S. Carbon nanotubes for next-generation electronics devices. *Science* 1997;278:77–78.
290. Kim P and Lieber CM. Nanotube nanotweezers. *Science* 1999;286:2148–2150.
291. Collins PG, Zettl A, Bando H, Thess A, Smalley RE. Nanotube nanodevice. *Science* 1997;278:100–102.
292. Mitchell DT, et al. Smart nanotubes for bioseparations and biocatalysis. *J Am Chem Soc* 2002;124:11864–11865.
293. Wu W, et al. Targeted delivery of amphotericin B to cells by using functionalized carbon nanotubes. *Angew Chem Int Ed* 2005;44:6358–6362.
294. Pastorin G, et al. Double functionalization of carbon nanotubes for multimodal drug delivery. *Chem Commun* 2006;11:1182–1184.
295. Yinghuai Z, et al. Substituted carborane-appended water-soluble single-wall carbon nanotubes: new approach to boron neutron capture therapy drug delivery. *J Am Chem Soc* 2005;127:9875–9880.
296. Rojas-Chapana J, Troszczynska J, Firkowska I, Morszeck C, Giersig M. Multi-walled carbon nanotubes for plasmid delivery into *Escherichia coli* cells. *Lab Chip* 2005;5:536–539.
297. Singh R, et al. Binding and condensation of plasmid DNA onto functionalized carbon nanotubes: toward the construction of nanotube-based gene delivery vectors. *J Am Chem Soc* 2005;127:4388–4396.
298. Kam NS, Liu Z, Dai H. Functionalization of carbon nanotubes via cleavable disulfide bonds for efficient intracellular delivery of siRNA and potent gene silencing. *J Am Chem Soc* 2005;127:12492–12493.
299. Kam NS and Dai H. Carbon nanotubes as intracellular protein transporters: generality and biological functionality. *J Am Chem Soc* 2005;127:6021–6026.

300. Kam NS, Jessop TC, Wender PA, Dai H. Nanotube molecular transporters: internalization of carbon nanotube–protein conjugates into mammalian cells. *J Am Chem Soc* 2004;126:6850–6851.
301. Pantarotto D, et al. Immunization with peptide-functionalized carbon nanotubes enhances virus-specific neutralizing antibody responses. *Chem Biol* 2003;10:961–966.
302. Rasenick MM, Watanabe M, Lazarevic MB, Hatta S, Hamm HE. Synthetic peptides as probes for g protein function. *J Biol Chem* 1994;269(34):21519–21525.
303. Bianco A, et al. Cationic carbon nanotubes bind to CpG oligodeoxynucleotides and enhance their immunostimulatory properties. *J Am Chem Soc* 2005;127:58–59.
304. Schergna S, et al. Enzymatic modification of fullerene derivatives. *Tetrahedron Lett* 1998;39(42):7791–7794.
305. Kurz AH, Halliwell CM, Davis JJ, Hill AO, Canters GW. A fullerene-modified protein. *Chem Commun* 1998;433–434.
306. Available at <http://www.csixty.com/development.html>.
307. Dugan LL, et al. Carboxyfullerenes as neuroprotective agents. *Proc Natl Acad Sci USA* 1997;94:9434–9439.
308. Foley S, et al. Cellular localisation of a water-soluble fullerene derivative. *Biochem Biophys Res Commun* 2002;294:116–119.
309. Friedman SH, et al. Inhibition of the HIV-1 protease by fullerene derivatives: model building studies and experimental verification. *J Am Chem Soc* 1993;115:6506–6509.
310. Gonzalez AK, Wilson LJ, Wu W, Nancollas GH. Synthesis and *in vitro* characterization of a tissue-selective fullerene: vectoring C₆₀(OH)₁₆AMBP to mineralized bone. *Bioorg Med Chem* 2002;10:1991–1997.
311. Tsao N, et al. *In vitro* action of carboxyfullerene. *J Antimicrob Chemother* 2002;49:641–649.
312. Isobe H, et al. Nonviral gene delivery by tetraamino fullerene. *Mol Pharmacol* 2006;3(2):124–134.
313. Ashcroft JM, et al. Fullerene (C₆₀) immunoconjugates: interaction of water-soluble C₆₀ derivatives with the murine anti-gp240 melanoma antibody. *Chem Commun* 2006;3004–3006.
314. Rancan F, et al. Fullerene-pyropheophorbide a complexes as sensitizer for photodynamic therapy: uptake and photo-induced cytotoxicity on Jurkat cells. *J Photochem Photobiol B: Biol* 2005;80:1–7.
315. Zakharian TY, et al. A fullerene–paclitaxel chemotherapeutic: synthesis, characterization, and study of biological activity in tissue culture. *J Am Chem Soc* 2005;127:12508–12509.
316. Cagle DW, Kennel SJ, Mirzadeh S, Michael Alford J, Wilson LJ. *In vivo* studies of fullerene-based materials using endohedral metallofullerene radiotracers. *Proc Natl Acad Sci* 1999;96:5182–5187.
317. Bolskar RD, et al. First soluble M@C₆₀ derivatives provide enhanced access to metallofullerenes and permit *in vivo* evaluation of Gd@C₆₀[C(COOH)₂]₁₀ as a MRI contrast agent. *J Am Chem Soc* 2003;125:5471–5478.

318. Kato H, et al. Lanthanoid endohedral metallofullerenols for MRI contrast agents. *J Am Chem Soc* 2003;125:4391–4397.
319. Lee I and Akiyoshi K. Single molecular mechanics of a cholesterol-bearing pullulan nanogel at the hydrophobic interfaces. *Biomaterials* 2004;25:2911–2918.
320. Candau F, Daoud M, Williams CE. *Soft Matter Physics*. New York: Springer; 1995.
321. Antonietti M, Bremser W, Schmid M. Clusters and colloids: from theory to applications. *Macromolecules* 1990;23:3796–3805.
322. Antonietti M. Microgels—colloidal models for the cross-linked state. *Macromol Symp* 1995;93:213–225.
323. Antonietti M, Pakula T, Bremser W. Rheology of small spherical polystyrene microgels: a direct proof for a new transport mechanism in bulk polymers besides reptation. *Macromolecules* 1995;28:4227–4233.
324. Kuckling D, Vo CD, Wohlrab SE. Preparation of nanogels with temperature-responsive core and pH responsive arms by photocrosslinking. *Langmuir* 2002; 18:4263–4269.
325. Zhou J, Li Z, Liu G. Diblock copolymer nanospheres with porous cores. *Macromolecules* 2002;35:3690–3696.
326. Daubresse C, Grandfils C, Jerome R, Teysse P. Enzyme immobilization in nanoparticles produced by inverse microemulsion polymerization. *J Colloid Interface Sci* 1994;168:222–229.
327. Daubresse C, et al. Synthesis and inverse emulsion polymerization of aminated acrylamidodextran. *J Pharm Pharmacol* 1993;45:1018–1023.
328. Gupta AK, Madan S, Majumdar DK, Maitra A. Ketorolac entrapped in polymeric micelles: preparation, characterisation and ocular anti-inflammatory studies. *Int J Pharm* 2000;209:1–14.
329. Gaur U, et al. Biodistribution of fluoresceinated dextran using novel nanoparticles evading reticuloendothelial system. *Int J Pharm* 2000;202:1–10.
330. Madan T, et al. Biodegradable nanoparticles as a sustained release system for the antigens/allergens of *Aspergillus fumigatus*: preparation and characterisation. *Int J Pharm* 1997;159:135–147.
331. Harth E, et al. A facile approach to architecturally defined nanoparticles via intramolecular chain collapse. *J Am Chem Soc* 124:8653–8660.
332. Mecerreyes D, et al. A novel approach to functionalized nanoparticles: self-crosslinking of macromolecules in ultradilute solution. *Adv Mater* 2001;13: 204–207.
333. Gregor HP, Samuelson E, Dalven PI, Gregor CD. Homopolymers and copolymers of acrylamide *N*-substituted acrylamide or *N*-substituted methacrylamide solid state cross-linked with polyamines or polyols. US patent 5,280,078. 1994.
334. Gan D and Lyon LA. Tunable swelling kinetics in core–shell hydrogel nanoparticles. *J Am Chem Soc* 2001;123:7511–7517.
335. Jones CD and Lyon LA. Synthesis and characterization of multiresponsive core–shell microgels. *Macromolecules* 2000;33:8301–8306.
336. Kadlubowski S, Grobelny J, Olejniczak W, Cichomski M, Ulanski P. Pulses of fast electrons as a tool to synthesize poly(acrylic acid) nanogels: intramolecular

- cross-linking of linear polymer chains in additive-free aqueous solution. *Macromolecules* 2003;36:2484–2492.
337. Ulanski P, Kadlubowski S, Rosiak JM. Synthesis of poly(acrylic acid) nanogels by preparative pulse radiolysis. *Radiat Phys Chem* 2002;63:533–537.
338. Corrigan VG and Zawacky SR. Cationic microgels and their use in electrodeposition. US patent 5,096,556. 1992.
339. Gajria C and Ozari Y. Water-swellable crosslinked polymeric microgel particles and aqueous dispersions of organic film-forming resins containing the same. US patent 4,560,714. 1985.
340. Quadrat O and Snuparek J. Structure and flow properties of latexes containing carboxylic groups. *Prog Org Coat* 1990;18:207–228.
341. Biffis A. Functionalised microgels: novel stabilizers for catalytically active metal colloids. *J Mol Catal A: Chem* 2001;165:303–307.
342. Morris GE, Vincent B, Snowden MJ. The interaction of nanothermosensitive, anionic microgels with metal ion solution species. *Prog Colloid Polym Sci* 1997; 105:16–22.
343. Sawai T, Ikariyama Y, Aizawa M. Electrically modulated/flocculation of ultra fine microgels. In: *Proceedings of the International Conference on Intelligent Materials*; 1993; p 279.
344. Peppas NA, Bures P, Leobandung W, Ichikawa H. Hydrogels in pharmaceutical formulations. *Eur J Pharm Biopharm* 2000;50:27–46.
345. Kiserab PF, Wilson G, Needham D. Lipid-coated microgels for the triggered release of doxorubicin. *J Control Release* 2000;68:9–22.
346. Guzman LA, et al. Local intraluminal infusion of biodegradable polymeric nanoparticles: a novel approach for prolonged drug delivery after balloon angioplasty. *Circulation* 1996;94:1441–1448.
347. Morimoto M, Endo T, Ohtomi M, Iwasaki Y, Akiyoshi K. Hybrid nanogels with physical and chemical cross-linking structures as nanocarriers. *Macromol Biosci* 2005;5:710–716.
348. Moshfeghi AA and Peyman GA. Micro- and nanoparticulates. *Adv Drug Deliv Rev* 2005;57:2047–2052.
349. Winet H, Hollinger JO, Stevanovic M. Incorporation of polylactide–polyglycolide in a cortical defect: neoangiogenesis and blood supply in a bone chamber. *J Orthop Res* 1995;13:679–689.
350. Kuckling D, Vo CD, Wohlrab SE. Preparation of nanogels with temperature-responsive core and pH-responsive arms by photo-cross-linking. *Langmuir* 2002; 18:4263–4269.
351. Shin Y, et al. Hybrid nanogels for sustainable positive thermosensitive drug release. *J Control Release* 2001;73:1–6.
352. Jeong B, Kim S, Bae YH. Thermosensitive sol–gel reversible hydrogels. *Adv Drug Deliv Rev* 2002;54:37–51.
353. Sershen S and West J. Implantable, polymeric systems for modulated drug delivery. *Adv Drug Deliv Rev* 2003;55:439–446.
354. Lowman AM, Takayama K, Nagai T, Peppas NA. Elucidation of the mechanism of incorporation of insulin in controlled release systems based on complexation polymers. *J Control Release* 2002;81:25–32.

355. Lowman AM, Morishita M, Kajita M, Nagai T, Peppas NA. Oral delivery of insulin using pH-responsive complexation gels. *J Pharm Sci* 2003;88(9):933–937.
356. Podual K, Doyle FJ, Peppas NA. Dynamic behavior of glucose oxidase-containing microparticles of poly(ethylene glycol)-grafted cationic hydrogels in an environment of changing pH. *Biomaterials* 2000;21:1439–1450.
357. Podual K, Doyle FJ, Peppas NA. Preparation and dynamic response of cationic copolymer hydrogels containing glucose oxidase. *Polymer* 2000;41:3975–3983.
358. Vinogradov SV, Batrakova EV, Kabanov AV. Nanogels for oligonucleotide delivery to the brain. *Bioconjug Chem* 2004;15:50–60.
359. Soni S, Babbar AK, Sharma AK, Maitra M. Delivery of hydrophobised 5-fluorouracil derivative to brain tissue through intravenous route using surface modified nanogels. *J Drug Target* 2006;14(2):87–95.
360. McAllister K, et al. Polymeric nanogels produced via inverse microemulsion polymerization as potential gene and antisense delivery agents. *J Am Chem Soc* 2002;124:15198–15207.
361. Bronich TK, Vinogradov SV, Kabanov AV. Interaction of nanosized copolymer networks with oppositely charged amphiphilic molecules. *Nano Lett* 2001;1:535–540.
362. Zuber G, Dauty E, Nothisen M, Belguise P, Behr JP. Towards synthetic viruses. *Adv Drug Deliv Rev* 2001;52:245–253.
363. Knowles MR, et al. Adenoviral-vector-mediated gene transfer for cystic fibrosis. *N Eng J Med* 1995;333(13):823–831.
364. Lai CM, et al. Controlled production of active cathepsin D in retinal pigment epithelial cells following adenovirus-mediated gene delivery. *Mol Ther* 2000;2(5):476–484.
365. Lazennec G and Katzenellenbogen BS. Expression of human estrogen receptor using an efficient adenoviral gene delivery system is able to restore hormone-dependent features to estrogen receptor-negative breast carcinoma cells. *Mol Cell Endocrinol* 1999;149:93–105.
366. Noad R and Roy P. Virus-like particles as immunogens. *Trends Microbiol* 2003; 11(9):438–444.
367. Garcea RL and Gasman L. Virus-like particles as vaccines and vessels for the delivery of small molecules. *Curr Opin Biotechnol* 2004;15:513–517.
368. Grinshtein N. Recombinant adenovirus vaccines can successfully elicit CD8+ T cell immunity under conditions of extreme leukopenia. *Mol Ther* 2006;13(2): 270–279.
369. Graham FL and Prevec L. Methods for construction of adenovirus vectors. *Mol Biotechnol* 1995;3:207–220.
370. Robbins PD and Ghivizzani SC. Viral vectors for gene therapy. *Pharmacol Ther* 1998;80(1):35–47.
371. Kamiya H, Tsuchiya H, Yamazaki J, Harashima H. Intracellular trafficking and transgene expression of viral and non-viral gene vectors. *Adv Drug Deliv Rev* 2001;52:153–164.
372. Verma IM and Somia N. Gene therapy: promises, problems and prospects. *Nature* 1997;398(18):239–242.

373. Hruby DE. Vaccinia virus vectors: new strategies for producing recombinant vaccines. *Clin Microbiol Rev* 1990;3(2):153–170.
374. Sandler VM, et al. Modified herpes simplex virus delivery of enhanced GFP into the central nervous system. *J Neurosci Methods* 2002;121:211–219.
375. Donofrio G, Martignani E, Cavirani S, Flammini CF. Exploiting persistent infection for selection of bovine herpesvirus 4 recombinants. *J Virol Methods* 2005;125:6–13.
376. Ketola A, Schlesinger S, Wahlfors J. Properties of Sindbis virus vectors produced with a chimeric split helper system. *Int J Mol Med* 2005;15(6):999–1003.
377. Chou AK, et al. Intrathecal gene delivery of glial cell line-derived neurotrophic factor ameliorated paraplegia in rats after spinal ischemia. *Mol Brain Res* 2005;133:198–207.
378. Morrison DF and Murtaugh MP. Adenovirus-mediated expression of interleukin-1 receptor antagonist in swine cells *in vitro* and *in vivo*. *Vet Immunol Immunopathol* 2001;78:71–81.
379. Wang C, Chao C, Chao L, Chao J. Expression of human tissue kallikrein in rat salivary glands and its secretion into circulation following adenovirus-mediated gene transfer. *Immunopharmacology* 1997;36:221–227.
380. Mason BB, et al. Adenovirus vaccine vectors expressing hepatitis B surface antigen: importance of regulatory elements in the adenovirus major late intron. *Virology* 1990;177:452–461.
381. Lubeck MD, et al. Immunogenicity and efficacy testing in chimpanzees of an oral hepatitis B vaccine based on live recombinant adenovirus. *Proc Natl Acad Sci USA* 1989;86:6763–6767.
382. Xiang ZQ, Yiping Y, Wilson JM, Ertl HJ. A replication-defective human adenovirus recombinant serves as a highly efficacious vaccine carrier. *Virology* 1996;219:220–227.
383. Wesley RD, Tang M, Lager KM. Protection of weaned pigs by vaccination with human adenovirus 5 recombinant viruses expressing the hemagglutinin and the nucleoprotein of H3N2 swine influenza virus. *Vaccine* 2004;22:3427–3434.
384. Imler JL. Adenovirus vectors as recombinant viral vaccines. *Vaccine* 1995;13(13):1143–1151.
385. McTaggart S and Rubeai ML. Retroviral vectors for human gene delivery. *Biotechnol Adv* 2002;20:1–31.
386. Nagano M, Shinohara T, Avarbock MR, Brinster RL. Retrovirus-mediated gene delivery into male germ line stem cells. *FEBS Lett* 2000;475:7–10.
387. Du L, et al. Differential myocardial gene delivery by recombinant serotype-specific adeno-associated viral vectors. *Mol Ther* 2004;10(3):604–608.
388. Rivera VM, et al. Long-term regulated expression of growth hormone in mice after intramuscular gene transfer. *Proc Natl Acad Sci USA* 1999;96:8657–8662.
389. Ye X, et al. Regulated delivery of therapeutic proteins after *in vivo* somatic cell gene transfer. *Science* 1999;283:88–91.
390. Auricchio A, et al. Constitutive and regulated expression of processed insulin following *in vivo* hepatic gene transfer. *Gene Ther* 2002;9:963–971.

391. Auricchio A, et al. Pharmacological regulation of protein expression from adeno-associated viral vectors in the eye. *Mol Ther* 2002;6(2):238–242.
392. During MJ. Adeno-associated virus as a gene delivery system. *Adv Drug Deliv Rev* 1997;27:83–94.
393. Desrosiers RC, et al. Synthesis of bovine growth hormone in primates by using a herpesvirus vector. *Mol Cell Biol* 1985;5:2796–2803.
394. Simmer B, et al. Persistence of selectable herpesvirus saimiri in various human haematopoietic and epithelial cell lines. *J Gen Virol* 1991;72:1953–1958.
395. Stevenson AJ, et al. Assessment of herpesvirus saimiri as a potential human gene therapy vector. *J Med Virol* 1999;57:269–277.
396. Donofrio G, Cavirani S, Simone T, Van Santen VL. Potential of bovine herpesvirus 4 as a gene delivery vector. *J Virol Methods* 2002;101:49–61.
397. Krisky DM, et al. Deletion of multiple immediate-early genes from herpes simplex virus reduces cytotoxicity and permits long-term gene expression in neurons. *Gene Ther* 1998;5(12):1593–1603.
398. Lilley CE, et al. Multiple immediate-early gene-deficient herpes simplex virus vectors allowing efficient gene delivery to neurons in culture and widespread gene delivery to the central nervous system *in vivo*. *J Virol* 2001;4343–4356.
399. Costantini C, et al. Gene transfer to the nigrostriatal system by hybrid herpes simplex virus/adeno-associated virus amplicon vectors. *Hum Gene Ther* 1999;10(15):2481–2494.
400. Emborg ME, Deglon N, Leventhal L, Aebischer P, Kordower JH. Viral vector-mediated gene therapy for Parkinson's disease. *Clin Neurosci Res* 2001;1:496–506.
401. Lesch KP. Gene transfer to the brain: emerging therapeutic strategy in psychiatry. *Soc Biol Psychiatry* 1999;45:247–253.
402. Feldman LJ and Steg G. Optimal techniques for arterial gene transfer. *Cardiovasc Res* 1997;35:391–404.
403. Parry S, Koi H, Strauss JF. Transplacental drug delivery: gene and virus delivery to the trophoblast. *Adv Drug Deliv Rev* 1999;38:69–80.
404. Ou WC, et al. The major capsid protein, VP1, of human JC virus expressed in *Escherichia coli* is able to self-assemble into a capsid-like particle and deliver exogenous DNA into human kidney cells. *J Gen Virol* 1999;80:39–46.
405. Touze A and Coursaget P. *In vitro* gene transfer using human papillomavirus-like particles. *Nucleic Acids Res* 1998;26(5):1317–1323.
406. Kirnbauer R, Booy G, Cheng N, Lowy DR, Schiller JT. Papillomavirus L1 major capsid protein self-assembles into virus-like particles that are highly immunogenic. *Proc Natl Acad Sci USA* 1992;89:12180–12184.
407. Rose RC, Bonneze R, Reichman C, Garcea RL. Expression of human papillomavirus type 11 L1 protein in insect cells: *in vivo* and *in vitro* assembly of viruslike particles. *J Virol* 1993;67:1936–1944.
408. Volpers CP, Schirmacher RE, Sapp M. Assembly of the major and the minor capsid protein of human papillomavirus type 33 into virus-like particles and tubular structures in insect cells. *Virology* 1994;200:504–512.
409. Zhou J, Stenzel DJ, Sun XY, Frazer IH. Synthesis and assembly of infectious bovine papillomavirus particles *in vitro*. *J Gen Virol* 1993;74:763–768.

410. Hagensee ME, Yaegashi N, Galloway DA. Self-assembly of human papilloma-virus type 1 capsids by expression of the L1 protein alone or by coexpression of the L1 and L2 capsid proteins. *J Virol* 1993;67:315–322.
411. Breitburd F, et al. Immunization with viruslike particles from cottontail rabbit papillomavirus (CRPV) can protect against experimental CRPV infection. *J Virol* 1995;69(6):3959–3963.
412. Christenson ND, Reed CA, Cladel NM, Han R, Kreider JW. Immunization with viruslike particles induces long-term protection of rabbits against challenge with cottontail rabbit papillomavirus. *J Virol* 1996;70(2):960–965.
413. Suzich JA, et al. Systemic immunization with papillomavirus L1 protein prevents the development of viral mucosal papillomas completely. *Proc Natl Acad Sci USA* 1995;92:11553–11557.
414. Balmelli C, Demotz S, Orbea HA, Grandi PD, Haefliger DN. Trachea, lung, and tracheobronchial lymph nodes are the major sites where antigen-presenting cells are detected after nasal vaccination of mice with human papillomavirus Type 16 virus-like particles. *J Virol* 2002;76(24):12596–12602.
415. Silva DD, et al. Physical interaction of human papillomavirus virus-like particles with immune cells. *Int Immunol* 2001;13(5):633–641.
416. Nicholls PK and Stanley MA. The immunology of animal papillomaviruses. *Vet Immunol Immunopathol* 2000;73:101–127.
417. Forstova J, et al. Cooperation of structural proteins during late events in the life cycle of polyomavirus. *J Virol* 1993;67(3):1405–1413.
418. Henke S, Rohmann A, Bertling WM, Dingermann T, Zimmer A. Enhanced *in vitro* oligonucleotide and plasmid DNA transport by VP1 virus-like particles. *Pharm Res* 2000;17(9):1062–1070.
419. Chang D, et al. Self-assembly of the JC virus major capsid protein, VP1, expressed in insect cells. *J Gen Virol* 1997;78:1435–1439.
420. Pawlita M, Müller M, Oppenlander M, Zentgraf H, Herrmann M. DNA encapsidation by viruslike particles assembled in insect cells from the major capsid protein VP1 of B-lymphotropic papovavirus. *J Virol* 1996;70(11):7517–7526.
421. Sandalon Z and Oppenheim A. Self-assembly and protein–protein interactions between the SV40 capsid proteins produced in insect cells. *Virology* 1997;237:414–421.
422. Rodgers RD, Chang D, Cai X, Consigli RA. Purification of recombinant budgerigar fledgling disease virus VP1 capsid protein and its ability for *in vitro* capsid assembly. *J Virol* 1994;68(5):3386–3390.
423. Schmidt U, Gunther C, Rudolph R, Bohm G. Protein and peptide delivery via engineered polyomavirus-like particles. *FASEB J* 2001;15:1646–1648.
424. Goldmann C, et al. Molecular cloning and expression of major structural protein VP1 of the human polyomavirus JC virus: formation of virus-like particles useful for immunological and therapeutic studies. *J Virol* 1999;73(5):4465–4469.
425. Abbing A, et al. Efficient intracellular delivery of a protein and a low molecular weight substance via recombinant polyomavirus-like particles. *J Biol Chem* 2004;279(26):27410–27421.

426. Merisko E. Liversidge nanocrystals: resolving pharmaceutical formulation issues associated with poorly water-soluble compounds. In: Marty JJ, editor. *Particles*. Orlando: Marcel Dekker; 2002.
427. Lee J. Drug nano- and microparticles processed into solid dosage forms: physical properties. *J Pharm Sci* 2003;92:2057–2068.
428. Lee J. Intrinsic adhesion force of lubricants to steel surface. *J Pharm Sci* 2004;93:2310–2318.
429. Liu R. *Water-Insoluble Drug Formation*. Buffalo, IL: Inter-Pharm Press; 2000. p 455.
430. Fromming KS and Fromming J. *Cyclodextrines in Pharmacy*. Dordrecht: Kluwer Academic Publishers; 1993.
431. Müller RH. Dispersions for the formulation of slightly or poorly soluble drugs. PCT/EP01/08726, Pharmasol GmbH Berlin; 2001.
432. Choi JY, Yoo JY, Kwak HS, Nam BU, Lee J. Role of polymeric stabilizers for drug nanocrystal dispersions. *Curr Appl Phys* 2005;5:472–474.
433. Sucker H and Gassmann P. Improvements in pharmaceutical compositions. GB patent 2,269,536. Sandozy Ltd;1994.
434. Buchmann S, Fischli W, Thiel FP, Alex R. Aqueous microsuspension, an alternative intravenous formulation for animal studies. In: 42nd Annual Congress of the International Association for Pharmaceutical Technology; Mainz;1996. p 124.
435. Müller RH, Becker R, Kruss B, Peters K. Pharmaceutical nanosuspensions for medicament administration as systems with increased saturation solubility and rate of solution. US patent 5,858,410. 1999.
436. Müller RH, Mader K, Krause K. Verfahren zur schonenden Herstellung von hochfeinen Micro-/Nanopartikeln. PCT application PCT/EP00/06535. Germany; 2000.
437. Rabinow BE. Nanosuspensions in drug delivery. *Nat Rev Drug Discov* 2004;3:785–796.
438. Müller RH and Peters K. Nanosuspensions for the formulation of poorly soluble drugs I. Preparation by a size-reduction technique. *Int J Pharm* 1998;60:229–237.

Bioconjugated Nanoparticles for Ultrasensitive Detection of Molecular Biomarkers and Infectious Agents

AMIT AGRAWAL, MAY DONGMEI WANG, and SHUMING NIE

8.1 INTRODUCTION

Infectious diseases are one of the major health problems in the world and have in recent years led to several epidemics including SARS, the West Nile virus, and the avian flu. An urgent need is to develop new technologies for detection and identification of infectious agents with high sensitivity and specificity. At the community level, early detection of communicable infections helps implement better quarantine measures. For individuals, early detection leads to effective treatment while at the cellular level sensitive detection and imaging of microbe–host cell interactions inside live cells helps to reveal infection mechanisms and to develop better drugs and vaccines. Several technologies based on DNA amplification and serological assays are currently available for detection, but target amplification (such as the polymerase chain reactions) often suffers from contamination, while serological assays are slow and are not as sensitive.

The ultimate limit in biomedical diagnostics is the ability to detect and identify single biomarker molecules and single intact viruses in complex samples. Recent advances have allowed detection of single dye molecules and fluorescent proteins, but these fluorescent tags are not bright or stable enough for routine single-molecule studies. Another problem is that target molecules often need to be chemically derivatized with a fluorophore, a difficult task for low abundance genes and proteins. A further challenge is the need to discriminate bound targets from excess unbound probes in complex mixtures or inside living cells.

In this chapter, we discuss the use of bioconjugated nanoparticles and two-color fluorescence coincidence for rapid detection of single *native* biomolecules and intact viruses. Recent research by us and others has shown that nanometer-sized particles such as quantum dots (QDs) can be covalently linked with biorecognition molecules such as peptides, antibodies, or nucleic acids for use as fluorescent probes [1–6]. In comparison with organic dyes and fluorescent proteins, quantum dots and related nanoparticles exhibit unique optical and electronic properties such as size and composition-tunable fluorescence emission, large absorption coefficients, and improved brightness and photostability [7–9]. By taking advantage of these properties, we have developed a nanoparticle “sandwich” assay in which two nanoparticle probes of different colors simultaneously recognize two binding sites on a single target molecule. This two-site sandwich method relies on a “double-selection” process to improve both detection sensitivity and specificity. Indeed, a number of powerful diagnostic technologies are based on this two-site sandwich format such as latex agglutination tests (LATs) [10], enzyme-linked immunoabsorbent assays (ELISAs) [11], luminescent oxygen channeling immunoassay (LOCI) [12, 13] (in which light emission arises from proximal diffusion of singlet oxygen species between two adjacent particles after target binding), and fluorescence cross-correlation spectroscopy (FCCS) [14, 15]. In this format, target molecules do not need to be chemically derivatized, but the bound targets must be differentiated from excess probe.

8.2 NOVEL PROPERTIES OF NANOPARTICLES

Fluorescent nanoparticles such as QDs have several unique properties that make them excellent labels for ultrasensitive optical detection (Fig. 8.1). Quantum dots have very large molar extinction coefficients on the order of $0.5\text{--}5 \times 10^6 \text{ M}^{-1}\text{cm}^{-1}$ [16], which makes them 10–50 times brighter probes than organic dye molecules. Quantum dots are also several thousand times more photostable than organic dye molecules [17, 18] so that a single nanoparticle can be imaged and tracked over a long period of time with continuous excitation (Fig. 8.1b). This allows one to use single nanoparticles as probes for ultrasensitive detection. The ability to collect higher number of photons from bright nanoparticles has allowed us to locate their position with errors less than 1 nm (discussed in the next section). Since QDs also have high absorption rates, they require lower excitation powers when used as a probe for biological systems. This minimizes photodamage of the biological sample in experiments that involve long-term, continuous observations.

Quantum dots have size and composition-tunable fluorescence emission from visible to infrared wavelengths (Fig. 8.1d) [21], with very broad absorbance profiles [22] (Fig. 8.1a). This leads to very large Stokes spectral shifts (up to 300–400 nm, measured by the distance between the excitation and emission peaks) so that single excitation source can be used to obtain multiple

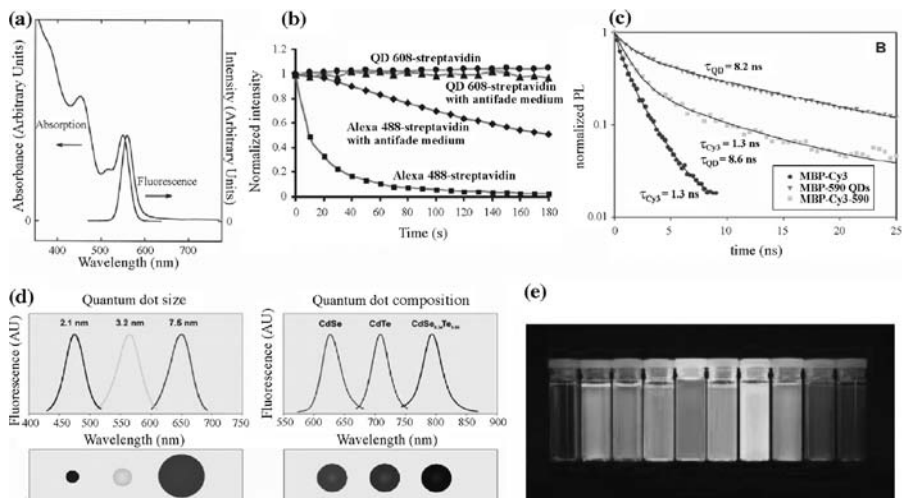


FIGURE 8.1 Novel optical properties of quantum dots. (a) Broad absorption and narrow and symmetric emission of quantum dots (reprinted from Murray et al. (1993), with permission of the American Chemical Society). (b) Photostability of QDs compared with the dye molecule Alexa-488 (reprinted from Reference [18], with permission from the Nature Publishing Group). (c) Fluorescence lifetime of protein-coated QDs compared with Cy3 (reprinted from [19], with permission of the American Chemical Society). (d) Size- or composition-based tuning of emission wavelength in QDs (reprinted from Reference [20]). (e) Bright QDs with emissions spanning the entire visible spectrum (reprinted from Reference [7]).

colors of fluorescence emission [7]. As a result, it is possible to prepare QD probes with maximum emission offset with the background signal resulting in improved signal-to-noise ratios (SNRs). In single-molecule detection (SMD), this eliminates the requirement for the expensive two-laser optical setup that is required to focus two different wavelengths in overlapping probe volumes [23, 24]. The large Stokes shift also becomes important for *in vivo* molecular imaging due to the high autofluorescence background often seen in complex biomedical specimens. Organic dye signals with a small Stokes shift are often buried by strong tissue autofluorescence, whereas QD signals with a large Stokes shift are clearly recognizable above the background. This “color contrast” is only available to QD probes because the signals and background can be separated by wavelength-resolved or spectral imaging [25].

To improve the SNR, one can either increase the signal or decrease the background noise. In SMD, a major challenge is to minimize the background noise. In this regard, the longer fluorescence lifetimes of QDs may be utilized to improve the SNR. As shown in Fig. 8.1c, the fluorescence lifetimes of QDs are roughly 10 ns while that of the dye molecules is 1–2 ns. Thus, if we excite the QD-labeled sample with a laser pulse and wait more than a nanosecond before collecting emission from the sample, the QD signal would still be strong

while the autofluorescent species would have decayed, resulting in improved SNRs.

Dye-doped nanobeads are another class of fluorescent nanoparticles that provide similar benefits as QDs. Since several thousands of dye molecules are doped into each bead, these particles are very bright and photostable. Multiple color emissions with the same excitation are enabled by fluorescence resonance energy transfer (FRET) between the donor–acceptor dye pairs inside the bead. These beads are available in the size range of 20 nm to 1 μm , and with various surface functions suitable for bioconjugation (Invitrogen, Inc.).

It is worth noting that quantum dots and color-coded nanobeads are in the same size regime as the biological molecules and are amenable to biological conjugation [1, 2]. The small size ensures minimal interference with the native biological system and allows tailoring of the QDs as a target-specific probe for protein, nucleic acid, or small molecule detection. By controlling the number of ligands on their surface, it is also possible to control the stability of the target-QD-probe binding strength. Further, by tailoring their surface chemistry, one can tune their biocompatibility and toxicity to suit the specific application [25, 26].

8.3 SINGLE-MOLECULE DETECTION

8.3.1 Instrumental Setup and Principles

Optical methods for SMD have been reported for nearly 40 years. In 1961, Rotman detected conversion of a nonfluorescent substrate into a fluorescent molecule by β -galactosidase enzyme encapsulated in microdroplets and measured the reaction rate for a single enzyme molecule [27]. In 1976, Hirshfield reported detection of 80–100 molecules of fluorescein isothiocyanate dye bound to an antibody molecule [28]. These pioneering experiments shared several features such as an optical setup to probe a very small volume, low concentration of fluorophores, and time-gated optical detection using a photomultiplier. SMD systems employ these basic principles even today. In 1990, Shera et al. reported the first efficient detection of individual rhodamine-6G dye molecules at 100 fM concentration [29]. In the following years, two broad approaches were devised for detection of single biomolecules: fluorescence correlation spectroscopy [30] and coincidence-based SMD [31]. Both of these approaches use a confocal optical setup and rely on photon burst analysis.

A typical setup for SMD is shown in Fig. 8.2a. A high numerical aperture objective focuses a laser beam into a small volume (<10 fl) in the solution. When the dye-labeled biomolecule enters this probe volume (Fig. 8.2b), it is repeatedly excited by the tightly focused laser beam and emits an intense fluorescence burst. The fluorescence signal is allowed to pass through a pinhole and optical filters to reduce background noise and is detected using a sensitive photon detector (such as a CCD, a photomultiplier tube, or an avalanche photodiode—APD).

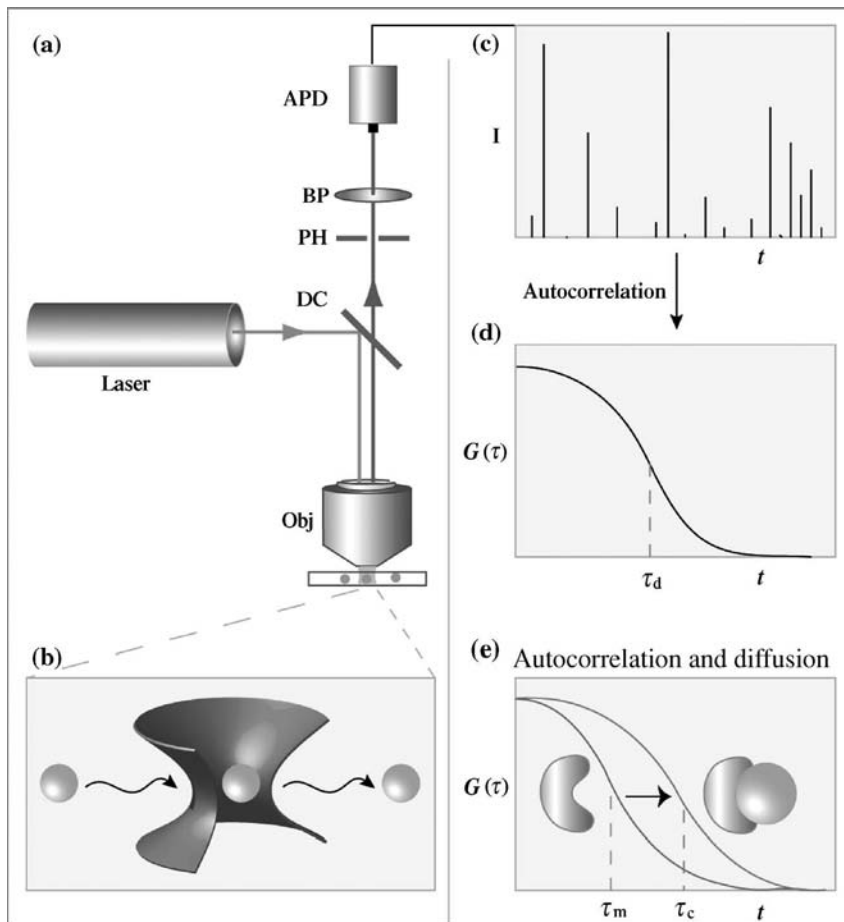


FIGURE 8.2 Instrumental setup and basic principles of single-molecule detection. (a) A laser light source excites a confocal volume (b) in solution containing dye-labeled molecules. The signal is filtered optically and detected on an avalanche photodiode (APD), and the photon burst data (c) are analyzed by using an autocorrelation device (d). (e) Target binding decreases the diffusion kinetics of the fluorescent probe and is measured as an increase in the autocorrelation time.

The train of photon bursts can be analyzed for autocorrelation ($G(\tau)$) using the following equation and a correlation curve is plotted.

$$G(\tau) = \frac{\langle \delta F(t) \cdot \delta F(t + \tau) \rangle}{\langle F(t) \rangle^2} \quad (8.1)$$

Here, $F(t)$ is the fluorescence burst signal obtained over time (t), and $\delta F(t)$ is the difference between the average of $F(t)$ and $F(t)$. In summary, the

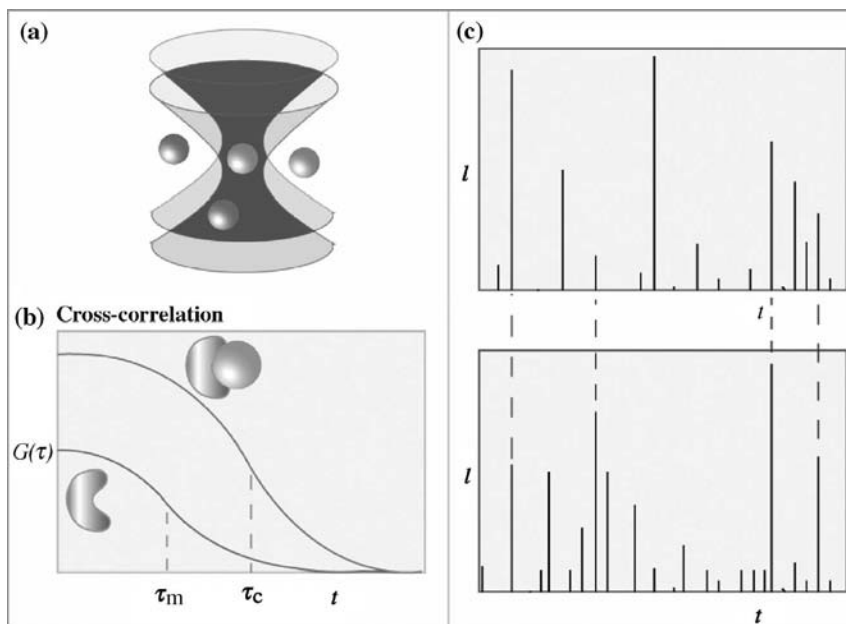


FIGURE 8.3 Single-molecule detection by two-color fluorescence correlation. (a) Difficulties in achieving par-focality and probe volume overlapping with two color lasers are used to excite two dyes, due to spherical and chromatic aberrations of the microscope objective. (b) Signals from the two color fluorophores are analyzed by cross-correlation or (c) by coincidence of arrival on two APD detectors.

autocorrelation function $G(\tau)$ represents the extent to which the photon burst signal is related to itself when shifted by time τ . The correlation curve is used to obtain the time (τ) the fluorophore spends in the probe volume. This time (τ) depends on diffusion and blinking characteristics of the fluorophore. Since biomolecular binding results in formation of a complex with higher mass and lower diffusion constant, the above methods can be used to detect biomolecular complex formation.

By using two-color labels and cross-correlation analysis, one can also measure biomolecular interactions and binding behavior, as shown schematically in Fig. 8.3. For a detailed account on fluorescence correlation spectroscopy, the reader is referred to the work of Schille and coworkers [32]. Recently, coincidence of two-color photon bursts has been used to study biomolecular interactions and to detect disease biomarkers in solution (Fig. 8.3c) [23, 24]. This is discussed in greater detail in a later section.

In the dual-color detection schemes, two complementary, target-specific probes are labeled with fluorescent dyes of different emission wavelengths. Because organic fluorophores usually have narrow excitation profiles, each dye needs to match a specific excitation wavelength. Weiss and coworkers [33] have

shown that the cofocusing of two laser beams (par-focality) is an exceedingly difficult task due to both chromatic and spherical aberrations of the microscope objective. Klenerman and coworkers [24, 34] reported that even under carefully matched conditions, the volume overlap for two excitation laser beams was less than 30%.

8.3.2 Color-Coded Nanoparticles

The basic principles of single-molecule counting using nanoparticle probes are shown in Fig. 8.4. In this scheme, two bioconjugated nanoparticles are designed to recognize the same target molecule at two different sites (antigenic sites or nucleic acid sequences). This sandwich-type binding brings two color-coded nanoparticles together to form a nanoparticle pair (Fig. 8.4a). This pair moves in solution as a single complex, and when excited by a laser beam, emits green and red fluorescence light simultaneously (i.e., spatial colocalization of two particles leads to time coincidence of their fluorescence signals). In contrast, unbound green and red particles move in a random fashion and are unlikely to pass through the laser beam at the same time (Fig. 8.4b). Thus, coincident green and red light emission allows one to discriminate bound targets from excess unbound probes in a homogeneous solution mixture.

Both QDs and energy-transfer nanoparticles are well suited for SMD. A major advantage is that a single light source can be used to excite two or more fluorescence colors (Fig. 8.4c). A single excitation beam produces only one probe volume, and this overcomes the difficulties in focusing two color laser beams into a small confocal volume (femtoliter or 10^{-15} l). QDs also have more symmetric and narrower emission spectra than single-color organic fluorophores, a feature that is important for minimizing spectral overlaps between two or more colors.

Single-molecule instrumentation is based on an inverted single-point confocal microscope, equipped with two photon-counting avalanche photodiodes (APD-1 and APD-2), a single-photon counting and coincidence analysis module (attached to the microscope side port), and a capillary flow channel placed on the microscope stage (Fig. 8.5). In the photon analysis module, fluorescence light emitted from green and red nanoparticles is separated by a dichroic filter (DC-2) and is detected in real time by APD-1 and APD-2. The single-photon output signal from APD-1 is used to trigger a delay generator, which produces a voltage pulse with a controllable width. This modified pulse is fed into a coincidence event detector, and its preset width is used as a time window to determine whether one or more photons are detected by APD-2 during this time period. Using a standard photon-counting device such as a multichannel scalar (MCS), the coincidence output signals are recorded over a period of time. At an integration time of 1 ms, this system permits high speed detection of single molecules in a flow channel at 1000 data points per second.

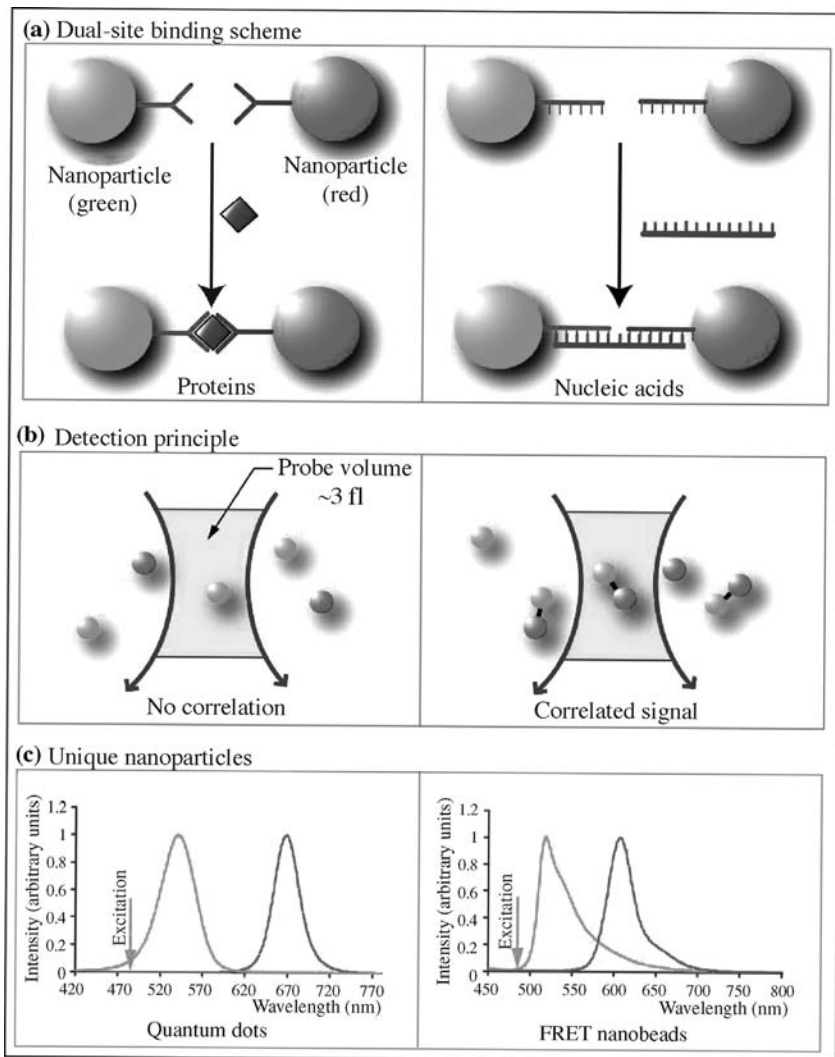


FIGURE 8.4 Single-molecule sandwich assays using color-coded nanoparticles. (a) Simultaneous double-site binding for protein and nucleic acid detection; (b) free nanoparticle probes and bound sandwich pairs moving across a tightly focused laser beam; and (c) fluorescence emission spectra of color-coded quantum dots and energy-transfer nanoparticles. The left panel shows green and red QDs simultaneously excited with a single light source at 420 nm, and the right panel shows green and red energy-transfer nanoparticles excited at the same wavelength. The arrows indicate the relative position of the excitation laser wavelength (488 nm) used in single-molecule detection.

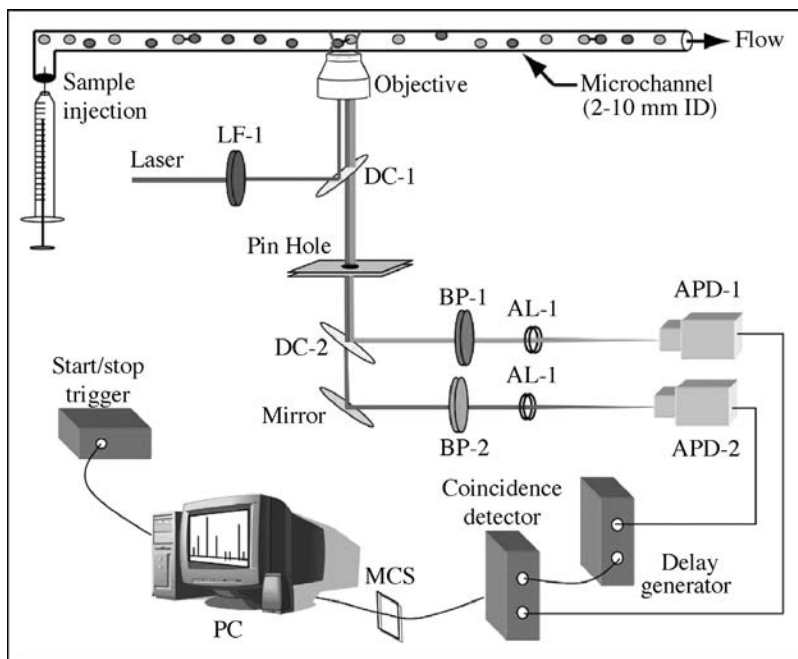


FIGURE 8.5 Instrumental diagram showing real-time detection of single nanoparticles and correlated sandwich pairs flowing in a small capillary. See the text for detailed discussion. LF-1 = laser filter; DC-1 = dichroic filter in the microscope filter cube; DC-2 = dichroic filter outside the microscope side port; BP-1 = bandpass filter (HQ514 M10); BP-2 = bandpass filter (D670 M40); AL-1 and AL-2 = aspheric focusing lenses; ADP-1 and APD-2 = single-photon counting avalanche photodiodes; MCS = multi-channel scalar; PC = personal computer.

8.3.3 Single-Molecule Imaging

The main concept is to determine the location of color-coded nanoparticles at nanometer precision. This is done by using a 2D Gaussian kernel convolution, local maxima-based centroid determination in the convolved image, followed by a Gaussian point spread function (PSF) fitting step to locate the position of the nanoparticles. The procedure is adapted from an astrophotometry package named DAOPHOT¹ developed by P.B. Stetson in 1987 [35]. Recent research by several groups has shown that the location of a single molecule can be determined at nanometer accuracy [33, 36–40], far beyond the ability to resolve objects located within the diffraction limit. Weiss and coworkers demonstrated highly accurate nanoparticle localization (error < 10 nm) and measured

¹DAOPHOT was developed at the Dominion Astrophysical Observatory for the photometric analysis.

distance between closely spaced two-color nanoparticles [33]. In 2002, Thompson et al. reported a framework for accurate localization of single fluorescent molecules and tested it using 30-nm fluorescent beads. The authors concluded that minimization of noise in the system and maximization of the photons collected from each fluorophore was the key for high accuracy in localization. Later, using photobleaching of one Cy3 dye molecule in a pair, Selvin and coworkers were able to localize the dye molecules with a precision of 1.5 nm [41]. In the same year, using similar approach, Scherer and coworkers localized Cy3 molecules with precision of 2.5 nm [36]. More recently, Spudich and co-workers have demonstrated use of Cy3 and Cy5 molecules for measuring intermolecular distances [38] and Ram et al. have proposed new resolution measures for locating single molecules with high accuracy [40]. In several of these reports, image of a fluorophore is fit to a 2D Gaussian profile and the center is estimated by finding the local maxima of the fit. The error in position of a single molecule is then given by the equation shown below [37].

$$\langle(\Delta x)^2\rangle = \frac{s^2 + a^2/12}{N} + \frac{4\sqrt{\pi}s^3b^2}{aN^2} \quad (8.2)$$

where Δx is the error in center localization, s is the standard deviation of a 2D Gaussian kernel used to fit the intensity profile, a is the pixel size in the image, b is the background noise, and N is the number of photons collected per nanoparticle. While advances in optics and imaging instrumentation have enabled data collection with minimal noise (b), high accuracy in localization is largely determined by the number of photons collected from the object being imaged, meaning that brighter and more photostable fluorophores can be localized with greater accuracy.

8.4 APPLICATIONS

8.4.1 Detection of Single Respiratory Syncytial Virus Particles

Respiratory syncytial virus (RSV) causes serious infection of the lower respiratory tract in young children and the immune compromised adults. However, no RSV vaccine is available at present, and diagnosis is often made based on symptoms or using serological studies. Serological approaches take a long time for disease diagnosis and may not be useful in acute illness. Thus, there is a pressing need to develop sensitive and rapid methods for detection of viral particles.

RSV has surface proteins that are used to fuse and attach with the host cell. Using antibodies against these proteins, RSV and the surface protein expression on its surface could be detected [42]. In this work, nanoparticles were functionalized with antibodies that specifically recognize either attachment protein or the fusion protein on the viral particle, as shown in Fig. 8.6. Then, two probes carrying nanoparticles with different emission profiles were allowed to form a sandwich with the viral particle. When RSV is present in the

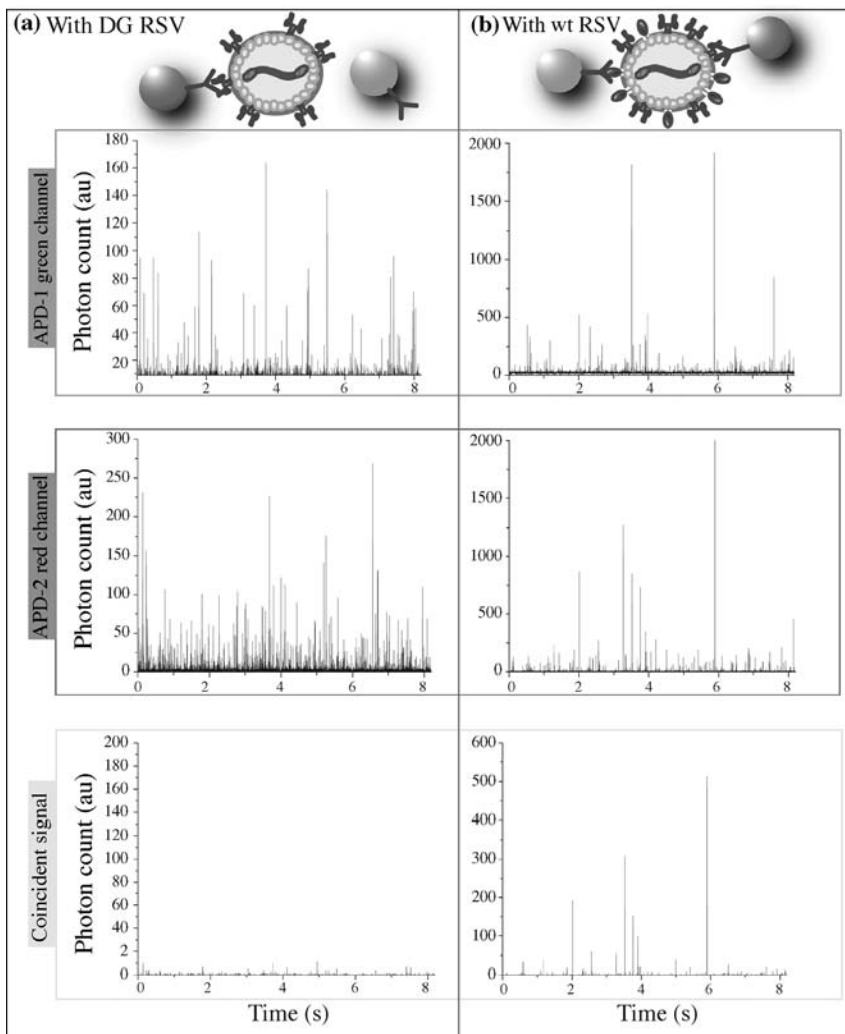


FIGURE 8.6 Counting viral particles in solution. The 40-nm nanoparticles conjugated to RSV anti-F or anti-G protein monoclonal antibodies were used to produce red or green photon emission, respectively. RSV Δ G, used as a control, produced low green photon counts as expected and did not show coincidence signals (a), while coincident peaks were observed for RSV/A2 (b).

solution, the two nanoparticles pass through the confocal probe volume at the same time and the photons emitted from them are coincident (Fig. 8.6b).

The SMD system used in the above studies not only removes the par-focality issue by using nanoparticles but also provides a single test for detecting presence of protein, DNA, or virus in solution in real time. Real-time data

processing with even counting and coincidence detection can enable multiplexed SMD and has been shown to provide wider dynamic range in comparison with cross-correlation [43]. However, flow-based molecule counting is slow because of the low sample throughput. For target concentrations below the femtomolar level, significant time may be required to achieve confidence in the detection. As shown in the next section, imaging-based single-molecule detection assays may provide a solution.

8.4.2 Single-Molecule Detection by Two-Color Imaging

Figure 8.7 shows the results obtained when complementary DNA sequences are coupled with dual-color nanoparticles. Several yellow spots indicating nanoparticle colocalization are seen only when the targets are complementary (Fig. 8.7a and b). The DNA hybrid was 24 base pair long, which is smaller than the persistence length of double-strand DNA [44]. Thus, it is like a “rigid rod” and one would expect the center of the two beads to appear at 54 nm distance. By using the above localization scheme, we find that the two beads are separated by 54-nm, which is consistent with the theoretical estimates.

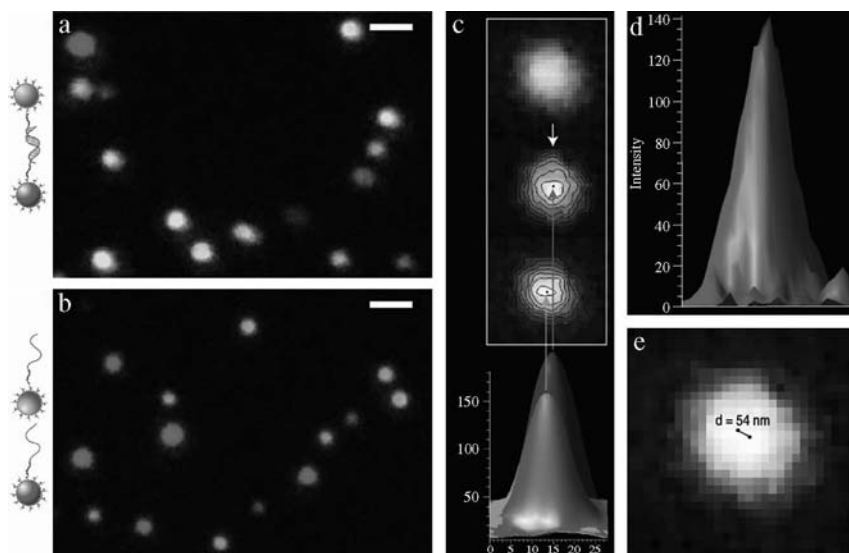


FIGURE 8.7 Dual-color imaging and colocalization of nanoparticle probes at nanometer precision. (a and b) Nanoparticles form diffraction-limited pairs resulting in color change only in presence of complementary sequences. (c) Image of a real R–G bead pair separated into red and green components that are convolved with a Gaussian kernel to determine center. (d) High SNR >60 allows highly accurate measurements. (e) Close-up of colocalization of the R–G bead pair.

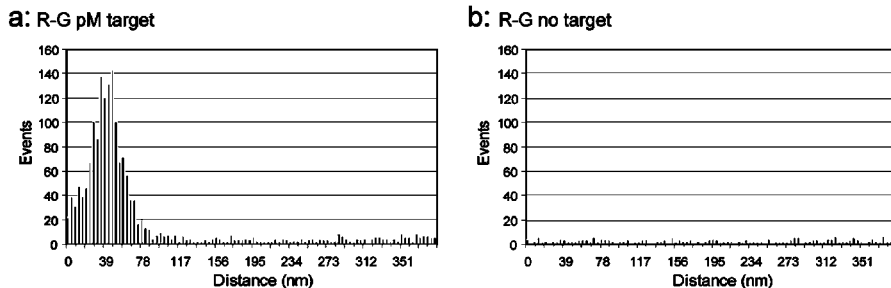


FIGURE 8.8 Rapid detection of DNA molecules. Nanoparticle labeled probes colocalize in target-dependent manner. R–G distance histogram (a) has a peak that is missing in the control experiment (b, no target present).

When this assay is performed for over nine million bead pairs to detect a segment of breast cancer antiestrogen resistance gene at picomolar concentrations, the image processing can be performed in under a minute on a desktop computer. The results are shown in Fig. 8.8. In the presence of the target molecule, a clear peak is seen in the R–G distance histogram which is absent when the target is absent. This approach is not limited to nucleic acid molecules but can be extended to protein and pathogen detection as well. Thus, single-molecule imaging allows quantitative and high throughput detection of biological targets. Since infectious agents lie in the same size range as nanoparticles, the use of color-coded nanoparticles should allow rapid and sensitive detection of infectious disease biomarkers and intact viruses.

8.5 CONCLUSION AND OUTLOOK

Quantum dots and other fluorescent nanoparticles have emerged as a new class of versatile biological probes for *in vitro* diagnostics [42] to molecular/cellular imaging [25]. By combining magnetic and optical nanoparticles, multimodality probes have also been prepared (Agrawal and Nie, unpublished data). Using magnetic enrichment and separation along with fluorescent detection and identification, highly multiplexed, ultrasensitive assays can be realized for clinical use. Advances in nanoparticle synthesis and instrumentation are likely to continue to open up new frontiers in ultrasensitive biological detection. Miniaturization of instruments and availability of safe nanoparticle probes will allow production of low cost, point-of-care, multifunctional diagnostic devices. Practical applications of these multifunctional nanodevices will not come without careful research, but the multidisciplinary nature of nanotechnology may expedite these goals by combining the great minds from many different fields. The results seen so far with QDs point toward the success of QDs in biological systems and also predict the success of other nanotechnologies for biomedical applications.

REFERENCES

1. Bruchez M, Moronne M, Gin P, Weiss S, Alivisatos AP. Semiconductor nanocrystals as fluorescent biological labels. *Science* 1998;281(5385):2013–2016.
2. Chan WCW, et al. Quantum dot bioconjugates for ultrasensitive non isotopic detection. *Science* 1998;281:2016–2018.
3. Dubertret B, et al. *In vivo* imaging of quantum dots encapsulated in phospholipid micelles. *Science* 2002;298(5599):1759–1762.
4. Jaiswal JK, Mattoussi H, Mauro JM, Simon SM. Long-term multiple color imaging of live cells using quantum dot bioconjugates. *Nat Biotechnol* 2003; 21(1):47–51.
5. Dahan M, et al. Diffusion dynamics of glycine receptors revealed by single-quantum dot tracking. *Science* 2003;302(5644):442–445.
6. Lidke DS, et al. Quantum dot ligands provide new insights into erbB/HER receptor-mediated signal transduction. *Nat Biotechnol* 2004;22(2):198–203.
7. Chan WCW, et al. Luminescent quantum dots for multiplexed biological detection and imaging. *Curr Opin Biotechnol* 2002;13(1):40–46.
8. Alivisatos P. The use of nanocrystals in biological detection. *Nat Biotechnol* 2004;22(1):47–52.
9. Michalet X, et al. Quantum dots for live cells, *in vivo* imaging, and diagnostics. *Science* 2005;307(5709):538–544.
10. Newman DJ, Henneberry H, Price CP. Particle enhanced light-scattering immunoassay. *Ann Clin Biochem* 1992;29:22–42.
11. Diamandis EP, Christopoulos TK, Immunoassay. San Diego: Academic Press; 1996. p 579.
12. Ullman EF, et al. Luminescent oxygen channeling assay (LOCI(TM)): sensitive, broadly applicable homogeneous immunoassay method. *Clin Chem* 1996;42(9): 1518–1526.
13. Ullman E, et al. Luminescent oxygen channeling immunoassay—measurement of particle binding-kinetics by chemiluminescence. *Proc Natl Acad Sci* 1994; 91(12): 5426–5430.
14. Schwille P, MeyerAlmes FJ, Rigler R. Dual-color fluorescence cross-correlation spectroscopy for multicomponent diffusional analysis in solution. *Biophys J* 1997;72(4):1878–1886.
15. Rigler R. Fluorescence correlations, single molecule detection and large number screening. Applications in biotechnology. *J Biotechnol* 1995;41(2–3):177–186.
16. Leatherdale CA, Woo WK, Mikulec FV, Bawendi MG. On the absorption cross section of CdSe nanocrystal quantum dots. *J Phys Chem B* 2002;106(31): 7619–7622.
17. Gao XH, et al. *In vivo* molecular and cellular imaging with quantum dots. *Curr Opin Biotechnol* 2005;16(1):63–72.
18. Wu XY, et al. Immunofluorescent labeling of cancer marker Her2 and other cellular targets with semiconductor quantum dots. *Nat Biotechnol* 2003;21(1):41–46.
19. Clapp AR, et al. Fluorescence resonance energy transfer between quantum dot donors and dye-labeled protein acceptors. *J Am Chem Soc* 2004;126(1):301–310.

20. Bailey RE, Smith AM, Nie SM. Quantum dots in biology and medicine. *Phys E Low Dimension Syst Nanostruct* 2004;25(1):1–12.
21. Smith AM, Gao X, Nie S. Quantum dot nanocrystals for *in vivo* molecular and cellular imaging. *Photochem Photobiol* 2004;80(3):377–385.
22. Smith AM and Nie S. Chemical analysis and cellular imaging with quantum dots. *Analyst* 2004;129(8):672–677.
23. Agrawal A, Zhang C, Byassee T, Tripp RA, Nie S. Counting single native biomolecules and intact viruses with color-coded nanoparticles. *Anal Chem* 2006;78(4):1061–1070.
24. Li HT, Ying LM, Green JJ, Balasubramanian S, Klenerman D. Ultrasensitive coincidence fluorescence detection of single DNA molecules. *Anal Chem* 2003;75(7):1664–1670.
25. Gao X, Cui Y, Levenson RM, Chung LW, Nie S. *In vivo* cancer targeting and imaging with semiconductor quantum dots. *Nat Biotechnol* 2004;22(8):969–976.
26. Smith AM, Ruan G, Rhyner MN, Nie S. Engineering luminescent quantum dots for *in vivo* molecular and cellular imaging. *Ann Biomed Eng* 2006;34(1):3–14.
27. Rotman B. Measurement of activity of single molecules of beta-D-galactosidase. *Proc Nat Acad Sci* 1961;47(12):1981.
28. Hirschfeld T. Optical microscopic observation of single small molecules. *Appl Opt* 1976;15(12):2965–2966.
29. Shera EB, Seitzinger NK, Davis LM, Keller RA, Soper SA. Detection of single fluorescent molecules. *Chem Phys Lett* 1990;174(6):553–557.
30. Schwille P and Kettling U. Analyzing single protein molecules using optical methods. *Curr Opin Biotechnol* 2001;12(4):382–386.
31. Castro A and Williams JG. Single-molecule detection of specific nucleic acid sequences in unamplified genomic DNA. *Anal Chem* 1997;69(19):3915–3920.
32. Medina MA and Schwille P. Fluorescence correlation spectroscopy for the detection and study of single molecules in biology. *Bioessays* 2002;24(8):758–764.
33. Lacoste TD, et al. Ultrahigh-resolution multicolor colocalization of single fluorescent probes. *Proc Natl Acad Sci USA* 2000;97(17):9461–9466.
34. Li H, Zhou D, Browne H, Balasubramanian S, Klenerman D. Molecule by molecule direct and quantitative counting of antibody-protein complexes in solution. *Anal Chem* 2004;76(15):4446–4451.
35. Stetson PB. Daophot—a computer-program for crowded-field stellar photometry. *Publ Astron Soc Pacific* 1987;99(613):191–222.
36. Qu X, Wu D, Mets L, Scherer NF. Nanometer-localized multiple single-molecule fluorescence microscopy. *Proc Natl Acad Sci USA* 2004;101(31):11298–11303.
37. Thompson RE, Larson DR, Webb WW. Precise nanometer localization analysis for individual fluorescent probes. *Biophys J* 2002;82(5):2775–2783.
38. Churchman LS, Okten Z, Rock RS, Dawson JF, Spudich JA. Single molecule high-resolution colocalization of Cy3 and Cy5 attached to macromolecules measures intramolecular distances through time. *Proc Natl Acad Sci USA* 2005;102(5):1419–1423.
39. Yildiz A, et al. Myosin V walks hand-over-hand: single fluorophore imaging with 1.5nm localization. *Science* 2003;300(5628):2061–2065.

40. Ram S, Ward ES, Ober RJ. Beyond Rayleigh's criterion: a resolution measure with application to single-molecule microscopy. *Proc Natl Acad Sci USA* 2006;103(12):4457–4462.
41. Gordon MP, Ha T, Selvin PR. Single-molecule high-resolution imaging with photobleaching. *Proc Natl Acad Sci USA* 2004;101(17):6462–6465.
42. Agrawal A, Tripp RA, Anderson LJ, Nie S. Real-time detection of virus particles and viral protein expression with two-color nanoparticle probes. *J Virol* 2005;79(13):8625–8628.
43. D'Antoni CM, et al. Rapid quantitative analysis using a single molecule counting approach. *Anal Biochem* 2006;352(1):97–109.
44. Hagerman PJ. Flexibility of DNA. *Annu Rev Biophys Biophys Chem* 1988;17:265–286.

PART II

Bio-Nano Interfaces

ECM Interactions with Cells from the Macro- to Nanoscale

STEVE MWENIFUMBO and MOLLY M. STEVENS

9.1 INTRODUCTION

Cells respond and interact with local chemical and topographical stimuli within their environment that range from the macro- to nanoscale. The extracellular matrix (ECM) plays a vital role in determining cell behavior through a melange of carefully choreographed extrinsic signals that orchestrate cellular functions in tissue development and homeostasis [1]. The significance of this role has become apparent in recent years, as the discovery and characterization of new ECM constituents, identification of novel receptors and signaling mechanisms, and the characterization of various effector molecules that regulate matrix assembly and turnover have brought new insights into ECM function.

The constituent molecules and architecture of ECM provide a dynamic environment that not only physically supports cells, but also guides cell behavior [2–7]. The numerous variants of the constituent molecules, their ratios, and relative arrangements give rise to considerable diversity in ECM form, each adapted for tissue specific biological, structural, mechanical, and functional requirements. This diversity generates a wealth of exposed and encoded information that is interpreted by a large number of cellular receptors such as transmembrane glycoproteins, proteoglycans, and glycolipids. A two-way flow of information ensues, which mediates gene and consequently protein expression that ultimately regulates cell processes such as cell migration or ECM remodelling [4]. The regulation of these processes requires both spatial and temporal coordination if cells are to form dynamic functional tissues [6].

This chapter aims to provide an up-to-date review of some of the significant developments in our understanding of the ECM and its interactions with cells from the macro- to nanoscale.

9.2 CELL MICROENVIRONMENT

Cells have diameters typically in the tens of microns and are not the only constituents of tissues. A large portion of tissue volume is often occupied by extracellular space, which contains a dynamic three-dimensional network of macromolecules that assemble to form the cell microenvironment—the ECM. Constant remodeling alters the constituent molecules and thus dictates the properties of the cellular environment.

The ECM is a diverse composite structure of cell-secreted proteins, glycosaminoglycans (GAGs), proteoglycans, and glycoproteins. Tissue-specific heterogeneity in its histoarchitecture has evolved to serve numerous functions ranging from supporting cells to intracellular signaling. Numerous proteins play a role in the activation of signaling pathways, with cell surface receptors serving as primary conduits for signal transduction between neighboring cells, secreted signaling molecules, and ligands in the surrounding matrix. These extrinsic factors extend profound influences on both gene expression and cell behavior and ultimately come together to form a dynamic cell microenvironment essential for tissue development and function.

9.2.1 ECM Compositional Diversity

Although the major constituents of ECM found in all metazoa can be grouped into four classes: collagens, glycoproteins, GAGs, and proteoglycans, evolutionary pressures have resulted in substantial diversity in the ECM structure. The many variations in ECM form may be explained by the numerous variants of each constituent class and the ability of cells to secrete different proportions of these ECM components, which then form various architectural configurations. ECM compositional diversity reflects the broad range of biofunctional requirements of the different organ systems.

9.2.1.1 Constituent Macromolecules Extensive evolutionary changes have occurred in metazoa, generating diversified matrix molecules with different structural properties and signaling domains. For example, fibrillar type I collagens found in tendons form rope-like structures to carry tensile loads [8], while nonfibrillar type IV collagens form a meshworks that act as size-selective filtration barriers in the basement membrane [9]. Many of the constituent macromolecules are the result of chimeric aggregations of structural domains that have formed by exon shuffling [10] and numerous isoforms have resulted through differential splicing of these domains and posttranslational modifications [11]. Collagens, for instance, have achieved considerable diversity, as more

than 27 distinct types have been characterized [12, 13]. Similar diversity through differential splicing has been found in numerous glycoproteins of the ECM, including fibronectins, laminins and tenascins, whereas GAG variation and number account for proteoglycan heterogeneity [11, 14].

9.2.1.2 Developmental Diversity In addition to the specific diversity found in the individual constituent macromolecules of the ECM, the matrix as a whole, can display considerable compositional diversity. Through differential production of particular ECM components, specific regions or boundaries within the tissue may be delineated.

ECM regulation of cell behavior has been observed in a number of developmental processes [5, 6, 15–17]. As developing cells move among microenvironments within the developing tissue, each with different markers/signals, they modulate their differentiating state and behavior accordingly. ECM signaling generates a unique biological and structural “niche” that directs cellular differentiation and maintains cellular phenotype. This cellular modulation is accompanied by dramatic changes in the types, ratios, and geometrical arrangements of the synthesized ECM macromolecules, giving rise to the specific biofunctional properties of the tissue in question.

Endochondral ossification is one developmental process that requires the coordination of a vast array of microenvironments and cell types. In the beginning, the hyaluronate- and type I collagen-rich matrix provides a supportive environment for mesenchymal cell migration and proliferation [18]. As bone development progresses, the mesenchymal cells migrate and aggregate into condensations that form the template for future skeletal elements [19, 20]. The cells at the center of these condensations then differentiate into chondrocytes, which subsequently leads to the removal of hyaluronate from the surrounding microenvironment and the secretion of large amounts of macromolecules including aggrecan and collagen II [21]. These macromolecules act as molecular markers that help distinguish the differentiating chondrocytes from the surrounding undifferentiated mesenchymal cells. Once fully differentiated, further complex transitions occur in the arrangement and composition of the cartilaginous ECM. The ECM surrounding the chondrocytes calcifies and the cells apoptose [17]. This calcified matrix favors vascular invasion from the bone collar and allows chondroclast and osteoblast invasion [15]. At this point, collagen synthesis reverts from type II to type I as the surrounding cartilaginous ECM degrades and is replaced with bone ECM [21]. Changes in composition are therefore important factors in the control of organogenesis as well as provide suitable structural properties to the developing skeletal tissues.

9.2.1.3 Tissue-Specific Diversity In complex organisms, the ECM of distinct tissue types has evolved into different forms. This is significant since the structure and function of a specific tissue will depend on the relative proportions of the constitutive molecules present. This is evident in tissue types

like articular cartilage or arterial walls, where ECM compositional diversity helps to engender their inherent structure and properties.

The unique blend of macromolecules, together with the ECM configuration, gives articular cartilage its important physical properties—compressive stiffness and friction-reduced movement of joints. In articular cartilage, the predominant collagen, type II, along with smaller amounts of other collagens (V, VI, IX, X, and XI), forms a fibrillar network [22] that is embedded with multimolecular aggregates that self-assemble from the proteoglycan, aggrecan, and the GAG, hyaluronan [23]. The fibrillar structure of the collagen network provides tensile strength to the tissue and resistance to the swelling pressures of the embedded proteoglycans, whilst the aggrecan surface, being highly sulfated and negatively charged, attracts cations to the matrix and in turn increases the osmotic swelling pressure [24]. This swelling property allows the dissipation of compressive loads through changes in osmotic and hydrostatic pressures.

Unlike the functional requirements of cartilage tissue, arterial walls must resist tensile forces, provide a barrier to blood cells, and be elastic enough to accommodate hemodynamic pressure [25] associated with blood flow from the heart. A hierarchical arrangement of endothelial cells (ECs), smooth muscle cells (SMCs), and ECM proteins come together to form the arterial walls in vascular systems [16]. Arterial walls are organized into three distinct layers: the intima, consisting of ECs and a hydrated matrix rich in hyaluronan and proteoglycans; the media, separated from the intima by a dense internal elastic lamina and composed of layers of SMCs and elastic fibers; and the adventitia, separated by an elastic lamina and composed primarily of fibrillar collagen and fibroblasts [26]. The integrated composition of collagens, fibrillins, and elastins help maintain vascular homeostasis and impart specific properties to the arterial walls. The predominant collagens type I and III assemble into fibrils that provide tensile strength to the walls [16], whereas type IV and VIII collagens within the basement membranes under the ECs, form three-dimensional networks that serve to anchor the cells and help control vascular permeability [26]. Fibrillins self-associate to form microfibrillar networks that stabilize elastic fiber structure [27, 28] and elastins assemble into elastic fibers that provide elasticity needed to accommodate hemodynamic pressure differences from blood flow [29].

ECM compositional diversity has therefore evolved as a mechanism to guide cell behavior through the organizational arrangement of developmental stage- and tissue-specific structures with the biofunctional properties of these tissues being dependent on the biochemical composition and architectural composition.

9.2.2 Nanoscaled Structures of the ECM

Interactions between cells and ECM occur over multiple length scales, where the hierarchical assembly of the various ECM constituents plays an essential

role in numerous cellular processes. Whether it is an intricate glycoprotein network providing adhesion points for cell binding and migration or a negatively charged matrix-embedded proteoglycan providing charge-selective filtration properties to the ECM, the constituent molecules that mobilize to form the nano- to macroscale structures of the ECM can be grouped into four major groups: proteins (collagens and elastins), GAGs, proteoglycans, and glycoproteins.

9.2.2.1 Proteins—Collagens and Elastins Numerous proteins are constituted in the ECM; however, the primary ones are collagens and elastins.

Collagens are the most abundant proteins in the human body and comprise a highly diverse superfamily of ECM proteins. Of the 27 different collagen types (I–XXVII), 42 distinct α -chains have been described [12, 30–33]. All collagen molecules consist of three homo- or heterotrimeric α -chain subunits that wind together to form triple-helix conformations [34]. Each α -chain subunit contains a $(\text{Gly-X-Y})_n$ repetitive sequence motif, where glycine is present every third position and X and Y are often the amino acids proline and hydroxyproline [35]. Hydroxyl groups in hydroxyproline are essential in forming H-bonds that stabilize the collagen triple-helix conformation, whereas lysine and hydroxylysine residues present in the structure are integral in forming covalent cross-links within and between collagen molecules in supramolecular form [36]. Most collagens associate into highly organized supramolecular structures and their triple-helical domains can vary in length and can be continuous or interrupted with nonhelical domains depending on collagen type.

The collagen superfamily can be divided into several subfamilies based on supramolecular structure and other properties. Table 9.1 presents a summary of these subfamilies and their known supramolecular structures.

The synthesis of collagen pro-alpha chains occurs by several co- and posttranslational modifications, in addition to established pathways for secretory proteins. These include the hydroxylation of secreted prolines and lysines, the glycosylation of selected hydroxylysine and asparagines residues, disulfide bond formation, and chain self-assembly into the procollagen triple helix. The procollagens are then secreted into the ECM where the protective N and C propeptides are cleaved and the collagen molecules are assembled into stable cross-linked fibrils or other supramolecular structures depending on collagen type. Further details of collagen biosynthesis may be found in the following reviews [13, 32, 36] and text [37, 40]. This section, however, will instead focus on the hierarchical structures of collagen and how they self-organize to interact with cells.

Collagens are primarily responsible for the structural integrity of ECM or the anchoring of cells to the matrix and have a tendency to form fibrils, filaments, or networks alone or in conjunction with other ECM proteins. Fibril-forming collagens are normally associated with the structural functions, whereas nonfibrillar collagens are often involved in the regulatory functions.

TABLE 9.1 Collagen Subfamilies and Known Supramolecular Structures

Subfamilies	Collagen type	Structural features	Representative tissues	Function
<i>Fibrillar collagens</i>				
Fibril forming	I	300 nm-long, staggered large-diameter banded fibrils	Skin, tendon, bone, lung, cornea	Supporting fibers recognized by integrin cell surface receptors
	II	300 nm-long, staggered small-diameter banded fibrils	Cartilage, vitreous humor	Supporting fibers
	III	300 nm-long, staggered small-diameter fibrils; often copolymer with type I	Skin, muscle, vascular, lung, kidney	Small supporting fibers
	V	390 nm-long fibrils with globular N-terminal extension; often copolymers with type I and III	Cornea, teeth, bone, skin, smooth muscle, tendon, liver	Small supporting pericellular fibers; interacts with thrombospondin
	XI	Small-diameter fibrils; can form molecules with type II, IX and V	Cartilage, vitreous humor	Possible core for type II regulating fibril diameter
	XXIV	Small-diameter fibrils; coexpressed with type I	Developing cornea and bone	Possible regulator of type I fibrillogenesis
	XXVII	Small-diameter fibrils	Cartilage, eye, ear, lung	Unknown
<i>Nonfibrillar collagens</i>				
FACIT ^a and related structural collagens	IX	FACIT; N-terminal globular domain; bound GAG	Cartilage, vitreous humor	Type II collagen fibril association and interaction with proteoglycans

XII	FACIT	Skin, tendon, cartilage, periodontal ligament	Type I collagen association and interaction with different ECM components
XIV	FACIT	Fetal skin, tendon, cartilage	Similar to type XII
XVI	FACIT	Heart, lung, pancreas, placenta	Stabilizing fibroblasts in dermal matrix
XIX	FACIT	Vascular, neuronal, and mesenchymal basement membrane zones	Cell-cell/cell-matrix adhesive protein; association with heparan sulfate proteoglycans
XX	FACIT	Corneal epithelium, skin, cartilage, tendon	Regulation of fibrillar diameter; similar to collagen XII and XVI
XXI	FACIT	Vascular walls, smooth muscle cells	Participation in ECM assembly of vascular networks during angiogenesis
XXII	FACIT	Tissue junctions	Cell adhesion ligand for skin epithelial cells and fibroblasts
XXVI	FACIT	Testis, ovary	Possible role in development of reproductive tissues

(continued)

TABLE 9.1 (Continued)

Subfamilies	Collagen type	Structural features	Representative tissues	Function
Sheet forming	IV	400 nm-long fibrils forming meshwork sheets	Basement membrane	Meshwork scaffolding; multiple cell-binding sites
	VIII	130 nm-long fibrils forming hexagonal network	Sclera, Descemet's membrane	Regulation of matrix environment; fibroblastic cell layers and Descemet's membrane thickness
	X	130 nm-long fibrils forming hexagonal network	Hypertrophic cartilage	Endochondral bone development; associates with type II collagen fibrils
Beaded filaments	VI	5–10 nm-diameter beaded filaments; periodic globular domains	Vessels, skin, intervertebral disc	Interfaces with major collagen fibrils and cells; multiple RGD motifs recognized by integrin receptors
Anchoring	VII	420 nm-long collagenous domains; forms anchoring filaments	Subbasal lamina of skin	Anchoring of dermal epithelial cells to underlying stroma
Transmembrane	XIII	Cell membrane protein	Fibroblasts, cartilage growth plate, epidermis, hair follicles	Cellular adhesion and migration; binds to fibronectin, heparin and basement membrane components

XVII	Cell membrane protein	Dermal–epidermal junction of skin in hemidesmosomes	Linkage of basal cells to stroma
XXIII	Cell membrane protein	Metastatic tumor cells, cornea, lung	May assist in enhancing the stability of corneal interfacial areas
XXV	Cell membrane protein	Neurons	May play a role in adheren junctions between neurons
XV	Core protein of chondroitin sulfate	Heart, placenta, endometrium, skeletal muscles	Regulates critical basement membrane functions; stabilizes muscle cells and microvessels
XVIII	Core protein of chondroitin sulfate	Lung, liver, kidney	Regulates critical basement membrane functions; maintains structural integrity

Multiplexins

Data compiled from multiple references and the references therein [13, 30, 32, 35–39].
 *Fibril-associated collagens with interrupted triple helices (FACIT).

Fibril-forming collagens (I, II, III, V, XI, XXIV, and XXVIII) represent major products synthesized by connective tissue cells and have the unique ability to associate into highly ordered fibrils and fibers. Their structural unit generally consists of a 300 nm-long, 1.5 nm-diameter triple helix, and the presence of the triple-helical domain provides these fibrils with stiff, rod-like regions. In addition, fibrils may be heterotypic aggregates of more than one collagen type organized into discrete tissue-specific configurations where their structure and biomechanical properties are governed by the specific ratios of collagen involved [35]. For example, diameter control was found to be an inherent property of the specific proportions of collagen type for heterotypic fibrils of embryonic cartilage formed from collagen types II, IX, and XI [41].

Interactions with fibril-associated collagens with interrupted triple-helix (FACIT) collagens and small proteoglycans have also been shown to regulate fibril properties [42]. FACITs (IX, XII, XIV, XVI, XIX, XX, XXI, XXII, and XXVI) are another subclass of collagens that do not form fibrils themselves, but are found attached to the surface of preexisting collagen fibrils. They are comprised of relatively short triple-helical (collageneous) domains connected by nontriple-helical (noncollageneous) sequences. FACITs help modulate ECM structure by forming molecular bridges between fibrillar collagens and other ECM components. Specifically, FACITs like collagen XVI may play an active role in anchoring microfibrils to basement membranes [43], while others like GAG carrying collagen IX help modulate the surface charge properties of fibrils [44].

Sheet-forming collagens (IV, VIII, and X) like those involved in forming basement membrane structures (IV) or hexagonal networks (VIII and X) can act as anchorage for cells, serve as molecular filters, or provide permeable barriers for developing embryos. Type IV collagen molecules in the basement membrane have collageneous domains longer than those of fibril-forming collagens, 400 nm long [45], and can self-assemble to form cross-linked network structures in which the monomers associate in end-to-end interactions and the helical domains intertwine to form super-coiled structures [36]. The other sheet-forming collagens type VIII and X are made up of almost the same sized 130-nm-long rod base units, where the collageneous domains contain eight imperfections in similar positions in the Gly-X-Y sequences [30] and assemble to form hexagonal lattices of type VIII or X collagen.

Beaded filament collagens (VI) are heterotrimeric molecules made up from three unique protein chains with very short triple-helical domains and large N- and C-terminal globular domains, which assemble into beaded microfibrils [36]. Type VI is the only known collagen to form beaded filaments and the presence of arginine–glycine–aspartate (RGD) motifs within its structure plays a central role in its interaction with other ECM constituents like fibronectin and with integrin cell surface receptors [30].

Anchoring collagens (VII) form anchoring fibrils that link the basement membrane to anchoring plaques in the underlying ECM [46]. Type VII collagen is a major component of anchoring fibrils, and the 420 nm-long triple-helical

domains are longer than any other collagen [30]. It is a homotrimeric molecule consisting of collagenous central domains flanked by two noncollagenous domain ends. Within the extracellular space, these type VII collagen molecules form antiparallel dimers, which then assemble laterally in a nonstaggered manner to form anchoring fibrils [47].

Transmembrane collagens (XIII, XVII, XXIII, and XXV) are homotrimeric cell surface molecules with multiple extracellular triple-helical domains that are connected to single hydrophobic transmembrane domains [35]. Within their ectodomains, which reside in the extracellular space, the triple-helical domains provide rigid rod-like structures, whereas the interruptions between these helical regions provide structural flexibility [48]. These collagens function as cell surface receptors and their ectodomains can be cleaved off from the cell surface to produce soluble extracellular molecules.

Multiplexins (XV and XVIII) are homotrimeric collagens with multiple triple-helical domains and interruptions. They have a large N-terminal globular domain, a highly interrupted triple helix, and a large C-terminal globular domain. In addition, multiplexins often carry GAG chains and are therefore referred to as proteoglycans.

For more comprehensive coverage of structure and function of the collagen superfamily, the reader is referred to previous reviews [13, 30, 32–34, 36, 48, 49].

Elastin is the major protein of elastic fibers in connective tissues like blood vessels and skin and is extremely rich in the hydrophobic amino acids glycine, valine, alanine, and proline [50, 51]. It is synthesized when the enzyme lysyl oxidase covalently cross-links its soluble precursor, tropoelastin, and forms an insoluble polypeptide [29]. Elastin, in association with other microfibrillar components, assembles to form elastic fibers, which then form a randomly oriented interconnected network. Elastin fibrillogenesis begins as 10–12-nm-diameter fibrillin microfibril bundles are secreted into the extracellular space near the cell surface and assemble into aggregates [29]. Fiber development progresses, as tropoelastins deposited at specific locations within the microfibril bundles progressively displace the microfibrils to the outer region of the fibers and covalently cross-link to form the elastin core. These elastin fibrous networks are highly insoluble and have the ability to undergo elastic recoil [52]. The unique intermolecular desmosine and isodesmosine cross-links and the high content of hydrophobic amino acids within elastin's structure account for these properties [53, 54]. Additionally, elastin peptides are known to enhance signaling pathways, with Val-Gly-Val-Ala-Pro-Gly (VGVAPG) known to upregulate metalloproteinases [55] and promote chemotactic activity with fibroblasts [56].

9.2.2.2 GAGs GAGs are long polymer chains of specific repeating disaccharides that are important in regulating biological functions. This may consist of creating permissive environments for cell migration and macromolecular transport through regulation of the size and properties of ECM spaces or binding to signaling molecules like growth factors to

modulate signaling pathways. This group of complex carbohydrates is classified based on the nature of their repeating disaccharide units and includes chondroitin sulfate, dermatan sulfate, heparan sulfate, hyaluronan, and keratan sulfate [57]. Due to their high sulfate content and/or the presence of uronic acid, GAGs bear many negative charges that enable them to associate with numerous ligands by electrostatic interactions. All GAGs are found in tissues as covalently attached components of proteoglycans, with the exception of hyaluronan. Hyaluronan is unique since it is secreted directly into the extracellular space by the cell membrane bound enzyme hyaluronan synthase and is able to function as a free carbohydrate [58, 59]. It is flexible, bending and twisting into many conformations forming random coils, and can self-associate to form networks. It has a strong affinity to water due to the large number of anionic residues on its surface and can bind cations by COO^- groups on its surface. Additionally, it can form superaggregates with a number of proteoglycans including aggrecan.

9.2.2.3 Proteoglycans Proteoglycans are a diverse group of molecules that are abundant in the ECM and expressed on cell surfaces. They represent a glycoprotein subset in which structure and function are mediated by protein cores and covalently linked GAG side chains. Numerous peptide motifs exist within these molecules and many of these are often found in the same protein core including epidermal growth factor (EGF) repeats, hyaluronan-binding, immunoglobulin-like, leucine-rich repeats, and sugar-binding lectin domains [60]. Several classes are present in the ECM and these may be divided into two subfamilies based on the typical features of the protein core arrangement (Table 9.2) [61].

The first family, the small leucine-rich proteoglycans, includes proteoglycans like biglycan, decorin, fibromodulin, and lumican. While the second family, the modular proteoglycans, can be further divided into the nonhyaluronate-binding proteoglycans like perlecan and agrin and the hyaluronan/lectin-binding proteoglycans like aggrecan, versican, and CD44 [2]. This diversity in protein core domains and GAG side chains enables proteoglycans to have a high affinity to binding of various ligands and accounts for many specific interactions in the matrix. Perlecan, for instance, is embedded in basement membranes and gives them a fixed negative electrostatic charge, which is responsible in part for their charge-selective filtration properties [63]. Whereas the small leucine-rich proteoglycan, decorin, can bind and regulate the fibrillogenesis of collagen [64, 65], other proteoglycans, like heparan sulfate proteoglycans, participate in fibroblast growth factor (FGF) signaling by directly interacting with FGFs and its receptors on the cell surface, subsequently increasing FGF's affinity for its associated receptors [57, 66].

9.2.2.4 Glycoproteins With the ability to organize collagens, elastins, proteoglycans, and cells into ordered structures, glycoproteins are also essential building blocks of the ECM. These macromolecules vary in size, structure, and

TABLE 9.2 General Properties of Selected Proteoglycans

Proteoglycan		Protein core (~kDa)	GAGs (number)	Representative tissue	Function
<i>Small leucine-rich proteoglycans</i>					
Biglycan		38–40	Chondroitin sulfate/ dermatan sulfate (2)	Muscle, bone, cartilage, epithelia	Associated with cell surfaces
Decorin		36–40	Chondroitin sulfate/ dermatan sulfate (1)	Collagenous matrices, bone, teeth	Binds collagen fibrils and modifies their assembly; binds to TGF-beta
Fibromodulin		42–43	Keratan sulfate (2–4)	Cartilage, skin, tendon	Binds collagen I and II; reduces size of collagen fibrils
<i>Modular proteoglycans</i>					
Nonhyaluronan binding	Agrin	200–250	Heparan sulfate (3)	Synaptic sites of neuromuscular junctions, renal basement membranes	Involved in the aggregation of acetylcholine receptors
	Perlecan	400–467	Chondroitin sulfate/ heparan (3)	Basement membranes, cell surfaces, cartilage	Self-associates; binds laminin in basement membranes; binds basic fibroblast growth factor
Hyaluronan and lectin binding	Aggrecan	220–250	Chondroitin sulfate (>150) and Keratin sulfate (100–150)	Cartilage, brain, blood	Binds hyaluronan, hydrates and fills ECM
	Versican	260–370	Chondroitin sulfate/ dermatan sulfate (10–30)	Blood vessels, brain, cartilage, skin	May bind hyaluronan

Data compiled from multiple references [2, 40, 61, 62].

distribution and are composed of a protein and covalently linked oligosaccharide(s). Glycoproteins are made up of multiple subunits colored with an assortment of distinct peptide motifs that interact with not only themselves, but also cells and other matrix proteins [6]. They may exist as large molecules with extended conformations that span distances of several hundred nanometers. A variety of glycoproteins are found in the ECM including fibronectin and laminin.

Fibronectin is one of the best studied glycoproteins, has multiple isoforms, and is composed of three modules, repeating motifs of type I, II, and III, separated by connecting sequences [67]. It is a large glycoprotein with numerous binding sites for collagens, proteoglycans, and cell surface receptors like integrins (Fig. 9.1). The type III module is the most abundant module in its structure and includes many aspartate-containing sequences such as RGD, which mediate cellular adhesion through integrins [68, 69]. Fibronectin is critical for numerous cellular functions and is one of the earliest macromolecules to be laid down in the ECM. It is required for the assembly of several ECM proteins like collagen I [70] and plays a role in regulating the incorporation of morphogens and growth factors into the ECM [71]. Its distribution in areas of skeletogenesis suggests that it may be involved in early stages of bone development [72] as well as continued mature bone homeostasis by regulating the differentiation and survival of osteoblasts [73].

Laminins are the primary adhesive matrix proteins in the basement membrane, exist in several isoforms, and are large heterotrimeric glycoproteins constituted by three genetically distinct polypeptide alpha, beta, and gamma

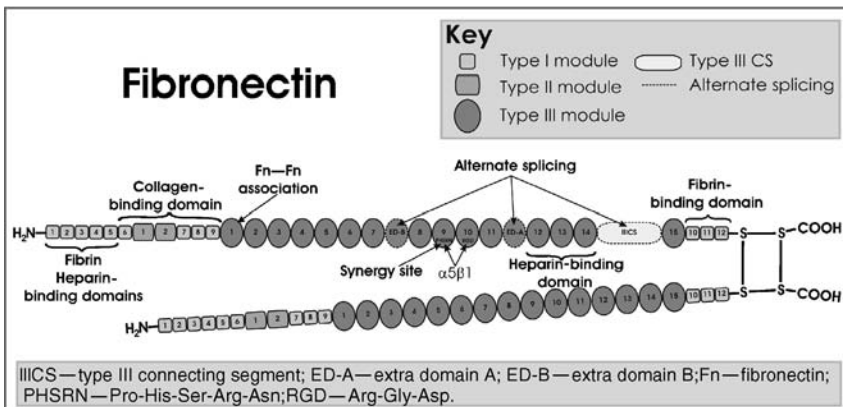


FIGURE 9.1 Schematic representation of fibronectin dimer. Depicts individual modules as well as a variety of binding domains specialized for particular macromolecules. Alternate splicing accounts for the differences in the two similar chains, which are joined by two disulfide bonds near the C-termini.

chains that assemble to form a cruciform structure with globular domains at each arm end (Fig. 9.1) [74, 75]. They contain multiple binding domains that participate in numerous biological activities (network and filament formation, cell binding through cell surface receptors, and binding to other matrix proteins in supramolecular assemblies), with the ECM structure-forming domains generally located on the short arms of all three subunits and cell-interacting domains mapped onto the N- and C-terminal domains of the alpha subunits [74]. For example, within the basement membrane, all three short arms (alpha1, beta1, and gamma1) of laminin-1 are involved in laminin self-assembly [76], while binding with entactin/nidogen is restricted to the short arm region of the gamma1 chain [77], and integrin cell surface receptors to the laminin G-domain-like (LG) modules of the alpha subunits [78, 79]. Such binding interactions are essential for proper assembly and function of the basement membrane, where type IV collagen, laminins, and entactins are thought to be the primary basement membrane scaffold, fibrous two-dimensional supramolecular networks where entactin binds the laminin and collagen networks with stable noncovalent bridges [78, 80].

9.2.3 Putting It All Together—Hierarchical Assembly

Hierarchy of scales is apparent in the biological structures formed during tissue development and homeostasis. Within the ECM, the multifunctional nature of matrix components is a direct reflection of their modular and hierarchical architecture. The multiple binding domains, chemistry, and topology of the various ECM constituents help regulate matrix assembly, stabilize ECM architecture, and modulate cell–matrix interactions. Some examples include fibrous structures that provide strength, elasticity, or cell permissivity, proteoglycans that act as reservoirs for morphogens or regulate osmotic pressure, and glycoproteins that stabilize fibrous structures or act as binding sites for cells. All of these structures combine together to give tissues their specialized properties. The significance of this relationship between ECM hierarchy and function is apparent in tissues like articular cartilage.

Articular cartilage is an avascular tissue containing a relatively sparse number of chondrocyte cells that covers the subchondral bone in diarthrodial joints [22]. In association with synovial fluid, it forms a wear-resistant, friction-reduced, load-bearing surface only a few millimeters thick [81, 82]. Its matrix and cells are organized into distinct zones: superficial, middle, deep, and calcified zones (Fig. 9.2) and these zones exhibit variations in biochemical composition, cell morphology, and cell–matrix structural organization [81, 83].

The superficial zone consists of a densely packed collagen fibrillar network with flattened chondrocytes that are aligned tangentially with the articulating surface [84]. Collagen fibril alignment within this zone enables the accommodation of high shear and tensile forces and type II collagen forms the bulk of the fibrils. Microfibril assembly is mediated in part by type XI collagen and decorin with the former regulating lateral growth and the latter regulating

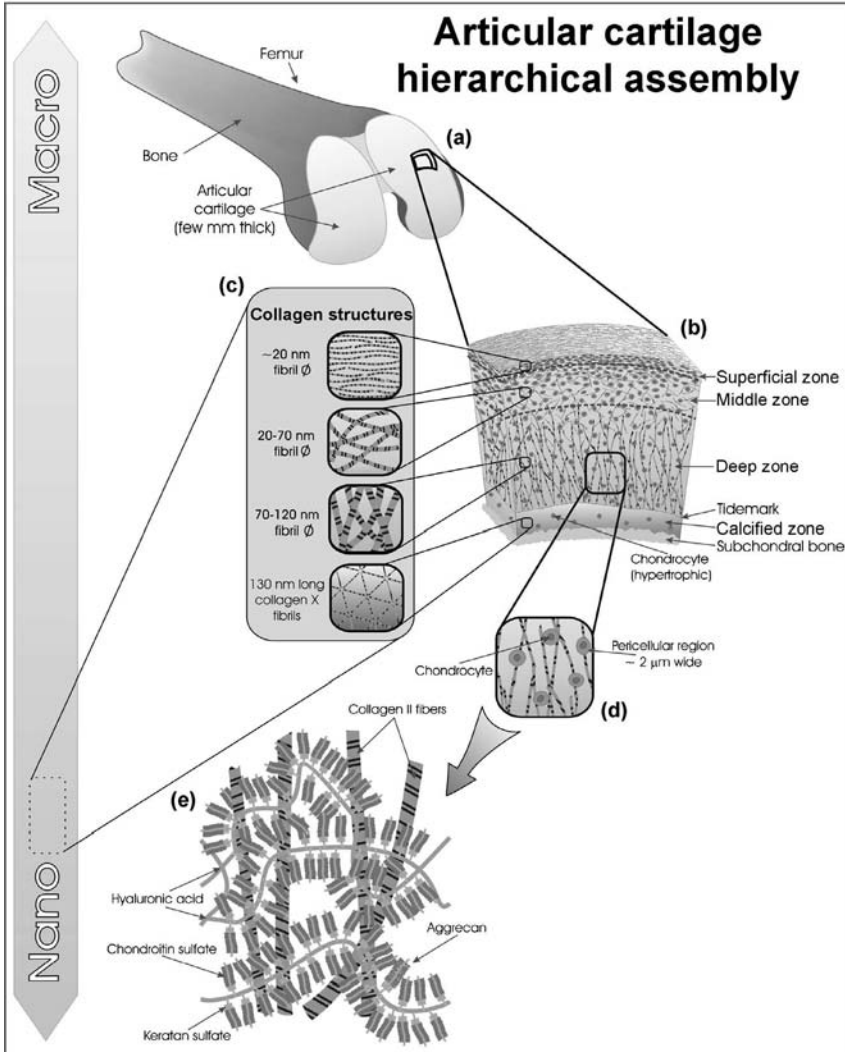


FIGURE 9.2 Hierarchical organization of articular cartilage over different length scales. Articular cartilage forms a wear-resistant, load-bearing surface that covers bone in diarthrodial joints (a). It is organized into distinct zones (b), where the organization of the collagen structures varies between zones (c). Resident chondrocytes are encased in pericellular regions (d), which are surrounded by a well-defined matrix nanoarchitecture of aggrecan/hyaluronic acid superaggregates and macrofibrillar collagen networks (e).

fibril diameter [41]. Fibrils are thinnest in this zone and measure approximately 20 nm in diameter [83].

The middle zone represents a transitional region from the tangential fiber orientation of the superficial zone to the radial fiber orientation of the deep

zone. Cells exhibit a round morphology and their density is lower than that in the superficial zone [85, 86]. The ECM within this region is aggrecan rich and the collagen fibrils are larger in diameter, randomly arranged, and loosely packed [84, 87].

Within the deep zone, the collagen fibers are perpendicularly oriented with the subchondral bone and attain a maximum diameter size that ranges from 70 to 120 nm [83]. Cell density is lowest in this region [86], whereas aggrecan content is at a maximum. Cartilage compressive stiffness is provided by the swelling pressure of hydrated aggregates of aggrecan and hyaluronan bound to the porous collagen II structure within this zone, where swelling is restricted by the collagen network. This hydrated fibrous proteoglycan structure, in conjunction with synovial fluid and articulating joint movements, allows nutrients to circulate and nourish cells [24].

The calcified zone provides a buffer region between the uncalcified cartilage and subchondral bone. The chondrocytes that reside in this region are in a hypertrophic phenotypic state. These cells secrete the hexagonal sheet forming collagen type X and participate in calcifying the ECM within this region [83].

Additionally, within the different zones a pericellular matrix region, approximately 2 μm wide, surrounds the chondrocytes [83]. This region varies in its structure compared to that of the surrounding matrix. Type VI collagen and decorin are concentrated in this region and assemble to form a microfilamentous network. The cell surface proteoglycan perlecan is also present within this region. It cross-links with ECM components such as type VI collagen, thereby linking cell surfaces with matrix organization.

Therefore, the highly specialized composition and structure of articular cartilage has evolved to enable joint mobility and gives an excellent example of the relationship between the ECM hierarchy and tissue function.

9.3 CELL—ECM INTERACTIONS—THE MULTIDIMENSIONAL MAP

Beyond its role in providing structural support and organization for resident cells and imparting tissues with specific biofunctional properties, the ECM also serves in an instructive capacity. A vast amount of information is encoded in the matrix architecture and this forms a multidimensional map (Fig. 9.3). Cells use this map to guide their behavior. The information within it is expressed in the form of signaling gradients, which may exist as chemical distributions or differential expressions of ECM components. Cell surface receptors interpret these gradients and respond accordingly with directionality being dictated by signaling gradient changes. A bidirectional flow of information between the cells and the ECM ensues where changes in the local microenvironment result in dynamic releases of information. This map may be perceived in a variety of different ways and its context is dependent on external events as well as specific cell types.

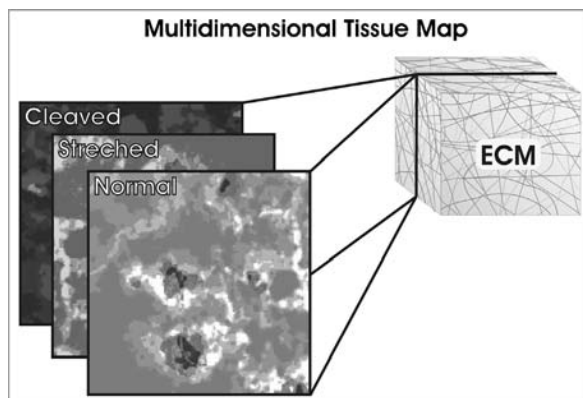


FIGURE 9.3 Multidimensional tissue map. By providing signaling gradients to cells, natural tissues effectively provide multiple behavioral maps, whose context is dependent on external events. These gradients present themselves in the form of different signaling molecules or binding opportunities that result from changes in the ECM through processes such as stretching and proteolytic cleavage. (Modified from Reference 7 with permission from AAAS).

9.3.1 Signaling Gradients

In order to direct cells into the desired mode of behavior, signaling cues need to be displayed within an appropriate context. This requires both spatial and temporal positioning of signals from different sources. Consequently, each cell type has evolved to produce their own network of precisely encoded ECM proteins. This enables the configuration of the structural properties and information content of distinct ECM microenvironments. The three-dimensional matrix architecture assembled from ECM constituents regulates the spatial and temporal signals that are derived from localized biochemical distributions and mechanical forces. Biochemically, the ECM interacts with cells to provide information on the microenvironment through soluble and insoluble effectors, while physically it achieves this action through structural and mechanical restraints. The mechanisms to establish gradients of signaling molecules within the matrix architecture coincide with the deposition of ECM constituents. This may involve sequestering effector molecules from cells, secreting them in activated or deactivated states, or varying concentrations within the local microenvironment. Autoregulation of these mechanisms occurs through incremental changes in which different levels of regulation help maintain a homeostatic balance between ECM remodeling and signaling molecule release during processes like morphogenesis and tissue remodeling.

A variety of extrinsic factors control cellular behavior. The major sources of these external signals are soluble factors, ECM components, environmental stresses, and cell–cell interactions (Fig. 9.4) [88]. The modulation and

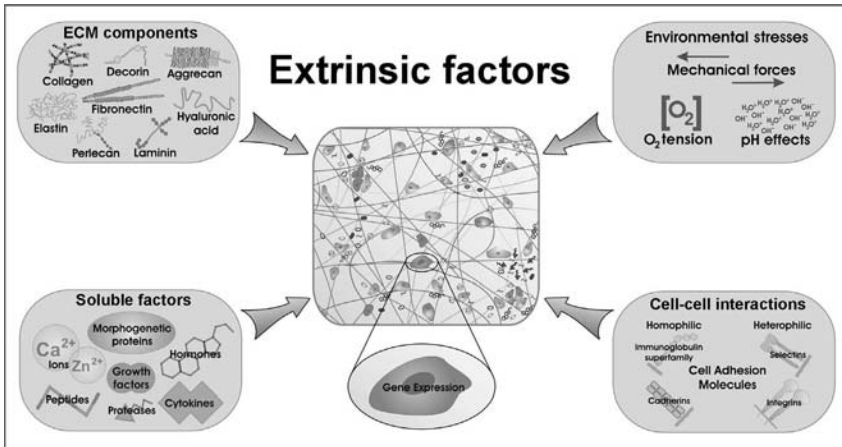


FIGURE 9.4 Extrinsic factors influencing cellular behavior. Four major sources of external signals regulate cell behavior: soluble factors, ECM components, environmental stresses, and cell–cell interactions. Soluble factors include growth factors, cytokines, morphogenetic proteins, peptides, hormones, proteases, and ions. ECM components include proteins, GAGs, proteoglycans, and glycoproteins. Environmental stresses include mechanical forces (dynamic and static), oxygen tension, and pH effects. Cell–cell interactions can be either homophilic or heterophilic and are regulated by cell adhesion molecules. These extrinsic factors in turn extend profound influences on gene expression and cell behavior, forming a dynamic cell microenvironment essential for tissue development and function.

presentation of these external factors within the local ECM microenvironments is of equal importance to the presence of the external signals themselves. This chapter, however, will primarily focus on those sources associated with ECM structures.

9.3.2 Soluble Factors

Secreted by cells, soluble factors (Fig. 9.4) feed into complex and overlapping signaling pathways that often share common receptors. The modulation of cellular activity by soluble factors is complex. Not only is the presence of the factors required, but they must be present at the appropriate times, concentrations, and ratios. These secreted molecules have a tendency to diffuse great distances, which potentially makes them unavailable or available in ineffective concentrations [89]. Consequently, a number of mechanisms have evolved to modulate their spatial and temporal distributions. These mechanisms include the production of molecules in an inactive form such as Transforming growth factor TGF- β [90], which activates only at the appropriate site of action; the requirement of cofactors such as heparan sulfate for receptor activation [57], and the localization of effector molecules like Ca²⁺ by binding to specific matrix constituents [91]. A direct or indirect relationship

can exist between ECM components and many of these soluble factors. For instance, interactions with GAGs and proteoglycans can lead to dynamic concentrations of free signaling molecules [88]. Additionally, signaling synergies often exist with ECM–soluble factor interactions. For example, cell adhesion has been shown to enhance autophosphorylation of the EGF receptor in response to its associated ligand [92]. Of the numerous soluble factors, growth factors are indicative of the necessity for spatial and temporal distribution in the modulation of cellular activities.

9.3.3 Growth Factors

Growth factors are specialized polypeptide molecules that bind to cell surface receptors and trigger intracellular signaling pathways [12]. The binding of growth factors to ECM structures is a major mechanism for regulating growth factor activity. Growth factors are essential for establishing signaling gradients during matrix synthesis. ECM–growth factor association enables the storage of large quantities of signals in readily available form. This association with matrix structures means the signals can prevent or slow down diffusion, thereby decreasing the loss of information [93]. Additionally, ECM–growth factor binding enables the transmission of signals to cells in contact with the same matrix region later, which is essential for the development of complex cellular structures.

Not all growth factors found within the matrix architecture are in an active state. This inertness may be attributed to a variety of factors. The growth factors may be concealed within the matrix only to be revealed during matrix degradation or cell movement. For instance, proteolysis of ECM-bound vascular endothelial growth factor (VEGF) by matrix metalloproteinase MMP-9 releases and increases VEGF bioavailability [94]. Similarly, an epidermal growth factor-like domain DIII, released through cleavage of laminin-5 by MMP-2, stimulates cell migration and changes in gene expression only upon its degradation [95]. A group effect may also occur where multiple signals from the matrix counteract each other and signaling activity would depend on the ratios of various growth factors (i.e. biological activity would require perturbations). For example, during angiogenesis, antiangiogenic factors dominate until the release of angiogenic growth factors by ECM proteinases causes a proangiogenic environment to ensue [96–100]. Finally, the growth factors can be latent with limited biological activity. For instance, TGF-beta is secreted by the majority of cells as latent complexes that are unable to interact with their corresponding signaling receptors until activated by processes like proteolysis [101].

Growth factor activity is primarily controlled by two biochemical mechanisms, release from the matrix architecture and activation. Release involves the dissociation of growth factors from matrix binding sites, while activation involves the dissociation of mature growth factors from dormant proteins or the induction of conformational changes that allow its binding to

receptors [93]. The release of growth factors from the matrix into biologically active form may occur via proteolytic enzymes. For example, cell surface localized matrix metalloproteinases such as MMP-9 and MMP-2 can release and activate TGF-beta by proteolytically cleaving its latent form [102]. This proteolytic release and activation of stored growth factors generates rapid localized signals. Proteolytic modulation is faster than simple control of gene expression, which is of particular importance in wound healing and immune system control [93].

9.3.4 ECM Components

ECM components can serve as landmarks for cells by leaving spatial and temporal cues. As discussed earlier, as cells migrate through the microenvironments within developing tissue, each with different ECM landmarks, they modulate their behavior accordingly, adjusting gene expression in response to the environmental cues. This creates a feedback loop as the responding cells also influence the surrounding ECM by differentially expressing particular ECM components and/or proteases. The stage- and tissue-specific assembly of matrix components therefore requires an intricate interplay between the residing cells and the signaling cues. With respect to the ECM components, these cues may emanate from the molecular composition, that is, multiple binding domains that may be apparent on the protein surface or concealed as cryptic sites or from the surface topography.

9.3.4.1 Binding Domains Numerous proteins are expressed in the ECM and each contains multiple motifs. These motifs are made up of specific amino acid sequences that present multiple binding sites for cell interactions with many distinct cell surface receptors. These interactions may directly or indirectly influence cellular activities such as adhesion, migration, proliferation, differentiation, and apoptosis. For instance, alpha5-beta1 integrin cell surface receptors bind directly to RGD sites on fibronectin molecules (10th type III repeating unit) [103], whereas tenascin indirectly interferes with cellular adhesion by binding to fibronectin [104], thus altering its ability to promote cell adhesion. The spatial proximity and regularity of binding domains has also been found to elicit different cellular responses. The migration of fibroblasts has been found to be a function of the average surface binding site density where cell speed varies with the spatial presentation of RGD binding sites and affected cell adhesion [105]. Colocalization of synergistic binding sites can also modulate cellular responses. For example, the synergistic Pro-His-Ser-Arg-Asn (PHSRN) site in the central cell-adhesive domain of fibronectin (9th type III repeating unit), although itself not biologically active, has been found to substantially enhance the cell-adhesive activity mediated by the alpha5-beta1 integrin cell surface receptor to its associated RGD binding site (10th type III repeating unit) [106]. The spacing between the PHSRN and RGD sites in the native conformation of fibronectin is approximately 4 nm [107].

9.3.4.2 Cryptic Sites Binding domains are also found encoded within the structures of ECM molecules. These domains, known as cryptic sites, are a result of convoluted protein folding and are not exposed on the protein surface (Fig. 9.5) [31, 108, 109]. The unmasking and activation of these sites occurs through structural modifications of ECM molecules that result from conformational changes or proteolytic cleavage. The conformational changes may be elicited by mechanical distortions and/or binding to other ECM molecules or cell membrane receptors, whereas proteolytic cleavage occurs during ECM degradation in processes like remodeling. Once exposed by either method, these cryptic sites become available for action. For example, conformational changes due to allosteric binding appear to reveal cryptic tenascin-binding sites on fibronectin molecules [110]. Binding with tenascin interferes with the cell adhesive properties of fibronectin and in turn influences cellular adhesion. Similarly, the proteolytically derived fragments from the noncollagenous domains (NC1) of basement membrane collagens (types IV, XV, and XVIII) also appear to act as regulators of biological activities such as angiogenesis [111]. Therefore, the spatial and temporal presentation of these binding domains ultimately depends on constituent molecule composition, mechanical distortions, as well as matrix assembly and turnover.

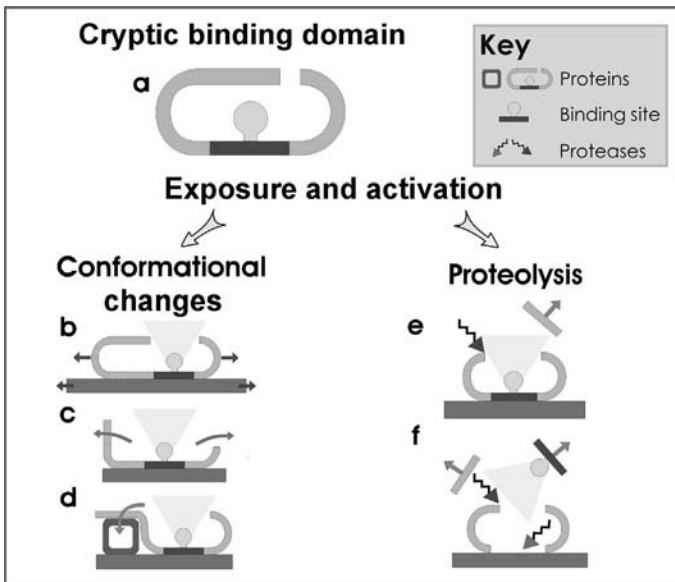


FIGURE 9.5 Mechanisms of cryptic site exposure. (a) Representation of protein structure encoded with a cryptic domain. Domains can be exposed through conformational changes due to (b) mechanical distortions, (c) surface adsorption, and (d) interactions with other proteins; or proteolytic cleavage that can (e) reveal hidden domains and may (f) release them as fragments, enabling the transport of signals into the local microenvironment. (Modified from Reference 7 with permission from AAAS).

9.3.4.3 Underlying Surface Chemistry ECM components also serve as a substrate for displaying signaling ligands. There are a variety of chemical signaling pathways through which cells receive information about the surfaces they contact and these generally involve the hierarchical assembly of molecular signaling molecules [69]. Numerous signaling ligands exhibit an environmental sensitivity to underlying surface chemistry. During adsorption processes, cell-secreted ECM proteins exhibit this sensitivity through conformational changes, which alter their receptor binding affinities. For example, integrin-binding specificities for adsorbed fibronectin were found to correlate with underlying surface chemistry [112]. Fibronectin conformational structure was altered in a manner that shifted the balance of preferential binding of one integrin over another. Surfaces predominant in OH- and NH₂-terminated groups were found to preferentially bind alpha5-beta1 integrins, while COOH- and CH₃-terminated surfaces were found to bind both alpha5-beta1 and alpha5-beta3 integrins. These differences in binding specificity were in turn transmitted to cells. The OH- and NH₂-terminated surfaces were found to upregulate osteoblast-specific gene expression, alkaline phosphatase enzymatic activity, and matrix mineralization compared with surfaces presenting COOH and CH₃ groups. Thus, surface-dependent differences in integrin binding enable the modulation of gene expression, ultimately allowing cells to sense structure and in turn regulate their own functions accordingly.

9.3.4.4 Topography In addition to molecular composition, surface topography is also capable of modulating cellular behavior. Termed topographic reaction, the reaction of cells to topography has been well documented in the literature for micrometer-scale features [113]. Recently, studies have explored topographic reactions at the nanoscale to investigate features with dimensions more relevant to native ECM—a three-dimensional structure exhibiting a rich complex topography of nanometer-scaled features, made up of interconnecting nanopores, fibers (10–300 nm in diameter), and nanoridges.

Topographic reactions including cell orientation, adhesion, motility, and morphology are elicited from micro- to nanoscale structures and these typically involve the activation of tyrosine kinases, cytoskeletal condensation, and further downstream modulation of gene expression [113]. Topographical scale (nanometer to micrometer range) is not the only topographical feature that modulates cellular behavior. The order and symmetry of the structures can also play a role [114]. Ordered structures occur naturally within the ECM, ranging from the highly ordered 67 nm repeat banded structure on collagen fibrils in the direction parallel to the fiber axis [115] to the collagen fibrils organized as aligned fibers in tendon ECM [42]. Cells appear to be able to distinguish between topological orders and symmetries, suggesting that interfacial forces between cells and ECM constituents may be organized by the nanostructures [116]. For example, the three-dimensional organization of the ECM environment also influences cell morphology and adhesion. Cell morphology and adhesion affect

gene expression and alter the protein expression of integrins, which in turn are important regulators of cell survival [117, 118]. It is likely that cells, which are sensitive to nanoscale features, require the full context of the three-dimensional nanofibrous matrix to maintain their phenotypic morphology and establish natural behavior patterns.

The nanoscale size of the ECM structures also means that overall surface area within the ECM is substantially larger relative to a comparable flat or microsized surface. This gives the matrix structure a larger surface area for storage and display of signaling molecules, which in turn increases the binding sites available for interactions with cell surface receptors. In addition to the increased surface area, the porosity of the structure also contributes to the diffusion and active transport of components, passage for cells, and the possibility of filtering functions.

The biological implications of topography are wide reaching and suggest that ECM components, which ultimately determine topographic features, modulate cellular behavior through ligand–receptor-mediated intracellular signaling pathways [31].

9.3.5 Environmental Stresses—Mechanical Stresses

Cells within the ECM are constantly exposed to mechanical signals that can be induced through contractile forces of resident cells (i.e., actomyosin contractility) or a variety of environmental factors (i.e., shear stresses produced by blood flow) [119]. These mechanical signals act at the interfaces between the cells and ECM and their bidirectional transduction modulates processes, that determine gene and protein expression [120]. The process by which physical signals are converted into the biochemical signals that cause cellular responses is called mechanotransduction. Mechanotransduction events span macro- to molecular size scales [3, 121] and this requires the coordination of the highly interconnected network of ECM molecules, cell surface receptors, and cell cytoskeleton in order to mediate the transmission of external forces to the cell nucleus via intracellular signaling pathways. The conversion of mechanical stresses into discrete signaling pathways is based on the molecular properties of cell–ECM contacts known as adhesion complexes. Application of intrinsic or extrinsic forces to these structures dramatically affects their assembly (maintained under a certain level of stress and disintegrate upon relaxation) and triggers adhesion-mediated signaling. Cell surface receptors are critical components to these structures.

9.3.6 Cell Surface Receptors

ECM constituents are recognized by a diverse variety of cell surface receptors. Numerous molecules are believed to function as cell surface receptors, such as transmembrane glycoproteins [122, 123], proteoglycans [124], and glycolipids. These receptors respond to a diverse set of structural and informational cues in

the ECM and their interactions lead to direct or indirect control of cellular activities such as adhesion, migration, differentiation, proliferation, gene expression, and apoptosis. Of the various cell surface molecules, integrin transmembrane receptors are the most prominent cell surface receptors in cell–ECM engagement.

9.3.6.1 Integrins Integrins are heterodimeric transmembrane molecules composed of alpha and beta subunits that recognize and bind to specific ECM ligands [125]. These subunits have large extracellular domains with transmembrane segments and short intracellular tails. Several isoforms of the alpha and beta subunits exist and integrin-binding specificity is dictated by the particular combination of these subunits. However, there exists a considerable overlap in binding specificity; that is, integrins can bind to several different types of ligands and many of those ligands are recognized by multiple integrins [126]. This suggests that in addition to mediating attachments to particular ECM proteins, different integrins perform multiple signaling functions. Over 24 distinct integrin receptors have been identified and these mediate interactions with ECM constituents and other cells [127].

9.3.6.2 Cell Adhesion—Adhesion Complexes The binding of ligands to the integrin extracellular domains leads to receptor conformation changes [128] and integrin clustering, which in turn initiate intracellular signaling pathways that regulate the formation of adhesion complexes. Integrin-mediated adhesions appear in different forms, including focal adhesions, focal complexes, and fibrillar adhesions [129]. Adhesion complexes link the ECM proteins with the actin cytoskeleton inside the cell and play an important role in governing the processes of cell survival [130]. Their assembly takes place in an ordered fashion indicating a hierarchical process that incorporates active feedback from cells—from increased/decreased protein expression to cytoskeletal driven spatial rearrangement of receptors and ligands.

9.3.6.3 Integrin Signaling In addition to cell adhesion, integrins also trigger many intracellular signaling pathways, including the activation of Rho-family GTPases as well as an array of protein and lipid kinases [129, 131, 132]. Signal transduction pathways are complex and poorly understood, but often involve a bidirectional flow of signaling information between the ECM, cytoskeleton, and nucleus [4]. In this cross talk, integrins are able to influence cell cycle progression, cell survival, and gene expression in addition to their effects on cell adhesion and morphology [122, 131, 133]. For example, alpha5-beta1 integrins, which are fibronectin receptors, suppress apoptotic cell death by triggering the B-cell lymphoma 2(Bcl-2) pathway and inducing the expression of the antiapoptotic protein Bcl-2 [134].

There are numerous signaling molecules native to adhesion sites that are also involved in growth factor and cytokine signaling pathways, suggesting overlapping pathways. The cross talk between soluble mediators and integrin

receptors enables the transduction of information about the extracellular microenvironment to cells and the subsequent control of cell behavior and survival in an intimately integrated fashion [123]. This exchange occurs at many levels, ranging from multiple inputs into common pathways to colocalization, where different types of receptors influence each other's activity. For instance, integrin-activated EGF receptors are capable of amplifying integrin signals [135]. In the absence of EGF receptor ligands, integrins can induce EGF receptor tyrosine phosphorylation, leading to downstream signaling (i.e., Shc phosphorylation and MAP kinase activation). This activation is important in anchorage-dependent cell survival, as it is sufficient to prevent apoptosis induced by cell–matrix detachment. Therefore, one must consider adhesion receptors and soluble mediator receptors as part of an integrated system, where integrins incorporate spatial signals provided by the matrix with those from soluble mediators.

9.3.7 Guided Activities of Cells—ECM Remodeling

ECM regulation of cell behavior is a complex process that involves the bidirectional flow of signals to and from the ECM and resident cells. Through receptor-mediated signaling and the mobilization of soluble signaling molecules, the ECM is able to mediate signals to migrating, proliferating, and differentiating cells. An excellent example of this is ECM remodeling.

9.3.7.1 ECM Remodeling ECM remodeling is extremely important for development, homeostasis, and wound repair. It is an intricately balanced process that is highly regulated by a complex network of enzymes and inhibitors. The ECM is constantly undergoing changes in response to intrinsic and extrinsic stimuli and these alterations in ECM microenvironment in turn help guide cellular activities such as migration, proliferation, and differentiation. Although, the structural and functional changes differ in response to different stimuli, a few key mechanistic features are common to tissue remodelling—the synthesis and deposition of ECM components and proteolytic breakdown [136]. Numerous proteases are involved in matrix remodeling; however, the most prominent are those of the matrix metalloproteinase (MMP) family.

Synthesized as secreted or transmembrane zymogens, these ECM-degrading enzymes share common activation mechanisms and functional domains [137]. They are generally grouped based on their perceived ECM protein specificity: collagenases, gelatinases, stromelysins, and matrilysins; however, these groups do present considerable amount of overlap between MMP specificities. MMP activity is primarily controlled through transcription, proenzyme activation, or enzyme activity inhibition by an array of inhibitors [138]. Activation largely occurs outside the cells [139], with numerous growth factors, cytokines, and physical cellular interactions providing cues that either induce or repress cellular transcription of metalloprotease genes [140]. For example, MMP cell

surface localization is one mechanism that controls MMP activity. Evidence suggests that cell surface association may be necessary for optimal MMP function. Indeed, MMPs have been shown to localize around cellular extensions and then lose their proteolytic activity when expressed in secreted form [141]. By linking MMP activity to locales of physical contacts between cells and the ECM, proteolytic activity may be concentrated at crucial sites. In essence, this provides cells with a means to control ECM degradation.

MMPs can influence cellular behavior by controlling cell adhesion through several mechanisms: changes in ECM structure, release and activation of soluble signaling molecules, and/or the potential activation or inactivation of cell surface receptors. For instance, proteolytic degradation processes that occur during remodeling permit cellular invasion by removing structural barriers within the ECM. Proteolytic activity may also influence migratory activity as matrix remodeling can lead to the dynamic exposure of cryptic sites previously unrecognizable by cell surface receptors. MMP-2 cleavage of laminin-5 has been shown to generate promigratory (integrin-binding sites) cryptic fragments that lead to the migration of breast epithelial cells [142]. In addition, MMP disruption of the matrix can also induce apoptosis in anchorage-dependent cells [143], subsequently playing an important role in normal physiological death in tissues.

Remodeling events also have the potential to control cellular phenotype by altering growth factor availability instead of directly affecting the cell–ECM interactions. By affecting the mobilization and/or activation of ECM sequestered growth factors, proteases can influence differentiation. For example, the binding of TGF-beta to decorin enables decorin to serve as a reservoir for growth factors. During degradation by various MMPs, the sequestered TGF-beta is made available to carry out its biological functions such as inducing differentiation and suppressing MMP expression [144]. A feedback mechanism is present in this process as MMP-mediated activation and release of TGF-beta also acts to limit further MMP expression and consequently TGF-beta release [138].

9.4 CONCLUSIONS

This chapter has considered recent advances in our knowledge of hierarchical ECM structures and cell–matrix interactions. Through a description of the main ECM constituents and structures, integrin cell surface receptors, and their role in the stimulation of various signaling pathways, an increased appreciation for the diversity and importance of the ECM in regulating development and physiological functioning is elucidated. In particular, the ability of the ECM to supply signaling cues that guide cellular responses ranging from gene expression to cell adhesion.

With respect to the ECM structures, the major finding has been the explosion in the elucidation of the number and categories of ECM constituents and binding

domains. Many of these appear to have evolved in response to particular evolutionary pressures, permitting organisms to function in specialized environments. Although the identification of matrix constituents is of importance, the identification and characterization of protein domain functions is also important. ECM proteins have a large number of domains with each domain seemingly capable of mediating interactions with cells and other macromolecules.

Despite recent advances, we are still a long way from understanding many of the dynamic mechanisms by which information is revealed in response to changes within the local microenvironment. Complicating our understanding is the diversity among cryptic motifs, the many types of cell surface receptors, and the complexity of cell signaling pathways. Additionally, the predominant focus has been placed on integrin cell surface receptors and their interactions; however, this should neither obscure the importance of other classes of receptors, nor should it distract from other aspects of cell–matrix interactions.

The study of fundamental matrix biology has implications for tissue engineering and biomedical nanostructures. By increasing our understanding of cell–matrix interactions from the macro- to nanolength scale, it may be possible to develop nanostructured biocomposites that effectively control the temporal and spatial signals presented to cells. A key challenge, however, will be to capture the degree of complexity that is required to functionally replicate the ECM of natural tissues. Advances in fundamental matrix biology, nanofabrication, synthetic molecular self-assembly, and recombinant DNA technologies should help realize this goal by enabling the generation of materials that can provide enhanced three-dimensional tissue context maps of molecular and structural information.

ACKNOWLEDGMENTS

The authors would like to thank Dr. Gavin Jell for constructive comments on the manuscript. SM would also like to acknowledge the Institute of Biomedical engineering (Imperial college London) and the Natural Sciences and Engineering Research Council of Canada (NSERC) for providing funding support.

REFERENCES

1. Lukashev ME and Werb Z. ECM signalling: orchestrating cell behaviour and misbehaviour. *Trends Cell Biol* 1998;8:437–441.
2. Aumailley M and Gayraud B. Structure and biological activity of the extracellular matrix. *J Mol Med* 1998;76:253–265.
3. Pizzo AM, Kokini K, Vaughn LC, Waisner BZ, Voytik-Harbin SL. Extracellular matrix (ECM) microstructural composition regulates local cell–ECM biomechanics and fundamental fibroblast behavior: a multidimensional perspective. *J Appl Physiol* 2005;98:1909–1921.

4. Roskelley CD, Srebrow A, Bissell MJ. A hierarchy of ECM-mediated signalling regulates tissue-specific gene expression. *Curr Opin Cell Biol* 1995;7:736–747.
5. Wallner EI, Yang Q, Peterson DR, Wada J, Kanwar YS. Relevance of extracellular matrix, its receptors, and cell adhesion molecules in mammalian nephrogenesis. *Am J Physiol* 1998;275:F467–F477.
6. Zagris N. Extracellular matrix in development of the early embryo. *Micron* 2001;32:427–438.
7. Stevens MM and George JH. Exploring and engineering the cell surface interface. *Science* 2005;310:1135–1138.
8. Provenzano PP and Vanderby R Jr. Collagen fibril morphology and organization: implications for force transmission in ligament and tendon. *Matrix Biol* 2006; 25:71–84.
9. Ayad S, Boot-Handford R, Humphries MJ, Kadler KE, Shuttleworth A. The Extracellular Matrix Facts Book. Academic Press; London: 2004; p 1–163.
10. Kolkman JA and Stemmer WP. Directed evolution of proteins by exon shuffling. *Nat Biotechnol* 2001;19:423–428.
11. Gerhart J and Kirschner M. Conditionality and Compartmentalization. *Cells, Embryos, and Evolution: Toward a Cellular and Developmental Understanding of Phenotypic Variation and Evolutionary Adaptability*. Blackwell Science; Malden: 1997; p 238–295.
12. Alberts B, et al. *Molecular Biology of the Cell*. Garland Science; New York: 2002;1–1463.
13. Myllyharju J and Kivirikko KI. Collagens and collagen-related diseases. *Ann Med* 2001;33:7–21
14. Reichardt LF. Extracellular matrix molecules introduction. In: Kreis T, Vale R, editors. *Guidebook to the Extracellular Matrix, Anchor, and Adhesion Proteins*. 2nd ed. Oxford University Press; New York; 1999. p 335–344.
15. Aszodi A, Bateman JF, Gustafsson E, Boot-Handford R, Fassler R. Mammalian skeletogenesis and extracellular matrix: what can we learn from knockout mice? *Cell Struct Funct* 2000;25:73–84.
16. Brooke BS, Karnik SK, Li DY. Extracellular matrix in vascular morphogenesis and disease: structure versus signal. *Trends Cell Biol* 2003;13:51–56
17. Behonick DJ and Werb Z. A bit of give and take: the relationship between the extracellular matrix and the developing chondrocyte. *Mech Dev* 2003;120:1327–1336.
18. Toole BP and Linsenmayer TF. Newer knowledge of skeletogenesis: macromolecular transitions in the extracellular matrix. *Clin Orthop Relat Res* 1977;258–278.
19. Erlebacher A, Filvaroff EH, Gitelman SE, Derynck R. Toward a molecular understanding of skeletal development. *Cell* 1995;80:371–378.
20. Hall BK and Miyake T. All for one and one for all: condensations and the initiation of skeletal development. *Bioessays* 2000;22:138–147.
21. Karsenty G and Wagner EF. Reaching a genetic and molecular understanding of skeletal development. *Dev Cell* 2002;2:389–406.
22. Leipzig ND and Athanasiou KA. Cartilage Regeneration. In: Wnek G, Bowlin GL, editors. *Encyclopedia of Biomaterials and Biomedical Engineering*. Marcell Dekker, Inc.; New York: 2004. p 283–291.

23. Knudson CB and Knudson W. Cartilage Proteoglycans. *Semin Cell Dev Biol* 2001;12:69–78.
24. Dudhia J. Aggrecan, aging and assembly in articular cartilage. *Cell Mol Life Sci* 2005;62:2241–2256.
25. Faury G. Function–structure relationship of elastic arteries in evolution: from microfibrils to elastin and elastic fibres. *Pathol Biol (Paris)* 2001;49:310–325.
26. Raines EW. The Extracellular matrix can regulate vascular cell migration, proliferation, and survival: relationships to vascular disease. *Int J Exp Pathol* 2000;81:173–182.
27. Handford PA, Downing AK, Reinhardt DP, Sakai LY. Fibrill: from domain structure to supramolecular assembly *Matrix Biol* 2000;19:457–470.
28. Reinhardt DP, Chalberg SC, Sakai LY. The structure and function of fibrillin. *Ciba Found Symp* 1995; 192:128–143.
29. Rosenbloom J, Abrams WR, Mecham R. Extracellular matrix 4: the elastic fiber. *FASEB J* 1993;7:1208–1218.
30. van der Rest M and Garrone R. collagen family of proteins. *FASEB J* 1991;5: 2814–2823.
31. Abrams GA, Goodman SL, Nealey PF, Franco M, Murphy CJ. Nanoscale topography of the basement membrane underlying the corneal epithelium of the rhesus macaque. *Cell Tissue Res* 2000;299:39–46.
32. Myllyharju J and Kivirikko KI. Collagens, modifying enzymes and their mutations in humans, flies and worms. *Trends Genet* 2004;20:33–43.
33. Kietly CM and Grant ME. The collagen family: structure, assembly, and organization in the extracellular matrix. In: Royce PM, Steinmann B, editors. *Connective tissue and its heritable disorders*. 2nd ed., New York: Wiley–Liss; 2002; p 159–221.
34. Exposito JY, Cluzel C, Garrone R, Lethias C. Evolution of collagens. *Anat Rec* 2002;268:302–316.
35. Ricard-Blum S and Ruggiero F. The collagen superfamily: from the extracellular matrix to the cell membrane. *Pathol Biol (Paris)* 2005;53:430–442.
36. Prockop DJ and Kivirikko KI. Collagens: molecular biology, diseases, and potentials for therapy. *Annu Rev Biochem* 1995;64:403–434.
37. Haralson MA and Hassell JR. The extracellular matrix—an overview. In: Haralson MA, Hassell JR, editors. *Extracellular Matrix: A Practical Approach*. Oxford University Press; New York: 1995; p 1–30.
38. Lodish H, et al. Integrating cells into tissues. *Molecular Cell Biology*. 5th ed., W. H. Freeman and Company; New York: 2003; p 197–243.
39. Koch M, et al. A novel marker of tissue junctions, collagen XXII. *J Biol Chem* 2004;279:22514–22521.
40. Pollard TD and Earnshaw WC. *Extracellular matrix molecules*. Cell Biology. Saunders; New York: 2002; p 485–506.
41. Blaschke UK, Eikenberry EF, Hulmes DJ, Galla HJ, Bruckner P. Collagen XI nucleates self-assembly and limits lateral growth of cartilage fibrils. *J Biol Chem* 2000;275:10370–10378.

42. Zhang G, et al. Development of tendon structure and function: regulation of collagen fibrillogenesis. *J Musculoskelet Neuronal Interact* 2005;5:5–21.
43. Kassner A, et al. Molecular structure and interaction of recombinant human type XVI collagen. *J Mol Biol* 2004;339:835–853.
44. Kassner A, et al. Discrete integration of collagen XVI into tissue-specific collagen fibrils or beaded microfibrils. *Matrix Biol* 2003;22:131–143.
45. Kuhn K. Basement membrane (type IV) collagen. *Matrix Biol* 1995;14:439–445.
46. Keene DR, Sakai LY, Lunstrum GP, Morris NP, Burgeson RE. Type VII collagen forms an extended network of anchoring fibrils. *J Cell Biol* 1987;104: 611–621.
47. Chen M, Keene DR, Costa FK, Tahk SH, Woodley DT. The carboxyl terminus of type VII collagen mediates antiparallel dimer formation and constitutes a new antigenic epitope for epidermolysis bullosa acquisita autoantibodies. *J Biol Chem* 2001;276:21649–21655.
48. Franzke CW, Bruckner P, Bruckner-Tuderman L. Collagenous transmembrane proteins: recent insights into biology and pathology. *J Biol Chem* 2005;280: 4005–4008.
49. Garrone R. Evolution of metazoan collagens. *Prog Mol Subcell Biol* 1998;21: 119–139.
50. Vrhovski B and Weiss AS. Biochemistry of tropoelastin. *Eur J Biochem* 1998;258:1–18
51. Li B and Daggett V. Molecular basis for the extensibility of elastin. *J Muscle Res Cell Motil* 2002;23:561–573.
52. Rodgers UR and Weiss AS. Cellular Interactions With Elastin. *Pathol Biol (Paris)* 2005;53:390–398.
53. Francis G, John R, Thomas J. Biosynthetic pathway of desmosines in elastin. *Biochem J* 1973;136:45–55.
54. Kielty CM, Sherratt MJ, Shuttleworth CA. Elastic fibres. *J Cell Sci* 2002;115: 2817–2828.
55. Floquet N, et al. Structural characterization of VGVAPG, an elastin-derived peptide. *Biopolymers* 2004;76:266–280.
56. Senior RM, et al. Val-Gly-Val-Ala-Pro-Gly, a repeating peptide in elastin, is chemotactic for fibroblasts and monocytes. *J Cell Biol* 1984;99:870–874.
57. Raman R, Sasisekharan V, Sasisekharan R. Structural insights into biological roles of protein–glycosaminoglycan interactions. *Chem Biol* 2005;12:267–277.
58. Taylor KR and Gallo RL. Glycosaminoglycans and their proteoglycans: host-associated molecular patterns for initiation and modulation of inflammation. *FASEB J* 2006;20:9–22.
59. Toole BP. Hyaluronan: from extracellular glue to pericellular cue. *Nat Rev Cancer* 2004;4:528–539.
60. Lander AD. Extracellular matrix molecules: proteoglycans. In: Kreis T, Vale R, editors. *Guidebook to the Extracellular Matrix, Anchor, and Adhesion Proteins*. 2nd ed. Oxford University Press; New York: 1999; p 351–356.
61. Iozzo RV and Murdoch AD. Proteoglycans of the extracellular environment: clues from the gene and protein side offer novel perspectives in molecular diversity and function. *FASEB J* 1996;10:598–614.

62. Iozzo RV. Matrix proteoglycans: from molecular design to cellular function. *Annu Rev Biochem* 1998;67:609–652.
63. Iozzo RV, Cohen IR, Grassel S, Murdoch AD. The biology of perlecan: the multifaceted heparan sulphate proteoglycan of basement membranes and pericellular matrices. *Biochem J* 1994;302(Pt 3):625–639.
64. Bhide VM, et al. Collagen phagocytosis by fibroblasts is regulated by decorin. *J Biol Chem* 2005;280:23103–23113.
65. Danielson KG, et al. Targeted disruption of decorin leads to abnormal collagen fibril morphology and skin fragility. *J Cell Biol* 1997;136:729–743.
66. Lin X. Functions of heparan sulfate proteoglycans in cell signaling during development. *Development* 2004;131:6009–6021.
67. Hynes R. Molecular biology of fibronectin. *Annu Rev Cell Biol* 1985;1:67–90.
68. Leahy DJ, Aukhil I, Erickson HP. 2.0 A crystal structure of a four-domain segment of human fibronectin encompassing the RGD loop and synergy region. *Cell* 1996;84:155–164.
69. Groves JT. Learning the chemical language of cell-surface interactions. *Sci STKE* 2005;2005:E45.
70. Velling T, Risteli J, Wennerberg K, Mosher DF, Johansson S. Polymerization of type I and III collagens is dependent on fibronectin and enhanced by integrins alpha 11beta 1 and alpha 2beta 1. *J Biol Chem* 2002;277:37377–37381.
71. Dallas SL, et al. Fibronectin regulates latent transforming growth factor-beta (TGF beta) by controlling matrix assembly of latent TGF beta-binding protein-1. *J Biol Chem* 2005;280:18871–18880.
72. Nordahl J, Mengarelli-Widholm S, Hultenby K, Reinholt FP. Ultrastructural immunolocalization of fibronectin in epiphyseal and metaphyseal bone of young rats. *Calcif Tissue Int* 1995;57:442–449.
73. Globus RK, et al. Fibronectin is a survival factor for differentiated osteoblasts. *J Cell Sci* 1998;111(Pt 10):1385–1393.
74. Miner JH and Yurchenco PD. Laminin functions in tissue morphogenesis. *Annu Rev Cell Dev Biol* 2004;20:255–284.
75. Jones JC, Dehart GW, Gonzales M, Goldfinger LE. Laminins: an overview. *Microsc Res Tech* 2000;51:211–213.
76. Cheng YS, Champlaud MF, Burgeson RE, Marinkovich MP, Yurchenco PD. Self-assembly of laminin isoforms. *J Biol Chem* 1997;272:31525–31532.
77. Mayer U, Kohfeldt E, Timpl R. Structural and genetic analysis of laminin–nidogen interaction. *Ann N Y Acad Sci* 1998;857:130–142.
78. Yurchenco PD, Amenta PS, Patton BL. Basement membrane assembly, Stability and activities observed through a developmental lens. *Matrix Biol* 2004;22: 521–538.
79. Timpl R, et al. Structure and function of laminin Ig modules. *Matrix Biol* 2000;19:309–317.
80. Timpl R and Brown JC. The laminins. *Matrix Biol* 1994;14:275–281.
81. Quinn TM, Hunziker EB, Hauselmann HJ. Variation of cell and matrix morphologies in articular cartilage among locations in the adult human knee. *Osteoarthritis Cartilage* 2005;13:672–678.

82. Wong M and Carter DR. Articular cartilage functional histomorphology and mechanobiology: a research perspective. *Bone* 2003;33:1–13.
83. Poole AR, et al. Composition and structure of articular cartilage: a template for tissue repair. *Clin Orthop Relat Res* 2001;S26–S33
84. Almarza AJ and Athanasiou KA. Design characteristics for the tissue engineering of cartilaginous tissues. *Ann Biomed Eng* 2004;32:2–17
85. Meachim G and Stockwell RA. The Matrix. In: Freeman MAR, editor. *Adult Articular Cartilage*. Pitman; London: 1973; p 1–50.
86. Stockwell RA and Meachim G. The chondrocytes. In: Freeman MAR, editor. *Adult Articular Cartilage*. Pitman; London: 1973; p 51–99.
87. Darling EM, Hu JC, Athanasiou KA. Zonal and topographical differences in articular cartilage gene expression. *J Orthop Res* 2004;22:1182–1187.
88. Bottaro DP, Liebmann-Vinson A, Heidaran MA. Molecular signaling in bioengineered tissue microenvironments. *Ann N Y Acad Sci* 2002;961:143–153.
89. Ramirez F and Rifkin DB. Cell signaling events: a view from the matrix. *Matrix Biol* 2003;22:101–107.
90. Hyytiainen M, Penttinen C, Keski-Oja J. Latent TGF-beta binding proteins: extracellular matrix association and roles in TGF-beta activation. *Crit Rev Clin Lab Sci* 2004;41:233–264.
91. Maurer P and Hohenester E. Structural and functional aspects of calcium binding in extracellular matrix proteins. *Matrix Biol* 1997;15:569–580.
92. Cybulsky AV, McTavish AJ, Cyr MD. Extracellular matrix modulates epidermal growth factor receptor activation in rat glomerular epithelial cells. *J Clin Invest* 1994;94:68–78
93. Taipale J and Keski-Oja J. Growth factors in the extracellular matrix. *FASEB J* 1997;11:51–59.
94. Bergers G, et al. Matrix metalloproteinase-9 triggers the angiogenic switch during carcinogenesis. *Nat Cell Biol* 2000;2:737–744.
95. Schenk S, et al. Binding to EGF receptor of a laminin-5 EGF-like fragment liberated during MMP-dependent mammary gland involution. *J Cell Biol* 2003;161:197–209.
96. Davis GE and Senger DR. Endothelial extracellular matrix: biosynthesis, remodeling, and functions during vascular morphogenesis and neovessel stabilization. *Circ Res* 2005;97:1093–1107.
97. Eliceiri BP and Cheresh DA. Adhesion events in angiogenesis. *Curr Opin Cell Biol* 2001;13:563–568.
98. Serini G, Valdembri D, Bussolino F. Integrins and angiogenesis: a sticky business. *Exp Cell Res* 2006;312:651–658.
99. Stupack DG and Cheresh DA. ECM remodeling regulates angiogenesis: endothelial integrins look for new ligands. *Sci STKE* 2002;2002:E7
100. Stupack DG and Cheresh DA. Apoptotic cues from the extracellular matrix: regulators of angiogenesis. *Oncogene* 2003;22:9022–9029.
101. Koli K, Saharinen J, Hyytiainen M, Penttinen C, Keski-Oja J. Latency, activation, and binding proteins of TGF-beta. *Microsc Res Tech* 2001;52:354–362.

102. Yu Q and Stamenkovic I. Cell surface-localized matrix metalloproteinase-9 proteolytically activates TGF-beta and promotes tumor invasion and angiogenesis. *Genes Dev* 2000;14:163–176.
103. Takagi J. Structural basis for ligand recognition by rgd (Arg-Gly-Asp)-dependent integrins. *Biochem Soc Trans* 2004;32:403–406.
104. Lightner VA and Erickson HP. Binding of hexabrachion (tenascin) to the extracellular matrix and substratum and its effect on cell adhesion. *J Cell Sci* 95:1990;(Pt 2):263–277.
105. Maheshwari G, Brown G, Lauffenburger DA, Wells A, Griffith LG. Cell adhesion and motility depend on nanoscale RGD clustering. *J Cell Sci* 2000;113(Pt 10):1677–1686.
106. Aota S, Nomizu M, Yamada KM. The short amino acid sequence Pro-His-Ser-Arg-Asn in human fibronectin enhances cell-adhesive function. *J Biol Chem* 1994;269:24756–24761.
107. Johansson S, Svineng G, Wennerberg K, Armulik A, Lohikangas L. Fibronectin-integrin interactions. *Front Biosci* 1997;2:d126–d146.
108. Schenk S and Quaranta V. Tales from the crypt [ic] sites of the extracellular matrix. *Trends Cell Biol* 2003;13:366–375.
109. Maquart FX, Pasco S, Ramont L, Hornebeck W, Monboisse JC. An introduction to matrikines: extracellular matrix-derived peptides which regulate cell activity, Implication in tumor invasion. *Crit Rev Oncol Hematol* 2004;49:199–202.
110. Ingham KC, Brew SA, Erickson HP. Localization of a cryptic binding site for tenascin on fibronectin. *J Biol Chem* 2004;279:28132–28135.
111. Marneros AG and Olsen BR. The role of collagen-derived proteolytic fragments in angiogenesis. *Matrix Biol* 2001;20:337–345.
112. Keselowsky BG, Collard DM, Garcia AJ. Integrin binding specificity regulates biomaterial surface chemistry effects on cell differentiation. *Proc Natl Acad Sci USA* 2005;102:5953–5957.
113. Curtis A and Wilkinson C. New depths in cell behaviour: reactions of cells to nanotopography. *Biochem Soc Symp* 1999;65:15–26.
114. Andersson AS, et al. Nanoscale features influence epithelial cell morphology and cytokine production. *Biomaterials* 2003;24:3427–3436.
115. Orgel JP, et al. The *in situ* supermolecular structure of type I collagen. *Structure* 2001;9:1061–1069.
116. Curtis AS, et al. Cells react to nanoscale order and symmetry in their surroundings. *IEEE Trans Nanobioscience* 2004;3:61–65.
117. Cukierman E, Pankov R, Yamada KM. Cell interactions with three-dimensional matrices. *Curr Opin Cell Biol* 2002;14:633–639.
118. Cukierman E, Pankov R, Stevens DR, Yamada KM. Taking cell–matrix adhesions to the third dimension. *Science* 2001;294:1708–1712.
119. Bershadsky AD, Balaban NQ, Geiger B. Adhesion-dependent cell mechanosensitivity. *Annu Rev Cell Dev Biol* 2003;19:677–695.
120. Alenghat FJ and Ingber DE. Mechanotransduction: all signals point to cytoskeleton, matrix, and integrins. *Sci STKE* 2002;2002:E6.

121. Ingber DE. Cellular mechanotransduction: putting all the pieces together again. *FASEB J* 2006;20:811–827.
122. Giancotti FG. Integrin signaling: specificity and control of cell survival and cell cycle progression. *Curr Opin Cell Biol* 1997;9:691–700.
123. Hynes RO. Integrins: bidirectional, allosteric signaling machines. *Cell* 2002;110:673–687.
124. Zimmermann P and David G. The syndecans, tuners of transmembrane signaling. *FASEB J* 1999;(13 Suppl):S91–S100.
125. Hynes RO. Integrins: versatility, modulation, and signaling in cell adhesion. *Cell* 1992;69:11–25.
126. Zamir E and Geiger B. Molecular complexity and dynamics of cell–matrix adhesions. *J Cell Sci* 2001;114:3583–3590.
127. Giancotti FG and Ruoslahti E. Integrin signaling. *Science* 1999;285:1028–1032.
128. Emsley J, Knight CG, Farndale RW, Barnes MJ, Liddington RC. Structural basis of collagen recognition by integrin alpha2beta1. *Cell* 2000;101:47–56.
129. Geiger B, Bershadsky A, Pankov R, Yamada KM. Transmembrane crosstalk between the extracellular matrix–cytoskeleton crosstalk. *Nat Rev Mol Cell Biol* 2001;2:793–805.
130. Gilmore AP, Anokis. *Cell Death Differ* 2005;12(2 Suppl):1473–1477.
131. Hynes RO. Cell adhesion: old and new questions. *Trends Cell Biol* 1999;9:M33–M37
132. Zamir E and Geiger B. Components of cell–matrix adhesions. *J Cell Sci* 2001;114:3577–3579.
133. Lin CQ and Bissell MJ. Multi-faceted regulation of cell differentiation by extracellular matrix. *FASEB J* 1993;7:737–743.
134. Zhang Z, Vuori K, Reed JC, Ruoslahti E. The alpha 5 beta 1 integrin supports survival of cells on fibronectin and up-regulates Bcl-2 expression. *Proc Natl Acad Sci USA* 1995;92:6161–6165.
135. Moro L, et al. Integrins induce activation of EGF receptor: role in MAP kinase induction and adhesion-dependent cell survival. *EMBO J* 1998;17:6622–6632.
136. Stamenkovic I. Extracellular matrix remodelling: the role of matrix metalloproteinases. *J Pathol* 2003;200:448–464.
137. Vu TH and Werb Z. Matrix metalloproteinases: effectors of development and normal physiology. *Genes Dev* 2000;14:2123–2133.
138. Sternlicht MD and Werb Z. How matrix metalloproteinases regulate cell behavior. *Annu Rev Cell Dev Biol* 2001;17:463–516.
139. Werb Z. ECM and cell surface proteolysis: regulating cellular ecology. *Cell* 1997;91:439–442.
140. Fini ME, Cook JR, Mohan R, Brinckerhoff CE. Regulation of matrix metalloproteinase gene expression. In: Mecham RP, Parks WC, editors. *Matrix Metalloproteinases*. Academic Press; New York: 1998; p 299–356.
141. Nakahara H, et al. Transmembrane/cytoplasmic domain-mediated membrane type 1-matrix metalloprotease docking to invadopodia is required for cell invasion. *Proc Natl Acad Sci U S A* 1997;94:7959–7964.

142. Giannelli G, Falk-Marzillier J, Schiraldi O, Stetler-Stevenson WG, Quaranta V. Induction of cell migration by matrix metalloprotease-2 cleavage of laminin-5. *Science* 1997;277:225–228.
143. Mannello F, Luchetti F, Falcieri E, Papa S. Multiple roles of matrix metalloproteinases during apoptosis. *Apoptosis* 2005;10:19–24
144. Imai K, Hiramatsu A, Fukushima D, Pierschbacher MD, Okada Y. Degradation of decorin by matrix metalloproteinases: identification of the cleavage sites. kinetic analyses and transforming growth factor-beta1 release. *Biochem J* 1997;322(Pt 3): 809–814.

Cell Behavior Toward Nanostructured Surfaces

SANGAMESH G. KUMBAR, MICHELLE D. KOFRON, LAKSHMI S. NAIR, and CATO T. LAURENCIN

10.1 INTRODUCTION

A basic understanding and knowledge of cell–biomaterial surface interaction is of immense interest in tissue engineering and other related biomedical applications. Studies have shown that cells respond to the surface topography and their performances vary with topographic features [1]. Such studies on cell–biomaterial surface interactions could better predict the cell behavior under *in vivo* conditions. Based on these interactions, many biological processes such as embryogenesis, angiogenesis, or tumor metastasis can also be elucidated. This knowledge will be useful in designing various structures with different surface topographies that can elicit the desired cellular behavior when implanted in the body. Further, these cellular interactions with surface topographies are also of prime importance in other related fields such as the production of pharmaceuticals, toxicology screening, and design of various prosthetic devices [2–4].

Basement membranes are unique extracellular matrices that support cell adhesion and provide an environment for the cells to interact with the surroundings. The extracellular matrix (ECM) is composed of specific proteins, several functional groups, and growth factor reservoirs along with many tropic agents that are responsible for cellular function. Several cellular activities such as adhesion, proliferation, migration, differentiation, and cell shape are influenced by the ECM in which they reside [5–9]. The ECM is principally composed of hierarchically arranged collagen, laminin, other fibrils, and proteoglycans in a complex topography in the nanometer range. Cells

experience nanotopography and interact with nanofeatures *in vivo* as evident from Fig. 10.1c. The basement membrane is an integrated component of the ECM and measures approximately 200 nm in thickness. The basement membrane separates various tissues such as epithelia, endothelia, muscle fibers, and the nervous system from connective tissue compartments. The basement membrane is characterized by a complex surface topography consisting of intertwining fibers, ridges, and pores in the nanometer scale as is evident from Fig. 10.1a–c. The corneal membrane of rhesus macaque is presented in Fig. 10.1a [10,11]. The topographical feature measured was 178 ± 57 nm for the basement membrane height, the interpore distance was 127 ± 54 nm, and fiber and pore diameters were 52 ± 28 nm and 82 ± 49 nm, respectively [10,11]. These measured topographic feature values are similar to

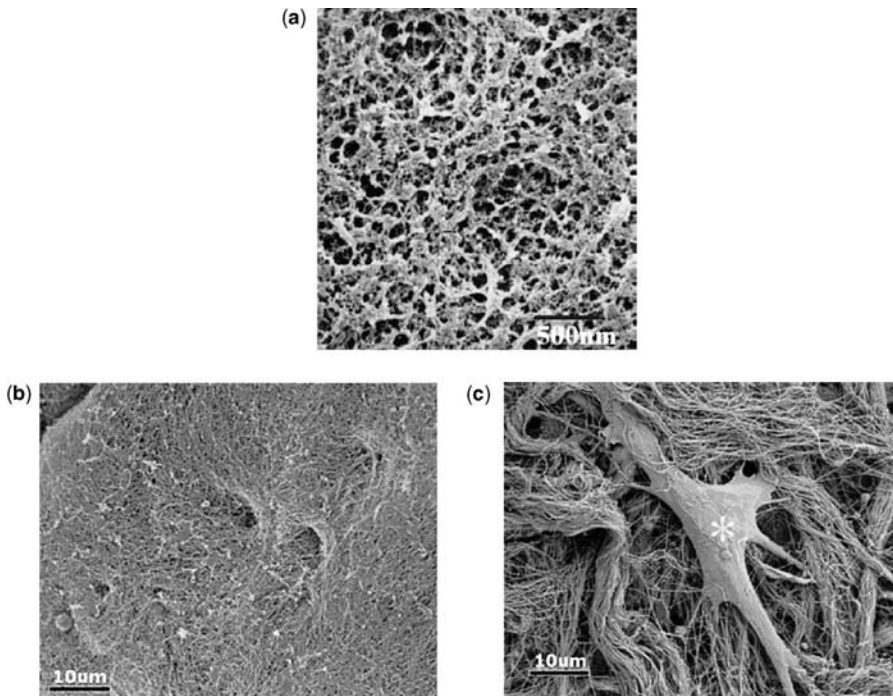


FIGURE 10.1 Scanning electron micrographs (SEM) of the basement membrane present (a) corneal of the rhesus macaque. The surface topography of the membrane is a mixture of ridges, pores, and fibers in the nanometer scale. SEM micrographs of the basement membrane from mice (b) and the dermis (c) present the dense collagen meshwork consisting of fibers and pore structures in nanometer scale. SEM (c) presents an attached fibroblast (asterisk) to the collagen meshwork (dermis). This explains the actual nanotopographic features experienced by micrometer dimension cells *in vivo*. (Reprinted with permission from (a) Reference [11], and (b and c), and Reference [12].)

the reported human basement membrane values [12, 13] SEM micrographs (b) and (c) represent the dense collagen nanofiber bundles present in the basement membrane and dermis of mouse skin. The collagen network appears less compact in the dermis (Fig. 10.1c), and a fibroblast attached to collagen nanofibrils can be seen. This explains the actual nanotopographic features experienced by micrometer dimension cells *in vivo*. This complex three-dimensional surface topography of the ECM provides not only the chemical stimulus but also biophysical cues for the cells attached to it. The ECM components and its topographic features are well characterized; however, the mechanisms that can predict the ECM–cell interactions are not well understood. The cell–ECM interaction based on integrin receptors that are associated with the cell membrane to specific sequences such as (RGD) arginine–glycine–aspartic acid part of the ECM is well characterized [14–17].

Cells produce ECM proteins to interact with the surfaces or the substrate on which they are growing. These ECM proteins act as transducers for extracellular signals, namely physical and chemical, through the cytosol membrane using focal contacts [18–20]. The cell–ECM–substrate interaction is shared among cell networks through intercellular communication. The cell–substrate interactions are critical for the integration and amplification of extracellular signals [21, 22]. Change in substrate surface properties, namely chemical composition, surface energy, surface roughness, and surface topography, can significantly affect cell–substrate interfacial characteristics and potentially influence cellular behavior and function [23]. These factors are more important when developing novel materials and surfaces for tissue engineering applications as well as prosthetic devices. Cells produce complex chemical and topographical cues in natural tissue and these cues will differ with the synthetic surfaces normally used for *in vitro* culture. Cells may encounter different surface topographies and that might vary from macro- to nano-size dimension, for example, macrotopographies experienced in bone or ligament shape, microtopographies with the shapes of other cells, and nanotopographies with protein folding and collagen banding [24].

Surface topography and biochemical cues have been shown previously to alter cell behaviors such as adhesion, orientation, cell activation, and migration significantly [25–32]. Furthermore, these topographical cues are shown to influence various modes of cell adhesion and consequently changes in cell shape, growth, apoptosis and regulation of certain gene expressions [28, 29, 33–35]. For instance, aligned fibroblasts on groove microtopography produced higher quantities of the adhesive protein fibronectin than the nonaligned cells on control plane surfaces [35, 36, 38].

Nanotopographical features of the ECM can significantly affect cellular behavior and were the inspiration for the favored nanoscale dimensions used in the design of new generation tissue engineering scaffolds and biomedical implants. Several evidences documented in the literature clearly showed the influence of nanotopography on cellular behavior that accounts for changes in morphology [25, 30], adhesion [26], motility [34], proliferation [36], endocytotic activity [37], and gene regulation [35] of various cell types, namely fibroblasts

[36, 38], osteoblasts [39], osteoclasts [40], endothelial [41], smooth muscle [42], epithelial [43, 44], and epitenon cells [45]. A detailed understanding of nanotopographical surface interaction with precursor cells and their differentiation is essential. In addition to fundamental understanding of cell–nanotopographic surface interactions, the nanotopographies may have potential applications in various biomedical fields.

10.2 NANOTOPOGRAPHIC SURFACES: FABRICATION TECHNIQUES

Presently, the experiments performed on conventional tissue culture polystyrene (TCPS) flat surfaces give an idea of cell–substrate interaction; however, they do not simulate the complex ECM topography and dimensions. Earlier studies have shown the effect of micro- and nanoscaled surface topographies on cellular functions including morphology, adhesion, motility, proliferation, and gene regulation [25–35]. Thus, various topographic features namely pores, ridges, grooves, fibers, nodes, and combinations of these features were created using a wide range of fabrication techniques [1, 46–54].

Advances in nanotechnology have enabled the fabrication of various structures in nanodimensions, and such structures vary from thin films to genetic constructs that are used for building biological molecules. All the nanofabrication techniques have been focused on two approaches, namely the top-down and bottom-up. The top-down approach includes lithographic techniques (e.g., soft, photo, colloidal, and electron beam lithography), electrospinning, polymer demixing, phase separation, evaporation techniques, and chemical etching. The bottom-up includes assembly process (supramolecular, assembly, monolayer, directed self-assembly), nanoparticle formation, and probe lithography to name a few. The resulting nanostructures may result in an ordered surface nanotopography or a random topography that will affect cellular functions, and thus cells behave according to the surface topography to which they are exposed. Nanofabrication techniques such as photolithography and electron beam lithography provide ordered nanotopographic surfaces. Recently, electrospinning has emerged as a promising technique to create nanofibers, and these nanofibers, can also be aligned to produce ordered nanotopographies [54]. Other techniques such as polymer demixing, phase separation, colloidal lithography, and self-assembly result in random surface topographies. Random topographies are created spontaneously during the process of fabrication or processing itself. These structures are randomly organized, arranged without any control on the geometry and reproducibility. However, creating these nanotopographic features is simple, inexpensive, and spontaneous. On the contrary, fabrication of ordered nanotopographic features requires complex and expensive equipments and sound technical knowledge. Table 10.1 summarizes various popularly studied nanotopography fabrication techniques, advantages, shortcomings, and observed changes in cellular behavior. We will discuss some of the most commonly used

TABLE 10.1 Summary of Nanotopographic Surfaces Created Using Different Fabrication Techniques and Observed Cellular Behavior

Technique	Topographic features	Merits	Shortcomings	Cell type used	Observed change in cellular behaviors	References
Ordered nanotopographic surfaces						
1 Electron beam lithography	Square groove, ridges, and nanopillars Dimensions 14 nm to several microns	With the aid of computer can create precise geometries and patterns without any mask	Expensive equipment, more time, lower resolution, hard to pattern large surface area	Gingival fibroblasts, embryonic <i>Xenopus</i> spinal cord neurons, rat hippocampal neurons, corneal epithelial cells, keratocytes	Strong alignment, migration, and orientation	[52, 55–62]
2 (a) Photolithography (near-UV) coupled with (b) etching	Square- and V-shaped grooves, ridges, round nodes Dimensions range between 30 nm to several microns and most frequently dimensions with few microns are created (b) Depends on the nature and time of etching agent used	(a) Create precise geometries and patterns (b) Fast, simple, and inexpensive	(a) Expensive and complicated instrumentation and nanodimensions at the higher side (b) Difficult to fabricate specific geometric features	Rat dermal fibroblasts, P388D1 macrophages, peritoneal macrophages, BHK, MDCK cells, chick embryo cerebral neuron, <i>Uromyces appendiculatus</i> fungus, murine macrophages, rat astrocytes	Improved orientation, faster spreading, migration into the structures and strong alignment	[63–69]

TABLE 10.1 (Continued)

Technique	Topographic features	Merits	Shortcomings	Cell type used	Observed change in cellular behaviors	References
3 Electrospinning (aligned nanofibers)	Aligned fibers in the nanometer dimension and can be extended to several micron thick fibers	Simple, facile, wide range of materials available for spinning ability to incorporate bioactive molecules	Can create only nonwoven fiber structures	Endothelial, neural stem cells, ligament fibroblast, smooth muscle cells, chondrocyte (HTB-94) osteoblast (MG-63)	Spreading, proliferation, phenotype expression, orientation, alignment	[70–77]
4 Nanoimprinting	Wide range of structures such as pillars, grooves, ridges possible in nanodimensions	Multilayer three-dimensional structures at comparatively lower cost than electron beam lithography	Expensive equipment and time consuming	Osteoblasts, smooth muscle cells	Strong alignment, spreading, migration, phenotype expression	[78–80]
Unordered nanotopographic surfaces						
5 Self-assembly	Can create fibers of any dimensions based on the start-up material	Process is simple, facile, low tech, can create complex functional structures. Structures are defect-free and self-healing	No direct control over fabrication, compared to lithography complex structure fabrication is difficult.	MC3T3-E1, neural, bladder, smooth muscle, aortic endothelia and neural progenitor cells. <i>In vivo</i> studies in Syrian hamsters	Adhesion, increased proliferation, differentiation, and phenotype expression.	[81–95]

6	Phase separation	Wide range of geometry and dimensions include pits, islands, fibers, and irregular pore structures	Simple, facile, no equipment needed, highly porous scaffolds with control on porosity, and scalable	No organized patterns	OCT-1 osteoblast-like cells, nerve stem cells, MC3T3-E1 preosteoblasts	Adhesion, proliferation, differentiation	[81, 96–99]
7	Colloidal lithography	Columns and islands can be created in nanometer ranges	Relatively cheap and less time consuming, can pattern large surface area with less effort	Specific feature geometries hard to design	Epitenon cells, pancreatic epithelial cells (AR4-2J), mammary epithelial cells (HC11), human bladder carcinoma, HTB-4, primary human osteoblasts, macrophages/monocytes human fibroblast	Interaction, spreading, alignment, migration, phenotype expression, and proliferation	(37, 43, 44, 100–105)
8	Electrospinning (random nanofibers)	Fibers in the nanometer dimension and can be extended to several micron thick fibers	Simple, facile, wide range of materials available for spinning ability to incorporate bioactive molecules	Can create only fibrous structures	Fibroblasts, MC3T3-E1 osteoblast-like, SMCs, NIH3T3, bone marrow stromal cells	Spreading, proliferation, phenotype expression, orientation,	[106–123]

(continued)

TABLE 10.1 (Continued)

Technique	Topographic features	Merits	Shortcomings	Cell type used	Observed change in cellular behaviors	References
9 Chemical etching	Depends on the nature and time of etching agent used	Fast, simple, and inexpensive	Difficult to get required geometry and features	Human osteoblasts CRL-11372, aortic smooth muscle cells, primary rat smooth muscle cells from thoracic aorta, bladder and cortical cells, LRM55	Adhesion, migration, proliferation and phenotype, expression	[124–127]
10 Carbon nanofibers/nanotubes	Fibers in nanodimensions 5 nm to several 100 nm in diameter and several microns in length. Various shapes straight, spiral, fishbone,	Excellent mechanical, electrical, and surface properties. Relatively easy to fabricate and no costly equipment needed	Can create only fibers and tubes and specific geometries not possible	Human osteoblasts, epidermal keratinocytes, macrophages and skin fibroblast rat astrocytes,	Compatibility, adhesion, proliferation, differentiation, morphology	[128–138]

<p>aortic smooth muscle cells, cardiac muscle cells and cortical cells, mouse skin fibroblasts, bovine bladder smooth muscle cells</p>	<p>Human fibroblasts, Adhesion, morphology, proliferation, differentiation, gene expression</p>	<p>[139–149]</p>
<p>Can only create pits, islands, or ribbons. No other specific geometries possible</p>	<p>Can pattern large surface area, low cost, high efficiency, less effort</p>	<p>Nanotopographic features such as pits, islands, or ribbons of wide range of height or depth possible</p>

nanofabrication techniques in brief while discussing the importance of nanotopographic features on cell behavior.

10.2.1 Cell Behavior Toward Nanotopographic Surfaces Created by Electron Beam Lithography

Electron beam lithography is an attractive computer-controlled technique to create precise geometries and patterns on nanoscale without the use of any mask. In brief, either positive or negative resists are used to create programmed nanotopographic features. Positive resists break down into lower molecular weight fragments when irradiated by a high energy electron beam, whereas negative resists form insoluble cross-linked networks. These irradiated resists are developed in a suitable developer. The preprogrammed nanotopographic features were created by leaching out of the resists in a developer. However, the use of negative controls limits the resolution of these features due to swelling while developing. Further, this technique requires expensive equipment and is time consuming. Many nanotopographic features including square grooves, ridges, and nanopillars, created using the current technique, were used to study *in vitro* cellular behavior to elicit the importance of nanoscale features for a variety of biomedical applications [52, 55–62].

Micro- and nanotopographic features containing grooves and ridges with dimensions varying from 400 to 4000 nm directed the alignment and migration of SV40-transformed human corneal epithelial cells along the grooves and ridges of all the dimensions [55]. It was observed that cell colonies migrated out along grooves and ridges in circular zones and migrated perpendicular to ridges in some cases. On flat controls equal migration was observed in all directions. Stress fibers and focal adhesions were also aligned along the ridges and groves [55]. Keratocytes showed a stronger alignment than epithelial cells to these nanotopographic surfaces [20]. Keratocytes presented fewer stress fibers and focal adhesions on nanodimensions when compared to micro and flat control surfaces [56]. Nanotopographic features containing varying widths of grooves and ridges ranging from nano- to micron dimensions provided stimulus for human corneal epithelial cells [57]. Cells were found to align along the grooves and the ridges of nanodimensions with elongated structures while rounded cells were observed on smooth surfaces as seen in Fig. 10.2. On the nanopatterned surfaces, cells periodically extend filopodia along the direction of the nanofeature as shown in Fig. 10.2c [57]. When the culture medium was changed from DMEM/F12 to Epilife medium, human corneal epithelial cells aligned perpendicular to the nanotopographic features as evident from Fig. 10.2d whereas parallel alignment was observed on microscale topographies [58]. Such an observed change in alignment is presumably due to a change in focal adhesion structure. Human gingival fibroblasts and rat neurons on patterned surfaces with grooves showed focal adhesion contacts and cells aligned to the grooves [59, 60]. *Xenopus* neuritis aligned parallel to all groove sizes whereas hippocampal neuritis aligned perpendicular to narrow, shallow

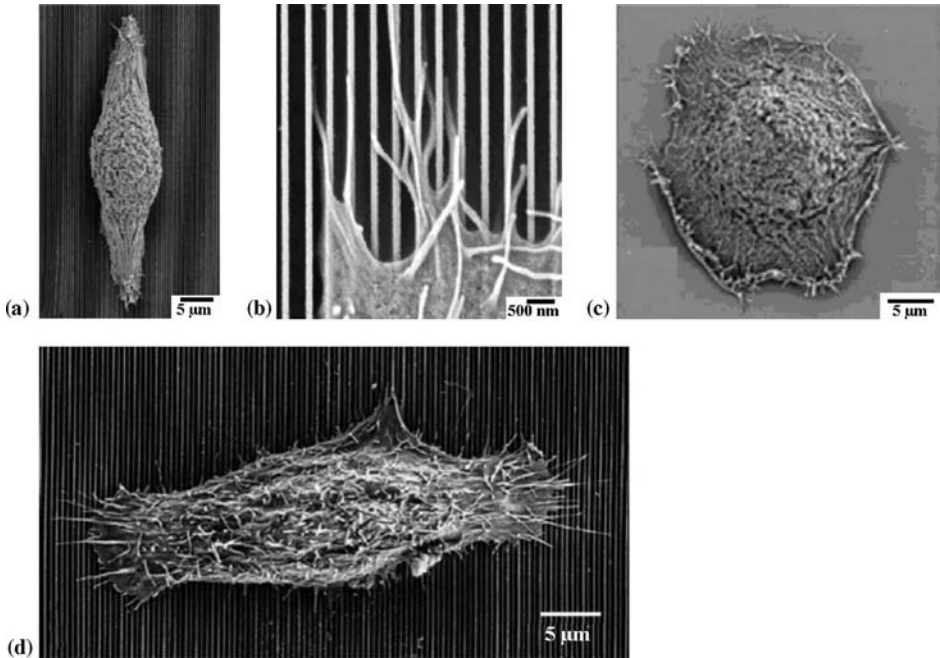


FIGURE 10.2 SEM micrographs of human corneal epithelial cells cultured in DMEM/F12 on (a) patterned nanotopography elongated and aligned (b) patterned surfaces filopodia extend in the direction of features. (c) Flat substrates with rounded morphology. (d) Patterned surfaces cultured in Epilife medium showing perpendicular alignment to nanotopographic features. (Reprinted with permission from (a, b and c) Reference [57] and (d) Reference [58].)

grooves [60, 61]. Nanotopographic surfaces containing ordered features of pillars, pits, cliffs, and random gold colloid particles showed topography dependence in their adhesion. Ordered cliffs showed enhanced adhesion at the cliff, edges. Reduction in cell adhesion was observed on pits and pillars when compared to flat and colloid particle surfaces [52]. Anisotropic features in the size range of 200–2000 nm on polyurethane surfaces showed decreasing proliferation of corneal epithelial cells with decreasing dimensions when compared to planar surfaces [62].

10.2.2 Cell Behavior Toward Nanotopographic Surfaces Created by Photolithography

Photolithography is one of the popular techniques to create nanotopographic surfaces containing many geometric features including grooves, ridges, and round nodes from nanometers to several microns in size. Photolithography involves a series of processes in brief; cleaned surfaces of silicon wafers are coated with photoresist and soft baked to remove the solvents from photoresist

that converts the resist photosensitive. The photomask containing previously defined geometric features aligned with the silicon surface and exposed to light source followed by etching and developing leaves the predetermined patterned surfaces. The hard baking process improves the adhesion of photoresist to silicon wafer and hardens the photoresist. Photolithography can create precise geometries and patterns but require expensive complicated instrumentation, and mostly microsized topographies can be created easily. Thus created nanotopographic features elicit changes in cellular functions including orientation, interaction, morphology, and differentiation based on the topography and dimensions they are exposed to [63–69].

Implant surfaces containing nodes of 2 and 5 μm diameter and having different heights in nanometer length showed fewer mononuclear cells and thinner fibrous capsules when implanted in a rabbit model than the control planar and 8- μm -diameter grooved surfaces [68]. Also, cells appeared to be elongated and with more number of filopodia on nanotextured surfaces, whereas cells assumed a rounded shape with less number of filopodia indicating less interaction with the implant surfaces [68]. Nanotopographic features containing rough surfaces were created by reactive ion etching, and smooth wet etched surfaces were created on silicon wafers showing surface-dependent adhesion behavior to rat astrocytes [69]. Transformed astrocytes showed preferential attachment and a spread morphology on wet etched surfaces. Columnar nanotopographic features created by reaction ion beam etching resulted in round morphology, loose attachment, and exhibition of complex surface projections of transformed cells [69]. Rat fibroblasts on square grooves with submicron dimension oriented and elongated along grooves [63]. P388D1 macrophages, rat peritoneal macrophages, and chick embryo cerebral neurons showed increasing orientation and spreading with increasing groove depth [64, 65]. Well-characterized cytoskeleton and F-actin and vinculin accumulation was observed along the edges of the grooves [64, 66]. *Uromyces appendiculatus* fungus cells showed a high degree of orientation to the polystyrene nanoridge spacing of 0.5–6.7 μm , whereas ridge height of 500 nm showed maximum cell differentiation compared to ridges of height greater than 1 μm or less than 0.25 μm [67].

10.2.3 Cell Behavior Toward Nanotopographic Surfaces Composed of Aligned Nanofibers by Electrospinning

Polymeric nanofibers are created using a variety of techniques such as template synthesis, phase separation, drawing, self-assembly, and electrospinning. Among these techniques, electrospinning is extensively studied since the process is simple, elegant, and facile, and can create polymeric fibers in the range of a few nanometers to several micron thicknesses using the same experimental setup [70–77]. During the process of electrospinning, fibers randomly deposited on the grounded collector create unordered surface topographies. Aligned nanofibers that could present ordered nanotopographies can be created by using a high speed rotating collector, applying an auxiliary

electric field, and using a sharp edged thin wheel collector or a frame collector in place of the stationary grounded collector [71–76]. Thus created nanostructured surfaces both aligned and random were used as tissue engineering constructs, and cells respond differently to the surfaces they were exposed to [71–76].

Human coronary artery endothelial cells on aligned gelatin-modified poly(caprolactone) (PCL) nanofibers in the diameter range of 200–1000 nm provided improved adhesion, spreading, and proliferation than the control PCL and random nanofibers [71]. These aligned nanofibers strongly cause the orientation of endothelial cells parallel to the nanofibers with spindle-like structures; also well-defined cytoskeleton and enhanced phenotypic expression were observed. Shear stress caused by the blood flow orients the endothelial cells in the flow direction *in vivo*, and surface-modified aligned nanofibers simulate the actual *in vivo* condition in a static culture that provides an alternative to complex dynamic culture [71]. Neonatal mouse cerebellum C17.2 stem cells (NSCs) on PLLA-aligned and random nanofibers attached well and changed their original round shape to elongated spindle-like shape that provided morphological evidence for NSC differentiation. The direction of NSC elongation and its neurite outgrowth was exactly parallel to the direction of aligned nanofibers with a higher rate of NSC differentiation than the control. Increased interaction between the filament-like structures produced by NSCs was observed on aligned fibers that were absent on random nanofibers as seen from Fig. 10.3 [72]. Such aligned nanofibers could be used as a potential

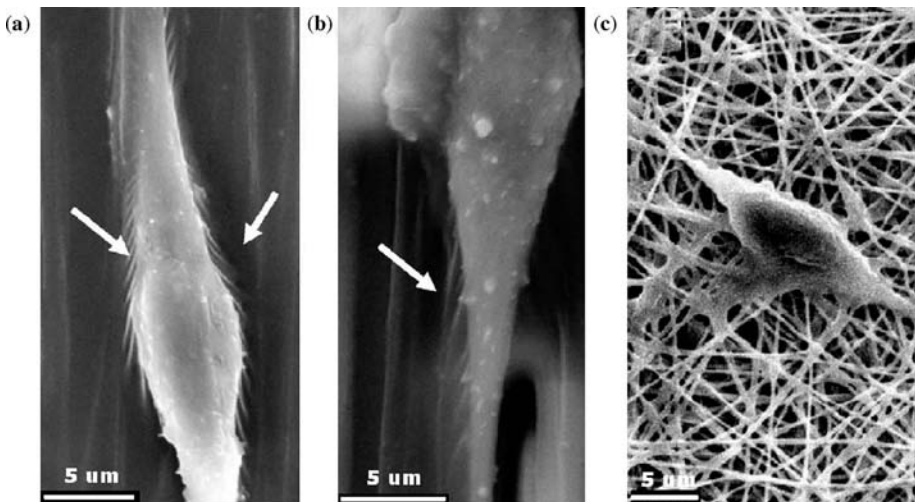


FIGURE 10.3 NSCs on PLLA-aligned fibers had an apparent bipolar elongated morphology with neuritis, and filament-like structures marked with arrows (a) attach to nanofibers and (b) microfibers, and (c) absence of filament-like structures on random nanofibers. (Reprinted with permission from Reference [72].)

cell carrier for neural tissue engineering. Human ligament fibroblast (HLF) on aligned polyurethane nanofibers also oriented in the direction of aligned nanofibers and had a spindle shape [73]. Fibroblasts synthesized significantly more collagen on aligned nanofibers, and further HLFs were more sensitive to the stress applied in longitudinal direction resulting in an increased production of collagen in response to applied strain [73]. Human coronary artery smooth muscle cells (SMCs) on poly(L-lactid-co-ε-caprolactone)-aligned nanofibers attached and migrated along the direction of the nanofiber orientation and maintained a spindle-like structure [74, 76]. SMCs resulted in increased adhesion and proliferation on aligned nanofibers, and cytoskeleton proteins inside SMCs were parallel to the direction of the nanofibers. Chitosan nanofibers and aligned nanofibers promoted the attachment of human osteoblasts and chondrocytes and maintained characteristic morphology throughout the study [75]. The observed cell orientation on aligned nanofibers presumably follows the contact guidance theory, which states that cells have a higher probability of migrating in directions of chemical, structural, and/or mechanical properties of the substratum [77].

10.2.4 Cell Behavior Toward Nanotopographic Surfaces Created by Nanoimprinting

Nanoimprint lithography can create ordered nanotopographic features such as pillars, grooves, and ridges at the required dimensions. In brief, the technique utilizes a hard mold containing previously defined nanoscale patterns. Wafer substrates covered by polymer cast under the controlled temperature and pressure will be imprinted by the hard mold. Hard mold embossing creates a thickness contrast on the polymer surface with the required nanotopographic features. It is possible to create multilayer three-dimensional structures using nanoimprint lithography at comparatively lower cost than electron beam lithography. However, the present technique also utilizes expensive equipment, and the process is time consuming. Thus, created ordered nanotopographic features elicit changes in cellular functions *in vitro* [78–80].

Nanopatterned gratings with 350 nm line width, 700 nm pitch, and 350 nm depth created on poly(methyl methacrylate) and poly(dimethylsiloxane) showed decreased proliferation of bovine pulmonary artery SMCs than the flat control [78]. More than 90% of the cells were aligned and assumed an elongated structure in both cytoskeleton and nuclei on nanopatterned surfaces as seen in Fig. 10.4 [78]. Also, the polarization of microtubule organizing centers of the SMCs associated with cell migration showed a preference toward the axis of cell alignment in an *in vitro* wound healing assay on nanopatterned surfaces. Polystyrene surfaces containing nanopillars in the diameter range of 160–1000 nm and 1000 nm height were tested as an alternative tissue culture plate by studying the *in vitro* behavior of epithelial-like cell line (HeLa) on the said topography [79]. HeLa cells adhered only to the heads of the nanopillar sheet with a significantly lower number of cells than the control and acquired

rounded morphology on nanopillars in comparison to a spread structure on the flat control. Also, actin molecules appeared to localize to the circumference of the nanopillar heads, whereas vinculin molecules were distributed homogeneously in regions away from the nanopillar heads [79]. Thus, the low adhesion properties exhibited by the cells might lead to alternative tissue culture plates that do not require conventional trypsin treatment to lift the cells. Polystyrene nanopatterned surfaces with grooves having two different depths of 50 and 150 nm with a periodicity of 500 ± 100 nm showed a strong

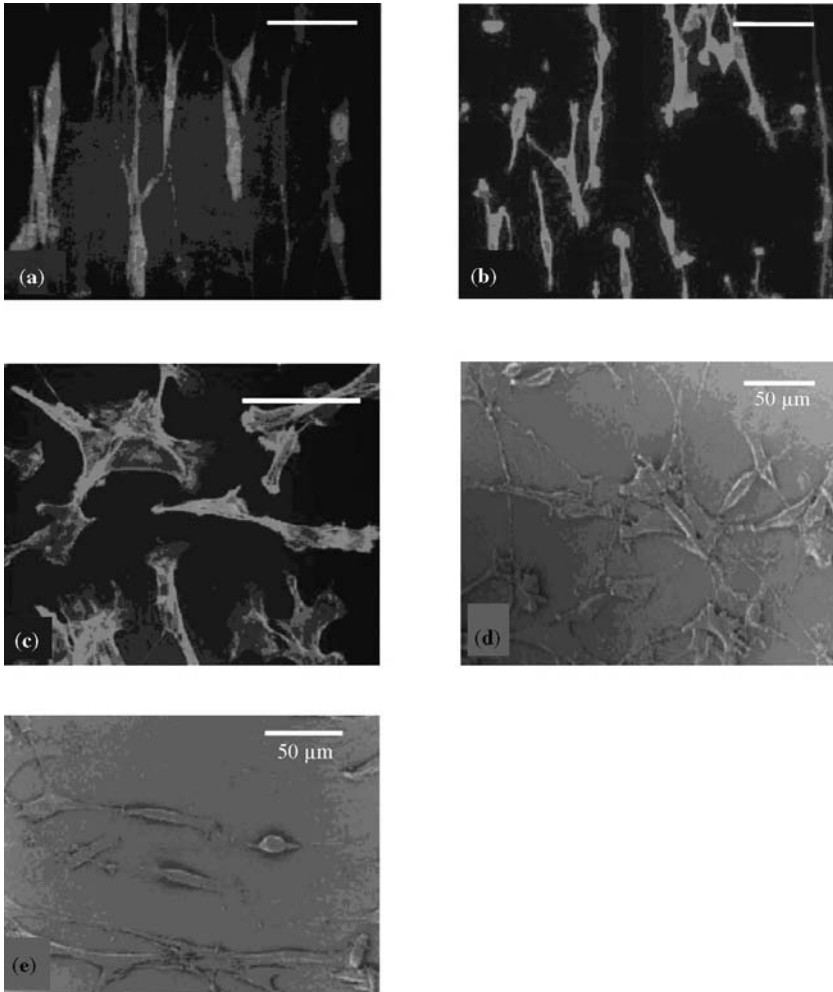


FIGURE 10.4 Confocal micrographs of F-actin stained SMCs on (a) nanoimprinted on PMMA, (b) PDMS, and (c) nonpatterned PMMA surfaces (scale bar $50 \mu\text{m}$). SEM micrographs on (d) nonpatterned PMMA and (e) nanoimprinted surfaces show elongated structures on patterned surfaces. (Reprinted with permission from Reference [78].)

alignment and orientation of primary osteoblasts in the direction of grooves [80]. The exposed patterned surface topography promoted the cell elongation, cytoskeleton actin, and actinin molecules' orientation in the direction of the grooves. However, vinculin, a protein associated with focal adhesions, appeared to concentrate at the opposite end of aligned cells presumably due to the balancing tension generated from the surface anisotropy [80]. The observed anisotropic behavior of osteoblasts on the nanogrooves might enhance cell settlement on the nanotopographic surface.

10.2.5 Cell Behavior Toward Nanotopographic Surfaces Created by Self-Assembly

Self-assembly is a powerful technique to create nanostructures from various polymers and biomolecules via molecular self-assembly. Molecules self-assemble by virtue of weak noncovalent bonds. Such interaction forces may be hydrogen bonds, electrostatic interactions, hydrophobic interactions, and van der Waals forces. All the biomacromolecules interact and self-assemble to create complex functional defect-free and self-healing nanostructures. The molecular self-assembly is simple, facile, and scalable. However, no direct control over the fabrication process is possible, and also it is not possible, to design specific geometric features. Using the bottom-up approach, many nanostructures created were studied as scaffold materials for various biomedical applications [81–95].

Self-assembled peptide nanofiber scaffolds (SAPNS) of branched and linear peptide-amphiphile molecules as coating on poly(glycolic acid) scaffolds resulted in preferential attachment of primary human smooth muscle cells on branched than on linear peptide amphiphile and control [88]. The SAPNS as sciatic nerve grafts could partially restore the optic tract and functional vision in brachium transected experimental adult animals *in vivo* [94]. Rat mesenchymal stem cells on SAPNS with RGD sequence resulted in increased attachment, alkaline phosphatase (ALP) activity, and osteocalcin content than the SAPNS without RGD sequence and tissue culture polystyrene [95]. Hybrid SAPNS scaffolds also supported MSC and resulted in homogeneous bone formation *in vivo* in a rat subcutaneous model. In perfusion, *in vitro* culture registered higher alkaline phosphatase activity and osteocalcin content indicated enhanced osteogenic differentiation of MSC than control and static culture [84]. The pentapeptide epitope isoleucine–lysine–valine–alanine–valine (IKVAV) containing SAPNS supported the neural progenitor cells and caused selective rapid differentiation into neurons with lesser number of astrocytes [87]. The IKVAV-incorporated SAPNS combine bioactive epitope and nanotopography elicits the observed advantages [87]. MC3T3-E1 cells not only survive and proliferate on SAPNS but also possibly utilize peptide molecules in their metabolic pathways [89]. Functionalized and biomimetic SAPNS can elicit cellular events such as wound healing and tissue regeneration by creating ECM recognition domains with nanofeatures [86].

10.2.6 Cell Behavior Toward Nanotopographic Surfaces Created by Phase Separation

The phase separation technique used for the fabrication of highly porous scaffolds with controllable porosity can create a wide range of geometries and dimensions including pits, fibers, and irregular pore structures [81, 96–99]. Phase separation either solid–liquid or liquid–liquid can be induced by lowering the solution temperature. In brief, to a polymer solution in a low melting point solvent, addition of a small quantity of water generates polymer-rich and polymer-poor phases. Such a system cooled below solvent melting point followed by vacuum drying to sublime the solvent produces the porous scaffolds of both micro- and nanostructures. The technique can create highly porous scaffolds with controllable porosity. The process is simple, facile, and scalable and does not require any costly equipment. The inability to fabricate well-organized patterns and specific geometric features is the limiting factor of this technique.

Nanostructures formed by phase separation technique favored the adhesion, proliferation, and differentiation of different cell lines studied. MC3T3-E1 showed better response on PLLA nanofiber scaffolds than the solid walled controls created using reverse solid freeform fabrication and thermal phase separation technique [96]. Significantly higher cell number, and osteocalcin and bone sialoprotein expressions were observed on nanofiber scaffolds. However, observed lower expression of type I collagen on nanofibers was presumably due to the quicker differentiation of preosteoblasts [96]. PLLA nanofiber scaffolds with an average diameter of 200 nm fabricated by phase separation technique supported the nerve stem cell differentiation and neurite outgrowth [99]. Figure 10.5 presents the neonatal mouse cerebellum C17-2 stem cells on PLLA nanofiber scaffolds presenting a differentiated cell with neurite penetration into the scaffolds [99]. Thus, the nanofiber structures could mimic the ECM

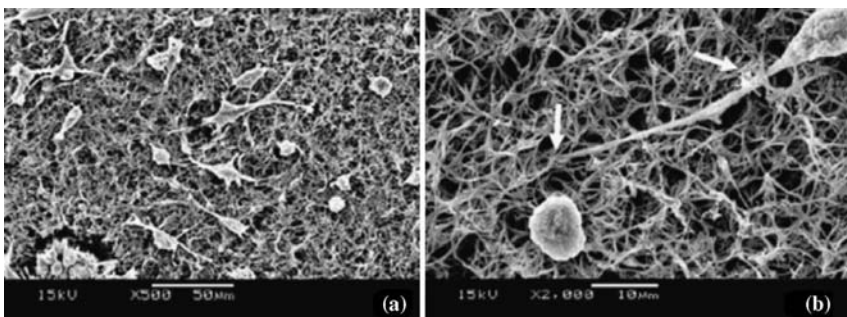


FIGURE 10.5 SEM micrographs of PLLA nanofiber scaffolds fabricated by the phase separation technique presenting neonatal mouse cerebellum stem cells seeded on these materials after 1 day in culture (a) at a magnification of 500 \times and (b) differentiated cells with neurite penetration into the nanofiber scaffolds identified by arrows at 2000 \times . (Reprinted with permission from Reference [99].)

structure and support the adhesion, proliferation, and phenotype expression of the cells.

10.2.7 Cell Behavior Toward Nanotopographic Surfaces Created by Colloidal Lithography

Colloidal lithography provides a means to pattern surfaces containing columns and pits with controllable dimensions. This technique utilizes nanocolloids as an etch mask that is dispersed and self-assembled electrostatically into a monolayer on the substrate surfaces. The area surrounding the nanocolloids is etched away along with the surface itself leaving a patterned substrate using a suitable etching technique. For example, surface nanotopographies containing columns can be created using chemically assisted ion beam etching or directed ion beam bombardment and pits with film evaporation technique. Patterned surface properties can be varied changing colloid size, colloid ionic strength, and the monolayer coverage on the substrate surface. Colloidal lithography is relatively cheap and less time consuming, and can pattern large surface area with less effort; however, it is difficult to create specific feature geometries. Cells on these columns and grooves in nanoscale showed interesting structural, morphological, and phenotypic behaviors on these nanotopographies [37, 43, 44, 100–105].

Columns with an average height of 160 nm, diameter of 100 nm and with a 230 nm spacing between the features produced by colloidal lithography resulted in less spreading of human fibroblasts (h-tert BJ1) compared to control plane surfaces [100]. Microarray analysis showed a shift in gene level expression when compared to microtopographic surfaces. Upregulation of several genes responsible for cell–cell signaling, wound healing, proliferation, and cell differentiation, and downregulation of several genes such as collagen, and cytoskeleton were observed. Such observed changes in gene level expression were presumably due to the decreased cell spreading on colloidal nanotopography [100]. The fibroblasts assumed more stellate and less well-spread morphology on these nanocolumns. Fibroblasts produced increased filopodia and were observed to interact with nanocolumns regularly with filopodia [103]. An attempt to endocytose the nanocolumns by fibroblasts failed; however, some cells appeared to try and go further producing high levels of Rac at sites of pseudopodia formation [37]. Human fibroblasts cultured for a short duration of time, 180 min, showed decreased cell adhesion and spreading on these nanocolumns than the planar control [101]. Fibroblasts showed less well-organized actin and vimentin cytoskeletons on these nanocolumns; however, tubulin cytoskeleton was well organized with least number of microtubules [101]. Silicon wafer surfaces modified with 50-nm colloidal gold particles resulted in the direct interaction with the primary rat epitenon cells at the peripheral cell membrane [102]. Nanocolumns with diameters of 58, 91, 111, and 166 nm resulted in increased spreading of rat pancreatic epithelial cells when compared to flat surfaces and spreading increased with increase in

column diameter [44]. Epithelial cells (human bladder carcinoma, HTB4) on nanotopographies containing continuous edged grooves with 184 nm depth were seen to become aligned [43]. Cells on nanotopographies containing hemispheres with 100 nm height and 167 nm diameter assumed less spread, less round, and more stellate morphology than the control. Cells registered no change in the production of cytokine on both the nanofeatures and a decreased production of IL-6 and IL-8 on the nanofeatures than the control [43]. Mouse mammary epithelial cells (HC11) on nanotopographies containing either continuous or discontinuous edges of various depths ranging from 40 to 400 nm were seen to align on the grooves than the control [104]. Grooved surfaces with continuous edges favored the orientation of cells with more elongated cells than grooves with discontinuous edges [104]. Nanotopographies containing hemispherical features with a height of 110 nm and various packing densities of these features were coated with Ti oxide thin films to obtain a single chemistry [105]. These nanotopographies induced the release of chemotactic macrophage activation agents and caused stress fiber and fibronectin formation from the primary human macrophages. Primary human osteoblasts were seen to migrate away from these nanofeatures [105]. The nanotopographies present physical cues for the cells that can elicit responses to align the cells, increase or reduce cell adhesion and proliferation, alter differentiation, and increase motility.

10.2.8 Cell Behavior Toward Nanotopographic Surfaces Composed of Random Nanofibers Created by Electrospinning

Cells identify the exposed surface topography and random nanofiber porous matrices influence the adhesion, spreading, proliferation, and gene expression of various cell types seeded on them. Mouse fibroblasts adhered, migrated through the pores, and integrated well with PLAGA nanofibers, and the development of the cell growth was guided by nanofiber architecture [106]. Fibroblasts changed morphology from a spread and flat to a long and spindle shape on nanofibers when adhered to the nanofibers detaching the flat surfaces [107]. Cross-linked gelatin nanofibers with improved mechanical properties and thermal stability supported human dermal fibroblast proliferation, and a linear increase in cell number was observed with time [108]. Scaffolds of polystyrene nanofiber resulted in a significant increase in smooth muscle cell attachment than control, and the ECN produced by oriented nanofibers was similar to native bladder tissue [109]. MC3T3-E1 cells showed significantly increased cell number and osteocalcin, alkaline phosphate production with increasing culture time on silk fibroin nanofibers [110, 111]. The silk fibroin nanofiber scaffolds *in vivo* showed good biocompatibility and enhanced bone regeneration without any inflammatory reaction [110]. Human coronary artery SMCs showed normal phenotypic shape on polycaprolactone and collagen nanofibers, and nanofibers coated with collagen resulted in the migration of SMCs inside the nanofiber scaffolds and formation of smooth muscle tissue [112–114]. NIH 3T3

fibroblasts and normal rat kidney cells showed the morphology and characteristics of their counterparts *in vivo* on polyamide nanofibers [115]. Bone marrow stromal cells' (BMSCs) attachment and proliferation was favored on gelatin/PCL nanofibers, and cells were able to migrate inside the scaffold [116]. Increased proliferation of H9c2 cardiac rat myoblasts was observed on polyaniline–gelatin blend nanofibers with different cell morphologies at the initial time point; however, similar cell density and morphology were attained after 1 week on all the nanofiber scaffolds as the cultures reached confluence [117, 118]. Cell–nanofiber interaction and orientation is more pronounced in the initial culture time, and once the confluence is reached it is difficult to identify morphological changes. Hepatocytes cultured on the galactosylated poly(ϵ -caprolactone-co-ethyl ethylene phosphate) (PCLEEP) nanofibers exhibited similar functional profiles as on flat control surfaces; however, morphological changes were observed. Hepatocytes formed 50–300- μm spheroids on flat surfaces whereas smaller aggregates of 20–100 μm were formed on nanofiber surfaces [119]. Random and fused surface topographies having fiber diameters in the range of 140 nm to 2.1 μm showed increased MC3T3-E1 osteoprogenitor cell density in the presence of osteogenic factors on the fibers than the smooth surfaces. The cell density increased with increasing fiber diameter while ALP expression was independent of surface topography [120]. Osteoblast-like cells on starch/polycaprolactone micronanofibers showed interesting morphological and phenotype expression behavior [121]. With the introduction of nanofiber structures on microfiber scaffolds, osteoblasts organized to bridge between microfibers and possessed much more spread and stretched morphology in contrast to continuous monolayer on microfibers. Additionally, the presence of nanostructure resulted in increased ALP activity than the microfibers. Nano–microscaffolds were fabricated by electrospinning nanofibers on PLAGA knitted scaffolds, and porcine bone marrow stromal cells showed improved cellular behavior on nanofiber combined scaffold than the control [122]. Increased cell attachment, faster cell proliferation, and higher expression of collagen I, decorin, and biglycan genes were observed on nanofiber-included scaffolds. Increased adhesion and proliferation of human umbilical vein endothelial cells were observed on poly(L-lactide-co- ϵ -caprolactone) nanofiber matrices (0.3–1.2 μm) whereas a decline in cell adhesion and restricted spreading was observed on larger fiber diameter (7.0 μm) [123].

10.2.9 Cell Behavior Toward Nanotopographic Surfaces Created by Chemical Etching

Chemical etching is a surface modification process to create surface roughness in nanometer scale length. In a typical procedure, material surfaces are soaked in a variety of etchants such as sodium hydroxide (NaOH), nitric acid (HNO_3), and hydrofluoric acid (HF) to name a few and the selection of the etchants depends on the material properties [124–127]. The material surface

disintegrated as they were exposed to etchants, and the surface became rough with pits and projections in nanometer scale length. It is possible to vary the surface roughness by varying exposure time, nature, and concentration of etchants to get various surface roughness dimensions in nanoscale. This process is fast, simple, and inexpensive; however, it is not possible to get required geometry features since it is a surface treatment phenomenon. Thus, created nanometer-scale roughness can potentially affect cellular behavior [124–127].

Compacts of selenium (Se) metal particles in micron- and nanometer-size range were tested as an anticarcinogenic orthopedic material [124]. These compacts were chemically etched with different concentrations of sodium hydroxide to create surface roughness in nanometer scale. Osteoblast densities increased on both nano- and microparticles with nanoscale roughness when compared to reference wrought titanium and Se microparticles after 24 h of cell culture under standard *in vitro* conditions [124]. The pillar patterned silicon wafers were subjected to wet chemical etch to produce nanometer-scale surface roughness, and astrocytes showed preferential attachment to these surfaces [125]. Transformed astrocytes preferred the wet etched surface to the unmodified silicon substrate as seen in Fig. 10.6 [125]. The degree of selective adhesion and spreading increased with duration of wet etch presumably due to the increased surface area. Primary cortical astrocytes from neonatal rats showed a preference for silicon glass over the wet etched surface. Such observed cellular behaviors are presumably due to the different cell types in the study [125]. Nanostructures created on PLAGA and PU surfaces by chemical etching showed improved adhesion and proliferation of bladder smooth muscle cells [126]. Surface chemistry and increased nanometer surface roughness created after prolonged chemical etching brought changes in the observed cellular behavior. Nanostructures produced after longer duration of etching on

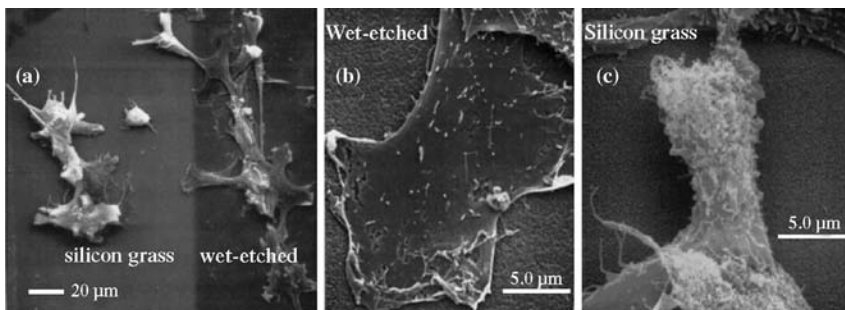


FIGURE 10.6 Transformed astrocytes cell line (LRM55) on (a) unmodified silicon glass and wet etched glass surface, and (b) the same at higher magnification. Cells appear flat and well attached showing very few projections on wet etched surfaces, whereas cells appear not closely adhered to the surface that contains the complex projections and ruffles. (Reprinted with permission from Reference [125].)

PLAGA surfaces registered significantly higher cell number compared to submicron surfaces, flat untreated and control glass surfaces. While nanostructured surfaces of PU did not show increasing proliferation trend with increasing nanometer surface roughness, chemically treated surfaces and submicron dimension surface roughness showed higher cell number than the control and conventional flat surfaces [126]. Further nanometer surface roughness on PLAGA resulted in absorption of significantly more vitronectin and fibronectin from serum compared to untreated flat PLAGA surfaces [127]. Significantly higher amounts of proteins, namely fibronectin and vitronectin adsorptions, enhanced the vascular smooth muscle cell and endothelial cell density presumably due to the cellular recognition sites present on the proteins. It is also observed that blocking of cell-binding epitopes of fibronectin and vitronectin on nanometer surface roughness resulted in significantly decreased vascular cell adhesion on nanostructured surfaces [127].

10.2.10 Cell Behavior Toward Nanotopographic Surfaces Created by Incorporating Carbon Nanotubes/Nanofibers

Carbon nanostructures such as carbon nanotubes and nanofibers possess outstanding physical and chemical properties and have a diversified application range. Carbon nanotubes can be either multiwalled nanotubes (MWNTs) or single-walled nanotubes (SWNTs). Carbon nanofibers are essentially of filamentous structure and can assume various shapes such as straight, spiral, or fishbone depending on the metal catalyst used. These carbon nanostructures are fabricated in industrial scale by three main methods, namely electric arc discharge, laser ablation, and catalytic chemical vapor deposition (CVD). Usually these processes simultaneously produce SWNTs, MWNTs, fullerenes, and a considerable amount of soot and carbon nanoparticles and need further purification to isolate each component. However, the yield of individual nanostructures varies depending on the method and fabrication condition used. Thus, produced carbon nanostructures are 5 nm to several 100 nm in diameter and several microns in length and have excellent mechanical, electrical, and surface properties and a potential utility in various biomedical applications including tissue engineering scaffolds [128–138].

Osteoblasts registered size-dependent behavior on multiwalled carbon nanofibers with diameters ranging from 60 to 200 nm in an *in vitro* culture of 21 days. Increased osteoblast proliferation, ALP synthesis, and calcium depositions were observed on carbon nanofibers with lesser diameter than the control (larger borosilicate glass) [129]. Osteoblasts, fibroblasts, chondrocytes, and smooth muscle cells showed dimension-dependent behavior on carbon nanofibers with the diameter range of 60–200 nm [130]. Osteoblasts adhesion increased with decreasing fiber diameter as previously observed [129], whereas other cells were not influenced by fiber dimension. Adhesion of fibroblasts, chondrocytes, and smooth muscle cells decreased with a decrease in nanofiber diameter and were dependent on carbon nanofiber chemistry. Further,

PLAGA carbon nanofiber composites enhanced the osteoblast adhesion that increased with lower diameter nanofiber dispersions [130]. SWNTs showed biocompatibility with cardiomyocytes in culture; however, slight modification in cell shape was observed microscopically due to the binding of carbon nanotubes to cell membranes that affected the cell count and viability only after 3 days of culture [128]. Polycarbonate urethane composites with different weight percentages of carbon nanofibers were used to study the adhesion behavior of astrocytes and osteoblasts on these composites and registered a size-dependent adhesion behavior [131, 132]. Astrocytes preferentially adhered and proliferated on carbon nanofibers with higher fiber diameter. Osteoblasts preferentially adhered and proliferated well on greater weight percentages of carbon nanofibers with least fiber diameter composites, whereas astrocytes showed reduced adhesion and proliferation on these composites [131, 132]. Neurons also showed improved adhesion and proliferation on these composites [131]. Such observed phenomenon is presumably due to the high degree of surface roughness in the nanometer scale. Osteosarcoma ROS 17/2.8 cells cultured on chemically modified SWNTs and MWNTs supported osteoblast proliferation. Nanotubes carrying neutral electric charge resulted in increased cell growth and produced plate-shaped crystals. Osteoblasts presented a dramatic change in cell morphology on MWNTs, which was correlated with changes in plasma membrane functions [133]. Osteoblasts and fibroblasts exhibited better viability for high purity MWNTs, and nanotubes induced an increase in collagen expression by these cells [135]. High purity SWNTs and fullerenes offered a very low toxicity to human macrophage cells and did not simulate nitric oxide release from murine macrophage cells *in vitro* [134]. MWNTs induced the release of the proinflammatory cytokine interleukin 8 from human epidermal keratinocytes [136]. Composites of collagen-SWNT gels showed biocompatibility and maintained smooth muscle cell viability more than 85% *in vitro* for 7 days [137]. MWNTs' and nano-onions' exposure resulted in increased apoptosis/necrosis of skin fibroblasts that indicated a strong immune and inflammatory response, which was further evident from the changes in the expression of genes involved in cellular transport, metabolism, cell cycle regulation, and stress response [138].

10.2.11 Cell Behavior Toward Nanotopographic Surfaces Created by Polymer Demixing

Polymer demixing is a widely studied nanofabricating technique to pattern large surface area with relatively low cost and high efficiency [139, 140]. In brief, in a typical experiment, polystyrene (PS) and poly(4-bromostyrene) blends undergo spontaneous phase separation during spin casting on silicon wafers. Various topographic features including pits, islands, or ribbons can be created with a wide range of height and depth by varying the blend concentration and composition. Different geometric shapes were fabricated by changing the blend ratio while the blend concentration changed the sizes of

these shapes. Thus, created nanotopographic features are unordered and covered randomly on the surfaces. This technique has precise control on patterning in the vertical direction as opposed to the horizontal, and thus allowed creating nanostructures with defined heights or depths. These unordered randomly placed nanotopographic features such as islands, pits, or ribbons of different heights or depths were utilized to evaluate cellular behavior [38, 41, 53, 139–149].

Dalby et al. have done extensive studies on fibroblast interaction and their behavior by changing heights of the islands [141–145, 149]. A detailed study was performed to know the effect of cell nanotopography interactions on different gene expressions. Human fibroblasts on 13-nm-high polymer demixed islands were studied for various gene expressions using a 1718-gene microarray analysis. Many changes in genes involved in signaling, cytoskeleton, ECM gene transcription, and protein translation were observed. A total of 584 genes showed an upregulation in their expression when compared to flat surfaces as control. The upregulation of these genes suggests that the fibroblasts were well differentiated on the studied nanotopography than the control. Fibroblasts on similar surface topography resulted in more spreading with the aid of many filopodia projecting from the cell membranes as seen in Fig. 10.7 [53]. Increased cell attachment, spreading, and well-developed cytoskeleton were also observed. Fibroblast interaction with nanoislands of different heights 13, 35, and 95 nm resulted in interesting cellular behavior [38]. Fibroblasts interaction seemed to increase with increasing island size, which is evident by the observed large pseudopodial projections on 95 nm. The 13-nm islands identified in the

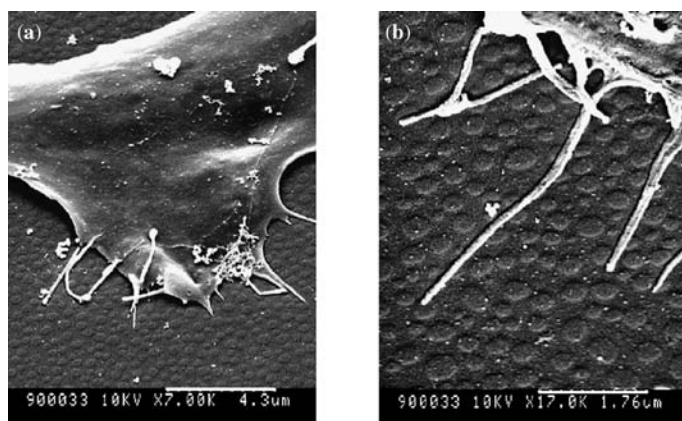


FIGURE 10.7 Scanning electron micrographs of human fibroblasts on 13-nm nanoislands created by polymer demixing of polystyrene–poly(4-bromostyrene) blends. Strong interaction between filopodia and nanoislands was seen on nanotopographies: (a) low magnification; (b) high magnification. (Reprinted with permission from Reference [53].)

most proliferative cell population had well-developed actin, tubulin, and vimentin cytoskeletons, whereas the 95-nm islands were characterized by a low level proliferative population and poorly developed cytoskeleton [38]. The nylon tubes of internal diameters 0.5 and 1.5 mm were used to create nanotopographic features with heights of 90 and 40 nm by polymer demixing using the blends of polystyrene poly(*n*-butylmethacrylate) (PS/PnBMA) [142]. Fibroblasts on control tubes showed better spreading, well-arranged β -tubulin, whereas nanotubular topographies assumed high stellate morphology with rounded cell structure and were poorly organized. The cell membranes on nanotubular topographies appeared ruffled with exceptionally long filopodia interacting with nanoislands. However, no significant differences in cellular responses were observed for both the diameters with varying island heights.

Primary human fibroblasts' interaction with the nanoislands of 10 nm height and controls resulted in increased cell adhesion, spreading, well-defined cytoskeleton formation, the fibroblastic morphologies were maintained, and produced lamellipodia with visible stress fibers at any given time point studied [143], whereas nanoislands with a height of 50 nm resulted in poor cell adhesion, low percentage of spreading, poorly defined cytoskeleton with very few lamellae, and developed no stress fibers at all the time points studied [143]. These topographies studied might help in designing surfaces with reduced cell adhesion and could be utilized in biomaterial design for stents and heart valves. Fibroblasts cultured for 4 days on the 27-nm nanoislands resulted in significantly greater areas than flat controls used in the study [144]. Well-organized cytoskeleton characterized by organized actin and tubulin on both the surfaces and stress fibers were more often observed in cells on the 27-nm islands. By day 30, vimentin was well organized on the control whereas poorly organized on the 27-nm islands. Fibroblasts on nanoislands of 95 nm height registered temporal changes in both morphology and cytoskeleton [145]. Fibroblasts on these islands started producing lamellae and filopodia after 5 min of seeding and with progressing time filopodia–island interactions increased. Fibroblasts assumed different morphologies with increasing time points and attained more stellate morphology with the large pseudopodial processes. Cultures even after 3 weeks had few patches of grouped cells and a large number of isolated cells. Isolated cells appeared to have a strong interaction with these nanoislands. On the contrary, flat control surfaces maintained normal fibroblast morphology and by 1 week cells were confluent. Many stress fibers around the cell periphery were observed, and these fibers were seen stretched across the cytoplasm on the cells on the nanoislands at the initial time points. At the later time points, controls had a matured cytoskeleton with distinct actin stress fibers and organized tubulin whereas cells on the nanoislands had less organized cytoskeleton [145]. Fibroblast interaction with the nanoislands can be summarized as presented in Fig. 10.8 that indicates that controlling the island height has a direct effect on different cellular activity.

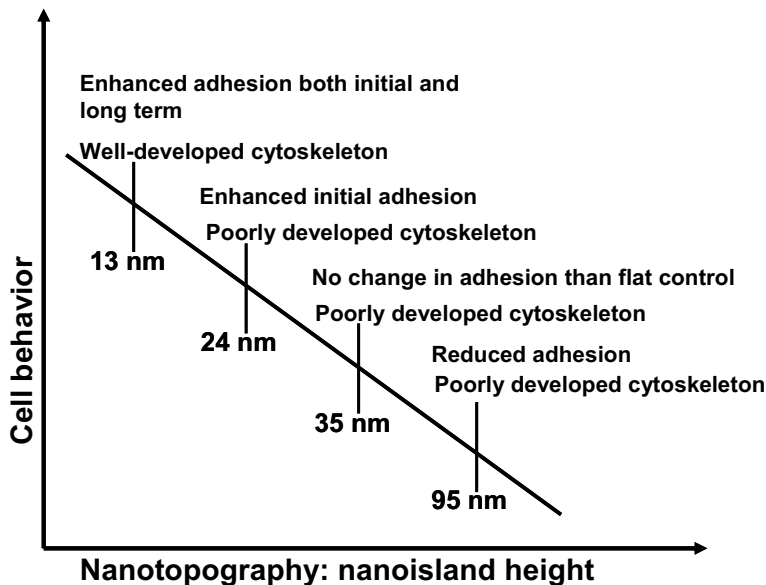


FIGURE 10.8 Human fibroblast behavior on nanotopographic features created by polymer demixing of polystyrene–poly(4-bromostyrene) blends. Fibroblast exhibited enhanced adhesion, proliferation, and well-developed cytoskeleton on 13-nm nanoislands, and with an increase in feature height, a decrease in all these above said properties were observed.

Osteoprogenitor, human bone marrow cells seeded on nanotopographies less than 10 nm showed similar features of extending filopodia toward nanostructures like fibroblasts [146]. Cells were seen to curl around nanostructures while maintaining their normal morphology and spreading on flat control surfaces. Well-defined cytoskeleton with increased actin stress fibers consisting of large networks of tubulin and vimentin were observed on nanostructures compared to the controls. Mesenchymal differentiation was demonstrated by the increased amount of osteocalcin and osteopontin expression by these cells on nanotopographies compared to the controls in a 21-day culture period [146]. With the PLLA-PS blends nanotopographic features were created using spin cast having the nanodimensions of 3–29 nm height or depth [147]. Human fetal osteoblasts adhesion was higher on nanostructures than the flat control surfaces, and nanoislands registered highest adhesion in all the cases studied. Cell adhesion was also dependent on many nonbiological cues including surface chemistry and wettability [147]. Human fetal osteoblasts on randomly distributed nanoisland topography with varying heights of 11, 38, and 85 nm also exhibited similar cellular behavior like fibroblasts previously discussed [148]. Osteoblasts showed filopodia projections and lamellipodia spreading in order to sense the nanotopography. Osteoblasts seeded on 11-nm-high islands showed significantly enhanced

spreading, proliferation, signal transmitting structures such as vinculin protein, actin stress fibers, and typical bone marker alkaline phosphatase (ALP) expression compared to the larger nanoislands or flat controls.

Dalby et al., studied human endothelial behavior on nanoislands of varying heights 13, 35, and 95 nm and observed size-dependent cellular behavior [41]. Endothelial cells also showed the largest cellular response on 13 nm with well-spread morphology and well-defined cytoskeleton than larger nanoislands and flat controls. Human mononuclear blood cells, platelets, fibroblasts, and endothelial cells were tested for their behavior on nanotopographies consisting of nanoislands of 95 nm [149]. No significant difference was observed in blood response to these nanoislands and flat control indicating minimum immunological difference. Fibroblasts were characterized by rounded morphology, reduced proliferation, and not well-developed cytoskeleton. Endothelial cells attained the characteristic curved morphologies in response to nanoislands.

10.3 CONCLUSIONS

Different nanofabrication methods need to be explored to pattern large surface areas with ease, precise control over geometries and shapes in a commercially viable manner. Many of these nanotopographical features including surface chemistry and properties should be further developed in order to control cell function at cell–biomaterial interfaces. Such an understanding will help to elicit desired cellular functions including preferential adhesion, migration, proliferation rate, and expression of specific cell phenotypes that can help in the design of a new generation of tissue engineering scaffolds and biomedical implants.

REFERENCES

1. Flemming RG, Murphy CJ, Abrams GA, Goodman SL, Nealey PF. Effects of synthetic micro- and nano-structured surfaces on cell behavior. *Biomaterials* 1999;20:573–588.
2. Valko K and Reynolds DP. High-throughput physicochemical and *in vitro* ADMET screening: a role in pharmaceutical profiling. *Am J Drug Deliv* 2005;3:83–100.
3. Riley RJ and Kenna JG. Cellular models for ADMET predictions and evaluation of drug–drug interactions. *Curr Opin Drug Discov Dev* 2004;7:86–99.
4. Zhu X. Cellular reactions of osteoblasts to micron- and submicron-scale porous structures of titanium surfaces. *Cells Tissues Organs* 2004;178:13–22.
5. Watt FM. The extracellular matrix and cell shape. *Trends Biochem Sci* 1986;11:482–485.
6. Adams JC. Cell–matrix contact structures. *Cell Mol Life Sci* 2001;58:371–392.
7. Streuli C. Extracellular matrix remodelling and cellular differentiation. *Curr Opin Cell Biol* 1999;11:634–640.

8. Mendes de Aguiar CBN, Lobao-Soares B, Alvarez-Silva M, Trentin AG. Glycosaminoglycans modulate C6 glioma cell adhesion to extracellular matrix components and alter cell proliferation and cell migration. *BMC Cell Biol* 2005;6:1–8.
9. Chiquet M. Regulation of extracellular matrix gene expression by mechanical stress. *Matrix Biol* 1999;18:417–426.
10. Abrams GA, Murphy CJ, Wang ZY, Nealey PF, Bjorling DE. Ultrastructural basement membrane topography of the bladder epithelium. *Urol Res* 2003;31:341–346.
11. Abrams GA, Goodman SL, Nealey PF, Franco M, Murphy CJ. Nanoscale topography of the basement membrane underlying the corneal epithelium of the rhesus macaque. *Cell Tissue Res* 2000;299:39–46.
12. Stoitzner P, Pfaller K, Stössel H, Romani N. A close-up view of migrating Langerhans cells in the skin. *J Invest Dermatol* 2002;118:117–125.
13. Abrams GA, Schaus SS, Goodman SL, Nealey PF, Murphy CJ. Nanoscale topography of the corneal epithelial basement membrane and Descemet's membrane of the human. *Cornea* 2000;19:57–64.
14. Askari JA and Humphries MJ. Cell–matrix interactions. *Encyclop Biol Chem* 2004;1:362–366.
15. Mueller U. Integrins and extracellular matrix in animal models. *Handbook Exp Pharmacol: Cell Adhes* 2004;165:217–241.
16. Juliano RL and Haskill S. Signal transduction from the extracellular matrix. *J Cell Biol* 1993;120:577–585.
17. Mousa SA and Cheresh DA. Recent advances in cell adhesion molecules and extracellular matrix proteins: potential clinical applications. *DDT* 1997;2:187–199.
18. Perris R and Perissinotto D. Role of the extracellular matrix during neural crest cell migration. *Mech Dev* 2000;95:3–21.
19. Boudreau NJ and Jones PL. Extracellular matrix and integrin signalling: the shape of things to come. *Biochem J* 1999;339:481–488.
20. Engel J. EGF-like domains in extracellular matrix proteins: localized signals for growth and differentiation? *FEBS Lett* 1989;251:1–7.
21. Yellowley CE, Hancox JC, Donahue HJ. Effects of cell swelling on intracellular calcium and membrane currents in bovine articular chondrocytes. *J Cell Biochem* 2002;86:290–301.
22. Yap AS and Kovacs EM. Direct cadherin-activated cell signaling: a view from the plasma membrane. *J Cell Biol* 2003;160:11–16.
23. Langer R and Vacanti JP. Tissue engineering. *Science* 1993;260:920–926.
24. Norman JJ and Desai TA. Methods for fabrication of nanoscale topography for tissue engineering scaffolds. *Ann Biomed Eng* 2006;34:89–101.
25. Vitte J, Benoliel AM, Pierres A, Bongrand P. Is there a predictable relationship between surface physical–chemical properties and cell behavior at the interface? *Eur Cell Mater* 2004;7:52–63.
26. Glass-Brudzinski J, Perizzolo D, Brunette DM. Effects of substratum surface topography on the organization of cells and collagen fibers in collagen gel cultures. *J Biomed Mater Res* 2002;61:608–618.

27. Kawahara H, et al. *In vitro* study on bone formation and surface topography from the standpoint of biomechanics. *J Mater Sci Mater Med* 2004;15: 1297–1307.
28. Berthiaume F, Moghe PV, Toner M, Yarmush ML. Effect of extracellular matrix topology on cell structure, function, and physiological responsiveness: hepatocytes cultured in a sandwich configuration. *FASEB J* 1996;10:1471–1484.
29. Braber den ET, et al. Effect of parallel surface microgrooves and surface energy on cell growth. *J Biomed Mater Res* 1995;29:511–518.
30. Karuri NW. Biological length scale topography enhances cell–substratum adhesion of human corneal epithelial cells. *J Cell Sci* 2004;117:3153–3164.
31. Tobasnick G and Curtis ASG. Chloride channels and the reactions of cells to topography. *Eur Cell Mater* 2001;2:49–61.
32. Curtis A and Wilkinson C. Topographical control of cells. *Biomaterials* 1998;18: 1573–1583.
33. Chen D, et al. Regulation of integrin expression by substrate adherence. *J Biol Chem* 1992;267:23502–23506.
34. Chen CS, Mrksich M, Huang S, Whitesides G, Ingber DE. Geometric control of cell life and death. *Science* 1997;276:1425–1428.
35. Chou L, Firth JD, Uitto VJ, Brunette DM. Effects of titanium substratum and grooved surface topography on metalloproteinase-2 expression in human fibroblasts. *J Biomed Mater Res* 1998;39:437–445.
36. Dalby MJ, et al. Increasing fibroblast response to materials using nanotopography: morphological and genetic measurements of cell response to 13-nm-high polymer demixed islands. *Exp Cell Res* 2002;276:1–9.
37. Dalby MJ, et al. Attempted endocytosis of nano-environment produced by colloidal lithography by human fibroblasts. *Exp Cell Res* 2004;295:387–394.
38. Dalby MJ, Riehle MO, Johnstone HJ, Affrossman S, Curtis AS. Polymer-demixed nanotopography: control of fibroblast spreading and proliferation. *Tissue Eng* 2002;8:1099–1108.
39. Price RL, Haberstroh KM, Webster TJ. Enhanced functions of osteoblasts on nanostructured surfaces of carbon and alumina. *Med Biol Eng Comput* 2003;41: 372–375.
40. Webster TJ, Ergun C, Doremus RH, Siegel RW, Bizios R. Enhanced osteoclast-like cell functions on nanophase ceramics. *Biomaterials* 2001;22:1327–1333.
41. Dalby MJ, Riehle MO, Johnstone H, Affrossman S, Curtis AS. *In vitro* reaction of endothelial cells to polymer demixed nanotopography. *Biomaterials* 2002;23: 2945–2954.
42. Thapa A, Webster TJ, Haberstroh KM. Polymers with nano-dimensional surface features enhance bladder smooth muscle cell adhesion. *J Biomed Mater Res* 2003;67A:1374–1383.
43. Andersson AS, et al. Nanoscale features influence epithelial cell morphology and cytokine production. *Biomaterials* 2003;24:3427–3436.
44. Andersson AS, Brink J, Lidberg U, Sutherland DS. Influence of systematically varied nanoscale topography on the morphology of epithelial cells. *IEEE Trans Nanobioscience* 2003;2:49–57.

45. Gallagher JO, McGhee KF, Wilkinson CDW, Riehle MO. Interaction of animal cells with ordered nanotopography. *IEEE Trans Nanobioscience* 2002;1:24–28.
46. Folch A and Toner M. Cellular micropatterns on biocompatible materials. *Biotechnol Prog* 1998;14:388–392.
47. Curtis A and Wilkinson C. Topographical control of cells. *Biomaterials* 1997;8:1573–1583.
48. Curtis A and Wilkinson C. Nanotechniques and approaches in biotechnology. *Trends Biotechnol* 2001;19:97–101.
49. Patel N, et al. Spatially controlled cell engineering on biodegradable polymer surfaces. *FASEB J* 1998;12:1447–1454.
50. Wilkinson CDW. Nanostructures in biology. *Microelectron Eng* 1995;27:61–65.
51. Barbucci R, et al. Micro and nano-structured surfaces. *J Mater Sci Mater Med* 2003;14:721–725.
52. Curtis ASG, et al. Substratum nanotopography and the adhesion of biological cells. Are symmetry or regularity of nanotopography important? *Biophys Chem* 2001;94:275–783.
53. Dalby MJ, et al. Increasing fibroblast response to materials using nanotopography: morphological and genetic measurements of cell response to 13-nm-high polymer demixed islands. *Exp Cell Res* 2002;276:1–9.
54. Nair LS, Bhattacharyya S, Laurencin CT. Development of novel tissue engineering scaffolds via electrospinning. *Expert Opin Biol Ther* 2004;4:659–668.
55. Diehl KA, Foley JD, Nealey PF, Murphy CJ. Nanoscale topography modulates corneal epithelial cell migration. *J Biomed Mater Res* 2005;75A:603–611.
56. Teixeira AI, Nealey PF, Murphy CJ. Responses of human keratocytes to micro- and nanostructured substrates. *J Biomed Mater Res* 2004;71A:369–376.
57. Teixeira AI, Abrams GA, Bertics PJ, Murphy CJ, Nealey PF. Epithelial contact guidance on well-defined micro- and nanostructured substrates. *J Cell Sci* 2003;116:1881–1892.
58. Teixeira AI, et al. The effect of environmental factors on the response of human corneal epithelial cells to nanoscale substrate topography. *Biomaterials* 2006;27:3945–3954.
59. Meyle J, Gultig K, Brich M, Hammerle H, Nisch W. Contact guidance of fibroblasts on biomaterial surfaces. *J Mater Sci Mater Med* 1994;5:463–466.
60. Rajniecek AM and McCraig CD. Guidance of CNS growth cones by substratum grooves and ridges: effects of inhibitors of the cytoskeleton, calcium channels and signal transduction pathways. *J Cell Sci* 1997;110:2915–2924.
61. Rajniecek AM, Britland S, McCraig CD. Contact guidance of CNS neurites on grooved quartz: influence of groove dimensions, neuronal age and cell type. *J Cell Sci* 1997;110:2905–2913.
62. Liliensiek SJ, Campbell S, Nealey PF, Murphy CJ. The scale of substratum topographic features modulates proliferation of corneal epithelial cells and corneal fibroblasts. *J Biomed Mater Res* 2006;79A:185–192.
63. Braber den ET, et al. Quantitative analysis of fibroblast morphology on microgrooved surfaces with various groove and ridge dimensions. *Biomaterials* 1996;17:2037–2044.

64. Wojciak-Stothard B, Curtis A, Monaghan W, MacDonald K, Wilkinson C. Guidance and activation of murine macrophages by nanometric scale topography. *Exp Cell Res* 1996;223:426–435.
65. Clark P, Connolly P, Curtis ASG, Dow JAT, Wilkinsin CDW. Topographical control of cell behavior. II. multiple grooved substrata. *Development* 1990;108:635–644.
66. Britland S, et al. Synergistic and hierarchical adhesive and topographic guidance of BHK cells. *Exp Cell Res* 1996;228:313–325.
67. Hoch HC, Staples RC, Whitehead B, Comeau J, Wolf ED. Signaling for growth orientation and cell differentiation by surface topography in *Uromyces*. *Science* 1997;235:1659–1662.
68. Schmidt JA and von Recum AF. Texturing of polymer surfaces at the cellular level. *Biomaterials* 1991;12:385–389.
69. Turner S, et al. Cell attachment on silicon nanostructures. *J Vac Sci Technol B* 1997;15:2848–2854.
70. Kumbhar SG, Nair LS, Bhattacharyya S, Laurencin CT. Polymeric nanofibers as novel carriers for the delivery of therapeutic molecules. *J Nanosci Nanotechnol* 2006;6:2591–2607.
71. Ma Z, He W, Young T, Ramakrishna S. Grafting of gelatin on electrospun poly(caprolactone) nanofibers to improve endothelial cell spreading and proliferation and to control cell orientation. *Tissue Eng* 2005;11:1149–1158.
72. Yang F, Murugan R, Wang S, Ramakrishna S. Electrospinning of nano/micro scale poly(L-lactic acid) aligned fibers and their potential in neural tissue engineering. *Biomaterials* 2005;26:2603–2610.
73. Lee CH, et al. Nanofiber alignment and direction of mechanical strain affect the ECM production of human ACL fibroblast. *Biomaterials* 2004;26:1261–1270.
74. Xu CY, Inai R, Kotaki M, Ramakrishna S. Aligned biodegradable nanofibrous structure: a potential scaffold for blood vessel engineering. *Biomaterials* 2004;25: 877–886.
75. Bhattarai N, Edmondson D, Veiseh O, Matsen FA, Zhang M. Electrospun chitosan-based nanofibers and their cellular compatibility. *Biomaterials* 2005;26:6176–6184.
76. Ma Z, Kotaki M, Inai R, Ramakrishna S. Potential of nanofiber matrix as tissue-engineering scaffolds. *Tissue Eng* 2005;11:101–109.
77. Dunn GA. Contact guidance of cultured tissue cells: a survey of potentially relevance properties of the substratum. In: Bellairs R, Curtis A, Dunn G, editors. *Cell Behavior*. Cambridge: Cambridge University Press; 1982. p 247–280.
78. Yim EKF, et al. Nanopattern-induced changes in morphology and motility of smooth muscle cells. *Biomaterials* 2005;26:5405–5413.
79. Nomura S, et al. Nanopillar sheets as a new type of cell culture dish: detailed study of HeLa cells cultured on nanopillar sheets. *J Artif Organs* 2006;9:90–96.
80. Lenhert S, Meier MB, Meyer U, Chi L, Wiesmann HP. Osteoblast alignment, elongation and migration on grooved polystyrene surfaces patterned by Langmuir–Blodgett lithography. *Biomaterials* 2005;26:563–570.
81. Liu X, Smith L, Wei G, Won Y, Ma PX. Surface engineering of nano-fibrous poly(L-lactic acid) scaffolds via self-assembly technique for bone tissue engineering. *J Biomed Nanotechnol* 2005;1:54–60.

82. Cui K, Zhu Y, Wang XH, Feng QL, Cui FZ. A porous scaffold from bone-like powder loaded in a collagen–chitosan matrix. *J Bioact Compat Polym* 2004;19:17–31.
83. Jun HW, Paramonov SE, Hartgerink JD. Biomimetic self-assembled nanofibers. *Soft Matter* 2006;2:177–181.
84. Hosseinkhani H, Hosseinkhani M, Tian F, Kobayashi H, Tabata Y. Ectopic bone formation in collagen sponge self-assembled peptide-amphiphile nanofibers hybrid scaffold in a perfusion culture bioreactor. *Biomaterials* 2006;27:5089–5098.
85. Hosseinkhani H, Kobayashi H, Tabata Y. Design of tissue-engineered nano-scaffold using peptide amphiphile for regenerative medicine. *Peptide Sci* 2005;42:341–344.
86. Genove E, Shen C, Zhang S, Semino CE. The effect of functionalized self-assembling peptide scaffolds on human aortic endothelial cell function. *Biomaterials* 2005;26:3341–3351.
87. Silva GA, et al. Selective differentiation of neural progenitor cells by high-epitope density nanofibers. *Science* 2004;303:1352–1355.
88. Harrington DA, et al. Branched peptide-amphiphilic as self-assembling coatings for tissue engineering scaffolds. *J Biomed Mater Res* 2006;78A:157–167.
89. Beniash E, Hartgerink JD, Storrer H, Stendahl JC, Stupp SI. Self-assembling peptide amphiphile nanofiber matrices for cell entrapment. *Acta Biomater* 2005;1:387–397.
90. Zhang S, Gelain F, Zhao X. Designer self-assembling peptide nanofiber scaffolds for 3D tissue cell cultures. *Semin Cancer Biol* 2005;15:413–420.
91. Smith LA and Ma PX. Nano-fibrous scaffolds for tissue engineering. *Colloids Surf B* 2004;39:125–131.
92. Zhang S. Fabrication of novel biomaterials through molecular self-assembly. *Nat Biotechnol* 2003;21:1171–1178.
93. Lutolf MP and Hubbell JA. Synthetic biomaterials as instructive extracellular microenvironments for morphogenesis in tissue engineering. *Nature Biotechnol* 2005;23:47–55.
94. Ellis-Behnke RG, et al. Nano neuro knitting: peptide nanofiber scaffold for brain repair and axon regeneration with functional return of vision. *Proc Nat Acad Sci* 2006;103:5054–5059.
95. Hosseinkhanian H, Hosseinkhanib M, Tianc F, Kobayashi H, Tabata Y. Osteogenic differentiation of mesenchymal stem cells in self-assembled peptide-amphiphile nanofibers. *Biomaterials* 2006;27:4079–4086.
96. Chen VJ, Smith LA, Ma PX. Bone regeneration on computer-designed nano-fibrous scaffolds. *Biomaterials* 2006;27:3973–3979.
97. Wei G and Ma PX. Structure and properties of nano-hydroxyapatite/polymer composite scaffolds for bone tissue engineering. *Biomaterials* 2004;25:4749–4757.
98. Chen VJ and Ma PX. Nano-fibrous poly(L-lactic acid) scaffolds with interconnected spherical macropores. *Biomaterials* 2004;25:2065–2073.
99. Yang F, et al. Fabrication of nano-structured porous PLLA scaffold intended for nerve tissue engineering. *Biomaterials* 2004;25:1891–1900.

100. Dalby MJ, Riehle MO, Sutherland DS, Agheli H, Curtis ASG. Morphological and microarray analysis of human fibroblasts cultured on nanocolumns produced by colloidal lithography. *Eur Cell Mater* 2005;9:1–8.
101. Dalby MJ, Riehle MO, Sutherland DS, Agheli H, Curtis ASG. Fibroblast response to a controlled nanoenvironment produced by colloidal lithography. *J Biomed Mater Res* 2004;69A:314–322.
102. Wood MA, Wilkinson CDW, Curtis ASG. The effects of colloidal nanotopography on initial fibroblast adhesion and morphology. *IEEE Trans Nanobioscience* 2006;5:20–31.
103. Dalby MJ, Riehle MO, Sutherland DS, Agheli H, Curtis ASG. Changes in fibroblast morphology in response to nano-columns produced by colloidal lithography. *Biomaterials* 2004;25:5415–5422.
104. Andersson AS, Olsson P, Lidberg U, Sutherland DS. The effects of discontinuous and continuous groove edges on cell shape and alignment. *Exp Cell Res* 2003;288:177–188.
105. Rice JM, et al. Quantitative assessment of the response of primary derived human osteoblasts and macrophages to a range of nanotopography surfaces in a single culture model *in vitro*. *Biomaterials* 2003;24:4799–4818.
106. Li WJ, Laurencin CT, Cateson ED, Tuan RS, Ko FK. Electrospun nanofibrous structure: a novel scaffold for tissue engineering. *J Biomed Mater Res* 2002;60:613–621.
107. Dalton PD, Klinkhammer K, Salber J, Klee D, Moeller M. Direct *in vitro* electrospinning with polymer melts. *Biomacromolecules* 2006;7:686–690.
108. Zhang YZ, Venugopal J, Huang ZM, Lim CT, Ramakrishna S. Crosslinking of the electrospun gelatin nanofibers. *Polymer* 2006;47:2911–2917.
109. Baker SC, et al. Characterisation of electrospun polystyrene scaffolds for three-dimensional *in vitro* biological studies. *Biomaterials* 2006;27:3136–3146.
110. Kim KH, et al. Biological efficacy of silk fibroin nanofiber membranes for guided bone regeneration. *J Biotechnol* 2005;120:327–339.
111. Min BM, et al. Electrospinning of silk fibroin nanofibers and its effect on the adhesion and spreading of normal human keratinocytes and fibroblasts *in vitro*. *Biomaterials* 2004;25:1289–1297.
112. Venugopal J, Ma LL, Yong T, Ramakrishna S. *In vitro* study of smooth muscle cells on polycaprolactone and collagen nanofibrous matrices. *Cell Biol Int* 2005;29:861–867.
113. Xu C, Yang F, Wang S, Ramakrishna S. *In vitro* study of human vascular endothelial cell function on materials with various surface roughnesses. *J Biomed Mater Res* 2004;71A:154–161.
114. Mo XM, Xu CY, Kotaki M, Ramakrishna S. Electrospun P(LLA-CL) nanofiber: a biomimetic extracellular matrix for smooth muscle cell and endothelial cell proliferation. *Biomaterials* 2004;25:1883–1890.
115. Schindler M, et al. A synthetic nanofibrillar matrix promotes *in vivo*-like organization and morphogenesis for cells in culture. *Biomaterials* 2005;26:5624–5631.
116. Zhang Y, Ouyang H, Lim CT, Ramakrishna S, Huang ZM. Electrospinning of gelatin fibers and gelatin/PCL composite fibrous scaffolds. *J Biomed Mater Res B* 2005;72:56–165.

117. Li M, Guo Y, Wei Y, MacDiarmid AG, Lelkes PI. Electrospinning polyaniline-contained gelatin nanofibers for tissue engineering applications. *Biomaterials* 2006;27:2705–2715.
118. Ma Z, Kotaki M, Yong T, He W, Ramakrishna S. Surface engineering of electrospun polyethylene terephthalate (PET) nanofibers towards development of a new material for blood vessel engineering. *Biomaterials* 26:2005;2527–2536.
119. Chua KN. Stable immobilization of rat hepatocyte spheroids on galactosylated nanofiber scaffold. *Biomaterials* 2005;26:2537–2547.
120. Badami AS, Kreke MR, Thompson MS, Riffle JS, Goldstein AS. Effect of fiber diameter on spreading, proliferation, and differentiation of osteoblastic cells on electrospun poly (lactic acid) substrates. *Biomaterials* 2006;27:596–606.
121. Tuzlakoglu K, et al. Nano- and micro-fiber combined scaffolds: a new architecture for bone tissue engineering. *J Mater Sci Mater in Med* 2005;16:1099–1104.
122. Sahoo S, Ouyang H, Goh James CH, Tay TE, Toh SL. Characterization of a novel polymeric scaffold for potential application in tendon/ligament tissue engineering. *Tissue Eng* 2006;12:91–99.
123. Kwon IK, Kidoaki S, Matsuda T. Electrospun nano- to microfiber fabrics made of biodegradable copolyesters: structural characteristics, mechanical properties and cell adhesion potential. *Biomaterials* 2005;26:3929–3939.
124. Perla V and Webster TJ. Better osteoblast adhesion on nanoparticulate selenium—a promising orthopedic implant material. *J Biomed Mater Res* 2005;75A:356–364.
125. Turner S, et al. Cell attachment on silicon nanostructures. *J Vac Sci Technol B Microelectronics and Nanometer Structures* 1997;15:2848–2854.
126. Thapa A, Miller DC, Webster TJ, Haberstroh KM. Nano-structured polymers enhance bladder smooth muscle cell function. *Biomaterials* 2003;24:2915–2926.
127. Miller DC, Haberstroh KM, Webster TJ. Mechanism(s) of increased vascular cell adhesion on nanostructured poly(lactic-co-glycolic acid) films. *J Biomed Mater Res* 2005;73A:476–484.
128. Garibaldi S, Brunelli C, Bavastrello V, Ghigliotti G, Nicolini C. Carbon nanotube biocompatibility with cardiac muscle cells. *Nanotechnol* 2006;17:391–397.
129. Elias KL, Price RL, Webster TJ. Enhanced functions of osteoblasts on nanometer diameter carbon fibers. *Biomaterials* 2002;23:3279–3287.
130. Price RJ, Ellison K, Haberstroh KM, Webster TJ. Nanometer surface roughness increases select osteoblast adhesion on carbon nanofiber compacts. *J Biomed Mater Res* 2004;70A:129–138.
131. McKenzie JL, Waid MC, Shi R, Webster TJ. Decreased functions of astrocytes on carbon nanofiber materials. *Biomaterials* 2004;25:1309–1317.
132. Price RL, Waid MC, Haberstroh KM, Webster TJ. Selective bone cell adhesion on formulations containing carbon nanofibers. *Biomaterials* 2003;24:1877–1887.
133. Zanello LP, Zhao B, Hu H, Haddon RC. Bone cell proliferation on carbon nanotubes. *Nano Letters* 2006;6:562–567.
134. Fiorito S, Serafino A, Andreola F, Bernier P. Effects of fullerenes and single-wall carbon nanotubes on murine and human macrophages. *Carbon* 2006;44:1100–1105.

135. Chopek J, et al. *In vitro* studies of carbon nanotubes biocompatibility. *Carbon* 2006;44:1106–1111.
136. Monteiro-Riviere NA, Nemanich RJ, Inman AO, Wang YY, Riviere JE. Multi-walled carbon nanotube interactions with human epidermal keratinocytes. *Toxicol Lett* 2005;155:377–384.
137. MacDonald RA, Laurenzi BF, Viswanathan G, Ajayan PM, Stegemann JP. Collagen–carbon nanotube composite materials as scaffolds in tissue engineering. *J Biomed Mater Res* 2005;74A:489–496.
138. Ding L, et al. Molecular characterization of the cytotoxic mechanism of multiwall carbon nanotubes and nano-onions on human skin fibroblast. *Nano Lett* 2005;5:2448–2464.
139. Muller-Buschbaum P, O’Neill SA, Affrossman S, Stamm M. Phase separation and dewetting of weakly incompatible polymer blend films. *Macromolecules* 1998;31:5003–5009.
140. Affrossman S, Henn G, O’Neill SA, Pethrick RA, Stamm M. Surface topography and composition of deuterated polystyrene-poly(bromostyrene) blends. *Macromolecules* 1996;29:5010–5016.
141. Dalby MJ, Yarwood SJ, Johnstone HJH, Affrossman S, Riehle MO. Fibroblast signaling events in response to nanotopography: a gene array study. *IEEE Trans Nanobioscience* 2002;1:12–17.
142. Berry CC, Dalby MJ, McCloy D, Affrossman S. The fibroblast response to tubes exhibiting internal nanotopography. *Biomaterials* 2005;26:4985–4992.
143. Dalby MJ, Riehle MO, Johnstone HJH, Affrossman S, Curtis ASG. Nonadhesive nanotopography: fibroblast response to poly(*n*-butyl methacrylate)-poly(styrene) demixed surface features. *J Biomed Mater Res* 2003;67A:1025–1032.
144. Dalby MJ, et al. Rapid fibroblast adhesion to 27 nm high polymer demixed nanotopography. *Biomaterials* 2004;25:77–83.
145. Dalby MJ, et al. Fibroblast reaction to island topography: changes in cytoskeleton and morphology with time. *Biomaterials* 2003;24:927–935.
146. Dalby MJ, et al. Osteoprogenitor response to semi-ordered and random nanotopographies. *Biomaterials* 2006;27:2980–2987.
147. Lim JY, et al. Osteoblast adhesion on poly(L-lactic acid)/polystyrene demixed thin film blends: effect of nanotopography, surface chemistry, and wettability. *Biomacromolecules* 2005;6:3319–3327.
148. Lim JY, Hansen JC, Siedlecki CA, Runt J, Donahue HJ. Human foetal osteoblastic cell response to polymer-demixed nanotopographic interfaces. *J R Soc Interface* 2005;2:97–108.
149. Dalby MJ, Marshall GE, Johnstone HJH, Affrossman S, Riehle MO. Interactions of human blood and tissue cell types with 95-nm-high nanotopography. *IEEE Trans Nanobioscience* 2002;1:18–23.

Cellular Behavior on Basement Membrane Inspired Topographically Patterned Synthetic Matrices

JOSHUA Z. GASIOROWSKI, JOHN D. FOLEY, PAUL RUSSELL,
SARA J. LILIENSIEK, PAUL F. NEALEY, and CHRISTOPHER J. MURPHY

11.1 INTRODUCTION

The basement membrane (BM) is a specialized layer composed of a complex web of extracellular matrix (ECM) proteins. It is through the basement membrane that a wide array of cells (e.g., epithelial, vascular endothelial cells) interact with their underlying stromal elements. Basement membranes have a number of intrinsic characteristics that can serve to regulate the behaviors of cells associated with them. These features include the presentation of ligand sequences for specific cell receptors, serving as a reservoir for soluble cytoactive factors such as polypeptide growth factors, and possessing physical characteristics that can modulate cell behaviors. Two key physical characteristics of the basement membrane shown to dramatically influence cell behaviors are compliance and the inherently complex three-dimensional topography that consists of feature types in the nano- through submicron-size scale [1].

This chapter will briefly review the biology of basement membranes and their biochemical and physical attributes. We then address the primary focus of this chapter, namely, the development of basement membrane inspired topographically patterned synthetic matrices for in vitro cell and tissue culture systems. A summary of cellular behaviors influenced by the topographic features of synthetic matrices is provided with an emphasis on the use of anisotropically grooved surfaces. Such surfaces allow for the rapid evaluation of cellular responses to topographic cues.

11.2 THE BASEMENT MEMBRANE

The evolution of the BM is likely driven by the need for the simple cell to interact with its environment. The earliest life forms on the planet were most likely acutely sensitive to changes in their environment. If the primordial milieu of simple molecules from which the first living cells arose did not supply enough nutrients at the appropriate pH, the earliest cells could not have survived. However, in order for life to evolve into complex organisms, cells needed to develop the ability to not only survive in their provided environment, but also alter and shape it to be more advantageous for cell growth and development. For this reason, secretion would appear to be a major step in evolution. With secretion, cells could utilize chemical signals to communicate with each other as well as deposit proteins onto surfaces to create attachment sites. By laying a protein coat down on a surface to create an anchor site, cells began to shape their environment to provide them with a selective advantage. Adherence to surfaces and to other cells could, in many instances, improve survival, change cellular behaviors, and lead to the evolution of multicellular organisms. This is still evident today as an individual bacterium that exists in our current world has different resistances and expression profiles than the same bacterium living within a thick, densely populated biofilm [2–4]. Without a doubt, the extracellular matrix and basement membrane have evolved to become integral to development and disease.

11.2.1 Significance of Basement Membranes in Disease

Besides providing cellular structural support, the functional importance of basement membranes is readily evident by their role in development and maintaining tissue homeostasis. One of the most well-known BM diseases is thin basement membrane disease, which is exactly what it implies, a decrease in basement membrane thickness. Thin basement membrane disease is characterized by a 100–200 nm glomeruli BM in the kidney, which ranges from half to a quarter of the normal size [5]. The decreased thickness can lead to blood in the urine as well as blood pressure complications [6].

The ECM and BMs also play roles in the orchestration of normal wound healing processes. Humans and rats with diabetes tend to have abnormally thick basement membranes in the cornea and glomerulus [7, 8]. Though not thoroughly investigated, thicker BMs may have altered topographical features and compliance. These features could contribute to improper wound healing, a common pathologic feature of diabetic patients. There are other cases, especially within the skin and bone, where extracellular matrix proteins are mutated or autoimmune reactions arise against matrix epitopes [9–12]. The result of these mutations and immune reactions are alterations of basement membrane function that can lead to disease. As such, it is important to characterize and understand the biochemical and physical properties of basement membranes.

11.2.2 Biochemical Attributes

Cells secrete many different fibrous proteins into the extracellular space and are constantly shaping and remodeling their surrounding environment. Collectively, this mix of secreted proteins is known as the extracellular matrix. A specialization of ECM proteins on the basal surface of many cells within a given tissue becomes the basement membrane. This layer provides tensile support, serves as a reservoir for signaling molecules, and presents biochemical and physical cues for cellular structures and tissues (Fig. 11.1). Transmission electron micrographs reveal that the basement membrane is comprised of an electron dense (lamina densa) and an electron lucid layer (lamina lucida) [13–15]. The biochemical composition of these layers will vary from tissue to tissue, but most BMs share the same fibrous protein components such as collagen, laminin, and proteoglycans [13, 16–18]. Type IV collagen is the main building block of all basement membranes and is highly conserved across species from *C. elegans* to humans. Collagen will self-assemble with itself, nidogen, the laminin family, and other proteins to form BMs of various functions and thicknesses that usually range from 50 to 150 nm in most tissues and up to 300–400 nm in glomerular BM or 8 μm in the human lens capsule [19–22, 55]. Many ECM proteins have whole domains or short conserved amino acid sequences that act as signaling antagonists or adherence ligands for cell membrane receptors. The slight biochemical differences that make up each BM account for many of the changes seen in cellular structures from one tissue to the next.

The majority of studies to date that have analyzed the impact of BMs on cell behavior have focused on the cellular response to the biochemical composition of the BM. The biochemical properties of ECMs and BMs that regulate cell behavior are better understood than the physical properties because they have historically been easier to manipulate and test. Typical experimental designs fall into three broad categories. First, most tests on ECM proteins have characterized changes in cells after they were transiently transfected with the

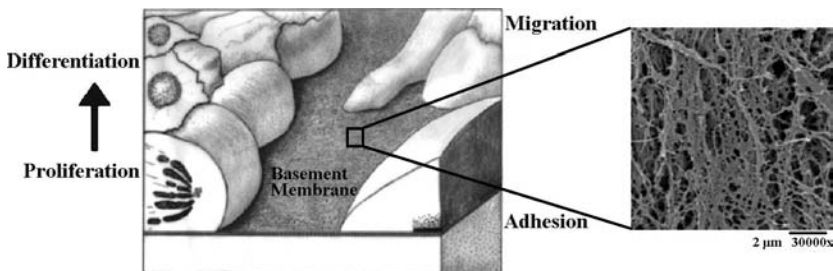


FIGURE 11.1 Schematic of cells on a basement membrane. The cartoon depicts cells adhering, proliferating, and migrating on a basement membrane. As cells expand in a basal to apical direction, they often begin to differentiate, as indicated by the arrow. The enlargement on the right is a 30,000 \times scanning electron micrograph of a rhesus aorta basement membrane.

protein in question, or subjected to various doses of recombinant protein added to the cell media. These experiments are often performed with cells plated onto flat surfaces and can reveal visual phenotypic changes. They also allow researchers to work out cell signaling pathways, such as how the proteolytic release of endostatin from collagen inhibits angiogenesis pathways [23–25]. Second, studies have been performed to characterize the effect of a growth factor or peptide on cellular migration using a Boyden chamber or experiments involving wound healing. These experiments typically measure the chemotactic potential of a signal protein to control immunocyte invasion or direct cells into a wound bed [26, 27]. Third, studies to measure the effect of a peptide signal on adherence are usually performed by seeding cells onto a surface coated with the protein being tested. Perhaps the best characterized ECM peptide signal from these types of experiments that has been shown to elicit a cellular adherence response is the arginine–glycine–aspartic acid (RGD) signal peptide. The RGD signal motif, found within many different ECM proteins, is a common ligand for several integrins, and can alter the ability of different cell types to adhere to a given surface [28, 29]. Experiments are commonly designed to measure RGD-dependent changes in cellular adhesion by coating a plastic surface with RGD signal peptides or full-length ECM proteins that contain the RGD domain, like fibronectin. However, while each of the aforementioned experimental strategies is designed to characterize the biochemical effects of individual ECMs, they rarely take into account the impact of the physical micron, submicron, and nanotopographic environments that cells are exposed to both *in vivo* and *in vitro*.

In addition to biochemical differences, BMs have unique physical characteristics: thickness, compliance, pore size, fiber width, and three-dimensional organization. These are all physical features that define a BM. Provided below is a concise summary of compliance followed by a presentation of the focus of this chapter, the topographic features of basement membranes, and their cellular consequences.

11.2.3 Physical Characteristics: Compliance

To date, the majority of studies on cells have been conducted on rigid surfaces such as silicon, polystyrene, and polyurethane. These surfaces have been coated with various ligands such as the RGD peptide to increase cell attachment or to alter cell behavior. It has become clear that mechanical compliance of cellular matrix may be as significant as ligand functionalization in impacting cell behavior [30, 31]. The compliance of a material relates the extent of deformation (strain) of the material to an imposed stress (force/unit area). A more rigid substratum has been shown to promote cell spreading and induce phosphorylation pathways [32]. The effects of compliance on differentiation have also been demonstrated with breast epithelial cells [33]. When these cells are cultured on floating gels, the cells differentiate into tubules. If the gels are attached to a substrate, this differentiation does not occur. Similarly, work on

human umbilical vein endothelial cells grown on polyacrylamide/gelatin supports has shown that by decreasing the rigidity of the support, cellular differentiation into tube-like structures will occur [34]. Increases in the traction forces of fibroblasts and the contractility of smooth muscle cells have been reported by altering the compliance of the substrata [31, 35–39]. Cortical neurons and glial cells are greatly influenced by compliance [40]. On hard gels, astrocytes will outgrow neurites and possess actin stress fibers. On soft matrix, astrocytes were rounded and showed few stress fibers similar to results observed with fibroblasts [31]. These characteristics are very different from their behavior on hard surfaces. However, neurites have robust actin filaments and enhanced F-actin protrusions on soft as well as hard surfaces.

Compliance of the matrix is probably vital in the organization of cells and tissues in living organisms. Neurons have been shown to grow into hydrogels in injured areas while astrocytes will not [41]. Certainly, the results with the brain cells suggest that the distribution and population sorting in the central nervous system may be closely related to compliance in particular areas. Work with stem cells has indicated that soft matrices similar to that of the brain induced neurogenic phenotypes [42]. Stiffer matrices similar to muscle were myogenic and rigid supports were osteogenic. Thus, the physical properties of cellular matrices as well as the biochemical ones are extremely important determinants of cell behavior. Despite the recent recognition that compliance is an essential property on the ECM, the compliance of native basement membranes has yet to be reported.

11.2.3.1 Physical Characteristics: Topography Basement membranes possess a complex “felt-like” three-dimensional topography. Individual features can range in scale from approximately 10 to 400 nm with the majority of features smaller than 100 nm [21, 22, 43, 44] (Fig. 11.2). The diameter of a primary epithelial cell in culture can average between 20 and 50 μm , depending

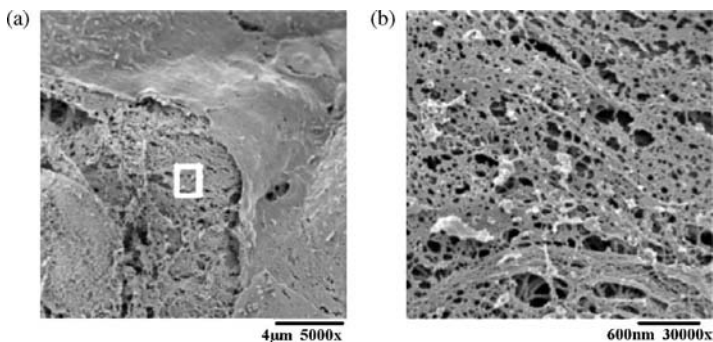


FIGURE 11.2 Electron micrographs of native basement membrane topography. (a) An SEM micrograph of cells covering the fibrous basement membrane. (b) An SEM magnified image of the window in (a) showing complex topography of the basement membrane.

on the cell type. This represents several orders of magnitude difference in scale between a cell and the basement membrane structural components and ensures that a single cell interfaces with thousands of nanoscale and submicron topographic features. Thus, in addition to a wide range of biochemical cueing, epithelial and endothelial cells are exposed to a complex information-rich topographic environment. Altogether, the integration of biochemical and physical cues provided by a BM plays a large role in development and disease by regulating cell behavior.

The physical features of BMs are believed to exert great control over cell behavior and development; however, it has been technically challenging to design controlled experiments to test these hypotheses. The ability to separate inherent chemical signals from purely physical ones for *in vitro* topography experiments has been a difficult task for cell biologists to overcome. Nevertheless, there has been nearly a century's worth of studies investigating the influence of topography on cellular behavior. As early as 1911, R.G. Harrison was using spider webs to study cellular responses to complex surface topography [45, 46]. What Harrison lacked was the ability to create controlled surfaces with precisely defined physical features for his experiments.

The interdisciplinary merging of engineering and cell biology has led to revolutionary bioengineering techniques, such as the use of photolithography and reactive ion etching, to create substrates to test the effects of topography on cell behavior. Due to recent innovative fabrication strategies, researchers can now produce the large number of nanostructured surfaces with controlled feature sizes required to conduct statistically robust cell behavior studies [1, 47]. Different surface features (e.g., surface roughness, grooves, pores, etc.) with dimensions ranging from tens to hundreds of nanometers have been reported to affect proliferation, alignment, adhesion, and cell viability [48–53]. However, the effects of physical features on cellular behaviors remain poorly understood for a number of reasons. First, the topographic layouts of many BMs have not been quantitatively analyzed. To date, the best characterized native BMs are skin, cornea, urothelium, vascular endothelium, and the glomerulus [19, 21, 22, 54, 55]. While some morphologic aspects of the BMs from other tissues have been characterized, a detailed quantitative description of their surface topographic features has not been reported. Second, research groups have been experimenting with different manufacturing protocols to produce the same type of topographical surfaces, with techniques such as UV or electron beam lithography, to fabricate nanogrooves from titanium or silicon chips. There are drawbacks and limitations for each and the result can lead to inconsistent surface types and feature sizes. This ultimately makes it difficult to draw direct conclusions between earlier studies. Third, bioengineers still face challenges in developing surfaces that reach the lower limit of physical features needed to recreate the full nanometer to submicron range of topographic features that define native basement membranes. Despite these limitations and shortcomings, biologists have made significant advances in understanding the interactions between the basement membrane and the cell. However, there is

still a strong need for further development of artificial surfaces that incorporate defined topographic features in order to fully characterize the role of the physical characteristics of BMs in development, disease, and maintenance of cell and tissue homeostasis.

11.3 HISTORY OF BIOMIMETIC SYNTHETIC MATRICES

Biological systems are comprised of entities whose scales range at least 10 orders of magnitude from the size of organisms down to the individual molecules that regulate cellular behaviors. At the level where cells interact with a basement membrane, most information is found at the submicron, nanoscale, and subnanoscale levels. Early attempts to create biomimetic synthetic matrices were limited by fabrication methods so that the manufactured surfaces had only micron-scale features. With the aid of new nanofabrication techniques, we have now been able to develop a generation of artificial surfaces that incorporate nano- through micron-scale topographies. The nano- and submicron features closely mimic the biologically relevant scale of physical features found in living tissues and the micron-scale features provide a connect to the bulk of the literature of topographic cueing.

To understand whether the scale of topographic features can influence cellular responses, one must first determine the relevant feature sizes of a cell's native microenvironment. Quantitative measurements of BM features such as pore diameter and fiber width are similar in scale for many tissues studied and also conserved across different species (Table 11.1). As more tissues have been analyzed, some differences have emerged. One of the best known exceptions to

TABLE 11.1 SEM Physical Feature Measurements of Several Basement Membranes

Species	Tissue BM	Mean feature height (nm)	Mean fiber diameter (nm)	Mean pore diameter (nm)	Reference
Rhesus	Cornea	191 ± 72	77 ± 44	72 ± 40	[22]
Human	Cornea	182 ± 49	46 ± 16	92 ± 34	[21]
Human	Descemet	131 ± 41	31 ± 9	38 ± 15	[21]
Human	Foreskin	—	24 ± 8	40 ± 17	^a
Porcine	Aortic valve	—	27 ± 12	38 ± 24	^a
Rhesus	Aorta	—	30 ± 11	62 ± 37	^a
Rhesus	Carotid	—	31 ± 11	60 ± 42	^a
Rhesus	Saphenous	—	27 ± 8	38 ± 16	^a
Rhesus	Bladder	178 ± 57	52 ± 28	82 ± 49	[43]
Bovine	Glomerulus	—	—	9 ± 3	[20]
Synthetic	Matrigel	162 ± 52	69 ± 35	105 ± 70	[44]

Most features are consistent in scale across different basement membranes and species. One noticeable difference is the average pore size of the glomerulus BM, which has a specialized role regulating solute transport.

^aLiliensiek SJ, Murphy CJ, personal communication.

date is the glomerulus BM, which has smaller pore diameters [19, 20]. This difference may be attributed to its specialized role as a selective diffusion barrier. In order to test the roles these physical features play in guiding cellular behavior, the features must be altered and arranged in a controlled fashion to produce a useful analytic end point. Unfortunately, the ability to manipulate the native BM of a tissue *in vivo* is limited with current biological techniques, hence the value of artificial surfaces that can be designed with varying physical features to exact specifications.

11.3.1 Matrigel and Randomly Ordered Arrays

Cells behave differently on flat tissue culture plastic than they will on a complex basement membrane *in vivo*. There is currently a demand for a more realistic *in vivo*-like environment that can be used for *in vitro* studies; however, this has proved to be a technically challenging task. Isolation of extracellular matrices from living tissue is difficult, often does not produce useful amounts of experimental material, and often contains contaminating cells. The first major breakthrough to address this problem was the development of Matrigel. Researchers discovered a tumor that was rich in basement membrane components and grew rapidly, but remained benign in mice [56, 57]. Extracts of that tumor were isolated, purified, and sterilized for *in vitro* use. It was found that the resultant gel would alter the morphology, behaviors, and expression patterns of cells that were plated onto it [58, 59]. For example, endothelial cells form a monolayer on tissue culture plastic, but arrange themselves into tube-like structures on Matrigel [59]. Although Matrigel is a commonly used reagent, the actual components cannot be easily manipulated and defined, demonstrating a need for alternative artificial BMs. Matrigel still remains one of the most useful artificial basement membrane-like complexes to study behaviors, but new nanotechnology manufacturing techniques are beginning to provide different options for cell biologists searching for *in vitro* ECM alternatives.

There have been other attempts to recreate the topographical environment of a basement membrane, with silicon grooves, ridges, and tubes replacing protein fibers and pores (Fig. 11.3). These projects have utilized micro- and nanomanufacturing techniques to produce surfaces that have randomly ordered arrays, such as carbon fibers, nanotubes, or nanocolumns. These arrays have been shown to influence the morphology and expression of certain cell types [60–62]. Artificial matrices that have isotropic randomly ordered arrays of physical features are valuable research tools to create tissue culture environments that more closely resemble *in vivo* environments. They are ideal for experiments where cells can respond to a drug or protein in question within a background more similar to *in vivo* conditions. Commercial stochastic surfaces are available using electrospun fibrillar structures as well as membranes containing specified feature dimensions that have been shown to impact cell behaviors [63, 64]. A stochastic surface has the advantage of better

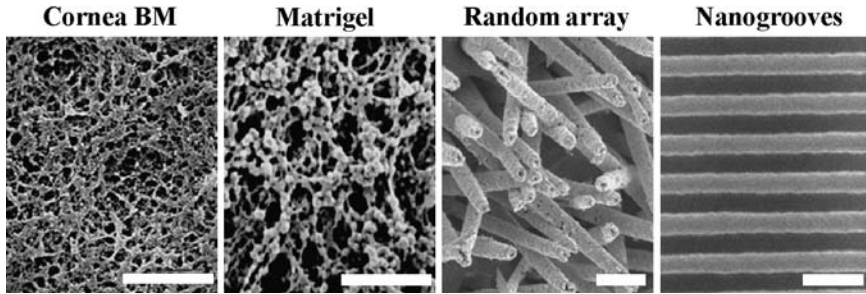


FIGURE 11.3 Scanning electron micrographs of native basement membrane, Matrigel, and bioinspired synthetic matrices. The topographical features of the corneal basement membrane compared to artificial surfaces. Matrigel biochemically and topographically mimics native BMs, but it is difficult to alter individual physical features. Synthetic isotropic surfaces, such as gold-coated “grass-like” fibers, can have some physical features altered, but still retain the random array appearance of native BMs. The physical features of anisotropic nanogrooves can be controlled and sized to study the effects of individual topographic features on cell behavior. Scale bars = 600 nm.

mimicking the surface order of the native basement membrane. These systems, however, are not ideal for studying the direct impact that physical ECM features have on cells. The drawback to these artificial systems is that there are too many variables to control in an attempt to isolate the effect of one individual feature. Pore sizes, fiber sizes, and depth are all randomly ordered and cannot be easily changed in these systems. With stochastic surfaces it is not possible to observe anisotropic cellular behaviors (such as alignment) that provide a rapid assessment of the cellular consequences of a surface structure. In order to answer specific questions about the individual physical features of BMs and their effects on cell behavior, new artificial systems had to be created. For this reason, several laboratories have focused on the modulation of cellular behaviors by nanogrooves.

Nanogrooves are repeating anisotropic ridges and channels that can be created with specified lengths and depths. While they do not simulate the surface order of the native BM, nanogrooves can be used to test a cellular response to a single anisotropic feature. For example, they can be used to test whether or not cells will align parallel to a topographic feature of a specific ridge size. The advantage of the nanogroove system is that it allows biologists to characterize cell behavior in response to a single topographic variable, thus defining basement membrane features through a reductionist approach.

11.3.2 Nanogroove Synthesis

Several laboratories have developed slightly different modifications to similar protocols in order to create grooved surfaces [65–72]. Most surface designs

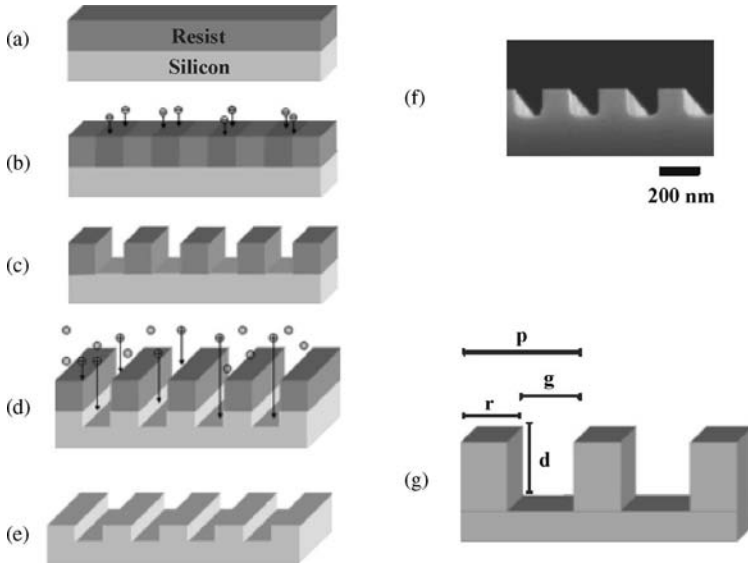


FIGURE 11.4 Fabrication of nanogrooved surface. (a–e) Sequential steps of nanogroove synthesis. (a) A photoresist is patterned on a silicon wafer. (b) The photoresist is exposed to radiation through a mask. (c) The resist is dissolved. (d) Reactive ion etching is used to produce grooves in the silicon wafer. (e) The remaining photoresist is removed to reveal a nanogrooved silicon surface. (f) Profile electron micrograph of a nanogrooved surface with 400 nm pitch. (g) Terminology of a nanogrooved surface: r = ridge, g = groove or channel, d = depth of groove or channel, p = pitch or the distance of one ridge plus one groove.

begin by patterning a photoresist on the surface of a silicon wafer via lithography (Fig. 11.4a). Briefly, the photoresist is exposed to radiation through a mask (Fig. 11.4b), and the exposed regions (for a positive tone resist) undergo chemical changes such that this material can be selectively removed by dissolving it with a developer solvent (Fig. 11.4c). For submicron- to micron-sized features, UV light can be used in the lithographic process, but for features under 100 nm, electron beam lithography is typically employed. The silicon that is not protected by the remaining photoresist can be etched to different depths by reactive ion etching to create three-dimensional relief structures (Fig. 11.4d). Finally, the remaining photoresist can be stripped to reveal a nanostructured surface comprised of controlled grooves and ridges (Fig. 11.4e–g). The silicon surface is typically coated with a compound, such as SiO_2 , or a self-assembled monolayer that makes it nontoxic and more favorable for cell attachment. Alternatively, the silicon surfaces can be used as masters in soft lithographic processes to make replicas of the original relief structures. For example, the master can be molded into polydimethylsiloxane (PDMS) stamps, and these stamps in turn can be molded into materials such as polyurethane [73, 74]. The end result is an optically clear polyurethane surface

with the same pitch and depth dimensions as the silicon master. Unfortunately, there are limitations with respect to the depth of the features that can be replicated with soft lithography. Still, these polyurethane substitutes can be made in mass quantities and are favorable to track quantitative and qualitative changes in cellular behavior with light and fluorescence microscopy methods. The rest of this chapter will summarize how specific cell types respond to known topographical features using nanogrooved surfaces.

11.4 CELL BEHAVIOR ON MANUFACTURED NANOGROOVE SURFACES

11.4.1 Nanoscale Topography Affects Cell Proliferation

The physical features of the native corneal BM have been well characterized in several species and thus serve as a rational starting point for the design of artificial BM surfaces [21, 22, 44]. The anterior corneal epithelium is a simple stratified epithelium that is continually renewed through proliferation of the basal cells. The basal cells are in contact with a basement membrane and require attachment to this substrate in order to proliferate. One recent study tested whether the scale of topographic features affects cellular proliferation. Primary human corneal epithelial cells (HCECs) seeded onto patterned polyurethane surfaces were measured for the percent increase in cell number from 4 h postplating through five days [75]. The percent increase in cell number was positively correlated with feature size such that cells on 4000 nm pitch surfaces (2200 nm ridges) had the highest percent increase while those on the 400 nm pitch (200 nm ridges) had a threefold decrease (Fig. 11.5a). A marked transition point in cellular behavior was noted between the 1200 and 1600 nm pitches (ridge widths of 400 and 900 nm) where cell proliferation on larger features was roughly identical to flat surfaces. The range of feature sizes over which the transition occurred (ridge widths of 400–900 nm) corresponds to some of the largest features present in the native basement membrane. The decreased proliferative potential for cells on 400 through 1200 nm pitch was significantly different than that found on flat surfaces, while the increase on larger features was not significant [75].

HCECs transformed by stable expression of the SV40 T-antigen exhibit a similar doubling time as primary cells [76]. Despite their transformed state, SV40 HCECs were also susceptible to topographic modulation of cellular proliferation. SV40 cells on 400 nm pitch had only about one third as many cells as those on flat surfaces, while cells on other feature sizes showed no inhibition [75]. The proliferation behavior was similar to primary HCECs, which was unexpected since the transformation with T-antigen acts to override the cells normal G1 to S-phase checkpoint [77]. This suggests that culturing cells on nanogrooved surfaces with 400 nm pitch sizes either slows the rate at which cells' progress through the cell cycle, or that other mitosis checkpoints

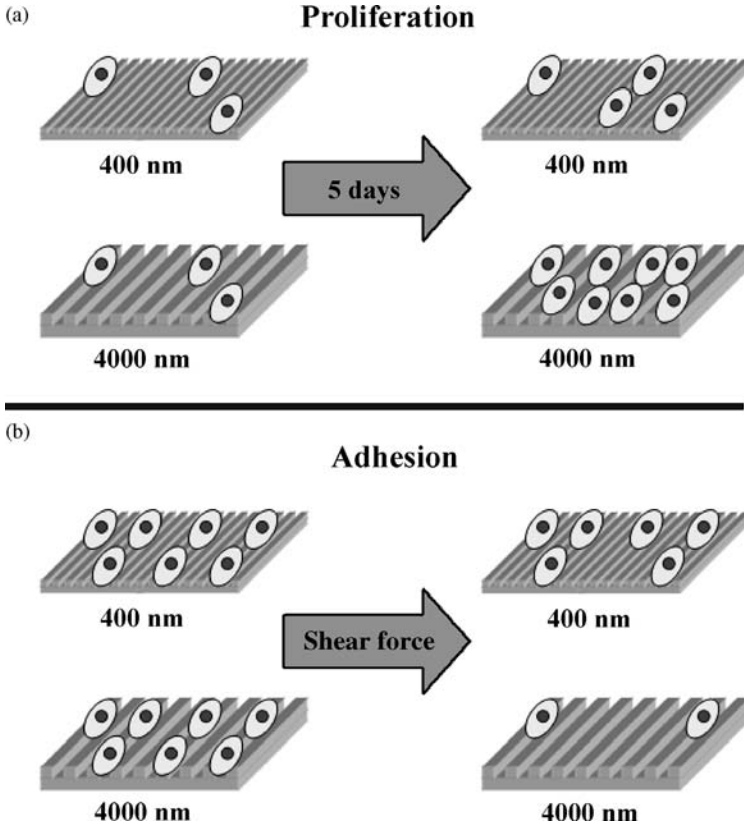


FIGURE 11.5 Cell behaviors on different scale nanogrooves. (a) Human corneal epithelial cells plated onto 4000 nm pitch grooved surfaces show a faster rate of proliferation than that on the 400 nm surfaces. (b) Cells plated onto the 4000 nm pitch surface detach easier than those plated on the 400 nm surface when subjected to 80 kPa of shear force.

are altered based on the topography of the underlying substratum. Taken as a whole, these results show that predictable modulation of cell proliferation may be accomplished through integration of specific topographic features into substrates.

11.4.2 Cellular Adhesive Strength on Nanogrooved Surfaces

Blinking of the eye results in HCECs being exposed to tear film shear forces [78, 79]. In the healthy cornea, the shear forces aid in desquamation of the outer layer of the cornea, but in a wounded cornea, blinking-induced shear might affect the ability of the underlying epithelial cells to migrate and reepithelialize the wound bed. Therefore, it is not surprising that the scale of substratum features affects the ability of cells to resist detachment under shear

flow conditions. At 400, 800, and 1200 nm (ridge widths of 70, 250, and 400 nm, respectively, with a constant depth of 600 nm), HCECs showed a marked resistance to shear flow forces at the highest forces of 80 Pa [80]. Again, a transition in cellular response to substratum features was observed around the 1200 and 1600 nm pitched grooves such that cells on 1600 nm and larger behave identically to cells plated onto flat surfaces (Fig. 11.5b).

Another influence in cellular adhesion may be due to the roughness of the surface that cells are exposed to. Nanogrooves generally have a uniform surface chemistry that is consistent between all pitch sizes; however, one study chemically modified the roughness of a flat polyurethane surface and showed enhanced adhesion of human umbilical vein endothelial cells (HUVECs) [81]. The rough surfaces were not as uniform as nanogrooves and had feature averages ranging from 2 to 40 nm. Current manufacturing techniques make it expensive and difficult to produce nanogrooved surfaces with uniform ridges much smaller than 70 nm, but very small topographical features likely play important roles in controlling cellular behaviors and must eventually be characterized.

11.4.3 Cellular Migration Rates on Nanogroove Surfaces

Migration requires cells to establish leading and trailing compartments and coordinate adhesion and deadhesion in the respective domains. For many cell types, the establishment of the orientation of these axes can be influenced by topographic cues [1]. HCECs respond to grooved substratum cues when establishing migration polarity and the scale of topographic features affects the rate of migration [82]. Individual HCECs have been shown to migrate preferentially along polyurethane ridges for all nanogroove feature sizes tested. The lowest percentage of migrating cells was found on surfaces with a 400 nm pitch (220 nm ridges), suggesting that the greater adhesive forces noted above have a negative impact on cell migration. The highest percentage of migrating cells was found on the 1600 nm pitch surfaces (900 nm ridges). In addition, the average rate of migration was found to be significantly stimulated on the 1600 nm pitch compared to the 4000, 800, and 400 nm pitches. In this situation, the divergent behavior occurs at the transition point of intermediate surface sizes. The reason for this observation may be due to the fact that migration requires two competing forces to promote efficient cell movement: sufficient adhesion to contract the leading edge of the cell and the ability of the trailing edge to detach. Thus, the optimal balance may occur somewhere between the two adhesive extremes demonstrated in the shear flow experiments.

11.4.4 Focal Adhesion Structure and Orientation are Dictated by Nanogroove Dimensions

The mechanisms by which the aforementioned HCEC responses were mediated are not clear, but may lie in the interface between the cells and the substratum.

Focal contacts and focal adhesions are sites of cell–matrix attachment and are important for regulating cytoskeletal architecture and intracellular signaling [83]. It is possible that topographic features of biologically relevant length scales affect the establishment, regulation, and persistence of signal transduction pathways. Studies have indeed shown that the size of the underlying nanogrooved ridges affects both the size and the organization of focal adhesion sites [49]. The average size of focal adhesions decreases in a linear fashion with decreasing ridge widths. The focal adhesions on 400 nm pitch (70 nm ridges) averaged 400 nm while those on 1600 nm pitch (650 nm ridges) and larger were over 800 nm. Interestingly, the orientation of the focal adhesions depends on the scale of the ridges. On 400 and 4000 nm pitches (70 and 1900 nm ridges), focal adhesions were assembled obliquely to the underlying pattern. On the 400 nm pitch (70 nm ridges), focal adhesions spanned several ridges while adhesion plaques assembled on 1900 nm ridges were confined to that single ridge (Fig. 11.6a). At the intermediate pitch, or transition zone (1200 nm pitch), focal contacts were parallel to the substratum features. These topographic cues may ultimately control focal adhesion size and lead to significant changes in cell signaling.

Besides ridge width, the importance of groove depth cannot be overlooked. Early studies have shown that fibroblasts seeded onto surfaces with 1 μm pitch

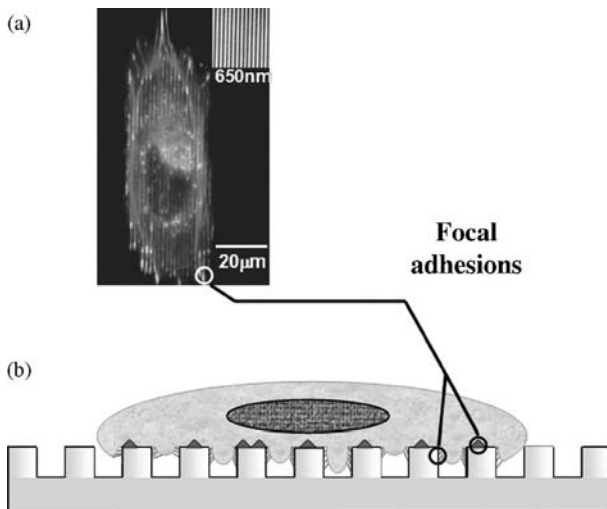


FIGURE 11.6 Focal adhesions anchor cells to nanogrooved surfaces. (a) Cells and their actin filaments (red) align parallel to grooves. Antibodies against vinculin (green) show focal adhesions are also aligned with the nanogrooved surface. (b) A side model of a cell growing on nanogrooved topography. The cell will form focal adhesions (red) on the top of the ridge and down along the walls of the groove. It should be noted that cells residing on the smallest nanoscale features usually lie across the ridges and do not invest the grooves with cellular elements.

and 1 μm depth have cellular processes that extend into the groove [84]. Another group created PDMS surfaces with ridge and groove width at a constant, albeit relatively large 3500 nm, but varied the channel depth. Bovine aortic endothelial cells cultured on these surfaces showed an increase in alignment with the grooves as the depth increased [85]. In addition, immunofluorescence images revealed that focal adhesions formed at the ridge edges and down along the walls of the channel (Fig. 11.6b). The focal adhesions could not reach the bottom of the deepest channel (5000 nm), but F-actin and vinculin were also aligned parallel to the grooves. In support of these data, recent experiments with HCECs found that cellular alignment to topography increased as nanogroove depth increased from 75 to 800 nm (Fraser SA, Murphy CJ, Nealey PF, personal communication). Undoubtedly, topographic features in all directional axes can affect cellular behavior and it is possible that the different focal adhesion architectures result in alterations in the initiation and duration of signals transduced through these complexes.

11.5 CELL SIGNALING AND EXPRESSION ON TOPOGRAPHICAL SURFACES

There is clearly a morphological difference between a cell plated onto a flat surface and a cell plated onto a nanogrooved surface. Surface topographies induce visible changes in the cytoskeleton. Recent studies have shown that cells grown on three-dimensional surfaces have sustained activation of cytoskeleton remodeling factors, such as the family of small GTPases [64]. How the physical environment is sensed by the cell and how these changes are regulated by downstream signals remain largely unknown. However, there have been several studies that have begun to characterize the translation of a physical surface cue into the enzymatic activation of a protein, a change in gene expression, or secretion of a signal.

11.5.1 Cell Morphology Changes Induced by Topography May Influence Gene Expression

Protocols to fabricate nanogrooved surfaces can be modified to produce slightly different topographic shapes and features. Instead of grooves, one modification uses electron beam lithography to create anisotropic patterns of circular or hexagonal nanopits with a specified diameter [86]. Nanopits with 120 nm diameters have been shown to limit fibroblast cell spreading. As a result of this reduced cell spreading, the nuclear area was also decreased and the centrosomes were spaced closer together [87]. The changes in cellular morphology induced by the nanopits were similar to the changes induced by cytoskeletal inhibitors [87]. These data suggest that topography alters the arrangement of microtubules and microfilaments within the cell, which in turn modulates the tension applied to the nucleus. Since many nuclear factors and

genes are regulated by their location within the nucleus, this is a possible mechanism for mechanotransduction. A hypothesized model that explains the influence a nanogrooved surface has on a cell could begin as a signal mechanically transduced from a topographical cue through the cytoskeleton and into the nucleus. A physical force transduced into the nucleus then can result in a transcription factor being “pushed” off of a compartment on the interior nuclear envelope and into the nucleoplasm in order to activate a specific gene. The end result is that a physical surface feature is translated into a change in gene expression and cell behavior.

11.5.2 Macrophages Are Stimulated by Nanoscale Topography

Macrophages have a unique ability to survive as both a suspended or an adherent cell on a variety of surfaces *in vivo*. Activated macrophages are typically recruited to an area by chemotaxic agents and need to interact with extracellular fibers and matrices to reach their target location. As a result, macrophages behave differently on artificial BM nanogrooved surfaces than on flat tissue culture plastic. P388D1 macrophage cells plated onto silicon nanogrooved surfaces of varying depth showed higher levels of phagocytosis when compared to a flat control surface [72]. Phagocytosis levels also increased as the depths of the nanogroove channels increased. The nanogroove surfaces stimulated an increase in the amount of F-actin filament present and the P388D1 cells were also able to adhere more strongly to the surfaces with deeper nanogrooves [72]. Nanoscale topographies appear to play a role in the macrophage production of inflammatory cytokines as well. J774A.1 macrophages on titanium surfaces with rough, irregular nanoscale topographies showed an increase in IL-1 β levels versus smooth surfaces during the first 48 h after plating [88]. The same rough titanium surfaces appeared to modestly decrease IL-6 production after 72 h [88]. These data further support the idea that many cellular processes that are related to adhesion can be manipulated and controlled by topographical cues on the surface substrata.

11.5.3 Osteoblast Expression on Nanoscale Surfaces

Another ideal tissue to model synthetic biomimetic surfaces after is bone because it is relatively well characterized and a common component of disease and wound healing. It is also structured like a large, continuously mineralized ECM. The mineralized fibers of bone are rich in nanoscale topography that likely influence osteoblast behavior. Researchers have used nanoscale surfaces in an attempt to study the effect of individual topographic features on bone cells. Mesenchymal stem cell-derived osteoblast-like cells align and elongate parallel to nanogrooved surfaces within 24 h of plating [89]. Additionally, the collagen matrix that these cells secrete aligned parallel to the nanogrooves. The collagen matrix produced by the same osteoblast-like cells growing on flat surfaces assembled in random directions [89]. In another

study, carbon nanofibers that possess crystalline lattice structures similar to those found in native bone ECM were used as a test substrate for osteoblasts. The carbon nanofibers, in addition to mimicking fibrous bone material, have a high degree of surface roughness. Compared to several cell types tested, osteoblasts had a stronger affinity for the nanofiber matrix due to their surface chemistry and topography [61]. Finally, osteoblast differentiation and gene expression have been shown to be modulated by topography. Osteoblasts seeded onto nanopatterned pores etched into titanium surfaces expressed increased levels of osteocalcin and alkaline phosphatase compared to flat surfaces [90]. Thus, *in vitro* nanosurfaces that closely mimic the ECM of bone are likely to yield more meaningful results that can be applied to *in vivo* models or implanted prosthetics.

11.5.4 The Addition of Soluble Factors Can Change Cellular Behavior on Nanogrooves

In initial studies of HCEC contact guidance, cells cultured in DMEM/F12 medium with serum preferentially aligned parallel to the long axis of all feature sizes [49]. Thus, contact guidance was a scale-independent phenomenon under these conditions. Unexpectedly, when HCECs were cultured in a serum-free medium, Epilife, the cells preferentially aligned parallel to micron-scale features, but perpendicular to nanometer length features [91]. At length scales of 1200–1600 nm pitch (400–650 nm ridges), the cells adopted an intermediate response with a roughly equal preference for both parallel and perpendicular orientations. On pitches below 1200 nm, the cells demonstrate a clear preference for perpendicular orientation to topographic features. Again, a clear transition in cell behavior is noted at intermediate length scales. Interestingly, intermediate orientation angles were not preferred by the HCECs on any feature sizes such that the cell alignment was either perpendicular or parallel.

As another example regarding the balance of topography and soluble factors, neurite formation in PC12 cells shows no scale-dependent effects on the percentage of cells forming neurites under standard culture conditions of 50 ng/ml of nerve growth factor (NGF). However, decreases in the concentration of NGF to suboptimal levels changed the cellular behavior of PC12 cells on surfaces with different nanogroove sizes. The most profound effects were noted when the cells were cultured in only 5 ng/ml of NGF. Under these conditions, neurite formation on nanoscale features (ridge widths of 70 and 250 nm, depth of 600 nm) was enhanced threefold over micron-scale and flat surfaces [92]. Both of these cases illustrate that a physical BM feature, such as nanogroove width, is only one component regulating complex cell behavior. Cell behaviors are augmented by soluble proteins and signal transduction pathways. In fact, the physical layout of the BM can also play a role in the dispersion of chemical signals near the cell surface interface. Brownian motion rates of solutes were twice as fast parallel to a nanogrooved surface compared

to perpendicular [93]. Therefore, the structure of artificial and native BM surfaces may also indirectly regulate biochemical signal propagation across a monolayer in tissue culture or within a stratified tissue.

11.6 CONCLUSIONS

Biological systems rely on more than just chemical signals to react and respond to their environment. At the cellular level, the physical topographical cues that lie within extracellular matrices and basement membrane surfaces can play a large role in defining migration, alignment, expression, and differentiation. Unfortunately, the direct effects that a signal feature such as fiber size, pore diameter, or pore depth can have on cell behavior remain poorly understood because researchers have had a difficult time trying to analyze and separate individual physical features from the structurally complex web of a BM. However, new manufacturing techniques have recently allowed the fabrication of nanogrooved surfaces that have repeating patterns of ridges and channels possessing feature dimensions in the biomimetic size scale that enable researchers to change one physical BM variable at a time. With a reductionist approach, the topographical cues that alter cell behavior can now be defined one feature at a time. The studies utilizing nanoscale manufacturing methods highlighted in this chapter have begun to characterize how a cell interacts with its physical environment. The fact that topographic cues that mimic the native basement membrane dramatically alter cell behaviors may provide a reason why *in vitro* studies sometimes fail to translate to an *in vivo* environment; cells within tissues never see flat surfaces. Furthermore, the knowledge gained from nanogroove *in vitro* systems may contribute to the genesis of novel strategies in cell, stem cell, and tissue engineering and advance the development of implanted prosthetics.

REFERENCES

1. Abrams GA, Teixeira AI, Nealey PF, Murphy CJ. The effects of substratum topography on cell behavior. In: Dillow A, Lowman A, editors, *Biomimetic Materials and Design*. New York Marcel Dekker; 2002;91–138.
2. Jefferson KK, Goldmann DA, Pier GB. Use of confocal microscopy to analyze the rate of vancomycin penetration through *Staphylococcus aureus* biofilms. *Antimicrob Agents Chemother* 2005;49:2467–2473.
3. Suci PA, Mittelman MW, Yu FP, Geesey GG. Investigation of ciprofloxacin penetration into *Pseudomonas aeruginosa* biofilms. *Antimicrob Agents Chemother* 1994;38:2125–2133.
4. Schembri MA, Kjaergaard K, Klemm P. Global gene expression in *Escherichia coli* biofilms. *Mol Microbiol* 2003;48:253–267.

5. Saxena S, Davies DJ, Kirsner RL. Thin basement membranes in minimally abnormal glomeruli. *J Clin Pathol* 1990;43:32–38.
6. Tonna S, et al. The risks of thin basement membrane nephropathy. *Semin Nephrol* 2005;25:171–175.
7. Taylor HR and Kimsey RA. Corneal epithelial basement membrane changes in diabetes. *Invest Ophthalmol Vis Sci* 1981;20:548–553.
8. Makino H, Yamasaki Y, Hironaka K, Ota Z. Glomerular extracellular matrices in rat diabetic glomerulopathy by scanning electron microscopy. *Virchows Arch B Cell Pathol Incl Mol Pathol* 1992;62:19–24.
9. Liu Z and Diaz LA. Bullous pemphigoid: end of the century overview. *J Dermatol* 2001;28:647–650.
10. Arikawa-Hirasawa E, Watanabe H, Takami H, Hassell JR, Yamada Y. Perlecan is essential for cartilage and cephalic development. *Nat Genet* 1999;23:354–358.
11. Boutboul S, et al. A subset of patients with epithelial basement membrane corneal dystrophy have mutations in TGFBI/BIGH3. *Hum Mutat* 2006;27:553–557.
12. Gould DB, et al. Role of COL4A1 in small-vessel disease and hemorrhagic stroke. *N Engl J Med* 2006;354:1489–1496.
13. Yurchenco PD and O'Rear JJ. Basal lamina assembly. *Curr Opin Cell Biol* 1994;6: 674–681.
14. Laurie GW, Leblond CP, Martin GR. Localization of type IV collagen, laminin, heparan sulfate proteoglycan, and fibronectin to the basal lamina of basement membranes. *J Cell Biol* 95:1982;340–344.
15. Laurie GW, Leblond CP, Inoue S, Martin GR, Chung A. Fine structure of the glomerular basement membrane and immunolocalization of five basement membrane components to the lamina densa (basal lamina) and its extensions in both glomeruli and tubules of the rat kidney. *Am J Anat* 1984;169:463–481.
16. Sanes JR and Hall ZW. Antibodies that bind specifically to synaptic sites on muscle fiber basal lamina. *J Cell Biol* 1979;83:357–370.
17. Sanes JR, Laminin, fibronectin, and collagen in synaptic and extrasynaptic portions of muscle fiber basement membrane. *J Cell Biol* 1982;93:442–451.
18. Noonan DM, et al. Identification of cDNA clones encoding different domains of the basement membrane heparan sulfate proteoglycan. *J Biol Chem* 1988;263:16379–16387.
19. Hironaka K, Makino H, Yamasaki Y, Ota Z. Pores in the glomerular basement membrane revealed by ultrahigh-resolution scanning electron microscopy. *Nephron* 1993;64:647–649.
20. Yamasaki Y, Makino H, Ota Z. Meshwork structures in bovine glomerular and tubular basement membrane as revealed by ultra-high-resolution scanning electron microscopy. *Nephron* 66:1994;189–199.
21. Abrams GA, Schaus SS, Goodman SL, Nealey PF, Murphy CJ. Nanoscale topography of the corneal epithelial basement membrane and Descemet's membrane of the human. *Cornea* 2000;19:57–64.
22. Abrams GA, Goodman SL, Nealey PF, Franco M, Murphy CJ. Nanoscale topography of the basement membrane underlying the corneal epithelium of the rhesus macaque. *Cell Tissue Res* 2000;299:39–46.

23. Pufe T, et al. Endostatin/collagen XVIII—an inhibitor of angiogenesis—is expressed in cartilage and fibrocartilage. *Matrix Biol* 2004;23:267–276.
24. Brammer RD, Bramhall SR, Eggo MC. Endostatin expression in a pancreatic cell line is modulated by a TNFalpha-dependent elastase. *Br J Cancer* 2005;93:1024–1028.
25. Brammer RD, Bramhall SR, Eggo MC. Endostatin expression in pancreatic tissue is modulated by elastase. *Br J Cancer* 2005;92:89–93.
26. Carlson MA and Longaker MT. The fibroblast-populated collagen matrix as a model of wound healing: a review of the evidence. *Wound Repair Regen* 2004;12:134–147.
27. Lackie JM, Chaabane N, Crocket KV. A critique of the methods used to assess leucocyte behaviour. *Biomed Pharmacother* 1987;41:265–278.
28. Presta M, Rusnati M, Urbinati C, Sommer A, Ragnotti G. Biologically active synthetic fragments of human basic fibroblast growth factor (BFGF): Identification of two Asp-Gly-Arg-containing domains involved in the mitogenic activity of BFGF in endothelial cells. *J Cell Physiol* 1991;149:512–524.
29. Nagayoshi T, et al. Human nidogen: complete amino acid sequence and structural domains deduced from cDNAs, and evidence for polymorphism of the gene. *DNA* 1989;8:581–594.
30. Thompson MT, et al. Biochemical functionalization of polymeric cell substrata can alter mechanical compliance. *Biomacromolecules* 2006;7:1990–1995.
31. Engler A, et al. Substrate compliance versus ligand density in cell on gel responses. *Biophys J* 2004;86:617–628.
32. Pelham RJ Jr and Wang Y. Cell locomotion and focal adhesions are regulated by substrate flexibility. *Proc Natl Acad Sci USA* 1997;94:13661–13665.
33. Wozniak MA, Desai R, Solski PA, Der CJ, Keely PJ. Rock-generated contractility regulates breast epithelial cell differentiation in response to the physical properties of a three-dimensional collagen matrix. *J Cell Biol* 2003;163:583–595.
34. Deroanne CF, Lapiere CM, Nusgens BV. *In vitro* tubulogenesis of endothelial cells by relaxation of the coupling extracellular matrix–cytoskeleton. *Cardiovasc Res* 2001;49:647–658.
35. Engler AJ, et al. Myotubes differentiate optimally on substrates with tissue-like stiffness: pathological implications for soft or stiff microenvironments. *J Cell Biol* 2004;166:877–887.
36. Polte TR, Eichler GS, Wang N, Ingber DE. Extracellular matrix controls myosin light chain phosphorylation and cell contractility through modulation of cell shape and cytoskeletal prestress. *Am J Physiol Cell Physiol* 2004;286:C518–528.
37. Wong GA, Tang V, El-Sabeawy F, Weiss RH. BMP-2 inhibits proliferation of human aortic smooth muscle cells via p21Cip1/Waf1. *Am J Physiol Endocrinol Metab* 2003;284:E972–979.
38. Damljanovic V, Lagerholm BC, Jacobson K. Fibroblast traction assays on modified polyacrylamide substrates. *Mol Biol Cell* 2004;15:160A.
39. Doyle AD and Lee J. Cyclic changes in keratocyte speed and traction stress arise from Ca²⁺-dependent regulation of cell adhesiveness. *J Cell Sci* 2005;118:369–379.

40. Georges PC, Miller WJ, Meaney DF, Sawyer ES, Janmey PA. Matrices with compliance comparable to that of brain tissue select neuronal over glial growth in mixed cortical cultures. *Biophys J* 2006;90:3012–3018.
41. Woerly S, Doan VD, Sosa N, de Vellis J, Espinosa-Jeffrey A. Prevention of gliotic scar formation by neurogel allows partial endogenous repair of transected cat spinal cord. *J Neurosci Res* 2004;75:262–272.
42. Engler AJ, Sen S, Sweeney HL, Discher DE. Matrix elasticity directs stem cell lineage specification. *Cell* 2006;126:677–689.
43. Abrams GA, Murphy CJ, Wang ZY, Nealey PF, Bjorling DE. Ultrastructural basement membrane topography of the bladder epithelium. *Urol Res* 2003;31:341–346.
44. Abrams GA, Bentley E, Nealey PF, Murphy CJ. Electron microscopy of the canine corneal basement membranes. *Cells Tissues Organs* 2002;170:251–257.
45. Harrison R. On the stereotropism of embryonic cells. *Science* 1911;34:279.
46. Harrison R. The reaction of the embryonic cells to solid structures. *J Exp Zool* 1921;17:521.
47. Curtis A and Wilkinson C. Topographical control of cells. *Biomaterials* 1997;18:1573–1583.
48. Washburn NR, Yamada KM, Simon CG Jr, Kennedy SB, Amis EJ. High-throughput investigation of osteoblast response to polymer crystallinity: influence of nanometer-scale roughness on proliferation. *Biomaterials* 2004;25:1215–1224.
49. Teixeira AI, Abrams GA, Bertics PJ, Murphy CJ, Nealey PF. Epithelial contact guidance on well-defined micro- and nanostructured substrates. *J Cell Sci* 2003;116:1881–1892.
50. Fan YW, et al. Culture of neural cells on silicon wafers with nano-scale surface topograph. *J Neurosci Methods* 2002;120:17–23.
51. Clark P, Connolly P, Curtis AS, Dow JA, Wilkinson CD. Cell guidance by ultrafine topography in vitro. *J Cell Sci* 1991;99: (Pt 1):73–77.
52. Dalby MJ, Riehle MO, Johnstone HJ, Affrossman S, Curtis AS. Polymer-demixed nanotopography: control of fibroblast spreading and proliferation. *Tissue Eng* 2002;8:1099–1108.
53. Dalby MJ, Yarwood SJ, Johnstone HJ, Affrossman S, Riehle MO. Fibroblast signaling events in response to nanotopography: a gene array study. *IEEE Trans Nanobioscience* 2002;1:12–17.
54. Bystrom B, Virtanen I, Rousselle P, Gullberg D, Pedrosa-Domellof F. Distribution of laminins in the developing human eye. *Invest Ophthalmol Vis Sci* 2006;47:777–785.
55. Ziebarth NM, Manns F, Uhlhorn SR, Venkatraman AS, Parel JM. Noncontact optical measurement of lens capsule thickness in human, monkey, and rabbit postmortem eyes. *Invest Ophthalmol Vis Sci* 2005;46:1690–1697.
56. Futaki S, et al. Molecular basis of constitutive production of basement membrane components. Gene expression profiles of Engelbreth–Holm–Swarm tumor and f9 embryonal carcinoma cells. *J Biol Chem* 2003;278:50691–50701.
57. Orkin RW, et al. A murine tumor producing a matrix of basement membrane. *J Exp Med* 1977;145:204–220.

58. Kleinman HK, et al. Basement membrane complexes with biological activity. *Biochemistry* 1986;25:312–318.
59. Kubota Y, Kleinman HK, Martin GR, Lawley TJ. Role of laminin and basement membrane in the morphological differentiation of human endothelial cells into capillary-like structures. *J Cell Biol* 1988;107:1589–1598.
60. Dalby MJ, Riehle MO, Sutherland DS, Agheli H, Curtis AS. Changes in fibroblast morphology in response to nano-columns produced by colloidal lithography. *Biomaterials* 25:2004;5415–5422.
61. Price RL, Ellison K, Haberstroh KM, Webster TJ. Nanometer surface roughness increases select osteoblast adhesion on carbon nanofiber compacts. *J Biomed Mater Res A* 2004;70:129–138.
62. Stevens MM and George JH. Exploring and engineering the cell surface interface. *Science* 2005;310:1135–1138.
63. Ahmed I, et al. Three-dimensional nanofibrillar surfaces covalently modified with tenascin-c-derived peptides enhance neuronal growth *in vitro*. *J Biomed Mater Res A* 2006;76:851–860.
64. Nur EKA, Ahmed I, Kamal J, Schindler M, Meiners S. Three dimensional nanofibrillar surfaces induce activation of Rac. *Biochem Biophys Res Commun* 2005;331:428–434.
65. Brunette DM. Spreading and orientation of epithelial cells on grooved substrata. *Exp Cell Res* 1986;167:203–217.
66. Chehroudi B, Gould TR, Brunette DM. Titanium-coated micromachined grooves of different dimensions affect epithelial and connective-tissue cells differently *in vivo*. *J Biomed Mater Res* 1990;24:1203–1219.
67. Chehroudi B, McDonnell D, Brunette DM. The effects of micromachined surfaces on formation of bonelike tissue on subcutaneous implants as assessed by radiography and computer image processing. *J Biomed Mater Res* 1997;34:279–290.
68. Dalby MJ, Riehle MO, Yarwood SJ, Wilkinson CD, Curtis AS. Nucleus alignment and cell signaling in fibroblasts: response to a micro-grooved topography. *Exp Cell Res* 2003;284:274–282.
69. den Braber ET, et al. Effect of parallel surface microgrooves and surface energy on cell growth. *J Biomed Mater Res* 1995;29:511–518.
70. Kim SO, et al. Epitaxial self-assembly of block copolymers on lithographically defined nanopatterned substrates. *Nature* 2003;424:411–414.
71. Pins GD, Bush KA, Cunningham LP, Campagnola PJ. Multiphoton excited fabricated nano and micropatterned extracellular matrix proteins direct cellular morphology. *J Biomed Mater Res A* 2006;78:194–204.
72. Wojciak-Stothard B, Curtis A, Monaghan W, MacDonald K, Wilkinson C. Guidance and activation of murine macrophages by nanometric scale topography. *Exp Cell Res* 1996;223:426–435.
73. Whitesides GM, Ostuni E, Takayama S, Jiang X, Ingber DE. Soft lithography in biology and biochemistry. *Annu Rev Biomed Eng* 2001;3:335–373.
74. Kane RS, Takayama S, Ostuni E, Ingber DE, Whitesides GM. Patterning proteins and cells using soft lithography. *Biomaterials* 1999;20:2363–2376.

75. Liliensiek SJ, Campbell S, Nealey PF, Murphy CJ. The scale of substratum topographic features modulates proliferation of corneal epithelial cells and corneal fibroblasts. *J Biomed Mater Res A* 2006;79:185–192.
76. Araki-Sasaki K, et al. An SV40-immortalized human corneal epithelial cell line and its characterization. *Invest Ophthalmol Vis Sci* 1995;36:614–621.
77. DeCaprio JA, et al. Sv40 large tumor antigen forms a specific complex with the product of the retinoblastoma susceptibility gene. *Cell* 1988;54:275–283.
78. Fatt I. Architecture of the lid-cornea juncture. *CLAO J* 1992;18:187–192.
79. King-Smith PE, et al. The thickness of the human precorneal tear film: evidence from reflection spectra. *Invest Ophthalmol Vis Sci* 2000;41:3348–3359.
80. Karuri NW, et al. Biological length scale topography enhances cell-substratum adhesion of human corneal epithelial cells. *J Cell Sci* 2004;117:3153–3164.
81. Chung TW, Liu DZ, Wang SY, Wang SS. Enhancement of the growth of human endothelial cells by surface roughness at nanometer scale. *Biomaterials* 2003;24:4655–4661.
82. Diehl KA, Foley JD, Nealey PF, Murphy CJ. Nanoscale topography modulates corneal epithelial cell migration. *J Biomed Mater Res A* 2005;75:603–611.
83. Sastry SK and Burridge K. Focal adhesions: a nexus for intracellular signaling and cytoskeletal dynamics. *Exp Cell Res* 2000;261:25–36.
84. Meyle J, Gultig K, Wolburg H, von Recum AF. Fibroblast anchorage to microtextured surfaces. *J Biomed Mater Res* 1993;27:1553–1557.
85. Uttayarat P, Toworfe GK, Dietrich F, Lelkes PI, Composto RJ. Topographic guidance of endothelial cells on silicone surfaces with micro- to nanogrooves: orientation of actin filaments and focal adhesions. *J Biomed Mater Res A* 2005;75:668–680.
86. Curtis AS, et al. Cells react to nanoscale order and symmetry in their surroundings. *IEEE Trans Nanobioscience* 2004;3:61–65.
87. Dalby MJ, et al. Nanotopographical stimulation of mechanotransduction and changes in interphase centromere positioning. *J Cell Biochem* 2006;100:326–338.
88. Tan KS, Qian L, Rosado R, Flood PM, Cooper LF. The role of titanium surface topography on J774A. 1 macrophage inflammatory cytokines and nitric oxide production. *Biomaterials* 2006;27:5170–5177.
89. Zhu B, Lu Q, Yin J, Hu J, Wang Z. Alignment of osteoblast-like cells and cell-produced collagen matrix induced by nanogrooves. *Tissue Eng* 2005;11:825–834.
90. Zinger O, et al. Differential regulation of osteoblasts by substrate microstructural features. *Biomaterials* 2005;26:1837–1847.
91. Teixeira AI, et al. The effect of environmental factors on the response of human corneal epithelial cells to nanoscale substrate topography. *Biomaterials* 2006;27:3945–3954.
92. Foley JD, Grunwald EW, Nealey PF, Murphy CJ. Cooperative modulation of neuritegenesis by PC12 cells by topography and nerve growth factor. *Biomaterials* 2005;26:3639–3644.
93. King MR. Anisotropic Brownian diffusion near a nanostructured surface. *J Colloid Interface Sci* 2006;296:374–376.

Focal Adhesions: Self-Assembling Nanoscale Mechanochemical Machines that Control Cell Function

TANMAY LELE and DONALD E. INGBER

12.1 INTRODUCTION

Living cells and organisms are constructed through hierarchical self-assembly of nanoscale molecular components. In the past, the primary focus in biology was on analysis of the composition and structure of individual biochemical constituents. However, it has become increasingly clear that the organic properties of living cells, including their ability to change shape, move, and grow, are a function of biological architecture — how these molecular components are positioned in space and connected to each other so as to produce structures with specialized forms and biochemical functions [1, 2]. This is true whether at the scale of a few molecules that come together to form a single multicomponent enzyme or at the level of the whole cell where different types of multimolecular, nanoscale filaments, bundles, and tubes join together to form the molecular framework of the cell, known as the “cytoskeleton”.

Because certain molecular filaments in the cytoskeleton actively generate mechanical (e.g., contractile) forces through an actomyosin filament sliding mechanism (like in muscle), all of the components of the cytoskeleton must physically resist these forces, as well as external mechanical stresses, to maintain cell shape stability [1]. At the same time, the cell possesses a mechanism to respond to these physical stresses by remodeling these very same structures (e.g., adding new components where they are needed and removing them where they are not). This ability to convert mechanical signals into biochemical signals and vice versa is one form of “mechanotransduction,” a fundamental property of

virtually all living materials [3]. If we could understand how structures are constructed at the nanometer scale so as to provide these linked mechanical and chemical functions, we might be able to revolutionize materials design by creating multifunctional “biomimetic” materials that mimic these properties for medical, industrial, and military applications.

Another key feature of living materials that makes it possible for them to interconvert mechanical and chemical energy is that the molecules that comprise many of structural scaffolds in cells, including the cytoskeleton, also carry out biochemical functions, or physically associate with chemically active molecules in the cytoplasm. This structure-based form of metabolism has been termed “solid-state biochemistry” [2]. Thus, for example, mechanical stresses that are exerted on the surface of the cell and transferred to the internal cytoskeleton can influence biochemical activities of some of its load-bearing components. Biochemical signaling may be triggered through stress-dependent alterations of molecular shape, which change biophysical parameters such as molecular binding affinities or opening and closing rates of ion channels [4]. Thus, to understand biological nanostructures and to mimic their novel properties in future man-made materials, it is necessary to understand how living cells are able to build and organize macromolecular scaffolds that provide critical structural and biochemical functions, as well as transduce mechanical and chemical signals at the nanometer scale.

In this chapter, we focus on specialized cell anchoring complexes, known as “focal adhesions,” as an example of self-assembling nanostructures that carry out all of these functions. These are particularly interesting because they physically bridge load-bearing extracellular matrix (ECM) scaffolds on the outside of the cell with the intracellular cytoskeleton as a result of binding interactions with transmembrane integrin receptors [5–7]. These multimolecular linkages provide a mechanism to channel mechanical stresses from ECM molecules to intracellular focal adhesion proteins that, in turn, anchor to the actin cytoskeleton [6]. In addition, the macromolecular scaffolds that comprise the focal adhesion grow and shrink when stresses applied to integrins are increased or decreased, respectively [8]; and numerous signal transducing molecules are concentrated within these structures [9, 10]. Thus, focal adhesions are a major site for mechanochemical conversion inside the cell, and the dynamic assembly of these structures is critical for whole cell behaviors, including growth, differentiation, and movement. In this chapter, we therefore review the concepts of solid-state biochemistry, macromolecular assembly, cellular mechanotransduction, and mechanoregulation of cell behavior using the focal adhesion as the paradigm for a self-assembling nanoscale mechanochemical machine. We also discuss the implications of these findings for future biomaterials design.

12.2 SOLID-STATE BIOCHEMISTRY IN FOCAL ADHESIONS

The control of cell behavior has been traditionally viewed as being triggered primarily by soluble stimuli (e.g., hormones, growth factors). These factors

bind to surface receptors on the outside of the cell and alter their conformation. This change in molecular shape triggers a cascade of biochemical events— a process known as signal transduction — that ultimately results in control of cell behavior. However, over the last decade, it has become clear that many of the molecules that mediate signal transduction are not floating free in the cytoplasm or lipid bilayer, and instead function when physically immobilized on insoluble molecular scaffolds inside the cytoplasm and nucleus, such as the cytoskeleton and nuclear matrix [11].

Signaling proceeds on these self-assembled, multimolecular scaffolds through binding interactions between several constituent macromolecules. Furthermore, there is an even higher level of complexity because the multiprotein complexes that form these insoluble scaffolds are constantly assembling and disassembling inside living cells, and this assembly may be controlled by physical cues like mechanical forces [12, 13]. Thus, the focal adhesion is an outstanding example of this type of insoluble multimolecular, mechanochemical scaffold that serves to mediate cell adhesion, spreading, contraction, and movement on ECM substrates.

Unlike a water droplet spreading on a surface, cells adhere to ECM at discrete sites. Cell–substrate adhesions assemble in these locations when transmembrane integrin receptors ligate ECM molecules (e.g., fibronectin, laminin, vitronectin, various collagen types) in the external environment and cluster together within the surface membrane [7]. This causes recruitment of a variety of molecules to the inner surface of the clustered integrins, including focal adhesion scaffold proteins that physically couple integrins to tensed actin microfilaments, such as talin, vinculin, α -actinin, paxillin, zyxin, and filamin, thereby mechanically anchoring the ECM to the cytoskeleton (Fig. 12.1). Other

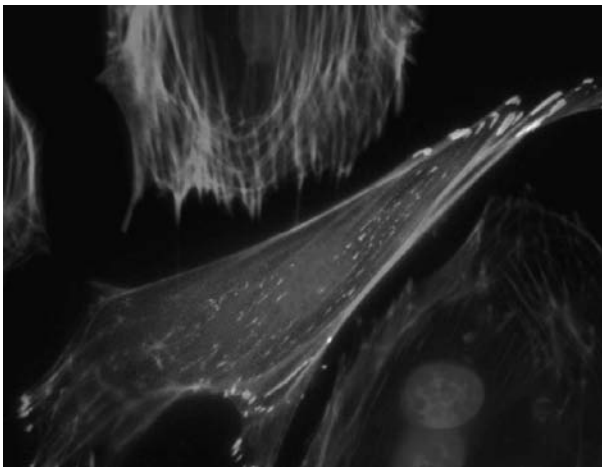


FIGURE 12.1 Fluorescence image of a single capillary endothelial cell expressing GFP-vinculin (green), stained for F-actin with Alexa 468-phalloidin (red), and nuclei with DAPI (blue). Note how each actin stress fiber anchors to focal adhesions at its distal ends (bar = 10 μm).

proteins that are simultaneously recruited to the cytoskeletal backbone of the integrin-associated focal adhesion include various signal transducing molecules, such as protein kinases (tyrosine, serine, and threonine), protein phosphatases, inositol lipid kinases, ion channels, G proteins, and certain growth factor receptors [14, 15]. In fact, it is now clear that focal adhesions are extremely complex macromolecular assemblies consisting of at least 50 different proteins [10]. These various proteins play unique functional roles in mediating focal adhesion assembly, as well as providing the crucial link between the cell–ECM interface and biochemical signaling pathways that regulate cellular behavior.

Ultrastructural studies of focal adhesion architecture have revealed that they measure ~ 60 nm in thickness, with areas of a few square micrometers in the plane parallel to the ECM substrate [16]. Use of two-photon microscopy with fluorescent membrane probes has also revealed that these are higher ordered portions of the cell membrane, which may, in turn, influence structural organization of associated lipid rafts [17]. These adhesion structures can vary in size and shape within the same cell because they form, mature, and disassemble over time [18].

A mature focal adhesion is the culmination of a complex process that begins with the formation of small dot-like adhesions, called “focal complexes,” at the leading edge of a motile cell [18], which differ in their chemical composition from mature focal adhesions [14]. Nascent focal complexes have significantly low concentrations of certain focal adhesion proteins, such as α -actinin, vinculin, paxillin, FAK, and VASP [14]. Interestingly, zyxin, a protein present abundantly in mature focal adhesions, is completely absent in focal complexes in certain cells. Many focal complexes are fated to dissolve away, but some survive and grow in size to form mature focal adhesions in a tension-dependent manner [14].

Exertion of sustained, polarized tensional forces by or on cells causes some focal adhesions to reorganize and move toward the nucleus, resulting into linear, streak-like shaped anchoring structures called fibrillar adhesions [19]. While focal complexes and focal adhesions are predominantly present close to the cell periphery, fibrillar adhesions are more localized in the central regions of the cell. Fibrillar adhesions are enriched in $\alpha 5\beta 1$ integrin as opposed to $\alpha V\beta 3$ integrin, which is primarily found in focal adhesions [20]. Fibrillar adhesions also have elevated levels of tensin and low levels of phosphotyrosine compared to focal adhesions [20]. Thus, focal complexes, focal adhesions, and fibrillar adhesions differ not only in their shape, size, and subcellular localization, but also in their molecular composition.

12.3 FOCAL ADHESION AS A MECHANOTRANSDUCTION MACHINE

Because focal adhesions form a molecular bridge between ECM, integrins, and the contractile actin cytoskeleton, they provide a preferential path for the

transfer of mechanical forces across the cell surface [6]. This is true whether it involves transmission of internal cytoskeletal traction forces to the ECM substrate, which are critical for cell migration, muscle contraction, and cell shape changes, or for transfer of external mechanical stresses to the cytoskeleton and nucleus [21].

Importantly, the focal adhesion does not just passively transmit force to associated biochemical signal transducing molecules, it also changes its own assembly in response to forces that impinge on it [22, 23]. For example, focal adhesion area directly correlates with the level of traction force exerted on these sites at the substrate interface in stationary (nonmotile) cells [24, 25]. When tension in contractile microfilaments is relaxed by chemically inhibiting myosin II-mediated contractility, time-dependent disassembly of preexisting focal adhesions occurs and new adhesions do not form [26, 27]. Application of fluid shear stresses to the apical cell surface or mechanical strain to whole cells causes remodeling of focal adhesions at the base, in part, through stress-dependent activation of additional integrin receptors [28, 29]. Forces applied to the apical surface of the cell through a micropipette can also induce adhesion assembly at the cell base in a myosin II-independent manner [8]. This appears to be mediated by force channeling through the cytoskeleton [5, 6, 21, 30–33]. When cells are cultured on ECMs that vary in stiffness, focal adhesions also have a smaller average size on soft versus rigid substrates; this is because cells are not able to exert significant traction forces on the softer matrices [34]. Taken together, these observations support the hypothesis that mechanical forces control focal adhesion assembly.

Various stimuli including externally applied mechanical forces, ECM ligand affinity [35], ECM mechanics [36], nanoscale ligand distribution, and substrate topology [37, 38] regulate the composition and the concentration of macromolecules that localize within focal adhesions. Focal adhesion assembly also regulates soluble signaling pathways, including Erk signaling that controls cell growth [39]. Integrin ligation triggers a variety of signal transduction pathways that modulate cell shape, gene expression, differentiation, and apoptosis [39–45]. However, the cell's response to soluble growth, motility, and survival factors also depends on the ability of integrins to transfer transmembrane mechanical signals across the cell surface and to the focal adhesion. For example, force transfer to the focal adhesion mediated by integrin–cytoskeletal connections induces a variety of responses including cAMP signaling [46, 47], Ca^{2+} influx (through mechanosensitive ion channels), cytoskeletal remodeling [48], alterations of cell shape [49, 50], and changes in nuclear morphology [21]. These latter effects on cell and nuclear shape are equally important regulators of cell growth, differentiation, contractility, motility, and survival as soluble cytokines and hormones [51–56]. Thus, the focal adhesion is really a nanoscale mechanochemical machine that transduces mechanical forces into intracellular biochemical signals, and therefore mediates both chemical and physical control of cellular physiology by ECM and mechanical forces.

12.4 MECHANICAL CONTROL OF MOLECULAR BINDING INTERACTIONS IN FOCAL ADHESIONS

How do mechanical forces control the assembly of complex nanoassemblies like focal adhesions? One possible mechanism is that force application may change macromolecular conformation [57, 58] and expose cryptic binding sites that promote recruitment of binding partners. For example, using fluorescence resonance energy transfer (FRET) to detect changes in protein conformation, mechanical forces were shown to locally unfold ECM molecules such as fibronectin, which promotes molecular self-assembly (fibronectin fibrillogenesis) outside the cell [59, 61]. Computational modeling studies suggest that an analogous process could occur inside the cell within the focal adhesion [57].

Alternatively, force-dependent changes in molecular conformation may alter the binding kinetics of certain load-bearing proteins within the focal adhesion. This could perturb the steady-state balance between binding and unbinding, and thereby result in a change in focal adhesion size and density. This concept is based, in part, on early work in the field of mechanoregulation that suggested that the dissociation rate constant k_{OFF} of a receptor from a ligand–receptor complex may rise exponentially with an increase in the imposed mechanical stress. This was shown to be experimentally valid for adhesive bonds between neutrophils in shear flow that tether transiently to P-selectin-coated substrates [62]. Such ligand–receptor bonds that break more easily under increasing force are termed slip bonds. However, increasing force can also make bonds stronger; these are termed catch bonds [63, 65]. Direct experimental evidence for the existence of catch bonds has come from studies that used atomic force microscopy to study bonds between purified P-selectin and P-selectin glycoprotein ligand-1 molecules [65].

We recently tested the hypothesis that intracellular mechanical forces alter the binding kinetics of focal adhesion proteins within living cells [12, 66]. To do this, we used fluorescence recovery after photobleaching (FRAP) to photobleach GFP-tagged proteins that localize to adhesions, such as vinculin and zyxin. In FRAP, fluorescently labeled molecules within a small region of the surface membrane, cytoplasm, or nucleus are exposed to a brief pulse of radiation from a laser beam. When the appropriate wavelength of light is utilized, this irradiation bleaches all of the molecules within the path of the beam without altering their structure or function [67]. Repeated fluorescence images of the bleached zone can be used to measure the rate at which remaining fluorescent molecules in the cytoplasm redistribute and replace photobleached ones on focal adhesion scaffolds.

We first confirmed that molecular diffusion was not rate limiting during FRAP recovery for zyxin and vinculin. Under these conditions, the normalized recovery during FRAP can be used to estimate the k_{OFF} of individual proteins inside living cells. We found that both zyxin and vinculin recover over timescales of several seconds inside focal adhesions in living capillary endothelial cells (Fig. 12.2a) [66]. To alter the tension exerted on these

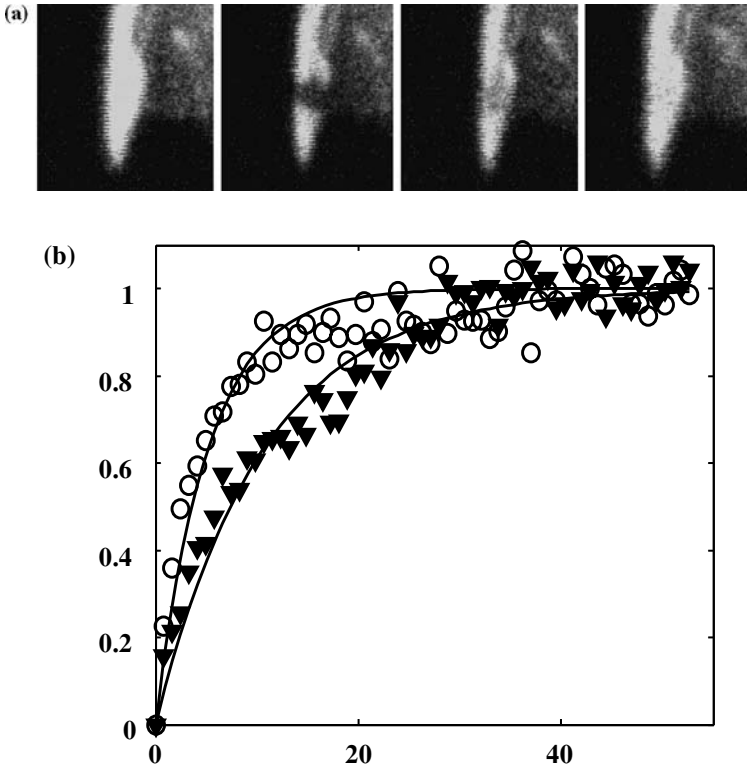


FIGURE 12.2 Tension dissipation accelerates FRAP recovery of zyxin in living cells. (a) Confocal fluorescence microscopic images of a single focal adhesion containing GFP-zyxin before (left) and 0, 12, and 40 s after (right) a small circular area ($<1 \mu\text{m}^2$) was photobleached with a high intensity laser pulse of wavelength 488 nm (white arrow) using a Zeiss LSM 510 meta laser scanning confocal microscope. Note that the fluorescence staining recovers over time. (b) Graph showing time-dependent recovery of fluorescence intensity for GFP-zyxin in control (open circles) versus cells in which tension was dissipated (closed triangles); solid lines are curve fits to $1 - e^{-k_{\text{OFF}}t}$ using the method of least squares to estimate k_{OFF} . See Reference [82] for more details.

adhesions, we either chemically inhibited actomyosin-based tension using pharmacological agents or physically severed individual stress fibers using a tightly focused femtosecond laser that vaporizes cellular structures with $\sim 300 \text{ nm}$ resolution [68,69]. Severing the stress fiber resulted in retraction of the cut ends (Fig. 12.3) and relaxation of traction stress at cell–substrate adhesion sites [70].

When we used this laser surgery method to sever a single stress fiber in a living cell and then immediately measured the effects of dissipating tension on individual focal adhesions on the binding kinetics of vinculin and zyxin using FRAP, we found that the dissociation rate constant of zyxin increased with

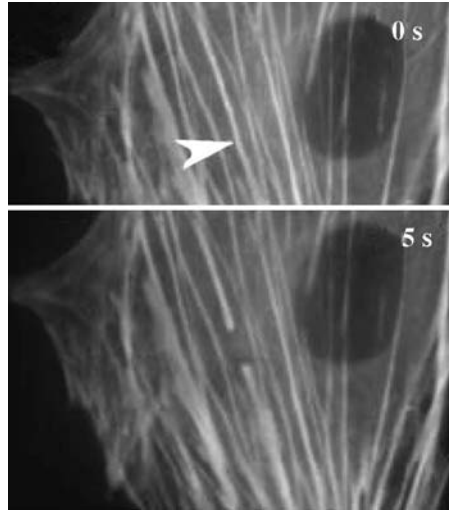


FIGURE 12.3 Tension dissipation in a living cell by mechanical disruption of a single stress fiber using laser nanosurgery. Fluorescence microscopic images of a living endothelial cell expressing YFP-actin before (top) and 5 s after (bottom) a single stress fiber (white arrow) was severed by applying light energy to the center of the fiber using a pulsed Ti:sapphire laser at 790 nm (bar = 10 μm). See Reference [70] for more details.

decreasing tension, as indicated by increased rates of fluorescence recovery (Fig. 12.2b) [66]. Interestingly, the dissociation rate constant of vinculin, another adhesion molecule that colocalizes with zyxin in the same focal adhesions, remained unchanged [66]. These effective dissociation rate constants arise due to binding interactions between the photobleached molecule and its binding partners. This suggests that assembly of at least a subset of adhesion proteins may be regulated by mechanical forces through changes in their binding kinetics. Importantly, our measured changes in the dissociation rate constant of zyxin can predict the overall tension-dependent disassembly rates of zyxin from focal adhesions observed over many minutes. Thus, our measured rate constants represent an essential input in developing systems-level models of dynamic assembly of complex macromolecular assemblies like focal adhesions.

12.5 THE FOCAL ADHESION AS A MULTIFUNCTIONAL BIOMATERIAL

Although biologists tend to think of the focal adhesion as a multimolecular signaling complex or a mechanotransduction organelle, it is in reality a biomaterial. Its material properties are as critical for its function (particularly its anchoring capability) as the chemical composition of its constituents. But it

has many novel features compared to man-made materials. One feature discussed already is its ability to dynamically assemble and disassemble in response to force application. This process can also be induced biochemically by triggering different signaling cascades, although these too may influence the assembly process in the end by regulating cell-generated tensional forces [8].

Another property of the focal adhesion is its ability to mediate mechanochemical transduction, apparently as a result of force-induced changes of conformation and binding kinetics of load-bearing molecules within this anchoring complex. However, this same anchoring scaffold can influence chemomechanical conversion in that chemical modification of focal adhesion mechanics or assembly will alter the level of cytoskeletal tension transferred to the ECM substrate and neighboring cells. This is one way in which biochemical signals may influence cell movement and contractility.

Importantly, focal adhesions can also mediate mechano-electrical conversion, for example, by force-dependent activation of membrane ion channels that can associate with integrins and change their activity when stresses are varied [71–73]. It is possible that electrical signals could similarly impact cell function by altering the structure, assembly, or biochemical signaling properties of focal adhesions, perhaps through stress-dependent changes in ion flux across the cell membrane.

It is also important to clarify that the focal adhesion represents a site for integration of different types of chemical signals, in particular, those conveyed by binding of both soluble and insoluble molecules to cell surface signaling receptors. For example, ligation and clustering of cell surface receptors by soluble growth factors (e.g., FGF, PDGF) can elicit distinct signals (e.g., changes of Na^+/H^+ exchange, inositol lipid modifications) from those produced by integrin binding to insoluble ECM molecules (independent of force application). Yet these signals integrate to control cell behavior, and the integration is mediated by enzymes and substrates that function when immobilized on the cytoskeletal backbone of the focal adhesion [74–78].

In summary, the focal adhesion is an amazing biomaterial in that it simultaneously provides sensing, processing, integration, and response functions. It is a material that provides the cell with the ability to fuse inputs, to integrate this information, and to change its structure to strengthen itself when needed, and to release itself and shut down the processing activity when not. These features are truly unique to living materials and represent a target for biomimicry in the future.

12.6 CONCLUSIONS

Controlling the mechanical properties of biomaterials is emerging as one of the most promising strategies for controlling cellular behavior in the field of tissue engineering [34]. Applications range from controlling stem cell fate switching and creating muscle tissue *in vitro* to promoting neuron differentiation [79–81].

The emerging theme is that cells prefer to attach to substrates that have mechanical properties similar to their natural microenvironment *in vivo*. This ability of cells to sense substrate stiffness is intimately linked to the ECM–cytoskeleton connection within focal adhesions. Thus, understanding how focal adhesions are assembled inside living cells is central to designing new therapeutic interventions for treating disease, developing new technologies that effectively interface with cells, and creating a more rational approach to biomaterials design for tissue engineering applications.

Supramolecular self-assembled structures like focal adhesions are a universal feature of living organisms. Such multiprotein complexes are assembled through transient binding interactions between constituent molecules. Mechanical forces generated through the actin cytoskeleton or transmitted to cells from their surrounding microenvironment can regulate these binding interactions, and hence control adhesion assembly. Given that adhesion assembly is intimately linked to intracellular signaling pathways that control cellular behaviors such as differentiation, growth, and apoptosis, a clearer understanding of how focal adhesions are assembled from their constituents so as to carry out mechanochemical conversion is of great interest in biology and medicine. A more complete understanding of this mechanism will come from multidisciplinary efforts that rely on quantitative experimentation, combined with molecular simulation techniques that predict how the conformation of adhesion proteins may change in response to applied forces. In this context, *in vitro* methods that permit more precise measures of changes of protein binding kinetics may prove invaluable.

But the goal for the future is to understand how force is channeled to particular molecules, or groups of molecules, within the focal adhesion so as to promote coordinated self-assembly, and simultaneously link structure to chemistry. It will be necessary to adapt techniques similar to those described here (e.g., FRAP, FRET, laser nanosurgery) to analyze how force application to integrins and the cytoskeleton results in changes in the activities of biochemical signaling molecules and cytoskeleton-associated enzymes, much like we characterized force-dependent effects on molecular self-assembly. However, to fully understand this complex physicochemical mechanism, it will likely be necessary to develop entirely new techniques for simultaneous visualization, perturbation, and analysis at the nanometer (even single molecule) scale.

Focal adhesions could also form the basis for the design of a new generation of intelligent biomaterials. Properties of such biomaterials would include the ability to self-assemble from diverse molecular components, to alter the rate of assembly in response to both physical and biochemical cues, and to interconvert mechanical and chemical energy. Incorporating these molecular processes into material design may allow the fabrication of multifunctional materials that can simultaneously carry out sensing, processing, and responder functions. Such intelligent materials would be useful for a variety of applications ranging from tissue engineering to biocomputing.

It is difficult to predict when man will build the first artificial, self-assembling, mechanochemical transduction machine. This will likely require advances in nanotechnology and controlled molecular assembly that are beyond those available today. However, clearly, the focal adhesion is an outstanding model system to attempt to mimic.

REFERENCES

1. Ingber DE. Tensegrity I. Cell structure and hierarchical systems biology. *J Cell Sci* 2003;116(Pt 7):1157–1173.
2. Ingber DE. Tensegrity II. How structural networks influence cellular information processing networks. *J Cell Sci* 2003;116(Pt 8):1397–1408.
3. Ingber DE. Cellular mechanotransduction: putting all the pieces together again. *FASEB J* 2006;20(7):811–827.
4. Ingber DE. Tensegrity: the architectural basis of cellular mechanotransduction. *Annu Rev Physiol* 1997;59:575–599.
5. Ingber DE. Integrins as mechanochemical transducers. *Curr Opin Cell Biol* 1991; 3(5):841–848.
6. Wang N, Butler JP, Ingber DE. Mechanotransduction across the cell surface and through the cytoskeleton. *Science* 1993;260(5111):1124–1127.
7. Hynes RO. Integrins: bidirectional, allosteric signaling machines. *Cell* 2002;110(6): 673–687.
8. Riveline D, et al. Focal contacts as mechanosensors: externally applied local mechanical force induces growth of focal contacts by an mDia1-dependent and ROCK-independent mechanism. *J Cell Biol* 2001;153(6):1175–1186.
9. Zamir E and Geiger B. Molecular complexity and dynamics of cell–matrix adhesions. *J Cell Sci* 2001;114(Pt 20):3583–3590.
10. Zamir E and Geiger B. Components of cell–matrix adhesions. *J Cell Sci* 2001; 114(Pt 20):3577–3579.
11. Alberts B. The cell as a collection of protein machines: preparing the next generation of molecular biologists. *Cell* 1998;92(3):291–294.
12. Lele T, Thodeti CK, Ingber DE. Force meets chemistry: analysis of mechanochemical conversion in focal adhesions using fluorescence recovery after photobleaching. *J Cell Biochem* 2006;97(6):1175–1183.
13. Rabut G, Doye V, Ellenberg J. Mapping the dynamic organization of the nuclear pore complex inside single living cells. *Nat Cell Biol* 2004;6(11):1114–1121.
14. Zaidel-Bar R, Ballestrem C, Kam Z, Geiger B. Early molecular events in the assembly of matrix adhesions at the leading edge of migrating cells. *J Cell Sci* 2003;116(Pt 22):4605–4613.
15. Bershadsky AD, Balaban NQ, Geiger B. Adhesion-dependent cell mechanosensitivity. *Annu Rev Cell Dev Biol* 2003;19:677–695.
16. Franz CM and Muller DJ. Analyzing focal adhesion structure by atomic force microscopy. *J Cell Sci* 2005;118(Pt 22):5315–5323.

17. Gaus K, Le Lay S, Balasubramanian N, Schwartz MA. Integrin-mediated adhesion regulates membrane order. *J Cell Biol* 2006;174(5):725–734.
18. Beningo KA, Dembo M, Kaverina I, Small JV, Wang YL. Nascent focal adhesions are responsible for the generation of strong propulsive forces in migrating fibroblasts. *J Cell Biol* 2001;153(4):881–888.
19. Smilenov LB, Mikhailov A, Pelham RJ, Marcantonio EE, Gundersen GG. Focal adhesion motility revealed in stationary fibroblasts. *Science* 1999;286(5442):1172–1174.
20. Zamir E, et al. Molecular diversity of cell–matrix adhesions. *J Cell Sci* 1999;112 (Pt 11):1655–1669.
21. Maniotis AJ, Chen CS, Ingber DE. Demonstration of mechanical connections between integrins, cytoskeletal filaments, and nucleoplasm that stabilize nuclear structure. *Proc Natl Acad Sci USA* 1997;94(3):849–854.
22. Choquet D, Felsenfeld DP, Sheetz MP. Extracellular matrix rigidity causes strengthening of integrin–cytoskeleton linkages. *Cell* 1997;88(1):39–48.
23. Wang N and Ingber DE. Probing transmembrane mechanical coupling and cytomechanics using magnetic twisting cytometry. *Biochem Cell Biol* 1995;73(7–8):327–335.
24. Balaban NQ, et al. Force and focal adhesion assembly: a close relationship studied using elastic micropatterned substrates. *Nat Cell Biol* 2001;3(5):466–472.
25. Schwarz US, et al. Calculation of forces at focal adhesions from elastic substrate data: the effect of localized force and the need for regularization. *Biophys J* 2002;83(3):1380–1394.
26. Etienne-Manneville S and Hall A. Rho GTPases in cell biology. *Nature* 2002;420(6916):629–635.
27. Hall A and Nobes CD. Rho GTPases: molecular switches that control the organization and dynamics of the actin cytoskeleton. *Philos Trans R Soc Lond B Biol Sci* 2000;355(1399):965–970.
28. Tzima E, del Pozo MA, Shattil SJ, Chien S, Schwartz MA. Activation of integrins in endothelial cells by fluid shear stress mediates Rho-dependent cytoskeletal alignment. *EMBO J* 2001;20(17):4639–4647.
29. Katsumi A, Naoe T, Matsushita T, Kaibuchi K, Schwartz MA. Integrin activation and matrix binding mediate cellular responses to mechanical stretch. *J Biol Chem* 2005;280(17):16546–16549.
30. Hu S, et al. Intracellular stress tomography reveals stress focusing and structural anisotropy in cytoskeleton of living cells. *Am J Physiol Cell Physiol* 2003;285(5):C1082–C1090.
31. Hu S, et al. Mechanical anisotropy of adherent cells probed by a three-dimensional magnetic twisting device. *Am J Physiol Cell Physiol* 2004;287(5):C1184–C1191.
32. Hu S, Chen J, Butler JP, Wang N. Prestress mediates force propagation into the nucleus. *Biochem Biophys Res Commun* 2005;329(2):423–428.
33. Ingber DE. Cellular tensegrity: defining new rules of biological design that govern the cytoskeleton. *J Cell Sci* 1993;104(Pt 3):613–627.
34. Discher DE, Janmey P, Wang YL. Tissue cells feel and respond to the stiffness of their substrate. *Science* 2005;310(5751):1139–1143.

35. Kato M and Mrksich M. Using model substrates to study the dependence of focal adhesion formation on the affinity of integrin–ligand complexes. *Biochemistry* 2004;43(10):2699–2707.
36. Reinhart-King CA, Dembo M, Hammer DA. The dynamics and mechanics of endothelial cell spreading. *Biophys J* 2005;89(1):676–689.
37. Dalby MJ, Riehle MO, Sutherland DS, Agheli H, Curtis AS. Use of nanotopography to study mechanotransduction in fibroblasts—methods and perspectives. *Eur J Cell Biol* 2004;83(4):159–169.
38. Teixeira AI, Abrams GA, Bertics PJ, Murphy CJ, Nealey PF. Epithelial contact guidance on well-defined micro- and nanostructured substrates. *J Cell Sci* 2003;116(Pt 10):1881–1892.
39. Chen Q, Kinch MS, Lin TH, Burrridge K, Juliano RL. Integrin-mediated cell adhesion activates mitogen-activated protein kinases. *J Biol Chem* 1994;269(43):26602–26605.
40. Burrridge K and Wennerberg K. Rho and Rac take center stage. *Cell* 2004;116(2):167–179.
41. Ridley AJ, et al. Cell migration: integrating signals from front to back. *Science* 2003;302(5651):1704–1709.
42. DeMali KA, Wennerberg K, Burrridge K. Integrin signaling to the actin cytoskeleton. *Curr Opin Cell Biol* 2003;15(5):572–582.
43. Sastry SK and Burrridge K. Focal adhesions: a nexus for intracellular signaling and cytoskeletal dynamics. *Exp Cell Res* 2000;261(1):25–36.
44. Burrridge K and Chrzanowska-Wodnicka M. Focal adhesions, contractility, and signalling. *Annu Rev Cell Dev Biol* 1996;12:463–518.
45. Romer LH, Burrridge K, Turner CE. Signaling between the extracellular matrix and the cytoskeleton: tyrosine phosphorylation and focal adhesion assembly. *Cold Spring Harb Symp Quant Biol* 1992;57:193–202.
46. Overby DR, et al. Magnetic cellular switches. *IEEE Transac Magn* 2004;40(4):2958–2960.
47. Matthews BD, Overby DR, Mannix R, Ingber DE. Cellular adaptation to mechanical stress: role of integrins, Rho, cytoskeletal tension, and mechanosensitive ion channels. *J Cell Sci* 2006;119(Pt 3):508–518.
48. Overby DR, Matthews BD, Alsberg E, Ingber DE. Novel dynamic rheological behavior of focal adhesions measured within single cells using electromagnetic pulling cytometry. *Acta Biomater* 2005;3:295–303.
49. Chen CS, Alonso JL, Ostuni E, Whitesides GM, Ingber DE. Cell shape provides global control of focal adhesion assembly. *Biochem Biophys Res Commun* 2003;307(2):355–361.
50. Brock A, et al. Geometric determinants of directional cell motility revealed using microcontact printing. *Langmuir* 2003;19(5):1611–1617.
51. Polte TR, Eichler GS, Wang N, Ingber DE. Extracellular matrix controls myosin light chain phosphorylation and cell contractility through modulation of cell shape and cytoskeletal prestress. *Am J Physiol Cell Physiol* 2004;286(3):C518–C528.
52. Parker KK, et al. Directional control of lamellipodia extension by constraining cell shape and orienting cell tractional forces. *FASEB J* 2002;16(10):1195–1204.

53. Chen CS, Mrksich M, Huang S, Whitesides GM, Ingber DE. Geometric control of cell life and death. *Science* 1997;276(5317):1425–1428.
54. Ingber DE and Folkman J. Mechanochemical switching between growth and differentiation during fibroblast growth factor-stimulated angiogenesis *in vitro*: role of extracellular matrix. *J Cell Biol* 1989;109(1):317–330.
55. Ingber DE and Folkman J. How does extracellular matrix control capillary morphogenesis? *Cell* 1989;58(5):803–805.
56. Singhvi R, et al. Engineering cell shape and function. *Science* 1994;264(5159): 696–698.
57. Kamm RD and Kaazempur-Mofrad MR. On the molecular basis for mechanotransduction. *Mech Chem Biosyst* 2004;1(3):201–209.
58. Zaman MH and Kaazempur-Mofrad MR. How flexible is alpha-actinin's rod domain? *Mech Chem Biosyst* 2004;1(4):291–302.
59. Baneyx G, Baugh L, Vogel V. Coexisting conformations of fibronectin in cell culture imaged using fluorescence resonance energy transfer. *Proc Natl Acad Sci USA* 2001;98(25):14464–14468.
60. Vogel V, Thomas WE, Craig DW, Krammer A, Baneyx G. Structural insights into the mechanical regulation of molecular recognition sites. *Trends Biotechnol* 2001;19(10):416–423.
61. Baneyx G, Baugh L, Vogel V. Fibronectin extension and unfolding within cell matrix fibrils controlled by cytoskeletal tension. *Proc Natl Acad Sci USA* 2002;99(8):5139–5143.
62. Chen S and Springer TA. Selectin receptor–ligand bonds: formation limited by shear rate and dissociation governed by the bell model. *Proc Natl Acad Sci USA* 2001;98(3):950–955.
63. Dembo M, Torney DC, Saxman K, Hammer D. The reaction-limited kinetics of membrane-to-surface adhesion and detachment. *Proc R Soc Lond B Biol Sci* 1988;234(1274):55–83.
64. Konstantopoulos K, Hanley WD, Wirtz D. Receptor–ligand binding: 'catch' bonds finally caught. *Curr Biol* 2003;13(15):R611–R613.
65. Marshall BT, et al. Direct observation of catch bonds involving cell-adhesion molecules. *Nature* 2003;423(6936):190–193.
66. Lele T, Pendse J, Kumar S, Salanga M, Ingber DE. Mechanical forces alter zyxin unbinding kinetics within focal adhesions in living cells. *J Cell Physiol* 2006; 207(1):187–194.
67. Phair RD and Misteli T. Kinetic modelling approaches to *in vivo* imaging. *Nat Rev Mol Cell Biol* 2001;2(12):898–907.
68. Shen N, et al. Ablation of cytoskeletal filaments and mitochondria in cells using a femtosecond laser nanoscissor. *Mech Chem Biosys* 2005;2:17–26.
69. Heisterkamp A, et al. Pulse energy dependence of subcellular dissection by femtosecond laser pulses. *Opt Expr* 2005;13(10):3690–3696.
70. Kumar S, et al. Viscoelastic retraction of single living stress fibers and its impact on cell shape, cytoskeletal organization, and extracellular matrix mechanics. *Biophys J* 2006;90(10):3762–3773.
71. Shakibaei M and Mobasheri A. Beta1-integrins colocalize with Na, K-ATPase, epithelial sodium channels (ENaC) and voltage activated calcium channels (VACC)

- in mechanoreceptor complexes of mouse limb-bud chondrocytes. *Histol Histopathol* 2003;18(2):343–351.
72. Alenghat FJ, Nauli SM, Kolb R, Zhou J, Ingber DE. Global cytoskeletal control of mechanotransduction in kidney epithelial cells. *Exp Cell Res* 2004;301(1):23–30.
 73. Chen J, Fabry B, Schiffrin EL, Wang N. Twisting integrin receptors increases endothelin-1 gene expression in endothelial cells. *Am J Physiol Cell Physiol* 2001;280(6):C1475–C1484.
 74. Ingber DE. Fibronectin controls capillary endothelial-cell growth by modulating cell shape. *Proc Nat Acad USA* 1990;87(9):3579–3583.
 75. Schwartz MA, Lechene C, Ingber DE. Insoluble fibronectin activates the Na/H antiporter by clustering and immobilizing integrin alpha 5 beta 1, independent of cell shape. *Proc Natl Acad Sci USA* 1991;88(17):7849–7853.
 76. McNamee HP, Liley HG, Ingber DE. Integrin-dependent control of inositol lipid synthesis in vascular endothelial cells and smooth muscle cells. *Exp Cell Res* 1996;224(1):116–122.
 77. McNamee HP, Ingber DE, Schwartz MA. Adhesion to fibronectin stimulates inositol lipid synthesis and enhances PDGF-induced inositol lipid breakdown. *J Cell Biol* 1993;121(3):673–678.
 78. Plopper GE, McNamee HP, Dike LE, Bojanowski K, Ingber DE. Convergence of integrin and growth factor receptor signaling pathways within the focal adhesion complex. *Mol Biol Cell* 1995;6(10):1349–1365.
 79. Engler AJ, et al. Matrix elasticity directs stem cell lineage specification. *Cell* 2006;126(4):677–689.
 80. Engler AJ, et al. Myotubes differentiate optimally on substrates with tissue-like stiffness: pathological implications for soft or stiff microenvironments. *J Cell Biol* 2004;166(6):877–887.
 81. Griffin MA, Sen S, Sweeney L, Discher DE. Adhesion-contractile balance in myotube differentiation. *J Cell Sci* 2004;117(Pt 24):5855–5863.
 82. Lele TP, et al. Mechanical forces alter zyxin unbinding kinetics within focal adhesions of living cells. *J Cell Physiol* 2006;207(1):187–194.

Controlling Cell Behavior via DNA and RNA Transfections

JASPREET K. VASIR and VINOD LABHASETWAR

13.1 INTRODUCTION

RNA and DNA are the basic genetic components of the cell machinery through which flows the information for the normal functioning of the cell. However, in disease conditions, there is often a misinterpretation of this information and malfunctioning of cell machinery. Elucidation of the human genome has identified a number of genes implicated in disease progression. This has offered new possibilities of treating the diseases by means of gene therapy (replacing a defective gene or modifying the expression of a gene by introducing genetic material/DNA into the cells). The introduction of foreign DNA or RNA molecules into cells is known as “transfection.” Transfection is now a commonly used method in laboratories for studying gene function, modulation of gene expression, biochemical mapping, and mutational analysis. Thus, it has now become possible to control cell behavior by means of DNA/RNA transfections. In this chapter, we discuss how DNA/RNA transfections can be used to alter cell behavior, their numerous applications as a research tool, and new therapeutic options.

13.2 METHODS OF DNA/RNA TRANSFECTION

Polynucleotide molecules (e.g. DNA or RNA) are large, hydrophilic macromolecules with a net negative charge. These are very labile in biological environment and do not cross biological membranes effectively. Thus, the need for an effective and safe transfection system/vector is quite obvious. In general,

transfection methods can be broadly categorized into viral-based gene transfer (retrovirus, adeno-associated virus, and lentivirus), chemical transfection methods (lipid- or polymer-mediated), and physical delivery methods (electroporation, microinjection, heat shock). Viral vectors include the use of genetically engineered retroviruses, adenoviruses, adeno-associated viruses (AAV), and other viruses that have been used for gene transfer procedures. Though the viruses are highly efficient for gene transfer to cells, their potential to induce drastic immune responses such as with adenovirus or the risk of insertional mutagenesis in the host genome with retroviral vectors [1] has sparked a major debate over their safety for human gene therapy. Thus, the current consensus is to develop suitable vector systems for DNA/RNA transfections, which are minimally invasive (safe) and highly efficient. This has steered research toward the development of nonviral vectors for gene delivery. Nonviral vectors include nanoparticles (NPs), liposomes, and complexes prepared using either cationic lipids (lipoplexes) or polymers (polyplexes), and also mechanical methods, such as electroporation or microneedle injections of plasmid, especially for transfection through the skin surface. Polymeric NPs for gene delivery can be formed (1) by simple condensation of polynucleotides (DNA/RNA) with polymers, like poly-L-lysine (PLL), polyethyleneimine (PEI), polyamidoamines, and polyimidazoles, (2) by encapsulating DNA into polymers, like polyethylene oxide, polylactide (PLA), poly-(lactic-co-glycolic acid) (PLGA), and polyalkylcyanoacrylates, or (3) by complexing DNA to the surface of preformed polymeric NPs grafted with cationic surfactants or polysaccharides. These are the three basic types of polymeric NPs, under investigation for DNA/RNA transfection [2]. The NPs formed by either condensation, encapsulation, or complexation of DNA have very distinct characteristics and varying transfection efficiencies, making them suitable for different transfection applications. These differences primarily arise due to the disparity in the basic chemical structure of polymers and the methods used to formulate NPs. Cationic polymers like PLL, and PEI that can effectively condense DNA often have limitations for *in vivo* applications due to their cytotoxicity, nonbiodegradable nature, and the possibility to aggregate in physiological conditions. On the contrary, NPs prepared with biodegradable polymers, like PLGA/PLA are stable in the blood stream, but have lower transfection efficiency as compared to cationic polymers like PEI. Nonetheless, one major advantage of PLGA/PLA NPs, which cannot be ignored, is the ability to protect and release DNA/RNA slowly inside the cells, thus sustaining transfection levels for a prolonged period of time. Recent efforts for synthesis of degradable, cationic polymers with low cytotoxicity and high transfection efficiency can provide new polymers to formulate NPs for efficient transfections. Furthermore, approaches, such as the use of cell-specific targeting moieties, can target polymeric NPs to particular cells and have helped to overcome some of the cellular barriers to gene delivery. Still nuclear membrane stands as an invincible barrier for DNA transfections. The use of nuclear localization signaling (NLS) peptides and the tissue-specific promoters, though in early stages of development, constitutes promising efforts at improving nuclear import of DNA.

Electroporation employs the use of an electrical field to create small pores in cellular membrane, also referred as electropores, enabling delivery of highly charged macromolecules, such as RNA or DNA to the cytoplasm and nuclei of the cell. Gene guns and manual microinjection are very efficient techniques for direct delivery of DNA to a specified target. The method is limited with regard to the number of cells applied and requires certain operator skill.

13.3 BARRIERS TO TRANSFECTION

To be successful, transfection methods/vectors need to overcome several physical and biological barriers before DNA/RNA can be delivered to its target site inside a cell. Physical barriers include the formulation of polymeric gene delivery systems, which in idealistic perspective, should be able to condense DNA/RNA to a size that can easily gain access into cells and can maintain its stability and biological activity.

Further upon introduction into cells, vectors are required to cross a series of hurdles in order to reach the cytoplasm or nucleus and during this process, lose significant portion of the DNA/RNA molecules at each successive step. These barriers include the physical and chemical stability of transfection vector in the cell culture media or in systemic circulation, association and internalization of the vectors into cells by endocytosis, intracellular trafficking and release of DNA/RNA into the cytoplasm, cytoplasmic translocation of DNA to nucleus, and the nuclear uptake of DNA [3]. The transfection methods for DNA and RNA differ in terms of the final target site for action. DNA needs to translocate to the nucleus of the cells, for expression of the gene; however, site of action of RNA is the cytoplasm. Thus, the vectors needed for RNA transfection are a little less complicated than those required for DNA transfection.

The transfection methods differ to a great extent in their efficiency, which in part depends on the association of the vector with cell membranes and its release from the endosomal compartment [4]. Cell recognition and association of NPs to cell membrane can be enhanced by the use of targeting ligands that can bind to specific receptors on cell membranes. This can not only promote the association and binding of NPs to the cell surface, but can also increase the cellular internalization by means of receptor-mediated endocytosis. The major bottleneck issue for polymeric transfection is that following endocytosis, the polymeric vectors may get sequestered within the endosomal compartment. Viruses have evolved highly efficient inherent mechanisms for escaping the endosomal compartments and reaching the cytoplasm. These include the presence of fusogenic or membrane disruptive peptides in the viral coats that allow the viral particles to readily escape into the cytoplasm. However, transfection efficiency of the nonviral vectors is highly dependent on the efficiency of endosomal escape of the vectors. This has galvanized active research to develop strategies to enhance the endosomal escape of nonviral polymeric vectors, in order to improve the efficiency of gene transfection. The

transfection methods face more challenges for *in vivo* studies. The physico-chemical characteristics of vectors have a major influence on their biodistribution and pharmacokinetics and thus, affect the therapeutic efficacy [5]. Thus, it is important to understand a correlation between transfection vector characteristics and the pharmacokinetics of their biodistribution to develop an efficient transfection system for DNA/RNA delivery *in vivo*.

13.4 DNA TRANSFECTION

Successful DNA transfections *in vitro* have demonstrated the potential of DNA transfections to control cell behavior in diseased and healthy cells. However, potential of DNA transfections *in vivo* is limited due to the availability of safe and efficient gene transfection methods. Here, we discuss the applications of DNA transfections in gene therapy, tissue engineering, and as an experimental tool for functional genomics.

13.4.1 Gene Therapy

DNA transfection holds the potential to alter cell behavior by expressing a gene deficient in cell types. DNA transfections have been attempted to correct the loss of genes responsible for tumor suppression (p53), receptor expression on cells, hormonal/ enzyme production, growth factor secretion, and also for DNA immunization strategies. Gene therapy is an approach for treating diseases at the genetic level, modifying the biology of the cells for a therapeutic benefit. This makes it all the more important to understand the biology of cells. For instance, in case of gene therapy approaches for correcting a genetic deficiency, it may be required to maintain the physiological concentrations of the expressed protein for a sustained period of time. Gene therapy strategies to correct hormone deficiencies would require not only the restoration of normal gene expression, but also strict control of physiological, pulsatile nature of hormone secretion [6]. A common biological effect of cell proliferation can also be a factor in different diseases. Rate and kinetics of cell proliferation in cancers may be quite different than that in other proliferative disorders like, restenosis, and this demands a consideration while selecting the gene delivery vectors. It has been shown that even a 50% reduction in the proliferating cells can reduce the neointimal volume to 90% in postangioplasty patients, which equates to a substantial therapeutic benefit [7]. Thus, clinically relevant reduction of neointima formation can be attained, with realistic transfection rates. In contrast, it is necessary that all the cancer cells be killed, in order to achieve a complete remission in patients presenting a disseminated disease.

Most often, emphasis is laid on the level of gene transfection; however, as indicated below, in certain disease conditions, the low level, but sustained gene expression could be more effective. Therapeutic angiogenesis is one such example, where a sustained, but low level of expression of genes encoding the angiogenic

factors (e.g., VEGF or FGF) is required. High levels of growth factors are known to form leaky vasculature, which are nonfunctional and regress with time. Therefore, it is considered that a low level of sustained gene expression could be more effective in forming mature and functional blood vessels [8].

DNA complexed with PEI has been used for *in vivo* delivery of therapeutic DNA, oligonucleotides, or therapeutic RNA molecules as a part of experimental gene therapy. For the delivery of plasmid DNA, PEI of any molecular weight can be used, while small nucleic acids, like RNA molecules, are preferentially complexed with low molecular weight PEI [9]. Systemic administration of PEI polyplexes with tumor suppressor gene p53 every 3 days for 3 weeks in an orthotopic bladder cancer model resulted in a 70% reduction in tumor size. A 14-fold higher reporter gene expression was observed in the tumor as compared to the lungs on intravenous injection of the respective polyplexes [10]. The authors of this study attributed the reason for preferential accumulation in tumors (as compared to lungs) and the low cytotoxicity to the use of low N/P ratio for polyplexes. This results in marginally positive zeta potential of polyplexes and can potentially reduce the interaction of polyplexes with the serum proteins, thus making it ideal for *in vivo* systemic delivery to the tumor.

Linear PEI of molecular weight 22 kDa was used for successful *in vivo* transfer of the cloned somatostatin receptor subtype 2 (sst2) gene in transplantable models of primary and metastatic pancreatic carcinomas in hamsters [11]. The peptide somatostatin negatively regulates cellular proliferation by means of its cell surface receptor subtypes (sst1, sst2, and sst5). It has also been observed that there is a loss of sst2 gene expression in human pancreatic adenocarcinoma and in pancreatic cancer derived cell lines. Thus, correcting the deficit of sst2 gene in pancreatic cancer cells can slow the tumor growth and can make the tumors responsive to somatostatin treatment. A plasmid DNA containing the murine sst2 gene was complexed with linear PEI. PEI–DNA complexes were injected intratumorally into the pancreatic tumor model in hamsters. This *in vivo* sst2 gene transfer resulted in significant inhibition of growth progression of pancreatic primary tumor as well as hepatic metastases, 6 days after the intratumoral injection of PEI–DNA polyplexes.

Biodegradable PLGA NPs have been shown to sustain the release of DNA inside the cells, thus enabling sustained gene expression. Such sustained gene expression is advantageous especially if the half-life of the expressed protein is very short and/or a chronic gene delivery is required for better therapeutic efficacy. Prabha and Labhsetwar have shown slow intracellular release of plasmid DNA from PLGA NPs, which resulted in sustained levels of DNA inside the cells. This could be easily related to the greater gene expression, quantitated by mRNA levels determined using RT-PCR. The *wt*-p53 gene-loaded NPs showed higher mRNA levels for p53, as compared to the liposomal formulation, even 5 days after transfection of the MDA-MB-435S breast cancer cells [12]. The sustained p53 expression levels resulted in greater and sustained inhibition of cell proliferation as compared to plasmid DNA alone

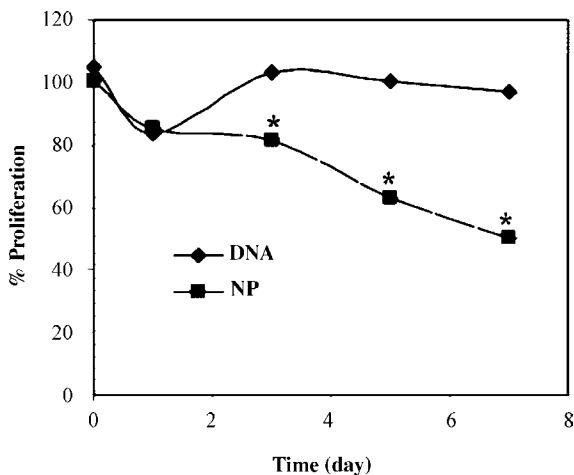


FIGURE 13.1 Antiproliferative activity of *wt*-p53 DNA-loaded nanoparticles (NP) and naked *wt*-p53 DNA (DNA) in MDAMB-435S cells. Cells (2500 cells/well) grown in 96-well plates were incubated with 500 $\mu\text{g}/\text{ml}$ nanoparticles and an equivalent amount of naked DNA (10.5 $\mu\text{g}/\text{ml}$). Medium control or NPs without DNA were used as controls. Cell growth was followed using a standard MTS assay, where the absorbance is directly proportional to the number of viable cells. Nanoparticles demonstrated an increase in antiproliferative activity with incubation time. Data are represented as the mean the standard error of the mean ($n = 6$; $p < 0.01$ for points marked with asterisks). (Reproduced with permission from Reference 12.)

(Fig. 13.1). Cohen et al. have shown that despite lower transfection levels observed *in vitro* with NPs as compared to liposomal formulations, the *in vivo* gene transfection with NPs was one to two orders of magnitude greater than that with liposomes, 7 days after an intramuscular injection in rats [13]. Their studies demonstrated gene expression sustaining over 28 days *in vivo* with a single dose of intramuscular injection of NPs.

DNA transfection is also a potential alternative for immunization strategies. Chitosan NPs are considered a very appealing carrier choice for orally delivered mucosal immunization strategies, owing to the mucoadhesive properties of chitosan. Orally administered chitosan–DNA NPs can adhere to the gastrointestinal epithelium and transfect epithelial or immune cells present in the gut-associated lymphoid tissue [14]. *In vitro* studies have shown that chitosan can enhance transcellular and paracellular transport of drugs across intestinal epithelial monolayers [15]. Roy et al. have demonstrated successful mucosal immunization via oral gene delivery, using DNA complexed with chitosan [16]. Chitosan–DNA NPs were administered orally in a murine model of peanut-allergen-induced hypersensitivity and levels of serum and secreted antibodies were detected 4 weeks after first immunization. Substantial differences in the antibody levels were found for NP immunized mice, and the control mice or the mice immunized with naked DNA. The efficiency of orally

administered chitosan–DNA NPs for gene expression was studied using the lacZ gene in the same mouse model. Mice fed with NPs showed high levels of gene expression in both stomach and small intestines as compared to mice fed with plasmid DNA.

13.4.2 Tissue Engineering

Cell-induced tissue regeneration is usually achieved by providing cells with a local environment of biological cues that enable cells to promote proliferation and differentiation. Such biological cues include growth factors, signaling molecules, and extracellular matrix (ECM) molecules. Transfection with plasmid DNA encoding for various growth factors has been used for tissue regeneration approach [17–19]. This strategy becomes more imperative when the protein/growth factor required for tissue growth has a short biological half-life. Plasmid DNA encoding for fibroblast growth factor-4 (FGF4) was delivered using hydrogel microspheres of cationized gelatin in a rabbit hind limb ischemia model [20]. This DNA transfection led to significantly greater angiogenesis due to greater expression of FGF4 at the injection site as compared to plasmid DNA in solution. The blood vessels formed by the DNA transfection were demonstrated to be completely functional and physiologically mature.

Another interesting application of DNA transfection in tissue engineering involves genetically manipulating the biological functions of stem cells. Stem cell therapy is promising, but often the stem cells need some kind of genetic modification to activate specific biological functions. One such example involves using the cells (endothelial progenitor cells (EPCs)) as a vehicle for DNA and also as a tissue engineering tool. EPCs were transfected with plasmid DNA encoding angiogenic adrenomedullin using cationized gelatin microspheres. Gene-transfected EPCs were then injected into a rat model of pulmonary hypertension. EPCs preferentially targeted the injured pulmonary endothelia and restored the intact endothelium [21].

13.4.3 Functional Genomics

High throughput transfected cell arrays can be used to correlate gene expression with functional cell responses. This approach can also be used for screening large collections of target sequences for therapeutic interventions [22, 23]. In one such study, cells were transfected by collagen mixed with plasmid DNA or viruses carrying the DNA. Collagen mixed with plasmids was spotted on glass slides or into wells and used to transfect the cells. Such transfected cell arrays can then be analyzed for cellular responses using imaging or biochemical techniques. Transfection methods required for such studies must result in a cost-effective and efficient transfection of a wide variety of primary cells and cell lines [24].

13.5 RNA TRANSFECTION

RNA interference (RNAi) is based on the premise that dsRNA can be used to bind to and promote the degradation of target mRNAs by harnessing an endogenous biological pathway, thus knocking down the expression of the respective genes. RNAi is an evolutionarily conserved gene-silencing phenomenon. Fire et al. were first to describe RNAi in animal cells, in the nematode *C. elegans* [25]. RNAi was later described to be also present in mammalian cells [26]. The effector molecules for this gene silencing phenomenon that guide mRNA degradation in a cell are small 21–30-nucleotide dsRNA, termed “small interfering RNAs” (siRNA). These siRNAs have nucleotide complementarity to the mRNA sequence of the protein whose transcription is to be blocked. Upon entry into cell, siRNA molecules are incorporated into a multisubunit ribonucleoprotein complex called RNA-induced silencing complex (RISC), which binds to and promotes the degradation of the target mRNA.

siRNA can be introduced into cells via transfection of chemically synthesized molecules or generated inside the cells from the enzymatic cleavage of long dsRNAs. Synthesizing siRNA molecules offers a precise control over the sequence of siRNA, purity, and the possibility to introduce chemical modifications to enhance the efficacy of siRNA. siRNA/shRNA (short hairpin RNA) can be produced intracellularly by transfecting the cells with plasmid DNA carrying the transcript encoding DNA. Chemically synthesized siRNA are less prone to nonspecific side effects due to greater control over the amount of transfected reagent. The duration of gene silencing is limited by the rate of cell division. The siRNA molecules hold immense potential for therapeutic applications due to their small size and chemical modifications that can confer more stability and high efficacy.

The basic chemical structure of effective siRNAs has been defined as 19-bp RNA duplex with a two-nucleotide overhang on the 3' ends. The potency of gene silencing depends on the sequence of siRNA and rules have been developed for the design of effective siRNA [27]. In the year 2002, Couzin et al. hailed dsRNA reagents as the “scientific breakthrough of the year” [28]. All this has raised the prospects of RNAi not only as a research tool, but also as a novel therapeutic option for many diseases.

13.5.1 As a Tool to Understand Gene Function

RNAi is a powerful research tool in “reverse genetic studies” whereby the function of a gene is determined by its disruption. Recently, RNAi screens have been developed in mammalian cells [29]. Libraries can be designed to silence expression of the mammalian genes by using retroviral vectors to express (shRNA) in cells. RNA interference has been extensively used for study of disease-associated genes for diseases, such as cancer, infectious diseases, and respiratory diseases. One of the mammalian screens identified new genes

involved in p53-mediated cell cycle arrest [30]. By varying the amount of siRNA expressed in the cell, it is now possible to determine the relative amount of gene product required for certain processes in a temporal and spatial manner [31]. This has broadened the horizons of the types of experiments that can be done in mammalian model systems. Thus, RNAi-directed gene silencing coupled with genomics data can provide functional determination of any gene expressed in a cell. High gene silencing efficiency at low concentration, high specificity and stability, and the low costs of custom siRNA synthesis are further promoting the use of siRNA in functional genomics [32]. RNAi is now the most preferred approach for functional genomics in mammalian tissue culture.

siRNA-mediated gene silencing can be a reliable and valuable approach for large-scale screening of gene function and drug–target identification and validation. RNAi can also be potentially used in drug discovery to evaluate the specificity and the mechanism of action of a new chemical entity before resources are spent to develop it into a drug [33]. Furthermore, transgenic mice with stably silenced gene expression have also been developed using RNAi. Inducible or tissue-specific promoters can be used to drive the intracellular production of siRNAs (from shRNAs), and thus, can be used to generate animals in which gene expression is silenced in particular cells/tissues [34]. Since RNAi sequences vary in their extent of silencing, transgenic mice with graded degrees of gene silencing can also be developed. The use of RNAi has also allowed the development of double-knockout mice of two genes that are located in close proximity on the same chromosome. Also, by targeting a conserved domain, an entire gene family can be knocked down using a single siRNA [32].

Although RNAi offers a potentially faster way to produce transgenic mice, it is not yet completely characterized as a robust approach. Further studies are needed to determine how reliably gene expression can be knocked down in all tissues/target tissue at all times, to produce a knockdown with a different phenotype.

13.5.2 As a Therapeutic

The widespread applicability, relative ease of synthesis, and low cost of production (as compared to recombinant proteins, monoclonal antibodies) make siRNA an attractive new class of therapeutic entities. siRNA can be used to direct silencing of genes responsible for induction or progression of disease [35]. Several studies have demonstrated the therapeutic potential of siRNAs: siRNAs protecting mice from fulminant hepatitis [36], viral infection [37], sepsis [38], tumor growth [39], and macular degeneration in eye [40]. siRNA-directed gene silencing of the Fas receptor (responsible for apoptosis of hepatocytes) can be of therapeutic value for preventing/treating acute and chronic liver injury, hepatitis, liver failure, and rejection of liver transplants. Such a therapeutic benefit was demonstrated by protection of mice from liver failure in two models of

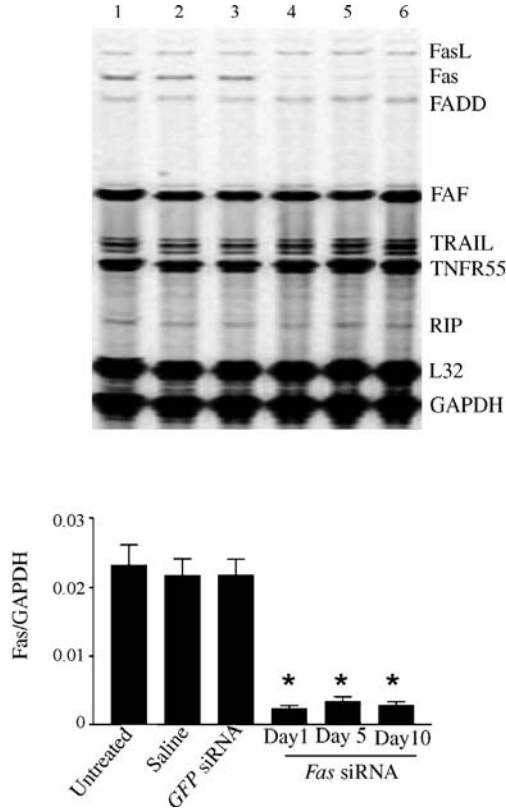


FIGURE 13.2 RPA for *Fas* mRNA expression in hepatocytes from mice that were untreated (lane 1) or were injected 24 h earlier with saline (lane 2), *GFP* (sequence 1) siRNA (lane 3) or *Fas* (sequence 1) siRNA (lane 4). Silencing of *Fas* expression in mice treated with *Fas* siRNA is maintained 5 (lane 5) or 10 days (lane 6) later. Expression of other genes involved in the *Fas* pathway and housekeeping genes (*L32* and *Gapd*) were unaffected (names of the corresponding proteins are listed at right). Similar results were obtained in three independent experiments. The graph shows results of densitometric quantification of the *Fas/GAPDH* ratios in three mice per condition. *Fas* mRNA levels in hepatocytes are significantly lower ($*P < 0.001$) at all times in mice treated with *Fas* siRNA mice than in control mice. (Reproduced with permission from Reference 36.)

autoimmune hepatitis, by injecting siRNA against the *Fas* gene [36]. siRNA was injected into mice via the hydrodynamic tail vein injection. The mRNA and protein levels of *Fas* were significantly reduced in the hepatocytes of mouse and the effects persisted for 10 days (Fig. 13.2). Fulminant hepatitis was induced in animals by injecting agonistic *Fas*-specific antibody; 82% of the animals treated with siRNA silencing *Fas* survived for 10 days, as compared to control animals, that died within 3 days (Fig. 13.3). This shows that effective gene silencing can be

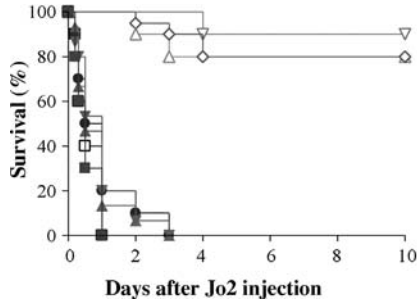


FIGURE 13.3 Survival advantage of mice injected with *Fas* siRNA as compared to saline or *GFP* siRNA after challenge by intraperitoneal injection with *Fas*-specific antibody and observation for 10 day before sacrifice. Sequences that silenced *Fas* by $\geq 80\%$ protected against fulminant hepatitis, whereas sequences that did not silence or silenced inefficiently provided no protection. * $P < 0.0001$. ■, *GFP* (dt) ($n = 10$); ▲, *GFP* (CU) ($n = 15$); ▼, saline ($n = 15$); ◆, *Fas* (sequence 1) ($n = 20$); ●, *Fas* (sequence 2) ($n = 10$); □, *Fas* (sequence 4) ($n = 10$); △ *Fas* (sequence 5) ($n = 10$); ▽, *Fas* (sequence 6) ($n = 10$). (Reproduced with permission from Reference 36.)

achieved in hepatocytes via the hydrodynamic tail vein injection and silencing effects are not diluted as the hepatocytes are mostly nondividing cells.

siRNA use can also potentiate/sensitize diseases to first line agents. Such studies have been shown with siRNAs potentiating the effects of imatinib (Ab1-kinase specific competitive inhibitor). siRNAs were used to decrease the protein levels of Bcr/Ab1, thus potentiating the effects of imatinib [41]. The major hurdle in cancer treatment with chemotherapeutic agents is the development of drug resistance, owing to the expression of *MDR1* (a multidrug transporter encoding P-glycoprotein). *In vitro* RNAi targeting of *MDR1* has been shown to overcome resistance to daunorubicin by over 90% in pancreatic and gastric carcinomas [42]. Currently, there are numerous studies with siRNA as a potential therapeutic in different stages of clinical studies.

13.5.3 RNA Transfection—Delivering siRNA Inside Cells

13.5.3.1 In vitro Efficient gene silencing can be achieved by transfecting the cells *in vitro* either using chemically synthesized siRNA or by transfecting the cells with transcript encoding plasmid DNA. Either way, the molecules to be introduced into cells—siRNA/plasmid DNA—are hydrophilic and polyanionic, and need some kind of transfecting agent/vector to achieve sufficient levels inside the cell. However, introducing chemically synthesized siRNA molecules may be less complicated than transfecting cells with transcript encoding plasmid DNA. The difference lies in the fact that siRNA molecules require cytoplasmic delivery for gene silencing; however, intracellular production of siRNA from plasmid DNA requires nuclear delivery of the plasmids.

Further, gene silencing achieved by transfecting mammalian cells with siRNA duplexes is transient and depends on the number of siRNA molecules transfected into the cells. The mammalian cell lacks the enzyme: RNA-dependent RNA polymerases (which can amplify the siRNA molecules inside a cell). Thus, the number of effective siRNA molecules present inside cells gets diluted with each cell division. Omi et al. have shown that siRNA activity lasts for 3–7 days in proliferating cells, but can persist for more than 3 weeks in terminally differentiated cells (such as in neurons) [43]. Gene expression can be knocked down in mammalian cell lines, primary cells, and even in embryonic stem cells [44].

Elbashir et al. were the first to report the transfection of siRNA duplexes in cultured mammalian cells [26]. siRNA duplexes were synthesized against the luciferase gene and cotransfected with the plasmid encoding luciferase. The transfections were performed with cationic liposomes in a variety of mammalian cell lines—NIH/3T3, COS-7, and HeLa S3 cells. Expression of luciferase gene was monitored 20 h after the transfection, and it was found that the siRNA duplexes can specifically inhibit the gene expression, but to a different extent in different cell lines. Another important finding of these experiments was that siRNAs are extraordinarily potent reagents for mediating gene silencing as they were found to be effective at concentrations that are several orders lower than that required for conventional antisense reagents.

siRNA can be transfected into mammalian cells using lipid-based formulations, conjugating with peptides, or by electroporation. Membrane permeant peptides (MPPs) are amphipathic peptides that can translocate across the lipid bilayers of cells in an energy-independent manner. Thiol-containing siRNAs were conjugated to MPPs (penetratin, transportan) via disulfide bonds [45]. The peptides allowed efficient cytoplasmic delivery of siRNAs, since upon entering the cells the disulfide bonds are reduced, releasing the siRNA molecules. MPP-siRNAs successfully silenced the expression of GFP and luciferase genes in stably transfected cell lines. Chinese hamster ovary cells (CHO-AA8-Luc Tet-Off) that stably expressed luciferase gene were used for the experiments to compare the transfection efficiency of MPP-siRNA and lipofectamine-delivered siRNAs. Lipofectamine-siRNA transfected cells showed a decrease in luciferase activity by 36%, 2 days after the transfection; however, the luciferase levels returned to the basal levels on the third day. On the contrary, penetratin-delivered siRNAs decreased the luciferase levels by 53% on second day after treatment and maintained these low levels of gene expression on the third day as well. These results indicate that MPPs have higher transfection efficiencies for siRNA as compared to lipofectamine in this cell line.

13.5.3.2 In vivo The first method to successfully deliver siRNA *in vivo* was the high pressure tail vein injection of siRNAs (in physiological solution) in mice. This method of rapid hydrodynamic infusion delivers siRNA to the highly vascularized organs, like liver, lung, kidney, spleen and pancreas.

Almost 90% reduction in target gene expression was observed in the liver of mice, though the effect was transient, lasting for about a week. Numerous studies have used this method to introduce siRNA/shRNA into rodents, achieving efficient delivery and silencing of target gene expression. Though quite successful for introducing siRNA in rodents, this method is not a clinically feasible option for humans.

Sorensen et al. were the first to show that cationic liposome-mediated delivery of synthetic siRNA molecules can specifically inhibit the expression of exogenous and endogenous gene in adult mice [38]. Cationic liposomes (DOTAP based) complexed with a plasmid encoding green fluorescent protein (GFP) and its cognate siRNA was injected intravenously into adult mice. GFP gene expression was found to be significantly inhibited with the siRNA in the liver and spleen of mice, 3 days after the injection, as compared to the mismatched/inactive siRNA as control. Furthermore, the therapeutic efficacy of synthetic siRNA molecules was investigated *in vivo* in a mouse model of sepsis. BALB/c mice were intraperitoneally pretreated with anti-TNF- α siRNA, prior to the injection of a lethal dose of lipopolysaccharide (LPS) capable of inducing septic shock. A significant protective effect of siRNA was found in terms of the number of mice surviving the septic shock, as compared to the inactive siRNA. Further this effect was attributed to the decreased levels of TNF- α as a result of the specific inhibition of TNF- α gene expression with siRNA.

Since high concentrations of siRNA can induce the nonspecific immune stimulation response, it is important that the vectors for *in vivo* delivery of siRNA can deliver siRNA even at low concentrations to the target site. Such an experiment was performed using a lipid-based vector for the delivery of siRNA to mouse brain. JetSITM (a mixture of cationic lipids) was used to complex plasmid DNA encoding luciferase gene and picomolar concentrations of siRNA against this gene [46]. These polyplexes were injected into the mouse brain using stereotaxic intracerebroventricular injections. A formulation of JetSITM with another fusogenic lipid dioleoylphosphatidylethanolamine (DOPE) was found to efficiently inhibit the expression of target gene *in vivo*, even at picomolar concentrations of siRNA. The gene silencing effect was found to be dose dependent and specific.

Most of the *in vivo* studies have been performed with rodents, but one recent study has demonstrated that RNAi-mediated gene silencing can be successfully achieved in nonhuman primates as well, thus highlighting the potential of siRNA as a therapeutic via systemic delivery in species higher than rodents. siRNA targeting the gene expressing apolipoprotein B (ApoB) was administered, as a liposomal formulation via a bolus intravenous injection into cynomolgus monkeys [47]. mRNA levels of the target gene in the liver were found to be reduced within 48 h of the injection. Significant reduction in the levels of ApoB protein was observed as early as 24 h after siRNA injection with the effects lasting for 11 days. Furthermore, there was no evidence of complement activation, proinflammatory cytokine production, or toxicities in

the animals. The only detected changes in the primates as a result of siRNA liposomal injections were the transient increase in the liver enzymes, which normalized to the basal levels within 6 days of treatment.

siRNAs can be complexed with polycationic polymers to form polyplexes. Self-assembling nanoparticles with siRNA were prepared with PEI that is PEGylated with an Arg–Gly–Asp (RGD) peptide ligand attached at the distal end of the PEG [48]. The use of RGD ligand allows targeting of integrins expressed on tumor neovasculature, thus selectively delivering siRNA to the tumor tissue. The polymer was prepared with three functionalities in order to obtain targeted self-assembling nanoplexes: (1) branched PEI—as the cationic complexing polymer, (2) PEG—steric protective surface layer, and (3) RGD peptide—targeting ligand. The nanoplexes were used to successfully deliver siRNA inhibiting the vascular endothelial growth factor receptor-2 (VEGF R2) expression, to the tumor neovasculature, and thereby inhibiting tumor angiogenesis. siRNA carrying nanoplexes were injected every 3 days into mice carrying subcutaneous tumor (developed by injecting N2A cells) by tail vein injection. There was a selective tumor uptake of the nanoplexes showing a sequence-specific inhibition of VEGF R2 expression and inhibition of both tumor angiogenesis and tumor growth (Fig.13.4).

Chemical modifications of siRNA have also been attempted to improve the delivery of siRNA without using any other transfecting agents. Lipophilic siRNAs were synthesized by covalently conjugating the 5'- ends of RNA with derivatives of cholesterol, lithocholic acid, or lauric acid [49]. These constructs were shown to improve the delivery of siRNA to liver cells and downregulate the expression of a LacZ expression construct. In another study, the 3'- end of siRNA was conjugated to cholesterol by means of a pyrrolidine linker. This improved the resistance of siRNA to nuclease degradation, increased its stability in blood circulation, and also, increased the uptake of siRNA by liver.

Recombinant viral vectors, such as AAV, can mediate the delivery and long-term silencing of a gene in both dividing and nondividing mammalian cells. siRNA-producing lentivirus can transduce nondividing cells and has been used to deliver siRNA into embryonic stem cells to create knockdown mice. Kunath et al. used viral constructs expressing shRNA for Ras GTPase-activating protein to transfect mouse embryonic stem cells [50]. The resulting mice showed defects similar to that of a knockout developed by the conventional homologous recombination. Despite the advantage of viral vectors to deliver siRNA to nontransfectable cells, their potential for therapeutic applications is reduced by the fact that this delivery method is more prone to nonspecific interferon response, owing to high expression of shRNA. Viral vectors expressing siRNA have been shown to markedly diminish the expression of exogenous and endogenous genes *in vitro* and *in vivo* in brain and in liver [51]. Recombinant adenoviral vectors were generated for intracellular expression of siRNA against GFP (siGFP) and β -glucouronidase. HeLa cells were infected with the viral vectors expressing siRNA against β -glucouronidase, and lysed

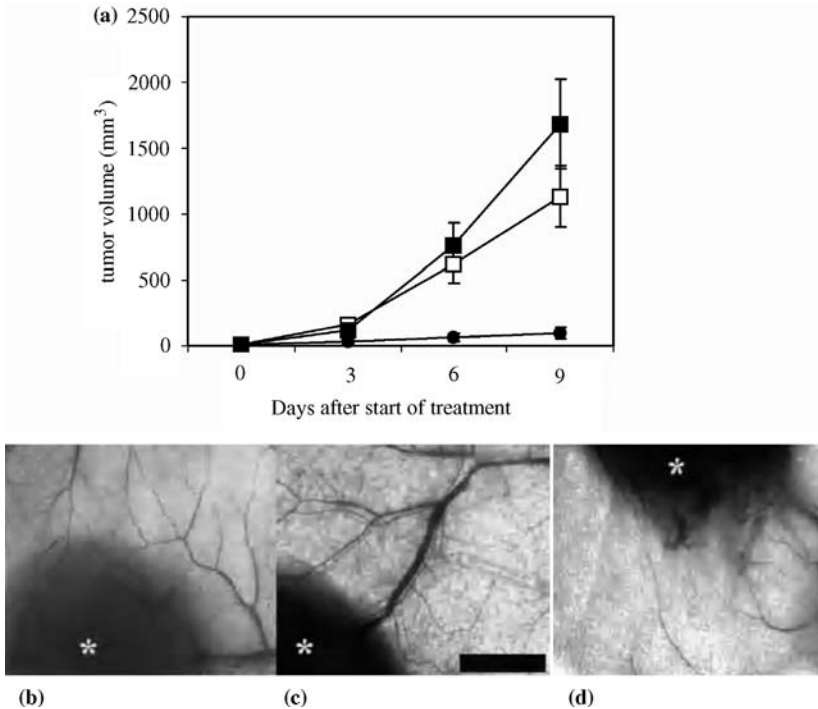


FIGURE 13.4 Tumor growth inhibition by VEGF R2 siRNA nanoplexes. (a) Tumor growth inhibition by siRNA RPP nanoplexes. Mice were inoculated with N2A tumor cells and left untreated (open squares) or treated every 3 days by tail vein injection with RPP-nanoplexes with siLacZ (filled squares) or siVEGF R2 (filled circles) at a dose of 40 μg per mouse. Treatment was started at the time point that the tumors became palpable ($\sim 20 \text{ mm}^3$). Only VEGF R2-sequence-specific siRNA inhibited tumor growth, whereas treatment with LacZ siRNA did not affect tumor growth rate as compared with untreated controls ($n = 5$). (b–d) Neovascularization in tumors treated with siRNA RPP nanoplexes. Representative tumors excised at the end of the tumor growth inhibition experiment (a) were examined using low magnification light microscopy. Transillumination of tumor and surrounding skin tissue shows strong neovascularization in mice left untreated (b) and mice treated with RPP nanoplexes with siRNA-LacZ (c). In contrast, mice treated with RPP nanoplexes with VEGF R2 siRNA showed low neovascularization and erratic branching of blood vessels (d). Asterisks indicate tumor tissue. Bar = 2 mm. (Reproduced with permission from Reference 48.)

72 h after treatment. This resulted in a specific reduction of β -glucuronidase gene expression, leading to a 60% reduction in β -glucuronidase activity. For *in vivo* studies, adenoviral vectors expressing siGFP were injected into the brain striatal regions of transgenic mice expressing eGFP. Effective gene silencing for up to 5 days was observed after a local injection of siRNA-producing AAV in mouse brain.

13.5.4 Issues

13.5.4.1 Specificity Nonspecific inhibition of gene expression is a problem with the use of dsRNAs for RNAi. dsRNAs are known to activate the dsRNA-dependent protein kinase (PKR), which results in a general inhibition of total protein synthesis and the nonspecific degradation of mRNAs present in the cells. However, the use of synthetic siRNA molecules is capable of bypassing the activation of this nonspecific pathway. Still there are numerous reports indicating the potential of siRNA molecules to produce some nonspecific and off-target effects. This may be due to partial homology of the siRNA sequences to mRNA sequences, other than the target mRNA [52,53]. Most nonspecific responses can be minimized with careful design of siRNA sequences. The nonspecific effects of siRNA on gene expression depend on the siRNA concentration, specific sequence, delivery method, and the cell type [54]. High siRNA concentrations enhance nonspecific effects.

13.5.4.2 Resistance Cells can develop resistance to the effect of siRNA by loss of genes required for RISC complex formation or by selection of suppressors that inhibit degradation [35]. Further, not all mRNA sequences can be targeted by siRNAs, due to lack of accessibility of the target sequences hidden by RNA-binding proteins or complex secondary structures. Recent reports have indicated that siRNA-resistant viral strains (HIV) can emerge in as few as 25 days [55]. To reduce the chances of such resistance, multiple sequences per target and multiple targets per viral genome would be required. On the contrary, so far there are no reports of resistance developing in mammalian cells upon introduction of siRNA.

13.5.4.3 Stability For successful *in vivo* use, siRNA molecules must have sufficient stability in systemic circulation and should have desirable pharmacokinetic properties. The molecules should bind blood proteins to an extent so that immediate loss by excretion is prevented, but at the same time, this degree of binding should not be toxic [56]. However, studies have shown that siRNA degradation peaks 36–48 h after introduction and diminishes around 96 h. Biodistribution of radiolabeled siRNA was studied by intravenous and intraperitoneal injections in mice [57]. siRNA primarily accumulated in the liver and kidney and was also detected in the heart, spleen, and lung. These biodistribution patterns demand an improvement in the pharmacokinetic properties of siRNA for successful *in vivo* gene silencing.

Chemical modifications are in pursuit for increasing the stability, of siRNA while maintaining an adequate gene-silencing activity for therapeutic applications. Such chemical modifications can be made throughout the siRNA duplex or at selected one or two bases, to alter the chemical properties of siRNA. This can potentially help to increase the resistance of siRNA to nuclease enzymes, impart serum stability, and also alter the biodistribution patterns. Further, by

directing the biodistribution of siRNA to target tissues, the nonspecific effects can also be effectively reduced. The introduction of phosphorothioate linkages enhance nuclease resistance and improve serum stability [57]. However, the use of such modifications often results in cellular and *in vivo* toxicity, also their effect on *in vivo* potency of siRNA is yet to be established. Chemical modifications to the sugar moiety of the siRNA sequence can also significantly alter thermal stability, and, potentially affect the gene silencing activity of siRNA. Jayasena and coworkers have demonstrated that functional and nonfunctional siRNAs show distinct thermodynamic profiles. Several 2' modifications have been tested for their effects on gene expression in cultured cells. Gene silencing activity is retained after partial substitution of bases with 2'-fluoro bases [58].

13.6 CONCLUSIONS

Advances in molecular biology and polymer chemistry have enabled controlling cell behavior via DNA/RNA transfections. This has steered research toward identifying new genes responsible for disease induction/progression. DNA/RNA transfections have now become a routine research tool, though its applications as a therapeutic intervention is limited by the availability of safe and efficient transfection methods.

ACKNOWLEDGMENTS

Grant support from the National Institutes of Health (R01 EB003975) and a predoctoral fellowship to JKV from the American Heart Association, Heartland Affiliate (Award #0515489Z).

REFERENCES

1. Li Z, et al. Murine leukemia induced by retroviral gene marking. *Science* 2002; 296:497.
2. Vasir JK and Labhasetwar V. Polymeric nanoparticles for gene delivery. *Expert Opin Drug Deliv* 2006;3:325–344.
3. Wiethoff CM and Middaugh CR. Barriers to nonviral gene delivery. *J Pharm Sci* 2003;92:203–217.
4. Lechardeur D and Lukacs GL. Intracellular barriers to non-viral gene transfer. *Curr Gene Ther* 2002;2:183–194.
5. Pouton CW and Seymour LW. Key issues in non-viral gene delivery. *Adv Drug Deliv Rev* 2001;46:187–203.
6. Lee EJ and Jameson JL. Gene therapy of pituitary diseases. *J Endocrinol* 2005; 185:353–362.

7. Ohno T, et al. Gene therapy for vascular smooth muscle cell proliferation after arterial injury. *Science* 1994;265:781–784.
8. Lee RJ, et al. VEGF gene delivery to myocardium: deleterious effects of unregulated expression. *Circulation* 2000;102:898–901.
9. Bettinger T, Carlisle RC, Read ML, Ogris M, Seymour LW. Peptide-mediated RNA delivery: a novel approach for enhanced transfection of primary and post-mitotic cells. *Nucleic Acids Res* 2001;29:3882–3891.
10. Sweeney P, et al. Efficient therapeutic gene delivery after systemic administration of a novel polyethyleneimine/DNA vector in an orthotopic bladder cancer model. *Cancer Res* 2003;63:4017–4020.
11. Vernejoul F, et al. Antitumor effect of *in vivo* somatostatin receptor subtype 2 gene transfer in primary and metastatic pancreatic cancer models. *Cancer Res* 2002;62:6124–6131.
12. Prabha S and Labhasetwar V. Nanoparticle-mediated wild-type p53 gene delivery results in sustained antiproliferative activity in breast cancer cells. *Mol Pharm* 2004;1:211–219.
13. Cohen H, et al. Sustained delivery and expression of DNA encapsulated in polymeric nanoparticles. *Gene Ther* 2000;7:1896–1905.
14. Bernkop-Schnurch A and Krajcicek ME. Mucoadhesive polymers as platforms for peroral peptide delivery and absorption: synthesis and evaluation of different chitosan–EDTA conjugates. *J Control Release* 1998;50:215–223.
15. Artursson P, Lindmark T, Davis SS, Illum L. Effect of chitosan on the permeability of monolayers of intestinal epithelial cells (Caco-2). *Pharm Res* 1994;11:1358–1361.
16. Roy K, Mao HQ, Huang SK, Leong KW. Oral gene delivery with chitosan–DNA nanoparticles generates immunologic protection in a murine model of peanut allergy. *Nat Med* 1999;5:387–391.
17. Roman S, Lindeman R, O’Toole G, Poole MD. Gene therapy in plastic and reconstructive surgery. *Curr Gene Ther* 2005;5:81–99.
18. Baltzer AW and Lieberman JR. Regional gene therapy to enhance bone repair. *Gene Ther* 2004;11:344–350.
19. Madeddu P. Therapeutic angiogenesis and vasculogenesis for tissue regeneration. *Exp Physiol* 2005;90:315–326.
20. Kasahara H, et al. Biodegradable gelatin hydrogel potentiates the angiogenic effect of fibroblast growth factor 4 plasmid in rabbit hindlimb ischemia. *J Am Coll Cardiol* 2003;41:1056–1062.
21. Nagaya N, et al. Hybrid cell–gene therapy for pulmonary hypertension based on phagocytosing action of endothelial progenitor cells. *Circulation* 2003;108:889–895.
22. Michiels F, et al. Arrayed adenoviral expression libraries for functional screening. *Nat Biotechnol* 2002;20:1154–1157.
23. Ziauddin J and Sabatini DM. Microarrays of cells expressing defined cDNAs. *Nature* 2001;411:107–110.
24. Honma K, et al. Atelocollagen-based gene transfer in cells allows high-throughput screening of gene functions. *Biochem Biophys Res Commun* 2001;289:1075–1081.
25. Fire A, et al. Potent and specific genetic interference by double-stranded RNA in *Caenorhabditis elegans*. *Nature* 1998;391:806–811.

26. Elbashir SM, et al. Duplexes of 21-nucleotide RNAs mediate RNA interference in cultured mammalian cells. *Nature* 2001;411:494–498.
27. Reynolds A, et al. Rational siRNA design for RNA interference. *Nat Biotechnol* 2004;22:326–330.
28. Couzin J. Breakthrough of the year. Small RNAs make big splash. *Science* 2002;298:2296–2297.
29. Paddison PJ, et al. A resource for large-scale RNA-interference-based screens in mammals. *Nature* 2004;428:427–431.
30. Berns K, et al. A large-scale RNAi screen in human cells identifies new components of the p53 pathway. *Nature* 2004;428:431–437.
31. Hemann MT, et al. An epi-allelic series of p53 hypomorphs created by stable RNAi produces distinct tumor phenotypes *in vivo*. *Nat Genet* 2003;33:396–400.
32. Dorsett Y and Tuschl T. siRNAs: applications in functional genomics and potential as therapeutics. *Nat Rev Drug Discov* 2004;3:318–329.
33. Wall NR and Shi Y. Small RNA: can RNA interference be exploited for therapy? *Lancet* 2003;362:1401–1403.
34. Gupta S, Schoer RA, Egan JE, Hannon GJ, Mittal V. Inducible, reversible, and stable RNA interference in mammalian cells. *Proc Natl Acad Sci USA* 2004;101:1927–1932.
35. Ryther RC, Flynt AS, Phillips JA, 3rd, Patton JG. siRNA therapeutics: big potential from small RNAs. *Gene Ther* 2005;12:5–11.
36. Song E, et al. RNA interference targeting Fas protects mice from fulminant hepatitis. *Nat Med* 2003;9:347–351.
37. Song E, et al. Sustained small interfering RNA-mediated human immunodeficiency virus type 1 inhibition in primary macrophages. *J Virol* 2003;77:7174–7181.
38. Sorensen DR, Leirdal M, Sioud M. Gene silencing by systemic delivery of synthetic siRNAs in adult mice. *J Mol Biol* 2003;327:761–766.
39. Yoshinouchi M, et al. *In vitro* and *in vivo* growth suppression of human papillomavirus 16-positive cervical cancer cells by E6 siRNA. *Mol Ther* 2003;8:762–768.
40. Reich SJ, et al. Small interfering RNA (siRNA) targeting VEGF effectively inhibits ocular neovascularization in a mouse model. *Mol Vis* 2003;9:210–216.
41. Wohlbold L, et al. Inhibition of bcr–abl gene expression by small interfering RNA sensitizes for imatinib mesylate (STI571). *Blood* 2003;102:2236–2239.
42. Wilda M, Fuchs U, Wossmann W, Borkhardt A. Killing of leukemic cells with a BCR/ABL fusion gene by RNA interference (RNAi). *Oncogene* 2002;21:5716–5724.
43. Omi K, Tokunaga K, Hohjoh H. Long-lasting RNAi activity in mammalian neurons. *FEBS Lett* 2004;558:89–95.
44. Leung RK and Whittaker PA. RNA interference: from gene silencing to gene-specific therapeutics. *Pharmacol Ther* 2005;107:222–239.
45. Muratovska A and Eccles MR. Conjugate for efficient delivery of short interfering RNA (siRNA) into mammalian cells. *FEBS Lett* 2004;558:63–68.
46. Hassani Z, et al. Lipid-mediated siRNA delivery down-regulates exogenous gene expression in the mouse brain at picomolar levels. *J Gene Med* 2005;7:198–207.

47. Zimmermann TS, et al. RNAi-mediated gene silencing in non-human primates. *Nature* 2006;441:111–114.
48. Schiffelers RM, et al. Cancer siRNA therapy by tumor selective delivery with ligand-targeted sterically stabilized nanoparticle. *Nucleic Acids Res* 2004;32:e149.
49. Lorenz C, Hadwiger P, John M, Vornlocher HP, Unverzagt C. Steroid and lipid conjugates of siRNAs to enhance cellular uptake and gene silencing in liver cells. *Bioorg Med Chem Lett* 2004;14:4975–4977.
50. Kunath T, et al. Transgenic RNA interference in ES cell-derived embryos recapitulates a genetic null phenotype. *Nat Biotechnol* 2003;21:559–561.
51. Xia H, Mao Q, Paulson HL, Davidson BL. siRNA-mediated gene silencing *in vitro* and *in vivo*. *Nat Biotechnol* 2002;20:1006–1010.
52. Bridge AJ, Pebernard S, Ducraux A, Nicoulaz AL, Iggo R. Induction of an interferon response by RNAi vectors in mammalian cells. *Nat Genet* 2003;34:263–264.
53. Sledz CA, Holko M, deVeer MJ, Silverman RH, Williams BR. Activation of the interferon system by short-interfering RNAs. *Nat Cell Biol* 2003;5:834–839.
54. Persengiev SP, Zhu X, Green MR. Nonspecific, concentration-dependent stimulation and repression of mammalian gene expression by small interfering RNAs (siRNAs). *RNA* 2004;10:12–18.
55. Boden D, Pusch O, Lee F, Tucker L, Ramratnam B. Human immunodeficiency virus type 1 escape from RNA interference. *J Virol* 2003;77:11531–11535.
56. Paroo Z and Corey DR. Challenges for RNAi *in vivo*. *Trends Biotechnol* 2004;22:390–394.
57. Braasch DA, et al. Biodistribution of phosphodiester and phosphorothioate siRNA. *Bioorg Med Chem Lett* 2004;14:1139–1143.
58. Harborth J, et al. Sequence, chemical, and structural variation of small interfering RNAs and short hairpin RNAs and the effect on mammalian gene silencing. *Antisense Nucleic Acid Drug Dev* 2003;13:83–105.

Multiscale Coculture Models for Orthopedic Interface Tissue Engineering

HELEN H. LU and I-NING E. WANG

14.1 INTRODUCTION

Biological tissues and organs are complex systems whose maintenance and repair are regulated through cell–cell, cell–matrix interactions, as well as physical and chemical stimuli. These extrinsic and intrinsic signals collectively contribute to organ homeostasis and physiological function. Cellular interactions, in general, consist of one or all of the following: direct cell–cell communications as well as extracellular matrix- and soluble factor-mediated effects. Cell–cell communications imply direct physical contact between cells, while cell–matrix interactions are initiated by the binding of transmembrane proteins such as integrins to the extracellular matrix or biomaterial surface. In addition, secreted soluble factors and cytokines serve as chemical messengers directing both local and systemic cellular communications. These signaling molecules can be classified as autocrine, paracrine, or endocrine factors. While cell-to-cell contact may be required to initiate one or all of the above interactions, the secretion of soluble factors enables interactions beyond the immediate vicinity of the cell population and facilitates communication between adjacent tissues and organ systems.

The manipulation of cell microenvironment via modulation of cell–cell communication and cell–matrix interaction is important for the regeneration of complex tissue systems [1–3]. Currently, the specific mechanisms underlying the interactions between different types of connective tissue cells are not well understood. Physiologically relevant *in vitro* and *in vivo* models are thus needed in order to investigate the role of cellular communications in multitissue

regeneration and organ homeostasis. This review will first discuss the relevance of cellular interactions for engineering complex tissues for orthopedic repair, focusing on the regeneration of the multitissue interface between bone and soft tissues such as ligaments and tendons. After a brief overview of the different types of coculture models, their application in elucidating the mechanisms of interface regeneration through controlled interactions between connective tissue cells (e.g., osteoblasts, fibroblast, and chondrocytes) will be reviewed, highlighting the potential of controlled heterotypic cellular interactions for interface tissue engineering and biological fixation of soft tissue grafts.

14.2 CELLULAR INTERACTIONS AND THE SOFT TISSUE-TO-BONE INTERFACE

Soft tissues such as tendons or ligaments insert into bone through a fibrocartilage interface [4–10], and the reestablishment of this physiologic interface is essential for the clinical efficacy of soft tissue-based grafts. This complex interface consists of several continuous yet distinct tissue regions, with each region exhibiting characteristic cellular phenotype and matrix composition. It is thus likely that heterotypic cellular interactions are essential for the maintenance and repair of the distinct matrix zones at the interface between soft tissue and bone. Using the insertion site of anterior cruciate ligament (ACL) to bone as a model system, this review highlights the utility of *in vitro* coculture models for elucidating the role of heterotypic cellular interactions in interface regeneration.

Anatomically, the ACL-to-bone interface consists of three distinct yet continuous tissue regions: ligament, fibrocartilage, and bone. The fibrocartilage region is further divided into nonmineralized and mineralized zones. The ligament proper contains fibroblasts embedded in collagen-rich matrix. The nonmineralized fibrocartilage matrix consists of ovoid chondrocytes, and collagen types I and II are found within the proteoglycan-rich matrix. Hypertrophic chondrocytes reside in the mineralized fibrocartilage zone with a pericellular matrix containing collagen type X [8, 11]. The last region is subchondral bone, within which osteoblasts, osteocytes, and osteoclasts are embedded in a type I collagen matrix. The multitissue organization and controlled heterogeneity are believed to be important for minimizing stress concentrations and facilitating the transfer of complex loads between soft and hard tissues [5, 12]. At present, it is not well understood how this complex interface is formed, and the inability to regenerate this interface following ligament reconstruction surgery is one of the primary causes of graft failure [13–16].

While the mechanism of interface regeneration is not known, it has been observed *in vivo* that tendon-to-bone healing following ACL reconstruction results in the formation of a fibrovascular tissue layer within the bone tunnel [17–20]. During the healing process, this layer reorganizes into a fibrocartilage-like tissue. Although the location of this neo-fibrocartilage is nonanatomical, these *in vivo* observations demonstrate that a fibrocartilage-like tissue can be

regenerated between the soft tissue and bone. Specifically, the formation of a fibrocartilage layer only at regions where the tendon graft *directly contacts* the bone tissue suggests that the interactions between cells derived from tendon (e.g., fibroblasts) and bone tissue (e.g., osteoblasts) are important for fibrocartilage regeneration [2]. In particular, osteoblast–fibroblast interactions may lead to the transdifferentiation of osteoblasts and/or fibroblasts, as well as the recruitment of progenitor or mesenchymal stem cells to the soft tissue-to-bone interface. These recruited progenitor or stem cells are likely to be responsible for fibrocartilage formation, and their eventual differentiation may also be regulated by osteoblast–fibroblast interactions.

To test the above hypothesis, *in vitro* coculture models have been reported, which evaluate the role of heterotypic cellular interactions on the development of fibrocartilage-specific markers [21–23]. The cell types prevalent at the native ligament-bone insertion include fibroblasts, fibrochondrocytes, and osteoblasts, each residing in their own phenotypic extracellular matrix. Therefore, the ideal coculture model for orthopedic interface tissue engineering must be able to recapitulate the complex three-dimensional and multiscale (macro-, micro-, and nanolevel) interactions between these distinct cell types.

14.3 TYPES OF COCULTURE MODELS

Cellular communications can be bidirectional or multidimensional and may be exercised at both macro- and microscales. Depending on the hypothesis of interest, coculture models may be used to discern the individual and collective effects of physical contact and soluble factors. Specifically, the types of existing coculture models can be classified as either systems that enable or prevent cell–cell contact (Fig. 14.1). The advantages and disadvantages of each type of model are briefly discussed below.

14.3.1 Coculture System with Cell–Cell Contact

14.3.1.1 Mixed Coculture The simplest coculture system that permits physical contact between cells consists of a mixed monolayer culture of the cell types of interest. This is achieved by combining the different cell suspensions at the desired coculture ratio, and then seeding the mixture in the well (Fig. 14.1). Alternatively, the second cell type can be plated directly atop of a preformed monolayer of the first cell type. The mixed coculture model has been used successfully to examine interactions between fibroblasts and hepatocytes [24–26], fibroblasts and bone marrow stromal cells [27], fibroblasts and chondrocytes [28], as well as osteoblast and chondrocyte interactions [21,29–31]. This simple and convenient model maximizes the local heterotypic interactions and can be used to control the level of heterotypic and homotypic interactions by altering the seeding densities of each cell type. Interpretation of these coculture results, however, must take into consideration any dilution

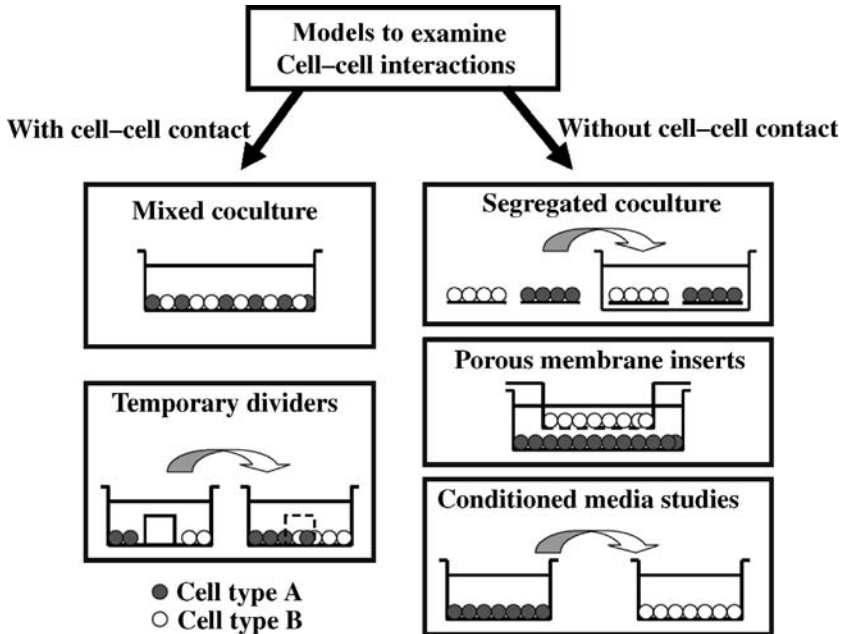


FIGURE 14.1 Schematic of models to evaluate heterotypic cell-cell interactions.

effect on cell response due to mixed culture as well as any metabolic differences between the various cell types.

14.3.1.2 Temporary Dividers Cell-cell contact can also be controlled by establishing physical barriers that are used to organize cell-seeding patterns in coculture (Fig. 14.1). The barrier may be removed later to permit cell migration and controlled cell-cell physical contact. This model has been used to examine interactions between fibroblasts and hepatocytes [26], as well as between osteoblast and fibroblast as shown in Fig. 14.2a [22]. It has the advantage of been able to excise greater control of the extent of heterotypic and homotypic interactions, while permitting both physical contact and soluble factor interactions. This system is, however, experimentally more challenging as a complete seal between the individual cell compartments is required. Moreover, cell response and soluble-factor transport in this model is a function of the physical and chemical properties of the divider material utilized.

14.3.2 Coculture System Without Cell-Cell Contact

14.3.2.1 Segregated Coculture To prevent cell-cell contact, a segregated coculture system may be established by first forming individual cultures

of each cell type, and later cocultivate them in the same environment. For example, monolayers of each cell type can be preformed on tissue culture coverslips, and then cocultured together to examine heterotypic cellular interactions. In contrast to the mixed coculture model, the primary advantage of this coverslip-based system is that the response of the subpopulation of cells in coculture can be analyzed. This coculture method has been used to determine the interactions between chondrocytes and synovial cells [32], as well as those of fibroblasts and osteoblasts [22]. A disadvantage of the segregated coculture model is that physical contact cannot be completely prevented in the long term, as the cells often migrate from the coverslips and form a heterogeneous culture on the coverslips or in the culture well.

14.3.2.2 Porous Membrane Inserts The advent of cell culture membrane inserts reduced many of the experimental difficulties associated with coculture and has led to the development of reliable and reproducible coculture systems. The transwell[®] inserts are designed with pores small enough to prevent cell migration, yet still large enough to permit transport of interactive factors and other biomolecules. The insert also provides an additional culturing surface, while effectively preventing heterotypic cell–cell contact. This method has been widely used to investigate the mechanism of endochondral ossification by examining the interactions between chondrocytes and mesenchymal stem cell [33, 34], chondrocytes, and osteoblasts [35, 36], and osteoblasts and fibroblasts [37], in addition to a variety of other cell types [38–40]. This coculture model is attractive due to its reproducibility and ease of experimentation, although the effects of soluble factors detected are unidirectional. Moreover, extensive cell growth can cover the pores of the inserts, limiting cellular interactions to only the bottom first monolayer of cells, which may be insufficient to elicit a significant response in coculture.

14.3.2.3 Conditioned Media Studies Another widely utilized method for determining soluble factor effects is through conditioned media studies, during which the culture media from one cell type is introduced into the culture of the second cell type. This method has been used in conjunction with direct physical contact models to investigate the mechanism of interaction between fibroblasts and stem cells [27, 41], fibroblasts and chondrocytes [28], as well as between osteoblasts and fibroblasts [42]. The advantages of this model include its simplicity and the ability to immediately discern any soluble factor-related effects, plus the potential for subsequent identification of relevant soluble factors using quantitative assays. An inherent limitation of conditioned media studies, however, is the issue of nutrient deficiency, as the experimental group is exposed to the conditioned media and only supplemented partially with fresh media. Additional challenges including the reproduction of both the temporal distribution and optimal concentrations of the secreted factors in conditioned media studies.

14.4 COCULTURE MODELS FOR ORTHOPEDIC INTERFACE TISSUE ENGINEERING

As discussed in Section 14.2, the ideal coculture model for evaluating the role of cellular communications in interface tissue engineering must be able to recapitulate the complex interactions inherent at the native soft tissue-to-bone interface. To this end, existing coculture models can be combined and optimized in conjunction with other systems in order to evaluate interactions between interface-relevant cells such as osteoblasts, fibroblasts, chondrocytes, and stem cells. The application of these models to determine the effects of cell–cell contact and soluble factors for interface tissue engineering are reviewed below.

14.4.1 Coculture Models of Osteoblasts and Fibroblasts

To determine the role of fibroblast and osteoblast interactions in fibrocartilage formation, a novel coculture model permitting both cell contact and paracrine interaction was reported by Wang et al. [22]. This model was designed to emulate the *in vivo* condition where the tendon is in direct contact with bone tissue during graft healing following ACL reconstruction. Briefly, as shown in Fig. 14.2a, osteoblasts and fibroblasts were first seeded on opposing sides of a tissue culture well. The cells were separated by a hydrogel divider preformed in the center of the well. Once the cells reached confluence on each side, the divider was removed, allowing the osteoblasts and fibroblasts to migrate and interact within the interface region. The two cell types communicated through paracrine and autocrine factors, as well as eventual physical contact in the interface region. It was found that osteoblast–fibroblast interaction led to a decrease in cell

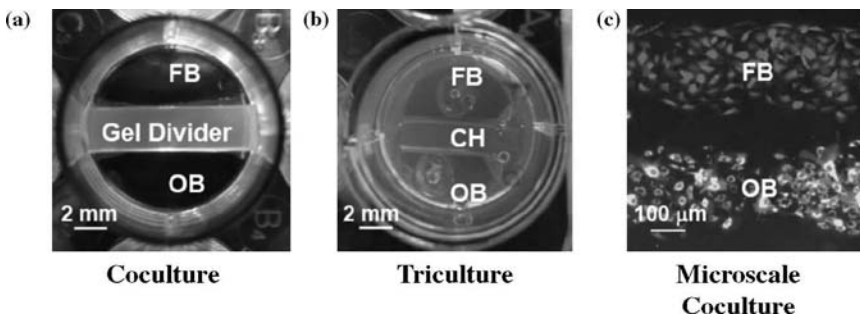


FIGURE 14.2 Examples of cell–cell interaction models used in interface tissue engineering: (a) Coculture of fibroblasts and osteoblasts with temporary agarose gel divider; (b) triculture of fibroblasts and osteoblasts with chondrocytes encapsulated in 3D hydrogel; (c) microscale coculture of fibroblasts and osteoblasts using microfluidic patterning techniques. FB: fibroblasts, OB: osteoblasts, CH: chondrocytes.

proliferation, a reduction in osteoblast-mediated mineralization, accompanied by an increase in the mineralization potential of fibroblasts [23].

This osteoblast–fibroblast model is limited in its ability to distill the relative contributions of soluble factor and cell–cell contact to these observed changes, and the specific response of each cell type in coculture is not known. Further refinement of the model using the coverslip-based segregated coculture system [22] revealed that the observed changes in cell phenotype are indeed cell type-specific. For example, doubling the number of osteoblasts in coculture resulted in greater suppression of cell proliferation, suggesting that the decreased mitotic activity is affected by osteoblasts instead of fibroblasts. In addition, conditioned media studies have been performed to investigate the relative contribution of cell–cell contact and soluble factors. Shan et al. introduced three types of conditioned media (osteoblasts, fibroblasts, and osteoblast–fibroblast coculture) to individual culture of fibroblasts or osteoblasts, and examined the proliferation and differentiation of each cell type over time [42]. It was found that both autocrine and paracrine effects were responsible for the changes in phenotype observed due to osteoblast–fibroblast coculture. The magnitude of response of the cultures treated with conditioned media was, however, significantly lower than those seen in coculture [42], suggesting that cell–cell contact also plays a role in cell transdifferentiation. Interestingly, the osteoblast–fibroblast cocultured media elicited distinct responses when compared to media from single cultures of either osteoblasts or fibroblasts. These observations confirm that osteoblast and fibroblast respond differently when they are in a cocultured or single-cultured environment.

Findings from these coculture studies collectively demonstrate that osteoblast–fibroblast interactions modulate cell phenotypes and may lead to transdifferentiation. While it is not known which or if any of these cells are directly responsible for interface regeneration, their interactions most likely have a downstream effect, either in terms of directing osteoblast or fibroblast transdifferentiation, or in the recruitment and induction of progenitor or stem cells for fibrocartilage formation.

14.4.2 Coculture Models of Osteoblasts and Chondrocytes

As the postnatal ligament-to-bone interface comprised chondrocyte-like cells [43], the effects of osteoblast and chondrocyte coculture also needs to be examined. Using a layered mixed coculture model, Jiang et al. seeded an osteoblast monolayer atop a condensed chondrocyte micromass [21]. This model permitted direct physical contact between these two cell types, while maintaining the required 3D culture for chondrocytes. It was found that while the chondrocytes continued to synthesize collagen type II, proteoglycan deposition was significantly lower in coculture. Alkaline phosphatase activity remained unchanged in the osteoblasts, while their mineralization potential was significantly reduced due to coculture. These results suggest that osteoblast–fibroblast and osteoblast–chondrocyte interactions are key modulators of cell phenotypes.

14.4.3 Coculture and Triculture Models of Osteoblasts, Chondrocytes, and Fibroblasts

Recently, Wang et al. reported on a triculture model of fibroblasts, chondrocytes, and osteoblasts; the three cell types dominant in their respective region of the interface, namely ligament, fibrocartilage, and bone (Fig. 14.2b) [44]. To ensure their phenotypic spherical morphology, chondrocytes were encapsulated within the hydrogel divider used in the previous osteoblast–fibroblast coculture model (Fig. 14.2a) [22]. Once again, a reduction in the proliferation of both osteoblasts and fibroblasts due to heterotypic cell interactions was found, while the number of chondrocytes remained relatively constant over time in the hydrogel. Triculture led to reduced osteoblast-mediated mineralization, accompanied by increased fibroblast mineralization. The chondrocytes continued to produce proteoglycans and the expression of both collagen types I and II were detected in the interfacial region.

This model was subsequently used to compare the effects of fibroblast–osteoblast interaction on the response of interface-relevant cells such as bone marrow stromal cells and ligament fibroblasts [45]. In this study, the stromal cells or fibroblasts were encapsulated in the hydrogel insert instead of chondrocytes. While minimal response was observed with fibroblasts, the stromal cells measured significantly higher ALP activity during triculture. Moreover, expressions of interface-relevant markers such as collagen type II and proteoglycans were detected in triculture with the bone marrow stromal cells. These results provide new evidence that osteoblast–fibroblast interactions may initiate the differentiation of stem cells or progenitor cells for fibrocartilage regeneration.

14.5 MACRO- AND MICROSCALE COCULTURE

The coculture models described above have evaluated cellular interactions only at the macroscopic level, while it is well known that physiologically relevant interactions are conducted at microscopic and nanolevels. Modern methods for spatial control over cell attachment and spreading have facilitated an unprecedented level of sophistication in the investigation of cell–cell interactions. Micropatterning and microfluidic models have been utilized for the microscale coculture of a variety of cells types [1, 23, 46–51]. Bioinspired micropatterning of cells have been reported using photolithography, microcontact printing, micromolding, inkjet printing, and dip-pen spotting [46–50, 52]. A distinct advantage of these microscale systems is that the diffusion distances between the different cell types can be controlled and designed to match the biological scenario, leading to physiologic and relatively rapid interaction times. Biomimetic pattern of cells can also be achieved with high fidelity. Moreover, the smaller solution volume and lower concentration of effector molecules required at the microscale level, increase

the overall sensitivity of the system in its ability to detect the local effects of cell–cell contact and secreted factors when compared to the macroscale models.

Although promising, micropatterning is limited by the fact that chemical or biochemical modification of the surface is usually required. Consequently, the selection of adhesion proteins, as well as the underlying chemistry and physical properties of the surface, have significant effects on the stability of the cell pattern and the eventual cell–cell interactions. Moreover, long term evaluation of cellular interactions is difficult as cell migration often disrupts the micropattern over time. Microfluidic systems have therefore been developed to circumvent these limitations associated with micropatterning. The primary advantage of the microfluidic model resides in its ability to provide high resolution spatial control of fluid flow and factor concentration, as well as the potential for long term microscale coculture.

For interface tissue engineering, a microscale coculture model is also physiologically more relevant, as the native human ligament-to-bone interface spans merely 200–300 μm [8]. Tsai et al. recently investigated the effects of osteoblast and fibroblast micropatterning on cellular function and organization [23]. This microscale coculture model (Fig. 14.2c) was fabricated using soft lithography and replica molding, and utilized microfluidics to exert spatial control and cell patterning. Not surprisingly, differences in cell growth and differentiation were detected at the microscale when compared to the macroscale model [22]. These observations emphasize the importance of considering interaction scale in coculture models.

14.6 TWO-DIMENSIONAL (2D) AND THREE-DIMENSIONAL (3D) COCULTURES

In addition to the interaction scale, the effects of 2D and 3D substrates on cellular communications during coculture must be considered. The majority of published coculture studies of connective tissue cells have been performed on 2D surfaces, while it is well known that cell response is distinctly different in the 3D environment. Cukierman et al., evaluated human foreskin fibroblast adhesion to various 2D and 3D matrices [53], and observed that a cell-derived 3D matrix was significantly more effective in promoting cell adhesion and migration. Similarly, Spalazzi et al. evaluated osteoblast and chondrocyte coculture as a function of scaffold architecture [3], and found temporal morphological changes in chondrocytes seeded on extracellular matrix preformed by osteoblasts on either a 2D (flat disc) or 3D (microsphere-based scaffold) substrate. Specifically, the time required for nonphenotypic chondrocyte spreading was prolonged on the microsphere scaffolds when compared to the 2D discs. The expression of adhesion complexes or the characteristics of the preformed extracellular matrix likely differ between 2D and 3D substrates [3, 53].

Recently, using a triphasic scaffold predesigned for interface tissue engineering, Spalazzi et al. evaluated the effects of osteoblast and fibroblast interactions in 3D coculture. It was found that phase-specific cell distribution and coculture resulted in the formation and maintenance of distinct yet continuous ligament, interface, and bone-like matrix regions on the scaffold [54]. In contrast to the 2D study, cell proliferation was not reduced in 3D coculture and consequently, the observed cell-matrix production was significantly more extensive. It is possible that the 3D coculture response is more representative of systemic effects of cellular interactions as opposed to the local effects seen in 2D coculture models. These observations highlight the importance of considering multiscale and multidimensional effects on cell–cell interactions and demonstrate the utility of *in vitro* coculture and triculture model systems for investigating the mechanisms of interface regeneration.

14.7 MECHANISM OF CELLULAR INTERACTIONS DURING COCULTURE

It has been well established that cell–cell physical contact and communications are regulated by a variety of cell-adhesion molecules and cell–cell junctions. Of these, cadherins, which represent a large family of calcium-dependent, transmembrane adhesion molecules, are particularly important in the dynamic regulation of cell–cell adhesion and communications. Cadherins are powerful modulators of tissue morphogenesis during embryonic development, as they direct cell sorting [55, 56], cell migration [57, 58] as well as cell adhesion [59, 60]. Cadherins are structurally classified into type I and type II subgroups, and are named in accordance to the tissue type from which they were first isolated. Type I cadherins consist of cadherin E (epithelial), N (neural), P (placental), and R (retinal) [61] while type II cadherins consist of cadherin-5, -6, -8, -11, and -12 [61]. During development, cell sorting is regulated by differential expression of cadherins, which in turn promotes tissue separation. For example, the selective expression of E-cadherin in the ectoderm versus N-cadherin in the developing neural epithelium allows the two regions to split and form separately [55, 56]. Compartmentalization of tissues and formation of tissue boundaries are also regulated by cadherins [62, 63]. In the adult tissue, cadherins are essential for tissue homeostasis in actively growing tissues such as the epidermis [64–66] and bone [67]. They also help to maintain tissue organization by promoting contact inhibition and preventing the invasion of tumor cells [60, 68]. The extracellular domains of cadherins interact with those of adjacent cells in order to mediate cell adhesion. The intracellular cadherin domain also binds to cytoplasmic proteins such as catenins (α, β) and p120, which in turn interacts with the cytoskeleton and facilitate cell migration and shape changes [69].

The mechanism of the various osteoblast, fibroblast, and chondrocyte interactions discussed in this chapter, in particular the mechanism related to heterotypic cellular interactions, is not known. In addition to above described cellular communication mediated by paracrine and autocrine factors during coculture, cell–cell interactions through cadherins will likely play a significant role, as post ligament reconstruction surgery, fibroblasts, and osteoblasts will come into physical contact with each other at the soft tissue-to-bone junction. Full elaboration of the osteoblast phenotype is directly regulated by N-cadherins [70–72], which is present or upregulated during osteogenic differentiation [67, 70, 73]. Cadherins are also believed to be involved in osteoinduction of mesenchymal stem cells by modulating β -catenin signalling [74]. Aside from cadherins, connexins which represent a family of gap junction proteins, are also important for directing adjacent osteoblast, osteocyte, and periosteal fibroblast communications. Interestingly, cadherins have also been reported to directly modulate the formation of tight junctions [75, 76].

Cell–cell adhesion is also essential for chondrogenesis [77–79], as N-cadherin expression has been reported in the developing chick limb mesenchyme, and its expression increases as condensation progresses [77, 78]. When the function of N-cadherin was neutralized through antibody binding, inhibition of condensation and chondrogenesis was reported [77]. Condensation is further mediated by parallel expression of Ca-independent membrane glycoproteins such as cell adhesion molecules (CAMs), in particular N-CAM, which has been reported to play a role in chondrogenesis [79–81].

Cadherin-11 (OB-Cadherin) is a marker of the loosely connected and migratory cellular elements of the mesenchyme, and it is consistently expressed in osteoblastic cells, directly affecting cell sorting, alignment, and separation through differentiation [82]. It has been reported to regulate osteogenesis and chondrogenesis of mesenchymal stem cells in the presence of N-cadherin and is functionally distinct from N-cadherin during endochondral ossification and chondrogenesis [82]. Gap junctions (connexins 32 and 43) have been identified in rat digital flexor tendons, suggesting the presence of a sophisticated cell communication network within the tissue, which may be critical for mechanotransduction [83]. Moreover, *in vitro* loading of tendon fibroblasts regulated N-cadherin and vinculin expression [84]. While the expression of adhesion molecules in ligament fibroblasts has not been examined, cadherin-11 expression has been identified in synoviocytes and are believed to be significant for synovial tissue organization [69]. Therefore, in the formation of the multitissue, multicell interface between ligament or tendon and bone, it is anticipated that cell–cell adhesions via cadherin complexes or gap junctions will facilitate critical cellular communications, which will control cell migration or dictate tissue organization at the interface.

The current understanding of cadherin function is deeply rooted in developmental biology, which may or may not be transferable to the case of tissue injury. While the injury model is a physiologically more relevant model for the soft tissue graft-to-bone junction, the expression and distribution of

cadherins and adherens junctions during tendon-to-bone healing are poorly understood. Nevertheless, the dynamic modulation of cadherin expression and associated changes in cell–cell communications will be essential in the regulation of multitissue organization formed via tissue engineering methods, and should be a critical focus in elucidating the mechanism for interface regeneration and homeostasis.

14.8 CONCLUSIONS

Multiscale and multidimensional cellular interactions are essential for organ homeostasis, repair, and regeneration. Biomimetic coculture models are powerful tools for deciphering the relative contributions of cell–cell contact, soluble factors, substrate geometry, as well as interaction scale. Studies utilizing coculture models have provided new insights into the role of cellular interactions in the regeneration of the multitissue interface between bone and soft tissue. As such, the precise mechanism of cellular interactions that drives tissue organization and homeostasis at the interface remains elusive. Findings from these and future studies in orthopedic interface tissue engineering will promote the design of a new generation of integrative fixation devices, as well as facilitating the development of modern tissue engineering strategies for the formation of complex tissues and functional organ systems.

ACKNOWLEDGMENTS

The authors would like to gratefully acknowledge funding support from the Wallace H. Coulter Foundation and the National Institutes of Health.

REFERENCES

1. Bhatia SN, Balis UJ, Yarmush ML, Toner M. Effect of cell–cell interactions in preservation of cellular phenotype: cocultivation of hepatocytes and nonparenchymal cells. *FASEB J* 1999;13:1883–1900.
2. Lu HH and Jiang J. Interface tissue engineering and the formulation of multiple-tissue systems. *Adv Biochem Eng Biotechnol* 2006;102:91–111.
3. Mikos AG, et al. Engineering complex tissues. *Tissue Eng* 2006;12:3307–3339.
4. Cooper RR and Misol S. Tendon and ligament insertion: a light and electron microscopic study. *J Bone Joint Surg Am* 1970;52:1–20.
5. Benjamin M, Evans EJ, Copp L. The histology of tendon attachments to bone in man. *J Anat* 1986;149:89–100.
6. Niyibizi C, Visconti CS, Kavalkovich K, Woo SL. Collagens in an adult bovine medial collateral ligament: immunofluorescence localization by confocal

- microscopy reveals that type XIV collagen predominates at the ligament-bone junction. *Matrix Biol* 1995;14:743–751.
7. Wei X and Messner K. The postnatal development of the insertions of the medial collateral ligament in the rat knee. *Anat Embryol (Berl)* 1996;193:53–59.
 8. Petersen W and Tillmann B. Structure and vascularization of the cruciate ligaments of the human knee joint. *Anat Embryol (Berl)* 1999;200:325–334.
 9. Thomopoulos S, Williams GR, Gimbel JA, Favata M, Soslowsky LJ. Variations of biomechanical, structural, and compositional properties along the tendon to bone insertion site. *J Orthop Res* 2003;21:413–419.
 10. Wang IN, Mitroo S, Chen FH, Lu HH, Doty SB. Age-dependent changes in matrix composition and organization at the ligament-to-bone insertion. *J Orthop Res* 2006;24:1745–1755.
 11. Niyibizi C, Sagarrigo VC, Gibson G, Kavalkovich K. Identification and immunolocalization of type X collagen at the ligament–bone interface. *Biochem Biophys Res Commun* 1996;222:584–589.
 12. Woo SL and Buckwalter JA. AAOS/NIH/ORS workshop. Injury and repair of the musculoskeletal soft tissues. Savannah, Georgia, June 18–20, 1987. *J Orthop Res* 1988;6:907–931.
 13. Friedman MJ, et al. Autogenic anterior cruciate ligament (ACL) anterior reconstruction of the knee: a review. *Clin Orthop*: 1985;9–14.
 14. Kurosaka M, Yoshiya S, Andrish JT. A biomechanical comparison of different surgical techniques of graft fixation in anterior cruciate ligament reconstruction. *Am J Sports Med* 1987;15:225–229.
 15. Robertson DB, Daniel DM, Biden E. Soft tissue fixation to bone. *Am J Sports Med* 1986;14:398–403.
 16. Yahia L. *Ligaments and Ligamentoplastics*. Springer Verlag; Berlin Heidelberg: 1997.
 17. Blickenstaff KR, Grana WA, Egle D. Analysis of a semitendinosus autograft in a rabbit model. *Am J Sports Med* 1997;25:554–559.
 18. Yoshiya S, Nagano M, Kurosaka M, Muratsu H, Mizuno K. Graft healing in the bone tunnel in anterior cruciate ligament reconstruction. *Clin Orthop* 2000;278–286.
 19. Eriksson K, Kindblom LG, Wredmark T. Semitendinosus tendon graft ingrowth in tibial tunnel following ACL reconstruction: a histological study of 2 patients with different types of early graft failure. *Acta Orthop Scand* 2000;71:275–279.
 20. Rodeo SA, Arnoczky SP, Torzilli PA, Hidaka C, Warren RF. Tendon-healing in a bone tunnel: a biomechanical and histological study in the dog. *J Bone Joint Surg Am* 1993;75:1795–1803.
 21. Jiang J, Nicoll SB, Lu HH. Co-culture of osteoblasts and chondrocytes modulates cellular differentiation *in vitro*. *Biochem Biophys Res Commun* 2005;338:762–770.
 22. Wang IE, et al. Role of osteoblast-fibroblast interactions in the regeneration of the ligament-to-bone interface. *J Orthop Res* 2007. (in press).
 23. Tsai J, Wang IE, Kam LC, Lu HH. Novel micropatterned microfluidic system for osteoblast and fibroblast co-culture. *Trans Soc Biomate* 2005, p. 30.
 24. Guguen-Guillouzo C, et al. Maintenance and reversibility of active albumin secretion by adult rat hepatocytes co-cultured with another liver epithelial cell type. *Exp Cell Res* 1983;143:47–54.

25. Langenbach R, et al. Maintenance of adult rat hepatocytes on C3H/10T1/2 cells. *Cancer Res* 1979;39:3509–3514.
26. Shimaoka S, Nakamura T, Ichihara A. Stimulation of growth of primary cultured adult rat hepatocytes without growth factors by coculture with nonparenchymal liver cells. *Exp Cell Res* 1987;172:228–242.
27. Ogiso B, Hughes FJ, Melcher AH, McCulloch CA. Fibroblasts inhibit mineralised bone nodule formation by rat bone marrow stromal cells *in vitro*. *J Cell Physiol* 1991;146:442–450.
28. Nevo Z, et al. Adhesion characteristics of chondrocytes cultured separately and in co-cultures with synovial fibroblasts. *Cell Biol Int* 1993;17:255–273.
29. Nakamata T, et al. *In vitro* demonstration of cell-to-cell interaction in growth plate cartilage using chondrocytes established from p53^{-/-} mice. *J Bone Miner Res* 2003;18:97–107.
30. Shimoaka T, et al. Regulation of osteoblast, chondrocyte, and osteoclast functions by fibroblast growth factor (FGF)-18 in comparison with FGF-2 and FGF-10. *J Biol Chem* 2002;277:7493–7500.
31. Jiang J, Leong NL, Mung J, Hidaka C, Lu HH. Interaction between zonal populations of articular chondrocytes suppresses chondrocyte mineralization and this process is mediated by PTHrP. *Osteoarthritis and Cartilage*. (in Press).
32. D'andrea P, Calabrese A, Grandolfo M. Intercellular calcium signalling between chondrocytes and synovial cells in co-culture. *Biochem J* 1998;329(Pt 3):681–687.
33. Gerstenfeld LC, et al. Chondrocytes provide morphogenic signals that selectively induce osteogenic differentiation of mesenchymal stem cells. *J Bone Miner Res* 2002;17:221–230.
34. Gerstenfeld LC, Barnes GL, Shea CM, Einhorn TA. Osteogenic differentiation is selectively promoted by morphogenetic signals from chondrocytes and synergized by a nutrient rich growth environment. *Connect Tissue Res* 2003;44 (1 Suppl): 85–91.
35. Lacombe-Gleize S, Gregoire M, Demignot S, Hecquet C, Adolphe M. Implication of TGF beta 1 in co-culture of chondrocytes-osteoblasts. *In Vitro Cell Dev Biol Anim* 1995;31:649–652.
36. Sanchez C, et al. Subchondral bone osteoblasts induce phenotypic changes in human osteoarthritic chondrocytes. *Osteoarthritis Cartilage* 2005;13:988–997.
37. Kinto N, et al. Fibroblasts expressing sonic hedgehog induce osteoblast differentiation and ectopic bone formation. *FEBS Lett* 1997;404:319–323.
38. Spector JA, et al. Co-culture of osteoblasts with immature dural cells causes an increased rate and degree of osteoblast differentiation. *Plas Reconstr Surg* 2002;109:631–642.
39. Fillinger MF, O'Connor SE, Wagner RJ, Cronenwett JL. The effect of endothelial cell coculture on smooth muscle cell proliferation. *J Vasc Surg* 1993;17: 1058–1067.
40. Burch MG, Pepe GJ, Dobrian AD, Lattanzio FA, Jr., Albrecht ED. Development of a coculture system and use of confocal laser fluorescent microscopy to study human microvascular endothelial cell and mural cell interaction. *Microvasc Res* 2005;70:43–52.

41. Sakai H, et al. Fibroblasts from the inner granulation tissue of the pseudocapsule in hips at revision arthroplasty induce osteoclast differentiation, as do stromal cells. *Ann Rheum Dis* 2002;61:103–109.
42. Shan JM, Wang IE, Lu HH. Osteoblast–fibroblast interactions modulate cell phenotypes through paracrine and autocrine regulations. *Trans Orthop Res Soc* 2007.
43. Sun WS, Moffat KL, Lu HH. Characterization of fibrochondrocytes derived from the ligament–bone insertion. *Trans Orthop Res Soc* 2007.
44. Wang IE and Lu HH. Triculture of bovine anterior cruciate ligament fibroblasts, osteoblasts and chondrocytes with application in interface tissue engineering. *Trans Orthop Res Soc* 2005.
45. Wang IE, Mitroo S, Poli R, Sun WS, Lu HH. Fibroblast and osteoblast interactions modulate the potential of bone marrow stromal cells to differentiation into fibrochondrocyte-like cells. *Trans Orthop Res Soc* 2007. (53rd meeting).
46. Bhatia SN, Yarmush ML, Toner M. Controlling cell interactions by micropatterning in co-cultures: hepatocytes and 3T3 fibroblasts. *J Biomed Mater Res* 1997;34:189–199.
47. Bhatia SN, Balis UJ, Yarmush ML, Toner M. Microfabrication of hepatocyte/fibroblast co-cultures: role of homotypic cell interactions. *Biotechnol Prog* 1998;14:378–387.
48. Yamato M, Konno C, Utsumi M, Kikuchi A, Okano T. Thermally responsive polymer-grafted surfaces facilitate patterned cell seeding and co-culture. *Biomaterials* 2002;23:561–567.
49. Khademhosseini A, et al. Layer-by-layer deposition of hyaluronic acid and poly-*L*-lysine for patterned cell co-cultures. *Biomaterials* 2004;25:3583–3592.
50. Whitesides GM, Ostuni E, Takayama S, Jiang X, Ingber DE. Soft lithography in biology and biochemistry. *Ann Rev Biomed Eng* 2001;3:335–373.
51. Albrecht DR, Tsang VL, Sah RL, Bhatia SN. Photo- and Electropatterning of Hydrogel-Encapsulated Living Cell Arrays. *Lab Chip* 2005;5(1):111–118.
52. Chen CS, Mrksich M, Huang S, Whitesides GM, Ingber DE. Geometric control of cell life and death. *Science* 1997;276:1425–1428.
53. Cukierman E, Pankov R, Stevens DR, Yamada KM. Taking cell–matrix adhesions to the third dimension. *Science* 2001;294:1708–12.
54. Spalazzi JP, Doty SB, Moffat KL, Levine WN, Lu HH. Development of controlled matrix heterogeneity on a triphasic scaffold orthopedic interface tissue engineering. *Tissue Eng* 2006;12:3497–3508.
55. Takeichi M. Morphogenetic roles of classic cadherins. *Curr Opin Cell Biol* 1995;7:619–627.
56. Price SR, De Marco Garcia NV, Ranscht B, Jessell TM. Regulation of motor neuron pool sorting by differential expression of type II cadherins. *Cell* 2002;109:205–216.
57. Keller R. Shaping the vertebrate body plan by polarized embryonic cell movements. *Science* 2002;298:1950–1954.
58. Zhong Y, Briehner WM, Gumbiner BM. Analysis of C-cadherin regulation during tissue morphogenesis with an activating antibody. *J Cell Biol* 1999;144:351–359.

59. Hay ED and Zuk A. Transformations between epithelium and mesenchyme: normal, pathological, and experimentally induced. *Am J Kidney Dis* 1995;26:678–690.
60. Cano A, et al. The transcription factor snail controls epithelial-mesenchymal transitions by repressing E-cadherin expression. *Nat Cell Biol* 2000;2:76–83.
61. Leckband D and Prakasam A. Mechanism and dynamics of cadherin adhesion. *Ann Rev Biomed Eng* 2006;8:259–287.
62. Kim SH, Jen WC, De Robertis EM, Kintner C. The protocadherin PAPC establishes segmental boundaries during somitogenesis in xenopus embryos. *Curr Biol* 2000;10:821–830.
63. Tepass U, Godt D, Winklbauer R. Cell sorting in animal development: signalling and adhesive mechanisms in the formation of tissue boundaries. *Curr Opin Genet Dev* 2002;12:572–582.
64. Hermiston ML, Wong MH, Gordon JI. Forced expression of E-cadherin in the mouse intestinal epithelium slows cell migration and provides evidence for nonautonomous regulation of cell fate in a self-renewing system. *Genes Dev* 1996;10:985–996.
65. Tinkle CL, Lechler T, Pasolli HA, Fuchs E. Conditional targeting of E-cadherin in skin: insights into hyperproliferative and degenerative responses. *Proc Natl Acad Sci USA* 2004;101:552–557.
66. Kobiela A and Fuchs E. Alpha-catenin: at the junction of intercellular adhesion and actin dynamics. *Nat Rev Mol Cell Biol* 2004;5:614–625.
67. Stains JP and Civitelli R. Cell–cell interactions in regulating osteogenesis and osteoblast function. *Birth Defects Res C Embryo Today* 2005;75:72–80.
68. Bex G, Nollet F, van RF. Dysregulation of the E-cadherin/catenin complex by irreversible mutations in human carcinomas. *Cell Adhes Commun* 1998;6:171–184.
69. Kiener HP and Brenner MB. Building the synovium: cadherin-11 mediates fibroblast-like synoviocyte cell-to-cell adhesion. *Arthritis Res Ther* 2005;7:49–54.
70. Ferrari SL, et al. A role for N-cadherin in the development of the differentiated osteoblastic phenotype. *J Bone Miner Res* 2000;15:198–208.
71. Marie PJ. Role of N-cadherin in bone formation. *J Cell Physiol* 2002;190:297–305.
72. Stains JP and Civitelli R. Cell-to-cell interactions in bone. *Biochem Biophys Res Commun* 2005;328:721–727.
73. Lin WL, Chien HH, Cho MI. N-cadherin expression during periodontal ligament cell differentiation *in vitro*. *J Periodontol* 1999;70:1039–1045.
74. Castro CH, et al. Targeted expression of a dominant-negative N-cadherin *in vivo* delays peak bone mass and increases adipogenesis. *J Cell Sci* 2004;117:2853–2864.
75. Siliciano JD and Goodenough DA. Localization of the tight junction protein, ZO-1, is modulated by extracellular calcium and cell–cell contact in Madin–Darby canine kidney epithelial cells. *J Cell Biol* 1988;107:2389–2399.
76. Troxell ML, et al. Inhibiting cadherin function by dominant mutant E-cadherin expression increases the extent of tight junction assembly. *J Cell Sci* 2000;113(Pt 6): 985–996.
77. Oberlender SA and Tuan RS. Spatiotemporal profile of N-cadherin expression in the developing limb mesenchyme. *Cell Adhes Commun* 1994;2:521–537.

78. Oberlender SA and Tuan RS. Expression and functional involvement of N-cadherin in embryonic limb chondrogenesis. *Development* 1994;120:177–187.
79. DeLise AM, Fischer L, Tuan RS. Cellular interactions and signaling in cartilage development. *Osteoarthritis Cartilage* 2000;8:309–334.
80. Tavella S, Raffo P, Tacchetti C, Cancedda R, Castagnola P. N-CAM and N-cadherin expression during *in vitro* chondrogenesis. *Exp Cell Res* 1994;215:354–362.
81. Chuong CM, et al. Roles of adhesion molecules NCAM and tenascin in limb skeletogenesis: analysis with antibody perturbation, exogenous gene expression, talpid mutants and activin stimulation. *Prog Clin Biol Res* 1993;383B:465–474.
82. Kii I, Amizuka N, Shimomura J, Saga Y, Kudo A. Cell–cell interaction mediated by cadherin-11 directly regulates the differentiation of mesenchymal cells into the cells of the osteo-lineage and the chondro-lineage. *J Bone Miner Res* 2004;19:1840–1849.
83. McNeilly CM, Banes AJ, Benjamin M, Ralphs JR. Tendon cells *in vivo* form a three dimensional network of cell processes linked by gap junctions. *J Anat* 1996;189(Pt 3):593–600.
84. Ralphs JR, Waggett AD, Benjamin M. Actin stress fibres and cell-cell adhesion molecules in tendons: organisation *in vivo* and response to mechanical loading of tendon cells *in vitro*. *Matrix Biol* 2002;21:67–74.

PART III

Clinical Applications of Nanostructures

Nanostructures for Tissue Engineering/Regenerative Medicine

SYAM P. NUKAVARAPU, SANGAMESH G. KUMBAR,
LAKSHMI S. NAIR, and CATO T. LAURENCIN

15.1 INTRODUCTION

15.1.1 Tissue Engineering/Regenerative Medicine

Tissue and organ failure has been a major health problem in the United States and worldwide. Autografting and allografting are the two main approaches currently used to repair or replace damaged or lost tissue and organs. However, limited availability and donor site morbidity are the problems associated with autografting, while disease transmission and foreign body response are associated with allografting. In addition, there is also a major concern about the growing number of patients waiting for an organ replacement. According to a recent report, in the United States alone 89,000 patients are waiting for an organ transplant and 17 people die every day waiting for a transplant of a vital organ such as a heart, liver, kidney, pancreas, lung, or bone marrow [1]. The viable solution to this problem is tissue engineering/regenerative medicine, which is defined as the application of biological, chemical, and engineering principles toward the repair, restoration, or regeneration of living tissues using biomaterials, cells, and factors, alone or in combination [2].

Researchers so far have identified three major strategies to regenerate tissues using tissue engineering principles [3]. The first approach involves injecting tissue-specific cells at the injury site. This is a noninvasive process and practiced in the repair of minor injuries, however not useful for regenerating complex tissues involving more than one cell type with a specific architecture. A second approach is guided tissue engineering, where biodegradable scaffolds made of

poly(L-lactic acid) (PLLA), polyglycolic acid (PGA), poly(D,L-lactide-co-glycolide) (PLGA), polycaprolactone (PCL), polyphosphazenes, and so on are used for guiding cellular in growth. The material selection is based on the desired application and is designed to permit scaffold disintegration by the time cells invade and completely repair the injured tissue.

Third and the most important strategy utilizes biodegradable scaffolds in combination with growth factors and tissue-specific cells or stem cells that ultimately differentiate into the required cell type. This approach is further divided into two kinds, one is a closed system and the other is an open system. In a closed system, cell-seeded scaffolds are encapsulated using a thin semipermeable membrane that acts as a barrier and protects cells from the host immune response while allowing nutrient transport and waste removal essential for cell survival. This approach is quite similar to extracorporeal device technology where particular organ functionality is temporarily restored. The open system is the most popular approach, where scaffolds are precultured *in vitro* before implantation. Based on the requirement, growth factors that are helpful in tissue regeneration are either released from the scaffold or delivered through programming cells via gene therapy [4]. Biodegradable scaffolds in combination with cells and growth factors have been used successfully to regenerate various tissues like skin, bone, cartilage, blood vessels, and heart valves. This method is further improved by replacing static culture methods with dynamic culture systems using bioreactors. These advanced culture systems not only mitigate nutrient transport limitations but also provide mechanical stimulation to seeded cells in the form of fluid shear stress [5]. Although tissue engineering approach has seen early success in the regeneration of simple tissues like skin and cartilage, there are however biological and engineering concerns to be addressed before the approach becomes a successful clinical alternative for regenerating complex tissues. In order to become a practical and successful procedure, scaffold selection, dosage of cells, and the amount and the kind of growth factors have to be optimized based on the particular application and the relative health status of the patient.

15.1.2 Scaffolds for Tissue Engineering

Tissue engineering involves assembling relevant cells into the required three-dimensional (3D) organs or tissue. Cells lack this ability to form a 3D tissue in culture and end up forming 2D layers with no anatomical features. The three-dimensionality can be achieved by seeding cells onto an artificial structure known as a scaffold that is capable of supporting 3D tissue formation, which is an important component in tissue engineering [6]. The required features of a scaffold are biocompatibility and bioactivity, biodegradability or bioresorbability, mechanical compatibility, interconnected porosity, and the nontoxic nature of the degradation products. Biocompatibility is defined as supporting the appropriate cellular activity without eliciting any undesirable effects in those cells and the host [7, 8]. Bioactivity refers to having appropriate surface chemistry that

favors cell attachment, proliferation, and differentiation [9, 10]. Controlled biodegradability is crucial because the rate of degradation of the scaffold should be in line with the neotissue formation, since scaffolds need to be absorbed by the surrounding tissues without the necessity of a surgical removal. High pore volume and an adequate pore size are necessary for cell infiltration and also for effective nutrient transport and waste removal. For example, scaffolds with 30% pore volume and 150 μm median pore size performed well for bone tissue regeneration [2]. Matching mechanical properties of the intended tissue (high modulus for bone and low modulus materials for vascular tissue engineering) is also critical for successful tissue engineering.

Synthetic polymers such as PGA, PLA, PLGA, PCL, polyphosphazenes, and polyanhydrides, and naturally derived proteins and carbohydrate polymers such as chitosan, alginate, and hyaluronic acid are the most commonly used biodegradable polymers for tissue engineering scaffold applications [11, 12]. Over the years, several techniques have been developed to fabricate synthetic and natural polymeric materials into 3D porous scaffolds. Some of the conventional scaffold fabrication techniques include solvent casting and particulate leaching [13], gas foaming [14], freeze drying [15], 3D printing (solid freeform fabrication) [16], and microsphere sintering [17]. It has been demonstrated that most of the 3D porous scaffolds were capable of supporting cellular adhesion and proliferation, but lack the ability to simulate the extracellular matrix (CM) like environment that is always in close proximity with cells in all the tissues. Therefore, the best alternative is nanofeatured scaffolds that not only mimic the ECM conditions but also show higher reactivity for proteins and ultimately enhances cell adhesion and thus regenerative capacity. Techniques like electrospinning [18], temperature-induced phase separation [19], molecular self-assembly [20], and surface patterning [21] are currently in practice for generating scaffolds with nano- and micron-size features for better mimicking the native ECM. In this chapter, we focus on the importance of nanofeatured scaffolds and their fabrication using various techniques. Further emphasis is also made on *in vitro* and *in vivo* studies where the tissue regenerative capacity is enhanced with these novel scaffolds.

15.1.3 Nanofeatures of ECM

ECM is a self-assembled nanofibrillar network composed of complex biomacromolecules that surround and support cells in tissues [22]. ECM is present in interstitial complex (IC) and basement membrane (BM) along with cells as shown in Fig. 15.1a. ECM is constructed with different classes of biomolecules such as structural proteins (collagen and elastin) and specialized proteins (fibrillin, fibronectin, and laminin) that help to structurally connect, bind, integrate cells to form tissues, and also provide a surface for cellular adhesion and migration. Proteoglycans are glycoaminoglycans like chondroitin sulfate and heparin sulfate linked with serine like core proteins that provide chemical cues and regulate cell growth, differentiation, and metabolic activity.

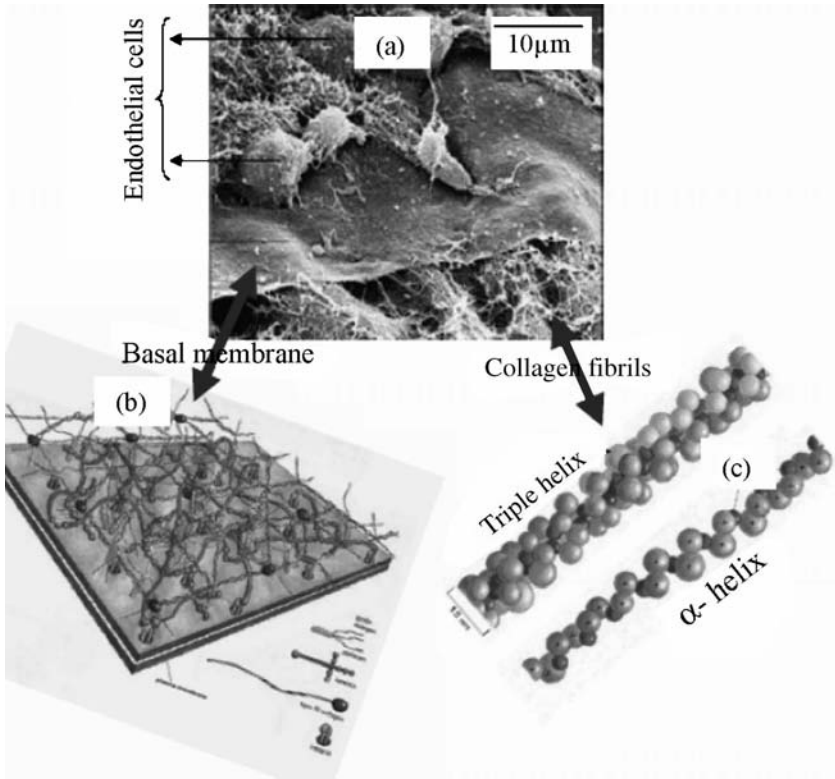


FIGURE 15.1 (a) SEM image of a chick embryo cornea showing epithelial cells, basal lamina, and network of collagen fibrils. Molecular structure of (b) basal lamina and (c) collagen. (Reproduced from Reference [22] with permission from (a) Dr. Robert Trelstad, (b) John Wiley & Sons Inc., and from (c) Garland Science Publishing).

The interstitial complex is mostly present in connective tissues like bone, cartilage, and ligaments, and present in association with a wide variety of cells and the above-mentioned proteins. BM supports a single layer of endothelial, epithelial, and some mesenchymal cells in many organs (Fig. 15.1b). BM's function is as an active barrier for cell infiltration and migration, and also acts as a reservoir for a variety of growth factors.

ECM and BM are comprised of fibrils made of proteins such as collagen, elastin, and fibronectin as shown in Fig. 15.1c. These fibrils are of nanosize and much smaller than micrometer-sized cells. The major component in the ECM is collagen, which is the fibrous backbone of the ECM and is at least available in 28 forms in our body. The abundant collagen is mostly in a fibril structure composed of 300-nm-long, 1.5-nm-diameter rodlike proteins consisting of three coiled chains. Each chain consists of 1050 amino acids that are wound around in a characteristic right-handed triplex. Further, interaction of triple helices of collagens results in the formation of fibrils that are roughly 50 nm in

diameter. The fibril packing is such that adjacent triple helix is displaced approximately 67 nm to yield a banded structure. Another important component in the ECM is fibronectin that acts as a glue between cells and the ECM by attaching cells to a variety of ECMs. Fibronectins (FNs) are dimers of two similar peptides that are 60–70 nm long and 2–3 nm thick. FN contains nanodomains with an arginine–glycine–aspartic–serine sequence that selectively exhibits high affinity for a particular substrate such as collagen, fibrin, and cell surface receptors. In addition, other proteins that are present in the ECM are also of nanosize and influence cell behavior at various levels.

15.2 NANOFIBROUS SCAFFOLDS

Cells within a tissue and organ are organized and encapsulated by the nanofibrous ECM. For example, a SEM of rat cornea tissue is shown in Fig. 15.2a that is composed of fibroblasts surrounded by ECM nanofibrils. A similar cellular arrangement is observed when cells are cultured *in vitro* on nanofibrous scaffolds (Fig. 15.2b). The tissue-like cellular organization observed with nanofibrous scaffolds prompted researchers to look for more sophisticated methods to fabricate nanofibrous structures that can better mimic the ECM and serve as potential scaffolds for tissue regeneration. Electrospinning, phase separation, and molecular self-assembly techniques that are currently popular for fabricating nanofiber-based scaffolds are described below.

15.2.1 Electrospinning

Electrospinning is a facile, efficient, and inexpensive technique for fabricating ultrafine fibers. A typical setup for electrospinning is shown in Fig. 15.3a. During electrospinning, a high electric potential in the order of few kilovolts is

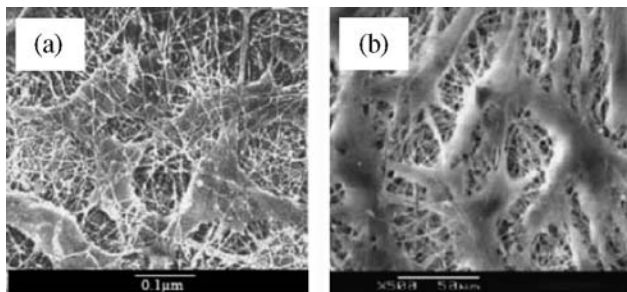


FIGURE 15.2 SEM of (a) the rat cornea tissue where fibroblasts are surrounded by extracellular matrix fibrils (reproduced from Reference [22] with permission, from Garland Science, publishing) and (b) human dermal fibroblasts cultured *in vitro* on PCL nanofibers (reproduced from Appl Biochem Biotechnol 2005;125:147–158 with permission, Humana Press Inc.)

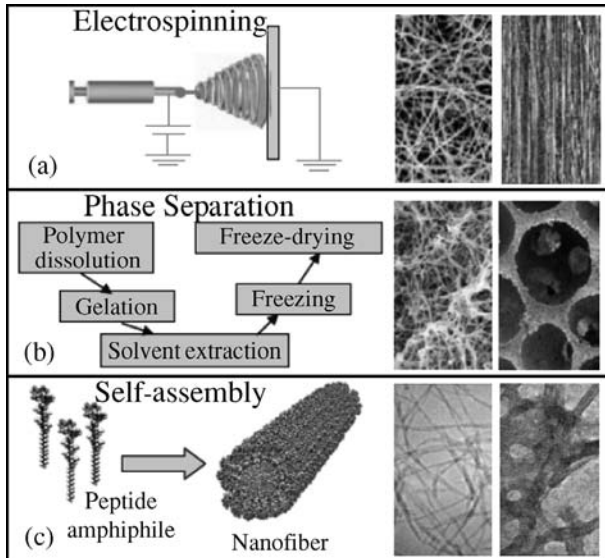


FIGURE 15.3 Nanofibrous scaffolding methodologies; (a) Typical setup for electrospinning and the resulting nonoriented and oriented nanofiber scaffolds (reproduced from Reference [33] with permission, from Elsevier). (b) Steps involved in the temperature-induced phase separation process, and the obtained nanofibrous and foams with spherical pore shape (reproduced from Reference [19] with permission, from Elsevier). (c) Self-assembly process and the derived individual nanofibers and the consolidated nanofibrous scaffold (reproduced from Reference [49] with permission from AAAS).

applied on the pendent drop of the polymer solution or melt held by surface tension. The applied field causes charge separation and hence causes repulsion within the polymer drop sitting at the nozzle of the spinneret. When the opposing electrostatic force overcomes the surface tension of the polymer solution, a thin polymer jet ejection initiates from the spinneret. The emerging jet undergoes a series of bending and stretching instabilities and becomes elongated until it is deposited on the grounded collector. Solvent evaporation occurs during the process, and eventually a polymer jet is deposited into long and ultrathin fibers with diameters ranging from tens of nanometers to a few micrometers. Recently, this approach has drawn much interest within the tissue engineering community. A number of synthetic and natural polymers have been spun into a variety of structures having fibers randomly oriented, oriented, core–shell structured, porous, and drug loaded that are suitable for tissue regeneration and drug delivery applications (Fig. 15.3a) [23–27].

Electrospun nonwoven nanofiber matrices are promising as scaffolds for tissue engineering since the fiber diameters are in line with most of the natural ECMs, and the resulting high surface area might allow a high percentage of

cellular attachment. In addition to the nanofibrous structure, the matrices also exhibit porosities greater than 90 % with adequate pore size for cell migration [27]. Thus, nanofiber matrices provide more structural space for cell accommodation and make the nutrient and metabolic waste exchange process efficient between the scaffold and the surroundings.

Electrospinning technique for creating tissue engineering scaffolds has been demonstrated and patented by Laurencin and Ko [28]. These authors demonstrated for the first time the formation of electrospun PLGA ultrafine fibers with morphological similarity to the ECM of natural tissue with a diameter ranging from 500 to 800 nm with porosity greater than 90% [27]. *In vitro* studies with mouse fibroblasts further indicated good cellular adherence and spreading onto PLGA nanofibers. Based on these results, it was hypothesized that 25–100 μm pore diameter that was observed is adequate for human mesenchymal stem cell migration and tissue ingrowth. Incorporation of drugs into these nanofibers has also been explored by these authors for wound healing applications [29]. In a recent study, Nair et al. from the same group developed polyphosphazene-based nanofiber scaffolds for tissue engineering applications. These novel scaffolds support the adhesion and proliferation of coronary artery endothelial cells and osteoblast-like MC3T3-E1 cells [30]. Currently, we are focusing on developing various polyphosphazene fiber scaffolds alone or in combination with PLGA for bone tissue engineering and wound dressing applications.

Many other research groups have also successfully electrospun biodegradable polyesters such as PLA, PGA, and their copolymer PLGA into nonwoven fiber scaffolds [31, 32]. PLLA is electrospun into aligned and random nanofiber mats with varied fiber diameters ranging from 300 to 700 nm. Ramakrishna et al. studied the cellular compatibility of PLLA nanofibers using neural stem cells [33]. It was noticed that cells adhered and proliferated on aligned and randomly oriented PLLA nanofibrous scaffolds. Other synthetic biodegradable polymers like PCL and PCL blends with polyorthoesters were also studied for their spinnability and cell interaction. Fetal bovine chondrocytes seeded on PCL nanofiber scaffolds, with an average fiber size of 700 nm, were able to maintain the chondrocytic phenotype during 3 weeks of culture period [34]. Geng et al. demonstrated better cell attachment and proliferation with human umbilical vein endothelial cells onto 50 : 50 poly(L-lactic acid-co- ϵ -caprolactone) (PLCL) fibers of 300 nm diameter when compared to the matrices with 7- μm fibers [35]. The observed better cellular performance on these nanofiber matrices is presumably due to the nanofiber structure that mimics the ECM.

Various natural polymers have also been considered for electrospinning because of their proven biocompatibility and biofunctionality. Natural polymers such as collagen, fibrinogen, alginate, hyaluronic acid, chitosan, and starch were electrospun alone or in combination with synthetic polymers to improve scaffold performance [36, 37]. Nanofiber scaffolds of ECM polymers may have added advantage of resembling not only the size scale but also the chemical and biological functions of the ECM. Collagen I and III were

electrospun using 1,1,1,3,3,3-hexafluoro-2-propanol (HFT) as a solvent that created type I collagen nanofibers with diameters in the range of 100 nm and type III collagen in the range of 250 nm [38]. The fabricated nanofiber scaffolds exhibited good cytocompatibility and proliferation with smooth muscle cells, and also showed cell infiltration into the collagen network. Efforts were made to improve the mechanical properties of the collagen nanofiber scaffolds by PCL coating. Coating imparted the right mechanical strength while retaining the collagen regions on the surface that maintained cell attachment and proliferation of human dermal fibroblasts for the purpose of dermal tissue engineering [39]. Even though electrospinning is a proven mild process, biological integrity of some polymers has been found to be lost during electrospinning. Such an adverse affect is presumably due to the harsh organic solvents like HFT used for electrospinning that could potentially denature the protein structures. Therefore, electrospinning of natural polymers is limited and still not versatile as compared to synthetic polymers.

15.2.2 Phase Separation

Polymer phase separation has been known for many years and is widely used for developing membranes for nonmedical applications [40]. Recently, thermally induced phase separation (TIPS) has become a popular technique for fabricating porous and nanofeatured 3D scaffolds for tissue engineering applications [41]. In this method, a polymer is first dissolved in a suitable solvent at high temperature. Lowering the solution temperature induces liquid–liquid or solid–liquid phase separation into two phases, one with a high polymer concentration and the other with a low polymer concentration. Subsequent solvent removal by exchange, evaporation, or sublimation from low polymer phase results in pores, whereas the high polymer phase solidifies into 3D interconnected fibrous networks as seen in Fig. 15.3b. Scaffold parameters such as porosity and fiber size can be controlled by varying the solvent, the polymer concentration, and the temperature for any polymer system.

Polymer phase separation has gained immense interest in recent days for developing tissue engineering scaffolds for two reasons. The first reason is that controlling scaffold porosity is ideal for supporting cell proliferation and 3D tissue formation. Second is the ability to form nanofibrous 3D structure, which mimics the fibrous 3D structure of natural collagen. Figure 15.3b shows SEM of highly porous scaffolds from aliphatic polyesters such as PLLA, poly(D-L-lactic acid) (PDLLA), and PLGA produced by phase separation [42–44]. However, the nanofibrillar structure is only observed with the highly crystalline polymer PLLA. Ma et al. extensively studied the effect of gelation temperature, polymer concentration, and solvents used on porosity and fiber diameters of scaffolds produced using PLLA. Combining the polymer with porogens further modified this process and achieved macroporous networks in scaffolds with nanofibrous pore walls [41].

15.2.3 Molecular Self-Assembly

Molecular self-assembly is the spontaneous organization of molecules into structurally well-defined and stable arrangements through weak and non-covalent interactions. Such interactions include hydrogen bonding, ionic bonding, hydrophobic interactions, van der Waals interactions, and water-mediated hydrogen bonding. Recently, molecular self-assembly has become one of the powerful methods to produce nanofibrous scaffolds for tissue engineering with properties similar in scale and chemistry to that of the natural ECM.

Proteins, peptides, and lipid molecules are commonly used as building blocks for forming nanofeatured scaffolds for tissue engineering applications. Nature has already used these molecules to produce various structures like collagen and keratin through molecular self-assembly [45]. For the first time, Zhang et al. produced 3D peptide scaffolds utilizing naturally occurring amino acids by exposing the self-assembling peptide ((Ala-Glu-Ala-Glu-Ala-Lys-Ala-Lys)₂ (EAK16)) to physiological media or a salt solution [46]. Peptides with alternating hydrophilic and hydrophobic amino acid moieties aggregated depending upon salt concentration and pH to form stable scaffolds consisting of interwoven nanofibers. This method has opened a new area of research where the peptide solution forms into a scaffold *in vivo* with ECM functionalities that would help in repair and regeneration of damaged or lost tissues. Based on this concept BD biosciences has commercialized a product “PuraMatrix peptide hydrogel” with fiber diameters of 10 nm and pores of 50–200 nm. This matrix has shown *in vitro* differentiation of hepatocyte progenitor cells into hepatocytes [47], neurons from hippocampal slices [48], and neurite out growth from PC12 cells [96].

Recently, Stupp et al. designed peptide-amphiphile (PA) nanocylinders adopting a composite approach with nonpolar hydrocarbon tails and hydrophilic peptide heads as seen from Fig. 15.3c [49]. The nanocylinder formation is induced through a pH change from 8 to 4. The produced fibers (diameter of 7.6 ± 1 nm) were cross-linked by oxidation to achieve structural integrity. Phosphorylated serine incorporation within the peptide end leads to the calciophilic nature of the scaffold with the ability to form hydroxyapatite mineral coating that promise a new approach for bone tissue engineering [50]. *In vitro* studies with different cell types on 3D peptide scaffolds exhibited interesting functional behavior such as good proliferation, functional differentiation, and active migration [51]. In a separate study with bovine chondrocytes encapsulated in a peptide scaffold, Kisiday et al. showed the extensive production of their own ECM (different types of collagen with glycosaminoglycans) while maintaining their phenotype [52]. The self-assembly process has also demonstrated the ability to present bioactive epitopes to cells. For example, the nanofiber scaffold containing the neurite-promoting laminin epitope isoleucine–lysine–valine–alanine–valine (IKVAV) pentapeptide selectively induced rapid differentiation of neural progenitor cells into neurons [99].

Electrospinning, phase separation, and self-assembly are useful methods to produce nanofibrous scaffolds with properties mimicking ECM in size and to some extent functionality. Electrospinning is a viable process to fabricate nanofiber scaffolds using both synthetic and natural polymers including collagen and fibrinogen. Although phase separation is limited for highly crystalline polymers, the process is economical and can be used to fabricate 3D scaffolds that directly fit into the anatomical shape of a body part using a mold. Molecular self-assembly has merits over other methods since the process involves body-friendly molecules such as protein, peptide, and lipids. Furthermore, scaffolds can be tissue specific by choosing the required building blocks and adopt the required shape *in vivo*. Even though above-mentioned techniques have demonstrated the versatility for creating ECM mimicking scaffolds, much work is required to improve the scaffold mechanical strength suitable for tissue engineering use.

15.3 SURFACE PATTERNED SCAFFOLDS

In tissue engineering, the surface is more important than the bulk properties because of the fact that cells land on the surface and look for specific cues before and after attachment. It is known that cells respond to spatially and temporally organized signals and can react to nanoscale surface features as small as 10 nm [53]. Patterned surfaces aim to recreate *in vivo* nano/microenvironments for optimum cell growth and functionality. These surfaces further control cell differentiation/proliferation and multicellular organization in building complex tissues that are otherwise not possible with uniform surfaces. Micro/nanofabrication methods include photolithography and soft lithography such as contact printing, replica molding, transfer molding, and imprint lithography are used to create nano/micropatterns in the form of gratings, wells, pits, grooves, and islands [54]. Traditionally, photolithography is used to generate nano/microsurface topologies for industrial and biomedical applications. Despite its popularity, the technique is limited in designing scaffolds for biospecific applications including tissue engineered scaffolds because of the nature of the process where high capital and operational costs are involved. Soft lithographic methods are useful because they permit direct construction of various shapes with precise control, and unlike in conventional lithography no biohazardous solvents are used in the process. Soft lithography refers to a set of methods for fabricating or replicating structures using elastomeric stamps, molds, and conformable photomasks using elastomers such as polydimethylsiloxane (PDMS) or fluorosilicone. Elastomeric molds are derived using a master that is generally prepared by either conventional photolithography or electron beam lithography techniques. In the last few years, soft lithography based techniques have been increasingly used for creating nano/micro featured surfaces [55,60,64]. Having seen the progress with surface patterning, it is time to combine lithography techniques with 3D

scaffolding methodologies for designing nanofeatured 3D scaffolds for tissue engineering applications.

15.3.1 Micro/Nanocontact Printing

In recent years, micro- and nanocontact printing have become an essential method for patterning surfaces for applications in tissue engineering and biology. Among the soft lithographic methods, contact printing was the first one to be used to pattern a self-assembled monolayer (SAM) of alkanethiols on gold substrate using a high resolution elastomeric stamp [55]. In brief, the PDMS stamp is inked with alkanethiol and printed onto a gold substrate to have the alkanethiol patterns in the regions where the stamp came in contact with the substrate. After washing, the remaining bare gold surface was exposed to another alkanethiol to obtain a surface patterned into two regions with different terminal groups. Patterned surfaces that resist nonspecific adsorption of proteins are further used for protein patterning. For example, when the surface with regions terminated in oligo(ethylene glycol) groups and methyl groups immersed in solutions of proteins such as fibrinogen, fibronectin, and immunoglobulin, proteins selectively adsorbed on the methyl-terminated regions as seen from Fig. 15.4a. Protein patterned surfaces were further used for patterning cells. In a study by Mrksich, bovine capillary endothelial cells were patterned on fibronectin-coated SAM surfaces [56]. Since most mammalian cells are anchorage dependent, endothelial cells attached only to the methyl-terminated fibronectin-coated regions of the patterned SAMs (Fig. 15.4b).

Micro/nanocontact printing is an inexpensive, simple, and effective tool for patterning planar and nonplanar tissue engineered surfaces. Lee et al. used printing inhibitory molecules to pattern the growth of retinal/iris pigment epithelial cells on human lens capsule for retinal cell transplantation [57]. This particular methodology of printing on autologous human tissue may find applications in the replacement of vital ocular tissues such as the retinal pigment epithelium in age-related macular degeneration. Recently, contact printing was further extended to produce nanostructures by adopting high elastic modulus PDMS and high molecular weight inks. Li et al. demonstrated the feasibility of nanocontact printing at a resolution of less than 50 nm via a combination of sharp and hard PDMS stamps using a diffusion limited high molecular weight ink [58]. Another modification to nanocontact printing came in the form of flexible PDMS stamps for printing on nonuniform surfaces that may find a myriad of applications in modifying tissue engineering scaffolds for clinical applications [59].

15.3.2 Capillary Force Lithography

The Langer's group at MIT has reported yet another simple lithographic method called capillary force lithography for protein and cell patterning [60]. This method involves a molding process in which a uniform polyethylene glycol

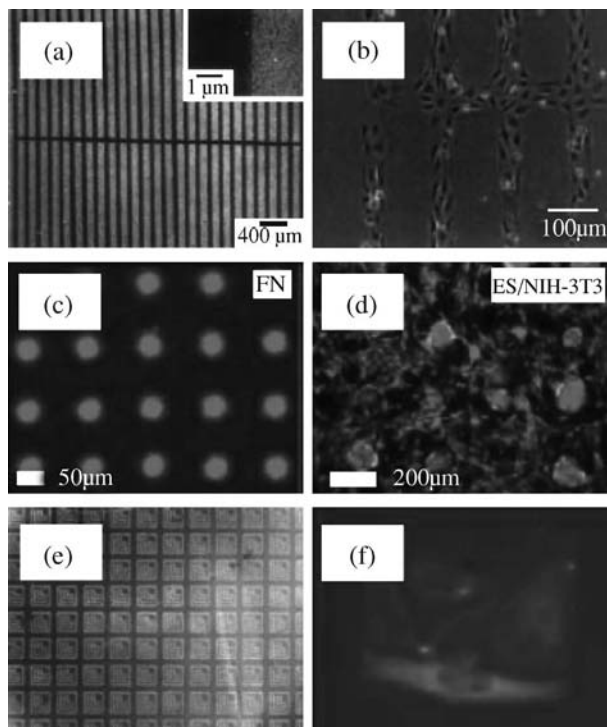


FIGURE 15.4 Surface patterning using various novel techniques. optical micrographs of microcontact printed SAMs on gold having patterned regions with (a) fibronectin (black in color) and (b) bovine capillary endothelial cells (reproduced from Reference [56] with permission, from Academic Press). Layer-by-layer deposition using capillary force lithography method; (c) fluorescence image of fibronectin adsorption on hyaluronic acid patterned surface and (d) fluorescent image of patterned 1-day-old cocultures of ES cells (red) with NIH-3T3 fibroblasts (green) (reproduced from Reference [62] with permission, from Elsevier). (e) Fluorescence micrograph showing selective protein adsorption to adhesive APS regions (line width of $L = 4 \mu\text{m}$) and (f) reflectance image of green fluorescence protein-tubulin transfected HeLa cells adhering to $100 \mu\text{m}^2$ island (reproduced from Reference [64] with permission, from Nano Science and Technology Institute.)

(PEG) or hyaluronic acid or chitosan films (above glass transition temperature) are molded using their capillarity and wettability properties with respect to the PDMS stamp. Due to the nonbiofouling property of polysaccharides when deposited as a film on a surface, hyaluronic acid and chitosan-molded regions exhibit protein or cell repellent properties [61] whereas bare substrate regions support cell or protein adsorption. In one study, PEG dimethacrylate was used as a cell repellent layer, and the substrate regions were modified with fibronectin for NIH3T3 cell patterning. In a more recent study, layer-by-layer deposition of hyaluronic acid and poly-L-lysine (PL) for micropatterned cocultures was

demonstrated and is shown in Fig. 15.4c [62]. The ionic adsorption of PL onto HA patterns was used to switch the HA surfaces from cell repulsive to adherent for the purpose of patterned cocultures. Fibronectin- and PL-coated patterned regions were selectively utilized for designing a coculture system with hepatocytes, murine embryonic stem cells (ES), and NIH3T3 fibroblasts as shown in Fig. 15.4d. The developed cocultures are independent of selective adhesion of the cell type, the seeding order, and notably remained stable for 5 days. Subsequently, the cytotoxic PL is replaced by collagen, a component of the natural ECM, and cationic in nature to form an ionic complex with HA [63]. Capillary force lithography is an inexpensive, simple, and powerful tool for designing micropatterned coculture systems for probing cell–cell and cell–ECM interactions for designing and engineering complex tissues.

15.3.3 Biomolecular Patterning

Organization of biomolecules such as proteins, DNA, and cells into ordered arrays on surfaces is called biomolecular patterning. This has been a subject of considerable interest in many areas including biology and medicine. Recently, photocatalytic lithography, scanning probe lithography, and computer-controlled laser ablation methods have been used for organizing biomolecules on silicon or glass surfaces. Photocatalytic lithography uses a specific wavelength of light to chemically activate material on a stamp in contact with an oxidizable thin film. In this method, a clean glass or silicon substrate is modified with nonfouling polyethylene glycol (PEG) thiol coatings [64]. Selective removal of light-exposed regions leads to the formation of a bare substrate and interpenetrating network of nonfouling regions. The bare glass or silicon regions are then backfilled with adhesive aminopropylsilane (APS). Subsequently, fluorescein isothiocyanate (FITC)-labeled neutravidin is spread on these surfaces and imaged using a fluorescence microscope. As shown in Fig. 15.4e, the protein is attached to adhesive L regions (bright) and was repelled by the PEG-based nonfouling regions (dark). Lipofectamine transfected HeLa cells attached to the substrate and cell proliferation occurred over time, as shown in Fig. 15.4f, which demonstrates that cell viability was maintained on these patterned regions that were backfilled with APS.

Patterning using scanning tunneling microscopy or atomic force microscopy (AFM) is known as scanning probe lithography. This particular lithographic approach is quite useful because the patterning, imaging, and pattern characterization can be carried out sequentially within the microscope chamber. This method allows making *in situ* observations of the material immobilized on the patterns. Choi et al. demonstrated patterning streptavidin on a PEG-modified Si surface using AFM. In this study, a silicon substrate was uniformly coated with low molecular weight protein repellent methoxy PEG silane [65]. Silane was converted into SiO₂ patterns by AFM anodic oxidation by applying a voltage of 10–20 V at the surface (anode) and the tip (cathode). The square SiO₂ patterns were 2–3 nm thick when formed with an applied

voltage of 14 V and observed to be more reactive than nonpatterned regions. These regions were chemically modified with functional groups having strong affinity for selective protein patterning. Oxide pattern was first modified with a self-assembled amine functional material. Protein patterning on these surfaces was done by two ways. The first method immobilized Au-conjugated streptavidin onto the amine-modified SiO₂. The second approach used glutaraldehyde to activate surface amino groups for protein attachment through selective covalent bonding between aldehyde and amino groups on streptavidin. These streptavidin patterns can be further utilized for the patterning of biotinylated materials. Various groups around the globe are working on creating features at 10–100 nm length scales for producing ultradense DNA and protein chips for various microarray and medical device applications.

15.4 RELEVANCE OF NANOSTRUCTURED SCAFFOLDS IN REGENERATIVE MEDICINE

In tissues and organs, cells are always surrounded and constantly in touch with the ECM, which is a self-assembled nanofibrillar matrix consisting of various proteins and polysaccharides. The ECM varies substantially in volume in organs: abundant in cartilage and bone, and rare in brain and spinal cord. It exhibits remarkable diversity and functional adaptation such as calcified in bone and teeth, transparent in cornea, ropelike in tendons, basal lamina between epithelium and connective tissue. Due to its ubiquitous nature and close association with cells, ECM controls cell functions and physical properties of tissues. In addition, high surface area of the ECM nanofibrils provides an opportunity to have proteins like proteoglycans, glycoaminoglycans, and integrins on the surface for better interaction with the cytoskeleton of cells.

Cellular functions *in vivo* are regulated by cell–cell communications and cell–substratum interactions and soluble factors. Ability to incorporate *in vivo*-like features in synthetic scaffolds for tissue engineering may lead to accelerated time regeneration. Cell–substratum interactions are influenced by topographical and chemical cues. Topographical cues dictate processes such as cell adhesion, proliferation, differentiation, migration, and gene expression based on the surface feature type and size. It is known that biological length scale topography that ranges from 10 nm to 100 μm influences the cytoskeletal organization and eventually cellular behavior [66]. Karuri et al. observed SV40 human corneal endothelial cell rounded morphology on flat surface (Fig. 15.5a), and elongated morphology on patterned surfaces (Fig. 15.5b). The inset shows the extended filopodia and lamellopodia on the patterned surfaces with grooves and ridges [67]. In a similar study with macrophage-like cells on nanogrooves, cells aligned to the long axis of grooves with

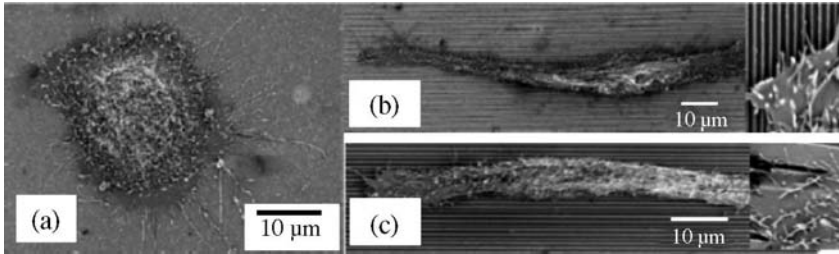


FIGURE 15.5 SEM of adherent SV40 human corneal epithelial cells on (a) planar surface and patterned surfaces with pitch size of (b) 400 nm and (c) 4000 nm. Inset shows the tip of an elongated cell. (Reproduced from Reference [67] with permission, from The Company of Biologists.)

organization of cytoskeletal elements parallel to the grooves [68]. Actin and microtubules were observed to align along the walls and edges of the grooves while actin condensations appeared at topographic discontinuities [69]. Some of the cells were also observed to have lamellae and filopodia bending around the edges. There are also reports on the effect of groove depth on baby hamster kidney (BHK) and Madin-Darby canine kidney (MDCK) cell orientation. For example, BHK cell alignment increased with depth but decreased with width, whereas width has no effect on MDCK cells [70]. Therefore, most of the cell types including fibroblasts, endothelial, smooth muscle, macrophage, leukocytes, osteoblasts, and mesenchymal stem cells respond to nanofeatured ridges, steps, wells, nodes, pillars, pores, and spheres by showing good adhesion, proliferation, migration, and differentiation. The cells have also shown to exhibit a broad gene upregulation and increased production of ECM proteins [71–74].

In vivo, cells are surrounded by the ECM and most of the cellular functions inside the complex organs are mediated by the ECM in association with signaling molecules and growth factors. In addition to the chemical cues, the ECM exhibits nanotopographical cues that influence various cellular functions including adhesion and differentiation. Therefore, there is a great need and demand for nanofeatured scaffolds that mimic and provide the same environment as the *in vivo* ECM for tissue engineering/regenerative medicine.

15.5 ROLE OF NANOSTRUCTURED SCAFFOLDS IN TISSUE ENGINEERING

Various *in vitro* and *in vivo* studies employed nanostructured scaffolds for engineering bone, cartilage, vascular, neural, cardiac, and bladder tissue. Some of the recent efforts where tissue regeneration was enhanced by mimicking the ECM topography via nanostructured scaffolds are discussed below.

15.5.1 Bone and Cartilage Tissue Engineering

Scaffold design and development for bone repair and regeneration has been a priority for the tissue engineering community for many years. Traditional methods like microsphere sintering, salt leaching, gas foaming, and freeze drying are employed for fabricating 3D scaffolds for bone tissue engineering applications [75]. Even though the fabricated scaffolds exhibit 3D pore structure, they lack the nanoscale topography that cells experience *in vivo*. In an attempt to mimic the ECM features, recently nanoscale features have been incorporated in the design of scaffolds [76]. The fabricated nanofeatured scaffolds were evaluated for their performance by culturing osteoblast and mesenchymal stem cells in an effort to engineer bone.

Li et al. used electrospinning for creating PLGA scaffolds for bone tissue engineering applications [27]. Using the same technique Vacanti et al. developed 3D nanofibrous biodegradable PCL scaffolds for regenerating bone [77]. The electrospun scaffold consists of fibers with diameters ranging from 20 nm to 5 μm with the average diameter of 400 nm. Mesenchymal stem cells (MSCs), derived from bone marrow of neonatal rats, were cultured with osteogenic supplements under dynamic culture conditions. This study has shown that nanofibrous scaffolds provide an environment that supports mineralized tissue formation. The cell–polymer nanofiber constructs obtained after the 4 weeks of *in vitro* dynamic culture were subsequently implanted in the omenta of rats to assess the bone formation *in vivo* [78]. Histological examination, on a specimen after 4 weeks of *in vitro* culture and 4 weeks of implantation, revealed the presence of osteocyte-like cells and the formation of mineralized bonelike tissue throughout the specimen confirming the suitability of a nanofibrous construct for the treatment of bone defects. A novel strategy that combined stem cell-based gene therapy with nanostructured scaffolds was recently developed for *in vivo* bone tissue engineering [79]. PLGA electrospun scaffolds seeded with transfected MSCs to express BMP2 were implanted in the thigh muscle of immunocompetent mice. After 4 weeks of implantation, animals were sacrificed and the ectopic bone formation was assessed via structural and nanoindentation studies. As shown in Fig. 15.6a, μCT (computed tomography) clearly shows the growth of ectopic bone at the transplantation site. Histological studies demonstrated the formation of bone marrow (Fig. 15.6b) and collagen (Fig. 15.6c) regions within the new bone. Ectopic bone further showed canaliculi structure as seen from Fig. 15.6d that is similar to the femoral bone. The similarity in mechanical properties (estimated by nano-indentation), nanoscale topographies, overall microstructure, and chemical composition between femoral and nanofiber-assisted engineered bone further reveals the nanostructured scaffold's potential in bone regeneration.

Self-assembly holds the reputation of creating 3D nanofibrous scaffolds with the fiber diameters that fall in the range of natural collagen present in the ECM. Self-assembled scaffolds have already been employed for regeneration of various tissues. Hosseinkhani et al. employed self-assembled peptide-amphiphile

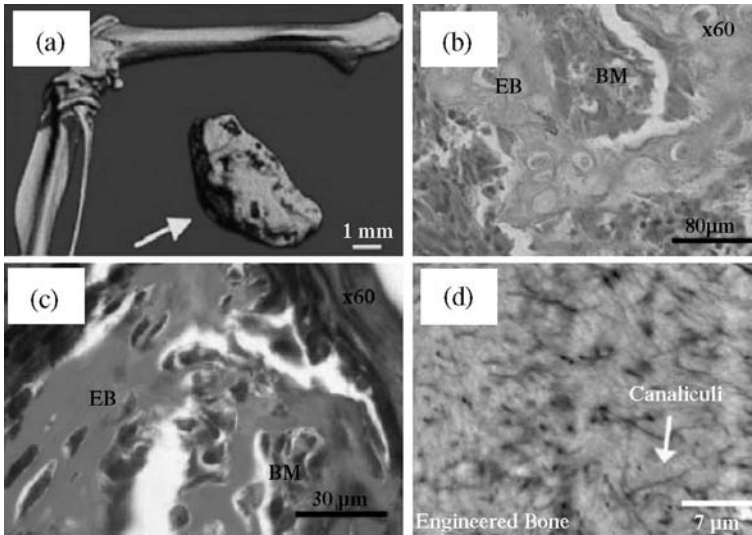


FIGURE 15.6 (a) μ CT image of a femoral and engineered bone. Histological evolution of the engineered bone. (b) Hematoxylin–eosin staining for bone marrow regions and (c) Masson’s trichrome staining for collagen regions (green in color). (d) Backscattered electron microscope image of an engineered bone showing canaliculi regions similar to the femoral bone (EB is engineered bone and BM is bone marrow). (Reproduced from Reference [79] with permission, from Elsevier).

nanofibrous scaffolds for osteogenic differentiation of mesenchymal stem cells [80]. A 3D network of cell–polymer nanofiber construct prepared by mixing cell suspension in media with dilute aqueous PA solution was used in this study. It has clearly demonstrated that PA nanofiber scaffolds significantly enhanced *in vitro* proliferation and osteogenic differentiation of MSC compared with a static culture. The response was further improved by functionalizing nanofibers with arginine–glycine–aspartic (RGD) sequence. Close resemblance of the *in vivo* situation resulted in an increased alkaline phosphatase (ALP) activity and osteocalcin expression. The authors further improved the mechanical strength by employing hybrid scaffolds consisting of a hydrogel formed through self-assembly of PA and the collagen sponge reinforced with PGA [81]. Hybrid scaffolds were precultured using bioreactor perfusion culture system and 3-week precultured scaffolds were used for the *in vivo* study. ALP activity and osteocalcin content of the subcutaneous tissues around the implant site clearly confirmed the ectopic bone-forming ability of these novel hybrid nanofibrous scaffolds. Though this study has focused more on evaluating the effectiveness of perfusion culturing system against the static culture, the observed *in vitro* and *in vivo* osteogenic differentiation of MSCs clearly demonstrated the bone-forming ability of nanofiber scaffolds.

Phase separation process has been recently employed to create highly porous (90% and above) nanofibrous PLLA scaffolds for bone tissue engineering. These scaffolds are three-dimensional with interconnected spheroid pores of diameter 250–420 μm and having pore walls with nanofibrous architecture with fiber diameter ranging from 50 to 500 nm. Nanofibrous scaffolds further showed improvement in protein adsorption with fibronectin and vitronectin that in turn enhanced osteoblast attachment as compared to the scaffolds with solid pore walls. Since the nanofibrous and nonfibrous scaffolds in this case are fabricated using the same base material PLLA, the difference observed in protein adsorption and cell attachment has been attributed to the nanoscale structure. Nanohydroxyapatite (NHAP)/PLLA composite scaffolds were also developed by the same group to better mimic the mineral component of the bone [82]. This modification has greatly enhanced the mechanical properties, and also the protein adsorption capacity. The similarity in microstructure and the bonelike composition makes NHAP/PLLA composite scaffold a better candidate for bone tissue regeneration. Li et al. in a related study investigated nanoscale scaffolds for cartilage tissue engineering [83]. The authors examined *in vitro* chondrogenesis of human MSCs cultured on electrospun PCL nanofibrous scaffold with an average fiber diameter of 700 nm. The level of chondrogenesis observed with nanofibrous scaffold was comparable to cell pellet cultures traditionally used in the study of MSC chondrogenesis [84]. But the advantage with nanofibrous scaffolds is that they are mechanically stable when compared to cell pellet cultures and can find clinical applications.

In vitro and *in vivo* studies conducted thus far clearly indicated that nanofibrous constructs are ideal candidates for bone and cartilage tissue engineering applications for the following reasons. Small fiber diameter resulted in high surface area, which is beneficial for better cell attachment and proliferation. Also, the high porosity associated with these constructs facilitated cell migration and effective nutrient and waste transport.

15.5.2 Vascular Tissue Engineering

Layered architecture and the unique mechanical properties present an enormous challenge to engineer blood vessels. The three types of blood vessels are arteries, capillaries, and veins. Each blood vessel consists of three layers: tunica intima, media, and adventitia that are built around endothelial, smooth muscle, and fibroblast cell layers, respectively. Over the last 20 years, the vascular tissue engineering community has been looking at various biodegradable vascular grafts that are biologically and mechanically sound, thrombosis resistant, and immunologically safe. With the advent of biodegradable polymer technology, various polymer candidates were developed with controllable properties that are suitable as graft materials for vascular tissue engineering. Initial studies indicated the usefulness of biodegradable PGA scaffolds seeded with vascular cells for vascular graft applications [85, 86]. Recently, nanostructured scaffolds were being investigated to mimic ECM until the

ECM secreted by the cells is capable of carrying out the required biomechanical functionalities of a blood vessel.

For this purpose, Mo et al. electrospun poly(L-lactide-co- ϵ -caprolactone) [P(LLA-CL)] (75:25) copolymer into randomly oriented nanofibers [87]. The biocompatibility of the nanofiber mats has been confirmed by culturing endothelial cells (ECs) and smooth muscle cells (SMCs). Both ECs and SMCs proliferated well on these surfaces and maintained normal phenotypic shape on the nanofibers. Simulation of the exact cell orientation present in tunica intima and media layers of a native blood vessel has been further achieved through oriented nanofiber matrices developed using a modified electrospinning process [88]. An interesting observation in this study was that SMCs seeded on oriented nanofiber mats proliferated along the longitudinal direction of the nanofiber length. SMCs are found to adhere well (Fig. 15.7a) to the nanofibers and also

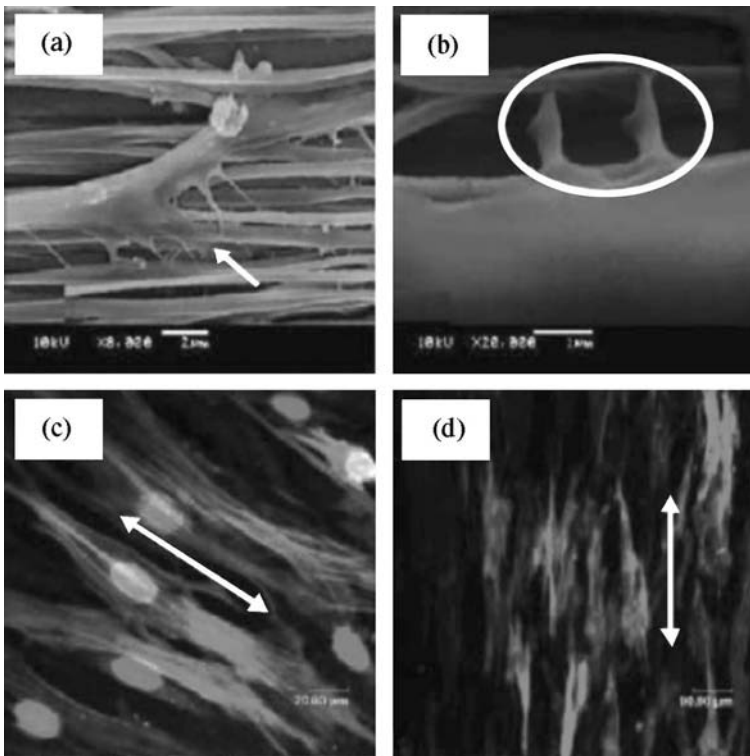


FIGURE 15.7 SEM micrographs showing the SMCs adhesion on the aligned P(LLA-CL) nanofibers: (a) SMC alignment along the fiber orientation with focal contacts and (b) close-up of SMC focal contacts that are attached to the surrounding fibers. Confocal micrographs of SMCs after 1 day culture immunostained for (c) α -actin and (d) myosin filaments. Arrow indicates the fiber orientation. (Reproduced from Reference [88] with permission, Elsevier)

observed to form bridges similar to focal contacts with the nearest fibers as seen in Fig. 15.7b. The expression and accumulation of cytoskeletal proteins such as α -actin (Fig. 15.7c) and myosin (Fig. 15.7d) inside the SMC in relation to the nanofiber orientation revealed the oriented fiber matrix effect on SMC expression. This is further assumed that cytoskeletal proteins expressed may have guided SMCs to orient along the fiber direction. In a native blood vessel, tunica intima consists of ECs aligned parallel to blood flow and in tunica media SMCs aligned perpendicular to the blood flow. Therefore, this particular study is very important as it could successfully align SMCs in a preferred direction so that the tissue engineered vascular grafts could better mimic the structure and also the cellular functionality of a native blood vessel.

Adding a cellular recognition layer to the internal surface of a vascular construct could significantly reduce intimal hyperplasia following scaffold implantation. Chemical and topographical simulation of the ECM may control ECs spreading, proliferation, and phenotype retention that are of great interest when designing biodegradable nanostructures for vascular graft applications. Therefore, an effective approach would be modifying the nanofiber mat surface with biocompatible layers such as gelatin and collagen to impart biofunctionality that ultimately prevent thrombosis and improve graft patency rate. Several studies thus far addressed mimicking the ECM topographically; however, Ma et al. grafted gelatin on to PCL nanofibers and created artificial basal lamina with both ECM-mimicking structure and cell-compatible surfaces [89]. Gelatin immobilization on random and oriented PCL nanofiber scaffolds was achieved via air plasma treatment to introduce $-\text{COOH}$ groups on PCL nanofiber surface, followed by covalent grafting of gelatin molecules. Gelatin grafting increased the wettability of PCL nanofiber mats and significantly improved EC spreading and growth, and also maintained their phenotypic character. Endothelialization of the vascular graft is one of the best ways to avoid coagulation and make these scaffolds ideal for blood vessel tissue engineering. For this reason, human coronary artery endothelial cells (HCAECs) were seeded onto the collagen-blended [P(LLA-CL), 70:30] electrospun nanofibers [90]. Cells on collagen-blended fibers showed better phenotypic spreading as compared to P(LLA-CL) nanofibers. Further, HCAECs observed to interconnect well with the nanofibers and also the pseudopods of the cells were oriented along the collagen-blended nanofibers. This study has confirmed that biocompatible layers such as gelatin and collagen in conjunction with nanofiber topography induce better phenotypic retention for longer time periods, which is a desirable feature for a vascular graft scaffold.

Angiogenesis, the process of forming new blood vessels from preexisting vessels, is essential in the repair and regeneration of tissues. For this reason, various scaffolds have been designed with the ability to deliver high concentrations of angiogenic growth factors locally [91]. Another important strategy is using heparin as a delivery agent for growth factors where vascular endothelial growth factor (VEGF) and fibroblast growth factor-2 (FGF-2) are

bonded through their heparin-binding domains [92, 93]. To better understand and control molecular-scale matrix–heparin microstructure, Rajangam et al. used heparin nucleated PA self-assembled nanofibrous scaffolds for effective binding of angiogenic growth factors [94]. In this process, aqueous solution containing heparin and growth factors is mixed with PA (specially designed to bind heparin) aqueous solution to form nanofibrous scaffold. Positively charged PA molecule aggregate is nucleated by negatively charged heparin and later bond to the resultant cylindrical nanostructure. The growth factor that is bonded to the rigid heparin on the nanofiber causes less Brownian motion that leads to a high ligand–receptor binding. This hypothesis was proven *in vitro* by a slow release of FGF-2 (57.1% in 10 days in presence of heparin) from a network of PA–heparin nanofibers compared to a faster release from PA–Na₂HPO₄ gel (98% in 10 days in the absence of heparin). A rat cornea angiogenesis assay was performed to test the angiogenesis capacity of heparin–PA system *in vivo*. It was observed that heparin-binding PA nanostructures combined with growth factors VEGF and FGF-2 promoted vascularization that is significantly higher than all the controls involved in this study. Thus, the self-assembled nanostructures cause extensive new blood vessel formation and might have potential as scaffolds for vascular tissue engineering.

15.5.3 Neural Tissue Engineering

Neural tissue regeneration is necessary in cases where scar tissue is formed after injury, gaps in the nervous system formed during phagocytosis, and failure of growth and extension of axons in the mature mammalian central nervous system [95]. As described in Section 15.2.3, a peptide hydrogel consists of standard amino acids (1% w/v) and 99% water. Under physiological conditions, the peptide component self-assembles into a 3D hydrogel that exhibits a nanometer-scale fibrous structure. Self-assembled peptide nanofiber scaffolds (SAPNS) are superior over the currently available scaffolding materials because they form a network of nanofibers that mimic the ECM, break into natural amino acids that can be effectively used by surrounding tissue, and are immunologically inert since they are free from chemical and biological contaminants.

Self-assembled scaffolds support the growth of PC12 cells and the formation of functional synapses *in vitro* with rat hippocampal neurons on arganine, alanine, aspartate, and alanine nanofiber scaffolds [96]. Extensive neurite outgrowth and active synapse formation encouraged similar studies in an *in vivo* model to demonstrate the suitability of these scaffolds for nano neuro knitting [97]. In this model, a wound was created in the mid brain superior colliculus (SC) region and SAPNS is inflicted to regenerate an optic tract in young and adult hamsters. The cavity that is seen with the control group (where 10 μ l of saline solution is injected) at 30-day time point showed the failure of tissue healing (Fig. 15.8a), whereas the site of the lesion has healed as

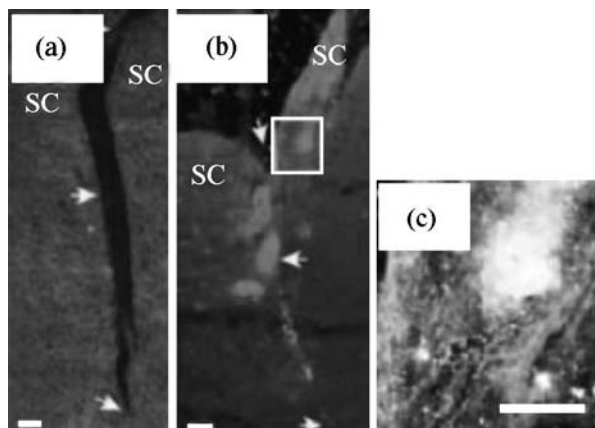


FIGURE 15.8 Dark field images of parasagittal sections from animals at day 30 after lesion and treatment. (a) Cavity in the retinal projections shows the failure of the tissue healing. (b) A similar lesion section injected with $10\ \mu\text{l}$ of 1% SAPNS. Axons that are indicated by light color have grown through the lesion and helped in tissue healing. Enlarged view of boxed area in (b) is shown in (c), which is an area of dense termination of axons (traced with cholera-toxin labeling) that have crossed the lesion. Scale bars, $100\ \mu\text{m}$ (SC, superior colliculus). (Reproduced from Reference [99] with permission, from The National Academy of Sciences of the USA.)

evident from Fig. 15.8b with the injection of $10\ \mu\text{l}$ of 1% SAPNS. In the case of SAPNS, axons have grown through the treated area and the tissue appeared to be knitted with little sign of the original lesion. Figure 15.9c clearly shows the innervation density, where the white regions correspond to axons or axon terminals labeled from the retina. This study has successfully demonstrated the feasibility of using SAPNS for axon repair and regeneration.

After CNS trauma, inhibition of astrocyte proliferation is important in preventing glial scar tissue formation. This is an important step since the newly formed scar tissue acts as a barrier to axon elongation [98]. Recently, many studies have aimed at achieving neural progenitor cell (NPC) differentiation into neurons while suppressing astrocyte differentiation. Silva et al. studied selective differentiation of NPCs using nanofibrous neurite promoting laminin epitope isoleucine–lysine–valine–alanine–valine (IKVAV-PA) self-assembled scaffolds [99]. Murine NPCs were mixed with 1 wt% of IKVAV-PA in 1:1 volume ratio in media or physiological fluids. The resulting transparent gel-like solid containing NPC clusters were encapsulated within a 3D network of nanofibers formed via self-assembly of PA molecules. NPCs survived the self-assembly process and showed differentiated neurons that were significantly larger than those of controls at both 1 and 7 days. In addition to the nanofibrous structure that simulates the ECM-like morphology, high content of water (99.5%) present in these scaffolds serves as a medium for nutrient diffusion and for cell migration. Differentiation and migration of NPC

neurospheres encapsulated in IKVAV-PA gel were observed to be significantly higher than the nonphysiological sequence glutamic acid–glutamine–serine (EQS) gel and poly(D-lysine) controls. In addition to the rapid selective differentiation, these scaffolds were further proven to be *in vivo* compatible and might find applications in neural tissue engineering where controlled neural differentiation and migration are required for treating CNS trauma conditions.

15.5.4 Cardiac Tissue Engineering

Myocardial infarction, fibrotic scar tissue formation (massive cell loss due to ischemia), and impaired cardiac function are common problems that lead to heart failure. This occurs because of the fact that cardiomyocytes (CMs) are terminally differentiated cells and unable to regenerate into myocardial tissue after infarction. Although heart transplantation is the ultimate cure to heart failure, lack of organ donors and complications associated with immune suppressive treatments are forcing scientists and surgeons to look for new strategies to regenerate the wounded heart [100]. Gene delivery techniques followed by cell transplantation techniques were considered in the mid-1990s to spark the failing heart [101, 102]. Recently, cardiac tissue engineering has emerged as a novel approach to repair and reinforce wounded cardiac tissue using embryonic or neonatal cardiomyocytes in combination with natural and synthetic biodegradable scaffolds [103]. This approach has been further modified by developing nanofeatured scaffolds that mimic certain features of the natural ECM and improve the regenerative capability of the tissue engineered cardiac constructs.

Collagen and gelatin-based tissue engineered patches have been recently reported [104, 105]. They exhibited good contraction and function, but are not popular for use due to the lack of stability required for handling. An alternative approach is using synthetic polymers that require physical properties such as stability and resistance to contractions [103]. Zong et al. seeded cardiomyocytes

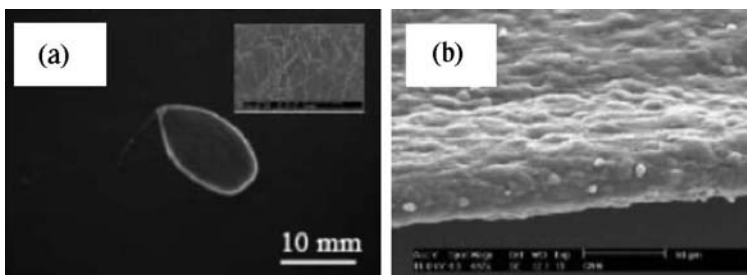


FIGURE 15.9 (a) A 10- μm -thick fibrous mesh suspended across a wire ring that acts as a passive load to condition cardiomyocytes during *in vitro* culture. Inset shows the SEM of an electrospun mesh with an average fiber diameter of 250 nm. (b) Cross-sectional SEM recorded on a cardiac nanofibrous mesh after 14 days of *in vitro* culture showing cardiomyocyte presence throughout the entire mesh. (Reproduced from Reference [107] with permission, from Elsevier)

on electrospun nanofiber scaffolds made of PLLA, PLGA (PLA10/PGA90) + PLLA, and PLGA(PLA75/PGA25) + PEG-PLA [106]. This study compared growth of cardiomyocytes on randomly oriented fiber scaffolds, and also on locally oriented fiber scaffolds where the microscale fiber orientation was achieved by uniaxial stretching. It was observed that the fiber orientation provided guidance for CM growth and showed sensitivity to the composition and degradation rate of the electrospun PLGA-based scaffolds. CM cell density was observed to be higher on relatively hydrophobic surfaces that in general exhibited slower degradation. Myocardial functional studies of CMs on different synthetic scaffolds showed PLLA as a better scaffold as compared to other candidates involved in this study.

Shin et al. electrospun PCL nanofiber meshes and seeded with cardiomyocytes isolated from neonatal Lewis rats [107]. ECM-like mesh with an average fiber diameter of 250 nm and a mesh thickness around 10 μm (inset of Fig. 15.9a) was suspended across a wire ring as shown in Fig. 15.9a. Cardiomyocytes attached well to these scaffolds and started contracting after 3 days of culture. After 14 days of culture, cardiomyocytes retained their phenotype, penetrated the entire scaffold, and stained positive for cardio typical proteins such as actin, tropomyosin, cardiac troponin-I, and connexin 43. Also, a cross-sectional view clearly confirms the presence of cells through the entire nanofibrous scaffold as presented in Fig. 15.9b. This study has established a versatile *in vitro* system to develop functional myocardial patches that may be used for healing and regeneration of wounded hearts.

As described in the previous sections, nanotechnology for tissue engineering/regenerative medicine is actively perused recently for multiple applications including the regeneration of bone, cartilage, neural, vascular and cardiac tissues. In addition, research is currently underway to regenerate skin, bladder and liver tissues using nanostructured scaffolds [108, 109, 110].

There have already been successful tissue engineering products that are clinically relevant, have achieved FDA approval, and are currently being marketed for tissue replacement. The most successful product is tissue engineered skin that is currently in clinical use (Dermagraft[®] and Apligraf[®]) for treating burn victims and patients with diabetic ulcers. Some of the products at advanced clinical stage are contractile patches for damaged heart, autologous chondrocytes in a polymer gel for treating urinary reflux in children, and urinary stress incontinence in adult women [111]. In addition, various other tissue engineered products are at preliminary stages of investigation (*in vitro* or animal studies) for regenerating tissues/organs such as bone, ligament, heart valves, heart muscles, blood vessels, and bladders [112]. Thus far, efforts have been on designing materials in combination with cells and factors to meet the targeted clinical application. The success of this approach can be further enhanced by creating cellular recognition nano/microtopographical features that aid in the control of cell functions and may lead to better tissue engineered products that meet future clinical needs.

15.6 CONCLUSIONS

The need for mimicking the ECM has led to the development of various scaffolding methodologies. These methods have helped in the creation of 3D scaffolds consisting of fibers, grooves, pits, and pillars in nanoscale for tissue engineering and biomedical applications. Due to the *in vivo*-like environment, cells seeded on nanofeatured scaffolds showed improved adhesion, proliferation, migration, differentiation, and phenotypic expression. These scaffolds with improved cellular compatibility can be directly translated into successful tissue constructs for restoration, repair, and regeneration of bone, cartilage, neural, vascular, and cardiac tissues. Even though scaffolds with nanofeatures have generated lot of interest and excitement, the future of tissue engineering will incorporate scaffolds with topographical and biochemical cues that would exactly duplicate the *in vivo* environment. Nanostructured scaffolds are still at their infancy stage and further work is required to answer questions such as what size is right for a desired cell response and how different cells react to the same topography.

REFERENCES

1. Data derived from American Association of Tissue Banks, Eye Bank Association of America, National Marrow Donor Program, National Kidney Foundation, Inc., and UNOS Scientific Registry; 2005.
2. Laurencin CT, Amborsio A, Borden MD, Cooper JA. Tissue engineering: orthopedic applications. *Anu Rev Biomed Eng* 1999;1:19–46.
3. Atala A and Lanza RP. *Methods of Tissue Engineering*. New York: Academic Press; 2002.
4. Kofron MD and Laurencin CT. Bone tissue engineering by gene delivery. *Adv Drug Deliv Rev* 2006;58:555–576.
5. Yu X, Botchwey EA, Levine EM, Pollack SR, Laurencin CT. Bioreactor-based bone tissue engineering: the influence of dynamic flow on osteoblast phenotypic expression and matrix mineralization. *Proc Natl Acad Sci USA* 2004;101:11203–11208.
6. Langer R and Vacanti JP. Tissue engineering. *Science* 1993;260:920–926.
7. Williams DF, *The Williams dictionary of Biomaterials*. Liverpool UK: Liverpool University Press; 1999.
8. Williams DF. Revisiting the definition of biocompatibility. *Med Device Technol* 2003;14:10–13.
9. Dankers PY, Harmsen MC, Brouwer LA, van Luyn MJ, Meijer EW. A modular and supramolecular approach to bioactive scaffolds for tissue engineering. *Nat Mater* 2005;4:568–574.
10. Livingston T, Ducheyne P, Garino J. *In vivo* evaluation of a bioactive scaffold for bone tissue engineering. *J Biomed Mater Res* 2002;62:1–13.
11. Griffith LG. Polymeric biomaterials. *Acta Mater* 2000;48:263–277.

12. Hayashi T. Biodegradable polymers for biomedical uses. *Prog Polym Sci* 1994;19:663–702.
13. Mikos AG, Thorsen AJ, Czerwonka LA, Bao Y, Langer R. Preparation and characterization of poly(L-lactic acid) foams. *Polymer* 1994;35:1068–1077.
14. Mooney DJ, Baldwin DF, Suh NP, Vacanti JP, Langer R. Novel approach to fabricate porous sponges of poly(D,L-lactic-co-glycolic acid) without the use of organic solvents. *Biomaterials* 1996;17:1417–1422.
15. Hsu YY, et al. DL Effect of polymer foam morphology and density on kinetics of *in vitro* controlled release of isoniazid from compressed foam matrices. *J Biomed Mater Sci* 1997;35:107–116.
16. Giordano RA, et al. Mechanical properties of dense polylactic acid structures fabricated by three dimensional printing. *J Biomat Sci Polym Ed* 1996;8:63–75.
17. Borden M, Attawia M, Khan Y, Laurencin CT. Tissue-engineered microsphere-based matrices for bone repair: design and evaluation. *Biomaterials* 2002;23:551–559.
18. Ramakrishna S, et al. *An Introduction to Electrospinning and Nanofibers*. Singapore: World Scientific Publishing Co. Pte. Ltd; 2005.
19. Ma PX. Scaffolds for tissue fabrication. *Mater Today* 2004;7:30–40.
20. Stupp SI, et al. Supramolecular materials: self-organized nanostructures. *Science* 1997;276:384–389.
21. Khademhosseini A, Langer R, Borenstein J, Vacanti JP. Microscale technologies for tissue engineering and biology. *Proc Natl Acad Sci USA* 2006;103:2480–2487.
22. Alberts B, et al. *Molecular Biology of the Cell*. New York: Garland Science; 2002. p 1090.
23. Murugan R and Ramakrishna S. Nano-featured scaffolds for tissue engineering: a review of spinning methodologies. *Tissue Eng* 2006;12:435–447.
24. Pham QP, Sharma U, Mikos AG. Electrospinning of polymeric nanofibers for tissue engineering applications: a review. *Tissue Eng* 2006;12:1197–1211.
25. Kumbhar SG, Nair LS, Bhattacharyya S, Laurencin CT. Polymeric nanofibers as novel carriers for the delivery of therapeutic molecules. *J Nanosci Nanotechnol* 2006;6:2591–2607.
26. Nair LS, Bhattacharyya S, Laurencin CT. Development of novel tissue engineering scaffolds via electrospinning. *Expert Opin Biol Ther* 2004;4:659–668.
27. Li WJ, Laurencin CT, Cateson EJ, Tuan RS, Ko FK. Electrospun nanofibrous structure: a novel scaffold for tissue engineering. *J Biomed Mater Res* 2002;60:613–621.
28. Laurencin CT and Ko FK. Hybrid nanofibril matrices for use as tissue engineering devices. *US Patent* 2004;6,689,166.
29. Katti DS, Robinson KW, Ko FK, Laurencin CT. Bioresorbable nanofiber-based systems for wound healing and drug delivery: optimization of fabrication parameters. *J Biomed Mater Res B Appl Biomater* 2004;70:286–296.
30. Nair LS, et al. Fabrication and optimization of methylphenoxy substituted polyphosphazene nanofibers for biomedical applications. *Biomacromolecules* 2004;5:2212–2220.

31. Bognitzki M, et al. Nanostructured fibers via electrospinning. *Adv Mater* 2001;13:70–72.
32. Boland ED, Wnek GE, Simpson DG, Pawlowski KJ, Bowlin GL. Tailoring tissue engineering scaffolds using electrostatic processing techniques: a study of poly(glycolic acid) electrospinning. *J Macromol Sci Pure Appl Chem* 2001;A38:1231–1243.
33. Yang F, Murugan R, Wang S, Ramakrishna S. Electrospinning of nano/micro scale poly(L-lactic acid) aligned fibers and their potential in neural tissue engineering. *Biomaterials* 2005;26:2603–2610.
34. Li WJ, Danielson KG, Alexander PG, Tuan RS. Biological response of chondrocytes cultured in three-dimensional nanofibrous poly(epsilon-caprolactone) scaffolds. *J Biomed Mater Res A* 2003;67:1105–1114.
35. Geng XY, Kwon OH, Jang JH. Electrospinning of chitosan dissolved in concentrated acetic acid solution. *Biomaterials* 2005;26:5427–5432.
36. Almany L and Seliktar D. Biosynthetic hydrogel scaffolds made from fibrinogen and polyethylene glycol for 3D cell cultures. *Biomaterials* 2005;26:2467–2477.
37. Schindler M, et al. A synthetic nanofibrillar matrix to promote *in vivo*-like organization and morphogenesis for cell in culture. *Biomaterials* 2005;26:5624–5631.
38. Matthews JA, Wnek GE, Simpson DG, Bowlin GL. Electrospinning of collagen nanofibers. *Biomacromolecules* 2002;3:232–238.
39. Venugopal J and Ramakrishna S. Biocompatible nanofiber matrices for the engineering of a dermal substitute for skin regeneration. *Tissue Eng* 2005;11:847–854.
40. Witte P, Dijkstra PJ, Berg JWA, Feijen J. Phase separation processes in polymer solutions in relation to membrane formation. *J Membr Sci* 1996;117:1–31.
41. Ma PX and Jennifer E. *Scaffolding in Tissue Engineering*. Boca Raton: CRC Press; 2006. p 125.
42. Ma PX and Zhang R. Synthetic nano-scale fibrous extracellular matrix. *J Biomed Mater Res* 1999;46:60–72.
43. Zhang R and Ma PX. Synthetic nano-fibrillar extracellular matrices with predesigned macroporous architectures. *J Biomed Mater Res* 2000;52:430–438.
44. Ma PX and Choi J. Biodegradable polymer scaffolds with well defined interconnected spherical pore network. *Tissue Eng* 2001;7:23–33.
45. Gross M. *Travels to the Nanoworld: Miniature Machinery in Nature and Technology*. New York: Perseus Books Group; 1999.
46. Zhang S, Holmes T, Lockshin L, Rich A. Spontaneous assembly of a self-complementary oligopeptide to form a stable macroscopic membrane. *Proc Natl Acad Sci USA* 1993;90:3334–3338.
47. Semino CE, Merok JR, Crane GG, Panagiotakos G, Zhang S. Functional differentiation of hepatocyte-like spheroid structures from putative liver progenitor cells in three-dimensional peptide scaffolds. *Differentiation* 2003;71:262–270.
48. Semino CE, et al. Entrapment of migrating hippocampal neural cells in 3D peptide nanofiber scaffold. *Tissue Eng* 2004;10:643–655.
49. Hartgerink JD, Beniash E, Stupp SI. Self-assembly and mineralization of peptide amphiphile nanofibers. *Science* 2001;294:1684–1688.

50. Murphy WL and Mooney DJ. Molecular scale bio-mimicry. *Nat Biotechnol* 2002;20:30–31.
51. Zhang S, et al. Self-complementary oligo peptides matrices support mammalian cell attachment. *Biomaterials* 1995;16:1385–1393.
52. Kisiday J, et al. Self assembling peptide hydrogel fosters chondrocyte extracellular matrix production and cell division: implications for cartilage tissue repair. *Proc Natl Acad Sci USA* 2002;99:9996–10001.
53. Dalby MJ, et al. Increasing fibroblast response to materials using nanotopography: morphological and genetic measurements of cell response to 13-nm-high polymer demixed islands. *Exp Cell Res* 2002;276:1–9.
54. Geissler M and Xia Y. Patterning: principles and some new developments. *Adv Mater* 2004;16:1249–1269.
55. Kane RS, Takayama S, Ostuni E, Ingber DE, Whitesides GM. Patterning proteins and cells using soft lithography. *Biomaterials* 1999;20:2363–2376.
56. Mrksich M, Dike LE, Tien J, Ingber DE, Whitesides GM. Using microcontact printing to pattern the attachment of mammalian cells to self-assembled monolayers of alkanethiolates on transparent films of gold and silver. *Exp Cell Res* 1997;235:305–313.
57. Lee CJ, et al. Microcontact printing on human tissue for retinal cell transplantation. *Arch Ophthalmol* 2002;120:1714–1718.
58. Li HW, Muir BVO, Fichet G, Huck WTS. Nanocontact printing: a route to sub-50-nm-scale chemical and biological patterning. *Langmuir* 2003;19:1963–1965.
59. Jo J, Kim KY, Lee ES, Choi BO. Nanocontact printing of nonplanar substrate by using flexible h-PDMS stamp. *Proc SPIE* 2005;6037:60371T.
60. Suh KY, Seong J, Khademhosseini A, Laibinis PE, Langer R. A simple soft lithographic route to fabrication of poly(ethylene glycol) microstructures for protein and cell patterning. *Biomaterials* 2004;25:557–563.
61. Morra M and Cassinelli C. Non-fouling properties of polysaccharide coated surfaces. *J Biomater Sci Polym Ed* 1999;10:1107–1124.
62. Khademhosseini A, et al. Layer-by-layer deposition of hyaluronic acid and poly-L-lysine for patterned cell co-cultures. *Biomaterials* 2004;25:3583–3592.
63. Fukuda J, et al. Micropatterned cell co-cultures using layer-by-layer deposition of extracellular matrix components. *Biomaterials* 2006;27:1479–1486.
64. Bearinger JP, et al. Biomolecular patterning via photocatalytic lithography. *Technical Proceedings of the NSTI Nanotechnology Conference and Trade Show. Volume 1;2005. p 339–342.*
65. Choi I, Kang SK, Lee J, Kim Y, Yi J. *In situ* observation of biomolecules patterned on a PEG-modified Si surface by scanning probe lithography. *Biomaterials* 2006;27:4655–4660.
66. Flemming RG, Murphy CJ, Abrams GA, Goodman SL, Nealey PF. Effects of synthetic micro and nano structured surfaces on cell behavior. *Biomaterials* 1999;20:573–588.
67. Karuri NW. Biological length scale topography enhances cell–substratum adhesion of human corneal epithelial cells. *J Cell Sci* 2004;117:3153–3164.

68. Wojciak-Stothard B, Madeja Z, Korohoda W, Curtis A, Wilkinson C. Activation of macrophage-like cells by multiple grooved substrata: topographical control of cell behaviour. *Cell Biol Int* 1995;19:485–490.
69. Wojciak-Stothard B, et al. Role of the cytoskeleton in the reaction of fibroblasts to multiple grooved substrata. *Cell Motil Cytoskeleton* 1995;31:147–158.
70. Clark P, Connolly P, Curtis A, Dow JAT, Wilkinsin C. Topographical control of cell behaviour. II. multiple grooved substrata. *Development* 1990;108:635–644.
71. Hoch HC, Staples RC, Whitehead B, Comeau J, Wolf ED. Signaling for growth orientation and cell differentiation by surface topography in *Uromyces*. *Science* 1997;235:1659–1662.
72. Clark P, Connolly P, Curtis A, Dow JAT, Wilkinson C. Topographical control of cell behavior. I. Simple step cues. *Development* 1987;99:439–448.
73. Rosdy M, Grisoni B, Clauss LC. Proliferation of normal human keratinocytes on silicone substrates. *Biomaterials* 1991;12:511–517.
74. Spaargaren M and Bos JL. Rab5 induces Rac dependant lamellipodia formation and cell migration. *Mol Biol Cell* 1999;10:3239–3250.
75. Liu X and Ma PX. Polymer scaffolds for bone tissue engineering. *Ann Biomedical Eng* 2004;32:477–486.
76. Christenson EM, et al. Nanobiomaterial applications in orthopedics. *J Orthop Res* 2007;25(1):11–22.
77. Yoshimoto H, Shin YM, Terai H, Vacanti JP. A biodegradable nanofiber scaffold by electrospinning and its potential for bone tissue engineering. *Biomaterials* 2003;24:2077–2082.
78. Shin M, Yoshimoto H, Vacanti JP. *In vivo* bone tissue engineering using mesenchymal stem cells on a novel electrospun nanofibrous scaffolds. *Tissue Eng* 2004;10:33–41.
79. Pelled G, et al. Structural and nanoindentation studies of stem cell-based tissue-engineered bone. *J Biomech* 2007;40:399–411.
80. Hosseinkhani H, Hosseinkhani M, Tian F, Kobayashi H, Tabata Y. Osteogenic differentiation of mesenchymal stem cells in self-assembled peptide-amphiphile nanofibers. *Biomaterials* 2006;27:4079–4086.
81. Hosseinkhani H, Hosseinkhani M, Tian F, Kobayashi H, Tabata Y. Ectopic bone formation in collagen sponge self-assembled peptide-amphiphile nanofibers hybrid scaffold in a perfusion culture bioreactor. *Biomaterials* 2006;27:5089–5098.
82. Wei G and Ma PX. Structure and properties of nano-hydroxyapatite/polymer composite scaffolds for tissue engineering. *Biomaterials* 2004;25:4749–4757.
83. Li WJ, et al. A three-dimensional nanofibrous scaffold for cartilage tissue engineering using human mesenchymal stem cells. *Biomaterials* 2005;26:599–609.
84. Muraglia A, et al. Formation of a chondroosseous rudiment in micromass cultures of human bone-marrow stromal cells. *J Cell Sci* 2003;116:2949–2955.
85. Niklason LE, et al. Functional arteries grown *in vitro*. *Science* 1999;284:489–493.
86. Watanabe M, et al. Tissue-engineered vascular autograft: inferior vena cava replacement in a dog model. *Tissue Eng* 2002;7:429–439.

87. Mo XM, Xu CY, Kotaki M, Ramakrishna S. Electrospun P(LLA-CL) nanofiber: a biomimetic extracellular matrix for smooth muscle cell and endothelial cell proliferation. *Biomaterials* 2004;25:1883–1890.
88. Xu CY, Inai R, Kotaki M, Ramakrishna S. Aligned biodegradable nanofibrous structure: a potential scaffold for blood vessel engineering. *Biomaterials* 2004;25: 877–886.
89. Ma Z, He W, Yong T, Ramakrishna S. Grafting of gelatin on electrospun poly(caprolactone) nanofibers to improve endothelial cell spreading and proliferation and to control cell orientation. *Tissue Eng* 2005;11:1149–1158.
90. He W, Yong T, Teo WE, Ma Z, Ramakrishna S. Fabrication and endothelialization of collagen-blended biodegradable polymer nanofibers: potential vascular graft for blood vessel tissue engineering. *Tissue Eng* 2005;11:1574–1588.
91. Lee KW. Sustained release of vascular endothelial growth factor from calcium-induced alginate hydrogels reinforced by heparin and chitosan. *Transplant Proc* 2004;36:2464–2465.
92. Ferrara N, Gerber HP, LeCouter J. The biology of VEGF and its receptors. *Nat Med* 2003;9:669–676.
93. Schlessinger J, et al. Crystal structure of a ternary FGF–FGFR–heparin complex reveals a dual role for heparin in FGFR binding and dimerization. *Mol Cell* 2000;6:743–750.
94. Rajangam K, et al. Heparin binding nanostructures to promote growth of blood vessels. *Nano Lett* 2006;6:2086–2090.
95. Fawcett JW and Asher RA. The glial scar and central nervous system repair. *Brain Res Bull* 1999;49:377–391.
96. Holmes TC, et al. Extensive neurite outgrowth and active synapse formation on self-assembling peptide scaffolds. *Proc Natl Acad Sci USA* 2000;97:6728–6733.
97. Ellis-Behnke RG, et al. Nano neuro knitting: peptide nanofiber scaffold for brain repair and axon regeneration with functional return of vision. *Proc Natl Acad Sci USA* 2006;103:5054–5059.
98. Chen ZJ, Ughrin Y, Levine JM. Inhibition of axon growth by oligodendrocyte precursor cells. *Mol Cell Neurosci* 2002;20:125–139.
99. Silva GA, et al. Selective differentiation of neural progenitor cells by high-epitope density nanofibers. *Science* 2004;303:1352–1355.
100. Koh GY, Soonpaa MH, Klug MG, Field LJ. Strategies for myocardial repair. *J Interv Cardiol* 1995;8:387–393.
101. Malosky S and Kolansky DM. Gene therapy for ischemic heart disease. *Curr Opin Cardiol* 1996;11:361–368.
102. Hassink RJ, Dowell JD, Riviere BA, Doevendans PA, Field LJ. Stem cell therapy for ischemic heart disease. *Trends Mol Med* 2003;9:436–441.
103. Leor J and Cohen S. Myocardial tissue engineering: creating a muscle patch for a wounded heart. *Ann N Y Acad Sci* 2004;1015:312–319.
104. Akhyari P, et al. Mechanical stretch regimen enhances the formation of bioengineered autologous cardiac muscle grafts. *Circulation* 2002;106:1137–1142.
105. Kofidis T, et al. *In vitro* engineering of heart muscle: artificial myocardial tissue. *J Thorac Cardiovasc Surg* 2002;124:63–69.

106. Zong X, et al. Electrospun fine-textured scaffolds for heart tissue constructs. *Biomaterials* 2005;26:5330–5338.
107. Shin M, Ishii O, Sueda T, Vacanti JP. Contractile cardiac grafts using a novel nanofibrous mesh. *Biomaterials* 2004;25:3717–3723.
108. Venugopal J and Ramakrishna S. Biocompatible nanofiber matrices for the engineering of a dermal substitute for skin regeneration. *Tissue Eng* 2005;11: 847–854.
109. Pattison MA, Wurster S, Webster TJ, Haberstroh KM. Three-dimensional, nano-structured PLGA scaffolds for bladder tissue replacement applications. *Biomaterials* 2005;26:2491–2500.
110. Berthiaume F, Moghe PV, Toner M, Yarmush ML. Effect of extracellular matrix topology on cell structure, function, and physiological responsiveness: hepatocytes cultured in a sandwich configuration. *FASEB J* 1996;10:1471–1484.
111. Langer R. Tissue engineering: status and challenges. *E-biomed: J Reg Med* 2000;1: 5–6.
112. Langer R, et al. Tissue Engineering: biomedical applications. *Tissue Eng* 1995;1: 151–162.

Nanostructures for Cancer Diagnostics and Therapy

KUMERASH S. SOPPIMATH and GURU V. BETAGERI

16.1 INTRODUCTION

In 2006, about 564,830 Americans were expected to die of cancer that is more than 1500 people a day. Cancer is the second most common cause of death in the United States, exceeded only by heart disease and accounts for one of every four deaths [1]. According to a worldwide survey published for the year 2001, there were 10.9 million new cases, 6.7 million deaths, and 24.6 million persons alive with cancer (within 3 years of diagnosis). The most commonly diagnosed cancers are lung (1.35 million), breast (1.15 million), and colorectal (1 million); the most common causes of cancer death are lung cancer (1.18 million deaths), stomach cancer (700,000 deaths), and liver cancer (598,000 deaths) [2]. The 5-year relative survival rate for all cancers diagnosed in the United States between year 1995 and 2001 is 65%, up from 50% in 1974–1976. The improvement in survival reflects progress in diagnosing certain kind of cancers at the early stage and the use of new and or improved treatments [1].

16.1.1 Cancer and Early Diagnosis

Despite recent progress in the treatment of cancer, the majority of cases are still diagnosed only after tumors have metastasized, leaving the patient with a grim prognosis. However, there may be an opportunity to drastically reduce the burden of cancer, if the disease can be detected early enough. Nanotechnology is in a unique position to transform cancer diagnostics and to produce a new generation of biosensors and medical imaging techniques with higher sensitivity and precision of recognition [3].

Cancer patients undergo many different types of tests in order to accurately diagnose their disease, determine their prognosis, and monitor their cancer for progression or recurrence. The term “diagnostic test” can be misleading, as these tests are used not only for diagnosing cancer, but also for monitoring cancer progression. There are many reasons for employing diagnostic tests, depending on whether the disease is active or progressing, being treated, or in remission. Diagnostic tests may be used to

- Diagnose primary disease—identify the disease the first time it occurs.
- Identify cancer subtype—some cancers are divided into subtypes that are more or less aggressive; identification of a more aggressive subtype may influence the type of treatment proposed.
- Predict prognosis—test results may indicate chance of cure, based on outcomes of other patients with similar results.
- Direct treatment—cancer is like many different diseases, all of which respond differently to various treatments. A diagnosis that accurately identifies the type of cancer and predicts prognosis will also help to identify the type of treatment that maximizes chance of cure.
- Evaluate response to treatment—some tests show whether the cancer is responding to treatment.
- Detect minimal residual disease—cancer cells that remain after treatment is completed are called MRD. Detection of MRD may indicate a higher likelihood of recurrence.
- Monitor remission or progression—if a cancer is in remission, frequent tests may help to detect the cancer if it returns and/or determine whether it is progressing.
- Screen at-risk individuals—identifying abnormalities in cells or the DNA of cells of asymptomatic (healthy) individuals may indicate an increased risk (although not a certainty) of developing disease.

Pathology tests: Pathology tests involve microscopic evaluation of abnormal cells.

Diagnostic imaging: Diagnostic imaging involves visualization of abnormal masses using high tech machines that create images. Examples of diagnostic imaging include X-rays, computed tomography (CT) scans, positron emission tomography (PET) scans, magnetic resonance imaging (MRI), and combined PET/CT scans.

Blood tests: Blood tests measure substances in the blood that may indicate how advanced the cancer is or other problems related to the cancer.

Tumor markers: Tumor marker tests detect substances in blood, urine, or other tissues that occur in higher than normal levels with certain cancers.

Genomics: Special laboratory evaluation of DNA involves the identification of the genetic makeup, the DNA of the abnormal cells [4].

Detection of cancer at early stages is a critical step in improving cancer treatment. Currently, detection and diagnosis of cancer usually depend on changes in cells and tissues that are detected by a doctor's physical touch or imaging expertise. Instead, scientists would like to make it possible to detect the earliest molecular changes, long before a physical exam or imaging technology is effective. To do this, they need a new set of tools. In order to successfully detect cancer at its earliest stages, scientists must be able to detect molecular changes, even when they occur only in a small percentage of cells. This means the necessary tools must be extremely sensitive. The potential for nanostructures to enter and analyze single cell suggests they could meet this need.

Nanomolecular diagnostics is the use of nanobiotechnology in molecular diagnostics and can be termed nanodiagnostics [3]. Numerous nanodevices and nanosystems for sequencing single molecules of DNA are feasible. Given the inherent nanoscale of receptors, pores, and other functional components of living cells, the detailed monitoring and analysis of these components will be made possible by the development of a new class of nanoscale probes. Because of the small dimension, most of the applications of nanobiotechnology in molecular diagnostics fall under the broad category of biochips/microarrays but are more correctly termed nanochips and nanoarrays. Nanotechnology-on-a-chip is a general description that can be applied to several methods. Some of these do not use nanotechnologies but merely have the capability to analyze nanoliter amounts of fluids. Potential applications in molecular diagnostics are listed in Table 16.1 [5]. In this chapter, we are discussing about some of the successful nanomolecular diagnostics.

16.1.2 Cancer and Chemotherapy

The clinical arsenal in treating cancer has been greatly extended in recent years with application of novel chemotherapy; however, the basic approaches continue to be (in order of success) surgical resection, radiation, and chemotherapy. Chemotherapy is the term broadly employed for the use of pharmaceutical agents that possess cytotoxic or cytotoxic activity. This systemic form of cancer treatment has evolved over more than half a century [6] and is undoubtedly the major weapon against most forms of cancer. It was indeed the accidental observation with the chemical weapon mustard gas that generated the idea that the systemic use of similar alkylating agents could be a potential way to poison cancerous cells [7]. Since the first clinical trials on nitrogen mustard by Gillman, there has been a continuous flow of novel compounds belonging to a variety of subclasses with the sole intent of finding a molecule or combination of molecules that could selectively knock out cancer cells with minimal damage to their normal counterparts.

Although, these agents have been developed keeping in mind the subtle differences between the biology of cancer cells and normal cells, a majority of the existing compounds do not exhibit the level of desirable selectivity. In addition, the probability of developing drug resistance is significantly higher if a single

TABLE 16.1 Nanotechnologies with Potential Applications in Molecular Diagnostics

Nanotechnology on a chip
Microfluidic chips for nanoliter volumes: NanoChip
Optical readout of nanoparticle labels
Nanoarrays
Protein nanoarrays
Nanoparticle technologies
Gold particles
Nanobarcodes
Magnetic nanoparticles: ferrofluids, supramagnetic particles combined with MRI
Quantum dot technology
Nanoparticle probes
Nanopore technology
Measuring length of DNA fragments in a high-throughput manner
DNA fingerprinting
Haplotyping
Cantilever arrays
Multiple combined tests (such as protein and DNA) to be performed on the same disposable chip
Prostate specific antigen binding to antibody
DNA nanomachines for molecular diagnostics
Nanoparticle-based immunoassays
DNA–protein and nanoparticle conjugates
Nanochip-based single-molecular interaction force assays
Resonance light scattering technology
Nanosensors
Living spores as nanodetectors
Nanopore nanosensors
Nanosensor glucose monitor
Optical biosensors: surface plasmon resonance technology
Probes Encapsulated by Biologically Localized Embedding (PEBBLE) nanosensors
Photostimulated luminescence in nanoparticles
Quartz nanobalance DNA sensor
SEnsing of Phage-Triggered Ion Cascade

Reprinted from Jain KK. Nanobiotechnology. Switzerland: Jain PharmaBiotech Publications; 2005, reproduced with permission of the publisher.

agent is used over a period of time [8]. The latter is somewhat circumvented by the routinely employed *combination chemotherapy*, the judicious cocktail of multiple anticancer agents administered simultaneously or sequentially [9].

Anticancer drug therapy is fraught with systemic toxicities, resulting from cytotoxicity to normal cells. Cancer cells share many common features with the

normal host cells from which they originate, so finding unique targets against which anticancer drugs can be selectively directed is difficult. Many anticancer drugs have a marginal selectivity for malignant cells because they target the reproductive apparatus in cells having high proliferation rates. However, anticancer drugs having this mechanism of action result in high toxicities against rapidly dividing normal cells, for example, hair follicles, germ cells, and hematopoietic cells, leading to dose-limiting side effects like mucositis, stomatitis, alopecia, and reproductive effects. The side effects associated with chemotherapy limit the dose or cumulative doses that can be administered to patients, which can lead to relapse of the tumor and often the development of drug resistance. [10].

Pharmacokinetics of anticancer drugs play an important role in determining the quantitative relationship between drug dose, exposure, and drug activity, thereby allowing adjustment of the dose to achieve maximum benefit [11, 12]. Improving the pharmacokinetics may result in enhanced antitumor activity and reduce toxicity (pharmacodynamics). Two important factors influencing the pharmacokinetics of antitumor drugs are route of administration and type of formulation [12]. Most anticancer drugs are administered intravenously (IV) due to its advantages of complete and immediate bioavailability and accurate dosing. However, due to large volumes of distribution and lower specificity, IV route exposes whole body with anticancer drugs to obtain high concentration of these drugs specialized parenteral routes such as intraarterial or intrathecal injection and direct injection to tumor are practiced [12, 13]. However, these routes of administrations have a limitation in accessing remote and deep cancer tissues.

The medical community has sought alternative therapies that improve selective toxicities against cancer cells, that is, therapies that increase efficacy and/or decrease toxicity, resulting in an increase in the therapeutic indices of the anticancer drugs. Hence, various drug carriers are developed for delivery of anticancer drugs and most of these carriers are in nanosize range.

16.1.3 Why Nanotechnology for Treating Cancer?

There are several reasons that nanotechnology could help transform cancer research and clinical approaches to cancer care [14]. Most biological processes, including those processes leading to cancer, occur at the nanoscale. For cancer researchers, the ability of nanoscale devices to easily access the interior of a living cell affords the opportunity for unprecedented gains on both clinical and basic research frontiers.

1. The ability to simultaneously interact with multiple critical proteins and nucleic acids at the molecular level will provide a better understanding of the complex regulatory and signaling patterns that govern the behavior of cells in their normal state as well as the transformation into malignant cells.
2. Nanotechnology provides a platform for integrating research in proteomics—the study of the structure and function of proteins, including the

way they work and interact with each other inside cells—with other scientific investigations into the molecular nature of cancer.

There are many nanotechnologies that are explored for delivery of anticancer drugs and some of the successful tools are explained in this chapter.

16.2 NANOTOOLS FOR EARLY CANCER DETECTION

16.2.1 Quantum Dots

Quantum dots (QDs) are semiconductor nanocrystals or particles, by adjusting their size and composition, QDs can be prepared to emit fluorescent light from the ultra violet (UV) light, through the visible and into the IR spectrum (400–4000 nm). They are composed of an inorganic elemental core (e.g., cadmium, mercury) with a surrounding metal shell [15–18]. QDs possess unique optical properties that not only allow them to be tunable to discreet narrow frequencies but also are an order of magnitude more resistant to photobleaching than their organic fluorophore counterparts [18, 19]. QDs find application in biological science as probes; QDs can absorb and emit light very efficiently allowing sensitive detection relative to conventionally used dyes. QDs have been found to be 10–20 times brighter than organic dyes [18–20]. QDs surface can be coated with hydrophilic polymers and linked with bioaffinity ligands such as monoclonal antibodies, peptides, oligonucleotides, or small molecular inhibitors. Due to higher surface area to volume ratio, QDs can be conjugated to obtain multifunctionality [20].

QDs find application in both *in vitro* and *in vivo* cancer diagnostics. *In vitro* screening of biological fluids for the presence of cancer markers is a commonly used diagnostic test for cancer, as sensitive and a specific test for cancer markers in biological fluids is laborious and time consuming by using conventional methods. Conjugated QDs are not only sensitive but also can detect multiple biomarkers [21]. Gerion et al. reported detection of specific single nucleotide polymorphisms of the human p53 tumor suppression gene using QDs in a microarray assay format and also demonstrated detection of two DNA sequences using two different QDs [22]. Another potential *in vitro* application of QDs is cellular imaging; recently water-soluble QDs for immunofluorescent labeling of cancer cells were successfully reported with very low nonspecific binding [23].

In vivo imaging of tumor tissue by tunable QDs is gaining lot of attention in recent days. QDs can detect multiple markers and increase the possibility of early detection of tumors, which is not possible by using conventional image contrasting agents. Figure 16.1 shows capability of multicolor QDs imaging in live animals [24, 25].

Qdot[®], PLxBeads[®] and BioPixels[®] are the brand names of some of the QDs that are commercially available for *in vitro*–*in vivo* applications. However, clinical success of QDs is impeded by their cytotoxicity. Besides

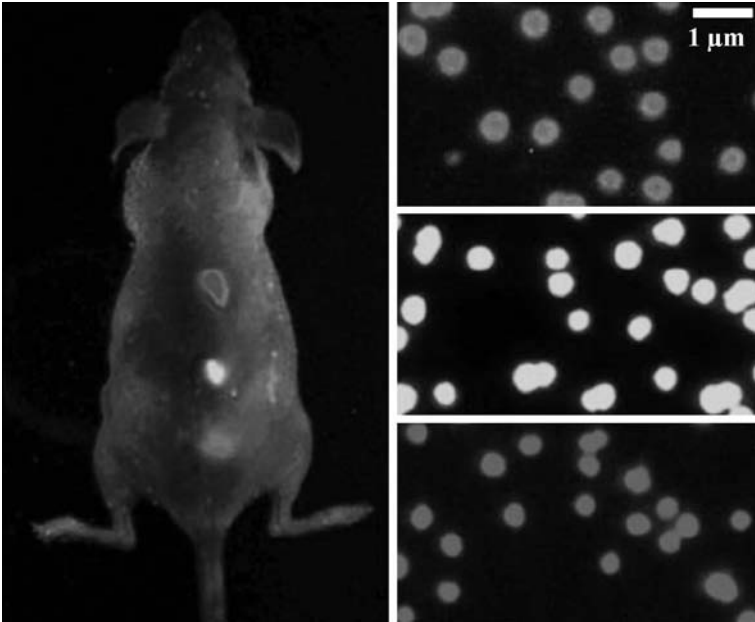


FIGURE 16.1 Multicolor quantum dot (QD) capability of QD imaging in live animals. Approximately one to two million in each color were injected subcutaneously at three adjacent locations on a host animal. Images were obtained with tungsten or mercury lamp excitation. (Reprinted from Reference [25], with permission from Macmillan Publisher Ltd.)

cytotoxicity, the degradation and metabolism of these QDs in the body remains to be investigated and there are reports that injected nanocrystals can accumulate in kidney, liver, and spleen [26]. Whether or not QDs can ultimately be cleared from the body is not known. More research in this area must be completed before they can be used as probes for diagnostic applications. However, advances in surface engineering and conjugation certain to aid in progress of QDs as clinical labels.

16.2.2 Nanoshells

Nanoshells are composed of a dielectric core, usually silica, surrounded by a thin metal shell, typically gold and in the size range of 10–300 nm [27, 28]. Nanoshells rely on the plasmon-mediated conversion of electrical energy into light. Similar to quantum dots, nanoshells have the ability to be tunable optically and have mission/absorption properties that range from the ultraviolet to the infrared [28]. Nanoshells are attractive because of their imaging potential and no heavy metal toxicity unlike QDs. However, large size compared with quantum dots, is the major disadvantage [28]. Polyethylene glycol (PEG)-coated long circulating [29, 30] nanoshells have been used *in vivo* as a contrast agent for imaging with optical

coherence tomography [31] and photoacoustic tomography [32]. Nanoshells also shown to have therapeutic application for cancer therapy by designing to carry antitumor agents and also specifically engineered to act as photoabsorbers with resultant heat generation have powerful potential therapeutic implications for the use in photothermal ablation [33–35]. AuroShellTM is one of the many nanoshells-based product that find application in cancer diagnostics and therapeutics. Human trial for the treatment of head and neck cancers will be commencing soon for this product. These AuroShell particles when injected intravenously and specifically collect in the tumor through enhanced permeation and retention (EPR) effect. After the particles accumulate in a tumor, the area is illuminated with a near-infrared laser at wavelengths chosen to allow the maximum penetration of light through tissue. Unlike solid metals and other materials, AuroShell particles are designed to specifically absorb this wavelength, converting the laser light into heat. This results in the rapid destruction of the tumor along its irregular boundaries [36].

16.2.3 Gold Nanoparticles

Gold nanoparticles (NPs) are one more promising technology to diagnose and treat cancer. The advantage of using gold is that nanoparticles of gold are easy to fabricate and they absorb or scatter light at a desired wavelength [37]. Another advantage of gold Nanoparticles is that gold as a metal is approved by FDA for some therapeutic application and are relatively less toxic than other metals used in constructing QDs. Gold Nanoparticles can be used for both *in vitro* diagnostics and *in vivo* tumor imaging [38–40]. Photoacoustic tomography has been used to image gold nanoparticles to a depth of few centimeters in experiments using gelatin phantoms. Based on this property, photoacoustic tomography may be useful for *in vivo* imaging of gold Nanoparticles [41]. Gold NPs absorb light much stronger than any organic dyes, which makes them a superior agent for tumor cells [42, 43], and with activation of laser, they inactivate cancer cells [44, 45]. Verigene AutoLab is a DNA functionalized gold nanoparticle-based sample-to-result platform technology. The mechanism involved in Verigene System's genomic detection technology is based on using DNA probes that identify a unique oligonucleotide sequence. Nanosphere coats DNA probes onto gold nanoparticles to create highly selective and sensitive nanoparticle probes. When the probes are combined with a sample, they target and bind only with the complementary genetic construct. The instrument is currently undergoing feasibility assessments and will soon be available for early detection of cancer [46].

16.2.4 Paramagnetic Nanoparticles

Magnetic nanoparticles are new generation MRI and CT imaging agents for cancer diagnostics. These particles are attractive because they have much greater magnetic susceptibility than traditional MR contrast agents, such as gadolinium. Gold Nanoparticles are gaining interest as lymphotropic

TABLE 16.2 Nanotechnology-Based Diagnostics for Early Detection of Cancer

Product	Technology	Application	Status	Company
Qdot	Quantum dots		In market	Invitrogen
Biopixel	Quantum dots	Cell assay detection	In market	Biocrystals
Plxbead	Quantum dots	Cancer diagnostics	In market	Crystalplex
Verigene	DNA functionalized Gold nanoparticles	Cancer diagnostics	In market	Nanosphere
Ferumoxtran-10	Iron oxide nanoparticles	Diagnostics of lymph cancer	In market	Advanced magnetics
Qdot 800	Near IR conjugated QDs	Lymph node mapping of colon, lung, and uterine cancer	Preclinical	Quantum dot

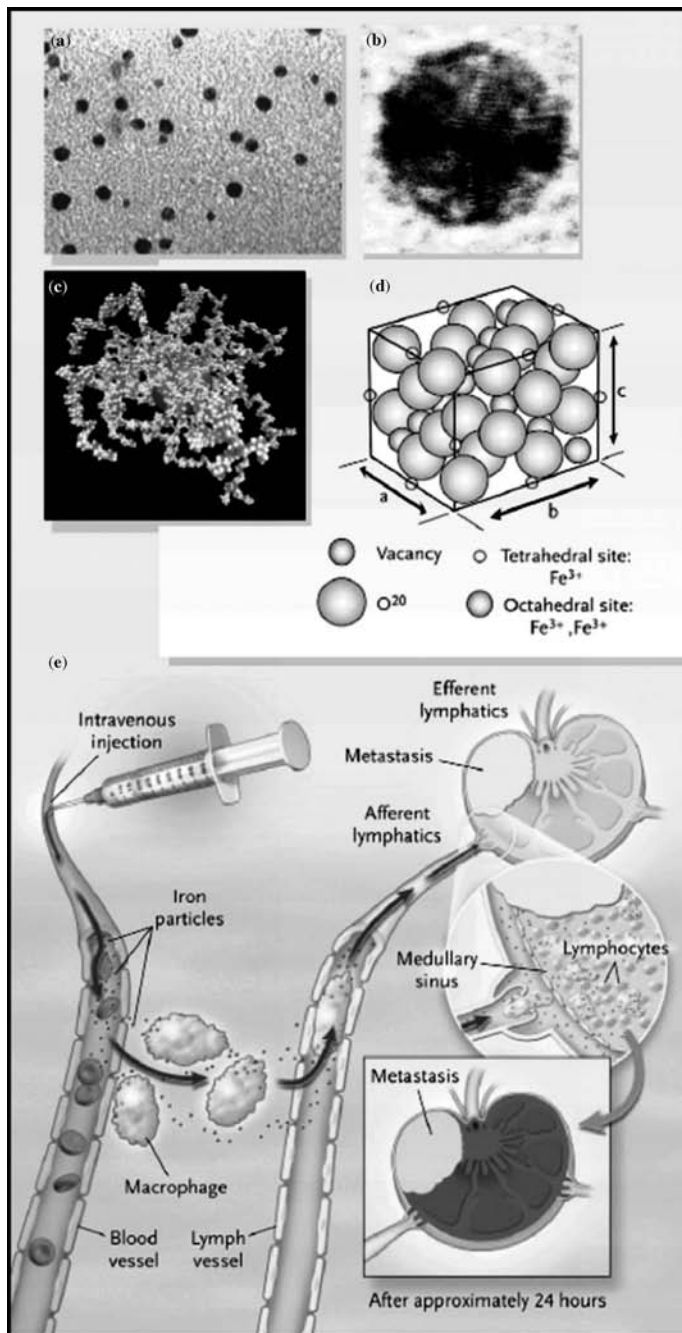
nanoparticles, which are a relatively new class of MR contrast agents with unique properties allowing them to be used in a wide variety of clinical applications [47]. Originally developed and tried for liver imaging, it became apparent that these nanosize supramagnetic iron oxide particles were small enough in size to migrate across the capillary walls and localize within lymph nodes allowing robust characterization of nodes independent of the size criterion. The mechanism of these Nanoparticles is illustrated in Fig. 16.2 [48–51]. Hence, they have emerged as a promising new technique for noninvasive nodal evaluation in patients undergoing staging for various malignancies [51, 52]. Magnetic nanoparticle technology is most successful among all other nanotechnologies in cancer diagnostics in bringing the product to market (ferumoxtran-10, AMI-227, Combidx[®]; by Advanced Magnetics Inc., and Sinerem[®], by Laboratoire Guerbet).

These nanotechnologies will extend the limits of current molecular diagnostics. Some of the potential diagnostics based on nanotechnology are listed in Table 16.2. The list will tend to grow very quickly as many products based on nanotechnologies are in pipeline. Combination of nanodiagnostics and nanotherapeutics will revolutionize diagnostics and treatment of cancer therapy.

16.3 NANOMEDICINE FOR CANCER TREATMENT

16.3.1 Liposomes

Since the pioneering observation of Alec Bangham roughly 40 years ago, that phospholipids in aqueous systems can form closed bilayered structures, liposomes have moved a long way from being just another exotic object of biophysical research to become a pharmaceutical carrier of choice for numerous practical applications. The use of liposomes as drug carriers for chemotherapeutic agents was proposed originally by Gregoriadis in 1981 [53]. Early studies, however, demonstrated rapid recognition and removal of liposomes from the circulation by the reticuloendothelial system (RES) [54, 55].



Other limitation of early liposomal formulations was premature leakage of the encapsulated drug and difficulty in extravasation of liposome from blood circulation into tumor interstitial fluid [56, 57].

However, various breakthrough developments in the area during the past 15 years have resulted in the approval of several liposomal drugs, and the appearance of many unique biomedical products and technologies involving liposomes. The whole process of development of liposomes from bench to product involved interdisciplinary research efforts both from academia and industry. These Herculean efforts lead to better understanding of some of the following critical aspects of nanosize carriers:

1. Design, manufacturing, and characterization of nanocarrier systems
2. Pharmacokinetics of nanocarriers
3. Mechanism of drug targeting Ex. passive targeting of liposomes in tumor tissue by enhanced permeation and retention

Liposomes are the first nanotechnology-based products that are approved for therapeutic application, and they are also the first nanopharmaceuticals for cancer chemotherapy. Topic of liposome and its application in biomedical field is broad and multidisciplinary. In this chapter, we are concentrating on application of liposomes in cancer chemotherapy and mainly on the products that have reached the market and those that have shown promising results in their clinical studies.

16.3.1.1 Long-Circulating Liposomes

Different methods have been suggested to achieve long circulation of liposomes *in vivo*, including coating the liposome surface with inert, biocompatible polymers. A major breakthrough in prolonging circulation time was the coating of liposomes with PEG, which form a protective layer over the liposome surface and slow down liposome recognition by opsonins and, therefore, subsequent clearance of liposomes from systemic circulation [58, 59]. Long-circulating liposomes are now being investigated in detail and are widely used in biomedical *in vitro* and *in vivo* studies; they have also found their way into clinical practice



FIGURE 16.2 Electron micrograph of hexagonal lymphotropic supramagnetic nanoparticles (panels (a) and (b)), molecular model of surface-bound 10 kD dextrans and packing of iron oxide crystals (panels (c) and (d)), and mechanism of action of lymphotropic supramagnetic nanoparticles (panel (e)). The model lymphotropic supramagnetic nanoparticles shown here measure 2–3 nm on average (panels (a) and (b)). The mean overall particle size of the 10 kD dextrans is 28 nm (panels (c) and (d)). In panel (e), the systemically injected long circulating particles gain access to the interstitium and are drained through lymphatic vessels. Disturbances in lymph flow or in nodal architecture caused by metastases lead to abnormal patterns of accumulation of lymphotropic supramagnetic nanoparticles, which are detectable by MRI (Reprinted with permission from Reference [51]).

[60]. These PEG-coated liposomes are referred as sterically stabilized or Stealth[®] liposomes. Stealth technology resulted in first commercial formulation based on liposome loaded with doxorubicin (Anticancer drug) known as Doxil, which was approved by FDA in year 1995.

Pharmacokinetics of drug encapsulated in liposomes depends upon following variables [61]:

1. The composition of lipid bilayer
2. Size of the liposomes
3. Nature of the drug
4. Nature of the interaction between the drug and the lipid

These variable influence liposome clearance and three main pathway are proposed as follows:

1. Uptake of liposomes from the circulation by RES of liver, spleen followed by metabolism, and excretion of the drug.
2. Leakage or release of the drug followed by tissue distribution and elimination of the free drug.
3. Accumulation of liposome-encapsulated drug in tissue with increased microvascular permeability other than RES, including tumor.

16.3.1.2 Size and Tumor Delivery

Particle size of the liposomes decides their fate in body, study showed that liposomes <200 nm can escape physical screening by liver. However, to facilitate delivery to tumors, liposomes require a diameter small enough to allow extravasation into malignant tissue through highly permeable tumor blood vessels [62, 63]. The cut-off size for particle extravasation based on the size of fenestrated liver sinusoids is <150 nm. However, one study of tumor xenografts, using the mouse skin fold chamber model, suggests that liposomes up to 400 nm diameter can extravasate across the tumor microvessels [64]. The overall conclusion from a large number of liposome pharmacological studies is that the smaller the vesicles, the better the chance of preventing nonspecific uptake by RES system.

16.3.1.3 Doxil

Doxorubicin hydrochloride (C₂₇H₂₉NO₁₁ HCl, molecular weight 579.99) is an established cytotoxicity anthracycline antibiotic obtained from *Streptomyces peucetius* var. *caesius*. Doxorubicin has shown a dose-dependent cardiotoxicity; a 7.5 % incidence of clinical cardiomyopathy was recorded at cumulative doxorubicin doses of 550 mg/m² [65]. This incidence rises to 20 % when careful prospective observations are made, including serial determinations of left ventricular ejection fractions, and close clinical follow-up [66]. These

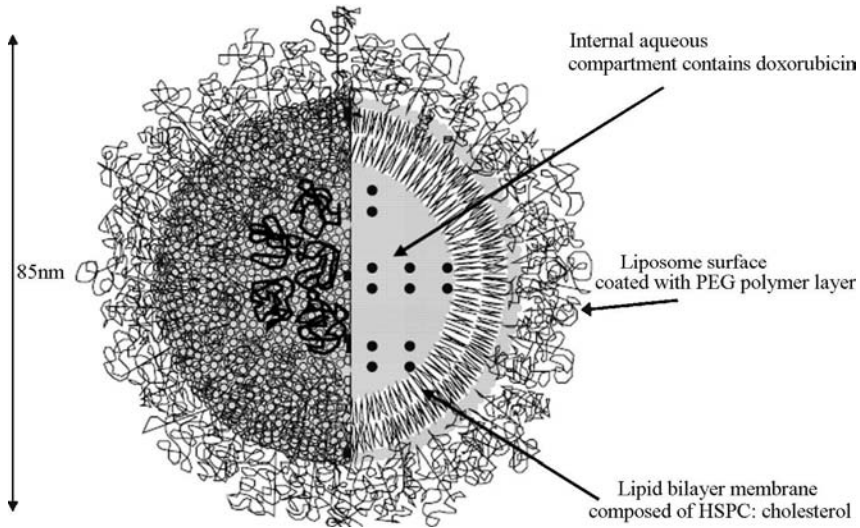


FIGURE 16.3 Dox loaded liposome. A single lipid bilayer membrane composed of hydrogenated soy phosphatidylcholine (HSPC) separates an internal aqueous compartment from the external medium. Doxorubicin is encapsulated in the internal compartment. Drug molecules are tightly packed (10,000–15,000 molecules per liposome) in a gel phase. Polymer groups (linear 2000 Da segments) of polyethylene glycol (PEG) are engrafted onto the liposome surface and form a protective hydrophilic layer providing stability to the vesicle. The mean diameter of the liposome is approximately 85 nm.

observations have led to setting cumulative dose limitations, generally 450–500 mg/m², for treatments employing free doxorubicin given by bolus every 3 weeks. Doxorubicin, on a weekly schedule [66] or prolonged infusions [67], allows exceeding these limits to a variable degree. By encapsulating doxorubicin HCl in liposomes drastically changed its pharmacokinetics, and FDA approved this formulation in year 1995 with brand name Doxil.

Doxil consists of a liquid suspension of single lamellar vesicles with an approximate mean size in the range of 80–90 nm loaded with doxorubicin HCl, schematics of liposome structure is shown in Fig. 16.3. The total lipid content of Doxil is approximately 16 mg/ml and the doxorubicin concentration is 2 mg/ml. There are three lipid components in Doxil: hydrogenated soy phosphatidylcholine (HSPC; T_m 52.5 °C), cholesterol, dis-stearoylphosphatidylethanolamine (DSPE) conjugated to PEG (*N*-carbamoylmethoxypolyethylene glycol 12000 1,2-distearoyl-*sn*-glycerol-3-phosphoethanolamine sodium salt) in a molar percentage ratio of 56:38:5 [68].

Phosphatidylcholine, cholesterol, and phosphatidylethanolamine are dietary lipids and normal components of the cellular plasma membrane. The ratio of HSPC and cholesterol used provides a rigid bilayer at 37 °C and below, promoting drug retention. DSPE is incorporated into the bilayer of the liposomes and provides a stable anchor for the hydrophilic PEG chains

(molecular weight 2000, 45 mers) covalently bound to the ethanolamine head of DSPE and extending into the inner and outer water phase. An efficient drug loading method was established where in doxorubicin HCl was loaded into liposomes by ammonium sulfate gradients that was achieved by incubating liposome preloaded with ammonium sulfate in presence of drug solution. Most of the drug (>90%) loaded was in the form of sulfate salt that is gel-like precipitate. Formation of salt not only helps increasing the encapsulation efficiency of drug loading but also prevents premature drug leakage [69–71].

Pharmacokinetics of Doxil The pharmacokinetics and mechanism of drug delivery to tumors of Doxil and other Stealth liposome preparations are drastically different from conventional chemotherapy [72]. There was a 1000-fold increase in the area under the plasma concentration-time curve (AUC) and a significant decrease in clearance and distribution in case of encapsulated drug. Half-life of drug was also increased remarkably, that is, to 60–80 h (see Table 16.3 for details). The long circulation time and stable drug retention of Doxil [73] is a key factor in enabling liposomes to reach the capillary bed of tissues with sluggish circulation as often is the case of tumors and other not well-stirred compartments [68]. Because, Stealth liposomes are very stable in plasma, most of the administered dose reaches tissues in liposome-encapsulated form with only minimal amounts of drug (5 %) leaking from liposomes during circulation and distributed to tissues as free drug [73]. It was also shown that when breast carcinoma patients were treated with Doxil, the drug concentration in the tumor tissue was approximately 10-fold greater than in the adjacent muscles [74], suggesting an enhancement of drug delivery to these tumors in line with extensive preclinical data [75]. Unfortunately, Stealth liposomes do also accumulate in large amounts in various healthy and susceptible tissues such as skin [76] and probably mucosa, accounting for the unique toxicity profile of Doxil. As a result, the maximal tolerated dose (MTD) of Doxil is actually lower than that of conventionally administered doxorubicin [77], whereas data from various clinical studies [77–79] suggest that the maximal cumulative dose of Doxil is substantially greater than that of free doxorubicin.

TABLE 16.3 Pharmacokinetics of Doxil and Free Doxorubicin [62, 74, 83, 85]

Pharmacokinetic parameter	Free doxorubicin	Doxil
AUC (mg h/l)	3.5	2325–4082
C_{\max} (mg/l)	5.9	21–33
Cl (ml/h)	25300	23–45
V_{ss} (l)	365	3–5
$T_{1/2}$ (h)	0.06/10.4 a	62–89

Free doxorubicin was administered at doses ranging from 50 mg/m² (slow infusion) and liposomal doxorubicin was administered at doses ranging from 60 mg/m² (slow infusion). Abbreviations: AUC = the area under the plasma concentration-time curve, C_{\max} = maximum measured concentration, $t_{1/2}$ = elimination half-life, Cl = total body clearance, V_{ss} = volume of distribution at study state, a = elimination phase.

Pharmacodynamics of Doxil Doxil is presently approved for the treatment of patients with ovarian cancer whose disease has progressed or recurred after platinum-based chemotherapy. Doxil is also indicated for the treatment of acquired immunodeficiency disease (AIDS)-related Kaposi's sarcoma in patients with disease that has progressed on prior combination chemotherapy or in patients who are intolerant to such therapy. More than three hundred clinical studies are under way for exploring possible application of Doxil either alone or in combination with other drugs for treating various cancers [80].

Liposomal doxorubicin in an early study in patients with AIDS-related Kaposi's sarcoma showed that pharmacokinetics of Doxil were best described by a two-compartment linear structural model. Lesion response was significantly related to both the average daily maximum doxorubicin concentration ($C_{\max, \text{avg}}$) and dose intensity [81]. Correlation analysis of dose and pharmacokinetic parameters with Doxil toxicities revealed that there was a decrease in the toxicity with improved antitumor activity, which was correlated significantly with $t_{1/2}$ in case of breast cancer patients [82]. Doxil showed a considerably lesser risk of cardiomyopathy than is generally associated with free doxorubicin when 500 mg/m² or more cumulative doses of Doxil were administered in patients in advanced solid tumors [83]. However, pegylated liposomal doxorubicin is associated with skin toxicity, referred to as plantar–palmar erythrodysesthesia or hand–foot syndrome, indistinguishable from that which is classically associated with infusional doxorubicin. The skin toxicity of pegylated liposomal doxorubicin is cumulative, and appears to be dose interval dependent [84]. Success story of Doxil not only encouraged researchers to engineer various liposomal systems but also other Nanocarrier for cancer therapy.

16.3.1.4 *Stealth Cisplatin Liposomes*

Cisplatin is one of the most widely used chemotherapeutic agents employed today in the clinical practice of human and veterinary oncology. It has a broad spectrum of activity and in particular is the cornerstone of adjuvant systemic therapy for osteosarcoma [85]. Its use is ultimately limited by dose-dependent toxicities, in particular nephrotoxicity [86]. Several strategies have been employed to abrogate or avoid the nephrotoxicity of cisplatin, including the development of less toxic and/or more efficacious platinum analogs, concurrent use of nephroprotective agents, and the use of time-consuming hydration protocols [85–87]. Another approach is to encapsulate cisplatin in liposomes in order to beneficially alter the toxicity profile, pharmacokinetics, and biodistribution [88, 89].

SPI-77 is a Stealth liposomal formulation of cisplatin, formulated in liposomes that contain a pegylated lipid [*N*-(carbamoyl-methoxypolyethylene glycol 2000)-1,2-distearoyl-*sn*-glycero-3-phosphoethanolamine sodium salt, MPEG-DSPE], another phospholipid (hydrogenated soy phosphatidylcholine, HSPC), and cholesterol. The total lipid content of the SPI-77 formulation is approximately 71 mg/ml, and the cisplatin concentration is 1 mg/ml with 110 nm in diameter [90]. Initial results of phase I clinical trial showed that the

pharmacokinetic behavior of capsulation is significantly altered by its encapsulation in Stealth liposomes. The pharmacokinetics of SPI-77 is mainly dominated by the liposomal properties, resulting in high cholesterol concentrations and relatively low concentrations of (free) platinum in plasma, white blood cells (WBC), and tumor tissue [91]. The lack of encouraging results from SPI-77 use in phase I and II clinical studies resulted in early closure of this trial by the manufacturer [92].

16.3.1.5 Vincristine Sphingomyelin Liposomes

Vinca alkaloid vincristine has significant activity against lymphomas and acute lymphocytic leukemia [93]. The dose intensity and delivery of conventional vincristine is limited by the disruption of axonal microtubules after vincristine binds to neuronal tubulin. This results in significant neurotoxicity at doses higher than the “capped” dose of 2.0 mg [94]. In most experimental models, the resistance of leukemia cells to vincristine is associated with decreased drug accumulation and retention; a phenomenon usually associated with the cellular expression of P-glycoprotein and the multidrug resistance (MDR) phenotype [95]. The pharmacokinetics of conventional vincristine given by bolus infusion is characterized by large interpatient and inpatient variations in drug clearance, volume of distribution, and elimination half-life [96–98].

To improve the pharmacokinetics of vincristine, it was encapsulated into sphingomyelin liposomes comprised sphingomyelin and cholesterol, and these liposomes are often called as “sphingosomes” [99]. Pharmacokinetic studies in animals demonstrated that sphingosomes administered intravenously had a significantly longer $t_{1/2}$ (approximately 12-fold longer) than conventional vincristine, which was attributed to the protection afforded by the liposome in abrogating the rapid initial elimination phase. A reduction in neurotoxicity compared with conventional vincristine was attributed to lower systemic levels of free vincristine with sphingosomes [100] and reduced dermatologic toxicity [101]. Increased plasma circulation of vincristine resulted in preferential accumulation of liposomal drug in tissues with permeable vasculature including tumor [102]. Same technology was used to deliver vinorelbine (VRL) and is a particularly lipophilic member of the vinca alkaloids. VRL was efficiently encapsulated (>90 %) into 100 nm liposomes using an ionophore-mediated loading method. The stability of the formulation was excellent (<5 % drug leakage, >99 % intact VRL, no changes in liposome size after 1 year at 2–8 °C). After successful preclinical studies, now phase I clinical study is underway [103].

16.3.1.6 Sustained Release Liposomes

Liposomes are also find application as sustained release delivery systems for anticancer drugs. DepoCyt[®] is first sustained-release injectable product to reach the market. DepoCyt features a sustained-release injectable technology

DepoFoamTM of Sky Pharma and is a treatment for lymphomatous meningitis, a complication of late-stage lymphoma. Lymphomatous meningitis can be controlled with cytarabine, but the drug's short half-life (plasma elimination half-life of = 7–20 min) requires a spinal injection every other day, distressing for the patient and incurring high nursing costs. DepoCyt cuts the injection frequency to every second week, allowing treatment on an outpatient. DepoCyt was introduced in the United States in 1999. DepoCyt consist of spherical particles composed of numerous nonconcentric internal aqueous chambers containing the encapsulated drug. Each chamber is separated from adjacent chambers by bilayer lipid membranes composed of synthetic analogs of naturally occurring lipids (dioleoyl phosphatidylcholine, dipalmitoyl phosphatidylglycerol, cholesterol, triolein) [104]. Studies have shown that, compared with unencapsulated cytarabine, intrathecal administration of DepoCyt provides a significant pharmacokinetic advantage that maximizes the therapeutic potential of cell cycle S-phase-specific cytotoxicity agents. In addition, the prolonged CSF $t_{1/2}$ of cytarabine provided by this novel formulation may permit less frequent dosing, which is particularly convenient for intrathecal administration [104, 105].

16.3.1.7 Liposome Vaccine

Known vaccines typically utilize either purified antigen or attenuated pathogen as the immunogen. However, attenuated vaccines can actually cause the infection against which a person is being immunized. On the contrary, purified antigens may not induce a long term immune response and sometimes induce no response at all. In contrast to the short-term immune response obtained by direct immunization with certain antigens, presentation of the antigen in the presence of liposomes can induce a long term response that is essential for any effective vaccine. Various studies showed that liposomes might also be formed, at least in part, from cell membranes of malignant cells that contain potential antigens. Due to the presence of membrane-associated antigens, these membrane-derived preparations may be used as malignancy-specific vaccines. Indeed, some types of membrane-derived preparations have been used as tumor-specific antigens to treat melanomas and murine SL2 lymphosarcoma [106–108].

In a study, a synthetic human MUC1 peptides (25 amino acid sequence) known as BLP 25 was studied for their therapeutic application as cancer vaccines. It was shown to render immunogenic by incorporation in liposomes, the effects of physical association of the peptide with liposomes on immune responses were investigated. Lipid conjugated and nonconjugated MUC1 peptides were incorporated in liposomes with a composition of distearoylphosphatidylcholine, cholesterol, dimyristoylphosphatidylglycerol (3:1:0.25, molar ratio) containing monophosphoryl lipid A (1% w/w of the total lipids). C57BL/6 mice were immunized with lipopeptide alone, peptide mixed with peptide-free liposomes, and peptide associated with liposomes in entrapped or

surface exposed forms. Results showed that immune responses were profoundly influenced by the liposome formulations. Physically associated, either encapsulated or surface exposed, peptide liposomes elicited strong antigen-specific T-cell responses, but not lipopeptide alone or peptide mixed with peptide-free liposomes. Thus, physical association of the peptide with liposomes was required for T-cell proliferative responses, but the mode of association was not critical. On the contrary, the nature of the association significantly affected humoral immune responses. Only the surface-exposed peptide liposomes induced MUC1-specific antibodies. These results support the hypothesis that different immune pathways are stimulated by different liposome formulations. This study demonstrated that a liposome delivery system could be tailored to induce either a preferential cellular or humoral immune response [109, 110].

Biomira, Inc., a Canadian-based company, is developing BLP25 liposome (L-BLP25) vaccine in collaboration with Merck KGaA, and the product is known as Stimuvax[®] for treating advanced-stage non-small cell lung cancer and prostate cancer. Results of phase IIa study demonstrate that L-BLP25 vaccine has the potential to extend the survival of patients with stage IIIB locoregional non-small cell lung cancer and maintain longer quality of life. L-BLP25 vaccine also shows promise for prostate cancer patients, having the potential to prolong prostate-specific antigen doubling time in men with biochemical failure postprostatectomy. These clinically meaningful results with a relatively nontoxic therapeutic vaccine are very encouraging and suggest potential for L-BLP25 to fulfill an unmet medical need [111–113].

16.3.1.8 Liposomes as Solubilizing Carrier for Water Insoluble Anticancer Drugs

Liposomes can be ideal delivery of water insoluble drugs by intravenous route of administration, by enhancing the physical and biological stabilities of the drug. One such example is liposomal annamycin. Annamycin is an anthracycline antibiotic that was selected for use for its lack of cross-resistant properties and a very high affinity for lipid membranes, making it an ideal compound for use in the liposome carrier. The drug is completely insoluble in water solution; therefore liposomes can be used as a carrier for its intravenous administration. The fundamental mechanism of action of annamycin appears to be inhibition of topoisomerase-II. Liposomal annamycin (L-annamycin) was developed to combine the intrinsic favorable properties of the compound (lack of cross-resistance) with the potential advantages associated with liposome delivery (reduced cardiotoxicity and preferential distribution to certain organs) [114]. A freeze dried prliposomal formulation shown to increase entrapment efficiency, physical stability, and chemical stability of the molecules [115]. Both in preclinical and clinical studies liposomes shown to enhance the *in vivo* antitumor properties of annamycin, and small liposomes are more effective than large liposomes and drug suspension in enhancing annamycin antitumor activity [116].

16.4 POLYMERIC NANOPARTICLES

With the experience of development of liposomal delivery systems and syntheses of various polymers over the past few decades, there has been considerable interest in developing biodegradable nanoparticles as effective drug delivery devices for cancer therapy. Many natural and synthetic polymers can be used to engineer nanocarriers for anticancer drugs of various physicochemical properties [117]. Few of these systems were successful in reaching the market and many of them are in various stages of clinical trials.

16.4.1 Albumin Nanoparticles

Paclitaxel is a chemotherapeutic agent with a wide spectrum of antitumor activity when used as monotherapy or in combination with chemotherapy regimens [118]. The drug is used extensively in the treatment of advanced carcinomas of the breast, ovary, head and neck, and lung. But taxanes cause serious side effects, including low white blood cell counts (neutropenia), weakness, and infection. They also cause extreme skin sensitivity, which can make them difficult to take [119–122].

The paclitaxel preparation in clinical use (Taxol[®]; Bristol-Myers Squibb, Princeton, NJ) is formulated in the nonionic surfactant Cremophor EL (polyoxyethylated castor oil) and ethanol to enhance drug solubility [123]. Cremophor EL may add to paclitaxel's toxic effects by producing or contributing to the well-described hypersensitivity reactions that commonly occur during infusion, affecting 25–30 % of treated patients [124,125].

To circumvent the toxic effect of Cremophore EL, many formulations were attempted for paclitaxel, one of the successful ones is albumin nanoparticle formulations of paclitaxel, nanoparticles of paclitaxel were formed by using cavitation and high shear forces during a sonication process. Thus, paclitaxel is dissolved in methylene chloride. The solution is added to human serum albumin solution. The mixture is homogenized in order to form a crude emulsion, and then sonicated. The mixture is transferred into a rotary evaporator, and methylene chloride is rapidly removed. The typical diameter of the resulting paclitaxel particles was 350–420 nm, which is complexed with albumin due to the negative zeta potential imparted by the albumin moiety particles are stable (Fig. 16.4). The dispersion was further lyophilized. The resulting cake could be easily reconstituted to the original dispersion by addition of sterile water or saline [126].

This paclitaxel formulation can be administered rapidly and safely without the risk of hypersensitivity reactions, eliminating the need for steroid and antihistamine premedication. Furthermore, the increased MTD and favorable toxicity profile of paclitaxel may ultimately prove advantageous in terms of rate and quality of response [127–129]. In January 2005, the U.S. FDA approved this formulation with the brand name Abraxane, the approval is for

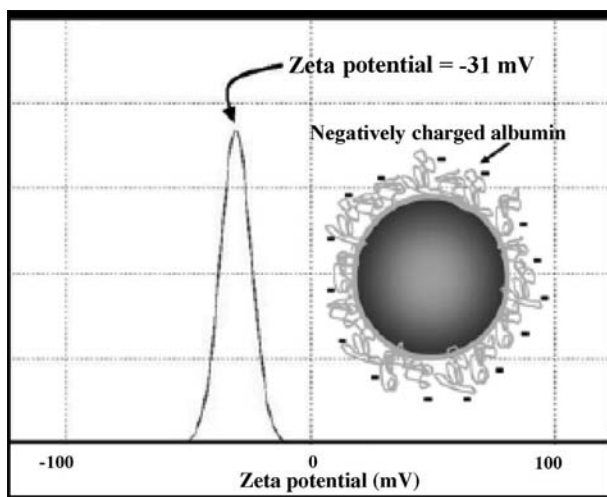


FIGURE 16.4 Diagram to show particle size distribution and albumin coated paclitaxel particles along with zeta potential.

secondline therapy—after another chemotherapy regimen has been used and stopped working.

16.4.2 Micellar Nanoparticles

Ampiphilic polymers are found to self-assemble to form polymeric micelle in aqueous environment and can encapsulate water insoluble drugs in their core. Polymeric micelles are stable compared to conventional surfactant micelle due to their lower critical micellar concentration [130]. A schematic of encapsulation of drugs in micellar nanoparticles is shown in Fig. 16.5. Micellar nanoparticles

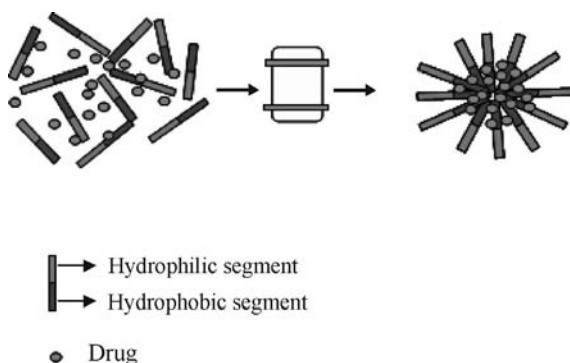


FIGURE 16.5 Schematics showing self assembly of polymeric micellar nanoparticles loaded with drug by dialysis method.

formed by self-assembly of biodegradable diblock copolymer composed of methoxy poly(ethylene glycol)-poly (lactide) [mPEG-PLA]. Particle size of these particles is in the range of 20–200 nm [131].

Compared with the Taxol, preclinical studies demonstrated that the polymeric micelle-formulated paclitaxel displayed a threefold increase in the MTD and a significantly increased antitumor efficacy [132]. In phase I clinical study, the formulation was found to be nontoxic at dosages up to 300 mg/m². However, at the MTD of 390 mg/m², a variety of dose-related toxicities were observed, which included neuropathy, myalgia, and neutropenia. Phase II studies with this formulation are currently underway for patients with advanced breast and non-small cell lung cancers [133]. Another promising micellar formulation is nanoparticles produced by block copolymers of

TABLE 16.4 Nanotechnology Based Pharmaceuticals for Treating Cancer

Drug	Product name	Application	Status	Company
Liposome				
Daunorubicin	DaunoXome	Kaposi's sarcoma	In market	Gilead Sciences
Doxorubicin	Doxil	Ovarian, recurrent breast cancer	In market	ALZA
Cytarabine	DepoCyt	Lymphomatous meningitis	In market	SkyePharma
Liposome Vaccine	BLP25	Non-small cell lung cancer	Phase III	Biomira Inc
Vincristine	Marqibo	Non-Hodgkin's lymphoma	Phase II	Inex Pharmaceuticals
Lurtotecan	NX211	Ovarian cancer	Phase II	Gilead Sciences
Irinotecan HCl and floxuridine	CombiPlex	Advanced colorectal carcinoma	Phase II	Celator Pharmaceuticals
TLK199 HCl	Telintra	Myelodysplastic syndrome	Phase II	Telik
Annamycin	–	lymphocytic leukemia	Phase II	Callisto Pharmaceuticals
Vinorelbine	–	Solid tumors	Phase I	Hana Biosciences
Oxaliplatin	MBP-426	Metastatic solid tumors	Phase I	Mebiopharm
Irinotecan	IHL-305	Solid tumor	Phase I	Yakult Honsha
Doxorubicin	ThermoDox	Breast and liver cancer	Phase I	Celsion
Polymeric Nanoparticles				
Paxlitaxel	Abraxane	Cancer treatment	In Market	Abraxis BioScience
Paclitaxel	Genexol	Non-small cell lung cancer	phase II	Samyang
Cisplatin	Nanoplatin	Treat wide range of cancer	Phase I	NanoCarrier

(polyethylene glycol) and a hydrophobic polymer (polyamino acid derivative) loaded with cisplatin. The formulation has size of approximately 30 nm, with a narrow size distribution and preserved the antitumor activity of cisplatin. Preclinical studies showed a reduced nephrotoxicity and neurotoxicity of cisplatin, which would therefore seem to suggest that encapsulation of cisplatin could allow the long term administration with low toxicity [134].

Liposomes and polymeric nanoparticles are two successful drug delivery systems till date; Table 16.4 enlists some of the important products based on these technologies. Other technologies are also under early stage of development.

16.5 CONCLUSIONS

The integration of nanotechnology into cancer diagnostics and therapeutics is a rapidly advancing field, and there is a need for wide understanding of these emerging concepts. The development of new nanoscale platforms offers great potential for improvements in the care of cancer patients in the near future. Eventhough *in vitro* nanodiagnostics has seen many successes, it is going to be a long road for *in vivo* diagnostics due to their possible systemic toxicity. Extensive research activities are under progress to deliver drugs with high precision by using various drug active targeting techniques, and these product are going to make a greatest clinical impact for cancer therapy. Because nanotechnology is a rapidly progressing field, future advances in nanotechnology research and development likely will be associated with the further development of novel, highimpact approaches to cancer diagnosis and treatment.

REFERENCES

1. Cancer facts and figures. 2006. Available at <http://www.cancer.org/downloads/STT/CAFF2006PWSecured.pdf>.
2. Parkin MD, Bray F, Ferlay J, Pisani P. Global cancer statistics, 2002. *CA Cancer J Clin* 2005;55:74–108.
3. Jain KK. Nanodiagnostics: application of nanotechnology in molecular diagnostics. *Expert Rev Mol Design* 2003;3:153–61.
4. Available at <http://www.ufscc.ufl.edu/Patient/content.aspx?section=testingid=31382>.
5. Jain KK. Nanotechnology in clinical laboratory diagnostics. *Clin Chim Acta* 2005;358:37–54.
6. Griswold DP Jr, Harrison SD Jr. *Cancer Metastasis Rev* 1991;10:255–261.
7. Workman P, Lewis AD, Caaseate F. Alkylating agents and related drugs. In: Peckham M, Pinedo HM, Veronesi U, editors. *Oxford Textbook of Oncology*. Volume 1. Oxford: Oxford University Press; 1995. p495–504.
8. Moscow JA and Cowan KH. Multidrug resistance. *J Natl Cancer Inst* 1988;80:14–20.

9. Shazib P. Anti-cancer drugs of today and tomorrow: are we close to making the turn from treating to curing cancer? *Curr Pharm Design* 2002;8:1723–1734.
10. Northfelt DW, et al. Doxorubicin encapsulated in liposomes containing surface-bound polyethylene glycol: pharmacokinetics, tumor localization, and safety in patients with AIDS-related Kaposi's sarcoma. *J Clin Pharmacol* 1996;36:55–63.
11. Katzung BG, Section I: basic principles In: Katzung BG, editor. *Basic and Clinical Pharmacology*. East Norwalk: Prentice-Hall international, Inc.; 1992. p4–5.
12. Terwogt MMM, Schellens JHM, ten Bokkel Huinink WW, Beijnen JH. Clinical pharmacology of anticancer agents in relation to formulation and administration routes. *Cancer Treat Rev* 1999;25:83–101.
13. Cavalheiro S. Use of interferon alpha in intratumoral chemotherapy for cystic craniopharyngioma. *Childs Nerv Syst* 2005;21:719–24.
14. Available at http://nano.cancer.gov/about_alliance/q-and-a.asp#3 (visited 09/20/06).
15. Bruchez M Jr, Moronne M, Gin P, Weiss S, Alivisatos AP. Semiconductor nanocrystals as fluorescent biological labels. *Science* 1998;281:2013–2016.
16. Seydel C. Quantum dots get wet. *Science* 2003;300:80–81.
17. Kim S, Fisher B, Elisler HJ, Bawendi M. Type II quantum dots: CdTe/CdSe (core/shell) and CdTe/ZnTe(core/shell) heterostructures. *J Am Chem Soc* 2003;125:11466–11467.
18. Andrew MS, Shivang D, Shuming N, Lawrence T, Xiaohu G. Multicolor quantum dots for molecular diagnostics of cancer. *Expert Rev Mol Diagn* 2006;6:231–244.
19. Qu L and Peng X. Control of photoluminescence properties of CdSe nanocrystals in growth. *J Am Chem Soc* 2002;124:2049–2055.
20. Bruchez M, Moronne M, Gin P, Weiss S, Alivisatos AP. Semiconductor nanocrystals as fluorescent biological labels. *Science* 1998;281:2013–2016.
21. Han My GX, Su JZ, Nie S. Quantum-dot-tagged microbeads for multiplexed optical coding of biomolecules. *Nat Biotechnol* 2001;19:631–635.
22. Gerion D, et al. Room-temperature single-nucleotide polymorphism and multi-allele DNA detection using fluorescent nanocrystals and microarrays. *Anal Chem* 2003;75:4766–4772.
23. Li Z, et al. Immuno-fluorescent labeling of cancer cells with quantum dots synthesized in aqueous solution. *Anal Biochem* 2006;354:169–174.
24. Weissleder RA. Clearer vision of *in vivo* imaging. *Nat Biotechnol* 2001;19:316–317.
25. Gao XH, Cui YY, Levenson RM, Chung LWK, Nie SM. *In vivo* cancer targeting and imaging with semiconductor quantum dots. *Nat Biotechnol* 2004;22:969–976.
26. Akerman ME, Chan WC, Laakkonen P, Bhatia SN, Ruoslahti E. Nanocrystal targeting *in vivo*. *Proc Natl Acad Sci USA*. 2002;99:12617–12621.
27. Hirsch LR, et al. Nanoshell mediated near-infrared thermal therapy of tumors under magnetic resonance guidance. *Proc Natl Acad Sci USA* 2003;100:13549–13554.
28. Cuenca AG, et al. Emerging implications of nanotechnology on cancer diagnostics and therapeutics. *Cancer* 2006;107:459–466.
29. Wang Y, et al. Photoacoustic tomography of a nanoshell contrast agent in the *in vivo* rat brain. *Nano Lett* 2004;4:1689–1692.

30. Loo C, Lowery A, Halas N, West J, Drezek R. Immunotargeted nanoshells for integrated cancer imaging and therapy. *Nano Lett* 2005;5:709–711.
31. Barton JK, Halas NJ, West JL, Drezek R. Nanoshells as an optical coherence tomography contrast agent. In: Tuchin VV, Izatt JA, Fujimoto JG. editors. *Coherence Domain Optical Methods and Optical Coherence Tomography in Biomedicine VIII*. Proc SPIE: 2004;5316:99–106.
32. Wu C, Liang X, Jiang H. Metal nanoshells as a contrast agent in near infra-red diffuse optical tomography. *Opt Commun* 2005;253:214–221.
33. Sengupta S, et al. Temporal targeting of tumour cells and neovasculature with a nanoscale delivery system. *Nature* 2005;436:568–572.
34. O'Neal DP, Hirsch LR, Halas NJ, Payne JD, West JL. Photothermal tumor ablation in mice using near infraredabsorbing nanoparticles. *Cancer Lett* 2004;209:171–176.
35. Hirsch LR, et al. Nanoshell mediated near-infrared thermal therapy of tumors under magnetic resonance guidance. *Proc Natl Acad Sci USA* 2003;100:13549–13554.
36. Hirsch LR, Jackson JB, Lee A, Halas NJ, West JL. A whole blood immunoassay using gold nanoshells. *Anal Chem* 2003;75:2377–2381.
37. Paciotti GF, et al. Colloidal gold: a novel nanoparticle vector for tumor directed drug delivery. *Drug Deliv* 2004;11:169–183.
38. Copland JA et al. Bioconjugated gold nanoparticles as a molecular based contrast agent: implications for imaging of deep tumors using optoacoustic tomography. *Mol Imaging Biol* 2004;6:341–349.
39. Hainfeld JF, Slatkin DN, Smilowitz HM. The use of gold nanoparticles to enhance radiotherapy in mice. *Phys Med Biol* 2004;49:N309–N315.
40. Hazarika P, Ceyhan B, Niemeyer CM. Reversible switching of DNA-gold nanoparticle aggregation. *Angew Chem Int* 2004;43:6469–6471.
41. Sokolov K et al. Real-time vital optical imaging of precancer using anti-epidermal growth factor receptor antibodies conjugated to gold nanoparticles. *Cancer Res* 2003;63:1999–2004.
42. Copland JA, et al. Bioconjugated gold nanoparticles as a molecular based contrast agent: implications for imaging of deep tumors using optoacoustic tomography. *Mol Imaging Biol* 2004;6:341–349.
43. O'Neal DP, Hirsch LR, Halas NJ, Payne JD, West JL. Photo-thermal tumor ablation in mice using near infraredabsorbing nanoparticles. *Cancer Lett* 2004;209:171–176.
44. Lapotko D, Lukianovaa E, Potapnev M, Aleinikovac O, Oraevsky A. Method of laser activated nano-thermolysis for elimination of tumor cells. *Cancer Lett* 2006;239:36–45.
45. El-Sayed IH, Huang X, El-Sayed MA. Selective laser photo-thermal therapy of epithelial carcinoma using anti-EGFR antibody conjugated gold nanoparticles. *Cancer Lett* 2006;239:129–135.
46. Jackson RA. Nanosphere readies Verigene system for commercialization. *Nanobiotech News* 2005;3:1–2.
47. Weissleder R, et al. Ultrasmall superparamagnetic iron oxide: characterization of a new class of contrast agents for MR imaging. *Radiology* 1990;175:489–493.

48. Michel SC, et al. Preoperative breast cancer staging: MR imaging of the axilla with ultrasmall superparamagnetic iron oxide enhancement. *Radiology* 2002;225: 527–536.
49. Saksena MA, Saokar A, Harisinghani MG. Lymphotropic nanoparticle enhanced MR imaging (LNMRI) technique for lymph node imaging. *Eur J Radio* 2006;58:367–374.
50. Nguyen BC, et al. Multicenter clinical trial of ultrasmall superparamagnetic iron oxide in the evaluation of mediastinal lymph nodes in patients with primary lung carcinoma. *J Magn Reson Imaging* 1999;10:468–473.
51. Harisinghani MG, et al. Noninvasive detection of clinically occult lymph-node metastases in prostate cancer. *N Engl J Med* 2003;348:2491–2499.
52. Rockall AG, et al. Diagnostic performance of nanoparticle-enhanced magnetic resonance imaging in the diagnosis of lymph node metastases in patients with endometrial and cervical cancer. *J Clin Oncol* 2005;23:2813–2821.
53. Gregoriadis G. Targeting of drugs: implications in medicine. *Lancet* 1981;II: 241–246.
54. Juliano R and Stamp D. The effect of particle size and charge on the clearance rates of liposomes and liposome encapsulated drugs. *Biochem Biophys Res Commun* 1975;63:651–658.
55. Poste G, et al. Analysis of the fate systemically administered liposomes and implications for their use in drug delivery. *Cancer Res* 1982;42:1412–1422.
56. Hwang KJ, et al. Uptake of small liposomes by non-reticuloendothelial tissues. *Biochim Biophys Acta* 1987;901:88–96.
57. Gabizon A and Papahadjopoulos D. Liposome formulations with prolonged circulation time in blood and enhanced uptake by tumors. *Proc Natl Acad Sci USA* 1988;85:6949–6953.
58. Klibanov AL, Maruyama K, Torchilin VP, Huang L. Amphipatic polyethyleneglycols effectively prolong the circulation time of liposomes. *FEBS Lett* 1990;268:235–238.
59. Blume G and Cevc G. Molecular mechanism of the lipid vesicle longevity *in vivo*. *Biochim Biophys Acta* 1993;1146:157–168.
60. Gabizon A. Pegylated liposomal doxorubicin: metamorphosis of an old drug into a new form of chemotherapy. *Cancer Invest* 2001;19:424–436.
61. Gabizon A, Shmeeda H, Barenholz Y. Pharmacokinetics of pegylated liposomal doxorubicin review of animal and human studies. *Clin Pharmacokinet* 2003;42: 419–436.
62. Hobbs SK, et al. Regulation of transport pathways in tumor vessels: role of tumor type and microenvironment. *Proc Natl Acad Sci USA* 1998;95:4607–4612.
63. Hashizume H, et al. Openings between defective endothelial cells explain tumor vessel leakiness. *Am J Pathol* 2000;156:1363–1380.
64. Yuan F, et al. Vascular permeability in a human tumor xenograft: molecular size dependence and cutoff size. *Cancer Res* 1995;55:3752–3756.
65. Von Ho DD, et al. Risk factors for doxorubicin-induced congestive heart failure. *Ann Intern Med* 1979;91:710–717.

66. Torti FM, et al. Reduced cardiotoxicity of doxorubicin delivered on a weekly schedule. *Ann Intern Med* 1999;99:745–749.
67. Legha SS, et al. Reduction of doxorubicin cardiotoxicity by prolonged continuous intravenous infusion. *Ann Intern Med* 1982;96:133–139.
68. Working PK and Dayan AD. Pharmacological–toxicological expert report. CAELYX. (Stealth liposomal doxorubicin HCl). *Hum Exp Toxicol* 1996;15:751–785.
69. Lasic DD, Frederik PM, Stuart MC, Barenholz Y, McIntosh TJ. Gelation of liposome interior: a novel method for drug encapsulation. *FEBS Lett* 1992;312:255–258.
70. Lasic DD, et al. Transmembrane gradient driven phase transitions within vesicles: lessons for drug delivery. *Biochim Biophys Acta* 1995;1239:145–156.
71. Haran G, Cohen R, Bar LK, Barenholz Y. Transmembrane ammonium sulfate gradients in liposomes produce efficient and stable entrapment of amphipathic weak bases. *Biochim Biophys Acta* 1993;1151:201–215.
72. Gabizon A. Liposomal anthracyclines. *Hematol Oncol Clin North Am* 1994;8:431–450.
73. Gabizon AA, et al. Prolonged circulation time and enhanced accumulation in malignant exudates of doxorubicin encapsulated in polyethylene-glycol coated liposomes. *Cancer Res* 1994;54:987–992.
74. Symon Z, et al. Selective delivery of doxorubicin to patients with breast carcinoma metastases by Stealth liposomes. *Cancer* 1999;86:72–78.
75. Gabizon A and Martin F. Polyethylene-glycol-coated (Pegylated) liposomal doxorubicin-rationale for use in solid tumors. *Drugs* 1997;54:15–21.
76. Gabizon A, et al. Long-circulating liposomes for drug delivery in cancer therapy: a review of biodistribution studies in tumor bearing animals. *Adv Drug Deliv Rev* 1997;24:337–344.
77. Uziely B, et al. Liposomal doxorubicin: antitumor activity and unique toxicities during two complementary phase I studies. *J Clin Oncol* 1995;13:1777–1785.
78. Berry G, et al. The use of cardiac biopsy to demonstrate reduced cardiotoxicity in AIDS Kaposi's sarcoma patients treated with pegylated liposomal doxorubicin. *Ann Oncol* 1998;9:711–716.
79. Muggia FM, et al. Phase II study of liposomal doxorubicin in refractory ovarian cancer: antitumor activity and toxicity modification by liposomal encapsulation. *J Clin Oncol* 1997;15:987–93.
80. Available at <http://www.clinicaltrials.gov> (visited 09/20/06).
81. Amantea MA, Forrest A, Northfelt DW, Mamelok R. Population pharmacokinetics and pharmacodynamics of pegylated-liposomal doxorubicin in patients with AIDS-related Kaposi's sarcoma. *Clin Pharmacol Ther* 1997;61:301–311.
82. Lyass O, et al. Correlation of toxicity with pharmacokinetics of pegylated liposomal doxorubicin (Doxil) in metastatic breast carcinoma. *Cancer* 2000;89:1037–1047.
83. Safra T, et al. Pegylated liposomal doxorubicin (doxil): reduced clinical cardiotoxicity in patients reaching or exceeding cumulative doses of 500 mg/m². *Ann Oncol* 2000;11:1029–1033.

84. Hamilton A, et al. EORTC 10968: a phase I clinical and pharmacokinetic study of polyethylene glycol liposomal doxorubicin (Caelyx[®], Doxil[®]) at a 6-week interval in patients with metastatic breast cancer. *Ann Oncol* 2002;13:910–918.
85. Malawer MM, Link MP, Donaldson SS. Sarcomas of bone. In: Devita VT, Hellman S, Rosenberg SA, editors. *Cancer Principles and Practice of Oncology*. 5th ed. Philadelphia: Lippincott-Raven; 1997. p1789–852.
86. Hacker MP, Toxicity of platinum-based anticancer drugs. In: Powis G, Hacker MP, editors. *The Toxicity of Anticancer Drugs*. New York: McGraw-Hill; 1991. p82–115.
87. Schilder RJ, et al. Phase I and pharmacokinetic study of ormaplatin (tetraplatin, NSC 363812) administered on a day 1 and 8 schedule. *Cancer Res* 1994;54:709–717.
88. Thamm DH and Vail DM. Preclinical evaluation of a sterically stabilized liposome-encapsulated cisplatin in clinically normal cats. *Am J Vet Res* 1998;59:286–289.
89. Working PK, et al. Comparative intravenous toxicity of cisplatin solution and cisplatin encapsulated in long-circulating, pegylated liposomes in cynomolgus monkeys. *Toxicol Sci* 1998;46:155–165.
90. Vail DM, et al. STEALTH liposome-encapsulated cisplatin (SPI-77) versus carboplatin as adjuvant therapy for spontaneously arising osteosarcoma (OSA) in the dog: a randomized multicenter clinical trial. *Cancer Chemother Pharmacol* 2002;50:131–136.
91. Terwogt JMM, et al. Phase I and pharmacokinetic study of SPI-77, a liposomal encapsulated dosage form of cisplatin. *Cancer Chemother Pharmacol* 2002;49:201–210.
92. Kim ES, et al. A phase II study of STEALTH cisplatin (SPI-77) in patients with advanced non-small cell lung cancer. *Lung cancer* 2001;34:427–432.
93. Carbone PP, Bono V, Frei E 3rd, Brindley CO. Clinical studies with vincristine. *Blood* 1963;21:640–647.
94. Haim N, et al. Full dose vincristine (without 2-mg dose limit) in the treatment of lymphomas. *Cancer* 1994;73:2515–2519.
95. Ronghe M, Burke GA, Lowis SP, Estlin EJ. Remission induction therapy for childhood acute lymphoblastic leukaemia: clinical and cellular pharmacology of vincristine, corticosteroids, L-asparaginase and anthracyclines. *Cancer Treat Rev* 2001;27:327–337.
96. Owellen RJ, Root MA, Hains FO. Pharmacokinetics of vindesine and vincristine in humans. *Cancer Res* 1977;37:2603–2607.
97. Gidding CE, et al. Vincristine pharmacokinetics after repetitive dosing in children. *Cancer Chemother Pharmacol* 1999;44:203–209.
98. Crom WR, et al. Pharmacokinetics of vincristine in children and adolescents with acute lymphocytic leukemia. *J Pediatr*. 1994;125:642–649.
99. Webb MS, Bally MB, Mayer LD. Sphingosomes for enhanced drug delivery. US Patent 5,543,152. 1996.
100. Krishna R, Webb MS, St. Onge G, Mayer LD. Liposomal and nonliposomal drug pharmacokinetics after administration of liposome-encapsulated vincristine and their contribution to drug tissue distribution properties. *J Pharmacol Exp Ther* 2001;298:1206–1212.

101. Boman NL, Tron VA, Bally MB, Cullis PR. Vincristine-induced dermal toxicity is significantly reduced when the drug is given in liposomes. *Cancer Chemother Pharmacol* 1996;37:351–355.
102. Krishna R, Webb MS, Onge GS, Mayer LD. Liposomal and nonliposomal drug pharmacokinetics after administration of liposome-encapsulated vincristine and their contribution to drug tissue distribution properties. *J Pharmacol Exp Ther* 2001;298:1206–1212.
103. Semple SC, et al. Optimization and characterization of a sphingomyelin/cholesterol liposome formulation of vinorelbine with promising antitumor activity. *J Pharm Sci* 2005;94:1024–1038.
104. Murry DJ and Blaney SM. Clinical pharmacology of encapsulated sustained-release cytarabine. *Ann Pharmacother* 2000;34:1173–1178.
105. Howell SB. Clinical applications of a novel sustained-release injectable drug delivery system: DepoFoam technology. *Cancer J* 2001;7:219–227.
106. Neil G, Dean J, Jean-Claude B. Potentiation of melanoma vaccine immunogenicity by interleukin 2 liposomes. *Vaccine Res* 1994;3:83–92.
107. Bergers, JJ, Den Otter W, Crommelin DJA. Vesicles for tumour-associated antigen presentation to induce protective immunity: preparation, characterization and enhancement of the immune response by immunomodulators. *J Control Rel* 1994;29:317–327.
108. Joep JB, Den Otter W, Crommelin DJA. Liposome-based cancer vaccines. *J Liposome Res* 1996;6:339–355.
109. Guan HH, et al. Liposomal formulations of synthetic MUC1 peptides: effects of encapsulation versus surface display of peptides on immune responses. *Bioconjug Chem* 1998;9:451–458.
110. Samuel J, et al. Immunogenicity and antitumor activity of a liposomal MUC1 peptide-based vaccine. *Int J Cancer*. 1998;75:295–302.
111. North S and Butts C. Vaccination with BLP25 liposome vaccine to treat non-small cell lung and prostate cancers. *Exp Rev Vaccines* 2005;4:249–257.
112. North SA, Graham K, Bodnar D, Venner P. A pilot study of the liposomal MUC1 vaccine BLP25 in prostate specific antigen failures after radical prostatectomy. *J Urol* 2006;176:91–95.
113. Butts C, et al. Randomized phase IIB trial of BLP25 liposome vaccine in stage IIIB and IV non-small-cell lung cancer. *J Clin Oncol* 2005;23:6674–6681.
114. Zou Y, Ling YH, Van NT, Priebe W, Perez-Soler R. Antitumor activity of free and liposome-entrapped annamycin, a lipophilic anthracycline antibiotic with non-cross-resistance properties. *Cancer Res* 1994;54:1479–1484.
115. Zou Y, Priebe W, Perez-Soler R. Submicron liposome Suspensions obtained from preliposome lyophilizates. 1999; US Patent 5,902,604. 1999.
116. Zou Y, Priebe W, Stephens LC, Perez-Soler R. Preclinical toxicity of liposome-incorporated annamycin: selective bone marrow toxicity with lack of cradiotoxicity. *Clin Cancer Res* 1995;1:1369–1374.
117. Soppimath KS, Aminabhavi TM, Kulkarni AR, Rudzinski WE. Biodegradable polymeric nanoparticles as drug delivery devices. *J Control Release* 2001;70:1–20.
118. Crown J and O'Leary M. The taxanes: an update. *Lancet* 2000;355:1176–1178.

119. Eisenhauer EA, et al. European–Canadian randomized trial of paclitaxel in relapsed ovarian cancer: high-dose versus low-dose and long versus short infusion. *J Clin Oncol* 1994;12:2654–2666.
120. Smith RE, et al. Randomized trial of 3-hour versus 24-hour infusion of high-dose paclitaxel in patients with metastatic or locally advanced breast cancer: national surgical adjuvant breast and bowel project Protocol B-26. *J Clin Oncol* 1999;17:3403–3411.
121. Wiernik PH, et al. Phase I trial of taxol given as a 24-hour infusion every 21 days: responses observed in metastatic melanoma. *J Clin Oncol* 1987;5:1232–1239.
122. Socinski, MA, et al. Phase I trial of a 96 h paclitaxel infusion with filgrastim support in refractory solid tumor patients. *Anticancer Drugs* 1998;9:611–619.
123. Dorr, RT, et al. Pharmacology and toxicology of Cremophor EL diluent. *Ann Pharmacother* 1994;28:S11–S14.
124. Weiss RB, et al. Hypersensitivity reactions from taxol. *J Clin Oncol* 1990;8:1263–1268.
125. Rowinsky EK and Donehower RC. Paclitaxel (taxol). *N Eng J Med* 1995;332:1004–1014.
126. Desai NP, et al. Protein stabilized pharmacologically active agents, methods for the preparation thereof and methods for the use thereof.; US Patent5,916,596. 1999.
127. Ibrahim NK, et al. Phase I and Pharmacokinetic Study of ABI-007, a cremophor-free, protein-stabilized, nanoparticle formulation of paclitaxel. *Clin Cancer Res* 2002;8:1038–1044.
128. Ibrahim NK, et al. Multicenter phase II trial of ABI-007, an albumin-bound paclitaxel, in women with metastatic breast cancer. *J Clin Oncol* 2005;23:6019–6026.
129. Gradishar et al. Superior efficacy of nanoparticle albumin-bound paclitaxel (Abraxane, ABI-007) compared with cremophor-based paclitaxel (Taxol) in women with metastatic breast cancer: Results of a phase III trial. *J Clin Oncol* 2005;23:7794–7803.
130. Aliabadi HM and Lavasanifar A. Polymeric micelles for drug delivery. *Expert Opin Drug Deliv* 2006;3:139–162.
131. Kim SC, Chang EO, Song IS, Pai CM. Biodegradable polymeric micelle-type drug composition and method for the preparation thereof. US Patent6,322,805. 2001.
132. Kim SC, et al. In vivo evaluation of polymeric micellar paclitaxel formulation: toxicity and efficacy. *J Control Release* 2001;72:191–202.
133. Kim TY, et al. Phase I and pharmacokinetic study of Genexol-PM, a cremophor-free, polymeric micelle-formulated paclitaxel, in patients with advanced malignancies. *Clin Cancer Res* 2004;10:3708–3716.
134. Uchino H, et al. Cisplatin-incorporating polymeric micelles (NC-6004) can reduce nephrotoxicity and neurotoxicity of cisplatin in rats. *Br J Cancer* 2005;199:678–687.

Clinical Applications of Micro- and Nanoscale Biosensors

DAVID W.G. MORRISON, MEHMET R. DOKMECI, UTKAN DEMIRCI,
and ALI KHADEMHOSEINI

17.1 INTRODUCTION

The ability to detect pathogenic and physiologically relevant molecules in the body with high sensitivity and specificity offers a powerful opportunity in early diagnosis and treatment of diseases. Early detection and diagnosis can be used to greatly reduce the cost of patient care associated with advanced stages of many diseases. These costs have been estimated to be ~\$75 billion [1] and ~\$90 billion [2] for cancer and diabetes, respectively. Currently, cancer can be detected by monitoring the concentration of certain antigens present in the bloodstream or other bodily fluids, or through tissue examinations. Correspondingly, diabetes is monitored by determining the glucose concentrations in the blood over time. However, despite their widespread clinical use, these techniques have a number of potential limitations. For example, a number of diagnostic devices have slow response times and are burdensome to patients. Furthermore, these assays are expensive and cost the health care industry billions of dollars every year. Therefore, there is a need to develop more efficient and reliable sensing and detection technologies.

A biosensor is commonly defined as an analytical device that uses a biological recognition system to target molecules or macromolecules. Biosensors can be coupled to a physiochemical transducer that converts this recognition into a detectable output signal [3]. Typically biosensors are comprised of three components: (1) the detector, which identifies the stimulus; (2) the transducer, which converts this stimulus to a useful output; and (3) the output system, which involves amplification and display of the output in an appropriate format [3].

Biomedical Nanostructures, Edited by Kenneth E. Gonsalves, Craig R. Halberstadt, Cato T. Laurencin,
and Lakshmi S. Nair

Copyright © 2008 John Wiley & Sons, Inc.

One of the earliest references to the concept of a biosensor appeared in 1962 when Clark and Lyons [4] coupled glucose oxidase to an amperometric electrode to measure oxygen pressures. The enzyme-catalyzed oxidation of glucose lowered the oxygen pressure in the test solution, which was then sensed by the electrode. This oxygen pressure reduction was then shown to be proportional to the declining glucose concentration in the sample. An early example of the use of cells as biosensors occurred in 1977 when Rechnitz et al. [5] coupled living microorganisms (*Streptococcus faecium*) on the surface of an ammonia gas-sensing membrane electrode. Rechnitz's electrode biosensor was capable of detecting the amino acid arginine.

The emergence of micro- and nanoscale technologies for biology has a great potential to lead to the development of next generation biosensors with improved sensitivity and reduced costs. Nanotechnology is the study, manipulation, creation, and use of materials, devices, and systems of dimensions less than 100 nm [6]. Nanoscale technologies could be developed either by using bottom-up molecular processes or by scaling down traditional microfabrication processes that have been commonly used in microelectronics [7].

Modern biosensors based on micro- and nanoscale techniques have the potential to greatly enhance methods of detecting foreign and potentially dangerous toxins and may result in cheaper, faster, and easier-to-use analytical tools. Furthermore, microscale biosensors may be more portable and scalable for point-of-care sample analysis and real-time diagnosis. The goal of this chapter is to give a brief description of the different types of biosensors and their roles regarding *in vitro* and *in vivo* diagnostics. Specifically, we will discuss the applications of micro- and nanotechnologies in the development of future biosensors and discuss the current and future clinical applications of these technologies and analyze their viability.

17.2 CLASSES OF BIOSENSORS

17.2.1 Method of Biological Signaling

Biosensors can be classified either by the type of biological signaling mechanism they utilize or by the type of signal transduction they employ. The biological signaling used by biosensors can be divided into five major mechanisms (Fig. 17.1). Here, we will discuss each of these mechanisms:

- (a) *Antibody/antigen*: The high specificity between an antibody and an antigen can be utilized in this type of sensor technology. Biosensors utilizing this specificity must ensure that binding occurs under conditions where nonspecific interactions are minimized [8]. Binding can be detected either through fluorescent labeling or by observing a refractive index or reflectivity change [9].
- (b) *Enzymes*: Enzyme-based biosensors are composed of enzyme bioreceptors that use their catalytic activity and binding capabilities for specific

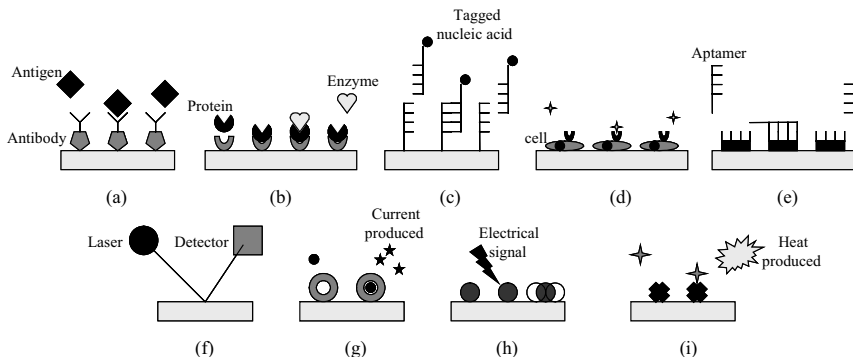


FIGURE 17.1 Biosensing and transduction classes for *in vitro* biosensors. Methods of biosensing: (a) antibody/antigen; (b) enzyme catalysed; (c) nucleic acid; (d) cell-based; (e) biomimetic. Methods of transduction; (f) optical; (g) electrochemical; (h) mass-sensitive; (i) thermal.

detection. The products of reactions catalyzed by enzymes can be detected either directly or in conjunction with an indicator [9]. The catalytic activity of the enzymes provides these types of biosensors with the ability to detect much lower limits than with normal binding techniques. This catalytic activity is related to the integrity of the native protein structure [10].

- (c) *Nucleic acids*: The complementary relationships between adenosine and thymine and cytosine and guanosine in DNA form the basis of specificity in nucleic acid-based biosensors. These sensors are capable of detecting trace amounts of microorganism DNA by comparing it to a complementary strand of known DNA [8]. By unwinding the target DNA strand, adding the DNA probe, and annealing the two strands, the probe will hybridize to the complementary sequence on the adjacent strand [10]. If the probe is tagged with a fluorescent compound, then this annealing can be visualized under a microscope. For accurate analysis, polymerase chain reaction (PCR) is often used to create multiple copies of the sample DNA.
- (d) *Cells and viruses*: Microorganisms such as bacteria and fungi can be used as biosensors to detect specific molecules or the overall “state” of the surrounding environment [10]. For example, cell behavior such as cell metabolism, cell viability, cell respiration, and bioluminescence can be used as indicators for the detection of heavy metals [10]. Furthermore, proteins that are present in cells can also be used as bioreceptors for the detection of specific analytes [11, 12].
- (e) *Biomimetic materials based*: A biomimetic biosensor is an artificial or synthetic sensor that mimics the function of a natural biosensor. These can include aptasensors, where aptasensors use aptamers as the biocomponent [8]. Aptamers are synthetic strands of nucleic acid that can be designed to recognize amino acids, oligosaccharides, peptides, and proteins [13].

17.2.2 Method of Transduction

Biosensors can also be classified according to their method of signal transduction. Typically, biosensors utilize one of following classes of signal transduction:

- (a) *Optical-detection*: Optical detection biosensors are the most diverse class of biosensors because they can be used for many different types of spectroscopy, such as absorption, fluorescence, phosphorescence, Raman, SERS, refraction, and dispersion spectrometry [8]. In addition, these spectroscopic methods can all measure different properties, such as energy, polarization, amplitude, decay time, and/or phase. Amplitude is the most commonly measured as it can easily be correlated to the concentration of the analyte of interest [8].
- (b) *Electrochemical*: Electrochemical biosensors measure the current produced from oxidation and reduction reactions. This current produced can be correlated to either the concentration of the electroactive species present or its rate of production/consumption [8].
- (c) *Mass-sensitive*: Biosensors that are based on mass-sensitive measurements detect small mass changes caused by chemical binding to small piezoelectric crystals. Initially, a specific electrical signal can be applied to the crystals to cause them to vibrate at a specific frequency. This frequency of oscillation depends on the electrical signal frequency and the mass of the crystal. As such, the binding of an analyte of interest will increase the mass of the crystal and subsequently change its frequency of oscillation, which can then be measured electrically and used to determine the mass of the analyte of interest bound to the crystal [10].
- (d) *Thermal detection*: Thermal biosensors measure the changes in temperature in the reaction between an enzyme molecule and a suitable analyte [14]. This change in temperature can be correlated to the amount of reactants consumed or products formed.

17.3 TYPES OF *IN VITRO* DIAGNOSTICS

Micro- and nanoscale technologies can be used to improve diagnostic efficiency and to develop novel portable devices for point-of-care applications. These devices can be used for a variety of common medical conditions such as diabetes, which currently comprises ~85% of the world biosensor market [15]. Here we will discuss three examples of these techniques.

17.3.1 Cantilever-Based Biosensors

The detection of molecular interactions between biomolecules by measuring their nanoscale mechanical forces offers exciting opportunities for the development of highly sensitive, miniature, and label-free biological sensors

[16]. Microscale cantilever beams can be used to detect biomolecules by deflecting upon interaction with a specific biomolecule. By measuring the amount of bending each cantilever beam experiences in response to interactions with the molecules, the amount of analyte in the solution can be quantified. Generally, there are three mechanisms to transduce the recognition of the analyte of interest into micromechanical bending of the cantilever. These include bending in response to a surface stress, bending in response to a mass loading, and bending as a result of a temperature change [17] (Fig. 17.2).

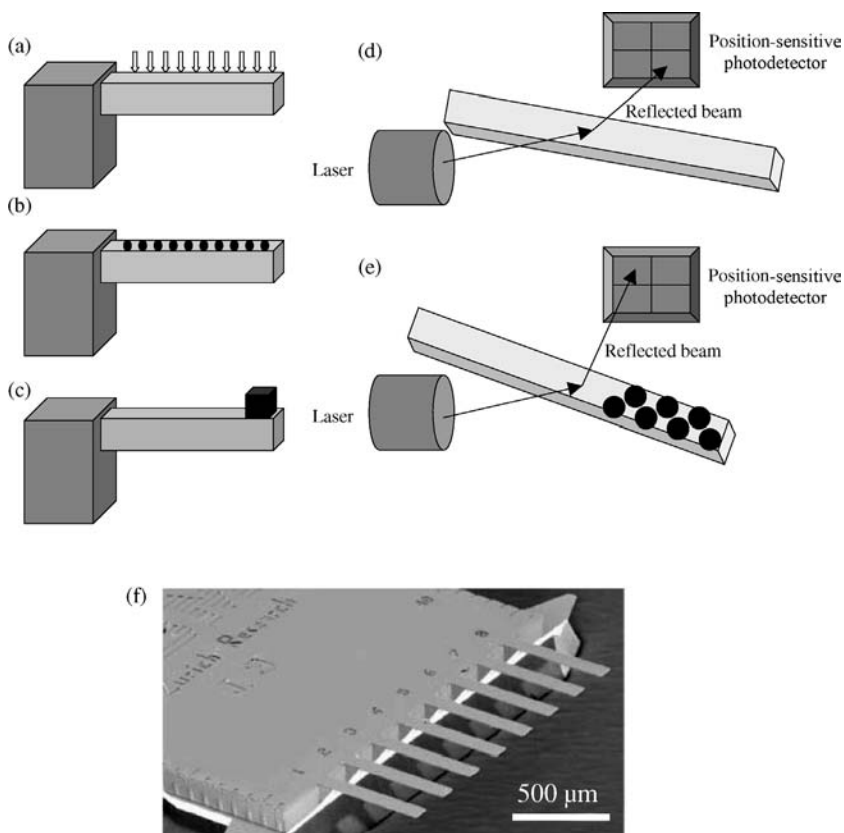


FIGURE 17.2 Microfabricated cantilevers for biosensing. Panels (a–c) illustrate various means of signal transduction: (a) a temperature and heat sensor, (b) a surface stress sensor, and (c) microbalance due to mass loading. Panels (d, e) illustrate the optical readout technique commonly used to measure deflections of cantilever biosensors; (d) optical deflection during normal cantilever conformation; (e) Optical deflection after the analyte binds to the end of the cantilever beam. (f) is an SEM micrograph of an array of eight silicon microcantilevers. (Reprinted with permission from Elsevier [115].)

Cantilever bending induced by surface stresses is caused by binding of the molecules of interest to one side of the cantilever. For example, specific binding of molecules such as streptavidin and biotin, L-cysteine [18], and prostate-specific antigen [19] can be detected by this mechanism. In addition, mass loading can be used to detect nanoscale deflections since the attachment of a larger mass causes the cantilever to oscillate at a different frequency. Also, a rapid, extreme temperature change around the cantilever can also cause it to bend.

Implementing different materials into the structure of the cantilever enhances its sensitivity to the aforementioned conditions. The most commonly used materials used for the construction of commercial micro- and nanoscale cantilevers are silicon, silicon nitride, and silicon oxide [17]. Although these cantilevers are extremely sensitive to different masses and stresses, they offer no chemical or biochemical specificity. By coating the surface of the cantilever with biological recognition molecules such as peptides, self-assembled monolayers, DNA probes, or antibodies, cantilevers can be built that detect specific molecules [20].

The degree of bending of the cantilevers can be registered using a wide range of detection techniques including optical laser based, piezoresistive, piezoelectric, and capacitive [21]. Deflection measurements based on optical beams are an efficient readout method for cantilevers with reflecting surfaces [22]. Here, a laser diode is focused at the free end of the cantilever (usually coated with gold) and the reflected beam is detected by a position-sensitive photodetector (Fig. 17.2) [22]. For additional sensitivity at nanoscale regimes, electron transfer methods can be used with cantilevers that are only a few hundred nanometers in length [22]. For piezoresistive detection, a resistor is embedded into a silicon cantilever, which changes its resistance as the cantilever bends. Accordingly, when the silicon cantilever is deformed, the change in resistance of the device reflects the degree of deformation [21]. These cantilevers typically have two legs that enable the resistance of a boron-doped channel to be successfully measured by wiring two conductive paths to the cantilever base next to the legs. Correspondingly, the piezoelectric method of detection requires the placement of a piezoelectric material, such as ZnO, onto the surface of the cantilever. When a stress is applied to piezoelectric materials, they respond by generating a voltage, which can then be measured and correlated to the amount of stress applied. Finally, the capacitance method of detecting cantilever bending is based on measuring the capacitance between a metal plate on the cantilever surface and another plate fixed on the substrate [22, 23]. The capacitance is inversely proportional to the distance between the substrate and the conductor on the surface of the cantilever. As the cantilever bends, the distance between the tip of the cantilever and the substrate changes, which results in changes in capacitance and can be correlated to the mass loading. This detection method is highly sensitive, yet only applies to small displacements and does not work in liquid solutions.

17.3.2 Cell and Protein Arrays

The use of live cells for biosensing applications is an exciting alternative to traditional biosensing approaches. These techniques may potentially enhance biosensor specificity and sensitivity [24]. Cell-based biosensors are also particularly useful in detecting unknown compounds and toxins since the behavior of the candidate molecules can be directly observed in tissues. Specific examples include the use of liver [25], cardiac [26–28], or immune cells [29, 30]. By using micro- and nanoscale devices it may be possible to mimic the function of cells *in vitro* as a means to develop more efficient sensor and transduction technologies [31].

By engineering the response of B lymphocytes, cells responsible for humoral immunity, Rider et al. have demonstrated that immunosensors can be developed using live cell arrays [24]. In this work, B lymphocytes were altered to recognize surface proteins of several different pathogens. They found that upon stimulation with specific test samples, the engineered cells responded within few seconds. These responses were visualized through the bioluminescence of a calcium-sensitive protein that the cells were engineered to express.

In addition, multiphenotype cell arrays have been fabricated for biosensing applications [32–34]. In one example, a biosensor was fabricated that incorporated B cells for the detection of specific analytes and T cells to convert the B-cell output signal into a readable form. This was accomplished through a similar mechanism as discussed previously. Kim et al. used the dose-dependence response of calcium released into the cytosol upon stimulation with T-cell receptor to engineer real-time biosensors [29]. By inserting calcium-sensitive dye (fura-2) into the T cells they were able to visualize the T-cell response to the peptide presentation from the B cells.

In addition to cellular arrays, there is significant interest in the use of protein arrays in biosensing applications [35]. Most studies on protein array biosensors have focused on the use of antibodies to create biosensors with the capability of performing multiple analyses simultaneously [36]. Ligler et al. reported their work regarding a single biosensor array capable of detecting multiple analytes on the same chip [37]. This was accomplished by immobilizing capture molecules onto the surface of an optical waveguide in stripes resembling “bar codes”. Each strip in the “bar codes” was directed against a different analyte of interest. The sample of interest was then loaded perpendicularly to these bar codes using flow chamber modules. This enabled each sample to encounter the “bar code” of columns and the specific binding of multiple analyte molecules to their corresponding capture molecule was achieved.

17.3.3 Nanoparticles

Nanoparticles have emerged as powerful and widely applicable materials in biosensing. Nanoparticles are generally defined as particles that range in size from 1 to 100 nm in diameter [38]. By conjugating specific molecules to the surface of nanoparticles, it is possible to engineer their biological functionality.

An exciting product of the progress in nanoparticles for *in vitro* diagnostic tools has been the emergence of probes encapsulated by biologically localized embedding (PEBBLEs). PEBBLEs are nanoscale polymer beads specifically designed to provide minimally invasive monitoring of specific analytes in single, viable cells with applications for real-time analysis of drugs, toxins, and environmental effects on cell function [39–45]. PEBBLEs typically encapsulate a dye sensitive to the analyte of interest and a dye to function as a reference. By encapsulating these within their biologically inert matrix, PEBBLEs avoid potential chemical interference from other cellular constituents [46]. Although PEBBLEs have been designed under multiple platforms [45, 47–49], most follow a parallel sensing format: analytes present in the cell diffuse through the PEBBLE matrix (which can be made from polyacrylamide, poly(decyl methacrylate) (PDMA), sol–gel or modified silicates [46]) and interact with the dyes contained within the nanoparticles. Interactions between the analytes and the sensing dye initiate conformational changes in the dye that are detectable through variations in excitation intensity. The reference dye is also affected by interactions and varying excitation intensities; however, the ratio between the two dyes helps to eliminate misrepresentation of the data [46]. In PEBBLE nanosensors, the sol–gel matrix can be modified to enable the encapsulation of both hydrophobic and hydrophilic dyes [39]. These gels can be heated to form high purity oxides that can then be combined with oxygen-sensitive dyes. Upon injection into rat C6-glioma cells, it was possible to detect intracellular oxygen concentrations with high accuracy and reproducibility [49]. This example shows the promise of PEBBLEs to detect and quantify the concentration of specific analytes.

Another group of nanoparticles for *in vitro* experimentation are quantum dots (QDs) [50–53]. QDs are semiconductor crystals (between 2 and 10 nm in diameter) that have unique electrical and optical properties. QDs are made from nanocrystals of CdS, CdSe, CdTe, or CdSe/ZnSe synthesized using different methods [54–57]. These materials exhibit unique optical and electronic properties through quantum mechanical scattering of valence shell electrons by the atomic cores [58] made possible due to their size. When excited with a beam of photons, they emit bright light at a distinct frequency on their own and hence are a promising technology for many biosensing applications [52]. In comparison to fluorescent labelling, QDs are less susceptible to photobleaching. Moreover, QDs have longer emission lifetimes and can be used in tracking cells for extended periods of time, and since they are small and emit light at a distinct color, multiple tagging experiments can be done simultaneously. Although examples of QDs in biosensing application are quickly emerging, the true promise of QDs is yet to be realized and they may lead to revolutionary advances in biosensing technology. We will discuss specific uses of QDs in Section 17.4.1.

17.4 IN VIVO DIAGNOSTICS

The advances in micro- and nanotechnologies can also be used for *in vivo* biosensing applications. With miniaturization, it is possible to fabricate novel

devices at low cost, with greater functionality and more reliability [34]. For instance, the ability to track the presence of fluorescent nanoparticles *in vivo* offers significant improvements in the detection, diagnosis, and treatment of diseases. Two types of nanoparticles that have been used *in vivo* for biosensing applications are QDs and MRI contrast agents.

17.4.1 Quantum Dots

QDs can be surface modified to enhance their biocompatibility, solubility, and functionality (Fig. 17.3a). For example, surface-modified QDs can be used as *in vivo* imaging tools capable of binding to specific targets [59]. The biological molecules can include peptides, antibodies, nucleic acids, or small-molecule ligands [60]. Recently, this technology has been used to image tumors *in vivo* (Fig. 17.3b) [60]. QDs have also been used for cell and tissue labeling [61], long-term cell trafficking, and multicolor cell imaging [62]. To increase the biocompatibility of QDs, the surface of QDs has been engineered with polyethylene glycol (PEG) molecules [60]. Using surface-modified approaches,

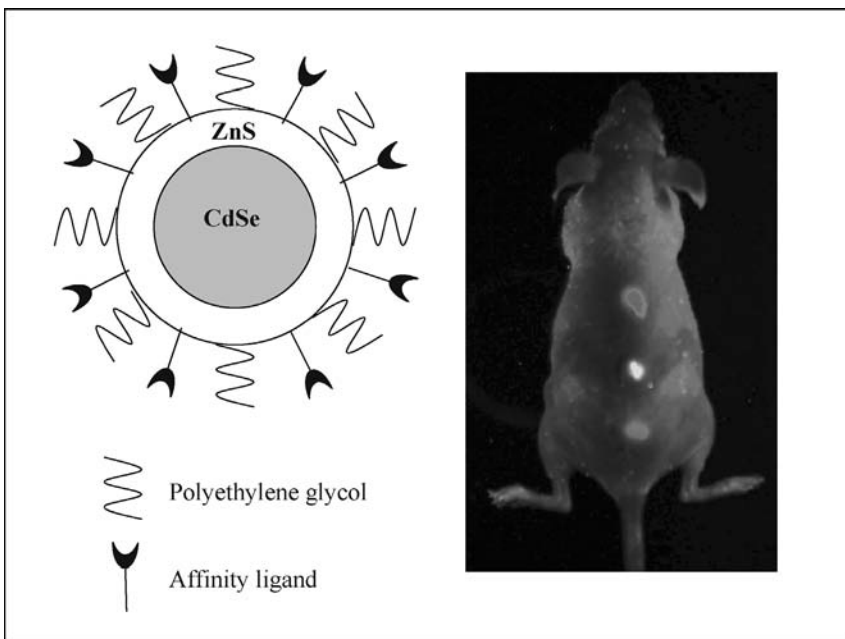


FIGURE 17.3 The basic structure of a quantum dot is provided. A cadmium selenide (CdSe) core is coated with zinc sulfide (ZnS) and polyethylene glycol (PEG) and affinity ligands are covalently coupled to the surface. The second image shows the capability of simultaneous *in vivo* imaging of QDs. The image was attained with either tungsten or mercury lamp excitation. (Used with permission from Gao et al. [60].)

Derfus et al. have demonstrated that QDs complexed with cationic liposomes can be used to target HeLa cells [63]. Thus, QDs complexed with transfection reagents are capable of entering the cytoplasm of cells.

Despite their success, a number of challenges exist for using QDs for *in vivo* applications. One of these challenges is that the core material for most QDs is a heavy metal that is toxic to cells, and accordingly, research is currently underway to produce nonheavy metal-based alternatives. Therefore, it may one day be possible to use QDs to detect, diagnose, and treat diseases in a minimally invasive manner.

17.4.2 MRI Contrast Agents

Cellular imaging with MRI contrast agents is used for many imaging and diagnostic applications [64–66]. MRI contrast agents are gaining popularity for *in vivo* diagnostics due to their high spatial resolution [67]. These particles are typically made from ferrous or ferric oxide coated with a polymeric material, such as dextran [67]. These particles have been shown to be nontoxic and inert for short durations, and after injection accumulate in the organ of interest [68]. In addition, these particles could be impregnated with a fluorescent agent to enable analysis by both fluorescent microscopy and MRI [69]. There are, however, a number of limitations to MRI tracking of cells. To effectively image a cell, a large number of nanoparticles need to be internalized by the cell. This requires a highly efficient labeling scheme [70]. Additionally, cell division dilutes the label once a cell has been effectively tagged [70]. These difficulties can hamper studies that aim to examine the long-term stability of cell labeling. A great deal of research is currently underway to overcome these limitations by engineering new contrast agents that are more stable, nontoxic, and functional *in vivo*.

17.5 CURRENT AND EMERGING CLINICAL APPLICATIONS OF MICRO- AND NANOSCALE BIOSENSORS

There are many applications of biosensor technologies in health care and for the treatment of infectious diseases. The current status and future potential of four of the most relevant applications are discussed below.

17.5.1 Glucose Detection *In Vivo*

One of the main clinical applications of biosensors is to develop point-of-care glucose concentration measuring devices for patients suffering from diabetes [71]. Originally introduced in the early 1980s [71], the latest generation of handheld glucose sensors has revolutionized the lifestyles of those suffering from diabetes. Patients are now able to self-monitor their glucose concentrations and self-administer insulin injections as required.

Most enzyme-based biosensors to detect glucose concentrations use enzymes known as oxidoreductases [72]. The most common enzymes used for glucose detection are glucose oxidase and glucose dehydrogenase [73]. Glucose biosensors generally make use of electrochemical transducers in their designs as they provide appropriate specificity and reproducibility and can easily be manufactured in large volumes at low costs [73].

These traditional amperometric-based biosensors have undergone recent miniaturization to enable subcutaneous implantation. In the minimed-medtronic continuous glucose monitoring system (CGMS), a needle-type amperometric enzyme electrode is coupled to a portable data logger [74]. The sensor is based on the aforementioned sensing technology and the data recorded from the logger can be downloaded to a portable computer after 3 days of sensing [74]. The monitor is implanted in the subcutaneous tissue to measure interstitial fluid glucose concentrations. Although interstitial fluid and blood concentrations are similar at steady state [75], there is a significant delay when the blood glucose concentration is rapidly changing as occurs after a meal.

Another microscale *in vivo* glucose monitor is the GlucoWatch (Cygnus, Inc.). This sensor operates by reverse iontophoresis, which utilizes a glucose-containing interstitial fluid that is lured to the skin surface by a small current passing between two electrodes [75]. Hydrogel pads containing a glucose oxidase biosensor are present on the surface and measure the glucose concentration present in the interstitial fluid. Again, the delay between the glucose concentrations variations in the interstitial fluid and corresponding changes in the blood creates a significant disadvantage.

There is a clinical need for future glucose sensors to become increasingly noninvasive and sensitive to rapid changes in glucose concentrations. It is anticipated that the development of microscale devices as well as emerging nano-based detection strategies will be useful as potential techniques for efficient glucose detection.

17.5.2 Bacterial Urinary Tract Infections

Bacterial infection in the urinary tract is the second most common organ system infection in the human body [76]. Microbial culture techniques are currently employed to identify urinary tract pathogens. These methods, however, are cumbersome and are accompanied by a 2-day lag period between the collection of the specimen and the identification of the pathogen [77]. As such, the development of tools to effectively decrease this lag period and increase diagnosis accuracy and efficiency is very appealing from an improved health care and reduced cost standpoint.

Electrochemical DNA biosensors have been documented in the literature to detect and identify pathogens [78, 79]. In these designs, a layer of oligonucleotide probes functions as the sensory receptor and the sensory input is detected through the use of an electrochemical transducer. There are two basic modes to detect DNA with this configuration. The first method requires target

immobilization followed by detection with a labeled probe [80]. In the second method, known as “sandwich” hybridization, the DNA target initially binds to a surface oligonucleotide through hybridization. This is followed by hybridization to a marker probe for signal transduction [80].

Liao et al. have used these concepts and methods to rapidly detect and identify molecular pathogens in clinical urine samples [77]. The authors successfully developed pairs of capture and detection oligonucleotides in an array for the detection of a 16S rRNA target. This “microchip” required 45 min after applying the sample to provide an output signal and did not require amplification or labeling of the target sequence. This biosensing technique confirms the capabilities of direct detection techniques for the identification of bacteria present in clinical samples and could be of great clinical potential.

17.5.3 Human Immunodeficiency Virus (HIV) Detection

More than 30 million HIV-infected people live in the developing world, where resources are scarce. In 2002, the U.S. National Intelligence Council (NIC) predicted that the number of HIV-infected individuals in the developing world would rise to 80 million by 2010. Effective antiretroviral therapy (ART) for HIV has been available in developing countries for more than a decade; however, only a small fraction of the infected people are currently receiving treatment due to lack of diagnostic tools and cost-effective therapies. To increase access to HIV care and improve treatment outcomes, there is an urgent need for low cost diagnostic tools that could be implemented in developing countries [81, 82].

Traditionally, HIV infections are diagnosed by either direct fluorescent antibody assays or viral load testing [83]. Direct fluorescent antibody assays, such as enzyme-linked immuno sorbent assay (ELISA), use two antibodies to identify the presence of a virus [84]. HIV presence *in vivo* can also be detected using viral load testing [85]. This technique detects cell-free plasma viral RNA with the use amplification techniques such as PCR. These types of diagnostic techniques provide rapid results, however, are generally not sensitive enough to provide reliable and consistent results [86].

The application of surface plasmon resonance-based (SPR) optical techniques could greatly enhance the understanding of HIV and lead to superior detection and quantification mechanisms [87]. In SPR, the surface of the biosensor is initially covered with immobilized ligands. Microfluidic channels then carry an analyte across the ligand and specific binding between the ligand and the analyte occurs. The SPR detector then measures changes in the refractive index of the biosensor as ligands and analytes bind and detach from one another [88] (Fig. 17.4).

This process has already had a tremendous impact on the understanding of HIV infections. Fagerstam et al. [89] initially used SPR to complete epitope mapping of monoclonal antibodies opposed to the HIV capsid protein. Subsequently, Alterman et al. studied the interaction of 17 inhibitors with differing structures on HIV protease immobilized onto electrodes during SPR

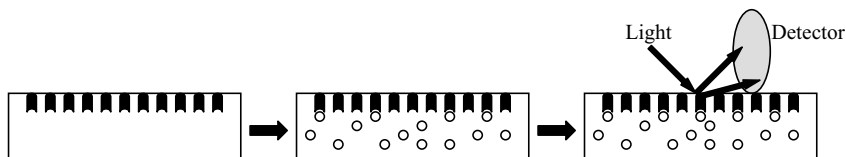


FIGURE 17.4 A schematic illustrating an SPR experiment. The ligand is initially immobilized on the surface of the biosensor chip. A microfluidic channel carries the analyte across the surface of the ligand and specific binding occurs. As the analyte binds and dissociates from the ligand, the refractive index is measured and recorded.

analysis [90]. This has potentially powerful applications in the development of HIV protease inhibitors, which may have profound impacts in the progress of therapies aimed at inhibiting the HIV replication cycle.

Another approach to evaluate HIV-infected patients is to measure the absolute number of CD4⁺ T lymphocytes in blood. The CD4 count is used to initiate treatment and to monitor the response to treatment. For instance, when the CD4 count falls below 200 cells/ μl , HIV-infected patients are at risk for severe opportunistic infections, and HIV treatment is drastically needed. In high income settings, CD4 counts rely on flow cytometry, which is expensive and not suitable for resource-limited countries. Handheld, reliable, and low cost CD4 counting devices for use in resource-scarce regions of the world are needed. There have been recent efforts to develop affordable CD4 counting methods by flow cytometry. Although these tools are more affordable than standard flow cytometers, they remain complex for district hospitals or point-of-care use in developing countries, require expensive reagents, involve several sample preparation steps, and are labor intensive and have low throughput. The need for simple CD4 counting solutions that satisfy requirements appropriate to point-of-care and developing world testing—such as high throughput, low fabrication cost, and device disposability—are made possible via microelectromechanical systems (MEMS) fabrication technologies. Microfluidics-based devices are being developed as tools to overcome these limitations since they can be fabricated cheaply, are portable, and have been engineered to perform variety of functions required to make biological measurements [91]. For instance, Demirci et al. demonstrated a microfluidic device that can separate and image CD4 T lymphocytes on a polycarbonate filter, to measure their concentration in the blood as shown in Fig. 17.5. In microfluidic devices, blood samples could be screened and partitioned. For example, by using an array of posts of defined sizes, red blood cells can be filtered from leukocytes [91]. Subsequently, leukocytes can be immobilized in microwells and stained to measure the number and frequency of the desired cell types.

17.5.4 Cancer Cell Targeting

Currently, 60% of patients diagnosed with breast, colon, lung, or ovarian cancer already have cell metastases forming in other locations of their body

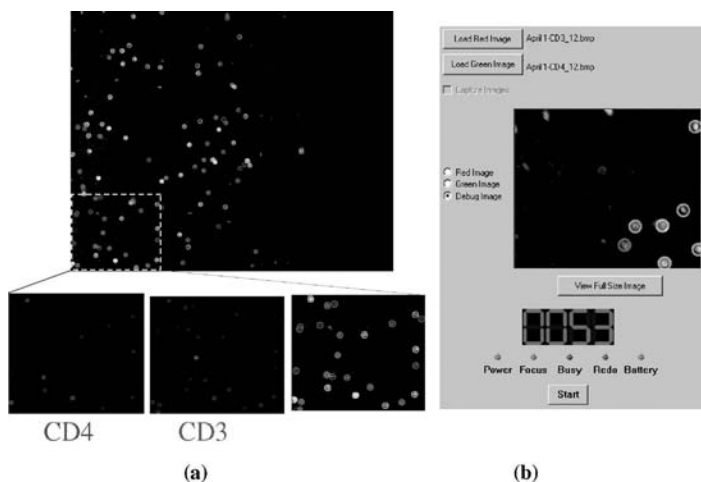


FIGURE 17.5 Detection of $CD4^+$ T lymphocytes in microfluidic-based devices for monitoring HIV. (a) Each location on the image is identified, where red marked cells correspond to $CD3^+$ cells, green marked cells correspond to $CD4^+$ cells, and the yellow marked locations on the image correspond to $CD3^+$ and $CD4^+$ T lymphocytes. (b) The software output is shown; the yellow circles are automatically drawn by the image recognition software and the $CD4^+$ T-cell count is displayed as 53 cells/ μ l of whole blood for this sample.

[92–103]. The development of effective diagnostic tools to detect these cells has been difficult due to the low number of circulating cancer cells and the lack of suitable markers to identify these cells. However, *in vivo* and *in vitro* applications of nanotechnology may be used to increase the selectivity and resolution and to make such diagnoses possible.

Currently, there are several techniques to isolate tumor cells. These require laborious manual sample preparation steps that result in variable results and low sensitivity. Circulating tumor cells (CTCs) are rare even in patients with advanced cancer, representing as low as 1–10 cells/ml [104] such that a reliable cell sorter for CTCs needs to detect approximately one CTC in one billion blood cells. The conventional cell separation methods rely on properties such as size, density and differential expression of surface antigens to isolate desired cell subpopulations, density gradient centrifugation, preferential lysis of red blood cells, ficoll-hypaque density, porous filters, immunomagnetic bead sorting, and cell filtration [105]. Molecular methods have also been developed that rely on PCR-based detection of tumor-associated RNA in blood as evidence of CTCs, including in melanoma, breast cancer and prostate cancer [14–17]. Moreover, methods that allow recovery of living or intact cells for further morphological, immunocytochemical, genome-wide expression profiling, or functional evaluation are significant. These studies could enhance the benefits of knowing the precise number of CTCs and circulating metastatic precursor cells.

There have been attempts to standardize the preparation steps, which target reduction in variations. For instance, Immunicon, Inc. has developed a semiautomated sample preparation and analysis system and has used it in multiple clinical or preclinical trials, which has been applied to several cancers [94, 96, 97, 101, 106]. The sample preparation steps include isolation of leukocytes followed by the incubation with antiepithelial cell adhesion molecule (EpCAM)-coated ferrofluid particles. Finally, the magnetic incubation and washing steps follow. EpCAM is a homotypic cell adhesion molecule with expression limited to and highly expressed by cells of epithelial origin [107–109]. It has also been shown to be expressed on CTCs [110]. To capture cells with low density of EpCAM receptors, the ferrofluid was modified to contain two distinct receptors, one monoclonal antibody for EpCAM and another receptor (biotin analog) that binds to a multivalent aggregator. This method increases the number of magnetic particles per target cell through controlled and reversible aggregation of the ferrofluid, which increases the capture efficiency.

The above studies demonstrate the potential use of EpCAM to isolate CTCs from blood. There is further room for improving the sensitivity of CTC detection and removing the variability for clinical applications. Among the new technologies with increasingly broader impact in biology, microfluidic lab-on-a-chip-type devices have potential for blood analysis. The use of physical properties for separation of cells takes advantage of the heterogeneity of blood cells [91]. The differences in the mechanical properties of cells, such as size, were tested for separation of larger tumor cells from blood samples [111]. Increased rigidity of blood cells was also used to distinguish and sort cells [112]. The advances in understanding of blood sample preparation and technological developments in microfabrication and microfluidics enable new capabilities for blood analysis.

In addition to utilizing antibodies for cancer cell detection, other biological molecules such as peptides and aptamers can be used. For example, nanoparticle–aptamer bioconjugates have been used to specifically target prostate cancer cells [113]. It was determined that nanoparticles with RNA aptamers experienced a significantly enhanced uptake in cells that expressed the prostate-specific membrane antigen, a prostate cancer tumor marker that is overexpressed on prostate cancer cells. This work is an exciting first step in targeting prostate cancer cells and could potentially be applied to numerous other important human diseases.

The early stage detection of certain cancer cells *in vivo* is difficult since these cells generally do not metastasize [92]. As such, there have been significant advances in the development of *in vivo* techniques of cancer cell imaging. For example, iron oxide particles have been used to identify lymph node metastases in male prostate cancer [114]. This group found that the distribution of the iron oxide particles was disrupted by malignant tumors present in the prostate, and that this disruption was detectable with MRI. Furthermore, prostate cancer cells have also been imaged using quantum dots in nude mice

[60]. In this case, quantum dot accumulation was achieved through two different mechanisms: by enhanced permeability and retention of tumor sites as well as by antibody binding to specific cancer cell surface biomarkers. These *in vivo* techniques are examples of noninvasive cancer imaging tools that may be enhanced to screen other cancer cell types in the future.

17.6 CONCLUSIONS

Biosensors are widely used in medicine to monitor or detect biological molecules for applications ranging from diabetes to cancer. The recent progress in micro- and nanoscale technologies shows significant promise in enabling a number of novel biosensing applications. For example, microcantilevers have been used to detect desired molecules without the need for a labeling agent, while nanoscale particles and cell/protein arrays have shown promise for improved sensing applications in biomedicine. Furthermore, through miniaturization, it is possible to fabricate biosensors that are portable, inexpensive, and highly sensitive that can be used for resource-poor settings for diagnosing diseases such as HIV/AIDS. Therefore, the continued progress in the development and use of micro- and nanotechnologies for biosensors shows great potential in improving methods to diagnose diseases or to monitor their progression.

ACKNOWLEDGMENTS

The authors would like to thank for funding from the Coulter Foundation, U.S. Army Corps of Engineers, CIMIT, and the Institute for Soldier Nanotechnology.

REFERENCES

1. American Cancer Society. Cancer Facts and Figures 2006. Atlanta: American Cancer Society; 2006.
2. Hogan P, Dall T, Nikolov P. Economic costs of diabetes in the US in 2002. *Diabetes Care* 2003;26:917–932.
3. Collings AF and Caruso F. Biosensors: recent advances. *Rep Prog Phys* 1997;60:1397–1445.
4. Clark LC Jr and Lyons C. Electrode systems for continuous monitoring in cardiovascular surgery. *Ann N Y Acad Sci* 1962;102:29–45.
5. Rechnitz GA, Kobos RK, Riechel SJ, Gebauer CR. A bio-selective membrane electrode prepared with living bacterial cells. *Anal Chim Acta* 1977;94:357–365.
6. Jianrong C, Yuqing M, Nongyue H, Xiaohua W, Sijiao L. Nanotechnology and biosensors. *Biotechnol Adv* 2004;22:505–518.

7. Whitesides GM, Ostuni E, Takayama S, Jiang XY, Ingber DE. Soft lithography in biology and biochemistry. *Annu Rev Biomed Eng* 2001;3:335–373.
8. Kubik T, Bogunia-Kubik K, Sugisaka M. Nanotechnology on duty in medical applications. *Curr Pharm Biotechnol* 2005;6:17–33.
9. Monk DJ and Walt DR. Optical fiber-based biosensors. *Anal Bioanal Chem* 2004;379:931–945.
10. Vo-Dinh T and Cullum B. Biosensors and biochips: advances in biological and medical diagnostics. *Fresenius J Anal Chem* 2000;366:540–551.
11. Suh KY, Khademhosseini A, Yoo PJ, Langer R. Fabrication of single or aggregated bacteria arrays using host–parasite and virus–antibody interactions. *Biomed Microdevices* 2004;6:223–229.
12. Suh KY, Khademhosseini A, Jon S, Langer R. Direct confinement of individual viruses within polyethylene glycol (PEG) nanowells. *Nano Lett* 2006;6:1196–1201.
13. Hermann T and Patel DJ. Adaptive recognition by nucleic acid aptamers. *Science* 2000;287:820–825.
14. Ramanathan K and Danielsson B. Principles and applications of thermal biosensors. *Biosens Bioelectron* 2001;16:417–423.
15. Newman JD, Warner PJ, Turner APF, Tigwell LJ. *Biosensors: A Clearer View*. UK: Cranfield University; 2004; p 216.
16. Cheng MM, et al. Nanotechnologies for biomolecular detection and medical diagnostics. *Curr Opin Chem Biol* 2006;10:11–19.
17. Ziegler C. Cantilever-based biosensors. *Anal Bioanal Chem* 2004;379:946–959.
18. Yang Y, Ji HF, Thundat T. Nerve agents detection using a Cu^{2+} /L-cysteine bilayer-coated microcantilever. *J Am Chem Soc* 2003;125:1124–1125.
19. Wu G, et al. Bioassay of prostate-specific antigen (PSA) using microcantilevers. *Nat Biotechnol* 2001;19:856–860.
20. Hansen KM and Thundat T. Microcantilever biosensors. *Methods* 2005;37:57–64.
21. Mukhopadhyay R, et al. Cantilever sensor for nanomechanical detection of specific protein conformations. *Nano Lett* 2005;5:2385–2388.
22. Lavrik NV, Separiak M, Datskos PG. Cantilever transducers as a platform for chemical and biological sensors. *Rev Sci Instrum* 2004;75:2229–2253.
23. Demirci U, Ergun A, Oralkan O, Karaman M, Khuri-Yakub B. Forward-viewing CMUT arrays for medical imaging. *IEEE Trans Ultrason Ferroelectr Freq Control* 2004;51:887–895.
24. Rider TH, et al. A B cell-based sensor for rapid identification of pathogens. *Science* 2003;301:213–215.
25. Powers MJ, et al. A microfabricated array bioreactor for perfused 3D liver culture. *Biotechnol Bioeng* 2002;78:257–269.
26. Natarajan A, Molnar P, Sieverdes K, Jamshidi A, Hickman JJ. Microelectrode array recordings of cardiac action potentials as a high throughput method to evaluate pesticide toxicity. *Toxicol In Vitro* 2006;20:375–381.
27. Fairey ER, Bottein Dechraoui MY, Sheets MF, Ramsdell JS. Modification of the cell based assay for brevetoxins using human cardiac voltage dependent sodium channels expressed in HEK-293 cells. *Biosens Bioelectron* 2001;16:579–586.

28. Gray SA, et al. Design and demonstration of an automated cell-based biosensor. *Biosens Bioelectron* 2001;16:535–542.
29. Kim H, Doh J, Irvine DJ, Cohen RE, Hammond PT. Large area two-dimensional B cell arrays for sensing and cell-sorting applications. *Biomacromolecules* 2004;5:822–827.
30. Doh J and Irvine DJ. Immunological synapse arrays: patterned protein surfaces that modulate immunological synapse structure formation in T cells. *Proc Natl Acad Sci USA* 2006;103:5700–5705.
31. Khademhosseini A, Langer R, Borenstein J, Vacanti JP. Microscale technologies for tissue engineering and biology. *Proc Natl Acad Sci USA* 2006;103:2480–2487.
32. Koh WG, Itle LJ, Pishko MV. Molding of hydrogel multiphenotype cell microstructures to create microarrays. *Anal Chem* 2003;75:5783–5789.
33. Kim H, Cohen RE, Hammond PT, Irvine DT. Live lymphocyte arrays for biosensing. *Adv Func Mater* 2006;16:1313–1323.
34. Khademhosseini A, et al. Cell docking inside microwells within reversibly sealed microfluidic channels for fabricating multiphenotype cell arrays. *Lab Chip* 2005;5:1380–1386.
35. Taitt CR, Anderson GP, Lingerfelt BM, Feldstein MJ, Ligler FS. Nine-analyte detection using an array-based biosensor. *Anal Chem* 2002;74:6114–6120.
36. Taitt CR, et al. A portable array biosensor for detecting multiple analytes in complex samples. *Microb Ecol* 2004;47:175–185.
37. Ligler FS, et al. Array biosensor for detection of toxins. *Anal Bioanal Chem* 2003;377:469–477.
38. Whitesides GM. The ‘right’ size in nanobiotechnology. *Nat Biotechnol* 2003; 21:1161–1165.
39. Monson E, Brasuel MA, Philbert A, Kopelman R. PEBBLE nanosensors for *in vitro* analysis. In: Vo-Dinh T, editor. *Biomedical Photonics Handbook*. Boca Raton, FL: CRC Press; 2003.
40. Cao Y, Lee Koo YE, Kopelman R. Poly(decyl methacrylate)-based fluorescent PEBBLE swarm nanosensors for measuring dissolved oxygen in biosamples. *Analyst* 2004;129:745–750.
41. Park EJ, Brasuel M, Behrend C, Philbert MA, Kopelman R. Ratiometric optical PEBBLE nanosensors for real-time magnesium ion concentrations inside viable cells. *Anal Chem* 2003;75:3784–3791.
42. Xu H, Aylott JW, Kopelman R. Fluorescent nano-PEBBLE sensors designed for intracellular glucose imaging. *Analyst* 2002;127:1471–1477.
43. Sumner JP, Aylott JW, Monson E, Kopelman R. A fluorescent PEBBLE nanosensor for intracellular free zinc. *Analyst* 2002;127:11–16.
44. Clark HA, Hoyer M, Philbert MA, Kopelman R. Optical nanosensors for chemical analysis inside single living cells. 1. Fabrication, characterization, and methods for intracellular delivery of PEBBLE sensors, *Anal Chem* 1999;71: 4831–4836.
45. Clark HA, Kopelman R, Tjalkens R, Philbert MA. Optical nanosensors for chemical analysis inside single living cells. 2. Sensors for pH and calcium and the intracellular application of PEBBLE sensors. *Anal Chem* 1999;71:4837–4843.

46. Buck SM, et al. Optochemical nanosensor PEBBLES: photonic explorers for bioanalysis with biologically localized embedding. *Curr Opin Chem Biol* 2004;8:540–546.
47. Wolfbeis OS. Fiber-optic chemical sensors and biosensors. *Anal Chem* 2000; 72:81R–89R.
48. Brasuel M, Kopelman R, Miller TJ, Tjalkens R, Philbert MA. Fluorescent nanosensors for intracellular chemical analysis: decyl methacrylate liquid polymer matrix and ion-exchange-based potassium PEBBLE sensors with real-time application to viable rat C6 glioma cells. *Anal Chem* 2001;73:2221–2228.
49. Xu H, Aylott JW, Kopelman R, Miller TJ, Philbert MA. A real-time ratiometric method for the determination of molecular oxygen inside living cells using sol–gel-based spherical optical nanosensors with applications to rat C6 glioma. *Anal Chem* 2001;73:4124–4133.
50. Alivisatos AP, Gu W, Larabell C. Quantum dots as cellular probes. *Annu Rev Biomed Eng* 2005;7:55–76.
51. Mansson A, et al. *In vitro* sliding of actin filaments labelled with single quantum dots. *Biochem Biophys Res Commun* 2004;314:529–534.
52. Smith AM, Dave S, Nie S, True L, Gao X. Multicolor quantum dots for molecular diagnostics of cancer. *Expert Rev Mol Diagn* 2006;6:231–244.
53. Tomlinson ID, Mason JN, Blakely RD, Rosenthal SJ. Peptide-conjugated quantum dots: imaging the angiotensin type 1 receptor in living cells. *Methods Mol Biol* 2005;303:51–60.
54. Dai Q, et al. Colloidal CdSe nanocrystals synthesized in noncoordinating solvents with the addition of a secondary ligand: exceptional growth kinetics. *J Phys Chem B Condens Matter Mater Surf Interfaces Biophys* 2006;110:16508–16513.
55. Jang E, Jun S, Pu L. High quality CdSeS nanocrystals synthesized by facile single injection process and their electroluminescence. *Chem Commun (Camb)* 2003: 2964–2965.
56. Skaff H, Sill K, Emrick T. Quantum dots tailored with poly(*para*-phenylene vinylene). *J Am Chem Soc* 2004;126:11322–11325.
57. Crouch D, Norager S, O'Brien P, Park JH, Pickett N. New synthetic routes for quantum dots. *Philos Trans A Math Phys Eng Sci* 2003;361:297–310. discussion 310
58. Alivisatos P. The use of nanocrystals in biological detection. *Nat Biotechnol* 2004;22:47–52.
59. Chan WC and Nie S. Quantum dot bioconjugates for ultrasensitive nonisotopic detection. *Science* 1998;281:2016–2018.
60. Gao X, Cui Y, Levenson RM, Chung LW, Nie S. *In vivo* cancer targeting and imaging with semiconductor quantum dots. *Nat Biotechnol* 2004;22:969–976.
61. Wu X, et al. Immunofluorescent labeling of cancer marker Her2 and other cellular targets with semiconductor quantum dots. *Nat Biotechnol* 2003;21:41–46.
62. Jaiswal JK, Mattoussi H, Mauro JM, Simon SM. Long-term multiple color imaging of live cells using quantum dot bioconjugates. *Nat Biotechnol* 2003;21:47–51.

63. Derfus AM, Chan WCW, Bhatia SN. Intracellular delivery of quantum dots for live cell labeling and organelle tracking. *Adv Mater* 2004;16:961–966.
64. Hoehn M, et al. Monitoring of implanted stem cell migration *in vivo*: a highly resolved *in vivo* magnetic resonance imaging investigation of experimental stroke in rat. *Proc Natl Acad Sci USA* 2002;99:16267–16272.
65. Yeh TC, Zhang W, Ildstad ST, Ho C. *In vivo* dynamic MRI tracking of rat T-cells labeled with superparamagnetic iron-oxide particles. *Magn Reson Med* 1995;33:200–208.
66. Dardzinski BJ, et al. MR imaging of murine arthritis using ultrasmall superparamagnetic iron oxide particles. *Magn Reson Imaging* 2001;19:1209–1216.
67. Ito A, Shinkai M, Honda H, Kobayashi T. Medical application of functionalized magnetic nanoparticles. *J Biosci Bioeng* 2005;100:1–11.
68. Hinds KA, et al. Highly efficient endosomal labeling of progenitor and stem cells with large magnetic particles allows magnetic resonance imaging of single cells. *Blood* 2003;102:867–872.
69. Shapiro EM, et al. MRI detection of single particles for cellular imaging. *Proc Natl Acad Sci USA* 2004;101:10901–10906.
70. Kalish H, et al. Combination of transfection agents and magnetic resonance contrast agents for cellular imaging: relationship between relaxivities, electrostatic forces, and chemical composition. *Magn Reson Med* 2003;50:275–282.
71. Turner AP, Chen B, Piletsky SA. *In vitro* diagnostics in diabetes: meeting the challenge. *Clin Chem* 1999;45:1596–1601.
72. Wilson GS and Hu Y. Enzyme-based biosensors for *in vivo* measurements. *Chem Rev* 2000;100:2693–2704.
73. Newman JD and Turner AP. Home blood glucose biosensors: a commercial perspective. *Biosens Bioelectron* 2005;20:2435–2453.
74. Pickup JC, Hussain F, Evans ND, Sachedina N. *In vivo* glucose monitoring: the clinical reality and the promise. *Biosens Bioelectron* 2005;20:1897–1902.
75. Bolinder J, Ungerstedt U, Arner P. Microdialysis measurement of the absolute glucose concentration in subcutaneous adipose tissue allowing glucose monitoring in diabetic patients. *Diabetologia* 1992;35:1177–1180.
76. Nicolle L. Epidemiology of urinary tract infection. *Infect Med* 2001;18:153–162.
77. Liao JC, et al. Use of electrochemical DNA biosensors for rapid molecular identification of uropathogens in clinical urine specimens. *J Clin Microbiol* 2006;44:561–570.
78. Wang J. Electrochemical nucleic acid biosensors. *Anal Chim Acta* 2002;469:63–71.
79. Drummond TG, Hill MG, Barton JK. Electrochemical DNA sensors. *Nat Biotechnol* 2003;21:1192–1199.
80. Campbell CN, Gal D, Cristler N, Banditrat C, Heller A. Enzyme-amplified amperometric sandwich test for RNA and DNA. *Anal Chem* 2002;74:158–162.
81. Sia SK, Linder V, Parviz BA, Siegel A, Whitesides GM. An integrated approach to a portable and low-cost immunoassay for resource-poor settings. *Angew Chem Int Ed Engl* 2004;43:498–502.

82. Christodoulides N, et al. A microchip-based multianalyte assay system for the assessment of cardiac risk. *Anal Chem* 2002;74:3030–3036.
83. Whiley DM and Sloots TP. A 5'-nuclease real-time reverse transcriptase-polymerase chain reaction assay for the detection of a broad range of influenza A subtypes, including H5N1. *Diagn Microbiol Infect Dis* 2005;53:335–337.
84. Ivanov AP and Dragunsky EM. ELISA as a possible alternative to the neutralization test for evaluating the immune response to poliovirus vaccines. *Expert Rev Vaccines* 2005;4:167–172.
85. Rich JD, et al. Misdiagnosis of HIV infection by HIV-1 plasma viral load testing: a case series. *Ann Intern Med* 1999;130:37–39.
86. van Elden LJ, Nijhuis M, Schipper P, Schuurman R, van Loon AM. Simultaneous detection of influenza viruses A and B using real-time quantitative PCR. *J Clin Microbiol* 2001;39:196–200.
87. Rich R.L and Myszka DG. Spying on HIV with SPR. *Trends Microbiol* 2003; 11:124–133.
88. Myszka DG and Rich RL. Implementing surface plasmon resonance biosensors in drug discovery. *Pharm Sci Technol Today* 2000;3:310–317.
89. Fagerstam LG, et al. Detection of antigen-antibody interactions by surface plasmon resonance. Application to epitope mapping. *J Mol Recognit* 1990;3: 208–214.
90. Alterman M, et al. P1/P1' modified HIV protease inhibitors as tools in two new sensitive surface plasmon resonance biosensor screening assays. *Eur J Pharm Sci* 2001;13:203–212.
91. Toner M and Irimia D. Blood-on-a-chip. *Annu Rev Biomed Eng* 2005;7:77–103.
92. Grodzinski P, Silver M, Molnar LK. Nanotechnology for cancer diagnostics: promises and challenges. *Expert Rev Mol Diagn* 2006;6:307–318.
93. Fehm T, et al. Cytogenetic evidence that circulating epithelial cells in patients with carcinoma are malignant. *Clin Cancer Res* 2002;8:2073–2084.
94. Cristofanilli M, et al. Circulating tumor cells, disease progression, and survival in metastatic breast cancer. *N Engl J Med* 2004;351:781–791.
95. Judson PL, et al. Preoperative detection of peripherally circulating cancer cells and its prognostic significance in ovarian cancer. *Gynecol Oncol* 2003;91:389–394.
96. Moreno JG, et al. Changes in circulating carcinoma cells in patients with metastatic prostate cancer correlate with disease status. *Urology* 2001;58:386–392.
97. Racila E, et al. Detection and characterization of carcinoma cells in the blood. *Proc Natl Acad Sci USA* 1998;95:4589–4594.
98. Raynor M, Stephenson SA, Walsh DC, Pittman KB, Dobrovic A. Optimisation of the RT-PCR detection of immunomagnetically enriched carcinoma cells. *BMC Cancer* 2002;2:14.
99. Smirnov DA, et al. Global gene expression profiling of circulating tumor cells. *Cancer Res* 2005;65:4993–4997.
100. Shigematsu H, et al. Clinical and biological features associated with epidermal growth factor receptor gene mutations in lung cancers. *J Natl Cancer Inst* 2005;97:339–346.

101. Moreno JG, et al. Circulating tumor cells predict survival in patients with metastatic prostate cancer. *Urology* 2005;65:713–718.
102. Vona G, et al. Impact of cytomorphological detection of circulating tumor cells in patients with liver cancer. *Hepatology* 2004;39:792–797.
103. Witzig T.E, et al. Detection of circulating cytokeratin-positive cells in the blood of breast cancer patients using immunomagnetic enrichment and digital microscopy. *Clin Cancer Res* 2002;8:1085–1091.
104. Zieglschmid V, Hollmann C, Bocher O. Detection of disseminated tumor cells in peripheral blood. *Crit Rev Clin Lab Sci* 2005;42:155–196.
105. Rolle A, et al. Increase in number of circulating disseminated epithelial cells after surgery for non-small cell lung cancer monitored by MAINTRAC is a predictor for relapse: a preliminary report. *World J Surg Oncol* 2005;3:18.
106. O'Hara SM, et al. Multigene reverse transcription-PCR profiling of circulating tumor cells in hormone-refractory prostate cancer. *Clin Chem* 2004;50:826–835.
107. Momburg F, Moldenhauer G, Hammerling GJ, Moller P. Immunohistochemical study of the expression of a Mr 34,000 human epithelium-specific surface glycoprotein in normal and malignant tissues. *Cancer Res* 1987;47:2883–2891.
108. Stoop JA, Hendriks JG, Berends D. Identification of malignant cells in serous effusions using a panel of monoclonal antibodies Ber-EP4, MCA-b-12 and EMA. *Cytopathology* 1992;3:297–302.
109. Gaffey MJ, et al. Immunoreactivity for BER-EP4 in adenocarcinomas, adenomatoid tumors, and malignant mesotheliomas. *Am J Surg Pathol* 1992;16:593–599.
110. Rao CG, et al. Expression of epithelial cell adhesion molecule in carcinoma cells present in blood and primary and metastatic tumors. *Int J Oncol* 2005;27:49–57.
111. Mohamed H, et al. Development of a rare cell fractionation device: application for cancer detection. *IEEE Trans Nanobiosci* 2004;3:251–256.
112. Shelby JP, White J, Ganesan K, Rathod PK, Chiu DT. A microfluidic model for single-cell capillary obstruction by *Plasmodium falciparum*-infected erythrocytes. *Proc Natl Acad Sci USA* 2003;100:14618–14622.
113. Farokhzad OC, et al. Nanoparticle–aptamer bioconjugates: a new approach for targeting prostate cancer cells. *Cancer Res* 2004;64:7668–7672.
114. Harishinghani MG, et al. Noninvasive detection of clinically occult lymph-node metastases in prostate cancer. *N Engl J Med* 2003; 348:2491–2499.
115. Battiston FM, et al. A chemical sensor based on a microfabricated cantilever array with simultaneous resonance-frequency and bending readout. *Sens Actuators* 2001;77:122–131.

Nanoscale Iron Compounds Related to Neurodegenerative Disorders

JOANNA F. COLLINGWOOD and JON DOBSON

18.1 INTRODUCTION

In this chapter, we consider the naturally occurring nanoscale iron biominerals and compounds in the human brain, and their incidence in a variety of neurodegenerative disorders. Some of the principal biogenic iron compounds, such as the iron cores in the ferritin iron storage protein, are common and necessary to most life forms and are modified according to purpose and environment [1]. However, biogenic iron compounds may also play a role in neurodegenerative processes. A disruption of normal iron metabolism can leave brain tissue vulnerable to oxidative stress damage [2–5], as can the brain iron accumulation associated with disease pathology in a wide range of neurodegenerative disorders [3, 4, 6–10]. While much remains to be understood about the role of iron in neurodegeneration, the regional accumulation of iron has been recognized as providing biomarker potential for detection, diagnosis, and staging [11, 12], and a potential target for therapeutic intervention with chelating agents [13]. Biogenic iron compounds are discussed from a biomedical imaging perspective, with direct relevance to disease detection and staging and to the application of magnetic iron nanoparticles to biomedical research [14–16].

18.2 IRON IN THE HUMAN BRAIN

18.2.1 General Overview

Iron is an essential element in the human body and has numerous functions that are beyond the scope of this (chapter 18). Unlike in other organs, brain

iron is unique in having specific patterns of distribution, both at the anatomical and at the cellular level [18], and is generally categorized either as “heme” or “nonheme” iron. The origin of this distinction is attributed to Zaleski [19], who demonstrated that iron in hemoglobin (“heme iron”) did not react with potassium ferrocyanide, and that the iron staining with Perls stain (see Section 18.5.2) must therefore be in another form (i.e. “non-heme”). This early discovery, and Zaleski’s deduction that the majority of brain iron was primarily ferric (Fe^{3+}), and linked to a protein, occurred many decades before the identification of ferritin as the principal iron storage protein in brain [18].

Heme iron includes the iron in hemoglobin, which is critical for transporting oxygen from the lungs to tissue, and the iron in enzymes such as peroxidases. Nonheme iron is present in a wide variety of forms including nanoscale particles. It plays a variety of essential roles in normal metabolism, from neurotransmitter synthesis to myelination, and contributes to cellular aerobic metabolism through its role in producing adenosine triphosphatase (ATP) [20]. Iron is unusual in that it adopts both the ferric and ferrous (Fe^{2+}) valence states *in vivo*, and utilizes this property in uptake, transport, and storage. An excess of ferrous iron can be toxic, leading to subsequent death of neurons by apoptosis [21]. For instance, ferrous iron reacting with hydrogen peroxide (H_2O_2) via the Fenton reaction, or with peroxy nitrates, catalyzes oxidant-mediated damage. In humans, nonheme brain iron tends to accumulate until the age of 40, with further region-specific increases in brain iron in later life [10, 22–24].

While some iron is bound in low molecular weight complexes, and on metalloproteins such as transferrin, lactoferrin, and melanotransferrin, a significant proportion of nonheme iron is present in iron storage proteins, predominantly ferritin, and arguably in hemosiderin [1]. The origins and form of hemosiderin are ambiguous and not well understood, as will be discussed later in this chapter. Large amounts of iron are contained in neuromelanin granules [25], and in addition to ferritin and hemosiderin, a mixed-valence iron compound has been found in brain tissue in the form of magnetite nanoparticles [26, 27]. Brain iron has also been reported bound in myelin, where it is thought to play an important role in the formation of the myelin sheath—an insulating layer surrounding axons [28]. Further evidence for this role is provided by studies of brain homogenates that have demonstrated comparatively high levels of H-ferritin mRNA in myelin (29).

18.2.2 Iron Storage

In this section, we discuss four forms of sequestered iron: ferritin, which is widely recognized as the primary form of iron storage; hemosiderin, which is less well understood; magnetite, a mixed-valence iron oxide that may signify disrupted iron metabolism; and neuromelanin, which is an example of a complex iron-rich molecular structure. Ferritin and hemosiderin are assumed to contain iron as superparamagnetic antiferromagnetic particulates, while

magnetite is ferrimagnetic. It should be noted that iron stores quantified in brain tissue appear several orders of magnitude higher than those required for known physiological processes [10]. On this basis, it appears that there are significant aspects of iron metabolism that are not yet understood.

18.2.2.1 Ferritin The majority of nonheme iron in the brain, as in the rest of the body, is thought to be present in the iron storage protein, ferritin—a spherical protein shell 12 nm in diameter with an 8-nm hollow cavity. As ferrous iron passes through one of the six channels in the protein shell, it is sequestered as a ferric iron core within the cavity. The biosynthesis of ferritin is dependent on translational control by iron regulatory protein 1 (IRP-1, the ferritin repressor protein) and IRP-2 [30–33], where IRP1 is most evident in astrocytes [34]. The ferritin iron cores are typically a few nanometers in diameter, where the internal protein core diameter limits them to 7–8 nm. The structure of the cores is not well established, but is generally accepted to be a hydrated ferric (ferrihydrite-like) iron oxide ($5\text{Fe}_2\text{O}_3 \cdot 9\text{H}_2\text{O}$), based primarily on X-ray and electron diffraction and high resolution electron microscopy studies [35–37]. Further information on the structure of ferritin cores has been obtained using electron nanodiffraction and electron energy loss spectroscopy, demonstrating that while the cores are predominantly ferrihydrite-like, other mineral phase crystal structures are also present including magnetite/maghemite-like structures, hematite, and a wüstite-like structure [38–40]. The ferritin protein stores excess iron and is understood to play a dual role in both preventing ferrous iron toxicity and providing an accessible source of iron for metabolic activities [1].

The protein shell (apoferritin) is composed of 24 subunits of two homologous polypeptides: light (L)-chain and heavy (H)-chain ferritin. Despite their names, there is only a slight difference in molecular weight between the H and L subunits (approximately 21 and 19 kDa, respectively). Separate genes are responsible for making the L and H ferritin, and the ratio of H:L in apoferritin varies with factors including region and age. H-chain ferritin is dominant in the brain, and its concentration increases with age in most regions of the brain, while L-chain only increases in the substantia nigra and globus pallidus [24, 23]. In the elderly, the ratio of H- to L-chain ferritin is between 1.5:1 and 3:1 depending on the region [12]. The subunits are thought to have distinct functions. The H-chain ferritin subunit has a ferroxidase center, providing it with the ability to rapidly sequester and utilize iron. It is associated with regions of stress, and the cores formed in H-chain-rich ferritin are typically smaller and less crystalline than those in L-chain. H-chain ferritin is therefore prominent in organs with high iron utilization. Conversely, the L-chain subunit is efficient at iron nucleation and is associated with long-term iron storage [1, 41, 42].

In human ferritin, the cores normally have a ferrihydrite-like structure. Cores with a ferrous component have been formed *in vitro*, either by incomplete oxidation of Fe^{2+} that is usually converted entirely to Fe^{3+}

during formation of the core or by reduction of an existing ferric iron core [43, 44]. Apoferritin (the empty shell prepared by removal of the ferrihydrite core) has also been used as a template for biomimetic synthesis of magnetite nanoparticles [16]. There is increasing evidence that ferrous components may occur in ferritin cores *in vivo*, particularly in the neurodegenerative state [40, 45], and the amyloid- $\beta_{(1-42)}$ peptide, a key component of Alzheimer's disease (AD) pathology, has been implicated in the reduction of ferric iron under physiological conditions [46].

The ultrastructure of both normal and pathogenic ferritin cores has been studied in detail using electron microscopy and diffraction [37, 38, 40]. The ferritin protein plays an active role in determining the properties of the core, as if cores are precipitated in the absence of ferritin, the hydrated iron oxides formed differ from normal ferritin cores and exhibit a lepidocrocite or goethite-like structure [47]. The ferrihydrite structure formed *in vivo* exhibits hydration and multiple lattice vacancies, which arguably enables rapid utilization of iron from ferritin, and also renders the cores less stable than other common iron oxide minerals such as maghemite, lepidocrocite, hematite, and goethite [42, 48]. The nanoscale particles have by definition a large surface: volume ratio, and it has been estimated that approximately 40% of the Fe atoms in a core of 2100 atoms are at the surface [49].

Originally, it was thought that two pathways were involved in the mineralization of ferritin cores, but at least one additional pathway has been demonstrated *in vitro* by Zhao et al. [50]. The mineralization of iron oxide cores in various recombinant H-chain and L-chain homopolymer and heteropolymer ferritins was investigated, with emphasis on iron oxidation and hydrolysis chemistry in association with iron flux into the protein. The first pathway concerns the H-subunit catalyzed ferroxidase reaction, which was evident for all levels of iron loading, but decreased with increasing addition of iron. The second pathway, concerning reaction at the mineral surface, dominated for loading of approximately 800 Fe^{2+} /protein and is the main means by which mineral cores are deposited for human L-chain ferritin and H-chain forms that lack functional nucleation and/or ferroxidase sites. The third pathway, involving $\text{Fe}^{2+} + \text{H}_2\text{O}_2$ detoxification, was predominantly evident for intermediate loadings of iron (100–500 Fe^{2+} /protein), where this reaction consumed some of the H_2O_2 from the ferroxidase reaction [50].

18.2.2.2 Hemosiderin Hemosiderin is widely considered to be an iron storage protein and/or a degradation product of ferritin. It is a poorly defined water-insoluble, iron-rich protein–mineral complex, associated in particular with sites of hemorrhage and iron overload, and is typically found in lysosomes and siderosomes in hemochromatosis. The nature of hemosiderin is not straightforward to characterize [51], and it is likely that the structure varies from one tissue to another. There is evidence to suggest that hemosiderin forms by several pathways, including lysosomal degradation of the ferritin shell [1] (which is responsive to immunostaining for the ferritin

protein), and another pathway that produces deposits that do not readily stain for ferritin. Chasteen found hemosiderin cores to be smaller than ferritin cores for a given tissue sample [42], and the structure of the hemosiderin cores to be ferrihydrite-like for healthy cases. *In vitro* work with human spleen ferritin and hemosiderin showed that conversion of ferritin into hemosiderin decreases the ability of iron to promote oxygen-radical reactions. It was suggested on this basis that hemosiderin might have a protective role in instances of iron overload [52].

Much of our understanding of ferritin and hemosiderin is gleaned from studies of the human liver and spleen. Hemosiderin is particularly prevalent in the liver in iron-overload diseases such as primary hemochromatosis and β -thalassemia, and therefore, many of our assumptions about brain hemosiderin are extrapolations from other organs. This is also the case to an extent for ferritin, although there have been studies looking at various properties of extracted human brain ferritin [39, 40, 53]. Pathological deposits of hemosiderin appear to be relatively inert and stable, based on studies of intracerebral hemorrhage and superficial siderosis (where slow chronic bleeding leads to extensive ferritin and hemosiderin deposition) [54]. It is not known whether hemosiderin accumulating via other pathways is as stable or inert. It has been claimed that hemosiderin is always related to an excess of iron, and that the iron in hemosiderin cores is more easily released than iron in ferritin [55].

As will be discussed in Section 18.5, the application of a variety of techniques to the study of iron compounds in brain tissue is necessary to fully characterize and distinguish between the forms of iron. Examples include Mössbauer spectroscopy, high resolution electron microscopy and diffraction, X-ray spectroscopy, superconducting quantum interference device (SQUID) magnetometry, and nuclear magnetic resonance (NMR) [53, 56–59]. Conventional descriptions of brain iron storage are usually limited to ferritin and hemosiderin, but the application of a variety of characterization techniques has allowed consideration of alternative forms, including iron bound to lipofuscin [60] and contained in neuromelanin (see Section 18.2.2.4). The ability to locate and characterize iron (structurally and chemically) *in situ* in unstained tissue at a subcellular resolution [58, 61], in combination with protein staining techniques, should enable an improved understanding of the role of these various iron compounds in brain tissue.

18.2.2.3 Magnetite Magnetite is a ferrimagnetic iron oxide that is present in many living creatures, from magnetotactic bacteria to pigeons and fish. It is often assumed, particularly from brain imaging and biohazard perspectives, that there are no ferromagnetic materials in human tissue. Contrary to this assumption, magnetite (including particles large enough to have a permanent magnetic alignment) has been extracted from human brain tissue [26, 27]. The magnetite crystal structure has also been observed in extracted human brain ferritin [39, 40], and magnetite has been demonstrated

by X-ray spectroscopy in intact human brain autopsy tissue [45]. Magnetite is a ferrimagnetic iron oxide (Fe_3O_4) formed from alternating lattices of Fe^{2+} and Fe^{3+} . The origins of magnetite in the human brain are unclear, although given that it has been identified in particularly iron-rich regions such as the hippocampus [27], and in AD brain tissue [45], its presence may be indicative of disrupted brain iron metabolism. It has been suggested that the precipitation of magnetite inside the ferritin shell, possibly due to a failure to fully oxidize Fe^{2+} on uptake into ferritin [1], may be a precursor for the formation of magnetite particles in the brain [8]. In 2002, preliminary data were reported that suggest concentrations of biogenic magnetite in males increase beyond age 40 in the hippocampus [62].

18.2.2.4 Neuromelanin Neuromelanin is a complex multilayer molecule that forms the pigment evident in high concentrations in both the dopaminergic neurons of the substantia nigra and the noradrenergic neurons of the locus coeruleus [63, 64]. Neuromelanin is typically present in organelles, known as neuromelanin granules, which also contain lipofuscin [63]. Neuromelanin binds a variety of toxic compounds and metals, modulating their effects [63]. Iron is a constituent of neuromelanin, where the molecule takes up redox-active Fe^{2+} and binds it as ferric iron to oxygen-derived phenol groups. The iron sites have a ferritin-like iron oxyhydroxide cluster form [24]. In Parkinson's disease (PD) tissue, some groups have reported a 30–35 % increase in nigral Fe, and the increased iron content in neuromelanin granules led to the conclusion that much of the additional iron was associated with the neuromelanin [57, 65]. However, the absolute nigral concentration of neuromelanin, while increasing with normal ageing, is observed to decrease significantly in PD [66]. The sequestering of redox-active metals and drugs indicates that neuromelanin may have a protective role and limit neuronal damage [63], although it arguably promotes the release of neurotoxins from microglia [10, 63].

18.2.3 Regional Distribution of Iron Compounds

The regional anatomical distribution of iron has been investigated in a number of ways. Originally, histochemical iron staining (Perls stain, see Section 18.5.2) was used to demonstrate strong regional variations in ferric iron throughout the brain architecture. The first color illustrations of the differential distribution of brain iron were produced by Spatz, where histochemical staining for iron in white matter was negligible, with some staining in the cerebral cortex and intense staining in regions of the extrapyramidal system [67]. Drayer subsequently used Perls stain to demonstrate significant iron staining in the temporal lobe and higher levels of iron in the frontal than occipital white matter regions [68]. By contrast, biochemical assay of postmortem brain revealed iron that had been unavailable for staining and provided a means of quantifying iron levels in specific regions. The highest

concentrations of brain iron revealed in this manner were $\sim 200 \mu\text{g/g}$ wet weight, notably in regions such as the globus pallidus, red nucleus, substantia nigra, and putamen. An extensive review of iron, ferritin, and transferrin concentrations by region is tabulated elsewhere [12], and perhaps the most striking difference between findings with biochemical assay and histochemical staining is for the white matter, where concentrations of iron are typically equivalent to those in the gray, and in specific regions such as the motor cortex can exceed those in adjacent gray matter [69, 70]. In the healthy brain, the extrapyramidal regions (associated with motor function) exhibit the highest concentrations of iron, although these high concentrations are not present at birth and tend to accumulate on approaching adulthood. The role of these high concentrations is not understood, as known processes utilizing brain iron only require 5–10% of that actually present [10]. In general, ferritin distribution closely matches iron distribution, with concentrations in the basal ganglia being two to three times those in the cerebral cortex. Ferritin levels in the cortical gray and adjacent white matter are also similar [12, 69].

At the cellular level, Perls staining originally demonstrated iron in microglia, oligodendrocytes, astrocytes, nerve cells, and possibly in axons and myelin sheaths [67]. Oligodendrocytes stain most intensely for iron in the human brain, although they exhibit patchy staining in white matter, and the significance of this is not known [18]. Expression of ferritin occurs in oligodendrocytes, neurons, and microglia, which suggests that all these cells have iron storage capacity [10]. Differences in the ferritin isoforms occur at the cellular as well as the regional level. Neurons are rich in H-chain ferritin, favoring high iron uptake and exhibiting peroxidase activity, while macrophages and microglia express primarily L-chain ferritin and are associated with iron storage [70]. Oligodendrocytes exhibit a mixture of H- and L-chain ferritin, and do so at a much higher level than neurons, although the H-chain-stained oligodendrocytes have a patchy distribution in white matter that parallels iron staining [71, 72]. Astrocytes are generally devoid of ferritin expression. From light microscopy observations of nonheme iron in brain tissue [73], it has been suggested that intracellular iron deposits are hemosiderin contained in siderosomes [10], as ferritin in the cytosol only produces a pale blue background. The reported nonuniformity of iron deposition in brain tissue [73] is significant for magnetic resonance imaging (MRI) iron concentration and T2 relaxation rate models, as it will lead to substantial variations in local iron concentration at the cellular level. Detailed ultrastructural (electron microscopy) studies have been performed of the nonuniform distribution of ferritin and hemosiderin in iron-overloaded liver, but similar studies of brain tissue are comparatively recent [55].

18.2.4 Iron Transport

Transferrin (Tf) is generally acknowledged as the primary protein responsible for transporting iron from the blood into brain tissue, via transferrin receptors

in the brain's microvasculature. Tf is composed from a single chain of amino acids and two carbohydrate groups onto each of which a single Fe^{3+} ion can bind. Only a tiny fraction of brain iron is bound to Tf at any instant, with Tf protein levels typically 10–50 times lower than ferritin concentrations per unit of protein [12]. The regional distribution of Tf and ferritin is also quite different. Typically, white matter demonstrates uniform staining for Tf and patchy staining for iron and ferritin, whereas gray matter has patchy staining for Tf and uniform staining for ferritin and iron. Levels of Tf in white matter are approximately three times higher than those in gray matter [23], and astrocytes tend to accumulate Tf with age [23, 71]. A detailed illustration of the Tf cycle is given by Zecca et al. [10], although as discussed in some detail by Burdo and Conner [74], there is compelling evidence for both Tf-bound and non-Tf-bound iron delivery, and the mechanisms by which brain iron homeostasis is maintained are only partially understood. A variety of iron transport proteins that can cross cell membranes and organelles have been identified, including divalent metal transporter 1 (DMT1), natural resistance associated macrophage protein 2 (NRAMP2), and ferroportin (MTP1), and these are reviewed elsewhere [75, 76]. There is immunohistochemical evidence for DMT1 in neurons, glial cells, and the cells of the vessel wall [77], while ferroportin appears to be present mainly in neurons [78], with further evidence for it in endothelial cells of the blood–brain barrier (BBB) and synaptic vessels within the CNS [76].

18.3 IRON COMPOUNDS IN NEURODEGENERATIVE DISORDERS

18.3.1 Overview

Neurodegenerative disorders exhibit disease-specific populations of neurons vulnerable to degeneration. Many are associated with regions exhibiting enhanced iron accumulation, particularly those areas associated with motor function that are normally rich in iron, such as the dopaminergic neurons of the substantia nigra in PD [103]. Other vulnerable populations include the neurons of the hippocampus in AD. The selective vulnerability of these cell populations is not fully understood, but the presence of high levels of iron may provide a catalyst for excess generation of reactive oxygen species and oxidant-mediated damage [2, 10].

The regional pattern of iron accumulation varies from one disease to another, even in similar recessive genetic disorders such as aceruloplasminemia and pantothenate kinase associated neurodegeneration (PKAN), but there are strong similarities in the local management of iron overload at the cellular level. There is evidence that tissue responds to excess iron by converting free iron to ferritin, uptake by microglia, and then astrocytes, followed by axonal expansions (spheroids). Iron is then thought to accumulate in neurons as a result of their increased permeability [18]. The form, including crystalline and

valence state, of accumulated nonheme iron is also critical in interpreting the origin and impact of the iron compounds.

We are still a long way from a thorough understanding of the nature of iron accumulations in neurodegenerative disease, and from knowing whether little-observed iron compounds such as magnetite, hemosiderin, and wüstite are normally present or indicative of the disease state. Ferritin levels normally increase with aging in the human brain [23, 79], but this does not appear to be the case in AD or PD [23, 80]. The failure to generate additional ferritin, despite recognized regional iron accumulation in these diseases, may lead to overloading of existing cores, to alternative forms of stored/bound iron, or to an excess of free iron and associated oxidant-mediated stress.

In iron-overload diseases such as hemochromatosis, hemosiderin is found in siderosomes and lysosomes, and is frequently cited as being a form of brain iron storage, even though there is very little direct evidence of hemosiderin deposition in brain tissue. The very presence of hemosiderin in brain tissue has recently been called into doubt [81], but various studies have provided experimental evidence for hemosiderin in human brain, including the demonstration of hemosiderin-rich lysosomes and siderosomes in the caudate nucleus in progressive supranuclear palsy (PSP), and of hemosiderin in hippocampal tissue from AD patients [40, 55]. The use of combined chemically and structurally sensitive techniques [45, 55, 88] may allow progress in understanding this rather ambiguous iron compound.

The extraction of a mixed valence iron oxide (magnetite), from human hippocampal tissue [27], and its observation in AD tissue [45] may be indicative of disruption iron homeostasis and a failure to fully oxidize redox-active iron in regions vulnerable to oxidative stress and neuronal atrophy [8]. Mechanisms by which excess iron influences neurodegeneration may include protein malfunction, for example, the aggregation of amyloid peptides that are associated with iron accumulation and neurotoxicity [46], and mutations in the genes encoding ferritin [82]. The isoforms of ferritin may also have an influence on the vulnerability of certain cell populations, as the relative levels of H and L-chain ferritin affect the local capacity to respond to excess iron. The protective role of H-ferritin has recently been illustrated, where Zhao et al. demonstrated that H-chain ferritin greatly attenuates $\bullet\text{OH}$ radical generation from the Fenton reaction. The ferroxidase site in the H-chain subunit was identified as being responsible for this activity [83]. It should be noted that many findings relating to iron overload in neurodegenerative disorders are based on iron sourced from human tissue other than the brain, or from animal models. The specificity of ferritin isoforms, and of local biochemistry in vulnerable regions of the brain, means that one cannot necessarily extrapolate these findings directly to brain tissue.

There is an increasing body of research looking at iron transport proteins, including IRP2 and DMT1, and the effects in either knockout or genetically deficient animal models. The consequences of knocking out IRP2 have

included neurodegenerative symptoms and evidence of brain iron accumulation [11, 33].

It is becoming more difficult to distinguish between rare forms of brain iron accumulation with a clear genetic basis (e.g., neuroferritinopathy), and other disorders exhibiting iron accumulation such as AD where iron-homeostasis-related genetic risk factors are increasingly evident. While accumulations of brain iron are only one component in a wide spectrum of disorders, understanding the origins of disrupted brain iron metabolism may provide stratagems for progress in detection, disease staging, and therapy.

18.3.2 Alzheimer's Disease

In AD, iron is seen to accumulate in the brain, but while in normal ageing there is an increase in both iron and ferritin, in AD there is some evidence that the increase in iron is not paralleled by an increase in ferritin [69]. This implies that ferritin loading may increase and/or that excess iron may not be stored in the usual fashion and may be a candidate for generating the oxidative damage observed in AD. Certainly, senile plaques exhibit a strong immunoreactivity for ferritin, and ferritin-containing cells are found in the periphery of the plaque core. There is evidence of iron-containing cells extending into the plaque cores: these are thought to be microglia [12], and iron-rich microglia have been demonstrated surrounding senile plaques [69, 84]. While iron and ferritin-reactive microglia are associated with destructive processes, and microglia may accumulate both iron and ferritin, this does not suggest that there is an overall increase in brain iron. Indeed, early research indicated that total brain iron does not alter in AD [22].

In addition to senile plaques, many blood vessels exhibit strong immunoreactivity for ferritin, and ferritin is found particularly in hippocampal gray matter. Intracellular accumulations of ferritin and hemosiderin were demonstrated in hippocampal tissue from AD [55], a key area of neurodegeneration and atrophy, indicating that these nanoscale iron oxide particle accumulations may play a role in AD pathogenesis. Notably, similarities were identified between isolated AD brain ferritin cores and hemosiderin cores from hemochromatosis sufferers, where the composition of the cores differed from the normal ferrihydrite-like structure, and included a wüstite-like Fe^{2+} -rich oxide [40]. *In vivo* work has revealed T2 shortening in MR images at 3 T from the hippocampus for AD compared to controls, supporting evidence for detectably elevated iron concentrations in hippocampal tissue in the disease state [85]. In many MRI studies of AD patients, autopsy tissue, and animal models of AD, small regions of hypointensity are frequently observed, with many of these being attributed to cerebral amyloid angiopathy associated microbleeds and corresponding accumulations of hemosiderin [86]. An apparent decline in myelin in both aging and AD has

also been demonstrated, with the suggestion that the decline may be linked to the iron content [87].

It has been shown *in vitro* that iron influences the processing of amyloid precursor protein (APP) via an iron-responsive element [88], and the aggregation of amyloid peptides found in senile plaques in AD [89–91]. In addition, Fe^{3+} can be reduced to Fe^{2+} by $\text{A}\beta_{(1-42)}$ aggregation under physiological conditions [46], a finding that is particularly interesting in that it provides a mechanism for the formation of toxic redox-active Fe^{2+} at pH 7.4 and involves the amyloid peptide most prominent in senile plaque pathology. The role of senile plaque formation is contentious, and while it is generally thought that initial oligomerization is toxic, the metal-sequestering abilities of senile plaques [69] may indicate a protective role for amyloid.

In addition to the presence of Fe^{2+} -rich oxides in AD ferritin cores [40], it has been further shown that Fe^{2+} iron is associated with the ribosomes of hippocampal pyramidal neurons in AD [5] and neurofibrillary tangles [3, 92]. Mixed-valence iron compounds have also been demonstrated, with a SQUID magnetometry study of tissue from the superior temporal gyrus revealing higher levels of magnetite in female AD cases compared to controls [93], and localized accumulations of magnetite and ferritin-like ferrihydrite being demonstrated in AD autopsy tissue from the superior frontal gyrus using X-ray spectroscopy [45].

18.3.3 Huntington's Disease

Huntington's disease (HD) is caused by genetic mutation of the huntingtin protein, with disease onset in middle to late age. Evidence exists at several levels for the involvement of iron in HD. Early postmortem studies of cerebral iron deposition in HD tissue revealed elevated levels of iron in the striatum [94, 95], and there is specific neurodegeneration of striatal neurons from an early stage in the disease process [96]. Disrupted expression of iron transport proteins has been implicated for HD, along with other disorders including AD, PD, and amyotrophic lateral sclerosis (ALS) [97]. Meanwhile, at the genetic level, huntingtin is reportedly iron responsive and involved in the regulation of iron homeostasis [98]. In clinical studies, early MRI investigations of HD patients identified abnormalities in the striatum [99], and more recent work has explored the potential of MRI to detect iron overload in the basal ganglia of HD patients using field-dependent relaxation rate increase (FDRI) [100].

18.3.4 Parkinson's Disease

Iron accumulation has been linked to cell death in both PD and other Lewy-body-related disorders [101]. It is often stated that levels of iron are increased in postmortem brains of PD patients compared with age-matched controls,

although these studies typically concern specific iron-rich and vulnerable regions such as the substantia nigra. A variety of techniques have been used to determine total nigral iron, and not all have shown a significant difference between disease and control, although this is usually for milder cases and may be in part due to the impact on iron of tissue processing and of the specific sensitivities of the techniques used [10, 64]. Another region exhibiting disease-specific iron accumulation is the lateral globus pallidus, which may be linked to the vulnerability of dopaminergic neurons [95]. Iron levels appear to increase in connection with pathological disease progression, with neurons being rich in iron-containing neuromelanin, and glial cells containing iron (Fe^{3+}) predominantly in ferritin. Neuromelanin is a strong iron chelator, so iron levels in the neuronal cytoplasm are low in PD [65]. It should be noted that the majority of these studies used formalin-fixed tissues, which generally leads to the loss and redistribution of iron. A recent electron microprobe study used unfixed frozen sections and demonstrated a doubling of iron concentrations in both individual neurons and surrounding neuropil of the SNzc [102].

Deposits of ferric iron have been found in oligodendrocytes, astrocytes in the vicinity of neurons, microglia, pigmented neurons [64], and in the rim of Lewy bodies in the SNzc of PD patients. Evidence from the pallidum and putamen supported these findings. As found for areas of damage in AD, there is an increased number of ferritin-loaded microglia in the SN in PD, and reactive microglia were found in connection with degenerating and neuromelanin-loaded dopaminergic cells [10]. Microglial activation by the neuromelanin–iron complex, particularly by neuromelanin released from dead and dying neurons, is thought to be responsible for the release of various neurotoxic compounds [10]. Protein aggregation is also a feature of PD, where a principal component of Lewy bodies (a pathological hallmark of PD and related disorders) is the α -synuclein protein. Extrapolating from *in vitro* findings, iron may contribute to toxicity *in vivo* through an influence on α -synuclein fibril formation and aggregation [91, 103].

Neurodegeneration in PD occurs prior to the onset of clinical symptoms, and early studies did not indicate an increase in total iron at this stage. However, it has been argued that iron mismanagement might occur at this early stage via intra- and intercellular translocation [10]. *In vivo* observations of elevated iron in PD patients have been performed using MRI [104], with evidence of correlation between basal ganglia iron and neurological symptoms [105]. The mechanisms leading to increased iron in the SN are currently unknown. While ferritin was not observed in demelanized neurons of the SN in PD [106], the iron loading of ferritin in PD has been shown to increase [107], and altered expression of various iron transport proteins has been observed, along with conflicting results from studies to determine whether upregulation of ferritin expression in the SN of PD patients occurs in response to iron elevation [10]. Gene mutations in iron proteins responsible for homeostasis have been implicated, along with the possibility of a “leaky” BBB [10].

18.3.5 Neurodegeneration with Brain Iron Accumulation

Neurodegeneration with brain iron accumulation (NBIA), formerly Hallervorden–Spatz syndrome, describes a rare disorder exhibiting excessive iron accumulation in brain regions including the globus pallidus and substantia nigra pars reticulata. These regions coincide with the primary sites of neuronal atrophy, and iron is implicated in the neurodegenerative process. There are strong regional similarities in iron accumulation between PD and NBIA, and the cellular pattern of iron staining is consistent with many other types of neurodegeneration with brain iron accumulation. Staining is particularly evident in hypertrophic microglia, macrophages, spheroids, and neurons. A genetic defect is evident in the gene encoding pantothenate kinase 2 (PANK2) in the majority of NBIA sufferers, with this recessive variant known as PKAN [108]. It has been suggested that perturbed cysteine modification may be at least in part responsible for iron accumulation in the basal ganglia [109]. The iron overload typically leads to an MRI signature in the globus pallidus exhibiting a hypointense region with a hyperintense core. This is termed the “Eye of the Tiger” and is increasingly being used as a principal diagnostic feature [108].

18.3.6 Aceruloplasminemia

Aceruloplasminemia is a rare autosomal recessive condition, with mutations in the ceruloplasmin gene leading to an absence of functional ceruloplasmin in plasma. Given that astrocyte-specific expression of ceruloplasmin has been shown to be essential for iron metabolism and neuronal survival in the CNS [110], systemic iron overload is a feature of the disorder, accompanied by neurologic symptoms. Iron overload is evident in neurons, astrocytes, microglia, and oligodendrocytes. The excessive regional accumulation of brain iron contradicts earlier assumptions that the adult BBB could protect against iron overload [111, 112]. Although the basal ganglia exhibit excessive iron accumulation, the specific pattern of iron accumulation is quite distinct from that in NBIA [113, 114], with an absence of accumulation in the globus pallidus. Intense staining occurs in the caudate nucleus, putamen, red nucleus, substantia nigra, and dentate nucleus. However, at a cellular level the findings parallel those in many other disorders with iron accumulating in microglia, astrocytes, spheroids, and neurons. As for PKAN, signal loss in MRI images has been used as an initial indicator of each of these diseases [11].

18.3.7 Neuroferritinopathy

Neuroferritinopathy is a rare dominantly inherited adult-onset form of neurodegeneration, and an example of a disease where iron dysmetabolism has been identified as the primary factor in pathogenesis. Neuroferritinopathy is caused by a mutation in the gene encoding L-chain ferritin [82, 115], leading to a breakdown in iron nucleation and storage, particularly evident in the basal

ganglia. Intense iron deposition is observed in the caudate nucleus, putamen, substantia nigra, and globus pallidus, including abnormal aggregates of ferritin in the latter two [82], with a pattern similar to the “Eye of the Tiger” (Section 18.3.5) appearing in the caudate nucleus [18]. These findings are accompanied by low serum ferritin concentrations [115]. At the cellular level, abnormal accumulations of ferritin have been observed within striatal and cortical neurons and glia, accompanied by extensive neurodegeneration [116].

18.3.8 Other Neurodegenerative Conditions

Other neurological conditions exhibiting disrupted brain iron include human immunodeficiency virus (HIV)-associated dementia (HAD), ALS (motor neuron disease), Friedreich’s ataxia, multiple sclerosis, PSP, cerebral infarction, and Down syndrome [12, 117].

HAD affects around one fifth of HIV patients, and MRI has indicated elevated iron concentration in the basal ganglia, particularly in the globus pallidus, for HIV patients compared to controls [118]. There is also evidence for iron-laden microglia in the white matter of brains of HIV patients [119]. The implications of iron overload in HIV, in conjunction with various types of anemia that also present in HIV disease, are discussed elsewhere [120].

In Friedreich’s ataxia, a defective protein, frataxin, is implicated in disrupted iron metabolism [121]. Mitochondrial iron accumulation is a primary feature in the disease, and frataxin, which has been postulated as being responsible for mitochondrial iron storage, iron export from mitochondria, and iron–sulfur cluster biosynthesis, is largely absent in Friedreich’s ataxia [122]. Iron accumulation occurs in the central nervous system and in the heart, accompanied by extensive neurodegeneration in the dentate nucleus [123]. However, the association between principal areas of neuropathology and of iron accumulation is not clear, and the role of frataxin in homeostasis, and its iron-binding properties, continues to be a matter of debate [81].

Multiple sclerosis (MS) is characterized by inflammation and demyelination of the axons of neurons. Axonal injury occurs during demyelination, followed by the formation of plaques. Redox-active metals, including iron, have been strongly implicated in MS pathogenesis, and globular structures of nonheme iron have been observed on the periphery of older MS plaques with deposition patterns not dissimilar to those seen in AD [70].

Another disorder linked to disrupted brain iron is restless legs syndrome (RLS), which is often linked to iron deficiency [124], but can also occur in conjunction with PD where regional brain iron accumulation is a key feature.

18.3.9 Hemochromatosis

Hemochromatosis is an iron-overload disease in which the absorption and accumulation of excessive dietary iron leads to organ failure from iron-related toxicity. Hemosiderin with ferrihydrite-like, goethite-like, and Fe^{2+} -rich

wüstite-like forms has been observed in hemochromatosis tissues, with evidence for disease-dependent structural differences in the cores [40, 42]. Variants of hemochromatosis include those with mutations in genes encoding HFE, transferrin receptor 2 (TfR2), hemojuvelin (HJV), and hepcidin [125].

While hemochromatosis is primarily associated with the liver, iron accumulation is also observed in other organs including the heart, pancreas, and brain. Altered brain iron concentrations have been demonstrated with MRI, including studies of the basal ganglia that indicated iron accumulation in association with hemochromatosis [126, 127] and decreased iron concentration in hemochromatosis associated with RLS [124].

There are indications that the HFE gene is a risk factor for, and affects the age of onset of, AD [128]. The HFE protein is reportedly expressed by cells associated with senile plaques and by reactive astrocytes in AD patients, and found in blood vessels in the brain and in the choroid plexus [10, 128]. The HFE mutation in AD provides further evidence that disrupted iron metabolism in the brain is a contributing factor, and the mutation may be a significant risk factor for the disease, as well as being associated with increased oxidative stress in neurodegeneration [129, 130]. PD is also linked with hemochromatosis, with evidence for both brain iron accumulation [126] and HFE-related genetic mutations [81].

18.4 MAGNETIC PROPERTIES OF NANOSCALE BRAIN IRON COMPOUNDS

Iron biominerals exhibit a range of magnetic properties. While human tissue is primarily constituted of diamagnetic material, the uncompensated spin associated with iron atoms gives iron-containing materials paramagnetic properties. Coupling between these spins depends on the crystallographic structure and gives rise to various forms of magnetic ordering. The degree of crystallinity is also important in determining the magnetic properties [42]. In the normal ferrihydrite-like cores of ferritin and hemosiderin, there is antiferromagnetic ordering at room (and body) temperature. The goethite-like structure, which is observed for some hemosiderin, is antiferromagnetic. However, the spin compensation is not perfect, which gives rise to weak ferromagnetism [131]. By contrast, magnetite displays ferrimagnetic order due to sublattices of iron where the spin coupling is mediated by the oxygen atoms. Magnetite has a comparatively high saturation magnetization ($\sim 90 \text{ A m}^2/\text{kg}$, compared to $<1 \text{ A m}^2/\text{kg}$ in goethite) at room temperature. These magnetic properties provide a means to distinguish between iron biominerals in tissue (see Section 18.5.3) and raise issues about the significance of magnetically ordered material in the brain [26]. The presence of magnetically ordered particles of magnetite, for example, may be important in the context of radio-frequency signal transduction [132] and in influencing region-specific brain biochemistry through the presence of strong local magnetic field gradients

[8, 133]. The size distribution of iron biominerals observed in human brain tissue is also important in determining their magnetic properties. The majority, including ferritin cores, are superparamagnetic by virtue of their small volume, which prevents the stabilization of magnetic domains. Also, the high surface to volume ratio of these particles means that the antiferromagnetic oxide particles in typical ferritin cores have a nonnegligible net magnetic moment due to uncompensated spins [42, 134]. An NMR magnetic susceptibility study of reconstituted ferritin iron cores demonstrated that antiferromagnetically coupled clusters were formed with as few as 8 Fe^{3+} ions per ferritin, and the limiting value of 3.8 Bohr magnetons per atom, as found in holoferritin, was achieved with only 24 Fe^{3+} ions per ferritin [44].

18.5 EXPERIMENTAL TECHNIQUES

Here we provide a brief overview of some standard and novel approaches. Aspects of the clinical determination of iron overload, and the detection and characterization of nanoscale iron compounds in autopsy tissue, are discussed in more detail elsewhere [58, 135].

18.5.1 Sample Integrity

In studies of iron compounds, it is important to avoid modification of valence state and crystal structure during tissue preparation or particle extraction, yet this is far from straightforward and is often overlooked [61]. Additionally, high resolution techniques typically involve the use of intense beams of electrons or X-rays. It is necessary to consider the potential of these high energy probes to alter the structures under investigation and to adapt experiment conditions or minimize beam exposure where this is demonstrated to be an issue [136].

18.5.2 Microscopy and Spectroscopy

Perls developed a method for staining “iron oxide” in tissue sections using a mixture of potassium ferrocyanide (1%) and hydrochloric acid (1%). The resulting blue stain (“Prussian Blue”) is still used as a principal method for staining iron in tissue [18, 137]. Although this approach reveals the distribution of much of the nonheme iron in tissue [73], it is not sensitive to both oxidation states, and not all forms of iron present in tissue are available for staining as evidenced by biochemical assay of iron in white and gray matter (Section 18.2.3). More recently, efforts have been made to develop techniques sensitive to the redox state of the iron [3, 92]. Fixation with aldehydes has been recommended to preserve iron in sections against the high solubility of ferritin in aqueous solvents [18], although fixation of tissue sections can significantly affect the iron content and distribution [138], with iron leaching and modification of iron compounds where conventional fixation techniques are employed [139].

Various microprobe techniques are used to quantify elemental concentrations of metals at cellular and subcellular resolution [140]. Recent studies have utilized frozen unfixed sections for microprobe studies [102], and the environmental constraints on high resolution microscopy and spectroscopy are improving, with the application of subcellular-resolution secondary ion mass spectrometry (nanoSIMS) to biological samples [55], and the facility to study fully hydrated samples with scanning electron microscopy [141]. Such techniques require an understanding of the variable yields obtained from inhomogeneous materials like human tissue if the spatial distribution of specific elements is to be quantified. Another technique, Mössbauer spectroscopy, has been used to study both structural and magnetic aspects of nanoscale iron compounds in tissue, including early structural studies of hemosiderin [142], investigations of iron-rich regions to establish the proportion of iron that was due to ferritin [56], and studies of the relative magnetic properties of natural and synthetic ferritin cores [36, 143].

High energy X-ray absorption spectroscopy has been used to study aspects of ferritin cores and their biomineralization [43, 107]. Aspects of this technique are now being applied to tissue, where a highly sensitive (<ppm) method to locate and characterize nanoscale iron compounds dispersed in autopsy tissue has been developed using a combination of synchrotron X-ray fluorescence and absorption spectroscopy [45, 58, 61]. This approach provides site-specific information on the chemical and structural state of iron compounds at subcellular resolution in the plane of measurement and can therefore identify spatial distributions of iron biominerals including ferrihydrite, magnetite, and wüstite-like structures [45].

18.5.3 Magnetic Characterization

The magnetic properties of iron compounds in the human brain are of interest for several reasons. First, disruption in iron metabolism appears to alter the forms of iron compounds present [39, 40], and so understanding which compounds occur is important for our understanding of, and ability to treat, syndromes where disrupted iron metabolism is a feature. Applications include the use of SQuID magnetometry in a preliminary study to demonstrate differences in magnetite concentrations for AD and control cases [93], and, incidentally, for the first demonstration of magnetite in the human brain [26]. Second, magnetic characterization techniques enable differences in iron loading and the magnetic properties of bulk tissue samples and extracts to be quantified in a nondestructive manner. For example, Dubiel et al. [56] used SQuID magnetometry and transmission electron microscopy (TEM) to demonstrate that the uniaxial magnetic anisotropy constant is an order of magnitude higher in brain tissue from the globus pallidus than it is in liver. Finally, the various magnetic properties of the nanoscale iron compounds present give us a means to detect and distinguish between them; for example, SQuID magnetometry can be used to quantify the various magnetic

“fractions” within tissue or extracted material [59], and differences in magnetic states will affect MR contrast for *in vivo* imaging as discussed below.

18.5.4 Clinical Imaging

There is great potential for clinical imaging of iron compounds in the brain using MRI, although quantifying the factors involved is far from trivial. For iron compounds embedded in tissue, it is important to assess how iron will affect the signal of the surrounding tissue via the MR relaxation mechanism. High iron concentrations, such as those observed in regions of the basal ganglia, lead to hypointense regions in T2-weighted MR images. Iron also influences the signal magnitude and phase of T2*-weighted gradient-echo images and the signal in diffusion-weighted spin-echo images. While ferritin induces hypointensity in T2 imaging, it can produce hyperintensity in T1-weighted images through its effect on T1 relaxation [12].

To study brain iron compounds using MRI, it is important to know the magnetic moment as defined by its molecular environment. *In vitro* studies of paramagnetic iron have demonstrated that it increases proton transverse relaxation rates (R_2 , where $R_2 = 1/T_2$). For normal ferritin, R_2 has a linear dependence on field strength [12] attributed to the antiferromagnetic superparamagnetic properties of the ferrihydrite-like cores, and a proton-exchange dephasing model (PEDM) [144] has been proposed to describe this behavior of R_2 for ferritin solutions. A detailed review of research exploring the relationship between brain iron and magnetic relaxation parameters can be found elsewhere [12].

Despite the various forms of iron in the human brain, only ferritin and hemosiderin are considered present in sufficient quantity to affect MR contrast [145] (where studies have suggested that >80 % of nonheme iron is ferritin-like [146]). The contributions from transferrin, free iron aqua ions, and nontransferrin bound iron are considered negligible in this context. In principle, iron is not the only paramagnetic ion that can affect relaxivities, other ions such as copper and manganese can also have an effect. However, these latter metals are considered too dilute in tissue to affect MR contrast [145]. In a recent study, MRI contrast due to ferritin and hemosiderin was compared using various sequences in patients with cavernous hemangioma, following on from previous work on the MRI of hemosiderin [147]. In T2*-weighted gradient-echo images, hemosiderin gave the best image contrast, but ferritin gave more prominent image contrast in the T2-weighted conventional spin-echo images [148].

18.6 APPLICATIONS

18.6.1 Iron Chelation

Chelation therapy is an attractive therapeutic concept for neurodegenerative disorders displaying regional iron accumulation; however, there are some

complex practical issues to overcome. For systemic iron-overload conditions, including inherited conditions such as β -thalassemia and transfusion-associated secondary iron overload, therapeutic chelators are successfully administered to manage iron concentrations in areas such as the liver and heart without leading to depletion of brain iron [149]. An important factor for consideration is the nature of the iron that is chelated. In general, the small labile iron pool present in most cells is the primary target of chelators such as DFO, and most storage iron is not easily available to chelators even when iron levels are significantly elevated. A further issue concerns lack of specificity of many chelators, leading to potential intracellular depletion of essential metals such as zinc.

Targeting specific regions of iron overload in the brain is not straightforward, and an ongoing area of research is to develop iron chelators that can cross the BBB [13, 150]. Typically, the less toxic chelators used in iron overload disorders, including deferoxamine (DFO), are bulky and do not easily cross the BBB. Recently, the idea of iron chelation using nanoparticles has been proposed and demonstrated *in vitro* in Alzheimer's tissue [151]. There may be several competing mechanisms by which nanoparticles can cross the BBB. It is known that polysorbate coating of nanoparticles aids their transport [152], and it has been proposed that the polysorbate allows the nanoparticles to mimic low density lipoproteins, facilitating their uptake and subsequent endocytosis by the endothelial cells lining the brain blood capillaries [152]. What is evident is that nanoparticles can provide a successful vehicle for compounds into the brain, and the viability of delivering and recovering chelators in this manner is being explored for iron and other metals in neurodegenerative disorders. Liu et al. have tested the viability of nanoparticle iron chelator systems for AD in their recent *in vitro* study with paraffin-embedded autopsy brain tissue [151], and the potential for nanoparticle copper chelation by D-penicillamine is being investigated [153].

While chelation mechanisms are still being explored, there is evidence from both animal model work and clinical trials for the beneficial effect of chelators. Clinical improvements have been observed in AD patients treated with DFO, ethylenediaminetetraacetic acid (EDTA), and iodochlorhydroxyquin (clioquinol) [151], and clioquinol has been used to reverse PD symptoms in transgenic mice [154]. There appear to be several biochemical pathways leading to senile plaque formation where clioquinol or equivalent chelators might slow the progression of AD [90, 155]. In addition, DFO is reported to have improved the neurologic symptoms of aceruloplasminemia, supporting the idea that modulating iron homeostasis can influence disease pathogenesis [156].

18.6.2 Detection and Diagnosis

Continued advances in MRI are providing a sound basis for *in vivo* imaging of brain iron [11, 12, 14, 108], and recent efforts have been made to quantify brain iron accumulation in neurodegenerative disorders using MRI. There is

increasingly strong evidence for a correlation between brain iron deposition patterns and signal hypointensity in T2-weighted MRI [12, 14] (although the converse cannot be assumed as T2 shortening can be due to a variety of factors). The correlation between iron concentration and T2 shortening is enhanced in higher fields, and the increasing availability of 3-T clinical scanners has led to MRI studies that use the field-enhanced effects to identify differences in the T2 shortening for the hippocampus in AD disease cases and controls [85], and to FDRI studies that use two different field strengths to quantify brain ferritin [100, 156]. In particular, strong correlations ($r > 0.99$) have been observed between postmortem brain iron levels and FDRI [14]. Currently, MRI is used diagnostically to detect atrophy in vulnerable regions such as the hippocampus or exclude other conditions such as tumor or stroke [11]. However, extracting specific information that can be used as a disease biomarker is increasingly a focus of research effort. Conceptually, biomarkers should allow accurate detection and disease staging, and may enable the efficacy of therapies on physiological condition to be assessed. While a wide range of imaging biomarkers have been proposed for AD and PD [11], the addition of brain iron imaging using approaches such as those pioneered by Bartzokis and Tishler [100] may prove a valuable tool for clinicians.

18.6.3 Nanoparticle Synthesis

Ferritin is of interest not only for its biological role, but also because the protein can be used to synthesize nanoparticles. Ferritin and other ferritin-like proteins such as the spherical cowpea chlorotic mottle viruses (CCMV) have been used as nanoscale reactors to produce quantum-sized inorganic particles [157]. Apoferritin can be obtained by reductive dissolution of the iron cores, and even when briefly subjected to high temperatures (up to 65 °C) and a wide spectrum of pH variation (4–9), it remains relatively intact [157]. Precipitation of cores, including ferrihydrite-like and magnetite-like (magnetoferritin), can then be achieved [16, 44]. As discussed elsewhere, biomedical applications of magnetic nanoparticles include targeted drug delivery, hyperthermia treatment, and contrast agents for MRI [15]. The effect of various iron compounds on MRI contrast continues to be explored [148], and the findings are important for both biogenic and synthetic sources of iron compounds in the human brain. For example, MRI can be used to confirm that magnetic particles introduced into the brain for hyperthermia treatment of cancerous cells have an appropriate concentration in the target region, and that they have not accumulated in vulnerable regions of healthy tissue [158].

18.6.4 Iron Nanoparticles as Contrast Agents

The use of superparamagnetic iron oxide nanoparticles as dedicated MRI contrast agents is being widely explored, where particle size, coating, charge, and so forth are critical for efficacy, stability, metabolism, and clearance [159].

Potential applications for neurodegenerative disorders include the uptake of the nanoparticles by elevated macrophage populations in degenerative tissue, providing negative T2/T2* enhancement of macrophage-rich regions, and the introduction of externally produced nanoparticle-laden progenitor and stem cells [160, 161]. The latter has particular relevance to neurodegeneration, where the use of stem and progenitor cells may enable replacement of those cell populations that are selectively targeted in disorders such as PD and HD [159]. Where these cells are introduced, it will be essential to monitor them *in vivo* to discover the proportion that reach their intended destination, and the timescale over which this occurs. The inclusion of iron oxide nanoparticles could provide a means of tracking these cell populations by MRI, although the implications of introducing iron-nanoparticle-laden cells to regions such as the substantia nigra in PD, where excess iron is implicated in the selective death of dopaminergic neurons [102], should not be overlooked.

18.7 CONCLUSIONS

The presence of elevated iron concentrations in neurodegenerative disorders alone does not confirm a role for iron in disease etiology. However, where nanoscale iron accumulations are implicated in oxidative stress damage, they may provide a target for chelation therapy. There is also increasing evidence for a genetic basis for disrupted brain iron metabolism, supporting the hypothesis that iron plays a key role in many of the disorders discussed above. A better understanding of pathogenesis, and of potential mechanisms for detection, diagnosis, and treatment, should be achievable through improved understanding of the various nanoscale iron compounds that form in these disorders.

REFERENCES

1. Harrison PM and Arosio P. The ferritins: molecular properties, iron storage function and cellular regulation. *Biochim Biophys Acta* 1996;1275:161–203.
2. Markesbery WR. Oxidative stress hypothesis in Alzheimer's disease. *Free Radic Biol Med* 1997;23:134–147.
3. Smith MA, Harris PLR, Sayre LM, Perry G. Iron accumulation in Alzheimer disease is a source of redox-generated free radicals. *Proc Natl Acad Sci U S A* 1997;94:9866–9868.
4. Ke Y and Qian Z. Iron misregulation in the brain: a primary cause of neurodegenerative disorders. *Lancet Neurol* 2003;2:246–253.
5. Honda K, et al. Ribosomal RNA in Alzheimer disease is oxidized by bound redoxactive iron. *J Biol Chem* 2005;280:20978–20986.
6. Goodman L. Alzheimer's disease—a clinicopathologic analysis of 23 cases with a theory on pathogenesis. *J Nerv Ment Dis* 1953;118:97–130.

7. Gorell JM, et al. Increased iron-related MRI contrast in the substantia nigra in Parkinson's disease. *Neurology* 1995;45:1138–1143.
8. Dobson J. Nanoscale biogenic iron oxides and neurodegenerative disease. *FEBS Lett* 2001;496:1–5.
9. Dobson J. Magnetic iron compounds in neurological disorders. *Ann N Y Acad Sci* 2004;1012:183–192.
10. Zecca L, Youdim MB, Riederer P, Connor JR, Crichton RR. Iron, brain ageing and neurodegenerative disorders. *Nat Rev Neurosci* 2004;5:863–873.
11. Schenck JF and Zimmerman EA. High-field magnetic resonance imaging of brain iron: birth of a biomarker? *NMR Biomed* 2004;17:433–445.
12. Haacke EM, et al. Imaging iron stores in the brain using magnetic resonance imaging. *Magn Reson Imaging* 2005;23:1–25.
13. Youdim MBH, Fridkin M, Zheng H. Novel bifunctional drugs targeting monoamine oxidase inhibition and iron chelation as an approach to neuroprotection in Parkinson's disease and other neurodegenerative diseases. *J Neural Transm* 2004;1435–1463 (Online).
14. Bartzokis G, et al. Brain ferritin iron may influence age- and gender-related risks of neurodegeneration. *Neurobiol Aging* 2007;28:414–423.
15. Pankhurst QA, Connolly J, Jones SJ, Dobson J. Applications of magnetic nanoparticles in biomedicine. *J Phys D: Appl Phys* 2003;36:R167–R181.
16. Douglas T, et al. Synthesis and structure of an iron(III) sulfide–ferritin bioinorganic nanocomposite. *Science* 1995;269:54–57.
17. Lieu P, Heiskala M, Peterson PA, Yang Y. The roles of iron in health and disease. *Mol Aspects Med* 2001;22:1–87.
18. Koeppe AH. A brief history of brain iron research. *J Neurol Sci* 2003;207:95–97.
19. Zaleski SS. Das Eisen der Organe beim Morbus maculosus Werlhofii (The iron of the organs in Werlhof's morbus maculosus). *Arch Exp Pathol Pharmacol* 1886;23:77–90.
20. Connor JR. Iron acquisition and expression of iron regulatory proteins in the developing brain: manipulation by ethanol exposure, iron deprivation, and cellular dysfunction. *Dev Neurosci* 1994;16:233–247.
21. Gelman BB. Iron in CNS disease. *J Neuropathol Exp Neurol* 1995;54:477–486.
22. Hallgren B and Sourander P. The non-haem iron in the cerebral cortex in Alzheimer's disease. *J Neurochem* 1958;3:41–51.
23. Connor JR, Snyder BS, Arosio P, Loeffler DA, LeWitt P. A quantitative analysis of iso-ferritins in selected regions of aged, parkinsonian, and Alzheimer's diseased brains. *J Neurochem* 1995;65:717–724.
24. Zecca L, et al. Iron, neuromelanin and ferritin in substantia nigra of normal subjects at different ages. Consequences for iron storage and neurodegenerative disorders. *J Neurochem* 2001;76:1766–1773.
25. Zecca L, et al. Interaction of neuromelanin and iron in substantia nigra and other areas of human brain. *Neuroscience* 1996;73:407–415.
26. Kirschvink JL, Kobayashi-Kirschvink A, Woodford BJ. Magnetite biomineralization in the human brain. *Proc Natl Acad Sci U S A* 1992;89:7683–7687.

27. Schultheiss-Grassi PP, Wessiken R, Dobson J. TEM observation of biogenic magnetite extracted from the human hippocampus. *Biochim Biophys Acta* 1999; 1426:212–216.
28. Connor JR, Pavlick G, Karli D, Menzies SL, Palmer C. A histochemical study of iron-positive cells in the developing rat brain. *J Comp Neurol* 1995;355:111–123.
29. Gould RM, Freund CM, Palmer F, Feinstein DL. Messenger RNAs located in myelin sheath assembly sites. *J Neurochem* 2000;75:1834–1844.
30. Patino MM and Walden WE. Cloning of a functional cDNA for the rabbit ferritin mRNA repressor protein. *J Biol Chem* 1992;267:19011–19016.
31. Guo B, Yu Y, Leibold EA. Iron regulates cytoplasmic levels of a novel iron-responsive element binding protein without aconitase activity. *J Biol Chem* 1994;269:24252–24260.
32. Guo B, Brown FM, Phillips JD, Yu Y, Leibold EA. Characterization and expression of iron regulatory protein 2 (IRP2). *J Biol Chem* 1995;270:16529–16535.
33. Rouault TA. The role of iron regulatory proteins in mammalian iron homeostasis and disease. *Nat Chem Biol* 2006;2:406–414.
34. Koepfen AH, Dickson AC, Chu RC, Thach RE. The pathogenesis of superficial siderosis of the central nervous system. *Ann Neurol* 1993;34:646–653.
35. Harrison PM, Fischbach FA, Hoy TG, Haggis GH. Ferric oxyhydroxide core of ferritin. *Nature* 1967;216:1188–1190.
36. St Pierre TG, Webb J, Mann S. Ferritin and hemosiderin: structural and magnetic studies of the iron core. In: Mann S, Webb J, Williams RJP, editors. *Bio-mineralization: Chemical and Biochemical Perspectives*. Germany: Weinheim, VCH; 1989. p 295–344.
37. Massover W and Cowley J. Ultrastructure of ferritin macromolecules–lattice structure of core crystallites. *Proc Natl Acad Sci U S A* 1973;70:3847–3851.
38. Cowley JM, Janney DE, Gerkin RC, Buseck PR. The structure of ferritin cores determined by electron nanodiffraction. *J Struct Biol* 2000;13:210–216.
39. Quintana C, et al. Preliminary high resolution TEM and electron energy loss spectroscopy studies of ferritin cores extracted from brain in patients with neurodegenerative PSP and Alzheimer diseases. *Cell Mol Biol* 2000;46:807–820.
40. Quintana C, Cowley JM, Marhic C. Electron diffraction and high-resolution electron microscopy studies of the structure and composition of physiological and pathological ferritin. *J Struct Biol* 2004;147:166–178.
41. Levi S, et al. Evidence that H- and L-chains have co-operative roles in the iron-uptake mechanism of human ferritin. *J Biochem* 1992;65:710–716.
42. Chasteen ND and Harrison PM. Mineralization in ferritin: an efficient means of iron storage. *J Struct Biol* 1999;126:182–194.
43. Rohrer JS, et al. Stabilization of iron in a ferrous form by ferritin. *J Biol Chem* 1987;262:13385–13387.
44. Hilty S, Webb B, Frankel RB, Watt GD. Iron core formation in horse spleen ferritin: magnetic susceptibility, pH, and compositional studies. *J Inorg Biochem* 1994;56:173–185.

45. Collingwood JF, et al. *In situ* characterization and mapping of iron compounds in Alzheimer's tissue. *J Alzheimer's Dis* 2005;7:267–272.
46. Khan A, Dobson J, Exley C. The redox cycling of Fe(II) by A β 42. *Free Rad Biol Med* 2005;40:557.
47. Macara IG, Hov TG, Harrison PM. The formation of ferritin from apoferritin. Kinetics and mechanism of iron uptake. *Biochem J* 1972;126:151–162.
48. Powell AK. Ferritin. Its mineralization. In: Sigel A, Sigel H, editors. *Iron Transport and Storage in Micro-Organisms, Plants, and Animals*. New York: Marcel Dekker; 1998.p 515–561.
49. Frankel RB, Papaefthymiou GC, Watt GD. Variation of superparamagnetic properties with iron loading in mammalian ferritin. *Hyperfine Interactions* 1991; 66:71–82.
50. Zhao G, et al. Multiple pathways for mineral core formation in mammalian apoferritin: the role of hydrogen peroxide. *Biochemistry* 2003;42:3142–3150.
51. Prutkin L and Munro HN. Hemosiderin: nature, formation, and significance. *Int Rev Exp Pathol* 1980;22:193–225.
52. O'Connell M, et al. Formation of hydroxyl radicals in the presence of ferritin and haemosiderin: is haemosiderin formation a biological protective mechanism? *Biochem J* 1986;234:727–731.
53. Gossuin Y, et al. Looking for biogenic magnetite in brain ferritin using NMR relaxometry. *NMR Biomed* 2005;18:469–472.
54. Koeppe AH and Dentinger MP. Brain hemosiderin and superficial siderosis of the central nervous system. *J Neuropathol Exp Neurol* 1988;47:249–270.
55. Quintana C, et al. Study of the localization of iron, ferritin and hemosiderin in Alzheimer's disease hippocampus by analytical microscopy at the subcellular level. *J Struct Biol* 2006;153:42–54.
56. Dubiel SM, Zablotna-Rypien B, Mackey JB. Magnetic properties of human liver and brain ferritin. *Eur Biophys J* 1999;28:263–267.
57. Jellinger K, et al. Iron–melanin complex in substantia nigra of parkinsonian brains: an X-ray microanalysis. *J Neurochem* 1992;59:1168–1171.
58. Collingwood JF and Dobson J. Mapping and characterization of iron compounds in Alzheimer's disease. *J Alzheimers Dis* 2006;10:215–222.
59. Hautot D, Pankhurst QA, Dobson J. Superconducting quantum interference device measurements of dilute magnetic materials in biological samples. *Rev Sci Instrum* 2005;76:045101.
60. Castelnaud PA, et al. Abnormal iron deposition associated with lipid peroxidation in transgenic mice expressing interleukin-6 in the brain. *J Neuropathol Exp Neurol* 1998;57:268–282.
61. Mikhaylova A, et al. Detection, identification and mapping of iron anomalies in brain tissue using X-ray absorption spectroscopy. *J R Soc Interface* 2005;2:33–37.
62. Dobson J. Investigation of age-related variations in biogenic magnetite levels in the human hippocampus. *Exp Brain Res* 2002;144:122–126.
63. Zecca L, Zucca FA, Wilms H, Sulzer D. Neuromelanin of the substantia nigra: a neuronal black hole with protective and toxic characteristics. *Trends Neurosci* 2003;26:578–580.

64. Götz M, Double K, Gerlach M, Youdim MBH, Reiderer P. The relevance of iron in the pathogenesis of Parkinson's disease. *Ann N Y Acad Sci* 2004;1012:193–208.
65. Good PF, Olanow CW, Perl DP. Neuromelanin-containing neurons of the substantia nigra accumulate iron and aluminum in Parkinson's disease: a LAMMA study. *Brain Res* 1992;593:343–346.
66. Zecca L, et al. The absolute concentration of nigral neuromelanin, assayed by a new sensitive method, increases throughout the life and is dramatically decreased in Parkinson's disease. *FEBS Lett* 2002;510:216–220.
67. Spatz H. Über den Eisennachweis in Gehirn, besonders in Zentren des extrapyramidal-motorischen Systems (On the visualization of iron in the brain, especially in the centers of the extrapyramidal motor system). *Z Ges Neurol Psychiatr* 1922;77:261–390.
68. Drayer B, et al. MRI of brain iron. *AJR Am J Roentgenol* 1986;147:103–110.
69. Connor JR, Snyder BS, Beard JL, Fine RE, Mufson EJ. Regional distribution of iron and iron-regulatory proteins in the brain in aging and disease. *J Neurosci Res* 1992;31:327–335.
70. Connor JR, Menzies SL, Burdo JR, Boyer PJ. Iron and iron management proteins in neurobiology. *Pediatr Neurol* 2001;25:118–129.
71. Connor JR, Boeshore KL, Benkovic SA. Isoforms of ferritin have a specific cellular distribution in the brain. *J Neurosci Res* 1994;37:461–465.
72. Connor JR and Menzies SL. Cellular management of iron in the brain. *J Neurol Sci* 1995;134(Suppl):33–44.
73. Morris CM, Candy JM, Oakley AE, Bloxham CA, Edwardson JA. Histochemical distribution of non-haem iron in the human brain. *Acta Anat Suppl (Basel)* 1992;144:235–257.
74. Burdo JR and Conner JR. Brain iron uptake and homeostatic mechanisms: an overview. *Biometals* 2003;16:63–75.
75. Kaplan J and Kushner JP. Mining the genome for iron. *Nature* 2000;403:711–713.
76. Wu LJ, et al. Expression of the iron transporter ferroportin in synaptic vesicles and the blood–brain barrier. *Brain Res* 2004;1001:108–117.
77. Moos T, Trinder D, Morgan EH. Cellular distribution of ferric iron, ferritin, transferrin and divalent metal transporter 1 (DMT1) in substantia nigra and basal ganglia of normal and beta 2-microglobulin deficient mouse brain. *Cell Mol Biol* 2000;46:549–561.
78. Burdo JR, et al. Distribution of divalent metal transporter 1 and metal transport protein 1 in the normal and Belgrade rat. *J Neurosci Res* 2001;66:1198–1207.
79. Focht SJ, et al. Regional distribution of iron, transferrin, ferritin and oxidatively modified proteins in young and aged Fischer 344 rat brains. *Neuroscience* 1997;79:255–261.
80. Connor JR, editor *Metals and Oxidative Damage in Neurological Disorders*. New York: Plenum Press; 1997.
81. Crichton RR, Ward RJ, *Metal-Based Neurodegeneration: From Molecular Mechanisms To Therapeutic Strategies*. Chichester; Hoboken, NJ: John Wiley Sons, Inc; 2006.

82. Curtis ARJ, et al. Mutations in the gene encoding ferritin light polypeptide causes dominant adult-onset basal ganglia disease. *Nat Genet* 2001;28:350–354.
83. Zhao G, Arosio P, Chasteen ND. Iron(II) and hydrogen peroxide detoxification by human H-chain ferritin. An EPR spin-trapping study. *Biochemistry* 2006;45:3429–3436.
84. Morris CM, Kerwin JM, Edwardson JA. Non-haem iron histochemistry of the normal and Alzheimer's disease hippocampus. *Neurodegeneration* 1994;3:267–275.
85. Zimmerman EA, Li Z, O'Keefe T, Schenck JF. High field strength (3 T) magnetic resonance imaging in Alzheimer's disease. *Ann Neurol* 2003;54(suppl 7):S68.
86. Nakata-Kudo Y, et al. Microbleeds in Alzheimer disease are more related to cerebral amyloid angiopathy than cerebrovascular disease. *Dement Geriatr Cogn Disord* 2006;22:8–14.
87. Bartzokis G. Age-related myelin breakdown: a developmental model of cognitive decline and Alzheimer's disease. *Neurobiol Aging* 2004;25:5–18.
88. Rogers JT, et al. An iron-responsive element type II in the 5'-untranslated region of the Alzheimer's amyloid precursor protein transcript. *J Biol Chem* 2002;277:45518–45528.
89. Mantyh PW, et al. Aluminum, iron and zinc ions promote aggregation of physiological concentrations of beta-amyloid peptide. *J Neurochem* 1993;61:1171–1174.
90. House E, et al. Aluminium, iron, zinc and copper influence the *in vitro* formation of amyloid fibrils of A β 42 in a manner which may have consequences for metal chelation therapy in Alzheimer's disease. *J Alzheimers Dis* 2004;6:291–301.
91. Khan A, Ashcroft AE, Higenell V, Korchazhkina OV, Exley C. Metals accelerate the formation and direct the structure of amyloid fibrils of NAC. *J Inorg Biochem* 2005;99:1920–1927.
92. Sayre LM, et al. In situ oxidative catalysis by neurofibrillary tangles and senile plaques in Alzheimer's disease: a central role for bound transition metals. *J Neurochem* 2000;74:270–279.
93. Hautot D, Pankhurst QA, Khan N, Dobson J. Preliminary evaluation of nanoscale biogenic magnetite and Alzheimer's disease. *Proc R Soc Lond B Biol Lett* 2003;270:S62–S64.
94. Klintworth GK. Cerebral iron deposition in Huntington's disease. In: Barbeau A, Brunette JR, editors. *Proceedings of the Second International Congress of Neurogenetics and Neuroophthalmology of the World Federation of Neurology*; Excerpta Medica Foundation; Amsterdam: 1969. p 589–596.
95. Dexter DT, et al. Alterations in the levels of iron, ferritin and other trace metals in Parkinson's disease and other neurodegenerative diseases affecting the basal ganglia. *Brain* 1991;114:1953–1975.
96. Bartzokis G, Cummings J, Perlman S, Hance DB, Mintz J. Increased basal ganglia iron levels in Huntington disease. *Arch Neurol* 1999;56:569–574.
97. Qian ZM and Wang Q. Expression of iron transport proteins and excessive iron accumulation in the brain in neurodegenerative disorders. *Brain Res Brain Res Rev* 1998;27:257–267.

98. Hilditch-Maguire P, et al. Huntingtin: an iron-regulated protein essential for normal nuclear and perinuclear organelles. *Hum Mol Genet* 2000;9:2789–2797.
99. Savoirdo M, Strada L, Oliva D, Girotti F, D'Incerti L. Abnormal MRI signal in the rigid form of Huntington's disease. *J Neurol Neurosurg Psychiatry* 1991;54:888–891.
100. Bartzokis G and Tishler TA. MRI evaluation of basal ganglia ferritin iron and neurotoxicity in Alzheimer's and Huntington's disease. *Cell Mol Biol* 2000;46:821–834.
101. Reiderer P, et al. Transition metals, ferritin, glutathione, and ascorbic acid in parkinsonian brains. *J Neurochem* 1989;52:515–520.
102. Oakley AE, et al. Individual dopaminergic neurons show raised iron levels in Parkinson disease. *Neurology* .2007;68:1820–1825.
103. Kaur D and Andersen J. Does cellular iron dysregulation play a causative role in Parkinson's disease? *Ageing Res Rev* 2004;3:327–343.
104. Bartzokis G, Tishler TA, Shin IS, Lu PH, Cummings JL. Brain ferritin iron as a risk factor for age at onset in neurodegenerative diseases. *Ann N Y Acad Sci* 2004;1012:224–236.
105. Costello DJ, Walsh SL, Harrington HJ, Walsh CH. Concurrent hereditary haemochromatosis and idiopathic Parkinson's disease: a case report series. *J Neurol Neurosurg Psychiatry* 2004;75:631–633.
106. Moos T and Morgan EH. The metabolism of neuronal iron and its pathogenic role in neurological disease: review. *Ann N Y Acad Sci* 2004;1012:1012–1014.
107. Griffiths PD, Dobson BR, Jones GR, Clarke DT. Iron in the basal ganglia in Parkinson's disease—an *in vitro* study using extended X-ray absorption fine structure and cryo-electron microscopy. *Brain* 1999;122:667–673.
108. Hayflick SJ, Hartman M, Coryell J, Gitschier J, Rowley H. Brain MRI in neurodegeneration with brain iron accumulation with and without PANK2 mutations. *AJNR Am J Neuroradiol* 2006;27:1230–1233.
109. Zhou B, et al. A novel pantothenate kinase gene (PANK2) is defective in Hallervorden–Spatz syndrome. *Nat Genet* 2001;4:345–349.
110. Harris ZL, Klomp LWJ, Gitlin JD. Aceruloplasminemia: an inherited neurodegenerative disease with impairment of iron homeostasis. *Am J Clin Nutr* 1998;67(Suppl):972S–977S.
111. Cammermeyer J. Deposition of iron in paraventricular areas of the human brain in hemochromatosis. *J Neuropathol Exp Neurol* 1947;6:111–127.
112. McDougal DB and Adams RD. The neuropathological changes in hemochromatosis. *J Neuropathol Exp Neurol* 1950;9:117–118.
113. Morita H, et al. Hereditary ceruloplasmin deficiency with hemosiderosis: a clinicopathological study of a Japanese family. *Ann Neurol* 1995;37:646–656.
114. Kawanami T, et al. Hereditary caeruloplasmin deficiency: clinicopathological study of a patient. *J Neurol Neurosurg Psychiatr* 1996;61:506–509.
115. Crompton DE, et al. Neuroferritinopathy: a window on the role of iron in neurodegeneration. *Blood Cells Mol Dis* 2002;29:522–531.

116. Vidal R, et al. Intracellular ferritin accumulation in neural and extraneural tissue characterizes a neurodegenerative disease associated with a mutation in the ferritin light polypeptide gene. *J Neuropathol Exp Neurol* 2004;63:363–380.
117. Perez M, et al. Ferritin is associated with aberrant tau filaments present in progressive supranuclear palsy. *Am. J Pathol* 1998;152:1531–1539.
118. Miskiel KA, et al. The measurement of R2, R2* and R2' in HIV-infected patients using the prime sequence as a measure of brain iron deposition. *Magn Reson Imaging* 1997;15:1113–1119.
119. Gelmann BB, et al. Siderotic cerebral macrophages in the acquired immunodeficiency syndrome. *Arch Pathol Lab Med* 1992;116:509–516.
120. Butensky E, Kennedy CM, Lee MM, Harmatz P, Miaskowski C. Potential mechanisms for altered iron metabolism in human immunodeficiency virus disease. *J Assoc Nurses AIDS Care* 2004;15:31–45.
121. Puccio H and Koenig M. Recent advances in the molecular pathogenesis of Friedreich ataxia. *Hum Mol Genet* 2000;9:887–892.
122. Campuzano V, et al. Friedreich's ataxia: autosomal recessive disease caused by an intronic GAA triplet repeat expansion. *Science* 1996;271:1423–1427.
123. Waldvogel D, van Gelderen P, Hallett M. Increased iron in the dentate nucleus of patients with Friedreich's ataxia. *Ann Neurol* 1999;46:123–125.
124. Haba-Rubio J, et al. Restless legs syndrome and low brain iron levels in patients with haemochromatosis. *J Neurol Neurosurg Psychiatry* 2005;76:1009–1010.
125. Camaschella C. Understanding iron homeostasis through genetic analysis of haemochromatosis and related disorders. *Blood* 2005;106:3710–3717.
126. Nielsen JE, Jensen LN, Krabbe K. Hereditary hemochromatosis: a case of iron accumulation in the basal ganglia associated with a parkinsonian syndrome. *J Neurol Neurosurg Psychiatry* 1995;59:318–321.
127. Berg D, et al. The basal ganglia in haemochromatosis. *Neuroradiology* 2000; 42: 9–13.
128. Connor JR, et al. Is hemochromatosis a risk factor for Alzheimer's disease? *J Alzheimer's Dis* 2001;3:471–477.
129. Moalem S, et al. Are hereditary hemochromatosis mutations involved in Alzheimer disease? *Am J Med Genet* 2000;93:58–66.
130. Pulliam JF, et al. Association of HFE mutations with neurodegeneration and oxidative stress in Alzheimer's disease and correlation with APOE. *Am J Med Genet* 119B:2003;48–53.
131. de Boer CB and Dekkers MJ. Thermomagnetic behaviour of haematite and goethite as a function of grain size in various non-saturating magnetic fields. *Geophys J Int* 1998;133:541–552.
132. Cranfield CG, et al. Biogenic magnetite in the nematode *Caenorhabditis elegans*. *Proc R Soc Lond B* 271:2004;S436–S439.
133. Till U, Timmel CR, Brocklehurst B, Hore PJ. The influence of very small magnetic fields on radical recombination reactions in the limit of slow recombination. *Chem Phys Lett* 1998;298:7–14.
134. Brooks RA, Vymaza J, Goldfarb RB, Bulte JWM, Aisen P. Relaxometry and magnetometry of ferritin. *Magn Reson Med* 1998;15:227–235.

135. Jensen PD. Evaluation of iron overload. *Br J Haematol* 2004;124:697–711.
136. Pan Y, et al. Electron beam damage studies of synthetic 6-line ferrihydrite and ferritin molecule cores within a human liver biopsy. *Micron* 2006;37:403–411.
137. Perls M. Nachweis von Eisenoxyd in gewissen Pigmenten (Demonstration of iron oxide in certain pigments). *Virchows Arch Pathol Anat Physiol Klin Med* 1867;39:42–48.
138. Chwiej J, et al. Preparation of tissue samples for X-ray fluorescence microscopy. *Spectrochim Acta B* 2005;60:1531–1537.
139. Dobson J and Grassi P. Magnetic properties of human hippocampal tissue: evaluation of artefact and contamination sources. *Brain Res Bull* 1996;39:255–259.
140. Watt F. Nuclear microscope analysis in Alzheimer's and Parkinson's disease: a review. *Cell Mol Biol (Noisy-le-grand)* 1996;42:17–26
141. Thiberge S, et al. Scanning electron microscopy of cells and tissues under fully hydrated conditions. *PNAS* 2004;101:3346–3351.
142. Dickson DPE, et al. Mössbauer spectroscopy, electron microscopy and electron diffraction studies of the iron cores in various human and animal haemosiderins. *Biochim Biophys Acta—Protein Struct Mol Enzymol* 1988;957:81–90.
143. Wade VJ, et al. Structure and composition of ferritin cores from pea seed. *Biochim Biophys Acta* 1993;1161:91–96.
144. Gossuin Y, Roch A, Bue FL, Muller RN, Gillis P. Nuclear magnetic relaxation dispersion of ferritin and ferritin like magnetic particle solutions: a pH-effect study. *Magn Reson Med* 2001;46:476–481.
145. Schenck JF. Magnetic resonance imaging of brain iron. *J Neurol Sci* 2003;207:99–102.
146. Dedman DJ, et al. Iron and aluminium in relation to brain ferritin in normal individuals and Alzheimer's-disease and chronic renal-dialysis patients. *Biochem J* 1992;287:509–514.
147. Vymazal J, Urgosik D, Bulte JW. Differentiation between haemosiderin and ferritin-bound brain iron using nuclear magnetic resonance and magnetic resonance imaging. *Cell Mol Biol* 2000;46:835–842.
148. Haque TL, et al. MR contrast of ferritin and haemosiderin in the brain: comparison among gradient-echo, conventional spin-echo and fast spin-echo sequences. *Eur J Radiol* 2003;48:230–236.
149. Porter JB, et al. Recent insights into interactions of deferoxamine with cellular and plasma iron pools: implications for clinical use. *Ann N Y Acad Sci* 2005;1054:155–168.
150. Bush AI. Metal complexing agents as therapies for Alzheimer's disease. *Neurobiol Aging* 2002;23:1031–1038.
151. Liu G, et al. Nanoparticle iron chelators: a new therapeutic approach in Alzheimer disease and other neurologic disorders associated with trace metal imbalance. *Neurosci Lett* 2006;406:189–193.
152. Kreuter J. Nanoparticulate systems for brain delivery of drugs. *Adv Drug Deliv Rev* 2001;47:65–81.

153. Cui ZR, et al. Novel D-penicillamine carrying nanoparticles for metal chelation therapy in Alzheimer's and other CNS diseases. *Eur J Pharm Biopharm* 2005;59:263–272.
154. Kaur D, et al. Genetic or pharmacological iron chelation prevents MPTP-induced neurotoxicity *in vivo*: a novel therapy for Parkinson's disease. *Neuron* 2003;37:899–909.
155. Richardson DR. Novel chelators for central nervous system disorders that involve alterations in the metabolism of iron and other metal ions. *Ann N Y Acad Sci* 2004;1012:326–341.
156. Bartzokis G, et al. MR evaluation of brain iron in young adults and older normal males. *Magn Reson Imaging* 1997;15:29–35.
157. Mayes EL, Mann S, Mineralization in nanostructured biocompartments: biomimetic ferritins for high density data storage. In: Niemeyer CM, Mirkin CA, editors. *John Wiley Nanobiotechnology: Concepts, Applications and Perspectives*. 2004. p 278–287.
158. St. Pierre TG, et al. Non-invasive measurement and imaging of tissue iron oxide nanoparticle concentrations *in vivo* using proton relaxometry. *J Phys: Conf Ser* 2005;17:122–126.
159. Corot C, Robert P, Idee JM, Port M. Recent advances in iron oxide nanocrystal technology for medical imaging. *Adv Drug Deliv Rev* 2006;58:1471–1504.
160. Bulte JW, Arbab AS, Douglas T, Frank JA. Preparation of magnetically labeled cells for cell tracking by magnetic resonance imaging. *Methods Enzymol* 2004; 386:275–299.
161. Daldrup-Link HE, et al. Targeting of hematopoietic progenitor cells with MR contrast agents. *Radiology* 2003;228:760–767.

Application of Nanotechnology into Life Science: Benefit or Risk

YOON-SIK LEE and MYUNG-HAING CHO

19.1 INTRODUCTION

The recent rapid shift in the focus of developing technology from microscale to nanoscale may change the very foundations of life science. Such a rapid development in nanotechnology will result in incredible changes such as nanoscale visualization, insight into living systems, revolutionary biotechnology, development of targeted delivery, and regenerative medicine and offer many other benefits [1]. In fact, the development level of nanomaterials is the most advanced at present, both in scientific knowledge and commercial applications [2, 3]. A representative list of applications of nanomaterials to life science is given below in Fig. 19.1.

As mentioned, the applicable areas of nanoparticles are broad. In this chapter, we will try to summarize the most recent and representative nanomaterial development in the field of life science, and discuss their potential concerns in order to facilitate the future development of nanotechnology. Therefore, we will give a broad prospective of nanomaterial application to life science. Then, we will overview the representative trend of recent developments in this field. In order to prevent potential problems, however, it is necessary to collect more information on the toxicological consequences and to investigate any possible side effects of these nanomaterials before introducing them into humans and the environment. Therefore, we will also briefly discuss the potential concerns of nanomaterials in the final part of this chapter.

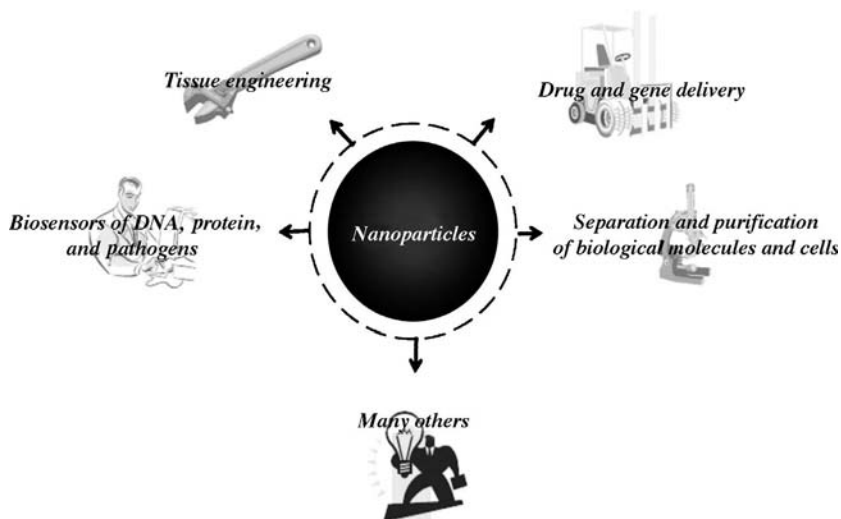


FIGURE 19.1 Ubiquitous applications of nanoparticles in life science.

19.2 DRUG OR GENE DELIVERY

Gene or drug delivery uses nucleic acids as a drug to treat or cure diseases. In most cases, the genetic materials should be packed in a delivery system to be protected from enzymatic digestion and to cross-physiological barriers, and/or cell membranes [4]. During the past years, two main approaches to gene delivery, viral and nonviral, have been developed. The primary advantages of viral delivery are efficient infection of cells/tissues and long-term gene expression [5]. Despite their usefulness in gene delivery, however, existing viral vectors have their downsides. To date, recombinant adenoviral vectors have been used for gene delivery because of their high affinity for airway epithelium and transfection efficiency for pulmonary cells [6]. However, the degree of toxicity and the subject's immune response against such vectors upon repeated administration have limited the application of such systems in practice [7–9]. Moreover, viral vectors are difficult to produce on a large scale [10]. Nonviral vectors, on the other hand, have been proposed as safer alternatives to viral vectors for their potential to be administered repeatedly with minimal host immune response. In addition, nonviral vectors have high specificity, targetability, stability in storage, and simplicity in large-scale production [11].

To improve the stability, efficiency, and uptake of drug- or gene-of-interest, numerous biomaterials have been used to create synthetic gene delivery vectors [12]. The main biomaterials that have been studied include cationic polymers, cationic lipids, liposomes, chitosans, inorganic nanoparticles, and dendrimers [5]. They have been proved to transfect the cells efficiently in cell culture.

However, most of these materials are practically ineffective for *in vivo* delivery due to the presence of physiological barriers such as interaction with serum and digestion by phagocytosis. Nanotechnology holds the promise to overcome the practical inefficiency because the nanotechnology may be able to provide the way of achieving satisfactory therapeutic outcome through improving the property of nanoparticles. Therefore, the spectrum of nanoparticle application in the fields of drug or gene delivery is as broad as it is promising.

The ability of nanoparticle drug or gene delivery carriers to target cells/tissues is very critical. The first thing to consider for effective target delivery is active tissue targeting with the aid of a specific ligand recognizing a receptor-of-interest. Second approach, passive tissue targeting, relies on the accumulation of drug or gene delivery carriers in targeted tissues due to nonspecific effects related to physicochemical characteristics of the carrier. Therefore, physicochemical properties of nanoparticles are major factors determining selective biodistribution in the living organism [13]. Other physicochemical properties such as surface charge [14], surface modification with polyethylene glycol as a particle stabilizer [15], and hydrophobicity [16] can also affect the bioavailability of nanoparticles. Therefore, synthesis of nanoparticles as a drug or gene delivery carrier should be based on optimal physicochemical properties of the nanoparticle candidate. In addition, the size of the nanoparticle is another important factor to consider in developing drug and gene delivery systems. If the size is too big (>200 nm), the particles cannot pass the cell membrane or are cleared rather quickly from the circulatory system. On the contrary, if the size of nanoparticles is less than 100 nm, the particles can be associated with variable levels of potential toxicity by different mechanisms. If we can apply a direct relationship with surface area, a 20-nm particle would have roughly 100 times the inherent toxicity of a 2- μ m particle [17].

Conventional delivery systems relies largely on oral and intravenous (i.v.) methods. However, such classical methods require larger amounts of drug than are necessary to be administered, thus, may cause unwanted effects such as toxicity with low specificity. Nanoparticle delivery using biodegradable polymers may provide efficient way to overcome the preexisting problems [18]. Tremendous improvements have been achieved and applied to various disease models including anticancer models. For example, administration of paclitaxel using emulsifying wax nanoparticles (PX NPs) has shown to overcome the drug resistance in human colon adenocarcinoma cells. Moreover, significant inhibition of tumor growth by PX NPs treatment has been shown in the mice bearing human colon cancer cells. This study demonstrated clearly that nanoparticle-based delivery of conventional cancer drug, paclitaxel, enhanced efficacy by overcoming resistance [19].

The lung is a highly accessible organ for the topical application of gene delivery system. For that reason, extensive efforts have been invested in the field of pulmonary medicine in the hopes of finding feasible therapeutic approaches for diverse lung diseases including cancer [20]. Different approaches for gene delivery to the lung such as intravenous injection and

nasal or intratracheal instillation have been reported in various animal models [21]. However, these strategies are invasive, or the methods may not be suitable for effective delivery of the gene-of-interest throughout pulmonary tissues. In recent years, a great deal of effort has focused on the development of aerosol gene delivery technology for the treatment of diverse lung diseases including cancer. This effort has involved finding appropriate nonviral DNA delivery nanovectors that both withstand the sheering force of nebulization and also function optimally in the lungs. Among several nonviral vectors, PEI derivatives were reported to be interesting vectors, and recently their efficacy has been reported to be increased by addition of sugar residues [22]. The high gene transfer efficiency of PEI derivatives is probably due to the buffering of endosomes through PEI that provokes a massive accumulation followed by passive chloride influx. Therefore, modification of PEI with glucose (glucosylated PEI, GPEI) showed high efficiency for aerosol gene delivery in a lung cancer mouse model [10, 23]. Together, aerosol delivery can deliver the gene-of-interest effectively and represents a noninvasive alternative for the targeting of genes to the lungs.

Drug delivery to the central nervous system (CNS) has been challenged by many scientists for the last decades [24, 25]. A number of hydrophilic agents such as antibiotics, anticancer agents, or newly developed biotechnology products do not penetrate the blood–brain barrier (BBB). Therefore, appropriate drug modification, opening of cerebral capillary endothelium, a critical composite of BBB, by osmotic change, and intracerebral delivery have been used to enhance the drug transport to the CNS [26]. However, the use of nanoparticles such as liposome, biocompatible nanoparticles, may provide the clue to overcome the limitations such as penetration of BBB while protecting the drug from degradation, and reducing the potential toxicity. In fact, a recent line of evidence demonstrated that orally administered antituberculosis drug by polylactide-*co*-glycolide nanoparticles was successfully delivered into the brain, thus, exhibited therapeutic effects against *Mycobacterium tuberculosis* H(37)Rv infected mice [27]. The nanoparticle-based delivery system should enable the transport of drugs-of-interest across the BBB that normally cannot cross this barrier in the future.

19.3 RAPID BIOASSAY

The rapid and sensitive determination of pathogenic microorganisms is quite important in life science, and the current war against bioterrorism as well. So far, several methods have been proposed for the detection of pathogens; however, many drawbacks such as low sensitivity, relatively long real-time detection, and low reproducibility hinder the practical application. Recently, nanomaterials have demonstrated their unique advantages in bioanalysis and biotechnology applications when they are combined with biomolecules. The urgent demand for developing highly sensitive nonisotopic bioanalysis

systems has driven nanomaterials more toward life science. Moreover, this nanotechnology can be applicable to the detection of a wide variety of bacterial pathogens that can be used as bioterror agents in food, clinical samples, and environmental samples [28]. For example, a recent report has introduced the quantum dot-based rapid immunoassays for the detection of *Listeria monocytogenes* that is an important food-borne pathogen with an extremely high mortality rate [29]. In addition, *Feline calicivirus* (FCV) has been detected by using monoclonal antibody-conjugated gold nanoparticles, which produce Raman signatures as a recognition tool [30]. Together, development of nanotechnology will be able to open the new era of biosensors for rapid and ultrasensitive determination of pathogenic microorganism.

Nanobiotechnology, which is related to the biomedical application of nanomaterials or nanostructures, is one of the rapidly growing branches within nanotechnology. With the development of this technology, important advances in the detection, diagnosis, and treatment of cancers are under progress. Moreover, nanoparticles are being actively developed for tumor targeting as well as tumor imaging *in vivo*, development of biomarkers, and targeted drug or gene delivery [31]. Thus, the nano-based techniques can be applied ubiquitously in the management of different malignant diseases. That is to say, the use of nanoparticles may provide the selective detection of critical tumor marker proteins for monitoring as well as efficient treatment options. In fact, nanotechnology-based approaches are being actively investigated in cancer imaging [32, 33]. For example, oligonucleotide-functionalized gold nanoparticles have been utilized for the multiplex detection of cancer biomarkers such as prostate specific antigen (PSA), human chorionic gonadotropin (HCG, testicular cancer marker), and α -fetoprotein (AFP, hepatocellular carcinoma marker) with high sensitivity and specificity [34]. Semiconductor quantum dots have been applied to detect the cancer biomarkers in blood and cancer biopsy samples with the aid of fluorescence [35]. Recently, active tumor targeting of nanoparticles has been achieved with direct targeting or pretargeting methods [36]. In direct targeting, nanoparticles are covalently coupled with the ligand of interest and the resulting drug carrier can be administered at once. In the pretargeting method, the therapeutic molecule is not coupled with the ligand and is administered after appropriate delay time because this delay will allow time for the antibody to localize and concentrate in tumor sites with the help of avidin–biotin system or specific antibody [37, 38]. There is a great need for the development of imaging techniques that specifically identify angiogenic blood vessels. A recent report demonstrates that MR molecular imaging of angiogenesis has been achieved by using a bimodal lipidic nanoparticles-labeled α v β 3-integrin [39]. Some research groups have described another novel technique, which uses folate-conjugated fluorescent silica nanoshells in order to detect malignant cells that overexpress folate receptors [40]. Nanoshells are composed of a dielectric silica core covered by a thin metal shell that is typically gold. Based on the relative dimensions of the core radius and shell thickness, nanoshells can be designed to

scatter and/or absorb light over a broad spectral range including near infrared, a wavelength of maximal penetration of light through tissues. With the aid of such characteristics of nanoshells in combination with a clinically relevant breast cancer biomarker, Loo et al. [41] reported that the dual functional (imaging/therapy) immunotargeted nanoshells could be used for the detection and selective destruction of breast carcinoma cells. Recently, nanoparticle probes, so called SERS Dots, which can produce a variety of vibrational information based on surface enhanced Raman scattering (SERS), have been utilized to the targeting of HER2 and CD10 cancer markers on living cells [42]. The nanoparticle probes are composed of silver nanoparticle-embedded silica nanospheres and organic Raman label compounds. In addition to these works, diverse diagnostic and therapeutic modalities are employed for the diagnosis and molecular imaging of cancer. However, at the present time, it is not possible to achieve the cancer cell targeting strategy, which is satisfactorily enough to be applicable to practice. Rather, more research needs to be performed; especially *in vivo* studies have to be undertaken in diverse animal tumor models. Nevertheless, the proof-of-concept of cancer cell targeting with nanoparticles has been suggested elsewhere.

19.4 TISSUE ENGINEERING

Biocompatible nanofibers have been proposed for the replacement of various tissues and organs in humans. Since the nanofibers made from biocompatible polymers have large surface area, the use of nanofibers in tissue regeneration/restoration seems highly plausible in diverse areas including construction of biocompatible prostheses, cosmetics, facemasks, bone substitutes, and artificial blood vessels [43]. Nanofibers can provide a link between nanoscale and microscale materials due to the versatile range of size. Therefore, a current focus of research is to find appropriate conditions for electrospinning various polymers for the application in many areas such as multifunctional membranes, biomedical structural elements, protective shields in specialty fabrics, filter media for submicron particles in the separation industry, composite reinforcement, and structures for nanoelectronic machines [44]. Recently, the use of a conductive polymer, polyaniline, has gained much attention. In fact, Li et al. [45] has shown that polyaniline-gelatin blend nanofibers may provide a novel conductive material, well suited as biocompatible scaffolds for tissue engineering. On the other hand, tremendous efforts have been focused on an efficient delivery of drugs using nanofibers. For such purpose, three-dimensional nanofibrous scaffolds incorporating controlled-release growth factors have been introduced successfully for complex tissue regeneration [46]. Thanks to the above efforts, many other applications of polymer nanofibers have been reported recently in the field of biomedicine and biotechnology.

19.5 POTENTIAL SAFETY ISSUES

To understand the potential adverse effects of nanomaterials on health, one must understand the general defense mechanism of living organism and the interactions between nanoparticles and the immune response. Based on much of evolutionary history, humans have been exposed to small particles, thus have developed appropriate defense mechanisms against these nanoparticles. The dominant routes of access to humans of nanoparticles include the lung (inhalation), skin (contact), or intestine (swallowing), which contain barriers to penetration by small particles [47]. Regardless of the presence of such defense mechanism, nanomaterials may cause potential problems for humans because defense mechanism may not work properly against the nanomaterials.

As mentioned briefly, widespread application of nanomaterials may cause significant potentials for human exposure and environmental release. Therefore, appropriate risk assessment and management of nanomaterials should be performed to assess and regulate these nanomaterials in order to protect human health and the environment. For the efficient risk assessment of nanomaterials, characterization of nanomaterials is essential because the reactivity of nanomaterials depends largely upon size, shape, and others. Complete characterization of nanomaterials includes measurements of size, shape, inborn chemistry of the nanomaterial, solubility, surface area, state of dispersion, surface chemistry, and other physicochemical properties. Complete characterization of nanomaterials to be tested may be time consuming, expensive, and complex; therefore, an agreeable basis of minimal characterization should be proposed for the safety evaluation of nanomaterials. Such properties should include the size, shape, state of dispersion, physicochemical properties, surface area, and surface chemistry [48].

As mentioned, the definition of a nanomaterial, which has been generally accepted, includes any material with at least one dimension smaller than 100 nm. Therefore, reliable methods for the size measurement should be developed. There are a wide variety of methods for determining nanoparticle size distribution, including light scattering, dynamic mobility analysis, electron microscopy, and many others. However, it is very important to recognize that measurement of size and shape of nanomaterials in the biological environment should be performed satisfactorily because the size and shape of the nanomaterial interacting with a biomolecule in living organism or with others may differ from their original form. Interactions between nanomaterials and biological organisms typically take place at the surface of nanomaterials; thus, surface area seems to be one of the primary factors in determining toxicity. Surface area can be characterized in two ways external surface area and internal surface area (porosity). The external and internal surface areas of nanomaterials can be measured by gas adsorption method, surface titrations, and aerosol diffusion [49, 50]. It is important to know that the practical surface area and porosity of nanomaterials in biological environments can be changed

due to the potential adsorption of biomolecules or self-agglomeration. Such changes may affect the toxicity of nanomaterials. Surface charge of nanomaterials is also critical to determine the toxicity because it is a major factor in determining the particle dispersion and will influence the behavior of nanomaterials in living organism.

19.6 CONCLUSIONS

Rapid development in nanotechnology will result in invaluable benefits for modern life. Simultaneously though, applications of nanotechnology should not produce adverse effects on human health and the environment. To predict and prevent the potential toxicity of nanomaterials, therefore, the complete characterization of nanomaterials should be elucidated under conditions as close to the point of application such as the biological environment. Therefore, new manufactured nanomaterials should be treated with caution and the toxic potential should be evaluated. Classical toxicity test battery may not be suitable to evaluate the potential impacts on humans and the environment. Therefore, it is highly recommended that the manufacture and release of nanomaterials should be regulated through multifunctional activities among academia, governmental regulatory agencies, and industries. Based on such concerted action, effective multidisciplinary collaborative research of the impacts of nanomaterials into humans should keep pace with the predicted development.

ACKNOWLEDGMENTS

Preparation of part of the current chapter is supported by Nano Systems Institute-National Core Research Center (NSI-NCRC) through KOSEF in Korea.

REFERENCES

1. Roco MC. Converging science and technology at the nanoscale: opportunities for education and training. *Nat Biotechnol* 2003;21(10):1247–1249.
2. La Van DA, McGuire T, Langer R. Small-scale systems for *in-vivo* drug delivery. *Nat Biotechnol* 2003;21(10):184–1191.
3. Nakanishi T, et al. Development of the polymer micelle carrier system for doxorubicin. *J Control Release* 2001;74:295–302.
4. Ruponen M, Honaski P, Ronko S, Tammi M, Urtti A. Extracellular and intracellular barriers in non-viral gene delivery. *J Control Release* 2003;93:213–217.
5. Partridge KA and Oreffo ROC. Gene delivery in bone tissue engineering: progress and prospects using viral and nonviral strategies. *Tissue Eng* 2004;10:295–307.

6. Bellon G, et al. Aerosol administration of a recombinant adenovirus expressing CFTR to cystic fibrosis patients: a phase I clinical trial. *Hum Gene Ther* 1997;8:15–25.
7. Crystal RG, et al. Administration of an adenovirus containing the human CFTR cDNA to the respiratory tract of individuals with cystic fibrosis. *Nat Genet* 1994;8:42–51.
8. Zabner J, et al. Repeat administration of an adenovirus vector encoding cystic fibrosis transmembrane conductance regulator to the nasal epithelium of patients with cystic fibrosis. *J Clin Invest* 1996;97:1504–1511.
9. Harvey BG, et al. Airway epithelial CFTR mRNA expression in cystic fibrosis patients after repetitive administration of a recombinant adenovirus. *J Clin Invest* 1999;104:1245–1255.
10. Kim HW, et al. Aerosol gene delivery of glucosylated polyethyleneimine/phosphatase and tensin homologue deleted on chromosome 10 complex suppressed Akt downstream pathways in the lungs of *K-ras* null mice. *Cancer Res* 2004;64(21):7971–7976.
11. Mao HQ, et al. Chitosan-DNA nanoparticles as gene carriers: synthesis, characterization and transfection efficiency. *J Control Release* 2001;70:399–421.
12. Green J, et al. Biodegradable polymeric vectors for gene delivery to human endothelial cells. *Bioconjugate Chem* 2006;19(5):1162–1169.
13. Bergen JM, von Recum HA, Goodman TT, Massey AP, Pun SH. Gold nanoparticles as a versatile platform for optimizing physicochemical parameters for targeted drug delivery. *Macromol Biosci* 2006;6(7):506–516.
14. Furumoto K, et al. Important role of serum proteins associated with on the surface of particles in their hepatic disposition. *J Control Release* 2002;83: 89–96.
15. Gbadamosi JK, Hunter AC, Moghimi SM. PEGylation of microspheres generates a heterogenous population of particles with differential surface characteristics and biological performance. *FEBS Lett* 2002;532(3):339–344.
16. Ogawara K, et al. Surface hydrophobicity of particles is not necessarily the most important determinant in their *in vivo* disposition after intravenous administration in rats. *J Control Release* 2001;77(3):191–198.
17. Emerich DF, Thanos CG. The pinpoint promise of nanoparticle-based drug delivery and molecular diagnosis. *Biomol Eng* 2006;23:171–184.
18. Soppimath KS, Aminabhavi TM, Kulkarni AR, Rudzinski WE. Biodegradable polymeric nanoparticles as drug delivery devices. *J Control Release* 2001;70: 1–20.
19. Koziara JM, Whisman TR, Tseng MT, Mumper RJ. *In-vivo* efficacy of novel paclitaxel nanoparticles in paclitaxel-resistant human colorectal tumors. *J Control Release* 2006;112(3):312–319.
20. Dailey LA, et al. Modified polyethylenimines as non viral gene delivery systems for aerosol therapy: effects of nebulization on cellular uptake and transfection efficiency. *J Control Release* 2004;100:425–436.
21. Gautam A, Densmore CL, Golunski E, Xu B, Waldrep JC. Transgene expression in mouse airway epithelium by aerosol gene therapy with PEI-DNA complexes. *Mol Ther* 2001;3:551–556.

22. Merlin JL, et al. Improvement of nonviral p53 gene transfer in human carcinoma cells using glucosylated polyethylenimine derivatives. *Cancer Gene Ther* 2001;8: 203–210.
23. Jin H, et al. Aerosol delivery of urocanic acid-modified chitosan/programmed cell death 4 complex regulated apoptosis, cell cycle, and angiogenesis in lungs of *K-ras* null mice. *Mol Cancer Ther* 2006;5(4):1041–1049.
24. Kreuter J. Nanoparticulate systems for brain delivery of drugs. *Adv Drug Deliv Rev* 2001;47:65–81.
25. Lockman PR, Mumper RJ, Khan MA, Allen DD. Nanoparticle technology for drug delivery across the blood–brain barrier. *Drug Del Ind Pharm* 2002;28:1–13.
26. Tiwari SB and Amiji MM. A review of nanocarrier-based CNS delivery systems. *Curr Drug Deliv* 2006;3(2):219–232.
27. Pandey R and Khuller GK. Oral nanoparticle-based antituberculosis drug delivery to the brain in an experimental model. *J Antimicrob Chemother* 2006;57(6): 1146–1152.
28. Zhao X, et al. A rapid bioassay for single bacterial cell quantitation using bioconjugated nanoparticles. *Proc Natl Acad Sci USA* 2004;101(42):15027–15032.
29. Tully E, Hearty S, Leonard P, O’Kennedy R. The development of rapid fluorescence-based immunoassays, using quantum dot-labelled antibodies for the detection of *Listeria monocytogenes* cell surface proteins. *Int J Biol Macromol* 2006;39(1–3): 127–143.
30. Driskell JD, et al. Low-level detection of viral pathogens by a surface-enhanced Raman scattering based immunoassay. *Anal Chem* 2005;77(19):6147–6154.
31. Yezhelyev MV, et al. Emerging use of nanoparticles in diagnosis and treatment of breast cancer. *Lancet Oncol* 2006;7(8):657–667.
32. Gao X, Cui Y, Levenson RM, Chung LW, Nie S. *In vivo* cancer targeting and imaging with semiconductor quantum dots. *Nat Biotechnol* 2004;22(8):969–976.
33. Fortina P, Kricka LJ, Surrey S, Grodzinski P. Nanobiotechnology: the promise and reality of new approaches to molecular recognition. *Trends Biotechnol* 2005;23(4): 168–173.
34. Stoeva SI, Lee JS, Smith JE, Rosen ST, Mirkin CA. Multiplexed detection of protein cancer markers with biobarcode nanoparticle probes. *J Am Chem Soc* 2006;128:8378–8379.
35. Smith AM, Dave S, Nie S, True L, Gao X. Multicolor quantum dots for molecular diagnostics of cancer. *Expert Rev Mol Diagn* 2006;6(2):231–244.
36. Nobs L, Buchegger F, Gurny R, Allemann E. Biodegradable nanoparticles for direct or two-step tumor immunotargeting. *Bioconjug Chem* 2006;17(1):139–145.
37. Goodwin DA and Meares CF. Advances in pretargeting biotechnology. *Biotechnol Adv* 2001;19:435–450.
38. Sharkey RM, et al. A universal pretargeting systems for cancer detection and therapy using bispecific antibody. *Cancer Res* 2003;63:354–363.
39. Mulder WJ, et al. MR molecular imaging and fluorescence microscopy for identification of activated tumor endothelium using a bimodal lipidic nanoparticle. *FASEB J* 2005;19(14):2008–2010.

40. Santra S, et al. Folate conjugated fluorescent silica nanoparticles for labeling neoplastic cells. *J Nanosci Nanotechnol* 2005;5(6):899–904.
41. Loo C, Lowery A, Halas N, West J, Drezek R. Immunotargeted nanoshells for integrated cancer imaging and therapy. *Nano Lett* 2005;5(4):709–711.
42. Kim JH, et al. Nanoparticle probes with surface enhanced Raman spectroscopic tags for cellular cancer targeting. *Anal Chem* 2006;78:6967–6973.
43. Venugopal J and Ramakrishna S. Application of polymer nanofibers in biomedicine and biotechnology. *Appl Biochem Biotechnol* 2005;125(3):147–158.
44. Jayaraman K, Kotaki M, Zhang Y, Mo X, Ramakrishna S. Recent advances in polymer nanofibers. *J Nanosci Nanotechnol* 2004;4(1–2):52–65.
45. Li M, Guo Y, Wei Y, MacDiarmid AG, Lelkes PI. Electrospinning polyaniline-contained gelatin nanofibers for tissue engineering applications. *Biomaterials* 2006;27(13):2705–2715.
46. Wei G, Jin Q, Giannobile WV, Ma PX. Nano-fibrous scaffold for controlled delivery of recombinant PDGF-BB. *J Control Release* 2006;112(1):103–110.
47. Oberdorster G, Oberdorster E, Oberdorster J. Nanotoxicology: an emerging discipline from studies of ultrafine particles. *Environ Health Perspect* 2005;113:823–839.
48. Powers KW, et al. Research strategies for safety evaluation of nanomaterials. Part VI: characterization of nanoscale particles for toxicological evaluation. *Toxicol Sci* 2006;90(2):296–303.
49. Allen T. Particle size measurement. Volume 2, Surface Area and Pore Size Determination 5th ed. ChapmanHall; 2004.
50. Burtscher H. Physical characterization of particulate emissions from diesel engines: a review. *J Aerosol Sci* 2005;36:896–932.

INDEX

- Aceruloplasminemia, 473
Acquired immunodeficiency disease (AIDS), 423
Active pharmaceutical ingredient (API), 94
Adeno-associated viruses (AAV), 175, 338
Adenosine triphosphatase (ATP), 462
Adenovirus-based vectors, 175
Alkaline phosphatase (ALP) activity, 276, 287, 393
Alzheimer's disease, 130, 470
Amyloid precursor protein (APP), 471
Amyotrophic lateral sclerosis (ALS), 471
Anterior cruciate ligament (ACL), 358
Antibody-based therapy, 101
Anticancer drug therapy, 412
Artery wall binding peptide (AWBP), 104
Atomic force microscope (AFM), 8, 53
Atom transfer radical polymerization (ATRP), 70
cis-Azobenzene moiety, 57
- Baby hamster kidney (BHK), 391
Basement membrane (BM), 297
Binding domains, 245, 246
 cryptic sites, 246
Biocompatible nanofibers, 496
Biosensor, 439, 441
 cantilever-based, 442
Black hole quencher (BHQ), 59
Blood-brain barrier (BBB), 118, 141, 468, 494
Blood-contacting devices, 32, 38
- Bovine brain microvessel endothelial cells (BBMECs), 173
Brain capillary epithelial cells (BCEC), 103
Brain iron accumulation, 473
- Cancer chemotherapy, 144, 411
Capillary force lithography, 387
Carbon nanotubes, 107, 162, 164
 biomedical applications, 165
 functionalization of, 164
Cardiac tissue engineering, 399
Cell-cell interactions, 242, 364, 365, 367
Central nervous system (CNS), 118, 144, 494
Chelation therapy, 478
Chemical vapor deposition (CVD), 162, 163
Colloidal lithography, 278
Computed tomography (CT) scans, 410
Cowpea chlorotic mottle viruses (CCMV), 480
Critical solution temperature (CST), 99
- Dendrimers, 152
Diethyl amino ethyl methacrylate (DEAEM), 172
Dioleoyl phosphatidyl ethanolamine (DOPE), 349
Dip pen lithography, 7, 8
DNA amplification, 207
DNA strand-exchanging reaction, 58
DNA transfection, 337, 342
 in vitro, 340
Dot-based rapid immunoassays, 495

- Doxil, 420
 pharmacodynamics, 422, 423
Drug-drug interactions, 97
Drug encapsulation, 143
Drug/gene delivery system (DGDS), 115
dsRNA-dependent protein kinase, 352
Dynamic light scattering (DLS), 67
- ECM-soluble factor interactions, 244, 360
Electric arc discharge, 17, 163
Electron beam lithography, 7, 270
 techniques, 386
Electroporation, 339
Electrospinning, 146, 264, 272, 279, 381,
 383, 386
Enhanced permeability and retention
 (EPR), 140, 416
Enzyme-based biosensors, 440
Enzyme-linked immunoabsorbent assays
 (ELISAs), 208
Epidermal growth factor (EGF) repeats, 236
Ethylenediaminetetraacetic acid
 (EDTA), 479
Extracellular matrix (ECM)
 molecules, 343
 proteins, 297
- Feline calicivirus (FCV), 495
Fetal bovine chondrocytes, 383
Fibril-forming collagens, 229, 234
Fibroblast growth factor (FGF), 236
Fibroblast-osteoblast interaction, 364
Field-dependent relaxation rate increase
 (FDRI), 471
Fluorescein isothiocyanate (FITC), 105
Fluorescence cross-correlation spectroscopy
 (FCCS), 208
Fluorescence recovery after photobleaching
 (FRAP), 326
Fluorescence resonance energy transfer
 (FRET), 210, 326
Focal adhesions, 322, 324
 as a mechanotransduction machine, 325
Folate receptors (FR), 102
Food and Drug Administration (FDA), 119
Foot-and-mouth disease virus (FMDV), 168
- Gaussian point spread function, 215
Gelatin immobilization, 396
- Gene delivery techniques, 399
Gene therapy, 337, 340
Gene-transfected EPCs, 343
Glial cell line-derived neurotrophic factor
 (GDNF), 176
Glucose-sensitive nanogels, 172
Glycoproteins, 236, 238, 239
Gram-positive bacteria, 169
Green fluorescent protein (GFP), 349
Growth factors, 151, 244
Guglielmi detachable platinum coils
 (GDCs), 38
Gut-associated lymphoid tissue, 342
- Hard baking process, 6, 272
Hemochromatosis, 474
Hemosiderin, 464
Hemosiderin-rich lysosomes, 469
Heterodimeric transmembrane mole-
 cules, 249
Heterotypic cell-cell contact, 361
Heterotypic cellular interactions, 358
 role of, 359
High pressure homogenization (HPH), 158
High speed stirring/ultrasonication, 159
HIV-associated dementia (HAD), 474
Horseradish peroxidase (HRP), 103
Human chorionic gonadotropin (HCG), 495
Human corneal epithelial cells
 (HCECs), 307
Human coronary artery endothelial cells
 (HCAECs), 273, 396
Human ligament fibroblast (HLF), 274
Human umbilical vein endothelial cells
 (HUVECs), 309
Huntington's disease, 471
Hydrogel nanoparticles, 68, 72, 75, 78
- Infectious diseases, 207
Integrin-activated EGF receptors, 250
Integrin-cytoskeletal connections, 325
Integrin signaling, 249
Interface-relevant cells, 362, 364
Interface-relevant markers, 364
Ion beam lithography, 7
Ion implantation process, 26, 31, 32, 38
Iron-overload disease, 465, 469, 473, 474
Iron-rich protein-mineral complex, 464
Iron-transporting serum glycoprotein, 102

- Keratin, 385
 Keratocytes, 270
 Kaposi's sarcoma, 423
- Laser ablation, 17, 163
 Latex agglutination tests (LATs), 208
 Ligand-mediated targeting, 140
 Ligand-receptor binding, 397
 Ligand-receptor bonds, 326
 Lipid-based delivery systems, 96
 Lipid-based vector, 349
 Lipid nanoparticles, 157
 drug delivery applications, 161
 Liposome(s), 72, 157, 160, 417, 419
 as solubilizing carrier, 426
 drug delivery applications, 159
 long-circulating, 419
 synthesis of, 158
 vaccine, 425
 Load-bearing extracellular matrix, 322
 Lower critical solution temperature (LCST), 64, 99, 172
 Luminescent oxygen channeling immunoassay (LOCI), 208
 Luteinizing hormone-releasing hormone (LHRH), 104
- Macrophages, 312
 Madin-Darby canine kidney (MDCK), 391
 Magnetic resonance imaging (MRI), 94, 410, 467
 Masked ion beam lithography (MIBL), 28
 Matrix metalloproteinase (MMP), 250
 Membrane permeant peptides (MPPs), 348
 Methotrexate-dendrimer conjugates, 154
 Micelle-based delivery systems, 96
 Microarray analysis, 278
 Microelectromechanical systems (MEMS), 3, 451
 Microemulsion method, 159
 Microfluidizer homogenizers, 181
 Micro/nanocontact printing, 387
 Molecular beacon, 55
 Molecular self-assembly techniques, 381, 385
 Monoclonal antibodies (mAb), 101
 Mononuclear phagocyte system (MPS), 140
 Multichannel scalar (MCS), 213
- Multidimensional cellular interactions, 370
 Multi-DNA nanomotors, 51
 Multidrug resistance (MDR), 121
 phenotype, 424
 Multifunctional nanoparticle systems, 105
 Multiphenotype cell arrays, 445
 Multiple sclerosis (MS), 474
 Multiwalled carbon nanotubes (MWNTs), 162
- Nanobiotechnology, 495
 Nanocrystal technology, 179, 182
 Nanoelectromechanical systems (NEMS), 3
 Nanoengineering techniques, 3, 131, 264
 Nanofiber-based carrier devices, 152
 Nanofibrous scaffolds, 381
 Nanogroove synthesis, 305
 Nanogroove system
 advantage of, 305
 Nanoimprint lithography (NIL), 41, 274
 Nanoparticle-aptamer conjugates, 103
 Nanosphere lithography, 7, 8
 Nanostructured lipid carriers (NLCs), 157
 Nanostructured scaffolds, 401
 Nanotechnology, 49, 93, 182, 409, 413, 440
 advent of nanotechnology, 141
 based drug delivery devices, 95, 96
 bioconjugated hydrogel particles in, 70
 Nerve growth factor (NGF), 151, 313, 398
 Neural progenitor cell (NPC), 398
 Neural tissue engineering, 397
 Neuroferritinopathy, 473
 Neuromelanin, 466, 472
 Next generation lithography (NGL), 25
 Nitroxide-mediated radical polymerization (NMRP), 70
 Noncollagenous domains, 246
 Nonsteroidal antiinflammatory drugs (NSAIDs), 155
 Nuclear localization signaling (NLS), 338
 Nuclear magnetic resonance (NMR), 465
 Nucleic acids, 441
 role in tissue engineering, 391
- Optical lithography, 4
 Osteoblast-fibroblast coculture model, 364
 Osteoblast-fibroblast interaction, 359, 362, 363, 364
 Osteoblast-fibroblast model, 363

- Osteoblast-mediated mineralization, 363
Osteoprogenitor, 286
Oxygen-radical reactions, 465
- Pantothenate kinase associated neurodegeneration (PKAN), 468
Parkinson's disease (PD) tissue, 466, 471
PEG-coated liposomes, 420
Phase-inversion technique, 126
Phase separation technique, 277, 384
Photochemical internalization (PI), 101
Photodynamic therapy (PDT), 101
Photolithography, 4, 271, 272, 386
Piston-gap homogenizers, 181
Planar microarray sensor, 3
Platelet-derived growth factor (PDGF), 152
Polyalkylcyanoacrylate (PACA), 119
Polyaniline-gelatin blend nanofibers, 280
Polycaprolactone (PCL), 119, 378
Polycation-DNA complexes, 145
Polydimethylsiloxane (PDMS), 386
Polyethylene glycol (PEG), 119
Polyethylene glycol-coupled transferrin (PEG-TF), 102
Polyglycolic acid (PGA), 378
Polylactic acid (PLA), 119
Polymerase chain reaction (PCR), 441
Polystyrene nanopatterned surfaces, 275
Positron emission tomography (PET) scans, 410
Polymer-polymer hydrophobic interactions, 64
Progressive supranuclear palsy (PSP), 469
Prostate specific antigen (PSA), 495
Prostate-specific membrane antigen (PSMA), 103
Protein arrays, 445
Proteoglycans, 236, 379
Proton-exchange dephasing model (PEDM), 478
- Quantum dots (QDs), 108, 208, 219, 414, 447
- Rapid bioassay, 494
Rayleigh equation, 7
Receptor-mediated endocytosis, 101, 103
Receptor-mediated signaling, 250
Recombinant herpesvirus vectors, 177
Redox-active metals, 474
Respiratory syncytial virus (RSV), 216
Restless legs syndrome (RLS), 474
Reticuloendothelial system (RES), 117, 144, 417
Retinal pigment epithelium, 387
Rhodamine-labeled dextran, 103
RNA-binding proteins, 352
RNA-induced silencing complex (RISC), 344
RNA interference (RNAi), 344
 directed gene silencing, 345, 349
RNA transfection, 344
- Serological assays, 207
Sandwich assay, 208
Secondary ion mass spectroscopy (SIMS), 30
Self-agglomeration, 498
Self-assembled monolayer (SAM), 387, 306
Self-assembled peptide nanofiber scaffolds (SAPNS), 397
Shell cross-linked knedels (SCK), 69
Signal-to-noise ratios (SNRs), 209
Single-molecule detection (SMD), 209
Single-stranded DNA (ssDNA), 55
Single-walled nanotubes (SWNTs), 282
Small angle neutron scattering (SANS), 67
Smooth muscle cells (SMCs), 228
Sodium dodecyl sulfate (SDS), 165
Solid lipid nanoparticles (SLNs), 157
Stem cell-based gene therapy, 392
Superconducting quantum interference device (SQUID), 465
Supercritical antisolvent precipitation (SAS), 120
Surface enhanced Raman scattering (SERS), 496
Surface of segmented polyurethane (SPU), 32
Surfactant-free emulsion polymerization (SFEP), 66
- Target-specific probes, 212
Temperature-sensitive core/shell microgel, 67
Therapeutic angiogenesis, 340

- Thermally induced phase separation (TIPS), 384
- Tissue culture polystyrene (TCPS), 264
- Tissue-like cellular organization, 381
- Transfection methods, 339
- Transferrin (TF), 102
bearing liposomes, 103
- Transforming growth factor, 152
- Transmembrane glycoproteins, 248
- Transmission electron micrographs, 299
- Ultrahigh molecular weight polyethylene (UHMWPE), 31
- Ultrasensitive assays, 219
- Ultrasound-mediated drug delivery, 101
- Vascular endothelial growth factor (VEGF), 152, 244, 396, 350
- Vincristine sphingomyelin liposomes, 424
- Viral-based gene transfer, 338
- Virus-based vectors, 130
- Virus-like particles (VLPs), 142, 174
- Volume phase transition temperature (VPTT), 64
- Water-containing hydrogels, 41
- Water-in-oil emulsification, 122
- Water-insoluble polymers, 119, 121
- Water-soluble carboxylic acid, 169
- Water-soluble polymers, 121
- Wheat germ agglutinin (WGA), 104
- Xenopus* neuritis, 270
- X-ray absorption spectroscopy, 477
- X-ray diffraction, 463
- X-ray photoelectron spectroscopy, 38
- Zeta potential, 143

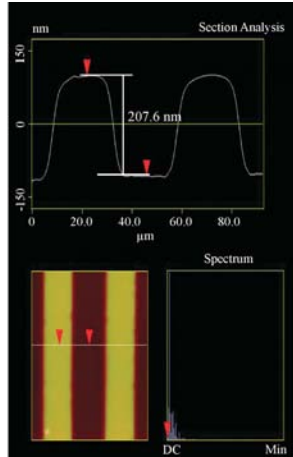
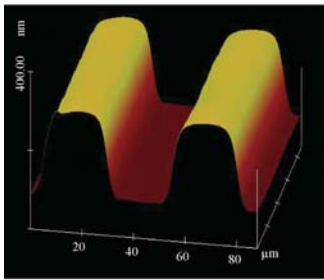


FIGURE 2.5 AFM micrographs of patterned poly(MMA-co-*t*-BOC-NVP) surface (25 μm line 50 μm space) showing section analysis.

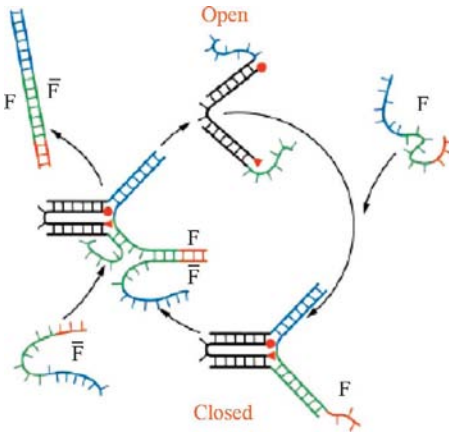


FIGURE 3.2 Operation of the molecular tweezers. Closing and opening the molecular tweezers. Closing strand F hybridizes with the dangling ends of strands B and C (shown in blue and green) to pull the tweezers closed. Hybridization with the overhang section of F (red) allows F strand to remove F from the tweezers, forming a double-stranded waste product FF and allowing the tweezers to open. Complementary sections of B, C, F, and F-bar that hybridize to close and open the tweezers are colored.

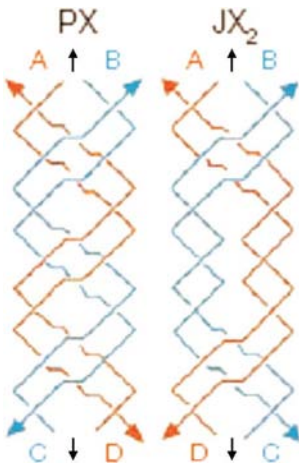


FIGURE 3.3 Schematic drawings of the device. The PX and JX₂ motifs. The PX motif, postulated to be involved in genetic recombination, consists of two helical domains formed by four strands that contain a central dyad axis (indicated by the vertical black arrows). Two strands are drawn in red and two in blue, where the arrowheads indicate the 3' ends of the strands. The Watson-Crick base pairing in which every nucleotide participates is indicated by the thin horizontal lines within the two double helical domains. Every possible crossover occurs between the two helical domains. The same conventions apply to the JX₂ domain, which lacks two crossovers in the middle. The letters A, B, C, and D, along with the color coding, show that the bottom of the JX₂ motif (C and D) are rotated 180° relative to the PX motif.

COLOR PLATES

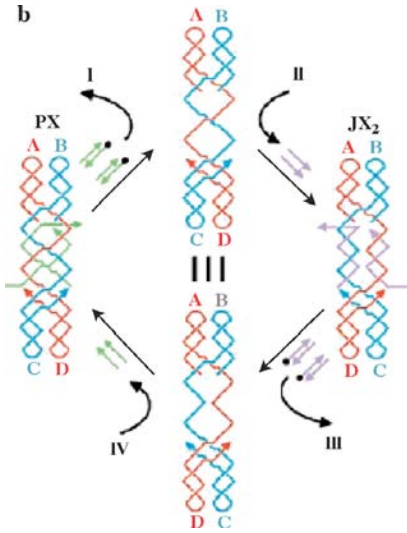


FIGURE 3.4 Principles of device operation. On the left is a PX molecule. The green set strands are removed by the addition of biotinylated green “fuel” strands (biotin indicated by black circles) in process I. The unstructured intermediate is converted to the JX₂ motif by the addition of the pale-purple set strands in process II. The JX₂ molecule is converted to the unstructured intermediate by the addition of biotinylated pale-purple “fuel” strands in process III. The identity of this intermediate and the one above it is indicated by the identity symbol between them. The cycle is completed by the addition of green set strands in process IV, restoring the PX device.

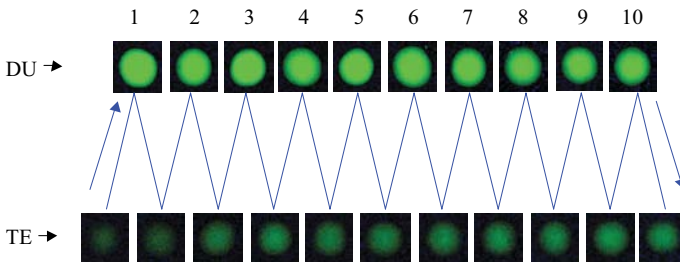


FIGURE 3.8 Cycling of the DNA motor. During the motor’s cycling, the motor molecules are imaged by a digital camera. Ten cycles were recorded here.

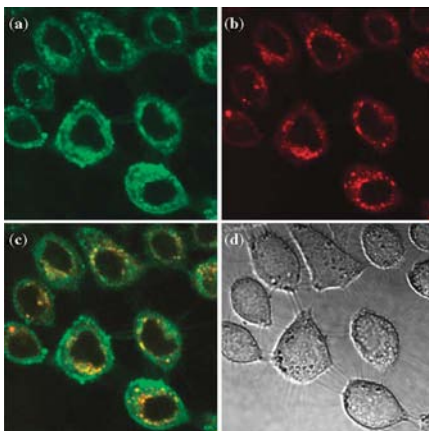


FIGURE 4.7 Confocal images of HeLa cells incubated with folate-conjugated nanoparticles. (a) Green fluorescent particle channel, (b) lysotracker red dye channel, (c) overlap of both the channels, and (d) transmittance image of the cells. Experiments performed in collaboration with Jean Chmielewski at Purdue University.

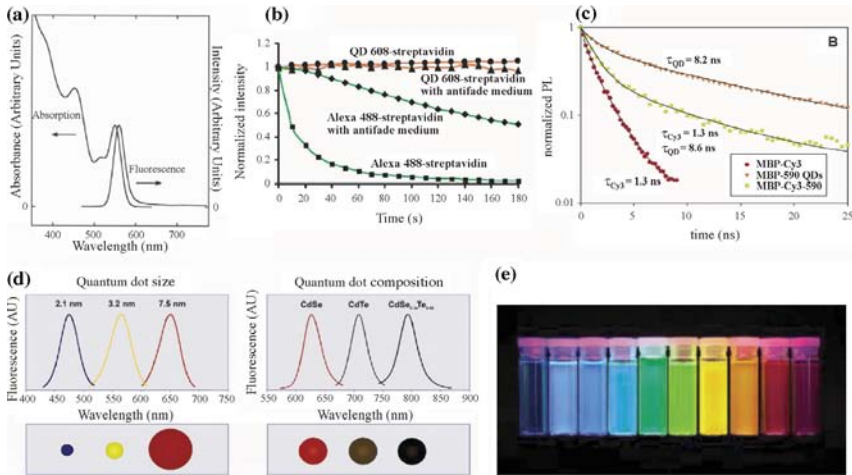


FIGURE 8.1 Novel optical properties of quantum dots. See text for full caption.

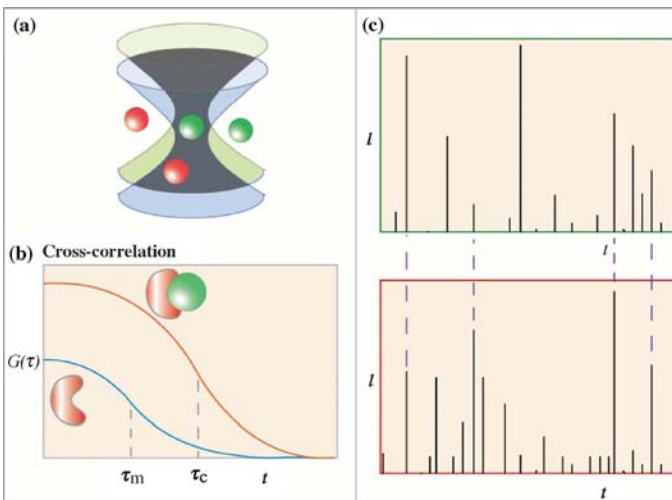


FIGURE 8.3 Single-molecule detection by two-color fluorescence correlation. (a) Difficulties in achieving par-focality and probe volume overlapping with two color lasers are used to excite two dyes, due to spherical and chromatic aberrations of the microscope objective. (b) Signals from the two color fluorophores are analyzed by cross-correlation or (c) by coincidence of arrival on two APD detectors.

COLOR PLATES

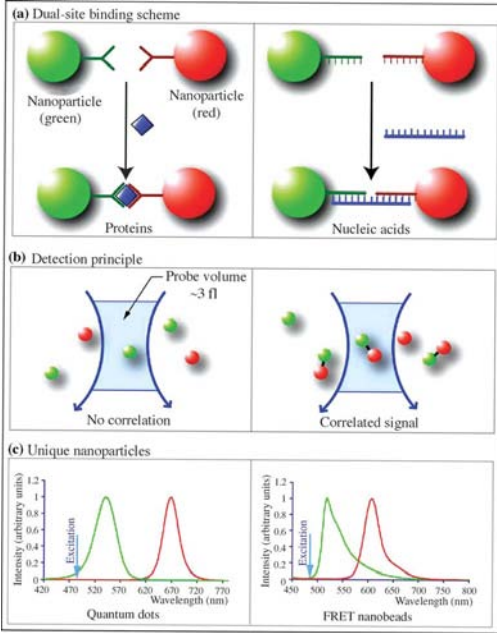


FIGURE 8.4 Single-molecule sandwich assays using color-coded nanoparticles. (a) Simultaneous double-site binding for protein and nucleic acid detection; (b) free nanoparticle probes and bound sandwich pairs moving across a tightly focused laser beam; and (c) fluorescence emission spectra of color-coded quantum dots and energy-transfer nanoparticles. The left panel shows green and red QDs simultaneously excited with a single light source at 420 nm, and the right panel shows green and red energy-transfer nanoparticles excited at the same wavelength. The arrows indicate the relative position of the excitation laser wavelength (488 nm) used in single-molecule detection.

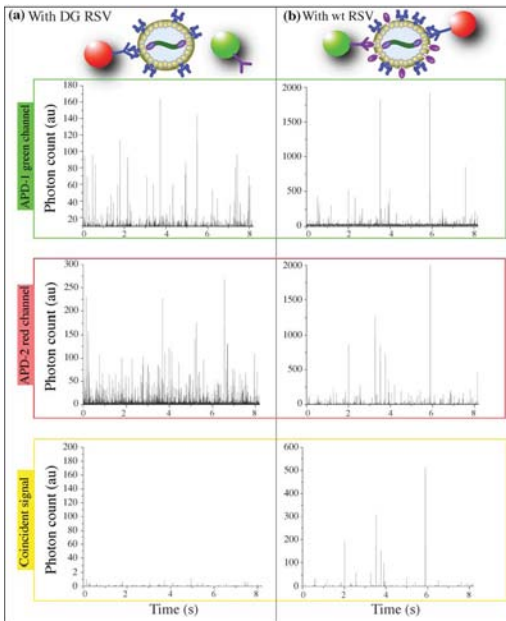


FIGURE 8.6 Counting viral particles in solution. The 40-nm nanoparticles conjugated to RSV anti-F or anti-G protein monoclonal antibodies were used to produce red or green photon emission, respectively. RSVΔG, used as a control, produced low green photon counts as expected and did not show coincidence signals (a), while coincident peaks were observed for RSV/A2 (b).

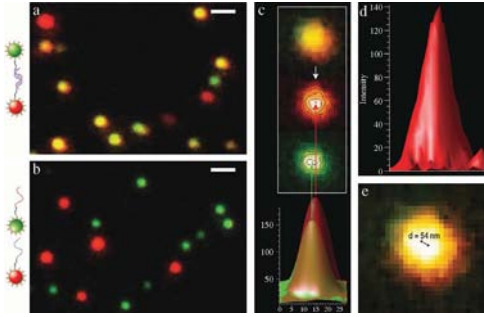


FIGURE 8.7 Dual-color imaging and colocalization of nanoparticle probes at nanometer precision. (a and b) Nanoparticles form diffraction-limited pairs resulting in color change only in presence of complementary sequences. (c) Image of a real R–G bead pair separated into red and green components that are convolved with a Gaussian kernel to determine center. (d) High SNR

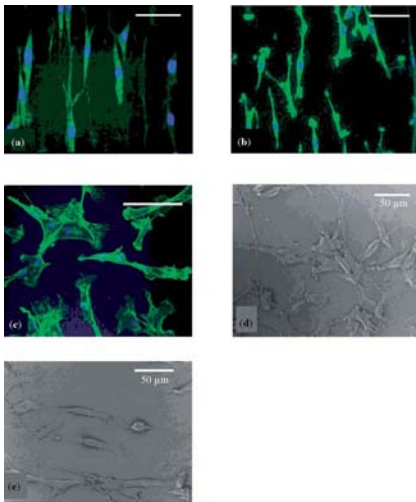


FIGURE 10.4 Confocal micrographs of F-actin stained SMCs on (a) nanoimprinted on PMMA, (b) PDMS, and (c) nonpatterned PMMA surfaces (scale bar 50 μm). SEM micrographs on (d) nonpatterned PMMA and (e) nanoimprinted surfaces show elongated structures on patterned surfaces. (Reprinted with permission from Reference [78].)

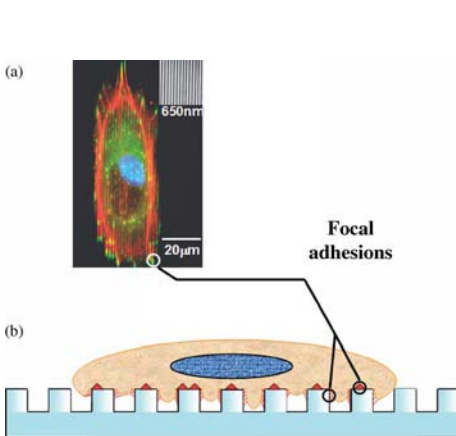


FIGURE 11.6 Focal adhesions anchor cells to nanogrooved surfaces. (a) Cells and their actin filaments (red) align parallel to grooves. Antibodies against vinculin (green) show focal adhesions are also aligned with the nanogrooved surface. (b) A side model of a cell growing on nanogrooved topography. The cell will form focal adhesions (red) on the top of the ridge and down along the walls of the groove. It should be noted that cells residing on the smallest nanoscale features usually lie across the ridges and do not invest the grooves with cellular elements.

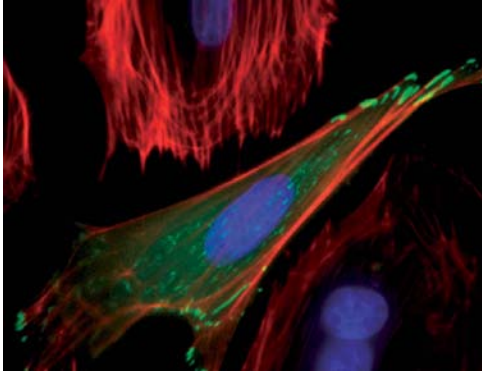


FIGURE 12.1 Fluorescence image of a single capillary endothelial cell expressing GFP-vinculin (green), stained for F-actin with Alexa 468-phalloidin (red), and nuclei with DAPI (blue). Note how each actin stress fiber anchors to focal adhesions at its distal ends (bar = 10 μm).

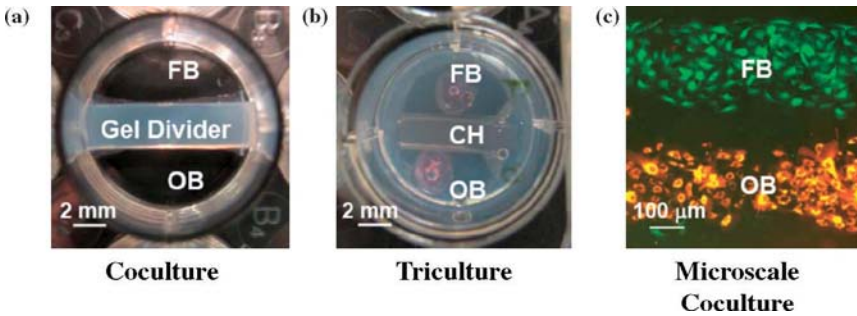


FIGURE 14.2 Examples of cell–cell interaction models used in interface tissue engineering: (a) Coculture of fibroblasts and osteoblasts with temporary agarose gel divider; (b) triculture of fibroblasts and osteoblasts with chondrocytes encapsulated in 3D hydrogel; (c) microscale coculture of fibroblasts and osteoblasts using microfluidic patterning techniques. FB: fibroblasts, OB: osteoblasts, CH: chondrocytes.

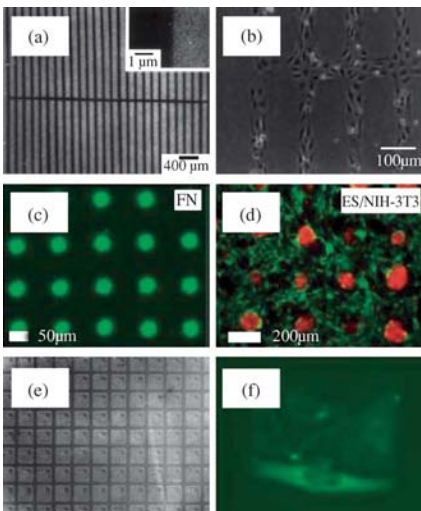


FIGURE 15.4 Surface patterning using various novel techniques, optical micrographs of microcontact printed SAMs on gold having patterned regions with (a) fibronectin (black in color) and (b) bovine capillary endothelial cells (reproduced from Reference [56] with permission, 1997, Academic Press). Layer-by-layer deposition using capillary force lithography method; (c) fluorescence image of fibronectin adsorption on hyaluronic acid patterned surface and (d) fluorescent image of patterned 1-day-old cocultures of ES cells (red) with NIH-3T3 fibroblasts (green) (reproduced from Reference [62] with permission, 2003, Elsevier Ltd). (e) Fluorescence micrograph showing selective protein adsorption to adhesive APS regions (line width of $L = 4 \mu\text{m}$) and (f) reflectance image of green fluorescence protein-tubulin transfected HeLa cells adhering to $100 \mu\text{m}^2$ island (reproduced from Reference [64] with permission, 2005, Nano Science and Technology Institute.)

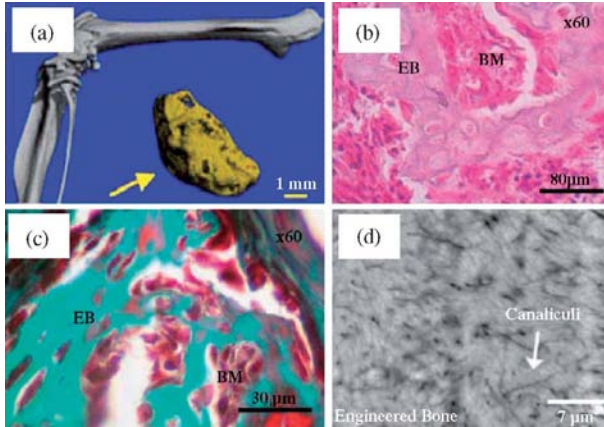


FIGURE 15.6 (a) μ CT image of a femoral and engineered bone. Histological evolution of the engineered bone. (b) Hematoxylin–eosin staining for bone marrow regions and (c) Masson’s trichrome staining for collagen regions (green in color). (d) Backscattered electron microscope image of an engineered bone showing canaliculi regions similar to the femoral bone (EB is engineered bone and BM is bone marrow). (Reproduced from Reference [79] with permission, 2006, Elsevier Ltd.).

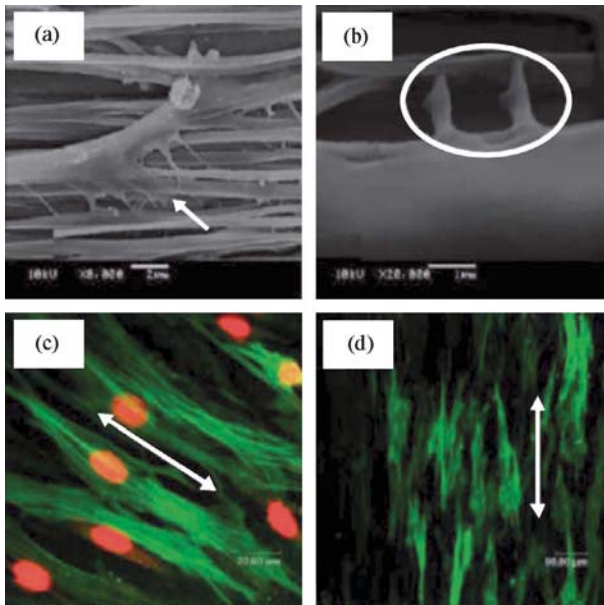


FIGURE 15.7 SEM micrographs showing the SMCs adhesion on the aligned P(LLA-CL) nanofibers: (a) SMC alignment along the fiber orientation with focal contacts and (b) close-up of SMC focal contacts that are attached to the surrounding fibers. Confocal micrographs of SMCs after 1 day culture immunostained for (c) α -actin and (d) myosin filaments. Arrow indicates the fiber orientation. (Reproduced from Reference [88] with permission, 2006, Elsevier Ltd.).

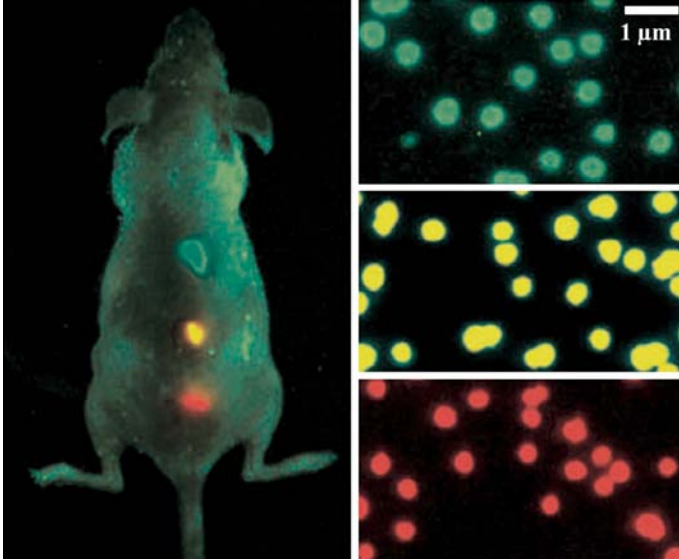


FIGURE 16.1 Multicolor quantum dot (QD) capability of QD imaging in live animals. Approximately one to two million in each color were injected subcutaneously at three adjacent locations on a host animal. Images were obtained with tungsten or mercury lamp excitation. (Reprinted from Reference [25], with permission from Macmillan Publisher Ltd.)

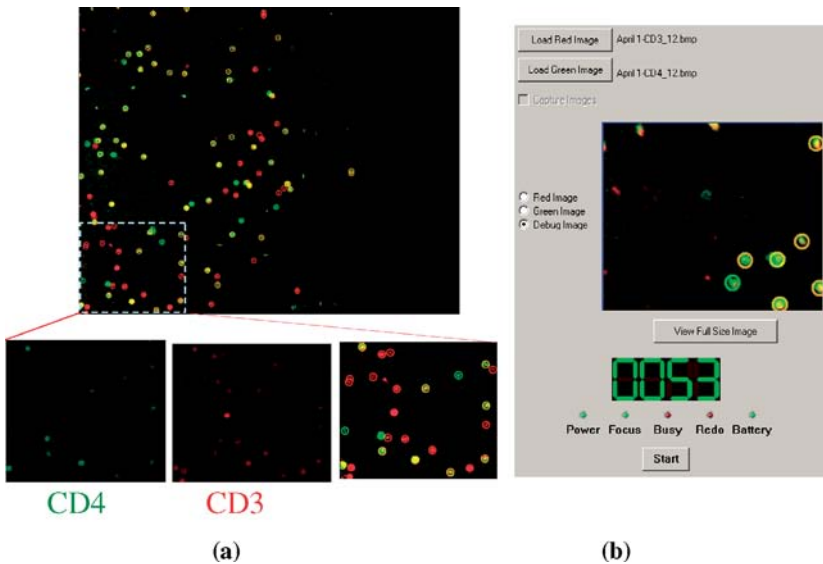


FIGURE 17.5 Detection of CD4⁺ T lymphocytes in microfluidic-based devices for monitoring HIV. See text for full caption.